

AD-A154 300

USAF/SCEEE GRADUATE STUDENT SUMMER RESEARCH PROGRAM  
(1984) PROGRAM MANAGE.. (U) SOUTHEASTERN CENTER FOR  
ELECTRICAL ENGINEERING EDUCATION INC 5..

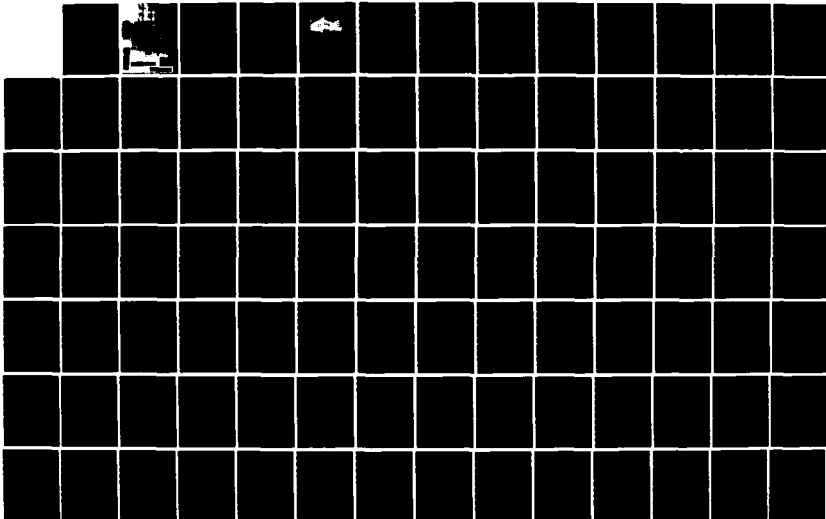
1/10

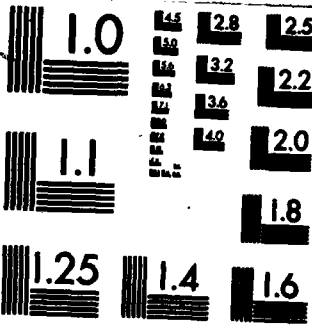
UNCLASSIFIED

W D PEELE ET AL. OCT 84 AFOSR-TR-85-0476

F/G 5/1

NL





MICROCOPY RESOLUTION TEST CHART  
NATIONAL BUREAU OF STANDARDS-1963-A

2

AIR FORCE OFFICE OF SCIENTIFIC RESEARCH

THE UNITED STATES AIR FORCE

GRADUATE STUDENT  
SUMMER RESEARCH PROGRAM

conducted by the  
SOUTHEASTERN CENTER,  
FOR ELECTRICAL ENGINEERING EDUCATION  
(SCEEE)

1984  
TECHNICAL REPORT  
VOLUME I  
OF II

SCEEE PROGRAM DIRECTORS:

WARREN D. PEELE

EARL L. STEELE

DISTRIBUTION STATEMENT A  
Approved for public release;  
Distribution Unlimited

DTIC  
ELECTE  
MAY 30 1985  
S D D

THE SCEEE

85 5 28 100

AD-A154 300

DTIC FILE COPY

UNCLASSIFIED

ADA 154 300

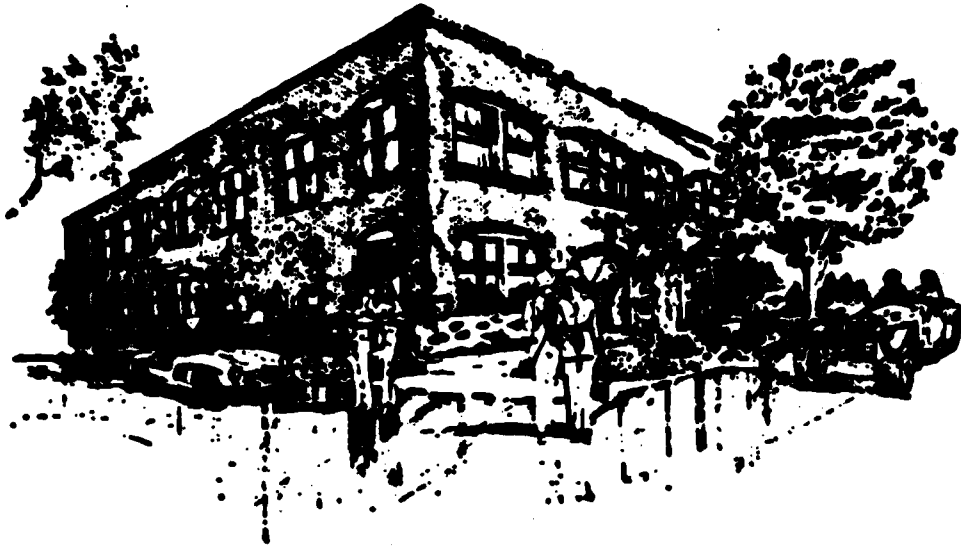
SECURITY CLASSIFICATION OF THIS PAGE

REPORT DOCUMENTATION PAGE

1a. REPORT SECURITY CLASSIFICATION <b>UNCLASSIFIED</b>		1b. RESTRICTIVE MARKINGS	
2a. SECURITY CLASSIFICATION AUTHORITY		3. DISTRIBUTION/AVAILABILITY OF REPORT <b>APPROVED FOR PUBLIC RELEASE; DISTRIBUTION UNLIMITED</b>	
2b. DECLASSIFICATION/DOWNGRADING SCHEDULE			
4. PERFORMING ORGANIZATION REPORT NUMBER(S)		5. MONITORING ORGANIZATION REPORT NUMBER(S) <b>AFOSR-TR- 85 - 0476</b>	
6a. NAME OF PERFORMING ORGANIZATION <b>Southeastern Center for Electrical Engineering Education</b>	6b. OFFICE SYMBOL <i>(If applicable)</i>	7a. NAME OF MONITORING ORGANIZATION <b>Air Force Office of Scientific Research/XOT</b>	
6c. ADDRESS (City, State and ZIP Code) <b>11th &amp; Massachusetts Ave: St. Cloud, FL 32769</b>		7b. ADDRESS (City, State and ZIP Code) <b>Building 410 Bolling AFB, DC 20332-6448</b>	
8a. NAME OF FUNDING/SPONSORING ORGANIZATION <b>AFOSR</b>	8b. OFFICE SYMBOL <i>(If applicable)</i> <b>XOT</b>	9. PROCUREMENT INSTRUMENT IDENTIFICATION NUMBER <b>F49620-82-C-0035</b>	
8c. ADDRESS (City, State and ZIP Code) <b>Building 410 Bolling AFB, DC 20332-6448</b>		10. SOURCE OF FUNDING NOS.	
		PROGRAM ELEMENT NO. <b>61102F</b>	PROJECT NO. <b>2301</b>
		TASK NO. <b>D5</b>	WORK UNIT NO.
11. TITLE (Include Security Classification) <b>United States Air Force Graduate Student Summer Research Program (1984) Volume 1</b>			
12. PERSONAL AUTHOR(S) <b>Warren D. Peele, Earl L. Steele, Major Amos L. Otis</b>			
13a. TYPE OF REPORT <b>FINAL</b>	13b. TIME COVERED FROM _____ TO _____	14. DATE OF REPORT (Yr., Mo., Day) <b>October 1984</b>	15. PAGE COUNT
16. SUPPLEMENTARY NOTATION			
17. COBATI CODES		18. SUBJECT TERMS (Continue on reverse if necessary and identify by block number)	
FIELD	GROUP	SUB. GR.	
19. ABSTRACT (Continue on reverse if necessary and identify by block number) <p>→ A pilot program for the Graduate Student Summer Research Program (GSSRP) was initiated by contract modification to the AFOSR Summer Faculty Research Program (SFRP) on 26 March, 1982. The program was developed as an adjunct effort to the SFRP. Its purpose is to provide funds for selected graduate students to do research at an appropriate Air Force laboratory or center with a supervising professor who holds a concurrent SFRP appointment. In the 1982 pilot program, SCEEE appointed 17 graduate students representing 15 schools and 10 disciplines in science and engineering. In 1983 the program was expanded to 53 students representing 36 schools and 18 disciplines. The 53 participants were selected from 117 applicants. In 1984 we had 112 applicants and made 84 graduate student appointments.</p>			
20. DISTRIBUTION/AVAILABILITY OF ABSTRACT <b>UNCLASSIFIED/UNLIMITED <input checked="" type="checkbox"/> SAME AS RPT. <input type="checkbox"/> DTIC USERS <input type="checkbox"/></b>		21. ABSTRACT SECURITY CLASSIFICATION <b>UNCLASSIFIED</b>	
22a. NAME OF RESPONSIBLE INDIVIDUAL <b>MAJOR AMOS L. OTIS</b>		22b. TELEPHONE NUMBER <i>(Include Area Code)</i> <b>(202) 767-4971</b>	22c. OFFICE SYMBOL <b>XOT</b>

AFOSR-TR- 85 - 0476

Approved for public release ;  
distribution unlimited.



SCEEE  
©  
1984



<b>Accession For</b>	
NTIS GRA&I	<input checked="" type="checkbox"/>
DTIC TAB	<input type="checkbox"/>
Unannounced	<input type="checkbox"/>
Justification	
By _____	
Distribution/	
Availability Codes	
Dist	Avail and/or Special
PA-1	

1984 USAF/SCEEE  
GRADUATE STUDENT SUMMER RESEARCH PROGRAM

Conducted by  
Southeastern Center for  
Electrical Engineering Education

under  
USAF Contract Number F49620-82-C-0035

PROGRAM MANAGEMENT REPORT

Volume I of II

Program Directors, SCEEE  
Warren D. Peele  
Earl L. Steele

Program Manager, AFOSR  
Major Amos L. Otis

Submitted to  
Air Force Office of Scientific Research  
Bolling Air Force Base  
Washington D.C.

by  
Southeastern Center for  
Electrical Engineering Education

October 1984

TABLE OF CONTENTS

<u>Section</u>		<u>Page</u>
I.	Introduction and History. . . . .	1
II.	List of 1984 Graduate Student Participants. . . . .	3
III.	Participant Laboratory Assignment . . . . .	14
IV.	Research Report Index . . . . .	17
V.	Graduate Student Research Reports . . . . .	24

## INTRODUCTION & HISTORY

A pilot program for the Graduate Student Summer Research Program (GSSRP) was initiated by contract modification to the AFOSR Summer Faculty Research Program (SFRP) on 26 March 1982. The program was developed as an adjunct effort to the SFRP. Its purpose is to provide funds for selected graduate students to do research at an appropriate Air Force laboratory or center with a supervising professor who holds a concurrent SFRP appointment. In the 1982 pilot program, SCEE appointed 17 graduate students representing 15 schools and 10 disciplines in science and engineering. In 1983 the program was expanded to 53 students representing 36 schools and 18 disciplines. The 53 participants were selected from 117 applicants. In 1984 we had 112 applicants and made 84 graduate student appointments.

To be eligible, all candidates had to be currently registered in a graduate program. The graduate students were selected from the fields of engineering, computer science, mathematics, or the physical sciences. They were supervised by a faculty member who held an appointment as a SCEE Fellow for the summer of 1984 under the Summer Faculty Research Program or an Air Force laboratory designated colleague. The students were U.S. citizens, working toward an appropriate graduate degree, and currently enrolled in the graduate school at their respective institutions.

The graduate student researchers in this program had the following specific obligations:

- 1) To participate in research under the direction of a faculty member or Air Force supervisor at an Air Force laboratory or center;
- 2) To prepare a report at the end of the summer period describing the summer research accomplishments. The report must have been approved by or co-authored with the supervising faculty member or Air Force supervisor;
- 3) To complete an evaluation questionnaire on the Graduate Student Summer Research Program.

1984 GSSRP OBJECTIVES: (1) To provide a productive means for a graduate student to participate in research under the direction of a faculty member or an Air Force designated supervisor at an Air Force laboratory or center; (2) to stimulate continuing professional association among graduate students, the supervising professors, and professional peers in the Air Force; and (3) to enhance the research productivity and capabilities of engineering and science graduate students.

**PREREQUISITES FOR APPOINTMENTS:** To qualify as a graduate researcher in the 1984 GSSR Program, applicants must be: (1) U.S. citizens; (2) holders of a B.S. or M.S. degree in an appropriate technical specialty; (3) registered in a graduate school working toward an appropriate graduate degree; and (4) willing to pursue their summer research work under the direction of a supervising professor who holds an appointment under the SFRP for the summer of 1984 or an assigned Air Force supervisor.

**RESEARCH PERIOD:** The period of the student appointments was for ten continuous weeks at the research site between May 1, 1984 and September 30, 1984. The student's research period coincided with the appointment period of the supervising professor with whom the student worked.

**APPLICATION DEADLINE:** April 15, 1984

**FINANCIAL TERMS:** Stipends for graduate student researchers were paid as follows:

\$55.00 per day (\$275 per week) for B.S. degree holders;  
\$65.00 per day (\$325 per week) for M.S. degree holders.

Travel expenses were reimbursed to the student for round trip travel between the researcher's school location and the Air Force facility in accordance with SCEEE travel policy. A living expense allowance of \$25.00 per day was paid for each day the researcher spent at the Air Force location.

Evaluations have been requested of the laboratory contacts and all have responded in writing or verbally. The common opinions among government laboratory scientists, faculty, and students are:

- (a) That the program is a valuable addition to the Summer Faculty Research Program;
- (b) That the program should be continued;
- (c) That students should be supervised by faculty researchers;
- (d) That the students are highly motivated and contribute significantly to the research effort;
- (e) That exposure to USAF R&D produces a positive student opinion of the USAF.

This report contains detailed and summarized data relevant to the 1984 Graduate Student Summer Research Program.

LIST OF 1984 GRADUATE STUDENT PARTICIPANTS

NAME/ADDRESS

DEGREE, SPECIALTY,  
LABORATORY ASSIGNED

Anton Ahrens  
University of Kansas  
Department of Chemistry  
Lawrence, KS 66045  
(913) 864-4220

Degree: B.S., Chemical Engineering,  
1980  
Specialty: Gas Phase Reaction Dynamics  
Assigned: GL

Jay Ambrose  
Washington State University  
Mechanical Engineering Department  
Pullman, WA 99164-2920  
(509) 335-8654

Degree: B.S., Mechanical Engineering,  
1984  
Specialty: Thermal Sciences  
Assigned: APL

Vicki Atkins  
University of Kentucky  
Dept. of Electrical Engineering  
Lexington, KY 40506  
(606) 257-1104

Degree: M.S., Mathematics,  
1981  
Specialty: Controls  
Assigned: FDL

Joseph Badalamenti  
University of Dayton  
Mechanical Engineering Dept.  
Dayton, OH 45409  
(513) 229-0123

Degree: B.S., Mechanical Engineering,  
1983  
Specialty: Mechanical Design  
Assigned: FDL

David Bauer  
California State University  
Computer Science Department  
Chico, CA 95925  
(916) 895-6442

Degree: B.S., Applied Physics,  
1982  
Specialty: Artificial Intelligence  
Assigned: RADC

Robert Bigelis  
Washington State University  
Civil & Environmental Eng. Dept.  
Pullman, WA 99164  
(509) 335-2576

Degree: B.S., Civil Engineering,  
1984  
Specialty: Structures  
Assigned: WL

Scott Bischoff  
Texas Lutheran College  
Department of Biology  
Sequin, TX 78155  
(512) 379-5675

Degree: B.S., Biology,  
1984  
Specialty: Medicine  
Assigned: SAM

Philip Blosser  
Wright State University  
School of Engineering  
Dayton, OH 45435  
(513) 873-2403

Degree: B.S., Material Science & Eng.,  
1984  
Specialty: Metals Processing  
Assigned: ML

LIST OF 1984 GRADUATE STUDENT PARTICIPANTS (continued)

NAME/ADDRESS	DEGREE, SPECIALTY, LABORATORY ASSIGNED
Donna Brandelik Wright State University Chemistry Department Dayton, OH 45435 (513) 873-2855	<u>Degree:</u> B.S., Chemistry, 1983 <u>Specialty:</u> Polymer Chemistry <u>Assigned:</u> Materials Laboratory
Frederick Breslin University of New Mexico Department of Mathematics Albuquerque, NM 87131 (505) 277-4613	<u>Degree:</u> M.A., Mathematics, 1983 <u>Specialty:</u> Statistics <u>Assigned:</u> Weapons Laboratory
Jan Brooks The University of Alabama Dept. of Management & Marketing University, AL 35486 (205) 348-6090	<u>Degree:</u> M.S., School of Social Work, 1974 <u>Specialty:</u> Organizational Behavior <u>Assigned:</u> Leadership & Mgmt. Dev. Ctr.
Howard Brown The Ohio State University Department of Civil Engineering Columbus, OH 43210 (614) 422-2771	<u>Degree:</u> M.S., Structural Eng., 1979 <u>Specialty:</u> Delamination & Failure of Angle Ply Laminated Comp. <u>Assigned:</u> Materials Laboratory
Robert Cheney University of Missouri Physics Department Rolla, MO 65401 (314) 341-4702	<u>Degree:</u> B.S., Physics, 1983 <u>Specialty:</u> Undecided <u>Assigned:</u> Aero Propulsion Laboratory
Susan Cheney The Ohio State University Department of Civil Engineering Columbus, OH 43210 (614) 422-2771	<u>Degree:</u> B.S., Civil Engineering, 1983 <u>Specialty:</u> Mechanics of Structural Composites <u>Assigned:</u> Materials Laboratory
Michael Coovert The Ohio State University Department of Psychology Columbus, OH 43210 (614) 422-8175	<u>Degree:</u> M.S., Psychology, 1981 <u>Specialty:</u> Ind./Organ. Psychology <u>Assigned:</u> Human Resources Laboratory
William Czelen Wright State University School of Medicine Dayton, OH 45401 (513) 278-9185	<u>Degree:</u> M.D., Aerospace Medicine, 1971 <u>Specialty:</u> Aerospace Medicine <u>Assigned:</u> USAF School of Aerospace Medicine

LIST OF 1984 GRADUATE STUDENT PARTICIPANTS (continued):

NAME/ADDRESS	DEGREE, SPECIALTY, LABORATORY ASSIGNED
Jennifer Davidson University of Florida Department of Mathematics Gainesville, FL 32611 (904) 392-0281	<u>Degree:</u> B.A., Physics, 1979 <u>Specialty:</u> Applied Mathematics <u>Assigned:</u> Armament Division
Timothy Downes North Dakota State University Dept. of Mathematical Sciences West Fargo, ND 58078 (701) 282-8519	<u>Degree:</u> M.B.A., Finance Marketing, 1978 <u>Specialty:</u> Computer <u>Assigned:</u> Science/Operations Research Logistics Command
Jon Ebert University of Oklahoma Aerospace, Mech., & Nuclear Eng. Norman, OK 73019 (405) 325-5011	<u>Degree:</u> M.S., Mechanical Eng., 1984 <u>Specialty:</u> Computational Fluid Dynam. <u>Assigned:</u> Aero Propulsion Laboratory
James Farmer University of Vermont Mechanical Engineering Dept. Burlington, VT 05405 (802) 656-3800	<u>Degree:</u> B.S., Mechanical Eng., 1983 <u>Specialty:</u> Thermal Sciences <u>Assigned:</u> Materials Laboratory
Mark Ferrel Kansas State University Nuclear Engineering Department Manhattan, KS 66502 (913) 776-1393	<u>Degree:</u> B.S., Physics, 1983 <u>Specialty:</u> Nuclear Engineering <u>Assigned:</u> F.J. Seiler Research Lab.
John Flach The Ohio State University Psychology Department Columbus, OH 43210 (614) 422-4131	<u>Degree:</u> M.A., Psychology, 1978 <u>Specialty:</u> Human Performance Theory <u>Assigned:</u> Aerospace Medical Rsch. Lab.
Paul Gader University of Florida Department of Mathematics Gainesville, FL 32611 (904) 392-0281	<u>Degree:</u> M.S., Mathematics, 1983 <u>Specialty:</u> Applied Mathematics <u>Assigned:</u> Armament Division
Carolyn Green Wayne State University School of Medicine Detroit, MI 48202 (313) 577-5115	<u>Degree:</u> B.A., Biochem. & Biology, 1982 <u>Specialty:</u> Medicine, Physiology <u>Assigned:</u> USAF School of Aerospace Medicine

LIST OF 1984 GRADUATE STUDENT PARTICIPANTS (continued)

NAME/ADDRESS	DEGREE, SPECIALTY, LABORATORY ASSIGNED
Bruce Harmon University of Cincinnati Department of Economics Cincinnati, OH 45263 (513) 475-4241	<u>Degree:</u> B.S., Economics, 1980 <u>Specialty:</u> Economics <u>Assigned:</u> Business Rsch. Mgmt. Center
Thomas Hayward University of Wyoming Dept. of Physics & Astronomy Laramie, WY 82071 (307) 766-6150	<u>Degree:</u> B.S., Physics & Astronomy, 1983 <u>Specialty:</u> Infrared Astronomy <u>Assigned:</u> Geophysics Laboratory
Ron Hightower Kansas State University Dept. of Electrical Engineering Manhattan, KS 66506 (913) 532-5600	<u>Degree:</u> B.S., Electrical Eng., 1983 <u>Specialty:</u> Electrical Engineering <u>Assigned:</u> Weapons Laboratory
Joseph Hjelm Wright State University School of Engineering Dayton, OH 45435 (513) 873-2403	<u>Degree:</u> B.S., Materials Sci. & Eng., 1984 <u>Specialty:</u> Metal Processing <u>Assigned:</u> Materials Laboratory
Arthur Hogan University of Alabama Dept. of Biomath. & Biostatistics Birmingham, AL 35294 (205) 934-4905	<u>Degree:</u> M.S., Biology, 1979 <u>Specialty:</u> Applied Stat. & Mathematics, <u>Assigned:</u> USAF School of Aerospace Medicine
Thomas Hopp Northwestern University Dept. of Mech. & Nuclear Eng. Evanston, IL 60201 (312) 492-7470	<u>Degree:</u> B.S., Mechanical Eng., 1982 <u>Specialty:</u> Control Systems Engineering <u>Assigned:</u> Flight Dynamics Laboratory
Robert Hoskin Purdue University Mechanical Engineering Department W. Lafayette, IN 47906 (317) 743-6558	<u>Degree:</u> B.S., Mechanical Eng., 1983 <u>Specialty:</u> Control Systems <u>Assigned:</u> Aero Propulsion Laboratory
George Howard, Jr. Meharry Medical College Div. of Biomedical Sciences Nashville, TN 37208 (615) 327-6212	<u>Degree:</u> B.A., Zoology, 1977 <u>Specialty:</u> Biochemical Toxicology <u>Assigned:</u> USAF School of Aerospace Medicine

LIST OF 1984 GRADUATE STUDENT PARTICIPANTS (continued)

NAME/ADDRESS	DEGREE, SPECIALTY, LABORATORY ASSIGNED
<p>Marc Hunter Southern Illinois University Psychology Department Edwardsville, IL 62025 (618) 656-5692</p>	<p><u>Degree:</u> B.S., Psychology, 1982 <u>Specialty:</u> Experimental Psychology <u>Assigned:</u> Human Resources Laboratory</p>
<p>Joseph Kager Auburn University Management Department Opelika, AL 36801 (205) 749-7909</p>	<p><u>Degree:</u> B.S., Ind./Organ. Psych., 1983 <u>Specialty:</u> Human Resource Management <u>Assigned:</u> Leadership and Management Development Center</p>
<p>John Kayser The Ohio State University Dept. of Chemical Engineering Columbus, OH 43210 (614) 422-6446</p>	<p><u>Degree:</u> B.S., Chemical Engineering, 1982 <u>Specialty:</u> Pressure Swing Adsorption <u>Assigned:</u> USAF School of Aerospace Medicine</p>
<p>Nancy Kirkwood Colorado State University Department of Mathematics Fort Collins, CO 80523 (303) 491-7617</p>	<p><u>Degree:</u> B.S., Computer Science, 1983 <u>Specialty:</u> Applied Discrete Math. <u>Assigned:</u> Rome Air Dev. Center</p>
<p>Guy Klose University of Vermont Dept. of Comp. Sci. &amp; Elec. Eng. Burlington, VT 05401 (802) 658-4250</p>	<p><u>Degree:</u> B.S., Electrical Eng., 1983 <u>Specialty:</u> Digital Signal Processing <u>Assigned:</u> Rome Air Development Center</p>
<p>John Kreuter Tulane University Computer Science Department New Orleans, LA 70118 (504) 865-5000</p>	<p><u>Degree:</u> B.S., Mathematics, 1972 <u>Specialty:</u> Computer Science <u>Assigned:</u> Human Resources Laboratory</p>
<p>Michael Lange University of New Mexico Physics &amp; Astronomy Dept. Albuquerque, NM 87131 (505) 277-2916</p>	<p><u>Degree:</u> M.A., Mechanical Eng., 1981 <u>Specialty:</u> Laser Physics <u>Assigned:</u> Weapons Laboratory</p>
<p>Barry Lemieux University of Lowell Computer Science Dept. Lowell, MA 01854 (617) 452-5000</p>	<p><u>Degree:</u> B.S., Electrical Eng., 1984 <u>Specialty:</u> Computer Science <u>Assigned:</u> Geophysics Laboratory</p>

LIST OF 1984 GRADUATE STUDENT PARTICIPANTS (continued)

NAME/ADDRESS

DEGREE, SPECIALTY,  
LABORATORY ASSIGNED

Eric Liverance  
Yale University  
Department of Mathematics  
New Haven, CT 06520  
(203) 436-1642

Degree: B.A., Mathematics,  
1983  
Specialty: Galois & Number Theory  
Assigned: Flight Dynamics Laboratory

Steven Lottes  
University of Illinois  
Department of Mechanical Eng.  
Naperville, IL 60540  
(312) 420-7610

Degree: M.S., Computer Science,  
1973  
Specialty: Combustion Modeling  
Assigned: Aero Propulsion Laboratory

James Lyne  
Vanderbilt University  
School of Medicine  
Nashville, TN 37203  
(615) 322-6109

Degree: M.S., Engineering Physics,  
1982  
Specialty: Medicine  
Assigned: Arnold Engineering  
Development Center

Duncan MacFarlane  
Brown University  
Electrical Engineering Dept.  
Providence, RI 02912  
(401) 273-4857

Degree: B.S., Electrical Eng.,  
1984  
Specialty: Quantum Electronics  
Assigned: Geophysics Laboratory

John McKelvey  
Wright State University  
School of Engineering  
Dayton, OH 45435  
(513) 873-2403

Degree: B.S., Materials Sci. & Eng.,  
1984  
Specialty: Metal Processing  
Assigned: Materials Laboratory

Steven Miller  
Washington State University  
Dept. of Civil & Environ. Eng.  
Pullman, WA 99164  
(509) 335-2576

Degree: B.S., Civil Engineering,  
1984  
Specialty: Structures  
Assigned: Weapons Laboratory

Margarita Miro-Julia  
University of Cincinnati  
Physics Department  
Cincinnati, OH 45221  
(513) 475-6912

Degree: M.S., Physics,  
1984  
Specialty: Many Body Theory  
Assigned: Aero Propulsion Laboratory

Paul Nichols  
The University of Iowa  
College of Education  
Iowa City, IA 52242  
(319) 353-6703

Degree: B.S., Psychology,  
1983  
Specialty: Information Theories of  
Learning  
Assigned: Human Resources Laboratory

LIST OF 1984 GRADUATE STUDENT PARTICIPANTS (continued)

NAME/ADDRESS

DEGREE, SPECIALTY,  
LABORATORY ASSIGNED

Edouard Noisin  
Meharry Medical College  
Department of Biochemistry  
Nashville, TN 37208  
(615) 327-6216

Degree: B.S., Biology, 1979  
Specialty: Neuronal Cell Membrane  
Receptors  
Assigned: USF School of Aerospace  
Medicine

David Norton  
Louisiana State University  
Dept. of Elec. & Computer Eng.  
Baton Rouge, LA 70816  
(504) 293-1540

Degree: B.S., Electrical Engineer,  
1984  
Specialty: Integrated Circuit  
Fabrication & Design  
Assigned: Avionics Laboratory

Raymond Patin  
Louisiana State University  
Mechanical Engineering Dept.  
Baton Rouge, LA 70803  
(504) 388-5792

Degree: B.S., Mechanical Engineering,  
1983  
Specialty: Thermal Science  
Assigned: Armament Division

David Patterson  
University of Oklahoma  
School of Industrial Engineering  
Norman, OK 73019  
(405) 325-3721

Degree: B.A., Psychology,  
1981  
Specialty: Human Factors  
Assigned: Aerospace Medical Research  
Laboratory

Michael Patterson  
Georgia Institute of Technology  
School of Psychology  
Atlanta, GA 30332  
(404) 894-2680

Degree: M.S., Psychology,  
1983  
Specialty: Engineering Psychology  
Assigned: Arnold Eng. Dev. Center

Jon Phillips  
Washington State University  
Mechanical Engineering Dept.  
Pullman, WA 99163  
(509) 335-3000

Degree: B.S., Mechanical Eng.,  
1984  
Specialty: Thermal Sciences  
Assigned: Aero Propulsion Laboratory

Debra Picklesimer  
Wright State University  
Department of Chemistry  
Dayton, OH 45435  
(513) 873-2855

Degree: B.S., Chemistry,  
1981  
Specialty: Organic/Polymer Chemistry  
Assigned: Materials Laboratory

Benjamin Pruitt  
University of Kentucky  
Electrical Engineering Dept.  
Lexington, KY 40506  
(606) 257-8042

Degree: B.S., Electrical Eng.,  
1982  
Specialty: Electro Physics  
Assigned: Rome Air Development Center

LIST OF 1984 GRADUATE STUDENT PARTICIPANTS (continued)

NAME/ADDRESS	DEGREE, SPECIALTY, LABORATORY ASSIGNED
William Rabinovich Brown University Department of Physics Providence of RI 02912 (401) 863-3078	<u>Degree:</u> B.S., Physics, 1982 <u>Specialty:</u> Quantum Optics <u>Assigned:</u> Geophysics Laboratory
John Ramsey The Ohio State University Aero. & Astro. Engineering Dept. Columbus, OH 43210 (614) 422-2691	<u>Degree:</u> B.S., Aeronautical & Astronautical Eng., 1982 <u>Specialty:</u> Structures <u>Assigned:</u> Aero Propulsion Laboratory
Christopher Reed University of Florida Dept. of Engineering Sciences Gainesville, FL 32211 (904) 392-0961	<u>Degree:</u> M.S., Engineering Science, 1984 <u>Specialty:</u> Aerodynamics <u>Assigned:</u> Armament Division
Joseph Rencis Case Western Reserve University Civil Engineering Department Cleveland, OH 44106 (216) 368-2952	<u>Degree:</u> B.S., Applied Mathematics, 1983 <u>Specialty:</u> Fluid Mechanics <u>Assigned:</u> Armament Division
Lila Roberts Old Dominion University Department of Mathematics Norfolk, VA 23508 (804) 440-3882	<u>Degree:</u> B.S., Mathematics, 1977 <u>Specialty:</u> Numerical Analysis <u>Assigned:</u> Avionics Laboratory
Karlin Roth University of Florida Department of Eng. Science Gainesville, FL 32611 (904) 392-0961	<u>Degree:</u> B.S., Applied Mathematics, 1983 <u>Specialty:</u> Fluid Mechanics <u>Assigned:</u> Armament Division
Debra Rotto Texas Lutheran College Department of Biology Seguin, TX 78155 (512) 379-4161	<u>Degree:</u> B.S., Biology, 1983 <u>Specialty:</u> Cardiovascular Physiology <u>Assigned:</u> USAF School of Aerospace Medicine
Diane Rotto Texas Lutheran College Department of Biology Seguin, TX 78155 (512) 379-4161	<u>Degree:</u> B.S., Biology, 1983 <u>Specialty:</u> Cardiovascular Physiology <u>Assigned:</u> USAF School of Aerospace Medicine

LIST OF 1984 GRADUATE STUDENT PARTICIPANTS (continued)

NAME/ADDRESS	DEGREE, SPECIALTY, LABORATORY ASSIGNED
Christine Ruben Texas Southern University Biology Department Houston, TX 77061 (713) 527-7005	<u>Degree:</u> B.S., Biology, 1980 <u>Specialty:</u> Undecided <u>Assigned:</u> Aerospace Medical Research Laboratory
Carlos Sanchez-Castro Michigan State University Physics Department East Lansing, MI 48825 (517) 355-3877	<u>Degree:</u> M.S., Physics, 1983 <u>Specialty:</u> Solid & Nuclear Physics <u>Assigned:</u> Flight Dynamics Laboratory
Randall Schadt University of Missouri Physics Department Rolla, MO 65401 (314) 341-4780	<u>Degree:</u> B.S., Physics, 1982 <u>Specialty:</u> Solid State Physics <u>Assigned:</u> Aero Propulsion Laboratory
Joshua Smith University of Vermont Mechanical Eng. Department Burlington, VT 05405 (802) 656-3800	<u>Degree:</u> B.S., Mechanical Eng., 1983 <u>Specialty:</u> Materials Processing <u>Assigned:</u> Materials Laboratory
Joseph Solomon University of Connecticut Department of Psychology Storrs, CT 06268 (203) 486-2337	<u>Degree:</u> M.A., Psychology, 1980 <u>Specialty:</u> Visual Perception <u>Assigned:</u> Aerospace Medical Research Laboratory
Lori Streit Arizona State University Department of Chemistry Tempe, AZ 85287 (602) 965-3461	<u>Degree:</u> B.S., Chemistry, 1983 <u>Specialty:</u> Analytical Chemistry <u>Assigned:</u> USAF School of Aerospace Medicine
Russell Thomas Kansas State University Department of Electrical Eng. Manhattan, KS 66502 (913) 539-3700	<u>Degree:</u> B.S., Electrical Eng., 1983 <u>Specialty:</u> Network Modeling & Analysis <u>Assigned:</u> Weapons Laboratory
Terry Thompson Meharry Medical College Department of Pharmacology Nashville, TN 37208 (615) 327-6979	<u>Degree:</u> B.S., Chemistry/Biology, 1979 <u>Specialty:</u> Neurotransmitter Regulation <u>Assigned:</u> USAF School of Aerospace Medicine

LIST OF 1984 GRADUATE STUDENT PARTICIPANTS (continued)

NAME/ADDRESS	DEGREE, SPECIALTY, LABORATORY ASSIGNED
Eric Utt University of Central Florida Dept. of Biological Sciences Orlando, FL 32816 (305) 275-2141	<u>Degree:</u> B.S., Microbiology, 1984 <u>Specialty:</u> Microbiology/Biotechnology <u>Assigned:</u> USAF School of Aerospace Medicine
Donald Varvel North Dakota State University Div. of Mathematical Sciences Fargo, ND 58105 (701) 777-3460	<u>Degree:</u> B.S., Computer Science, 1978 <u>Specialty:</u> Database Systems <u>Assigned:</u> Electronics Systems Div.
Peggy Vaughn Alabama A&M University Department of Psychology Normal, AL 35762 (205) 859-7336	<u>Degree:</u> B.S., Psychology, 1982 <u>Specialty:</u> Clinical Psychology <u>Assigned:</u> Leadership & Management Development Center
Kevin Verfaillie University of Vermont Department of Electrical Eng. Burlington, VT 05405 (802) 656-3330	<u>Degree:</u> B.S., Electrical Eng., 1981 <u>Specialty:</u> Signal Processing <u>Assigned:</u> Rome Air Development Ctr.
Michael Wager University of Dayton Engineering Department Dayton, OH 45469 (513) 229-2311	<u>Degree:</u> B.S., Physics, 1983 <u>Specialty:</u> Electro-Optics <u>Assigned:</u> Materials Laboratory
Ronald Wasserstein Kansas State University Department of Statistics Manhattan, KS 66502 (913) 532-6883	<u>Degree:</u> M.S., Statistics, 1983 <u>Specialty:</u> Regression Analysis <u>Assigned:</u> USAF School of Aerospace Medicine
Kenneth Wauchope Tulane University Department of Computer Science New Orleans, LA 70118 (504) 865-5100	<u>Degree:</u> B.A., Speech, 1971 <u>Specialty:</u> Artificial Intelligence <u>Assigned:</u> Human Resources Laboratory
Dennis Weatherby University of Dayton Chemical Engineering Department Dayton, OH 45469 (513) 229-2627	<u>Degree:</u> B.S., Chemistry, 1982 <u>Specialty:</u> Polymer Science <u>Assigned:</u> Materials Laboratory

LIST OF 1984 GRADUATE STUDENT PARTICIPANTS (continued)

NAME/ADDRESS

DEGREE, SPECIALTY,  
LABORATORY ASSIGNED

Paul Wetzel  
University of Illinois  
Department of Bioengineering  
Chicago, IL 60680  
(312) 787-9346

Degree: M.S., Bioengineering,  
1979  
Specialty: Oculomotor Control  
Assigned: Human Resources Laboratory

Kevin White  
University of Oklahoma  
Mechanical Engineering Dept.  
Norman, OK 73069  
(405) 325-5011

Degree: B.S., Mechanical Eng.,  
1979  
Specialty: Solid Mechanics  
Assigned: Materials Laboratory

Kurt Ziegler  
Kansas State University  
Department of Electrical Eng.  
Manhattan, KS 66502  
(913) 532-5600

Degree: B.S., Electrical Eng.,  
1984  
Specialty: Computer Science  
Assigned: Weapons Laboratory

Kevin Zook  
Kansas State University  
Department of Nuclear Engineering  
Manhattan, KS 66502  
(913) 776-0438

Degree: B.S., Nuclear Engineering,  
1984  
Specialty: Laser Research  
Assigned: F.J. Seiler Research  
Laboratory

**PARTICIPANT LABORATORY ASSIGNMENT**

**1984 USAF/SCEEE GRADUATE STUDENT SUMMER RESEARCH PROGRAM**

**AEROPROPULSION LABORATORY**

(Wright-Patterson Air Force Base)

1. Jay Ambrose
2. Robert Cheney
3. Jon Ebert
4. Robert Hoskin
5. Stephen Lottes
6. Margarita Miro-Julia
7. Jon Philips
8. Jon Ramsey
9. Randall Schadt

Washington State University  
University of Missouri  
University of Oklahoma  
Purdue University  
University of Illinois  
University of Cincinnati  
Washington State University  
Ohio State University  
University of Missouri

**AEROSPACE MEDICAL RESEARCH LABORATORY**

(Wright-Patterson Air Force Base)

1. John Flach
2. David Patterson
3. Christine Ruben
4. Joseph Solomon

Ohio State University  
University of Oklahoma  
Texas Southern University  
University of Connecticut

**ARNOLD ENGINEERING DEVELOPMENT CENTER**

(Arnold Air Force Station)

1. James Lyne
2. Michael Patterson

Vanderbilt University  
Georgia Institute of Technology

**ARMAMENT DIVISION**

(Eglin Air Force Base)

1. Jennifer Davidson
2. Paul Gader
3. Raymond Patin
4. Christopher Reed
5. Karlin Roth

University of Florida  
University of Florida  
Louisiana State University  
University of Florida  
University of Florida

**AVIONICS LABORATORY**

(Wright-Patterson Air Force Base)

1. David Norton
2. Lila Roberts

Louisiana State University  
Old Dominion University

**BUSINESS RESEARCH MANAGEMENT CENTER**

(Wright Patterson Air Force Base)

1. Bruce Harmon

University of Cincinnati

**ELECTRONICS SYSTEMS DIVISION**

(Hanscom Air Force Base)

1. Donald Varvell

North Dakota State University

**ENGINEERING AND SERVICES CENTER**

(Tyndall Air Force Base)

1. Susan Cheney

Ohio State University

PARTICIPANT LABORATORY ASSIGNMENT (continued)

FLIGHT DYNAMICS LABORATORY

(Wright-Patterson Air Force Base)

- |                          |                            |
|--------------------------|----------------------------|
| 1. Vicki Atkins          | University of Kentucky     |
| 2. Joseph Badalamenti    | University of Dayton       |
| 3. Thomas Hopp           | Northwestern University    |
| 4. Eric Liverance        | Yale University            |
| 5. Joseph Rencis         | Case Western Reserve Univ. |
| 6. Carlos Sanchez-Castro | Michigan State University  |

FRANK J. SEILER RESEARCH LABORATORY

(United States Air Force Academy)

- |                |                         |
|----------------|-------------------------|
| 1. Mark Ferrel | Kansas State University |
| 2. Kevin Zook  | Kansas State University |

GEOPHYSICS LABORATORY

(Hanscom Air Force Base)

- |                       |                       |
|-----------------------|-----------------------|
| 1. Anton Ahrens       | University of Kansas  |
| 2. Thomas Hayward     | University of Wyoming |
| 3. Barry Lemieux      | University of Lowell  |
| 4. Duncan MacFarlane  | Brown University      |
| 5. William Rabinovich | Brown University      |

HUMAN RESOURCES LABORATORY

(Brooks Air Force Base)

- |                    |                       |
|--------------------|-----------------------|
| 1. Michael Coovert | Ohio State University |
| 2. Paul Nichols    | University of Iowa    |

HUMAN RESOURCES LABORATORY

(Lowry Air Force Base)

- |                     |                   |
|---------------------|-------------------|
| 1. John Kreuter     | Tulane University |
| 2. Kenneth Wauchope | Tulane University |

HUMAN RESOURCES LABORATORY

(Williams Air Force Base)

- |                |                              |
|----------------|------------------------------|
| 1. Marc Hunter | Southern Illinois University |
| 2. Paul Wetzal | University of Illinois       |

LEADERSHIP & MANAGEMENT DEVELOPMENT CENTER

(Maxwell Air Force Base)

- |                 |                        |
|-----------------|------------------------|
| 1. Jan Brooks   | University of Alabama  |
| 2. Joseph Kager | Auburn University      |
| 3. Peggy Vaughn | Alabama A&M University |

LOGISTICS COMMAND

(Wright-Patterson Air Force Base)

- |                   |                               |
|-------------------|-------------------------------|
| 1. Timothy Downes | North Dakota State University |
|-------------------|-------------------------------|

PARTICIPANT LABORATORY ASSIGNMENT (continued)

MATERIALS LABORATORY

(Wright-Patterson Air Force Base)

- |                      |                         |
|----------------------|-------------------------|
| 1. Philip Blosser    | Wright State University |
| 2. Donna Brandelik   | Wright State University |
| 3. Howard Brown      | Ohio State University   |
| 4. James Farmer      | University of Vermont   |
| 5. Joseph Hjelm      | Wright State University |
| 6. John McKelvey     | Wright State University |
| 7. Debra Picklesimer | Wright State University |
| 8. Joshua Smith      | University of Vermont   |
| 9. Michael Wager     | University of Dayton    |
| 10. Dennis Weatherby | University of Dayton    |
| 11. Kevin White      | University of Oklahoma  |

ROME AIR DEVELOPMENT CENTER

(Griffiss Air Force Base)

- |                    |                             |
|--------------------|-----------------------------|
| 1. David Bauer     | California State University |
| 2. Kevin Verfaille | University of Vermont       |
| 3. Nancy Kirkwood  | Colorado State University   |
| 4. Guy Klose       | University of Vermont       |
| 5. Benjamin Pruitt | University of Kentucky      |

USAF SCHOOL OF AEROSPACE MEDICINE

(Brooks Air Force Base)

- |                        |                               |
|------------------------|-------------------------------|
| 1. Scott Bischoff      | Texas Lutheran College        |
| 2. William Czelen      | Wright State University       |
| 3. Carolyn Green       | Wayne State University        |
| 4. Arthur Hogan        | University of Alabama         |
| 5. George Howard       | Meharry Medical College       |
| 6. John Kayser         | Ohio State University         |
| 7. Edouard Noisin      | Meharry Medical College       |
| 8. Debra Rotto         | Texas Lutheran College        |
| 9. Diane Rotto         | Texas Lutheran College        |
| 10. Lori Streit        | Arizona State University      |
| 11. Terry Thompson     | Meharry Medical College       |
| 12. Eric Utt           | University of Central Florida |
| 13. Ronald Wasserstein | Kansas State University       |

WEAPONS LABORATORY

(Kirtland Air Force Base)

- |                      |                             |
|----------------------|-----------------------------|
| 1. Robert Bigelis    | Washington State University |
| 2. Frederick Breslin | University of New Mexico    |
| 3. Ron Hightower     | Kansas State University     |
| 4. Michael Lange     | University of New Mexico    |
| 5. Steven Miller     | Washington State University |
| 6. Russell Thomas    | Kansas State University     |
| 7. Kurt Ziegler      | Kansas State University     |

RESEARCH REPORTS

1984 GRADUATE STUDENT SUMMER RESEARCH PROGRAM

<u>Technical Report Number</u>	<u>Title</u>	<u>Graduate Researcher</u>
Volume I		
1	Effects of Temperature and Reactant Solvation Upon the Rates of Gas-phase Ion-Molecule Reactions	Anton F. Ahrens
2	Boiling Heat Transfer in Heat Pipe Evaporator	Jay Ambrose
3	Development of a Method for Constructing the Observer Matrix for Large Order Systems	Vicki Atkins
4	Improvements in Tire/Soil Modeling Techniques	Joseph Badalamenti
5	Computer Implementation of Nonparameteric Radar Detectors	David C. Bauer
6	Research into the Development of a Structure-Media Interaction for Dynamic Finite Element Analysis	Robert L. Bigelis
7	Phospholipid Metabolism in a Synaptic Membrane Preparation Isolated from Cerebellar Cortex	Scott B. Bischoff
8	Aging Behavior of Rapidly Solidified Ti-Co and Ti-Cr-Al Alloys	Philip E. Blosser
9	New Phenoxy Substituted Dianhydrides	Donna Brandelik
10	Stochastic Behavior of Random Lay Cables	Frederick C. Breslin
11	The USAF Organizational Assessment Package: Four Critical Decisions	Jan Leeman Brooks
12	The Uniqueness of Phase Retrieval from Intensity Measurements	Howard W. Brown

<u>Technical Report Number</u>	<u>Title</u>	<u>Graduate Researcher</u>
13	Infrared Measurements of Disilane Production From a A.D.C. Discharge in Silane	Robert F. Cheney
14	Finite Element Modeling of a Wall Under Blast Loads	Susan M. Cheney
15	Analysis of the J-79, J-57, and TF-33 Job Analysis Questionnaire Assessing Task Difficulty	Michael D. Coovert
16	The Physiologic Characterization, Prediction, and Biofeedback Treatment of Motion Sickness	William E. Czelen
17	An Algorithm for Segmenting Flir Imagery Containing Bridges	Jennifer Davidson
18	Computer-Based Optimization Algorithm for LOGAIR Cargo Allocation	Timothy R. Downes
19	Calculation of Enhanced Heating in Turbulent Boundary Layers Influenced by Free Stream Turbulence	Jon L. Ebert
20	Multiple Turbine Disk Simulation Using Alpid	James R. Farmer
21	The Effects of Nuclear Radiation on the Optical Characteristics of (SiO <sub>2</sub> -ZrO <sub>2</sub> on Si Substrate) Mirrors	Mark A. Ferrel
22	The Effects of Psychophysical Matching on the Transfer of Training Between Alternative Motion Simulators	John M. Flach
23	An Algorithm for Segmenting Flir Imagery Containing Bridges	Paul Gader

<u>Technical Report Number</u>	<u>Title</u>	<u>Graduate Researcher</u>
24	Neurotransmitter Systems in the Cerebellar Glomerulus: Analysis of Gaba Uptake, Exchange, and Release	Carolyn L. Green
25	A Dynamic Approach to Airframe Cost Estimation	Bruce Harmon
26	A Readout Electronics Design for an Infrared Array	Thomas L. Hayward
27	The Factor Analysis Methodology Applied to Moe Categorization and Evaluation	Ron R. Hightower
28	The "Processing Window" for the Near Beta Ti-10V-2Fe-3Al Alloy	Joseph M. Hjelm
29	Vehicle and Crew Scheduling in Airlift Operations	Arthur M.B. Hogan
30	A Design for Minimum Eigenvalue Sensitivity Subject to Selected Modal Insensitivity	Thomas Hopp
31	Digital LQR Design for Advanced Tactical Aircraft-Stol Approach	Robert F. Hoskin
32	The Role of Antioxidant Nutrients in Preventing Hyperbaric Oxygen Damage to the Retina	George Howard, Jr.
33	The Distributional Analysis of Contrast Sensitivity Measures	Marc W. Hunter
34	Individual and Group Dynamics: A Consideration of Climate, Task Design, and Combat Readiness Factors of the OAP/OAS	Joseph F. Kager
35	Experimental Analysis of Pressure Swing Adsorption	John C. Kayser

<u>Technical Report Number</u>	<u>Title</u>	<u>Graduate Researcher</u>
36	Tackling The I/O Bottleneck	Nancy K. Kirkwood
37	A Range Update Algorithm for the Data Handling/Recording System	Guy F. Klose
38	Pattern Matching Algorithms in ADA	John Kreuter
39	Optical Thin Film Coating Damage Via Pulsed Lasers	Michael R. Lange
40	Reprocessing of Barnes Transmissometer Data	Barry R. Lemieux
41	A Computer Search for $M_{11}$ as a Galois Group Over $Q$	Eric E. Liverance
Volume II		
42	Dynamic Flow Structures in a Bluff-Body Combustor	Steven A. Lottes
43	Thermal Mapping Data Reduction in Non-Semi-Infinite Solid Regions of Wind Tunnel Models	James E. Lyne
44	Optical Bistability with Liquid Media: Experimental Studies and Theoretical Predictions	Duncan L. MacFarlane
45	The "Processing Window" for the Near Beta Ti-10V-2Fe-3Al Alloy	John K. McKelvey
46	Incorporating the Matrix Difference Equation Theory into the Samson2 Dynamic Finite Element Computer Code	Steven S. Miller
47	Calculation of Correlation Function and Self-Energy Contribution for Non-Diagonal Response Functions	Margarita Miro-Julia
48	Individual Differences in Spatial Ability: The Roles of Practice and Synthesis	Paul D. Nichols

<u>Technical Report Number</u>	<u>Title</u>	<u>Graduate Researcher</u>
49	Acetylcholine as a Neurotransmitter in Purified Bovine Glomerulus Particles	Edouard L. Noisin
50	Semi-Insulating GaAs Chromium-Doped Buffer Layers	David P. Norton
51	An Elementary Model of the Interior Ballistics of a Two-Stage Light Gas Gun	Raymond M. Patin
52	Evaluation of Training Performance for the USAF Criterion Task Set (CTS)	David W. Patterson
53	The Function of Human Operators in the Control Facilities of Wind Tunnel 4T	Michael Patterson
54	The Effective Conductivity of Layered Cloth Heat Pipe Wicks	Jon R. Phillips
55	Synthesis of Acetylene Terminated (ATS) Candidates	Debra K. Picklesimer
56	Dye Laser System Development and Beam Data Acquisition Methods	Benjamin Pruitt
57	Optical Bistability with Liquid Media: Experimental Studies and Theoretical Predictions:	William S. Rabinovich
58	Normal Modes Analysis of a 12-Bladed Disk Using the Substructuring Technique of Nastran	John K. Ramsey
59	Application of the Thin Layer Navier Stokes Code	Christopher W. Reed
60	Three Dimensional Finite Element Acoustic Analysis	Joseph J. Rencis
61	An Optimal Trajectory Problem	Lila F. Roberts

<u>Technical Report Number</u>	<u>Title</u>	<u>Graduate Researcher</u>
62	An Evaluation of a Parabolized Navier-Stokes Code for Three-Dimensional Flared Geometries	Karlin R. Roth
63	Cardiovascular Responses of High- and Low-Fit Men to Head-Down Rest Followed by Orthostasis and Exercise	Debra K. Rotto
64	Cardiovascular Responses of High- and Low-Fit Men to Head-Down Rest Followed by Orthostasis and Exercise	Diane M. Rotto
65	The Role of the Periosteum in Bone Demineralization	Christine J. Ruben
66	Simulation of Lightning Striking a C-580 Aircraft	Carlos Sanchez-Castro
67	Infrared Absorption Measurements of the $V_4$ Band of Silane in a Heated Cell	Randall J. Schadt
68	Characterization of 6061 Aluminum During Hot Deformation with Emphasis on Identification of Optimum Processing Parameters	Joshua W. Smith
69	Kinematics of the Visual Flow Field	Joseph Solomon
70	Method Validation to Detect Chemical Warfare Agent Simulants	Lori A. Streit
71	Computer Network Measures of Effectiveness	Russell D. Thomas
72	The Effect of Soman on Rat Brain Levels of Acetylcholinesterase and Choline Acetyltransferase	Terry L. Thompson
73	Bacteriologic Techniques for the Isolation and Identification of Legionellae	Eric A. Utt

<u>Technical Report Number</u>	<u>Title</u>	<u>Graduate Researcher</u>
74	Future Tactical Air Control System Database Design	Donald A. Varvel
75	Expanded Content Domains for the Air Force Spouse Survey	Peggy J. Vaughn
76	Median Filter Enhancement for Computer Recognition	Kevin J. Verfaillie
77	Raman Spectroscopy Studies of Extrinsic P-Type Silicon	Michael Wager
78	Tactical-Surge Sortie Simulation Using OGERT	Ronald L. Wasserstein
79	Pattern-Directed List Processing in Ada	Kenneth Wauchope
80	Thermal Stability Characteristics of Silahydrocarbons	Dennis W. Weatherby
81	Coordinated Head and Eye Movement Position Measurement in a Visual Flight Simulator	Paul A. Wetzel
82	Acoustic Emission in Composites	Kevin M. White
83	A Delphi Methodology for Identifying and Prioritizing Network MOEs	Kurt Ziegler
84	The Effects of Nuclear Radiation on the Optical Characteristics of Poly-Methyl Methacrylate (PMMA)	Kevin D. Zook

V. Graduate Student Research Reports

**1984 USAF-SCREE GRADUATE STUDENT SUMMER SUPPORT PROGRAM**

Sponsored by the

**AIR FORCE OFFICE OF SCIENTIFIC RESEARCH**

Conducted by the

**SOUTHEASTERN CENTER FOR ELECTRICAL ENGINEERING EDUCATION**

**FINAL REPORT**

**EFFECTS OF TEMPERATURE AND REACTANT SOLVATION UPON**

**THE RATES OF GAS-PHASE ION-MOLECULE REACTIONS**

Prepared by: Anton F. Ahrens  
and Peter M. Hierl

Academic Rank: (A.F.A.) Graduate Student  
(P.M.H.) Professor (SFRP Supervising  
Faculty Member)

Department and University: Department of Chemistry  
University of Kansas

Research Location: Air Force Geophysics Laboratory (LID)  
Hanscom Air Force Base, Massachusetts

USAF Research: Dr. John F. Paulson

Date: September 8, 1984

Contract No.: F49620-82-C-0035

EFFECTS OF TEMPERATURE AND REACTANT SOLVATION UPON  
THE RATES OF GAS-PHASE ION-MOLECULE REACTIONS

by

Anton F. Ahrens and Peter M. Hierl

ABSTRACT

The rate constants and the product branching ratios for the nucleophilic displacement reactions of  $\text{CH}_3\text{O}^-$  and  $\text{OH}^-(\text{H}_2\text{O})_n$  (where  $n = 0, 1,$  or  $2$ ) with the methyl halides, and for the proton transfer reactions of  $\text{CH}_3\text{O}^-$  and  $\text{OH}^-(\text{H}_2\text{O})_n$  with acetonitrile and the hydrogen halides have been measured in the gas phase over the temperature range 200-500 K, using the AFGL selected ion flow tube (SIFT). The rate constants of the fastest reactions were found to be very close to the collision rate. Reactant solvation was found to decrease the rates of the nucleophilic displacement reactions, most significantly in the case of the least exothermic reactions, but was found to have little effect upon the rates of the proton transfer reactions. Likewise, increased temperatures decreased slightly the rates of the nucleophilic displacement reactions but had less effect upon the rates of the proton transfer reactions.

ACKNOWLEDGMENT

The authors would like to thank the Air Force System Command, the Air Force Office of Scientific Research, and the Southeastern Center for Electrical Engineering Education for providing them with the opportunity to spend a stimulating and productive summer at the Air Force Geophysics Laboratory (LID), Hanscom AFB, MA. They would like to acknowledge the laboratory for its hospitality and excellent working conditions.

Finally, they would like to thank Dr. John F. Paulson for his valuable suggestions and his guidance, and to thank their colleagues, Prof. Michael J. Henchman, Dr. Albert A. Viggiano, and Mr. Fred Dale for their invaluable assistance.

## I. INTRODUCTION

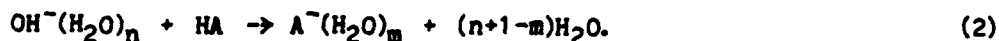
Gas-phase reactions between ions and neutral molecules play a significant role in atmospheric chemistry, radiation chemistry, combustion chemistry, and chemical processes occurring in lasers and in electrical discharges. Moreover, studies of ion-molecule reactions can provide important basic data on the energetics and mechanisms of gas-phase reactions in general, as well as provide valuable insight into ionic reactions occurring in solution. Consequently, gas-phase ion chemistry has been an active and rapidly growing field of chemical research for the past several decades.<sup>1</sup>

An important recent advance in this field has been the development of experimental techniques by which selectively solvated ions can be formed and the resulting effect of solvation upon the ion's reactivity can be studied.<sup>2</sup> These studies have been motivated both by the recognition that solvated ions play an important role in the chemistry of the lower ionosphere,<sup>3</sup> and by the hope that such studies might help elucidate the nature of the solvent effects which often dominate the rates of ionic reactions in solution.<sup>2,4,5</sup>

The present project is primarily concerned with investigating the effects of solvation and of temperature upon the reactivity of the hydroxide anion, OH<sup>-</sup>, in the gas phase. Two common types of ionic reactions were chosen for this study: (1) nucleophilic displacement (S<sub>N</sub>2) reactions between hydrated OH<sup>-</sup> and the methyl halides, which can be represented by the general equation



where  $n = 0, 1, 2,$  or  $3,$  and  $X = F, Cl, Br,$  or  $I;$  and (2) proton transfer reactions between hydrated  $OH^-$  and various proton donors, including the hydrogen halides,



The rate constants for the nucleophilic displacement reactions of the solvated hydroxide anion with  $CH_3Cl, CH_3Br,$  and  $CH_3I,$  have been measured in a flowing afterglow at room temperature by Bohme and coworkers,<sup>2,5-7</sup> who also measured room temperature rate constants for a number of proton transfer reactions involving  $OH^-(H_2O)_n$ .<sup>2,8,9</sup> We have measured, using the AFGL tandem mass spectrometer, integral cross sections and product branching ratios as a function of reactant translational energy (0.03 - 5 eV center-of-mass) for the reactions of  $OH^-(H_2O)_{0,1,2}$  with  $CH_3Cl$  and  $CH_3Br$ .<sup>10</sup>

## II. OBJECTIVES OF THE RESEARCH EFFORT

The objectives of this project were to investigate the following phenomena for the reactions described in Section I:

- (1) The effect of solvation ( $n = 0, 1, 2,$  or  $3$ ) upon the rate constant of the reaction.
- (2) The effect of temperature upon the rate constant.
- (3) The degree to which the product anion is solvated (i.e., the relative abundances of the various possible products  $Y^-, Y^-(H_2O),$  etc.) in a given reaction.
- (4) The effect of reaction exothermicity (varied by changing the identity of the halogen atom  $Y$  or  $A$ ) upon each of the three previously listed phenomena.

### III. EXPERIMENTAL

The rate constant measurements were carried out using the AFGL Selected Ion Flow Tube (SIFT) apparatus, which is similar to that described by Adams and Smith.<sup>11</sup> Briefly, the reactant ions are generated in a high-pressure ion source, mass-selected by a quadrupole mass filter, and then injected into the flow tube through a venturi-type aspirator. The injected ions are brought into thermal equilibrium through multiple collisions with the carrier gas (He or H<sub>2</sub>), the temperature of which can be varied over the range 200K - 500K. The thermalized reactant ions are then carried downstream past the inlet where the neutral reactant is admitted at a measured flow rate. Further downstream ionic reactants and products are mass analyzed by a second quadrupole mass spectrometer and are detected by conventional pulse counting techniques.

Data for a particular reaction at a given temperature are obtained for a number N (typically, N = 3-10) of replicate runs in each of which the intensity of the reactant ion is measured at eight different flow rates of the neutral reactant. The total rate constant for the selected ion-molecule reaction is determined from the decrease of the reactant ion signal as a function of the neutral reactant's concentration.

Calibration of the neutral reactant flow meter showed that the actual flow rate was approximately 20% less than that indicated by the meter, when the most sensitive scale of the meter was used; no error was found on the other 2 scales. Consequently, rate constants reported here for those experiments in which the flow meter was operated on the most sensitive scale have been multiplied by 1.2 to correct for the error in the flow measurement.

## IV. RESULTS AND DISCUSSION

### A. CALIBRATION EXPERIMENTS

To test the accuracy of the techniques employed in this experiment, rate constants were measured at room temperature (298K) for several negative ion-molecule reactions for which reliable rate constant measurements have been reported from other laboratories. In most cases, calibration reactions were chosen which involved the same neutral reactants to be studied in the present work. Table I lists these calibration experiments and compares the present results with those obtained elsewhere.

TABLE 1. Rate Constants for Calibration Reactions at 298K.

Reaction	Rate Constant ( $10^{-10}$ cm <sup>3</sup> /molec-s)	
	This Work	Other Work
(1) $F^- + HCl \rightarrow HF + Cl^-$	15.6	15.5 <sup>a</sup>
(2) $F^- + HBr \rightarrow HF + Br^-$	11.9	12.4 <sup>a</sup>
(3) $F^- + HI \rightarrow HF + I^-$	7.0	10.1 <sup>a</sup>
(4) $F^- + CH_3Cl \rightarrow CH_3F + Cl^-$	18.1	8.0 <sup>b</sup> 18.0 <sup>c</sup> 19.0 <sup>d</sup>
(5) $F^- + CH_3Br \rightarrow CH_3F + Br^-$	22.2	6.0 <sup>b</sup> 12.0 <sup>d</sup>
(6) $F^- + CH_3I \rightarrow CH_3F + I^-$	23.4	
(7) $OH^-(H_2O) + CO_2 \rightarrow HCO_3^- + H_2O$	8.3	6 <sup>e</sup>
(8) $OH^-(H_2O) + SO_2 \rightarrow HSO_3^- + H_2O$	18.1	20 <sup>e</sup>

<sup>a</sup> Reference 12

<sup>b</sup> Reference 13

<sup>c</sup> Reference 6

<sup>d</sup> Reference 14

<sup>e</sup> Reference 15

In most cases the present results agree very well with the previously reported rate constants; there are, however, several noteworthy exceptions. First, the rate constant measured for Reaction (3) is about 30% less than that reported by Weishaar et al.<sup>12</sup> It is possible that this discrepancy is caused by impurities in the HI used in the present study, and analysis of this HI should be made. Second, the rate constant measured for Reaction (4) agrees very well with that obtained by Bohme and coworkers<sup>6,14</sup> from a flowing afterglow experiment, but is much larger than the value obtained by Olmsted and Brauman<sup>13</sup> in an ion-cyclotron resonance (ICR) experiment. This discrepancy raises the possibility that the reactant ions in an ICR cell do not achieve true thermal equilibrium. Third, the rate constant measured for Reaction (5) is considerably larger than the values previously reported by either Bohme<sup>14</sup> or Olmsted and Brauman.<sup>13</sup> Although the discrepancy with the ICR result might be rationalized by the failure to achieve thermal equilibrium in the ICR cell, the discrepancy with Bohme's flowing afterglow measurement is less easy to explain.

#### B. REACTIONS OF $\text{OH}^-(\text{H}_2\text{O})_n$ WITH THE HYDROGEN HALIDES, METHYL HALIDES, AND ACETONITRILE

The major portion of this project was concerned with the temperature dependence of the rate constants and product branching ratios for the reactions of the solvated anion  $\text{OH}^-(\text{H}_2\text{O})_n$  with the hydrogen halides, the methyl halides, and acetonitrile. The reactant systems studied and the number of temperatures at which rate constants were measured for each system are summarized in Table 2.

TABLE 2: REACTIONS OF  $\text{OH}^-(\text{H}_2\text{O})_n$  STUDIED AS A FUNCTION OF TEMPERATURE\*

Neutral Reactant	Degree of Solvation			
	n = 0	n = 1	n = 2	n = 3
(9) HF	6	6	4	3
(10) HCl	5	4	4	0
(11) HBr	6	8	7	3
(12) HI	1	1	1	1
(13) $\text{CH}_3\text{F}$	0	4	1	0
(14) $\text{CH}_3\text{Br}$	5	5	7	0
(15) $\text{CH}_3\text{Cl}$	5	4	4	0
(16) $\text{CH}_3\text{CN}$	0	4	1	0

\* Each numerical entry in this table indicates the number of temperatures in the range 200 - 500K for which rate constants were measured for a given pair of reactants.

Because of the very large amount of data collected for these reactions, only a preliminary analysis has been performed at this time. However, some representative results are included in this report.

The effect of stepwise solvation of the reactant anion  $\text{OH}^-$  upon the rates of its reactions with HBr and with  $\text{CH}_3\text{Br}$  at room temperature is illustrated in Figure 1. Increasing reactant solvation can be seen to cause only a slight decrease in the rate constant for the proton transfer reaction with HBr. By contrast, the rate of the nucleophilic displacement reaction with  $\text{CH}_3\text{Br}$  is reduced by a factor of 2 by the addition of a single  $\text{H}_2\text{O}$  molecule to the  $\text{OH}^-$ , and is further reduced by

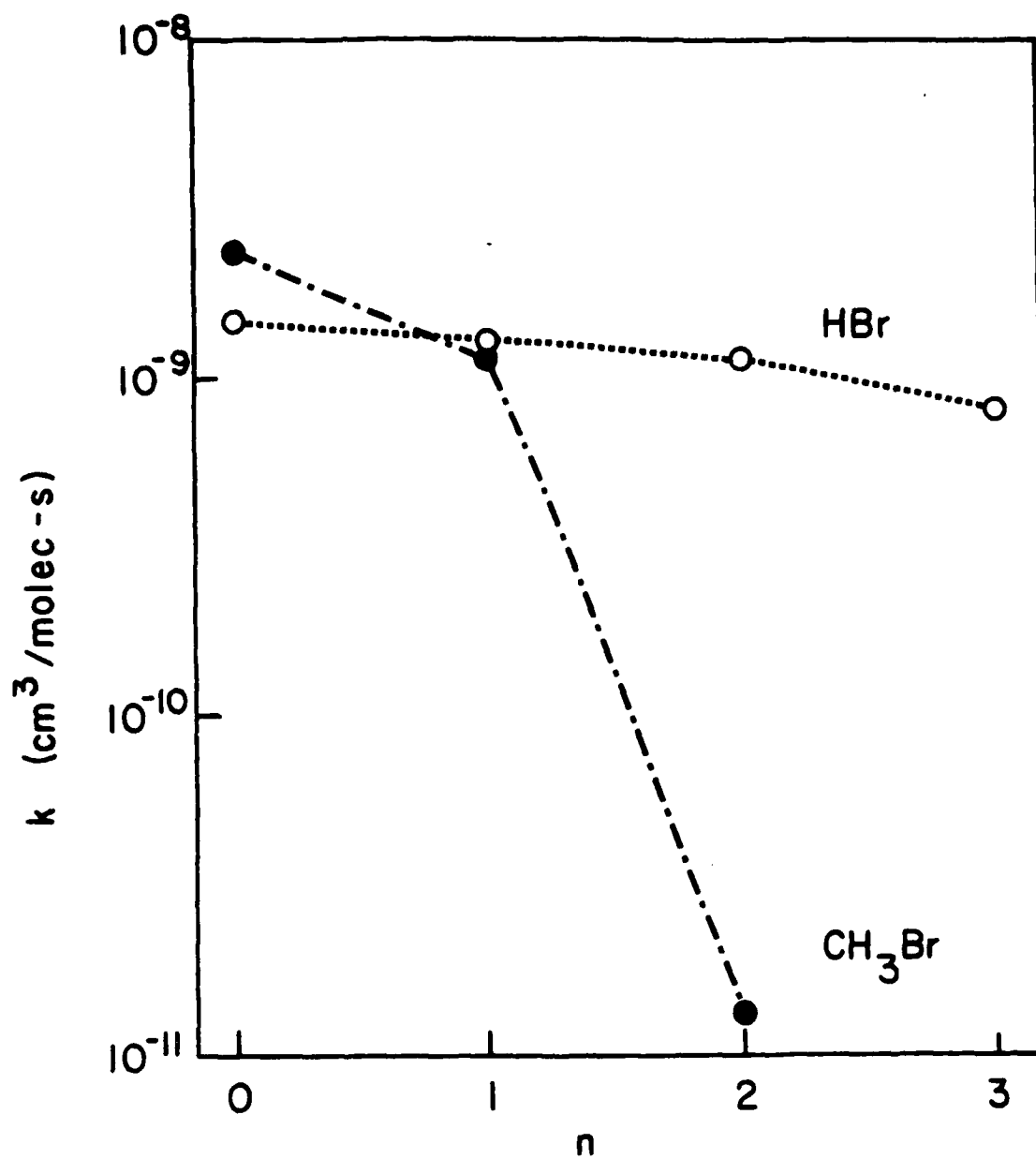


Figure 1. Effect of reactant solvation upon the rate constant  $k$  at 298K for the reactions of  $\text{OH}^-(\text{H}_2\text{O})_n$  with HBr and  $\text{CH}_3\text{Br}$ .

a factor of 100 by the addition of a second H<sub>2</sub>O molecule, despite the fact that formation of the unsolvated product ion, Br<sup>-</sup>, is still exothermic by more than 14 kcal/mole . Qualitatively similar behavior is also observed for the reactions of the other hydrogen halides and methyl halides with hydrated OH<sup>-</sup>.

The effect of temperature upon the rate constants for the reactions of OH<sup>-</sup> with HBr and CH<sub>3</sub>Br is illustrated in Figure 2. The rate constant for the proton transfer reaction with HBr shows little or no temperature dependence over the temperature range studied, while that for the nucleophilic displacement reaction with CH<sub>3</sub>Br is seen to decrease with increasing temperature over this range. Again, similar behavior is observed for the reactions of the other hydrogen halides and methyl halides with OH<sup>-</sup> and its solvates.

Although quantitative evaluation of the product branching ratios requires further data analysis, several qualitative generalizations can be made at this time. In all cases where formation of the unsolvated product anion Y<sup>-</sup> is energetically possible, it is found to be the dominant ionic product, although small amounts (5-20%) of the singly solvated product anion were observed. In those cases where solvation of the reactant anion caused formation of the unsolvated product anion to be endothermic, the proton transfer reactions of the hydrogen halides were found to occur rapidly and with efficient transfer to the product anion of the number of H<sub>2</sub>O molecules necessary for the reaction to be exothermic. By contrast, the rate constant for the nucleophilic displacement reactions became immeasurably small when reactant solvation caused formation of the unsolvated product anion to be endothermic.

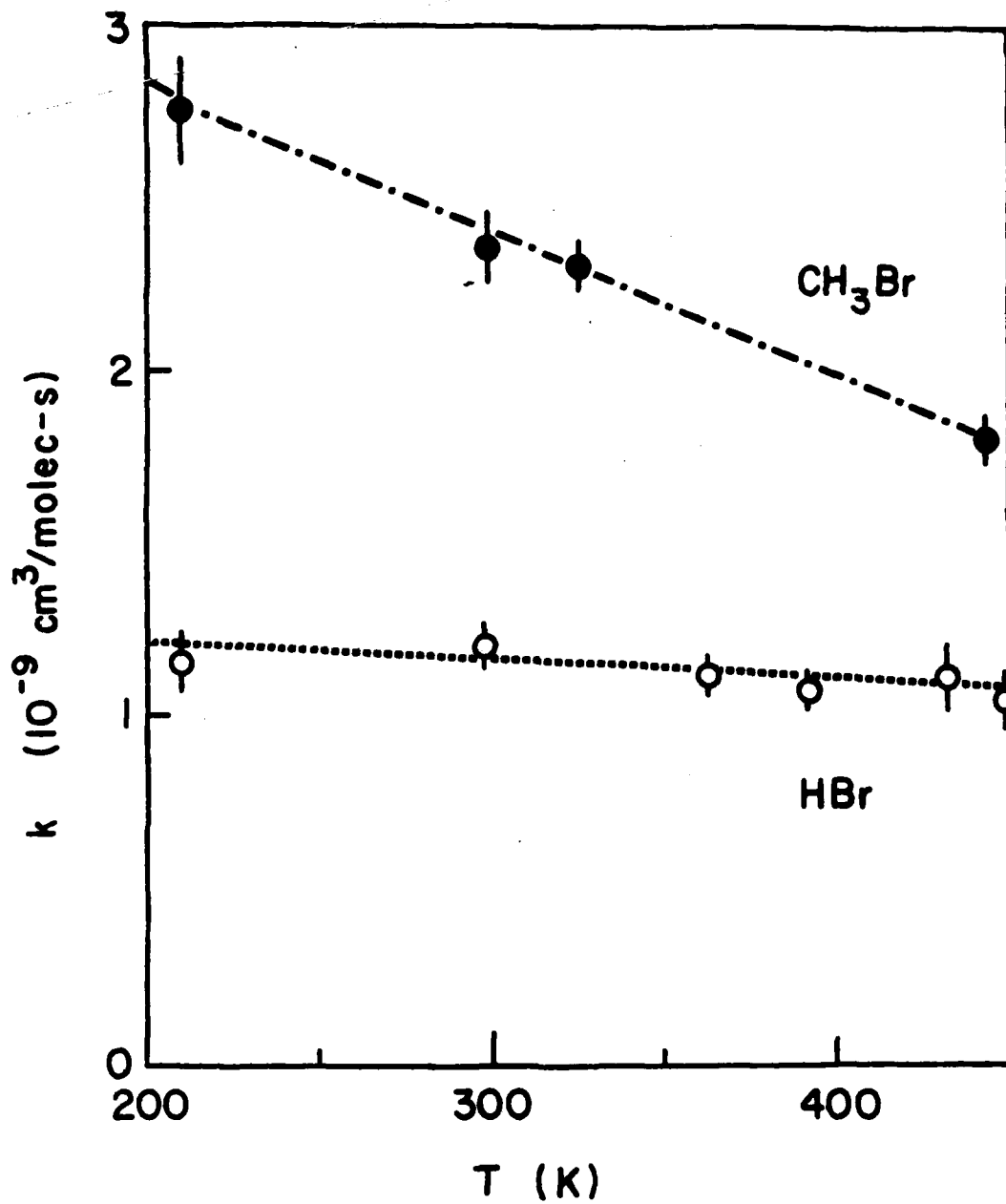


Figure 2. Effect of temperature  $T$  upon the rate constant  $k$  for the reactions of  $\text{OH}^-$  with  $\text{HBr}$  and  $\text{CH}_3\text{Br}$ .

### C. REACTIONS OF $\text{CH}_3\text{O}^-(\text{CH}_2\text{OH})_n$ WITH THE METHYL HALIDES

In order to investigate the effects of solvation and temperature upon the reactions of a nucleophile other than  $\text{OH}^-$ , rate constants were measured for the reactions of the unsolvated and the singly-solvated methoxide anion,  $\text{CH}_3\text{O}^-$ , with the methyl halides as a function of temperature over the range 200 - 500K (see Table 3).

TABLE 3: REACTIONS OF  $\text{CH}_3\text{O}^-(\text{CH}_2\text{OH})_n$  STUDIED AS FUNCTION OF TEMPERATURE\*

Neutral Reactant	Degree of Solvation	
	n = 0	n = 1
(17) $\text{CH}_3\text{Cl}$	6	4
(18) $\text{CH}_3\text{Br}$	7	1
(19) $\text{CH}_3\text{I}$	6	2

\*Each numerical entry in this table indicates the number of temperatures in the range 200-500K for which rate constants were measured for a given pair of reactants.

Qualitatively, the effects of temperature and reactant solvation upon the reactions of  $\text{CH}_3\text{O}^-$  with these molecules are quite similar to those observed for the corresponding reactions of hydrated  $\text{OH}^-$ . The unsolvated  $\text{CH}_3\text{O}^-$  ion reacted at nearly the collision rate, but addition of one solvent molecule decreased the rate constant, most appreciably in the case of the least exothermic reaction. Further data analysis is required, however, before a more quantitative characterization of these reactions can be made.

#### D. MISCELLANEOUS REACTIONS AT ROOM TEMPERATURE (298K)

Rate constants and product branching ratios (where appropriate) were measured at room temperature for the reactant systems listed in Table 4:

TABLE 4: REACTANT SYSTEMS STUDIED AT ROOM TEMPERATURE (298K)

- 
- (20)  $\text{OH}^-(\text{H}_2\text{O})_{2,3} + \text{CH}_3\text{OH}$
  - (21)  $\text{OH}^-(\text{H}_2\text{O})_{0,1} + \text{CH}_2\text{Cl}_2$
  - (22)  $\text{OH}^-(\text{H}_2\text{O})_{0,1} + \text{CHCl}_3$
  - (23)  $\text{OH}^-(\text{H}_2\text{O})_{0,1} + \text{CCl}_4$
  - (24)  $\text{OH}^-(\text{H}_2\text{O})_{0,1} + \text{SiCl}_4$
  - (25)  $\text{OH}^-(\text{H}_2\text{O}) + \text{C}_2\text{H}_2$
  - (26)  $\text{OH}^-(\text{H}_2\text{O})_{0,1} + \text{CH}_3\text{CCH}$
  - (27)  $\text{OH}^-(\text{H}_2\text{O}) + \text{CH}_2=\text{C}=\text{CH}_2$
  - (28)  $\text{CH}_3\text{O}^-(\text{CH}_3\text{OH})_{0,1} + \text{HF}$
  - (29)  $\text{CH}_3\text{O}^-(\text{CH}_3\text{OH})_{0,1} + \text{HCl}$
  - (30)  $\text{CH}_3\text{O}^-(\text{CH}_3\text{OH})_{0,1} + \text{HBr}$
  - (31)  $\text{CH}_3\text{O}^-(\text{CH}_3\text{OH})_{0,1} + \text{HI}$
- 

Reaction (20), which involves proton transfer from the  $\text{CH}_3\text{OH}$  to the reactant anion, is of interest because simultaneous transfer of at least 2 water molecules to the  $\text{CH}_3\text{O}^-$  product anion is required for the reaction to be exothermic. We find reaction to occur on essentially every collision, indicating that such solvent transfer, although appearing to be rather complex, is actually quite facile.

Reactions (21) - (23) were studied to determine the effect of

increased substitution upon the reactivity of neutral substrate. With  $\text{CH}_3\text{Cl}$  as the neutral reactant, proton transfer was endothermic and only nucleophilic displacement was observed. With  $\text{CH}_2\text{Cl}_2$ , however, proton transfer is evidently exothermic (or at least thermoneutral), for we observe very rapid reaction to form roughly equal amounts of the proton transfer and the nucleophilic displacement products; this finding appears to be an exception to the general rule<sup>16</sup> that proton transfer, when exothermic, always pre-empts nucleophilic displacement.

Reactions (25) - (27), which also proceed via proton transfer, were found to occur with a collision efficiency considerably less than unity, and to become less efficient with increasing solvation of the reactant anion. These results are similar to those reported previously by Bohme and co-workers.<sup>9</sup>

Reactions (28) - (31) involve proton transfer to the methoxide anion from the hydrogen halides, and give results very similar to those reported above for the proton transfer reactions of these neutrals with the hydroxide anion (and its hydrated forms): reaction occurs with nearly unit efficiency and is little affected by the addition of a single solvent molecule to the reactant anion.

A more detailed characterization of these reactions requires further analysis of the data collected this summer.

## V. RECOMMENDATIONS

During the relatively short period of this project, a very large amount of data has been collected on the effects of temperature and reactant solvation upon the rates of gas-phase ion-molecule reactions. These results, although only preliminary in scope and, as yet, incompletely analyzed, have greatly increased the available body of

data on such effects and amply demonstrate the suitability of instruments such as the AFGL SIFT for such studies. Because such studies are vitally important for an improved understanding of ionic reactions, both in the gas-phase and in solution, the following recommendations are made:

(1) The data collected this summer should be analyzed and the results disseminated by publication in scientific journals. Analysis would involve both the averaging of the rate constants measured in the  $N$  replicate runs for each reaction studied, and the evaluation of the product branching ratios for those reactions in which more than one set of products are formed. Publication would involve the preparation of manuscripts in which the present results are presented and compared with any related studies previously published.

(2) The present experimentally measured rate constants should be compared with those calculated from current theoretical models. A measure of the efficiency of a given reaction can be obtained by comparing the measured rate with the collision rate, which might, for example, be calculated from the AADO theory.<sup>17</sup> The collision efficiency and its measured temperature dependence might then be compared with the predictions of a model such as the "double-minimum" model proposed by Brauman and co-workers.<sup>13,18</sup>

(3) Experimental studies of the type reported here should be continued and extended. Such future studies should not only fill in the gaps in this preliminary study, but should also be extended to include other reactant anions (such as  $F^-$ ,  $Cl^-$ ,  $Br^-$ ,  $C_2H_5O^-$ , etc.), other solvent molecules (such as the hydrogen halides, ethanol, acetone, etc.), and/or other neutral reactants.

## REFERENCES

1. For recent reviews, see (a) Ionic Processes in the Gas Phase, edited by M. A. Almoester Ferreira, Reidel Publ. Co., Dordrecht (1984); (b) Gas Phase Ion Chemistry, edited by M. T. Bowers, Academic Press, New York (1979).
2. D. K. Bohme, "Gas-Phase Studies of the Influence of Solvation on Ion Reactivity," in Ref. 1(a).
3. See, for example, F. C. Fehsenfeld and D. L. Albritton, in Atmospheric Water Vapor, edited by A. Deepak, T. D. Wilkerson, and L. H. Ruhrike, Academic Press, New York (1980), pp. 587-597.
4. G. I. Mackay and D. K. Bohme, *J. Am. Chem. Soc.* 100, 327 (1978).
5. D. K. Bohme and G. I. Mackay, *J. Am. Chem. Soc.* 103, 978 (1981).
6. K. Tanaka, G. I. Mackay, J. D. Payzant, and D. K. Bohme, *Can. J. Chem.* 54, 1643 (1976).
7. D. K. Bohme and A. B. Rakshit, *J. Am. Chem. Soc.* 106, 3447 (1984).
8. S. D. Tanner, G. I. Mackay, and D. K. Bohme, *Can. J. Chem.* 59, 1615 (1981).
9. D. K. Bohme, A. B. Rakshit, and G. I. Mackay, *J. Am. Chem. Soc.* 104, 1100 (1982).
10. M. Henchman, J. F. Paulson, and P. M. Hierl, *J. Am. Chem. Soc.* 105, 5509 (1983).
11. N. G. Adams and D. Smith, *Int. J. Mass Spectrom. Ion Phys.* 21, 349 (1976).
12. J. C. Weisshaar, T. S. Zwier, and S. R. Leone, *J. Chem. Phys.* 75, 4873 (1981).
13. W. N. Olmsted and J. I. Brauman, *J. Am. Chem. Soc.* 99, 4219 (1977).
14. D. K. Bohme and A. B. Rakshit, *J. Am. Chem. Soc.* 106, 3447 (1984).
15. F. C. Fehsenfeld and E. E. Ferguson, *J. Chem. Phys.* 61, 3181 (1973).
16. J. L. Beauchamp, in Interactions Between Ions and Molecules, edited by P. Ausloos, Plenum Press, New York (1975), p. 425 ff.

17. W. J. Chesnavich, T. Su, and M. T. Bowers, in Kinetics of Ion-Molecule Reactions, edited by P. Ausloos, Plenum Press, New York (1979), p. 31 ff.
18. W. P. Olmsted, Ph.D. thesis, Stanford University, 1977 (University Microfilms, Ann Arbor, MI #77-12679).

1984 USAF-SCEEE GRADUATE STUDENT SUMMER SUPPORT PROGRAM

Sponsored by the

AIR FORCE OFFICE OF SCIENTIFIC RESEARCH

Conducted by the

SOUTHEASTERN CENTER FOR ELECTRICAL ENGINEERING EDUCATION

FINAL REPORT

BOILING HEAT TRANSFER IN HEAT PIPE EVAPORATOR

Prepared by:	Jay Ambrose
Academic Department:	Mechanical Engineering
University:	Washington State University
Research Location:	Aero Propulsion Laboratory Wright-Patterson Air Force Base
USAF Research Contact:	Dr. E. T. Mahefkey Mr. R. Ponnappan
SFRP Supervising Faculty Member:	Dr. Louis C. Chow Assistant Professor
Date:	September 24, 1984
Contract No.:	F49620-82-C-0035

BOILING HEAT TRANSFER IN HEAT PIPE EVAPORATOR

by

Jay Ambrose

ABSTRACT

Efforts are described to further the development of the Double-Wall Artery Heat Pipe (DWAHP). This is a unique new design which has shown much potential as a high heat flux device. A correlation is presented which relates the evaporator temperature drop for a water saturated screen wick to the heat flux. This correlation provides good results for different screen materials and mesh sizes. In addition, a computer program was written to perform the basic standard design calculations and simulate operating temperatures of the DWAHP.

ACKNOWLEDGMENTS

Many thanks go to the Graduate Student Summer Support Program of the S.C.E.E.E. and the Air Force Systems Command, Air Force Office of Scientific Research, Aero Propulsion Laboratory, for affording me the opportunity to begin my graduate research and career in Mechanical Engineering. My grateful appreciation goes to Dr. Louis C. Chow, supervising professor, Dr. Tom Mahefkey, Mr. Jerry Beam and Mr. R. Ponnappan, for their helpful guidance, and to my faithful typist and wife, Vicki.

Research sponsored by the Air Force Office of Scientific Research/AFSC, United States Air Force, under Contract F49620-82-C-0035. The United States Government is authorized to reproduce and distribute reprints for governmental purposes notwithstanding any copyright notation hereon.

## I. INTRODUCTION

Over the last decade, many advances have been made in heat pipe technology. Heat pipes play an important role in thermal energy management (waste heat rejection). They can transport thermal loads through finite distances with a minimal temperature drop and low space requirements. This has made them very attractive for use in spacecraft.

The increasing complexity of military space missions will require greater heat rejection. Capacity limits of current heat pipes set the performance limit of large heat transport and radiator components<sup>1</sup> which motivates the development of high-capacity heat pipes.

The Thermal Systems Group of the Aero Propulsion Laboratory is responsible for the invention and development of the Double-Wall Artery Heat Pipe<sup>2</sup> (DWAHP). The unique new design of the DWAHP is easily fabricated and tested, and virtually free of entrainment effects. Arteries provide a plentiful liquid return path. Both features (arteries and double wall) are reasonable approaches to the optimization of a copper/water heat pipe because of the capillary limit, which is the dominating factor for operation in the 40 to 250°C range.<sup>2</sup> Development of the DWAHP is aimed at testing these design concepts.

From initial calculations, it is clear that the effective thermal conductivity model adapted by Chi<sup>3</sup> and others<sup>4</sup> is incorrect for the heat pipe evaporator or condenser. Their model did not explain the  $\Delta T$ 's (temperature drop) observed for the copper/water system. Chi's model may work for a liquid-metal heat pipe but only because of the very large conductivity of the liquid within the wick. Obviously, a more complex mechanism exists in the heat pipe wick.

Numerous advantages are found with the double-wall design and it may prove to be a major development in heat pipes if optimized successfully. But the processes of boiling and condensation within heat pipes are not well understood. This is due to the scarcity of experimental data available. Additional research in this area will be required to fully understand this phenomenon.

## II. OBJECTIVES

The main objective of this project was to aid in the development process of the DWAHP. Efforts are being made to increase the understanding of the heat pipe's operation and to increase the performance of the device. Specifically, the objectives set at the beginning of the research period were to:

- (i) develop an understanding of the process occurring in the evaporator
- (ii) develop a correlation to describe this heat transfer process
- (iii) modify a heat pipe design computer program for use with the DWAHP

## III. HEAT TRANSFER MECHANISM - IMPORTANT PARAMETERS

Many researchers have postulated that nucleate boiling may occur in heat pipe wicks. This, of course, is dependent on working fluid and geometry as well as heat flux. In the case of water heat pipes, the effective thermal conductivity of the wick is low<sup>5</sup>, thus conduction through the saturated wick would cause a large temperature drop. The fine circumferential grooves on the evaporator wall provide excellent nucleation sites. Nucleate boiling is therefore highly probable even for modest superheat levels.

Agreement with the correlation suggests that this is a good hypothesis. A correlation was developed based on nucleate boiling and is similar to the pool-boiling correlation.

Since nucleate boiling was assessed to be important, the next step was an attempt to explain qualitatively the boiling process in the wick. All properties which would directly influence the heat transfer were examined. The process is dominated by surface tension because of the porous lattice of the screen. Any bubbles which escape the wall must enter the void space of the screen. The surface tension force on a vapor bubble is approximately:

$$F_{st} \cong \sigma \pi d_b$$

where the bubble diameter,  $d_b$  is of the order of the screen opening, and  $\sigma$  is the surface tension coefficient. The buoyancy force on the bubble is given by:

$$F_b \cong \rho_l g V_b$$

where  $\rho_l$  is the liquid density and  $V_b$  is the bubble volume. The ratio of surface tension to buoyant force  $F_{s.t.}/F_b$  is of the order  $10^3$ .

It was first thought that the vapor would push through the wick to the vapor slots and escape to the core, forming vapor channels. Formation of vapor channels was thought to increase the heat transfer coefficient, allowing higher heat fluxes. It is not clear what would drive the vapor to break clear through the liquid/wick layer since the buoyancy force is not significant. It is now recognized that the vapor release process need not be dominating; sensible heat absorbed by the liquid near the wall is larger than the latent heat contained in a bubble of equal volume as shown below. The latent heat released by a departing bubble is given by:

$$\rho_v V_b h_{fg}$$

where  $\rho_v$  is the vapor density,  $h_{fg}$  is the heat of vaporization, while the heat absorbed by an equal volume of liquid is

$$\rho_l V_b c_{pl} \Delta T_l$$

where  $c_{pl}$  is the liquid specific heat and the liquid heated by an amount  $\Delta T_l$ . Thus the ratio

$$\text{@ } 100^\circ\text{C} \quad \frac{\text{Sensible heat}}{\text{Latent heat}} = \frac{\rho_l c_{pl} \Delta T_l}{\rho_v h_{fg}} \approx 3 \Delta T_l$$

The major factor, then, is the heating of the returning liquid which is pumped about by the vapor release from the wall. The dominating process is a vapor-liquid pumping action such as that proposed by Engleberg-Forster and Grief<sup>6</sup>. Any vapor which leaves the wall probably moves into the screen and collapses, giving off its heat to the next layer of liquid. As this process repeats, liquid is heated successively. The liquid pumping mechanism is very efficient indeed, and creates a very effective convection process. This, coupled with limited conduction through the wick (solid), gives the heat needed to

evaporate liquid at the surface menisci in an amount sufficient to transport the heat to the condenser region.

#### IV. RELATED EXPERIMENTS

Two correlations have been presented to relate the heat flux and  $\Delta T$  for boiling in screen wicks<sup>7,8</sup>. Both correlations are similar and show good agreement with the experimental data used. Neither group of experimenters applied their correlation to heat pipe data or data obtained from a different type of apparatus. Fair agreement was found with the DWAHP data<sup>2</sup> but insufficient information was given for their correlation to be applied accurately. In the future, data from these two papers may be incorporated into the present correlation.

Data given by Abhat and Seban<sup>9</sup> showed good agreement with the DWAHP data. The apparatus for their experiment was a vertical tube with external wick and an internal heater. It was used with different screen types and working fluids to obtain  $q$  vs  $\Delta T$  curves for boiling in a screen wick. Their data for boiling of water into its vapor was used along with DWAHP data in the present correlation.

#### V. CORRELATION

Since liquid agitation, or pumping action, plays an important role in boiling in the wick, the first step was to check for similarities to the pool-boiling process. It has been assumed that buoyancy forces are unimportant. Calculations show that these forces are very small compared to surface tension. In pool-boiling, the buoyancy is used in a force balance on the vapor bubble in order to obtain the Reynolds No. for bubbles. In the case of a screen-wick, the bubble diameter is of the same order as the mesh opening. An alternative Reynolds No. is defined based on this dimension. Consider the liquid-vapor exchange process caused by bubble movement. By continuity, the mass of vapor entering the bubble must equal the mass of liquid replacing it,

$$\rho_l \dot{V}_l = \rho_v \dot{V}_v$$

where  $\dot{V}$  indicates the volume flow rate. The heat flux required to form vapor at the wall is equal to some fraction of the total heat flux, or equivalently,

$$\rho_v \dot{V}_v = f \frac{\dot{q}}{h_{fg}}$$

where  $\dot{q}$  is the heat flux and where the fraction  $f$  of the heat carried away from the wall by vapor is not a strong function of Reynolds No. As the rate of vapor formation at the wall is increasing so is the agitation of and heat transfer through the liquid. Since the liquid must flow through the screen opening denoted by  $w$ , a Reynolds No. for the liquid may be formed as:

$$Re = \frac{\rho_l \dot{V}_l w}{\mu_l} = \frac{f \dot{q} w}{\mu_l h_{fg}}$$

or,

$$Re = \frac{\dot{q} w}{\mu_l h_{fg}} \quad (1)$$

if  $f$  is absorbed into the lead constant of the correlation.

A slightly modified form of Rohsenow's pool-boiling correlation,

$$\frac{C_m \Delta T}{h_{fg}} = C Re^a Pr^b \quad (2)$$

where  $Pr$  is the liquid Prandtl No. and the Reynolds No. is defined by equation (1), showed fair agreement with the DWAHP data. Therefore, a regression analysis was performed using a form similar to equation (2), with the addition of three extra terms: the screen geometry ratio, the liquid to vapor density ratio, and the effective conductivity ratio. The geometry term ( $\delta/w$ ) is the ratio of the thickness of one screen layer to the size of the mesh opening and accounts for the relative thickness of the screen. The liquid to vapor density ratio ( $\rho_l/\rho_v$ ) is important to the momentum exchange between the two phases, while the effective conductivity ratio ( $k_e/k_l$ ) controls the vapor growth near the wall. Heat must conduct through a thin layer of liquid/wick to create vapor during the bubble growth.

The resulting correlation gives the evaporator temperature drop as:

$$\frac{C_{PI} \Delta T}{h_{fg}} = 0.656 Re^{0.69} Pr^{0.6} \left(\frac{\delta}{W}\right)^{2.2} \left(\frac{\rho_s}{\rho_w}\right)^{-0.45} \left(\frac{k_s}{k_w}\right)^{-1.17}$$

Data used from DWHP #1<sup>2</sup> and Abhat and Seban<sup>9</sup> includes screens of copper, stainless steel and phosphor bronze, and mesh sizes of 100, 150 and 325 in<sup>-1</sup>. Range of the variables used in the correlation are:

Re	: 2x10 <sup>4</sup> - 5.6x10 <sup>5</sup>	$\frac{\rho_s}{\rho_w}$	: 2.2x10 <sup>2</sup> - 3.3x10 <sup>3</sup>
Pr	: 0.9 - 2.8	$\frac{k_s}{k_w}$	: 1.5 - 2.5
$\delta/W$	: 1.42 - 1.95		

The boiling correlation has so far been used only for water. It can be used to predict the temperature drop across the heat pipe evaporator for the case of water working fluid and screen wick.

Fig. 1 shows the predicted values of  $\frac{C_{PI} \Delta T}{h_{fg}}$  for the data of the first DWHP prototype and the data of Abhat and Seban<sup>9</sup>. It is seen that most points fall within  $\pm 30\%$  of the prediction.

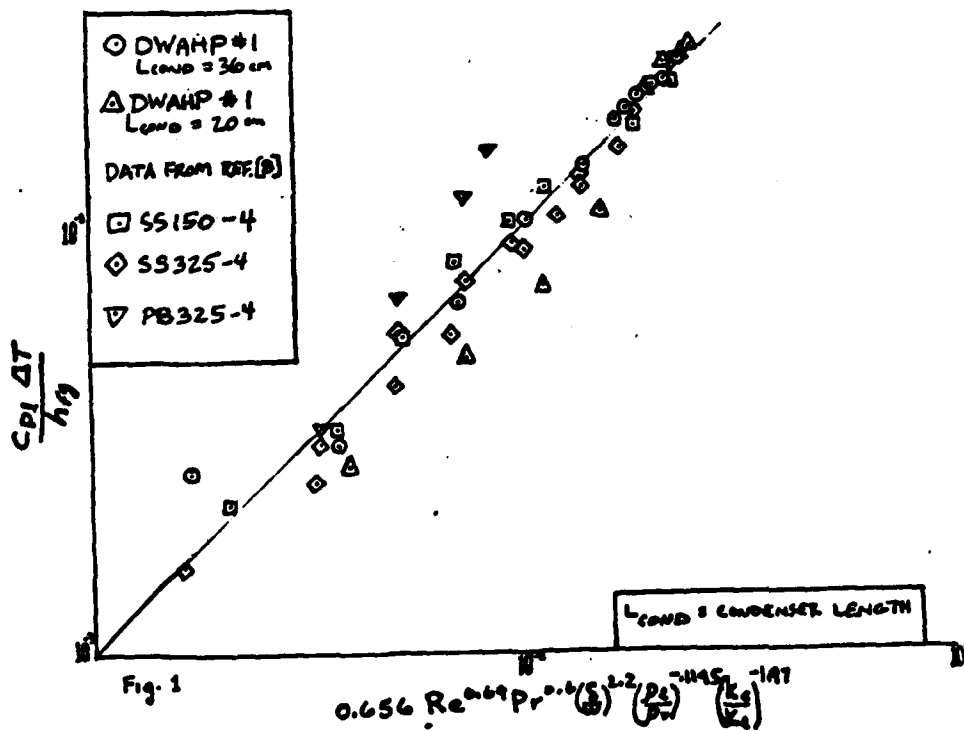
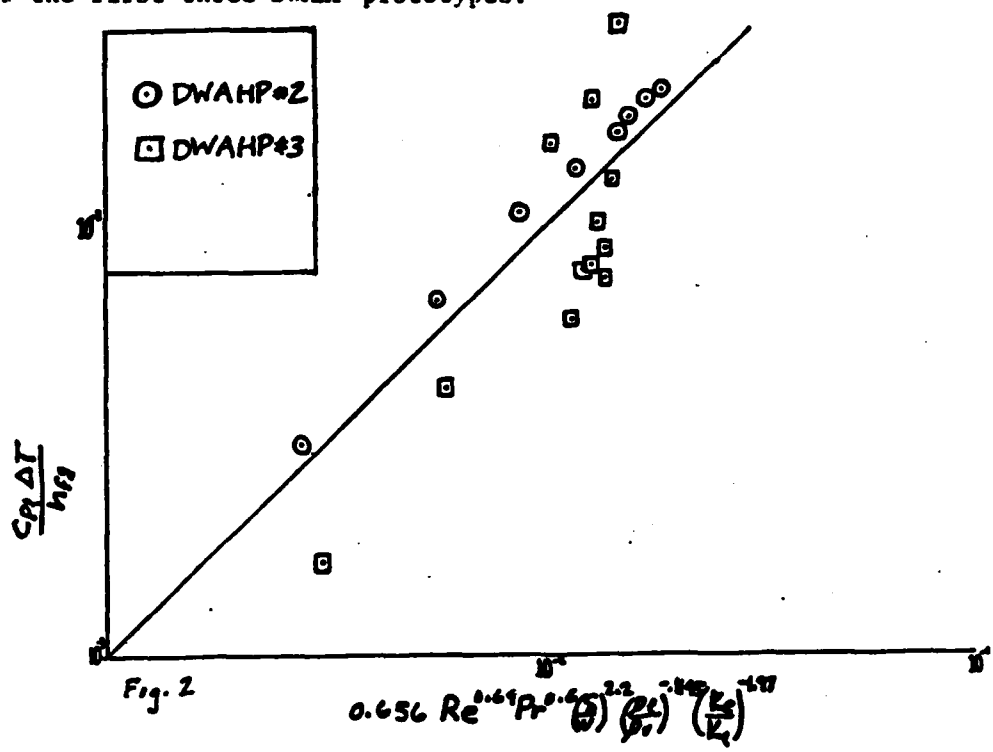


Fig. 1

Fig. 2 shows the measured vs. predicted values of  $\frac{Cp \Delta T}{h q}$  for the data of the first three DWHP prototypes.



Data of HP#2<sup>10</sup> is in good agreement with the correlation and found to be above predicted values. This was expected because of the absence of the fine circumferential grooves on the evaporator wall. HP#3<sup>11</sup> shows poor agreement with the prediction. It is likely that this heat pipe was not operating with uniform wetting conditions due to the absence of screen in the condenser and adiabatic sections. If this is the case, the heat is effectively choked off at the dry evaporator zones and must conduct through the wall to the wetted section before it can pass to the fluid. The variations in HP#3 data support a non-saturated wick operating mode.  $\Delta T$ 's for a given  $q$  vary from below predicted for low  $q$  to well above for high  $q$ . These conditions correspond to either a thin-film wetting condition on the evaporator top or a no-wetting condition. If the evaporator is not uniformly wetted, the mechanism of heat transfer will change significantly. The correlation works well in predicting the heat transfer when the evaporator operates under desirable (fully wetted) conditions.

## VI. COMPUTER PROGRAM - HEAT PIPE DESIGN

The purpose of this program is to perform the basic design calculations for the double-wall artery heat pipe. Standard calculations simulate the operating temperatures for different temperatures and heat inputs. The various operating limits are calculated to check if they have been exceeded. The equations used are taken from references<sup>3,4</sup>.

Input parameters include power level, sink temperature and heat pipe geometry. This information is read from a separate data file so they may be changed independently. A list of these variables is included for reference. The program returns the evaporator and condenser temperature drops, adiabatic and source temperatures.

Subroutines. Subroutine DELP calculates the pressure profiles of both the liquid and the vapor along the pipe's length. Pressure drop calculations are similar to those in equations<sup>3</sup> with the addition of a radial pressure drop correction and a liquid friction coefficient based on both groove and screen permeabilities. The temperature drop across the adiabatic section is calculated using the maximum vapor pressure drop. The pressure profile from DELP is used in subroutine LIMITS to determine the capillary limitation.

In subroutine LIMITS, the absolute vapor pressure profile is obtained by setting the vapor pressure equal to the saturation pressure at the evaporator end. The difference between the liquid and vapor pressures at the evaporator end is set equal to the maximum capillary pressure to obtain the absolute liquid pressure profile. Liquid and vapor pressures are then checked to make sure the vapor pressure is greater than or equal to that of the liquid everywhere along the pipe. If the liquid pressure is greater, the pipe is capillary limited. Other limits calculated using equations from<sup>3,4</sup> are boiling limit, sonic limit, entrainment limit and viscous limit.

Subroutine EVAP uses the screen-wick boiling correlation to calculate the  $\Delta T$  across the evaporator. Subroutine COND uses the effective conductivity model to calculate the  $\Delta T$  across the condenser wick. It uses a thermal boundary layer thickness theory to provide a reasonable estimate of the temperature drop. A layer of stagnant liquid

exists near the wall which must conduct heat while a moving layer is dominated by convection. The thickness of the conduction dominated layer was correlated with the heat flux using a second-order polynomial. Thermal resistance of the wick is calculated using the effective conductivity model from<sup>3</sup> and this thickness.

Modifications. The various operating limits may be calculated and printed out for different temperatures. This will require iteration on heat input to determine the capillary limit using subroutines DELP and LIMITS.

Different operating modes may be added such as input power level and adiabatic temperature or input source and sink temperatures. In the latter case, subroutine EVAP should be modified to return heat flux as a function of  $\Delta T$  in addition to the present method.

## VII. RECOMMENDATIONS

In all previous tests of the DWAHP design, heat input was provided by electrical resistance heaters wrapped around the evaporator. The independent parameter is therefore the heat flux, which is easily measured as the electrical power input to the heater divided by the heater area. If, as the power input is increased, observed  $\Delta T$ 's begin to increase rapidly, it is taken as an indication that the maximum flux has been reached. Although the correlation gives a relationship between heat flux and temperature drop for the heat pipe evaporator, it does not provide information as to the maximum heat flux ( $q_{\max}$ ). Prediction of the maximum heat flux is of prime importance because it determines the power capability of the heat pipe design.

The following project is recommended to give a more accurate determination of the maximum heat flux and also aid in the development of a prediction for  $q_{\max}$ . This will be accomplished by enclosing the evaporator within a variable pressure steam condenser, with power input to the heat pipe as the dependent parameter and where the temperature is controlled independently. Pressure of the steam will be controlled to provide a constant temperature heat source. The mass flow rate and temperature of the steam provide a measurement of heat input. With this apparatus, as the maximum flux is reached, a decrease in  $q$  will be

observed when  $\Delta T$  is further increased. This method is clearly advantageous for examining  $q_{\max}$  because it gives a better indication when  $q_{\max}$  is reached.

A follow-up research project has been initiated which will involve further testing of the DWHP prototype design. For the proposed testing, facilities have been made available at Washington State University, including high pressure steam (up to 600 psi) from the nearby power plant and laboratory space and equipment. This author's summer research project will continue through the year as he seeks his Masters in Mechanical Engineering with this research as his thesis topic.

## REFERENCES

1. E.T. Mahefkey, "Military Spacecraft Thermal Management? The Evolving Requirements and Challenges," In Spacecraft Thermal Control, Design, and Operation, Progress in Astronautics and Aeronautics, Vol. 56, 1983.
2. R. Ponnappan and E.T. Mahefkey, "Development of a Double-Wall Artery High-Capacity Heat Pipe," Progress in Astronautics and Aeronautics, Vol. 86, 1983.
3. S.W. Chi, Heat Pipe Theory and Practice, McGraw-Hill, 1976.
4. P.D. Dunn and D.A. Reay, Heat Pipes, Pergamon Press, 1978.
5. J.H. VanSant and J.R. Malet, "Thermal Conductivity of Some Heat Pipe Wicks," Letters in Heat and Mass Transfer, Vol. 2, 1975.
6. K. Engelberg-Forster and R. Grief, "Heat Transfer to a Boiling Liquid - Mechanics and Correlations," Journal of Heat Transfer, Feb., 1959.
7. M. Rannenber and H. Beer, "Heat Transfer by Evaporation in Capillary Porous Wire Mesh Structures," Letters in Heat and Mass Transfer, Vol. 7, 1980.
8. M.D. Zin, H.D. Xie, and Y.G. Chen, "Boiling Heat Transfer on Heating Surfaces Covered by Metal Screens," 5th Intl. Heat Pipe Conference, Tsukuba, Japan, May 14-17, 1984.
9. A. Abhat and R.A. Seban, "Boiling and Evaporation from Heat Pipe Wicks with Water and Acetane," Journal of Heat Transfer, Vol. 96, Aug., 1974.
10. R. Ponnappan and T. Mahefkey, "Performance Characteristics of the Double-Wall Artery High-Capacity Heat Pipe," AIAA 21st Aerospace Sciences Meeting, Reno, Nevada, Jan. 10-13, 1983.
11. R. Ponnappan, J. Beam and T. Mahefkey, "Improved Double-Wall Artery High-Capacity Heat Pipe," AIAA 19th Thermophysics Conference, Snowmass, Colorado, June 25-28, 1984.

DEVELOPMENT OF A METHOD FOR CONSTRUCTING THE  
OBSERVER MATRIX FOR LARGE ORDER SYSTEMS\*

by

Vicki Atkins

ABSTRACT

Controls are an important consideration in the design of dynamic systems. Currently control laws exist when there is complete knowledge of the components of the state vector associated with a system. But without enough sensors to measure the entire state accurately we must in some way reconstruct the state. The question is then, how do we build the observer matrix with the information that we do know? It is also important that the method used be capable of handling a large number of state variables. I will approach the problem by studying the Luenberg Observer and examining its limitations. Perhaps through modification of this technique I can develop an improved, more efficient, and more practical method. Hopefully significant performance as well as cost improvements can be realized.

\*Miss Atkins experienced a personal tragedy during the summer which resulted in her early withdrawal from the program. Consequently no final report is available.

**1984 USAF-SCEEE GRADUATE STUDENT SUMMER SUPPORT PROGRAM**

**Sponsored by the**

**AIR FORCE OFFICE OF SCIENTIFIC RESEARCH**

**Conducted by the**

**SOUTHEASTERN CENTER FOR ELECTRICAL ENGINEERING EDUCATION**

**FINAL REPORT**

**IMPROVEMENTS IN TIRE/SOIL MODELING TECHNIQUES**

**Prepared by:** Joseph M. Badalamenti

**Academic Department:** Mechanical Engineering

**University:** University of Dayton

**Research Location:** Air Force Wright Aeronautical Laboratory  
Air Force Flight Dynamics Laboratory  
Mechanical Branch

**USAF Research Contact:** George J. Sperry

**SFRP Supervising  
Faculty Member:** Dr. George R. Doyle, Associate Professor

**Date:** July 27, 1984

**Contract No.:** F49620-82-C-0035

IMPROVEMENTS IN TIRE/SOIL MODELING TECHNIQUES

by

Joseph M. Badalamenti

ABSTRACT

A review of current tire/soil mathematical modeling techniques is presented along with comments on their areas of applicability and their inaccuracies. A radial-interradial spring tire model is developed that uses linear springs to interconnect the radial linear or quadratic springs. This causes one radial element's deflection to be dependent upon its neighbors' deflections, improving the accuracy of the vertical and drag force predictions.

## I. INTRODUCTION

Aircraft tire/soil interaction has been the subject of increasing study in recent years. Most current fighter aircraft in the Air Force inventory were designed for operation on smooth, rigid, paved surfaces, but they also have a limited capability for operation on lower strength surfaces. Since main operating base runways would most probably be heavily damaged by an enemy attack, the Air Force has placed a greater emphasis on aircraft ground operations over unimproved surfaces. Therefore, the need exists for validated techniques for simulating aircraft ground operations over bomb-damage repaired or soil runways. Mathematical tire models are the hearts of current state of the art simulations. Accurate prediction of the forces developed by the tire, when traversing rough, rigid or compliant soil surfaces, is needed to evaluate strut loads, airframe dynamics, and loads.

## II. OBJECTIVES

The main objective of this project was to review existing tire modeling techniques, and identify needed improvements that should be made. Reasonably accurate models have been developed for the aircraft frame (rigid body and/or flexible) and the oleo-pneumatic strut, but a mathematical model of the tire/ground interaction has proven to be a more difficult problem. Several tire models have been used with some degree of

success. However, an improved computationally efficient tire model is still needed to increase the accuracy of the predicted tire deformations, and predicted vertical and drag loads transmitted to the strut.

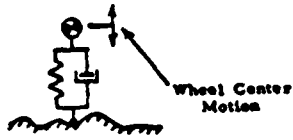
### III. POINT CONTACT FOLLOWER AND ITS VARIATIONS

The most extensively used tire models for aircraft taxi/tow simulations have been the point contact follower and its variations<sup>1</sup>, Figure 1a. These models generally represent the effects of inflation pressure and tire stiffness by using a spring and dashpot in parallel, giving fairly good results for smooth undulating surfaces. Drag forces are predicted by assuming that the resultant tire force is always normal to the local ground profile. However, since these models do not have the ability to envelop small wavelength bumps (smaller than the tire footprint length), they tend to give poor estimates of the forces generated over rough terrain.

The rigid tread band tire model, Figure 1b, also uses a parallel spring-dashpot combination. However, the spring and dashpot see a forcing function that is due to the vertical motion of a rigid wheel as it rolls over the terrain. In this model, the ground contact point is not constrained to lie directly beneath the wheel axle, but is free to move fore and aft due to encounters with local ground geometry. Small wavelength bumps are filtered out by this movement, and the tire

Figure 1. Tire Model Schematics

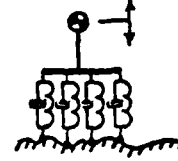
a) Point Contact Tire Model



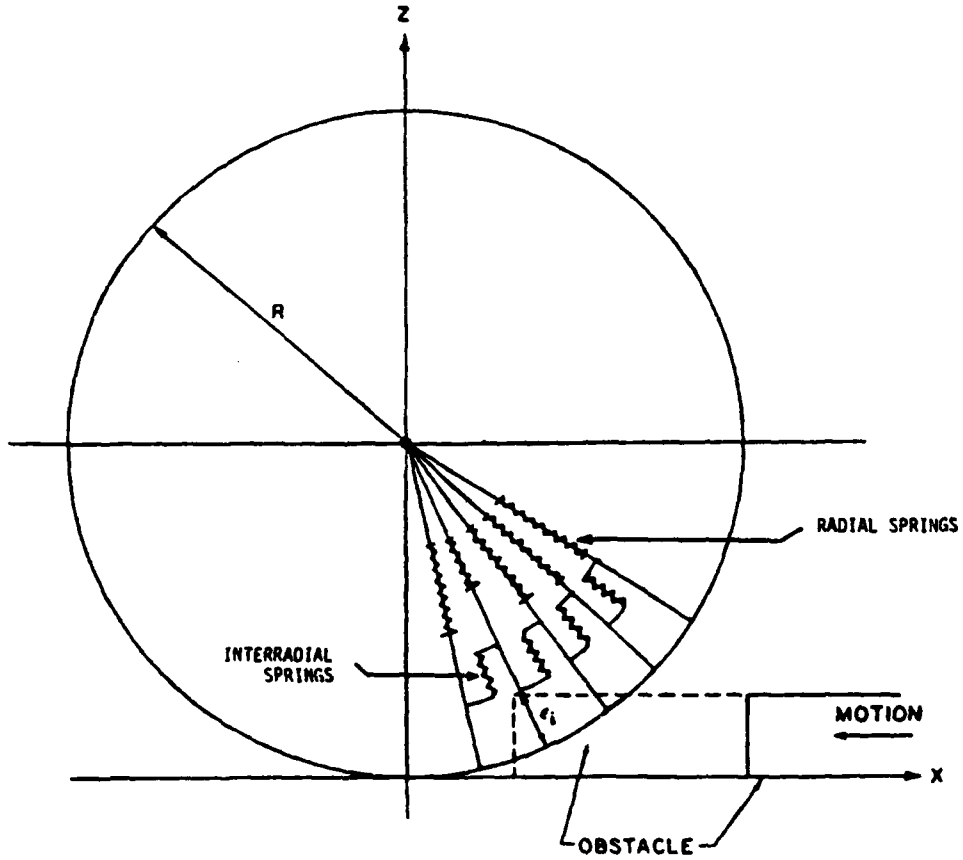
b) Rigid Tread Band Tire Model



c) Fixed Footprint Tire Model



d) Radial-Interradial Tire Model



forces become less exaggerated over rough terrain. Like the point contact model, drag forces are obtained by assuming that the resultant tire force is always normal to the terrain at the contact point.

The fixed footprint tire model, Figure 1c, uses linearly distributed stiffness and damping in the contact area. As its name implies, the footprint area is of constant size, independent of the tire deflection. Ground profile heights within the tire/soil contact area are averaged by the distributed springs and dampers, so that, like the rigid tread band tire model, the movement that the wheel sees is due to a modified ground profile. Drag forces are predicted by this model using the same assumptions listed for the point contact and the rigid tread band tire models.

#### IV. TOROIDAL MEMBRANE TIRE MODEL

A model proposed by J.R. Kilner<sup>2</sup> represented the tire as a toroidal membrane. In this model, pneumatic pressure was calculated by first finding the footprint area for the membrane in contact with a predefined rigid surface. A change in tire volume was found, which then resulted in a change in the pneumatic pressure. The vertical and drag forces were obtained by computing the product of the pneumatic pressure and the vertical and horizontal projections of the tire/ground contact area, respectively.

The forces predicted by this model for a tire rolling over a rigid obstacle compared favorably with experimental data obtained from the Flight Dynamics Laboratory at Wright-Patterson Air Force Base.<sup>2</sup> However, the toroidal membrane model can not be used for simulation of aircraft operation on soil or grass covered surfaces, since the governing equations were derived assuming a rigid surface profile.

#### V. RADIAL STIFFNESS TIRE MODELS

A radial stiffness tire model<sup>3</sup> was proposed that uses angularly distributed, linear spring elements to represent the tire stiffness characteristics. Vertical and drag forces are the result of the summations of the vertical and horizontal components of force in each element due to local radial spring deflections. This model has the capability to envelop short wavelength bumps and consequently filters the effects of small irregularities. This gives the model the potential to accurately predict resultant tire forces over rough terrain. However, in some simulations the load-deflection curve for this model does not agree well with the actual load-deflection curve of the tire it is to represent, limiting the accuracy of the predicted forces.

Phillips and Cook<sup>4</sup> recently suggested using radial quadratic spring elements to better approximate a measured load-deflection curve for a given tire. This model was extended

further by incorporating a Maxwell model (a spring and dashpot in series) of the soil for simulation of aircraft operations over compliant surfaces. A rut depth could then be generated by iterating on the vertical forces in the tire and soil elements. Rut depths predicted by this model correlated well with results from other prediction techniques.<sup>5,6</sup>

On the other hand, a review of the results of rigid obstacle encounters in Phillips' and Cook's work revealed some deficiencies in the model's ability to predict accurate loads. The model assumes that as a spring element encounters the obstacle, its deflection is independent of its neighbors' deflections. Only the elements in contact with the obstacle are affected. The neighboring noncontacting elements are fully extended to the radius of the tire. The end result is that smaller vertical loads are predicted when the tire is not wholly supported by the obstacle (as in obstacle encounter and departure, and where obstacle length is less than the tire footprint length). Also, computed drag loads are slower to increase and quicker to decrease than the measured loads.

#### VI. BACKGROUND SUMMARY

Use of the point contact follower as a tire model has been the most popular technique in dynamic simulations, not only because it is conceptually simple, but also because it is efficient. Aircraft operation over smooth, undulating surfaces

can be simulated using this model, giving very reasonable results. Simulations run over a rough surface profile, however, should not be made when using the point contact follower.

The concept of a toroidal membrane tire model was developed to be efficient for use on both smooth undulating surfaces, and austere surfaces. But since it can only be used over rigid profiles, its main area of effectiveness lies in predicting tire response to rigid obstacle encounters (spalls, rectangular bumps, haversines). This may be particularly useful for designing a test program using bumps and dips of varying geometries and of multiple configurations.

Although the radial stiffness tire models are more time consuming than the point contact and the toroidal membrane models, they can be used for simulations over rigid paved and soft soil surfaces. The main fault with these models lies in the assumption that an element's deflection is entirely independent of its neighbor's deflections, causing inaccuracies in the resulting tire force predictions.

#### VII. RADIAL-INTERRADIAL SPRING TIRE MODEL

A technique that would resolve the problem with the radial stiffness tire model would be to include interradiial springs, Figure 1d. These interradiial springs would inter-connect the main radial springs making the element deflections dependent upon one another. The radial-interradiial spring tire model

would therefore predict higher vertical and drag forces than those predicted by the radial element tire model, when the tire is not wholly supported by the ground or an obstacle.

Two separate models can be developed. The first would use linear radial and linear interradiial springs. This model has a load-deflection curve that adequately approximates a tire's actual load-deflection curve. Its main advantage is that all resultant forces and displacements can be solved directly for any imposed displacement state. This model should give very good results for a small amount of computer time.

The second model to be developed would use quadratic radial springs and linear interradiial springs. The load-deflection curve provided by this model closely resembles that of the tire's actual load-deflection curve. However, because of the quadratic relationship between force and displacement in the radial springs, the model's unknown displacements and forces cannot be solved for directly. An iteration process must be used for every tire/ground configuration. The computer run time for this model would therefore be higher than that of the linear-linear type model, but its force and displacement predictions would be more accurate.

#### VIII. DERIVATION OF EQUATIONS

Letting,

$\mathcal{E}_r$  = radial element deflection,

$k$  = interradsial linear spring constant

$C_1, C_2$  = radial quadratic spring constant

the radial force in element "i" can be written as:

$$F_{Ri} = C_1 \epsilon_{Ri} + C_2 \epsilon_{Ri}^2 + 2k\epsilon_{Ri} - k\epsilon_{Ri-1} - k\epsilon_{Ri+1} \quad (1)$$

Since the vertical force in element "i" is

$$F_{Vi} = F_{Ri} \sin \theta_i, \quad (2)$$

Equation (1) can be written as,

$$F_{Vi} = (C_1 \epsilon_{Ri} + C_2 \epsilon_{Ri}^2 + 2k\epsilon_{Ri} - k\epsilon_{Ri-1} - k\epsilon_{Ri+1}) \sin \theta_i \quad (3)$$

and since,

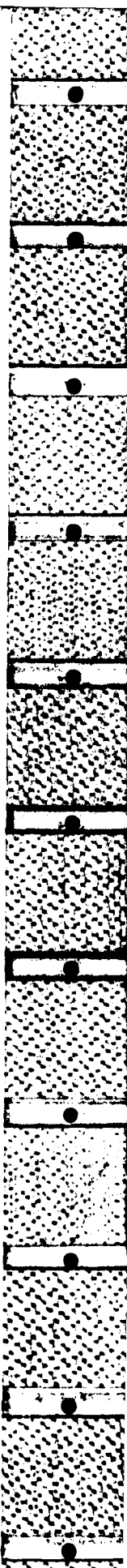
$$\epsilon_{Vi} = \epsilon_{Ri} \sin \theta_i, \quad (4)$$

the total vertical force on the wheel axle, due to 'N' radial elements is:

$$F_V = \sum_{i=1}^N \left[ C_1 \epsilon_{Vi} + \frac{C_2 \epsilon_{Vi}^2}{\sin \theta_i} + k \left( 2\epsilon_{Vi} - \epsilon_{Vi-1} \frac{\sin \theta_i}{\sin \theta_{i-1}} - \epsilon_{Vi+1} \frac{\sin \theta_i}{\sin \theta_{i+1}} \right) \right] \quad (5)$$

The vertical displacement of element "i" due to the tire/ground contact is:

$$\epsilon_{Vi} = z_{pi} - y_i - z_w \quad (6)$$



where

$z_{pi}$  = the ground profile height

$z_w$  = the wheel axle vertical displacement

and  $\gamma_i = R(1 - \sin\theta_i)$

Substituting Equation (6) into Equation (5) results in:

$$F_v = \sum_{i=1}^N \left\{ C_1 \left[ z_{pi} - R(1 - \sin\theta_i) - z_w \right] + \frac{C_2}{\sin\theta_i} \left[ z_{pi} - R(1 - \sin\theta_i) - z_w \right]^2 + k \left[ 2 \left[ z_{pi} - R(1 - \sin\theta_i) - z_w \right] - \frac{\sin\theta_i}{\sin\theta_{i-1}} \left[ z_{p_{i-1}} - R(1 - \sin\theta_{i-1}) - z_w \right] - \frac{\sin\theta_i}{\sin\theta_{i+1}} \left[ z_{p_{i+1}} - R(1 - \sin\theta_{i+1}) - z_w \right] \right\} \quad (7)$$

To evaluate the spring constants  $C_1$ ,  $C_2$ , and  $k$ , it is necessary to obtain three equations to be solved simultaneously. If the ground profile height is set equal to zero, the wheel axle displacement and force ( $z_w$  and  $F_v$ ) can be obtained from a tire load-deflection curve.

Using a 20-20 Type III tire load-deflection curve at a pressure of 125 psi, and a radius of 27.84 inches, three pairs of load deflection values can be obtained:

$F_{v1} = 54,000$ lb.	$z_{w1} = 6.0$ inches
$F_{v2} = 22,500$ lb.	$z_{w2} = 3.0$ inches
$F_{v3} = 12,800$ lb.	$z_{w3} = 2.0$ inches

Using these values in Equation (7) results in:

$$60.941 C_1 + 301.048 C_2 + 2.703 k = 54000 \quad (8a)$$

$$21.478 C_1 + 52.072 C_2 + 1.849 k = 22500 \quad (8b)$$

$$11.687 C_1 + 18.761 C_2 + 1.47 k = 12800 \quad (8c)$$

The constants  $C_1$ ,  $C_2$  and  $k$  can be solved for by using

Cramer's rule to obtain:

$$C_1 = 1227.17$$

$$C_2 = -67.34$$

and  $k = -189.66$

Substituting these values into Equation (5) results in:

$$F_v = \sum_{i=1}^N \left[ 847.85 \epsilon_{vi} - \frac{67.34 \epsilon_{vi}^2}{\sin \theta_i} + 189.66 \left( \epsilon_{v_{i-1}} \frac{\sin \theta_i}{\sin \theta_{i-1}} + \epsilon_{v_{i+1}} \frac{\sin \theta_i}{\sin \theta_{i+1}} \right) \right] \quad (9)$$

This equation can now be used to provide an analytical tire load-deflection curve for a 20-20 Type III tire at 125 psi.

#### IX. COMPUTER PROGRAM STRUCTURE

The computer program to be developed would rely heavily on the use of FORTRAN subroutines. Each subroutine would act as an independent module, with a minimum number of variables to be transferred among the subroutines. This will allow for program changes to be made quickly and easily, and also for easy substitution of all or part of the program into existing vehicle dynamics simulations.

An outline of the program flow can be found in Figure 2. The main program will consist of the necessary control statements, and one call statement to subroutine CONTRL. The CONTRL subroutine will read input data and CALL other subroutines based on options specified by the user.

The first option allows the user to choose one of three models to be included in this program (MODOPT = 1,2,or 3). MODOPT = 1 specifies the linear radial-linear interradiial spring tire model. If MODOPT = 2, then the user has chosen the quadratic radial-linear interradiial spring tire model. A third possibility, MODOPT = 3, directs the computer to use the quadratic radial spring tire model developed by R.F. Cook.<sup>4</sup> This third option would allow a direct comparison of the radial-interradiial spring tire models with the present state of the art modeling technique.

A second option to be specified indicates the type of surface to be used for the simulation (ISURF = 1 or 2). ISURF = 1 specifies a rigid surface for encounters with rigid obstacles (bumps and dips) or simulated operation over paved runways/taxiways. Soil surfaces of different strengths could be simulated by setting ISURF = 2.

#### X. RECOMMENDATIONS

It is recommended that the radial-interradiial spring tire model be developed and implemented as described in the previous

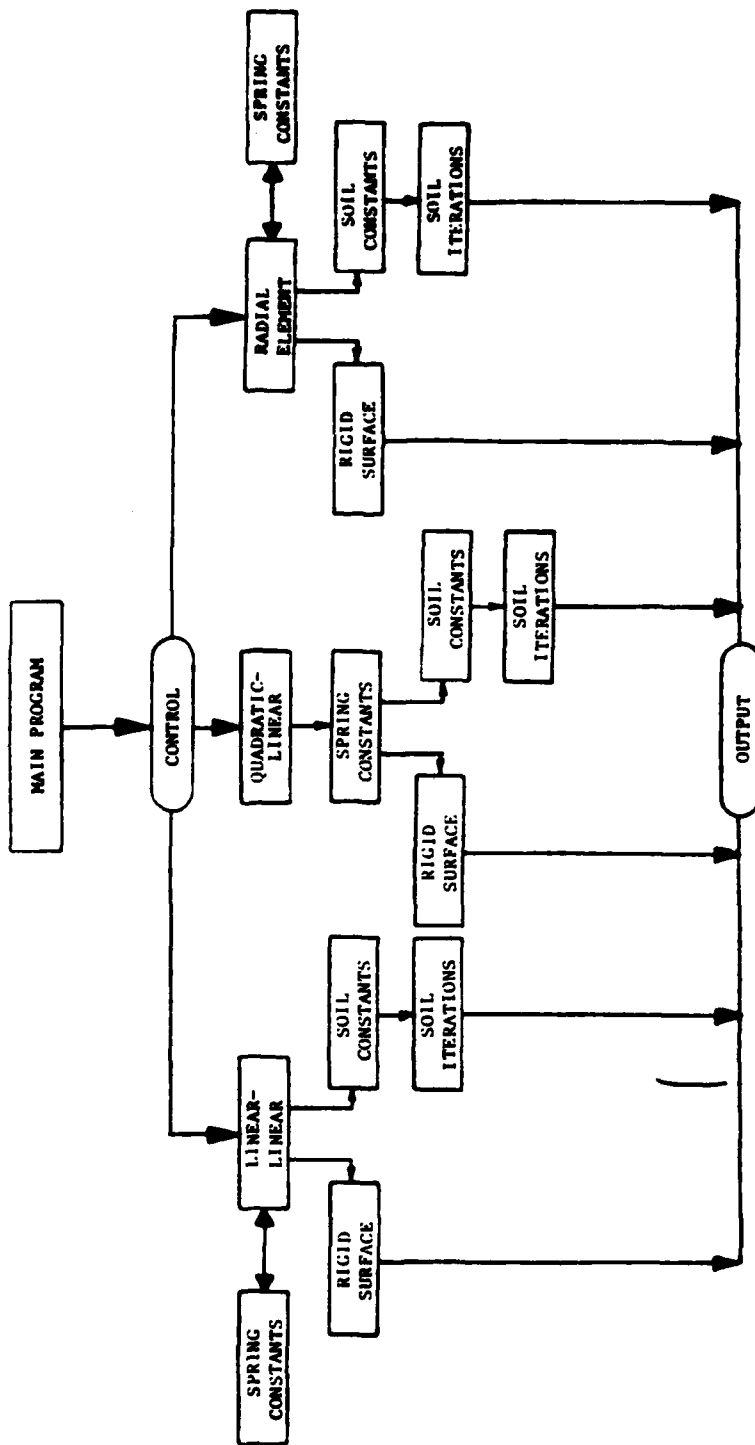


Figure 2. Computer Program Flow Chart

sections. Development of computer software for these models in the form presented above would allow direct comparison of different models and easy substitution into existing vehicle dynamics simulations. Adequate tire testing should continue so that the models' range of applicability can be defined and validated.

ACKNOWLEDGEMENTS

The author would like to acknowledge the Air Force Systems Command, the Air Force Office of Scientific Research, and the Southeastern Center for Electrical Engineering Education for enabling him to spend a very worthwhile summer at the Flight Dynamics Laboratory, Wright-Patterson Air Force Base, Ohio. He would also like to specifically thank the people at the Mechanical Branch for their hospitality and excellent working environment. Special thanks must go to both Dr. George R. Doyle, Jr., and Mr. George J. Sperry for suggesting this area of research, and their guidance throughout this research effort.

#### REFERENCES

- 1 Captain, K.M., Wormley, D.N., Grande, E., "The Development and Comparative Evaluation of Analytical tire Models for Dynamic Vehicle Simulation," U.S. Army TACOM, May 1974.
- 2 Kilner, J.R., "Pneumatic Tire Model for Aircraft Simulation," Journal of Aircraft, Vol. 9, Number 10, Pg. 851, October 1982.
- 3 Ingram, W.F., "A Numerical Model of the Ride Dynamics of a Vehicle using a Segmented Tire Concept," U.S. Army Waterways Experiment Station, TRM-73-5, August 1973.
- 4 Phillips, N.S., Cook, R.F., "Aircraft Operation on Soil Surfaces-- Computer Routine Revisions and Improvements," Volumes I and II, University of Dayton, March 1984.
- 5 Richmond, L.D., et. al., "Development of Tire-Soil Mathematical Model," AFFDL-TR-67-145 (II), September 1968.
- 6 Kraft, D.C., "Analytical landing Gear-Soils Interaction--Phase I," AFFDL-TR-68-88, August 1968.

1984 USAF-SCEEE GRADUATE STUDENT SUMMER SUPPORT PROGRAM

Sponsored by the

AIR FORCE OFFICE OF SCIENTIFIC RESEARCH

conducted by the

SOUTHEASTERN CENTER FOR ELECTRICAL ENGINEERING EDUCATION

FINAL REPORT

COMPUTER IMPLEMENTATION OF NONPARAMETERIC RADAR DETECTORS

Prepared by:	David C. Bauer
Academic Department:	Computer Science
University:	California State University, Chico
Research Location:	Rome Air Development Center
SFRP Supervising Faculty Member:	Dr. Basil Gala
Date:	September 21, 1984
Contractor Number:	F449620-82-C-0035

COMPUTER IMPLEMENTATION OF NONPARAMETRIC RADAR DETECTORS

by

David C. Bauer

ABSTRACT

Radar detection performance degrades when the target signal contains high levels of nonstationary surface clutter. However, many nonparametric statistics exist which may help improve radar performance. This report describes an existing detection program used as the baseline for this project and an existing signal generation program used to generate the data for the project. It discusses some of the nonparametric statistics, a detection algorithm that uses these statistics and a method of converting computer generated input signals with stationary clutter to signals with nonstationary clutter. In particular, it discusses the methods and the motivation for implementing these concepts on a computer. Finally, it proposes possible further research areas.

## I. Introduction

In an environment with a low signal-to-clutter ratio, surface clutter can significantly reduce the effectiveness of most techniques for analyzing radar data. This occurs partially because the clutter distribution function varies depending on the surface behind the suspect target space.

The model of radar used in this project sends a batch of several signal pulses and measures the power of the individual pulses as they return.

One approach to analyzing radar signals involves transforming the signals from the time domain into the frequency domain using an FFT (Fast Fourier Transform). The frequency bin in which the target appears indicates the doppler shift of the signal due to the relative velocities of the target and the source of the radar signal. The detector can then search for the target in each individual bin while ignoring the irrelevant signals in the other bins.

If the detector knows what the distribution of the noise, the surface clutter and the chaff (volume clutter) look like then it can simply compare the signals to the appropriate values to determine a detection.

Two major attributes of a detector help measure its performance. First, the detector should indicate a target as often as possible when and where one exists; i.e. high probability of detection. Second, the detector should indicate a target as seldom as possible when one does not exist; i.e. low false alarm rate. A good measure of the relative performance between two or more detectors involves adjusting them so they each have the same false alarm rate and measuring the probability of detecting the target for each.

## II. The Objectives

This project sought to find and evaluate four nonparametric statistics which would aid in the analysis of radar detection. These statistics would require a detection algorithm. The testing would involve implementing the detection algorithm on a computer and running it with data simulating radar signals with nonstationary clutter.

## III. The Existing Software

The MTI (Moving Target Indicator) program and the SSG (Statistical Radar Signal Generation) program, both written by the Motorola Corporation, implement a detection algorithm and generate simulated radar data, respectively.

The SSG program generates simulated radar signals based on parameter values chosen by the user. The data has the form of signal batches consisting of numerous individual pulses. The user can indicate the statistical model and parameters required by that model for the target(s), the noise, surface clutter and chaff as well as the number of signal pulses in a batch. The user does this by editing a PID (Primary Input Data) file prior to running the program. The SSG program then uses the information in the PID file to formulate its model for the signals.

The MTI program implements a simple, parametric detector on the data produced by the SSG program. The algorithm used by the MTI program requires data in the form of PSD's (Power Spectral Densities) that represent pulse batches transformed into doppler frequency bins. The MTI program does this transformation by using one of several Fourier Transformation schemes. The MTI program can run in two distinct modes - threshold generation and detection. In the threshold generation mode, it saves the ten largest values from each bin of the transformed target free data. The tenth largest value from each bin becomes the threshold for that bin. In the detection mode, the MTI program counts the number of times a value from a bin in the transformed target data equals or exceeds the corresponding

threshold. Each instance of this constitutes a detection. The MTI program divides the counts for each bin by the number of trials producing a probability of detection for that bin and prints them as part of its detection stage output. (Note: Each MTI trial consists of one batch of signals generated by the SSG program. When the programs that create data files for this project transfer data from one file to another, they do so one block at a time. Each block contains one batch of signals.) The parametric nature of this detection algorithm comes from its assumption that the clutter distribution does not vary between the threshold generation and the detection.

The SSG program runs as a subprogram of the MTI program and the MTI PID determines the value of some of the SSG variables. These variables include the number and existence of targets and the presence of noise clutter and chaff in the signal model. The MTI PID also determines the run mode, the number of trials and the number of points and the scheme used for the Fourier Transformation.

The user sets the False Alarm Rate for the MTI program by adjusting the number of trials to conform to the equation:  $(\text{False Alarm Rate}) = 10 / (\text{number of trials})$ . Using this measure, the MTI detector performs very well when the clutter model does not vary between the target

free data and the target data. However, in a low signal to clutter ratio environment with nonstationary clutter, the MTI detector performance reduces significantly.

#### IV. The Algorithm

The algorithm used for this project differs from that used by the MTI detector in only one significant way. The MTI detector did not use any actual statistic whereas the algorithm used for this project implements any of several different statistic that use a number of frequency bins. Therefore, this algorithm must set a criteria for determining from which bins to take data.

The analysis of data containing information with a nonstationary distribution function requires some assumptions about that function. The algorithm discussed here assumes the continuity of the clutter distribution function. More precisely, it assumes that the value of the clutter does not vary much between two doppler frequency bins near one another. This assumption allows the algorithm to neglect the different effect of the clutter on the data over a small range of frequencies.

This algorithm also considers the effect of the spreading of the target over more than one bin. To do this, it simply disregards the nearest few bins on either side of a test bin. This prevents a target in one bin from

affecting the detection of that target in an adjacent or nearly adjacent bin.

The use of multiple frequency bins produced one other effect not encountered by the MTI detector. The power from the noise in the bins near the center of the frequency exceeds the power due to the target in the target bins. Comparison of this large value with values from neighboring bins gives an unnaturally large value for the statistic. Fortunately, the noise distribution function does not vary as does the clutter distribution. Using this fact, the algorithm eliminates the effect of the noise by normalizing the data. The normalization process involves subtraction from each datum the mean of the target free data from the corresponding bin and dividing the difference by the standard deviation of the target free data from that bin. In this way, the algorithm solves a stationary problem with a parametric statistic.

#### V. The Testing Process

The testing process included setting a threshold based on 500 batches of target free data with a constant Weibull clutter parameter. The program repeated this process with the same data after normalizing it using the method discussed above. Those detectors that required data from

more than one batch of signals used overlapping batches. For example, if one test used batches one through five, the next test would use batches two through six.

Most of the detectors tested for this project suffered excessively high false alarm rates. This occurred in both the stationary and the nonstationary target data. This problem results from the small maximum value of the statistics. For example, if the sum runs over twelve bins (as it did for most of the tests) and a single batch of signals, the statistic can only attain twelve distinct values. With 500 trials to divide among the twelve values, even the maximum value attained will likely have well more than ten entries. Although a 100 way tie for the maximum would not raise the threshold beyond that value, each one of those 100 measurements would count as a detection. Thus, the algorithm does not insure the false alarm rate.

If the statistics could attain higher values, either by using more bins or by looking at more signal batches, they probably would perform better. However, increasing the number of bins used by the detector would tend to dismiss the assumption of continuity. Therefore, the detectors should look at more signal batches. This would increase the amount of overlapping of batches and might

reduce the accuracy of the tests because each consecutive test would use almost the same data.

VI. The Statistics

This project included testing four nonparametric statistics--the Generalized Sign Test, the Mann-Whitney test, the Wilcoxon test and the Mode test.

The statistic for the Generalized sign test is:

$$t = \sum_{i=1}^N \sum_{k=1}^K U(x_{ni} - x_{nk}), \quad (1)$$

where  $t_i$  is the value of the statistic in the  $i$ th bin,

$N$  is the number of batches looked at,  
 $K$  is the number of bins used,

$U(x)$  is the Unit function:  $U(x)=0$  for  $x<0$   
 $U(x)=1$  for  $x \geq 0$ , and

$x_{ni}$  is the value for the  $i$ th bin of the  $n$ th batch.

As with most of the other statistics discussed here, it had an unacceptable false alarm rate.

The statistic for the Mann-Whitney test is:

$$t = \sum_{l=1}^N \sum_{m=1}^N \sum_{k=1}^K U(x_{lk} - x_{mk}). \quad (2)$$

This statistic performed better than the others and has a particularly beneficial feature. In the bins near the target bin, excluding those containing target data, the probability of detection becomes very low. This highlights the target. This should have occurred in all of the

detectors, but the False Alarm Rate overshadowed it in the others.

The static for the Wilcoxon test is:

$$t = \sum_{i=1}^K k * U(y_{nik}), \quad (3)$$

where  $y_{nik}$  is the  $k$ th value of the sorted differences  $(x_{ni} - x_{nk})$ .

This statistic acts exactly like the Generalized Sign Test does with  $N=1$ . Each can attain only  $K+1$  distinct values and, therefore, neither can discriminate better than the other.

The statistic for the Mode Test is:

$$t = \sum_{i=1}^K U(M(x_{ni} - x_{nk})), \quad (4)$$

where  $M(x)$  is the mode over 100 batches.

This performed worst and requires the most information to make a decision. Possibly, it performed so poorly because the relatively small effect of the target could not change the value of the target bin enough to increase the mode for that bin. This could result from too few bins. However, too many bins could result in ties between bins, and the statistic would need a tie breaking criteria.

## VII. Programming the Detectors

The general approach taken in programming the algorithm stressed compatibility and modularity. Compatibility with the data format of the MTI program allows relative ease in the generation of input data and use of the MTI plot routine, INTERPLOT.COM (Note: Any string consisting entirely of upper case letters represents a file or subroutine. If a '.COM', a '.DAT', or a '.FOR' follows the string, it represents a Command procedure, a data file or a Fortran source program, respectively. If the string has no suffix, it represents a Fortran subroutine. The MTI program acts like a Command procedure and the SSG program acts like a subroutine.) Compatibility with each other allows for minimization of redundant code. Modularity makes the code easier to understand and modify. One effect of the modularity shows in the fact that the subroutines for each detector spread over three files.

Each detector requires one file called XMAIN.FOR (where the 'X' stands in place of the 'GST', 'MANN', 'COX' or 'GALA' for the Generalized Sign Test, the Mann-Whitney test, the Wilcoxon Test or the Mode Test, respectively) which contains the mainline and subroutines unique to that program. PREPARE does any initialization required specifically for a particular detector. FINDT calculates

the statistic used by a detector. FINDT in the Wilcoxon detector requires a routine to sort a small number of values, so COXMAIN.FOR contains a subroutine, BUBBLEY, that performs a Bubble sort. The mode statistic needs routines to make bins, find which bin a value belongs in and to delete a value from a bin and to find which bin contains the model value, so GALAMAIN.FOR contains the subroutines, MAKEBIN, FINDBIN and DELFTEBIN, and the function, MODE.

The file MASK.FOR contains the source code for most of the subroutines shared by the four detector programs. GPINIT opens the PID file and the output data file and initializes the arrays used in the normalization process. It also writes the 'Axis for the Plots' into the output data file. READX and WRITEX read and write data in almost the same format as the MTI program does. The output from WRITEX differs from that of the MTI program only in that WRITEX puts a blank line between the string used to find a block of data (the finder) and the first line of that block; the MTI program does not. WRITEX does this because INTERPLOT.COM appears to assume that such a blank line exists. FOPEN opens a file in the MTIPT.DIR directory for reading. THRESH and DETECT do almost the same things. They each initialize an array, call PREPARE and call FINDT once for each batch of signals. They differ in that TRESH

initialized the threshold array, ITHR, calls MISC to find the mean and standard deviation for the normalization and calls FINDT in the threshold generation mode. Whereas, DETECT initializes the detection array, ICNT and calls FINDT in the detection mode. MISC serves two major functions. It does the mathematics for the normalization statistics and it transfers data from one array to another for WRITEEX.

The third file of subroutines used by the detectors, UTILITIES.FOR, contains the source code for the subroutines, READTO, ADJFIN and REPLACE. The detectors use only the first two of these, whereas the data generation programs also use the third. The next section contains a discussion of all three.

#### VIII. The Data

The detection programs require data in the form of a series of signal batches transformed into PSD's. Also, some of the data must contain nonstationary clutter. Unfortunately, the SSG program produces data in the time domain and can not vary its parameters while it runs, and the MTI program only prints a PSD for the maximum and the average power of the signals. Thus, production of the data files for the detectors requires a large amount of editing of PID files and output files. The programs and routines

discussed in this section help make this process as painless and as efficient as possible.

Generation of the signal batches containing nonstationary clutter requires concatenation of several files of signal batches - each file generated with a different Weibull clutter parameter. The transformation to doppler frequency bins requires running the MTI program once for each batch and concatenation of one block of output data from each run. BLDIN.FOR, BLDDAT.FOR and BLDINDAT.FOR perform these tasks. A user can write a command procedure that calls these programs along with the MTI program and the SSG program in batch mode.

BLDIN.FOR edits the MTI PID file and the SSG PID file. It keeps count of how many times it has run by updating the value of a single integer in the file INDAT.DAT. Based on this value, it searches through a file called IFDATA.DAT to determine which file it should edit, into which which file it should write the edited version and in which file it can find the desired changes. Each record of the change file contains an eight character finder field and a ten character data field. BLDIN.FOR calls REPLACE to find the line with the finder as its first ten characters and replaces the data field from the old PID with the data field from the change file in the new PID.

AD-A154 300

USAF/SCEEE GRADUATE STUDENT SUMMER RESEARCH PROGRAM  
(1984) PROGRAM MANAGE. (U) SOUTHEASTERN CENTER FOR  
ELECTRICAL ENGINEERING EDUCATION INC S.

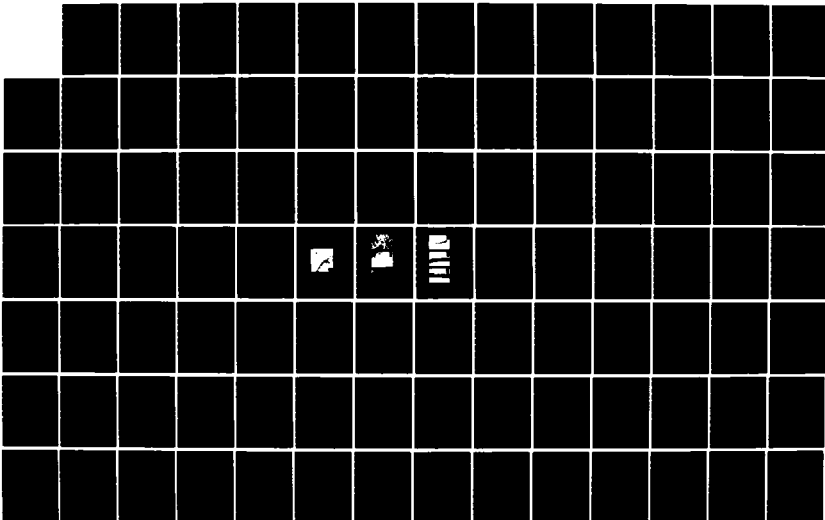
2/16

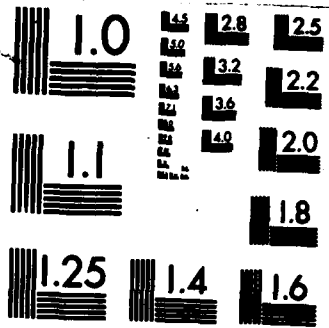
UNCLASSIFIED

W D PEELE ET AL. OCT 84 AFOSR-TR-85-0476

F/G 5/1

NL





MICROCOPY RESOLUTION TEST CHART  
NATIONAL BUREAU OF STANDARDS-1963-A

BLDDAT.FOR edits and concatenates MTI output files and SSG output files. It uses the value in INDAT.DAT for the file from which to read, the file to which to write and some information concerning the data transfer. That information consists of an eight character finder, the number of blocks of data already transferred, the number of blocks to transfer and the number of lines in each block of data.

BLDINDAT.FOR also transfers SSG output data from one file to another file, but it does so for a different purpose than BLDDAT.FOR does. When the MTI program reads data to transform into PSD's, it starts with the first block of data in the SSG output file. This appears to contradict the MTI program users manual that indicates that the MTI program begins reading the block corresponding to the variable NBATCH in the MTI PID file. The value in INDAT.DAT tell BLDINDAT where in MDAT.DAT to find the names of the input file and the output file and other information concerning the transfer.

UTILITIES.FOR contains the source code for two subroutines shared by the detection program and the data generation programs and a third used only by BLDIN.FOR. READTO reads records from one file and writes them to an optional second file until it matches one eight character

parameter with an eight character field (Note: The finder for the PID files contains a variable name. The finder for an output file consists of a space, followed by an integer of up to three digits followed by the string, '<>'.) in the first file. This match must start in the column indicated by one of READTO's parameters. REPLACE also copies data from one file to another, but when it finds a match, it replaces the last ten characters of the line containing the match with a string or a number indicated by one of REPLACE's parameters. ADJFIN changes the three digit portion of a finder for a block of data in an MTI output file or an SSG output file. This allows the data generation programs to put a unique finders on each block of data and allows the detection programs to find the next block of data.

#### IX. Recommendations

One approach to try involves taking the sum of the differences between the test bin and its neighboring bins. This would have the same effect as averaging the values in the neighboring bins and subtracting that average from the value in the test bin. As the number of neighboring bins increases, their average approach a constant for a

particular batch, and this statistic acts more like the MTI detector.

One might also try weighting the effects of the nearer neighbors more than the effects of the further neighbors. This would emphasize the continuity of the clutter distribution function. One could do this with the statistics discussed in this report or the one just recommended.

### ACKNOWLEDGEMENTS

I thank the USAF Office of Scientific Research for their sponsorship of the project. I thank the administrative and technical staff of RADC, especially Jim Michels and Janet Boyd, for their guidance and assistance. And I thank my SFRP Supervising Faculty Member, Dr. Basil Gala, for his encouragement.

1984 USAF-SCEEE GRADUATE STUDENT SUMMER SUPPORT PROGRAM

Sponsored by the  
AIR FORCE OFFICE OF SCIENTIFIC RESEARCH

Conducted by the  
SOUTHEASTERN CENTER FOR ELECTRICAL ENGINEERING EDUCATION

FINAL REPORT  
RESEARCH INTO THE DEVELOPMENT OF A STRUCTURE-MEDIA  
INTERACTION MODEL FOR DYNAMIC FINITE ELEMENT ANALYSIS

Prepared by:	Robert L. Bigelis
Academic Department:	Civil and Environmental Engineering
University:	Washington State University
Research Location:	Air Force Weapons Laboratory Civil Engineering Research Division (NTE) Kirtland Air Force Base, NM
USAF Research Contact:	Dr. Timothy J. Ross
SFRP Supervising Faculty Member:	Harold C. Sorensen, Associate Professor Department of Civil and Environmental Engineering Washington State University
Date:	September 18, 1984
Contract No.:	F49620-82-C-0035

RESEARCH INTO THE DEVELOPMENT OF A STRUCTURE-MEDIA  
INTERACTION MODEL FOR DYNAMIC FINITE ELEMENT ANALYSIS

by

Robert L. Bigelis

ABSTRACT

The various parameters which have been used to characterize structure-media interaction (S.M.I.) modeling is investigated. The SAMSON2 dynamic finite element code used by AFWL for S.M.I. problems uses a slideline model to determine interface behavior. It is recommended that the slideline algorithms in SAMSON2 be modified to model both the friction associated with soil failure and sliding near the interface and the friction associated with interface failure and sliding. This is in contrast to the single general friction model currently in the code. A S.M.I. element should then be developed and installed into the code together with the Matrix Difference Equation Theory algorithms. Experimental testing of soil-structure interaction behavior should then be conducted in order to better estimate the parameters governing the newly installed element.

### Acknowledgement

I would like to thank the Air Force Systems Command, Air Force Office of Scientific Research and the Southeastern Center for Electrical Engineering Education for providing me with this great learning experience at the Air Force Weapons Laboratory, Kirtland AFB, N.M. I would like to acknowledge the laboratory, in particular the Civil Engineering Research Division, for its hospitality and tolerance of my continual questioning.

I would also like to thank Dr. Timothy J. Ross, Mr. Doug Seeman, and Dr. Howard L. Schreyer for their guidance and patience.

Finally, I would like to especially thank Dr. Harold C. Sorensen for his help. He made all of this possible.

## I. INTRODUCTION:

The behavior of a structure placed on or buried in soil is dependent upon the material properties of both the structure and the soil, as well as the characteristics of the applied loads. Under dynamic loading, structure-media interfaces may separate, exhibit relative displacement, and impact together many times during the loading duration. This type of interface behavior is very difficult to model for analysis, and computer codes that have capabilities to simulate these phenomena require a comparatively large amount of computational time to determine this behavior. Ultimately, the goal of Structure-Media Interaction (S.M.I.) research is to develop a computer model which correctly simulates test data of interface behavior, while minimizing computer computational time required for obtaining a solution.

Employees at the Air Force Weapons Laboratory (AFWL) at Kirtland Air Force Base currently use the SAMSON2 computer code for dynamic finite element analysis of soil-structure interface effects on structural response (1). AFWL personnel use this code extensively in the analysis of structures subject to nuclear blast loadings. Much of the computational time required for solution by SAMSON2 is used by the complex algorithms that model S.M.I. These two facts show that there is a definite need to make the SAMSON2 S.M.I. model more accurate and time efficient.

## II. OBJECTIVES OF THE RESEARCH EFFORT:

The initial goal of the research effort was to effect computational efficiencies in the numerical algorithms of continuum finite element computer codes used in dynamic S.M.I. analysis. As a means of accomplishing this goal the SAMSON2 code was used. This code is a state-of-the-art dynamic finite element computer code undergoing development within AFWL/NTE.

The goal stated above was to be accomplished by investigating three research task areas. These three task areas were all under the direction of Professor Harold C. Sorensen, SFRP. This paper deals specifically with Task Area Number 2 of the goal:

Task Area No. 2 - Begin the development of a soil-structure interaction element which is both compatible with the Matrix Difference Equation (M.D.E.)

theory and the current numerical integration schemes of the SAMSON2 code.

- a. Become familiar with the parameters which have been used to characterize S.M.I. modeling.
- b. Formulate an element which takes these parameters into consideration for use in the SAMSON2 code.
- c. Implement the new element into the SAMSON2 code and run test solutions.

This description provided an initial scope and direction for the research.

As research progressed it became apparent that the S.M.I. model currently used in the SAMSON2 code contained inaccuracies that could be solved relatively quickly. (The S.M.I. slideline and the S.M.I. element are two unique types of modeling techniques; they will be discussed in detail later.) Thus the objectives for this research were slightly changed so that the existing model could be modified. This would result in a more immediate improvement to the SAMSON2 code than the development and installation of an S.M.I. element.

Since research was focused on the current S.M.I. slideline model, the objective concerning S.M.I. models and M.D.E. theory compatibility was temporarily dropped from consideration. This dismissal was due to the fact that the M.D.E. theory involves element numerical algorithms while the slideline concept involves boundary conditions and interface failure models only. However, the ultimate goal is still to develop a S.M.I. element compatible to both the current SAMSON2 code and a SAMSON2 code utilizing M.D.E. theory.

### III. APPROACHES TO LEARNING THE SAMSON2 CODE AND S.M.I. MODELING THEORIES

In order to implement any modifications to the SAMSON2 code it became necessary to understand the theory and input parameters associated with the code. This task seemed of primary importance since the research period was only ten weeks long and most of the experts on the code were employees at AFWL. The first four weeks of the research period were used primarily for running sample problems, reading both the SAMSON2 Theory Manual (1) and the User's Manual (12), and discussing difficult concepts with AFWL personnel for greater understanding.

Figure 1. Slideline Model Example

After this initial learning period, I began to study the S.M.I. slideline theory and the failure theories that are used in the SAMSON2 code. This period consisted of approximately three weeks.

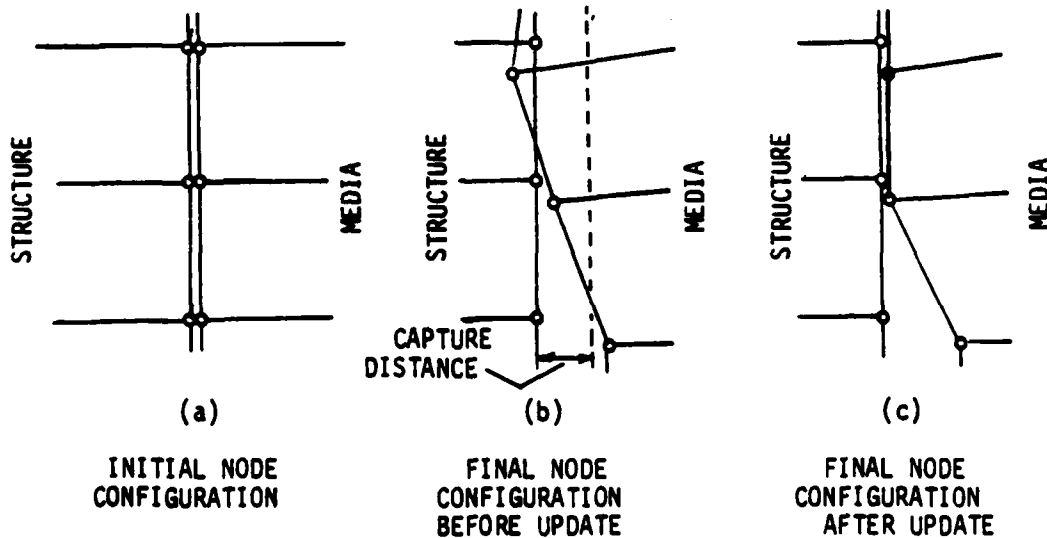
The final three weeks were then used to learn the different models that have been developed for S.M.I. problems. During this period, work was also done toward compiling existing S.M.I. test data and preparing this final report.

#### IV. STRUCTURE-MEDIA INTERACTION MODELS

The present version of the SAMSON2 code uses a slideline interface model to simulate S.M.I. Other models have been developed. One is a S.M.I. finite element which would have the properties of the S.M.I. interface. Another approach is to use special constitutive equations for the media elements directly adjacent to the structure. What follows is a brief explanation of the slideline, the finite element, and the constitutive equation modeling methods.

##### A. Slideline Model

The slideline interface model allows structure nodes and media nodes to relatively displace, separate and impact. Initially, the media nodes and structure nodes occupy the same coordinates as shown in Figure 1(a). During the analysis the media nodes are allowed to



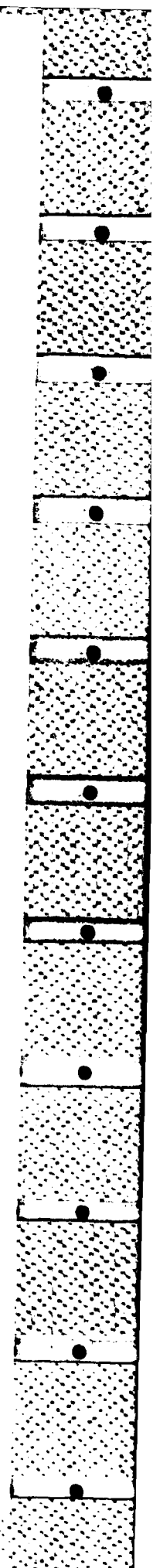
break free from the structure material if the stress state exceeds a prescribed failure envelope. If the node breaks free, it is displaced freely over the time step duration and the coordinates of the final position are stored as in Figure 1(b). If the node does not break free, it is considered fixed to the structure and the regular dynamic finite element method utilized by SAMSON2 is applied to determine element stresses.

After the free nodes are displaced, the final coordinates of these nodes are checked against two boundary conditions. The first test is to determine if the media node entered the structural material as the top node has in Figure 1(b). If the coordinates of the node are determined to exist inside the structure, the media node is simply put back on the slideline at a location nearest to the displaced coordinates. A friction law is applied during the sliding and the final coordinates are stored.

If the coordinates of the node are determined to not be inside the structure, then the node is checked to see if it is within a perpendicular "capture" distance of the structure. The capture distance is a numerical parameter used to determine if a structure-media friction law should apply over the movement. If the node exists within the capture distance, the friction law is applied over the movement and the node is placed back on the slideline. If the node is outside the capture distance, then it is said to be free and its final coordinates are not changed. The capture distance dimension is usually taken to be  $C.D. \approx (1 \times 10^{-7}) \times D$  where D is the nodal spacing (2).

The interface failure model used in the SAMSON2 code is a bi-linear failure envelope initially developed by Robert Frank (5). The envelope is shown in Figure 2. This failure envelope simulates interface failure as well as soil failure near the interface. The normal and shear stresses existing across the interface are compared with this envelope governed by the equation:

$$\tau_F = \text{MIN} \begin{cases} C + \sigma_N \text{TAN } \phi \\ \alpha + \sigma_N \text{TAN } \delta \end{cases} \quad (1)$$



where

- $\tau_F$  = failure shear stress at interface
- $C$  = soil cohesion
- $\alpha$  = adhesion at interface
- $\sigma_N$  = compressive normal stress at interface
- $\phi$  = internal angle of friction of soil
- $\delta$  = angle of friction at interface

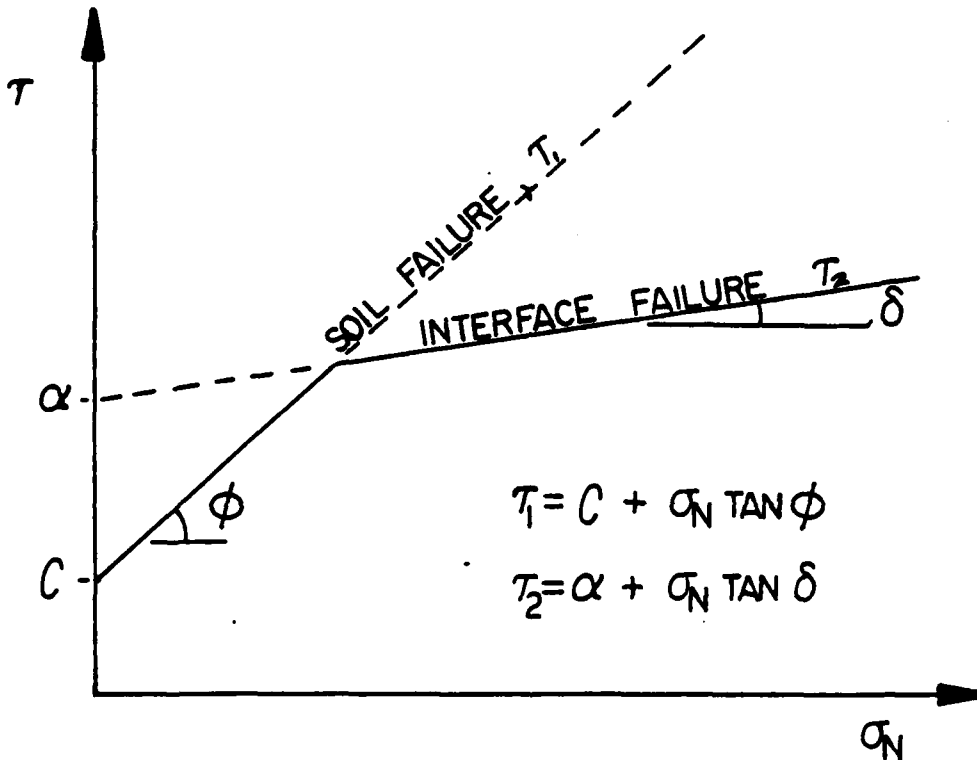


Figure 2 - BILINEAR S.M.I. FAILURE ENVELOPE

If the interface tangential stress  $T < \tau_F$ , then the interface remains bonded and no slip occurs. If  $T \geq \tau_F$ , then slip occurs and frictional stresses act on either side of the interface according to the maximum value calculated from the equation:

$$T = \text{MAX} \left\{ \begin{array}{l} \rho C \Delta V \\ \mu \sigma \frac{\Delta V}{|\Delta V|} \end{array} \right. \quad (2)$$

where

- $T$  = shear friction transferred
- $\rho C$  = soil shear impedance
- $\Delta V$  = relative tangential velocity of the two surfaces across the interface
- $\mu$  = coefficient of kinetic friction
- $\sigma_N$  = compressive normal stress at interface

According to an unfinished report written by AFWL personnel (8) the  $\rho C \Delta V$  friction model does not work properly in the current version of the SAMSON2 code. Current practice at AFWL is to use  $\mu = 0.2$  and set the shear impedance to zero.

Major problems with the slideline interface model include energy losses due to node updating, inadequate friction modeling and large computational times required to keep track of the movements of the nodes. However, the advantages of the slideline model are its ease of concept and the simplicity associated with the governing parameters.

#### B. Structure-Media Interaction Element

Another method of S.M.I. modeling is to place a unique finite element between each of the structure elements and the interacting media elements. Figure 3 shows its location in the model. This element should possess the unique properties of the structure-media interface. Future model development should allow for element expansion, contraction, large relative displacement between structure and media, plastic flow, and shear and normal stress transfer.

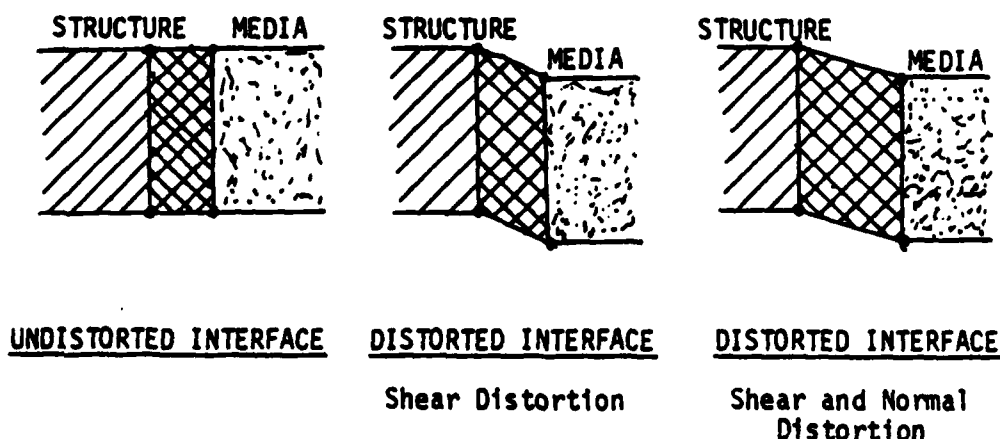


Figure 3. STRUCTURE-MEDIA INTERACTION ELEMENT EXAMPLE

One disadvantage of the S.M.I. element is its aspect ratio. Dynamic finite element analysis uses time step integration techniques. Since the S.M.I. element has one relatively short side, the allowable time step for the entire structure would be governed by this element, although multiple integration time step capabilities built into the SAMSON2 code would help decrease this problem. Another disadvantage of the S.M.I. element is the inability of the model to handle large relative displacements. However, the primary advantage of the S.M.I. element is the small amount of computational time required for solution compared to the time required by the slideline algorithms. These slideline algorithms must perform a computational search to determine the nearest structural element to each media node. This function is quite cumbersome since the code must do this for every time step. However, each S.M.I. element is geometrically defined by nodes which are associated with the element during the entire analysis, thus eliminating the need for searching algorithms.

#### C. Constitutive Equations Model

Professor Howard L. Schreyer, an associate of the New Mexico Engineering Research Institute (N.M.E.R.I.) has recently conducted some studies involving a constitutive model approach. The following information was gathered during an interview with Professor Schreyer (11).

Assume that the media being analyzed is soil. It is "reasonable to assume" that the soil near the interface deforms more than the soil further away. This is depicted graphically in Figure 4. If we observed the actual deformation of the element, we might see the deformation in Figure 4(b). This type of deformation cannot be modeled using linear displacement functions, and quadratic displacement functions would increase computational times excessively. Professor Schreyer suggests that we model the deformation with linear displacement functions, but model the internal stresses with constitutive equations that simulate the curved dashed lines as in Figure 4(c). This method has been

designated as the "smeared" approach. Since this theory is still under development, no advantages or disadvantages of the approach can be given.

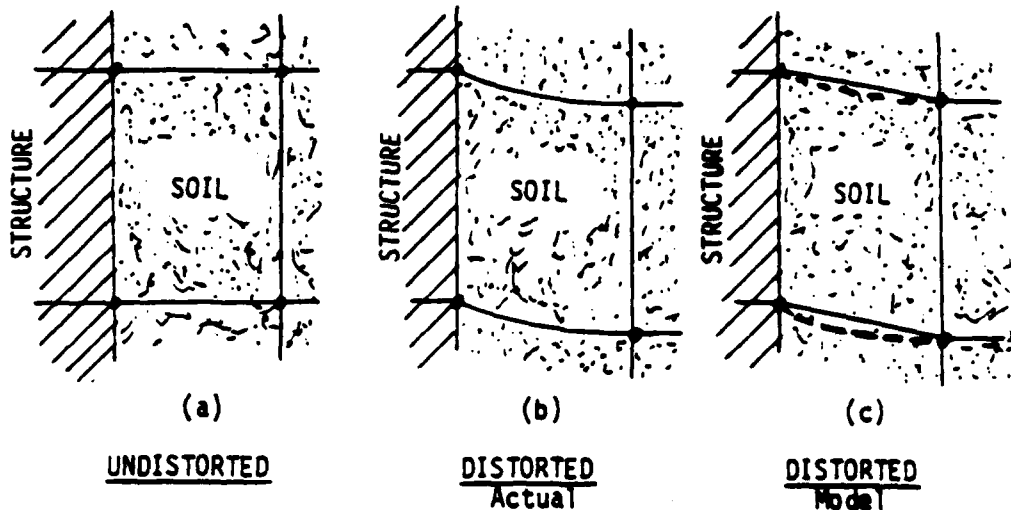


Figure 4. CONSTITUTIVE EQUATIONS APPROACH EXAMPLE

#### V. RECOMMENDATIONS

At this point a review of the main objective of this research is in order, i.e., to effect computational efficiencies in the numerical algorithms of continuum finite element computer codes used in dynamic soil-structure interaction analyses. This paper deals specifically with Task Area Number 2 which is to begin the development of a soil-structure interaction element which is both compatible with the Matrix Difference Equation theory and the current numerical integration schemes of the SAMSON2 code. The following recommendations pertain to these areas.

1. Modify the Current Slideline Model in the SAMSON2 Code. While the concept of the slideline is designed to model both media and interface failure as depicted in Figure 5, the friction equation employed after failure is the same for both media and interface sliding. This model, which is utilized in the current version of SAMSON2, uses  $\mu\sigma_N$  or  $\rho C\Delta V$  for shear stress transfer regardless of which mode of failure has occurred. It seems

reasonable to assume that using different friction equations for different failure modes would be more accurate. This area should be investigated.

At AFWL, the  $\rho C \Delta V$  equation for sliding friction is not used since the portion of the code containing this equation does not work properly. This is documented in an AFWL report written by Lt. G. Leiker (8). This situation should be corrected since the  $\rho C \Delta V$  model was stated as being the most theoretically accurate in another AFWL study (7). Current practice at AFWL is to set  $\rho C$  equal to zero and assign  $\mu = 0.2$  (9).

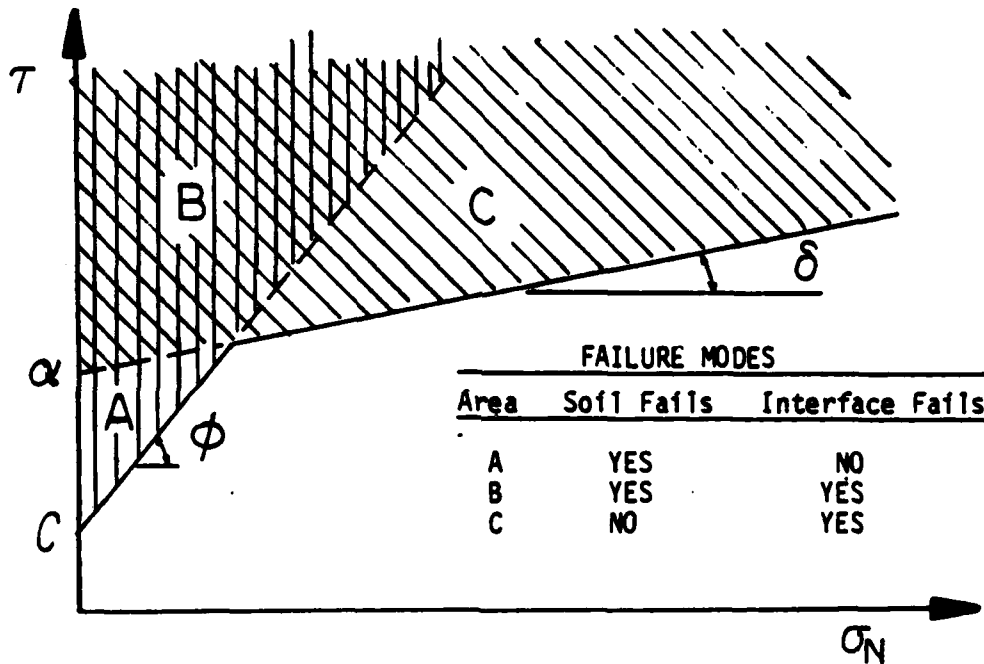


Figure 5. SCHEMATIC OF FAILURE MODES

2. Develop a Structure-Media Interaction Element and Install it into the SAMSON2 Code. Once the parameters which govern the movement of the slideline are better known, the development of a new S.M.I. element should begin. This element will be computationally more efficient than the slideline. The new element should also be compatible with the Matrix Difference Equation theory which is described under Task Area Number 1 of

the main objective. This theory is quite new and quite complicated and, hopefully, the time associated with fixing the sideline first will provide enough time for the Matrix Difference Equations installation and the S.M.I. element installation to begin concurrently.

3. Begin an Experimental Test Program to Better Estimate the Parameters Governing Soil-Structure Interaction. Currently, there is only a small reservoir of accurate structure-media interaction test data. Although models have been developed from these data, more tests need to be conducted to decrease the inaccuracies involved with S.M.I. modeling.

## REFERENCES

1. Belytschko, T., R.R. Robinson, SAMSON2: A Nonlinear Two Dimensional Structure/Media Interaction Code, AFWL-TR-81-109, Air Force Weapons Laboratory, Kirtland Air Force Base, New Mexico, January 1982.
2. Berglund, J., D. Rudeen, Installation of a Large-Displacement Slideline into the SAMSON2 Computer Code, Letter Report, Air Force Weapons Laboratory, Kirtland Air Force Base, New Mexico, October 31, 1983.
3. Drumm, E.C., C.S. Desai, Testing and Constitutive Modeling for Interface Behavior in Dynamic Soil-Structure Interaction, Report to the National Science Foundation, Dept. of Civil Engineering, University of Arizona, Tucson, Arizona, 1983
4. England, R.H., Y.M. Ito, Analysis of Small-Scale Experiments on MX Vertical Shelter Structures, Defense Nuclear Agency Report, DNA 5318f, Washington, DC, February 1980.
5. Frank, R., Analysis of Structure-Media Interaction Data Measured in MX Horizontal Shelter Tests, AFWL-TR-82-105, Air Force Weapons Laboratory, Kirtland Air Force Base, New Mexico, December 1982.
6. Hofmann, R., STEALTH - A Lagrange Explicit Finite Difference Code for Solids, Structural, and Thermohydraulic Analysis, Volume IB, Appendix B1A, EPRI NP-2080, Electric Power Research Institute, 3412 Hillview Avenue, Palo Alto, California, November 1981.
7. Huck, et al., Dynamic Response of Soil/Concrete Interfaces at High Pressure, AFWL-TR-73-264, Air Force Weapons Laboratory, Kirtland Air Force Base, New Mexico, December 1973.
8. Leiker, Lt. G., Model Development of AFWL Structure Pretest Predictions, an unfinished report, Air Force Weapons Laboratory, Kirtland Air Force Base, New Mexico, August 1984.
9. Leiker, Lt. G., Notes from an informal study used to determine a proper friction coefficient for the SAMSON2 slideline, Air Force Weapons Laboratory, Kirtland Air Force Base, New Mexico, date unknown.
10. Nelson, I., Analysis of Soil-Structure Interaction on Site Defense (SD) Type Semi Buried Structures, Department of the Army Corps of Engineers, Huntsville Division, Huntsville, Alabama, March 1975.
11. Shreyer, H.L., Personal interview with H.L. Schreyer, August 9, 1984.
12. Schreyer, H.L., et al., SAMSON2, A Nonlinear Two Dimensional Structure-Media Interaction Code: User's Manual, AFWL-TN-82, Air Force Weapons Laboratory, Kirtland Air Force Base, New Mexico, September 1982.

**1984 USAF-SCEEE GRADUATE STUDENT SUMMER SUPPORT PROGRAM**

**Sponsored by the**

**AIR FORCE OFFICE OF SCIENTIFIC RESEARCH**

**Conducted by the**

**SOUTHEASTERN CENTER FOR ELECTRICAL ENGINEERING EDUCATION**

**FINAL REPORT**

**PHOSPHOLIPID METABOLISM IN A SYNAPTIC MEMBRANE**

**PREPARATION ISOLATED FROM CEREBELLAR CORTEX**

**Prepared by:** Scott B. Bischoff  
**Academic Department:** Medicine  
**University:** University of Texas  
Medical School at Houston  
**Research Location:** USAF School of Aerospace Medicine,  
Clinical Sciences Division, Neurosciences  
Branch  
**USAF Research Contact:** Dr. David M. Terrian  
**SFRP Supervising  
Faculty Member:** Dr. Robert V. Dorman, Assistant Professor  
**Date:** August 15, 1984  
**Contract No.** F49620-82-C-0035

PHOSPHOLIPID METABOLISM IN A SYNAPTIC MEMBRANE  
PREPARATION ISOLATED FROM CEREBELLAR CORTEX

by  
Scott B. Bischoff  
and  
Robert V. Dorman Ph.D.

ABSTRACT

The cerebellum is involved in the control of voluntary motor activity. In turn, the functioning of the cerebellum depends on the membrane phenomena related to the uptake, release and effects of neurotransmitters. We have examined some aspects of membrane biochemistry in a synaptic preparation isolated from bovine cerebellar cortex. We have detailed some metabolic pathways, in order to obtain basic information on the interactions of neurotransmitters and excitable membranes. We employed a purified glomeruli fraction, which contains intact synaptic structures, for investigation of phospholipid metabolism.

The purified glomeruli fraction contains the ethanolamine and choline phosphotransferase enzymes. These enzymes are necessary for the synthesis of the major membrane phospholipid components. We characterized these enzymes and estimated their kinetic constants. The properties of these enzymes are similar to those reported for other brain regions. We also found that the glomeruli particles can incorporate exogenous fatty acids into the membrane lipids. This mechanism may be used for further studies on the complex relationship between neurotransmission and membrane lipid metabolism.

Acknowledgement

I would like to thank the Air Force Systems Command, the Air Force Office of Scientific Research and the Southeastern Center for Electrical Engineering for providing the opportunity to work on an interesting and worthwhile project at the USAF School of Aerospace Medicine, Brooks AFB, TX. I would also like to thank Dr. David M. Terrian and Dr. Robert V. Dorman. They provided me with a stimulating research environment and generously gave of their time and effort to insure my summer visit was rewarding in all respects.

## I. INTRODUCTION:

Describing the mechanisms involved in the uptake, release and effects of neurotransmitters are important problems in neuroscience research. Neurotransmitters are synthesized, stored and released by neurons. They act as chemical signals for interneuronal communications, by interacting first with the plasma membrane of the target cells. Opportunities for controlling nervous system activities can be logically developed only through an understanding of the complex processes involved in the movement, binding and metabolism of the neurotransmitters.

The uptake and release of neurotransmitters requires alterations in the structure of the membranes involved. Biological membranes act as barriers to molecular movement due to the presence of the hydrophobic core of the phospholipid bilayer. Large, or charged components, such as neurotransmitters, require special mechanisms for transmembrane movement. The processes that neuronal membranes use for such transport activities are unclear. However, a role for the bilayer phospholipids in such mechanisms is certain.

The structure of all biological membranes depends on an exact complement of the various phospholipid classes. The proportion of each class, and the molecular species within each class varies with the cell type. It has been shown that the phospholipids are more metabolically active in cells which require more transmembrane molecular movement. For example, neurons synthesize and degrade phospholipids at a faster rate than glial cells<sup>1,2</sup>, and neurotransmitters have been shown to stimulate phospholipid metabolism<sup>3,4,5</sup>.

The exact relationship between lipid metabolism and nervous system functions is poorly defined. It is uncertain which phospholipids and which metabolic pathways are involved in the processes of transmembrane molecular movement and signalling. Discrepancies have arisen due to the lack of a reliable model system. Reports have been described for different membrane preparations, tissue sources and analytical procedures.

In order to investigate membrane biochemistry, as it is related to chemical transmission, an appropriate model must be used. The integrity of the pre- and post-synaptic connections should be maintained. Peri-

peral interference in metabolic studies should be minimized. The membranes must be intact, easily extracted and accessible to manipulations. Synaptosomal preparations are commonly used to study the biochemical mechanisms related to neurotransmitter uptake and stimulation-secretion coupling in neurons. However, most synaptosomal preparations are heterogenous in source and are usually devoid of intact synaptic connections.

The purified glomeruli fraction (PGF) used in the following studies provides a useful model for investigations of synaptic biochemistry. The PGF is prepared from cerebellar cortex and contains the synaptic elements from the connections of the mossy fiber neurons with the granule cells.<sup>6</sup> This area of the cerebellum shows convergence and divergence of electrical information, which indicates integrative capabilities. The isolated glomeruli particles have been shown to be morphologically intact, highly purified and metabolically preserved.<sup>7,8,9,10,11</sup> Thus, the PGF is a synaptic preparation derived from a homogenous and morphologically well-defined source, and yet is metabolically active and diverse.

In order to use PGF for biochemical investigations of lipid involvement in neurotransmission, some amount of characterization must be done. Although the phospholipid content and composition of the cerebellum is similar to that in other brain regions,<sup>12</sup> there are no studies available on the normal phospholipid synthetic pathways in this brain region. The investigations described in this report were designed to examine the rates of synthesis of some major membrane phospholipids and to determine the ability of the synaptic fraction to incorporate radiolabeled fatty acids into the complex lipids. Completion of these studies provides the basis for more detailed investigations into the relationship between membrane phospholipids and neurotransmitter actions in the purified glomeruli fraction.

## II. OBJECTIVES:

The general goal of this research project was to investigate some of the phospholipid metabolic pathways in a synaptic preparation from cerebellar cortex, and relate these findings to the uptake and release



of neurotransmitter/membrane interactions in the glomeruli synaptic fraction.

(b) Methods and Results:

The membrane preparation employed was the purified glomeruli particles isolated from bovine cerebellar cortex. The PGF was prepared as follows: Bovine cerebellar vermis was removed by dissection and homogenized in 9 volumes of 0.3 M sucrose. The homogenate was filtered to remove debris, then was centrifuged at 1000 g for 10 minutes. The pellet was resuspended in 0.3 M sucrose and was centrifuged again at 1000 g for 10 minutes. The resultant pellet was resuspended in 18% Ficoll, dissolved in 0.3 M sucrose, and was centrifuged at 7500 g for 40 minutes. The supernatant was diluted 50% in 0.3 M sucrose and was centrifuged at 20,000 g for 20 minutes. That pellet was resuspended in 30 ml of 0.3 M sucrose and 5 ml aliquots were layered onto 25 ml of 1.2 M sucrose. The PGF was pelleted by centrifugation at 53,000 g for 60 minutes. The PGF was resuspended in 0.32 M glucose and this suspension was diluted 10-fold in buffer for the enzyme assays.

The phosphotransferase assays were carried out at 37°C in a volume of 1.0 ml. Typical incubations contained 1-2 mg of PGF protein and 40 nCi of either <sup>14</sup>C-CDPethanolamine or <sup>14</sup>C-CDPcholine (both at 2 nCi/nmol) in 10 mM Tris-HCl buffer at pH 7.45. Choline phosphotransferase (CPT) assays normally contained 100 mM MgCl<sub>2</sub>, while ethanolamine phosphotransferase (EPT) assays contained 10 mM MnCl<sub>2</sub>. The incubations were stopped by the addition of 5 ml of chloroform:methanol (2:1, v:v) and the total lipids were extracted according to Folch *et al.*<sup>16</sup> The incorporation of radiolabeled substrates was determined by liquid scintillation counting of the total lipid extract in a Beckman LS-230 counter. Aquasol II was the cocktail used. The results are typically expressed as nmol lipid synthesized/hour/mg PGF protein.

1. Time course of isotope incorporation:

Ethanolamine and choline phosphotransferase enzymes incorporated the radiolabeled precursors in a linear fashion for up to 30 minutes (Fig. 2). Subsequent assays were performed for 30 minutes to insure adequate isotope incorporation without risking the loss of enzyme activities.

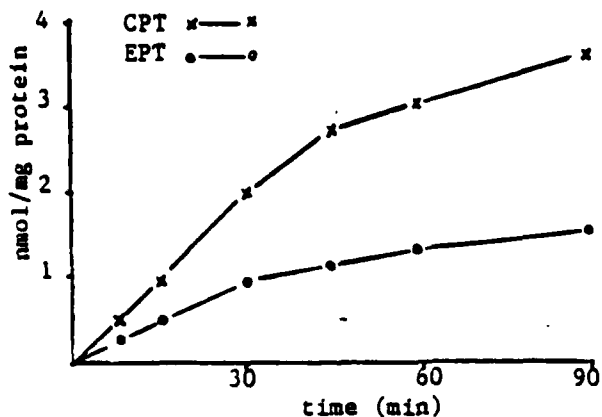


Figure 2. Time course of incorporation of either  $^{14}\text{C}$ -CDPcholine or  $^{14}\text{C}$ -CDPethanolamine into the corresponding phospholipids by PGF. The assay conditions are described above.

2. Protein dependence of isotope incorporation:

Assays were performed to determine if the incorporation of isotopes was dependent on the concentration of enzymes. We found that the rates of phospholipid synthesis were dependent on the amount of enzyme present (Fig. 3). We also found that both EPT and CPT were completely inhibited by exposure to  $100^\circ\text{C}$  for 10 minutes.

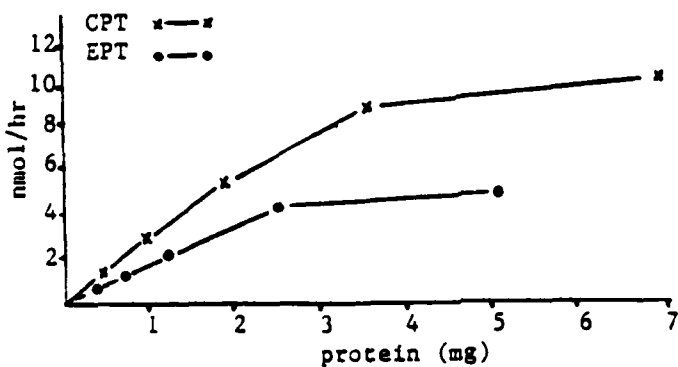


Figure 3. The dependence of EPT and CPT activities on the concentration of PGF protein. Assays were the same as described, except the concentration of PGF protein was varied.

### 3. Cation effects on phosphotransferase activities:

Both enzymes were assayed in the presence of various concentrations of  $\text{Ca}^{++}$ ,  $\text{Mg}^{++}$  and  $\text{Mn}^{++}$ , as well as EDTA, a cation chelator. EPT was most active in the presence of  $\text{Mn}^{++}$ , while CPT required  $\text{Mg}^{++}$  for optimal activity. The presence of  $\text{Ca}^{++}$  or EDTA markedly inhibited both enzymes (Table 1).

Table 1. Cation dependence of EPT and CPT. Assays were performed as previously described, except the cations, and their concentrations, were varied.

Addition (mM)	nmol/hr/mg protein						
	0.01	0.1	1.0	10	20	100	200
CPT	-	-	0.184	2.059	3.103	4.341	4.302
Mg <sup>++</sup> :							
EPT	-	-	0.863	0.839	0.831	0.686	-
CPT	0.226	1.544	2.376	2.366	2.064	-	-
Mn <sup>++</sup> :							
EPT	0.799	0.946	1.252	1.280	1.139	-	-
CPT	0.037	0.029	0.020	0.028	-	-	-
Ca <sup>++</sup> :							
EPT	0.827	0.731	0.467	0.175	0.152	-	-

### 4. The pH optima of CPT and EPT:

Enzyme assays were performed at various pH in order to determine the optimum pH for the activity of each enzyme. Both enzymes showed a pH optimum near 7.4 (Fig. 4).

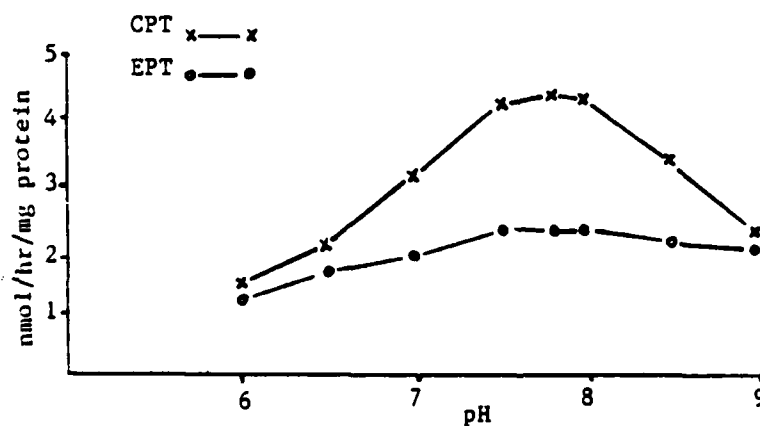


Figure 4. The pH dependence of the phosphotransferase enzymes. Assays were performed as before, but the pH of the incubations varied.

5. Enzyme kinetics for EPT and CPT:

The final step in characterizing the phosphotransferase enzymes in PGF was determination of the kinetic constants  $K_m$  and  $V_{max}$ . Apparent  $K_m$  values were estimated for both substrates with each enzyme by varying the concentrations of exogenous diacylglycerol and  $^{14}C$ -CDP-amines. The  $K_m$  values for diacylglycerol were determined by incubating the PGF with 0.5 - 10.0 mM diolein. CDPamine concentrations were varied from 5 - 100  $\mu M$ . The estimated kinetic constants are shown in Table 2.

Table 2. Kinetic estimates of apparent  $K_m$  and  $V_{max}$  for CPT and EPT. Assays were performed as before, except the concentrations of CDP-amines and diolein were varied. The diolein was suspended in 0.02% Triton X-100.

	$V_{max}$ (nmol/hr/mg prot)	$K_m$ diolein (mM)	$K_m$ CDPamine ( $\mu M$ )
EPT	10.0	2.1	8.3
CPT	35.9	2.9	28.6

6. The effects of hypotonic lysis of PGF vesicles on phosphotransferases activities.

It has previously been shown that hypotonic lysis of cerebral cortical synaptosomes resulted in a 3-fold increase in the activities of the phosphotransferase enzymes.<sup>16</sup> The authors suggested that most of the enzyme molecules were sequestered inside the synaptosomes and were unavailable to the radioactive substrates. We lysed our PGF vesicles by placing them in 5 mM Tris buffer and storing them at 4°C for 60 minutes prior to incubation. Unlike what was found with cerebral cortex synaptosomes, we found no enhancement of enzyme activities following hypotonic lysis (Table 3). The phosphotransferases in the PGF are readily accessible to exogenous substrates. Therefore, the glomeruli particles are devoid of trapped membranes, such as endoplasmic reticulum.

Table 3. Effects of hypotonic lysis and various buffer concentrations on the activities of CPT and EPT.

Tris (mM)	nmol/hr/mg protein					
	5	10	50	(60' lysis) 5	10	50
CPT	2.993	4.247	4.265	2.748	3.615	3.968
EPT	2.217	2.299	2.125	1.776	1.874	1.850

7. The effects of nucleotides and neurotransmitters on CPT and EPT:

Changes in the activities of CPT and EPT would alter the structure of the synaptic membranes. Any changes in structure would alter the permeability properties of the membrane, as well as the activities of membrane-bound enzymes. Therefore, phospholipid metabolism, through alterations of phosphotransferase activities, may provide a mechanism for the membrane changes related to neurotransmitter functions. We examined the effects of various neurotransmitters and nucleotides on the activities of CPT and EPT in the synaptic membrane preparation. We found that the enzymes were affected by some of these compounds (Table 4).

Table 4. The effects of neurotransmitters, agonists and nucleotides on phosphotransferase activities in PGF. The assays were performed as before, except for the additions listed in the table and the use of 20  $\mu$ M CDPcholine and CDPethanolamine.

Addition(1.0 mM)	nmol/hr/mg protein $\pm$ SD	
	EPT	CPT
none	1.425 $\pm$ 0.085	2.608 $\pm$ 0.102
ATP	1.599 $\pm$ 0.063	2.652 $\pm$ 0.098
cAMP	1.490 $\pm$ 0.074	2.746 $\pm$ 0.053
CTP	1.147 $\pm$ 0.113	3.548 $\pm$ 0.352
CDP	1.212 $\pm$ 0.052	3.776 $\pm$ 0.499
CMP	0.931 $\pm$ 0.024	3.755 $\pm$ 0.371
5-HT	1.427 $\pm$ 0.058	2.619 $\pm$ 0.112
GABA	1.439 $\pm$ 0.055	2.703 $\pm$ 0.086
Muscimol	1.440 $\pm$ 0.059	2.625 $\pm$ 0.081
Carbamylcholine	1.461 $\pm$ 0.086	2.729 $\pm$ 0.093

Summary of results of the experiments with EPT and CPT:

1. Bovine cerebellum contains EPT and CPT
2. CPT is approximately twice as active as EPT
3. Both enzymes have pH optimums near 7.45
4. EPT is most active in the presence of  $Mn^{++}$ , CPT requires  $Mg^{++}$
5. The kinetic parameters for both enzymes are similar to those reported for other brain regions.
6. Both phosphotransferases are readily available to exogenous substrates.
7. Both enzymes were influenced by some nucleotides and neurotransmitters.

#### IV. INCORPORATION OF $^{14}\text{C}$ -ARACHIDONIC ACID INTO PGF MEMBRANES:

(a) The release of free fatty acids (FFA), in particular arachidonic acid, has been shown to occur in nervous tissue during conditions known to elicit the release of neurotransmitters. Electroconvulsive shock, bicuculline induced seizures and acute cerebral ischemia all stimulate the release of unesterified fatty acids from membrane phospholipids.<sup>18,19,20</sup> We began experiments designed to investigate the relationships between phospholipid metabolism and depolarization stimulated neurotransmitter release.

PGF phospholipids were radiolabeled with  $^{14}\text{C}$ -arachidonic acid. Incubations were performed at  $37^{\circ}\text{C}$  in Krebs-Ringer buffer containing 1 mM CoA, 0.1 mM dithiothrietal,  $5 \times 10^5$  dpm  $^{14}\text{C}$ -arachidonic acid (52 nCi/nmol), and approximately 1 - 2 mg PGF protein. The PGF membranes were pelleted by centrifugation and were washed 3 times with Krebs-Ringer buffer containing 1.0% fatty acid free bovine serum albumin, in an attempt to remove unincorporated isotope. Lipids were extracted from the final PGF pellet as previously described. The non-polar and phospholipids were separated by thin layer chromatography and the radioactivity in each lipid was determined by liquid scintillation counting as previously described.

##### (b) Results:

##### 1. Removal of unincorporated $^{14}\text{C}$ -arachidonic acid:

The radioactivity in the supernatants produced by the centrifugation steps was determined in order to measure residual isotope. This was an important consideration, since the accumulation of free fatty acids is a primary criteria for assessing the membrane effects related to neurotransmission. The wash procedures did remove most of the unincorporated isotope. However, this technique left substantial amounts of radioactivity in the free fatty acid pool (Table 5).

Table 5. Removal of unincorporated  $^{14}\text{C}$ -arachidonic acid from radio-labeled PGF. The methods are described above. Incubation times were 15, 30 and 60 minutes.

supernatant	time (min)	dpm/mg protein		
		15	30	60
1		337841	333518	334490
2		10963	11895	10952
3		1153	1324	1036
4		435	431	313

2. Time course of incorporation of  $^{14}\text{C}$ -arachidonic acid into PGF lipids:

The incorporation of radiolabeled arachidonic acid into PGF lipids was determined following 15, 30, 60, 90 and 120 minute incubations at  $37^{\circ}\text{C}$ . The level of incorporation was near maximum by 60 minutes of incubation (Table 6).

Table 6. The incorporation of  $^{14}\text{C}$ -arachidonic acid into phospholipids and free fatty acids at various times of incubation. The methods are described above.

Time (min)	dpm/mg protein	
	Phospholipid	Free Fatty Acid
15	531	673
30	1377	629
60	1679	715
90	1688	488
120	1476	516

3. Incorporation of arachidonic acid into PGF phospholipids:

The incorporation of isotope into various phospholipids was determined following 30 and 60 minutes of incubation. The procedures used are described above. We found that the level of incorporation was greatest into the choline glycerophospholipids, followed by the inositol and ethanolamine glycerophospholipids (Table 7).

Table 7. Incorporation of  $^{14}\text{C}$ -arachidonic acid into the major PGF phospholipids. The methods are described above.

glycerophospholipid	dpm/ml incubation	
	30'	60'
choline	483	691
ethanolamine	116	206
inositol, serine & sphingomyelin	404	600

Summary of results of the experiments on the incorporation of  $^{14}\text{C}$ -arachidonic acid into PGF lipids:

1. PGF membranes actively incorporate exogenous arachidonic acid into complex lipids.

2. The incorporation of isotope into PGF lipids increased for up to 60 minutes of incubation.
3. Although four washes of the PGF did substantially reduce the level of unincorporated  $^{14}\text{C}$ -arachidonic acid, the removal was incomplete, and this preparation is unsuitable for investigations of the effects of depolarization on membrane lipid metabolism.

V. EFFECTS OF EXOGENOUS PHOSPHOLIPIDS ON NEUROTRANSMITTER UPTAKE:

(a) Exogenous phospholipid vesicles have been shown to enhance the uptake of neurotransmitters by neuronal membranes in vivo and in vitro.<sup>21,22</sup> We wanted to study this interesting phenomenon using the purified glomeruli. However, time limitations prevented any substantial effort in this direction. These studies will have to be performed at a later date.

VI. RECOMMENDATIONS:

The mechanisms of membrane alterations related to cerebellar function have not been resolved by the present research. We have identified some potential controls for membrane permeability changes by showing the presence and characteristics of the choline and ethanolamine phosphotransferase enzymes in cerebellar membrane preparations. We also showed that the purified glomeruli fraction can incorporate arachidonic acid into its complex lipids. This should provide an approach for further studies relating membrane metabolism to neurotransmitter effects, uptake and release. Some suggestions for follow-on research are:

1. Develop a method for the in vivo radiolabeling of PGF lipids with arachidonic acid.
2. Examine the effects of depolarization on the metabolism of PGF lipids, using the pre-labeled membranes. Of particular interest will be the loss of radioactivity from the complex lipids and the accumulation of label in the free fatty acid pool, as well as in their oxidized derivatives, the prostaglandins, thromboxanes and related compounds.
3. Determine the effects of neurotransmitters, analogues and inhibitors on the metabolism of pre-labeled PGF lipids, as described above.

Future investigations should include attempts to relate the biochemical data from this, and the follow-on research to electrophysiological studies. The goal of such investigations would be to make the biochemical-physiological correlations necessary to develop an approach for the manipulation of cerebellar functions, for the enhancement of voluntary motor activity.

## REFERENCES

1. Binaglia, L., Goracci, G., Porcellati, G., Roberti, R. and Woelk, H. (1973) The synthesis of choline and ethanolamine phosphoglycerides in neuronal and glial cells in vitro. J. Neurochem. 21: 1067-1082.
2. Freysz, L., Bieth, R. and Mandel, P. (1969) Kinetics of the biosynthesis of phospholipids in neurons and glial cells isolated from rat brain cortex. J. Neurochem. 16: 1417-1424.
3. Hokin, L.E. and Hokin, M.R. (1955) Effects of acetylcholine on the turnover of phosphoryl units in individual phospholipids of pancreas slices and brain cortex slices. Biochim. Biophys. Acta 18: 102-111.
4. Hokin, M.R. (1969) Effect of norepinephrine on <sup>32</sup>P incorporation into individual phosphatides in slices from different areas of the guinea pig brain. J. Neurochem. 16: 127-134.
5. Abdel-Latif, A.A., Yau, S.-J. and Smith, J.P. (1974) Effect of neurotransmitters on phospholipid metabolism in rat cerebral-cortex slices: cellular and subcellular distribution. J. Neurochem. 22: 383-393.
6. Llinas, R.R. and Simpson, J.I. (1981) Cerebellar control of movement. In "Handbook of Behavioral Neurobiology" 5: 231-302.
7. Hajos, F., Tapia, R., Wilkin, G., Johnson, A.L. and Balazs, R. (1974) Subcellular fractionation of rat cerebellum: an electron microscopic and biochemical investigation. Brain Res. 70: 261-279.
8. Hajos, F., Wilkin, G., Wilson, J. and Balazs, R. (1975) A rapid procedure for obtaining a preparation of large fragments of the cerebellar glomeruli in high purity. J. Neurochem. 24: 1277-1278.
9. Kingsbury, A.E., Wilkin, G.P., Patel, A. and Balazs, R. (1980) Distribution of GABA receptors in the rat cerebellum. J. Neurochem. 35: 739-742.
10. Tapia, R., Hajos, F., Wilkin, G., Johnson, A. and Balazs, R. (1974) Subcellular fractionation of rat cerebellum: an electron microscopic and biochemical investigation. Brain Res. 70: 285-299.
11. Wilson, J.E., Wilkin, G.P. and Balazs, R. (1976) Metabolic properties of a purified preparation of large fragments of the cerebellar glomeruli: glucose metabolism and amino acid uptake. J. Neurochem. 26: 957-965.

12. Geisen, R.L., Flangos, A.L. and Kornguth, S.E. (1974) Total glycerophospholipid fatty acid and phospholipid class composition of nerve ending and related fractions from fetal and adult pig cerebellum and adult pig whole brain cortex. *Lipids* 9: 756-764.
13. Kennedy, E.P. and Weiss, S.B. (1956) The function of cytidine coenzymes in the biosynthesis of phospholipids. *J. Biol. Chem.* 222: 193-214.
14. Porcellati, G., Biasion, M.G. and Pirota, M. (1970) The labelling of brain ethanolamine phosphoglycerides from cytidine diphosphate ethanolamine in vitro. *Lipids* 5: 734-742.
15. Wu, P.-S. and Ledeen, R.W. (1980) Evidence for the presence of CDP-ethanolamine: 1,2-diacyl-sn-glycerol ethanolamine phosphotransferase in rat central nervous system myelin. *J. Neurochem.* 35: 659-666.
16. Strosznajder, J., Radomska-Pyrek, A. and Horrocks, L.A. (1979) Choline and ethanolamine glycerophospholipid synthesis in isolated synaptosomes of rat brain. *Biochim. Biophys. Acta* 574: 48-55.
17. Folch, J., Lees, M. and Sloane-Stanley, G.H. (1957) A simple method for the isolation and purification of total lipids from animal tissues. *J. Biol. Chem.* 226: 497-509.
18. Bazan, N.G. (1970) Effects of ischemia and electroconvulsive shock on free fatty acid pool in the brain. *Biochim. Biophys. Acta* 218: 1-10.
19. Bazan, N.G., Aveldano de Caldironi, M.I., Cascone de Suarez, G.D. and Rodriguez de Turco, E.B. (1980) Transient modifications in brain free arachidonic acid in experimental animals during convulsions. In "Neurochemical and Clinical Neurology", Alan R. Liss Co., N.Y., N.Y., pp. 167-169.
20. Siesjo, Bo K., Ingvar, M. and Westerberg, E. (1982) The influence of bicuculline-induced seizures on free fatty acid concentrations in cerebral cortex. *J. Neurochem.* 39: 796-802.
21. Toffano, G., Leon, A., Benvegna, D., Borato, E. and Azzore, G.F. (1976) Effect of brain cortex phospholipids on catecholamine content of mouse brain. *Pharmac. Res. Commun.* 8: 581-590.
22. Bruni, A., Toffano, G., Leon, A. and Borato, E. (1976) Pharmacological effects of phosphatidylserine liposomes. *Nature, Lond.* 260: 331-333.

**1984 USAF-SCEE GRADUATE STUDENT SUMMER SUPPORT PROGRAM**

**Sponsored by the**

**AIR FORCE OFFICE OF SCIENTIFIC RESEARCH**

**Conducted by the**

**SOUTHEASTERN CENTER FOR ELECTRICAL ENGINEERING EDUCATION**

**FINAL REPORT**

**Aging Behavior Of Rapidly Solidified Ti-Co and Ti-Cr-Al Alloys**

**Prepared by:** Philip E. Blosser

**Academic Department:** Materials Science and Engineering

**University:** Wright State University

**Research Location:** Air Force Wright Aeronautical Laboratories,  
Materials Laboratory

**USAF Research Contact:** Dr. F.H. Froes

**SFRP Supervising  
Faculty Member:** Dr. Isaac Weiss  
Asst. Professor of Engineering

**Date:** August 17, 1984

**Contract No:** F49620-82-C-0035

AGING BEHAVIOR OF RAPIDLY SOLIDIFIED

Ti-Co AND Ti-Cr-Al ALLOYS

BY

Philip & Blosser

ABSTRACT

The feasibility of developing high strength titanium alloys containing eutectoid-forming elements is being explored via rapid solidification (RS) processing. Near eutectoid Ti-Co and Ti-Cr-Al alloys were both conventionally cast and rapidly solidified into ribbons by the melt spinning process. Aging treatments were carried out on these specimens at sub-eutectoid temperatures for varying times. Microstructural characterization was carried out by optical microscopy using the Nomarski interference contrast technique, scanning electron microscopy and transmission electron microscopy. The aging hardening response was studied by measuring microhardness values.

The as-quenched ribbon and solution treat/quenched bulk specimens of both alloys showed a retained beta microstructure. Aging below the eutectoid temperature resulted in rapid precipitation of a very fine proeutectoid alpha phase followed by a eutectoid decomposition of the beta phase into alpha and intermetallic compound ( $Ti_2Co$  and  $TiCr_2$ ). In the RS ribbons precipitation occurs more rapidly and more uniformly in comparison to conventionally cast specimens. The hardness peak for the Ti-Co alloy was found to occur at times which are three orders of magnitude shorter than for the Ti-Cr-Al systems. The hardness peak for both alloys corresponds to the formation of fine proeutectoid alpha phase. No hardening due to intermetallic compound was evident.

ACKNOWLEDGEMENT

The author would like to thank the Air Force Systems Command, Air Force Office of Scientific Research and the Southeastern Center for Electrical Engineering Education for allowing him to spend a challenging but rewarding summer at the Materials Laboratory (AFWAL/MLLS), Wright-Patterson AFB, Ohio. The council and suggestions by professor Isaac Weiss, Wright State University, and Dr. S. Krishnamurthy were very helpful in establishing direction for this project.

132

## I. INTRODUCTION

Ti-Co and Ti-Cr-Al alloys possess the microstructural characteristics necessary for use in many high strength applications. However, conventional ingot metallurgy (IM) processes result in grain boundary segregation of the eutectoid-forming elements. Rapid solidification techniques circumvents the segregation problem by producing a homogeneous microstructure while extending the solubility limits.<sup>1,2,3,4,5</sup> Development of alloys is always of interest to the Air Force mainly for aircraft application.

Little is known about the effects of aging rapidly solidified materials. In the past, there has been only limited research on the effects of eutectoid decomposition in titanium alloys.<sup>6,7</sup> Studies were limited to conventionally cast/homogenized alloys evaluated by standard optical metallographic techniques.

The addition of a eutectoid-forming compound lowers both the melting and transformation temperatures of pure titanium, Fig. 1. Precipitation of alpha (HCP structure) within the beta phase (BCC structure) achieves solid solution strengthening. The component,  $Ti_2Co$  and  $TiCr_2$ , are complex FCC structures which do not aid in strengthening the alloy.

## II. OBJECTIVE

The main objective of this project was to develop testing procedures to evaluate eutectoid-forming alloys. Specific objectives were;

(1) Development of procedures to age RS materials for times shorter than five minutes.

(2) Establishment of electropolishing/etching techniques for both conventional cast and RS material.

## III. MATERIAL HISTORY

The starting material was produced by utilizing a tungsten arc melting process followed by a homogenization treatment and hot swaging. Swaged

material was remelted and rapidly solidified in the form of ribbons by melt-spinning procedures. In order to compare aging characteristics of RS material and IM alloys, swaged alloy samples were beta solution treated prior to aging characteristics of RS material and IM alloys, swaged alloy samples were beta solution treated prior to aging, fig. 2.

#### IV. DEVELOPMENT OF AGING PROCEDURES

Isothermal aging of RS material was found to be rapid. As a result, treatments of less than 300 seconds are required. Three hundred seconds has been found to be the minimum practical aging time for convection air box furnaces. Since titanium oxidizes rapidly at elevated temperatures, aging must be carried out in vacuum.

Satisfactory results have been obtained by aging in a salt bath using encapsulated specimens in evacuated Vycor<sup>TM</sup> tubing. Prior to encapsulation, ribbons were wrapped in CP-titanium to act as an oxygen absorber. Quenching was performed in ice brine solution. Extended aging treatments were conducted in a box furnace using encapsulated specimens.

#### V. ELECTROPOLISHING AND ETCHING TECHNIQUES

Standard chemical etching can severely destroy the true microstructure studied. Hydride formation, chemical staining and precipitate leaching occurs as the result of standard chemical etching. These problems can be eliminated by using electropolishing techniques.

Electropolishing practices for RS materials were established. Specific problems such as edge retention and good electrical contact were considered. The use of Konductomet<sup>TM</sup>, a carbon impregnated Bakelite produced by Buehler was found to be part of the solution. Best results have been obtained by using an electrolyte of 6% perchloric acid, 35% butyrcellosolve and 59% methanol at a temperature of -55°C. A polishing curve for each alloy/aging treatment was obtained.

#### VI. HARDNESS TESTING

Comparison of the hardening response between RS and ingot materials requires a consistent approach to hardness testing. Whereas the

microstructure of the RS material is nearly homogenous, this is not the case for IM materials. Hardness variations occurs between grain boundary and interior regions. Variations greater than twenty percent were evaluated using the rule of mixtures;

$$\text{Hardness} = V_{f(\text{gb})} \text{HV}_{(\text{gb})} + V_{f(\text{gi})} \text{HV}_{(\text{gi})} \quad (1)$$

$V_{f(\text{gb})}$  = Volume fraction of grain boundaries

$V_{f(\text{gi})}$  = Volume fraction of grain interior

$\text{HV}_{(\text{gb})}$  = Average hardness of grain boundary

$\text{HV}_{(\text{gi})}$  = Average hardness of grain interior

All hardness measurements were obtained using a Vickers indenter and a 25 g load.

## VII. RESULTS

The eutectoid decomposition mechanism for both the Ti-Co and the Ti-CR-Al systems was found to be similar. Proeutectoid alpha forms from the beta phase upon aging at subeutectoid temperatures. Alpha precipitates in an ordered manner along grain boundaries while creating a basketweave pattern within the grain interior. Prolonged aging resulted in coarsening, Figures 3-5.

The occurrence of a hardening peak mainly corresponds to the formation of fine proeutectoid alpha phase. No hardening due to an intermetallic compound is evident. Precipitation occurs more rapidly and more uniformly in RS materials than in IM specimens, Figures 6 & 7. An increase in aging temperature resulted in coarsening of the alpha phase and subsequent decrease in hardness. The overall rate of reaction appears to be controlled by the structure complexity of the intermetallic compound.

RECOMMENDATIONS

This project established the ground work whereby other eutectoid-former alloys can be evaluated. "Short time" aging of RS materials can be accomplished via encapsulation and salt bath heat treatments. Lower aging temperatures consistently increase hardness values. Therefore, further studies should concentrate on aging temperatures above the omega formation range but well below the eutectoid temperature.

The choice of specimens for metallographic study should be judiciously made. Electropolishing procedures for new alloys are labor intensive. However, the results obtained in this project demonstrate the necessity to electropolish/etch instead of using mechanical polishing and chemical etching procedures.

## REFERENCES

1. S. Krishnamurthy, R.G. Vogt, D. Eylon, and F.H. Froes: "Developments in Titanium Powder Metallurgy". Structural Metals Branch, Metals and Ceramics Division, Materials Laboratory, AFWAL, Wright Patterson AFB, OH 45433, unpublished research, 1983.
2. S.M.L. Sastry, T.C. Peng, P.J. Maschter, and J.E. O'Neal: "Rapid Solidification Processing of Titanium Alloys". Journal of Metals, 1983, 35(9), pp. 21-28.
3. F.H. Froes and J.R. Pickens: "Powder Metallurgy of Light Metal Alloys for Demanding Applications". Journal of Metals, 1984, 36 (1), pp. 14-28.
4. S. Krishnamurthy: "Microstructural Characterization of Rapidly Solidified Titanium-Eutectoid Former Alloys". Structural Metals Branch, Metals and Ceramics Division, Materials Laboratory, AFWAL, Wright Patterson AFB, OH 45433, unpublished research, 1983.
5. N.J. Grant: "Rapid Solidification of Metallic particulates". Journal of Metals, 1983, 35 (1), pp. 20-27.
6. G.W. Franti, J.C. Williams, and H.I. Arronson: "A Survey of Eutectoid Decomposition in Ten Ti-X Systems". Met. Trans., 1978, Vol. 9A, pp.1641-1649.
7. D.J. Maykuth, H.R. Ogden, and R.I. Jaffee: "The Effects of Alloying Elements in Titanium, Volume A, Constitution". DMIL Report 136A pp. 39-41, Defense Materials Information Center, Battelle Memorial Institute, Columbus, OH, 1960.
8. F.L. Orrell Jr. and M.G. Fontana: "The Titanium-Cobalt System" Transactions ASM, 1955, (47) pp. 554-563.

Figure 1

**THE TI-Co PHASE DIAGRAM**

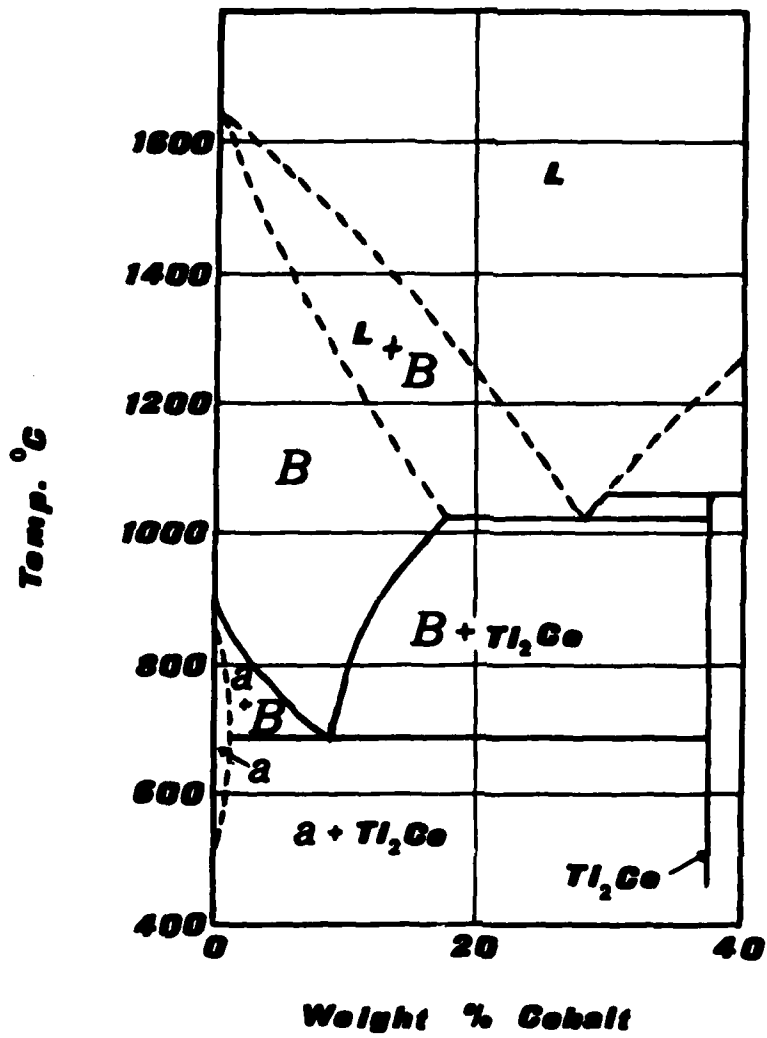
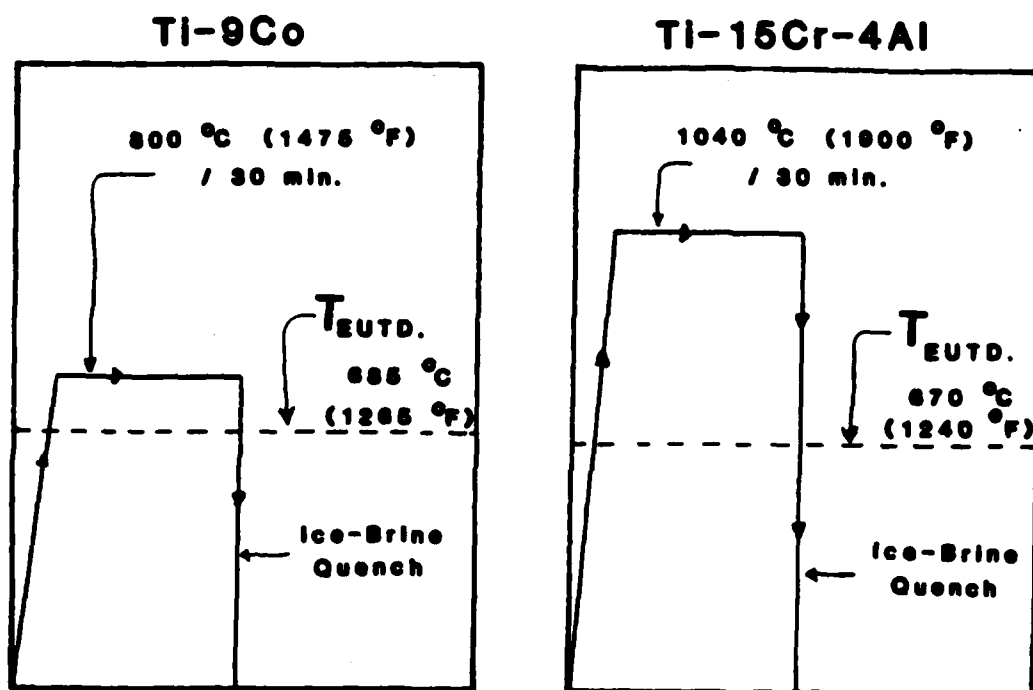


Figure 2

Beta Solution Heat Treatment



**Figure 3**

**SEM Micrograph  
Ti-9Co Bulk Sample**

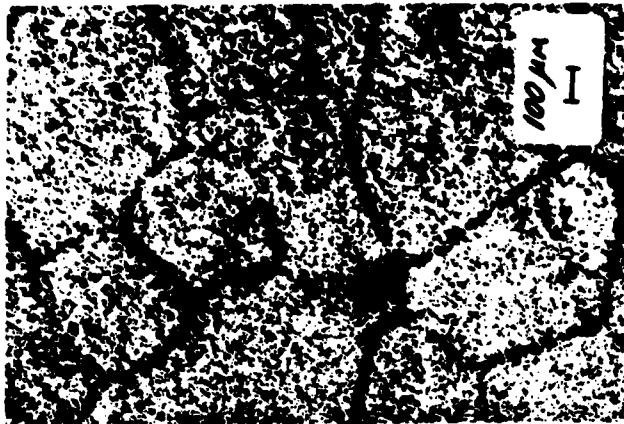
**3 min. Aging at 575 °C**



**Lenticular and basketweave alpha precipitation.**

**No intermetallic compound ( $Ti_2Co$ ) is present.**

**Figure 4**  
**Optical Micrographs of Ti-9Co Bulk Material**



**Solution Treated**

**10 sec. Aging**  
**575 °C**

**4 hour Aging**  
**525 °C**

**Fine alpha precipitates from all beta structure.**  
**Extended aging results in coarsening.**

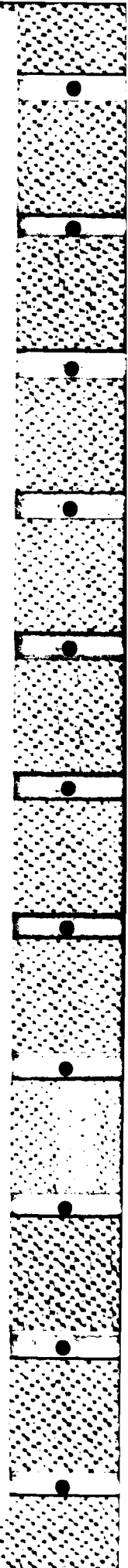
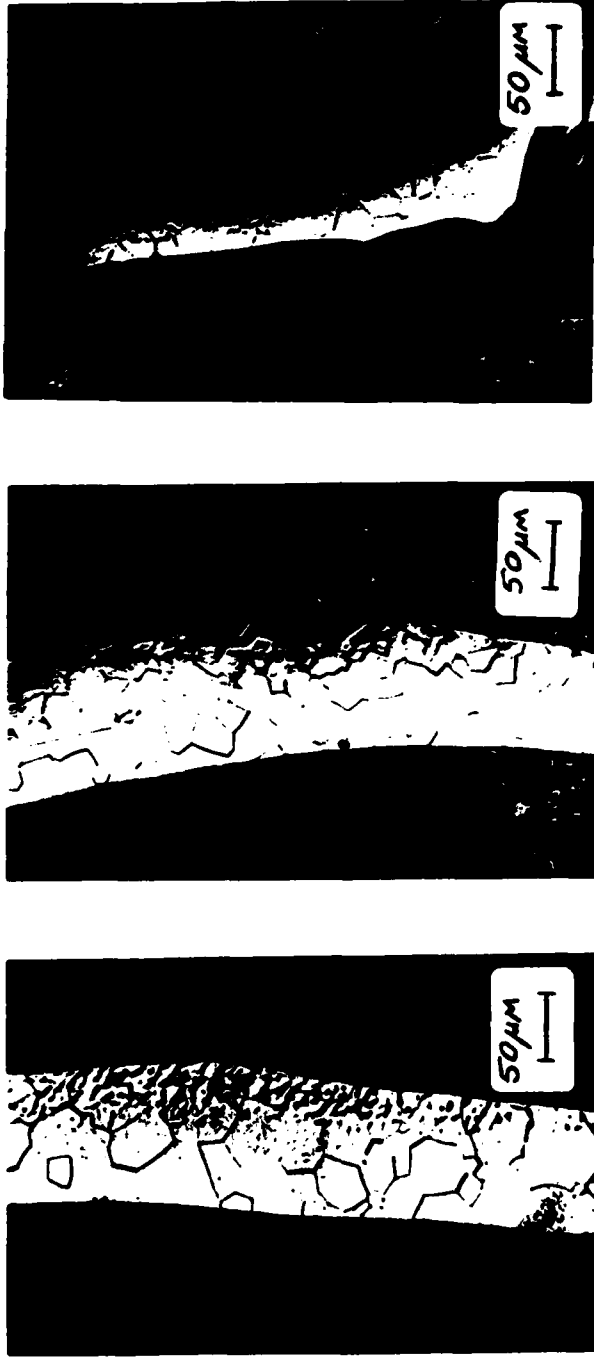


Figure 6

Optical Micrographs of Ti-15Cr-4Al Ribbon Material



As Cast

10 min. Aging  
/ 500 °C

10 Day Aging  
/ 500 °C

Fine alpha precipitates from all beta structure.

Extended aging results in coarsening.

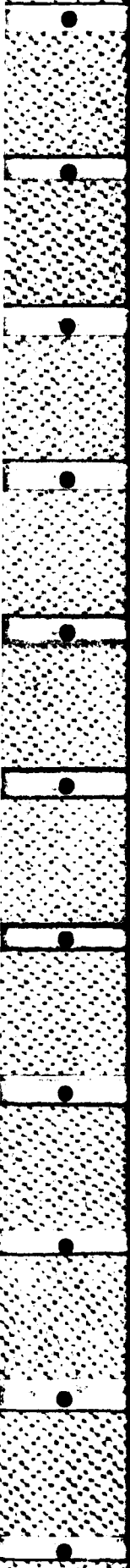


Figure 6  
Age Hardening Response of Ti-9Co

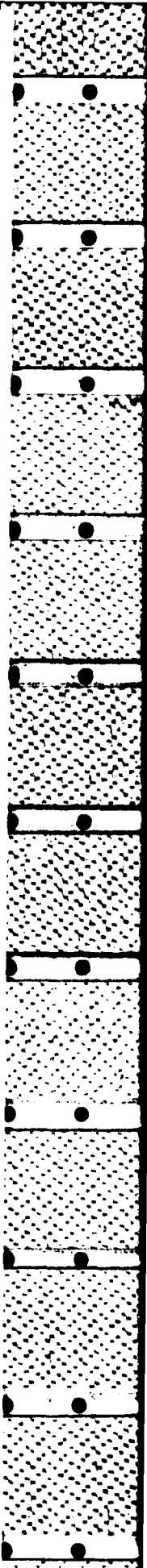
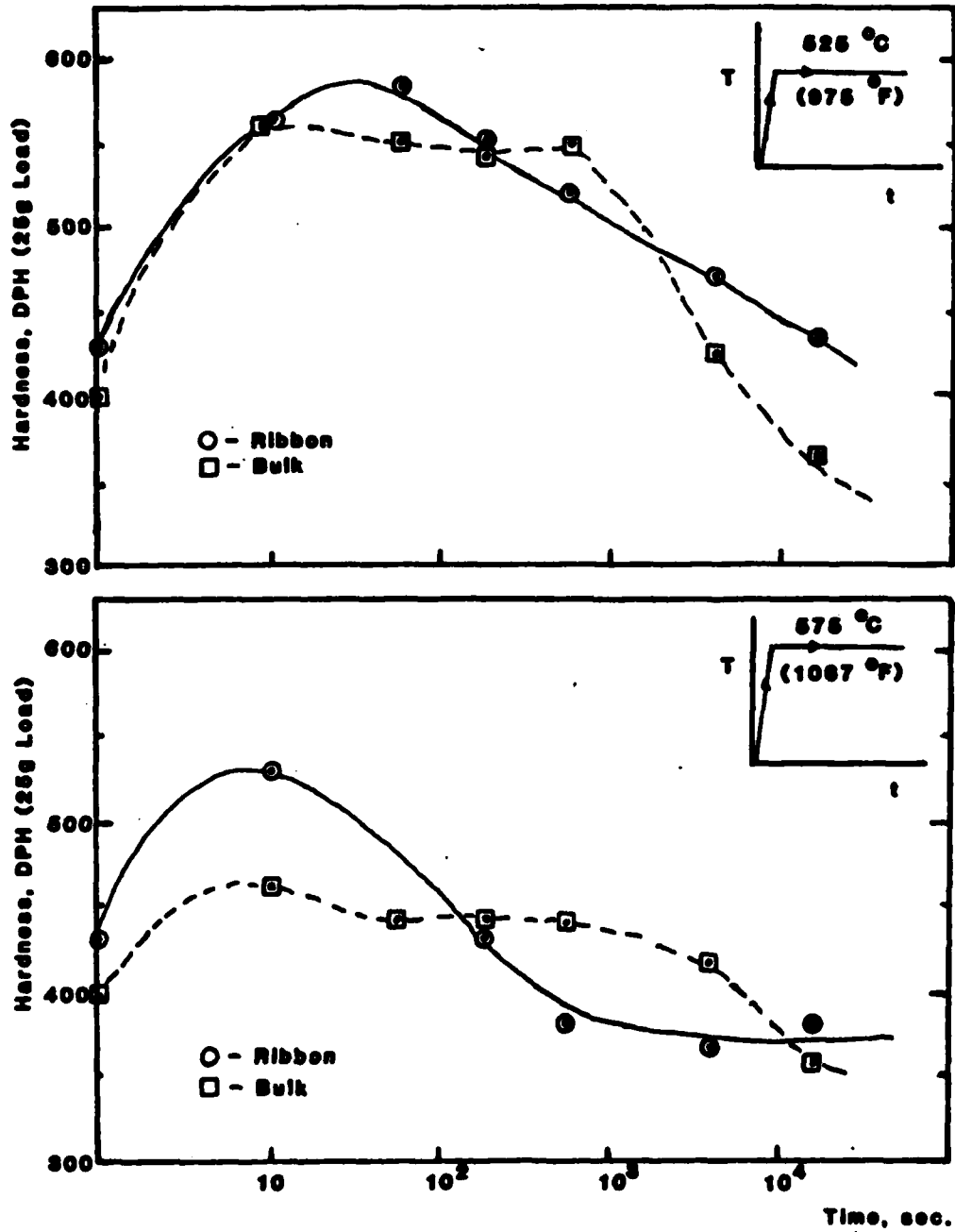
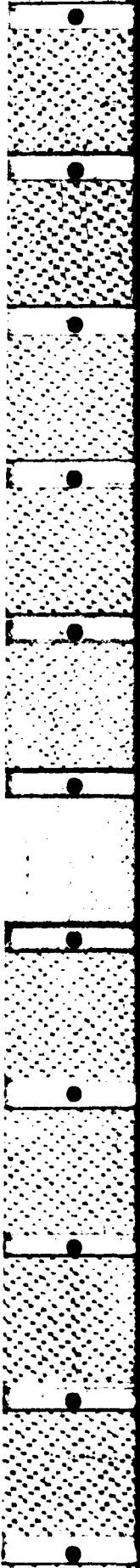
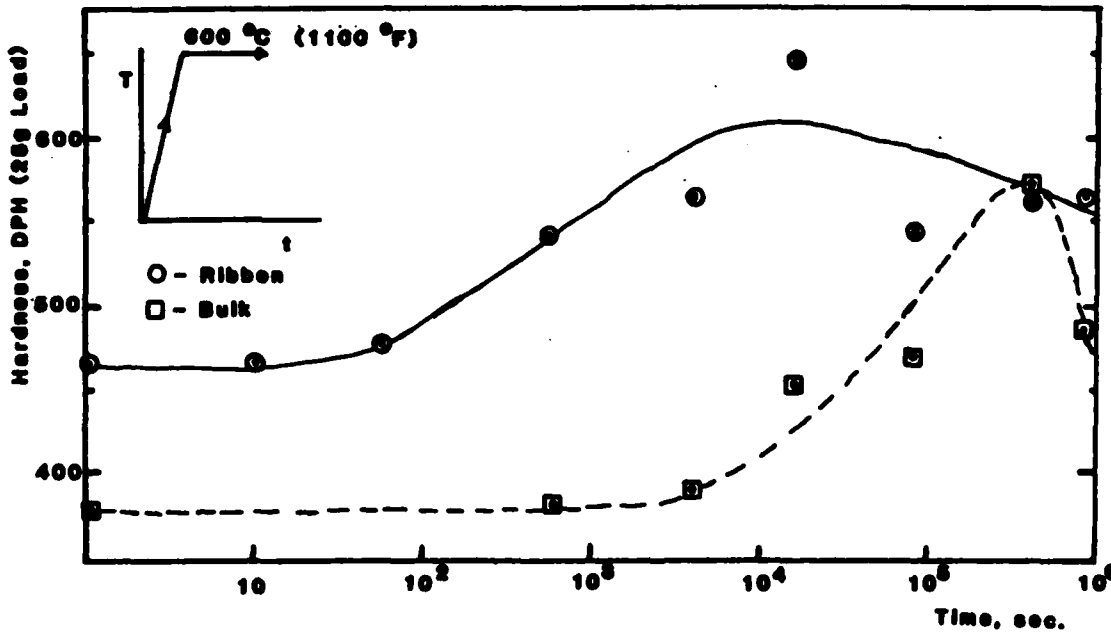
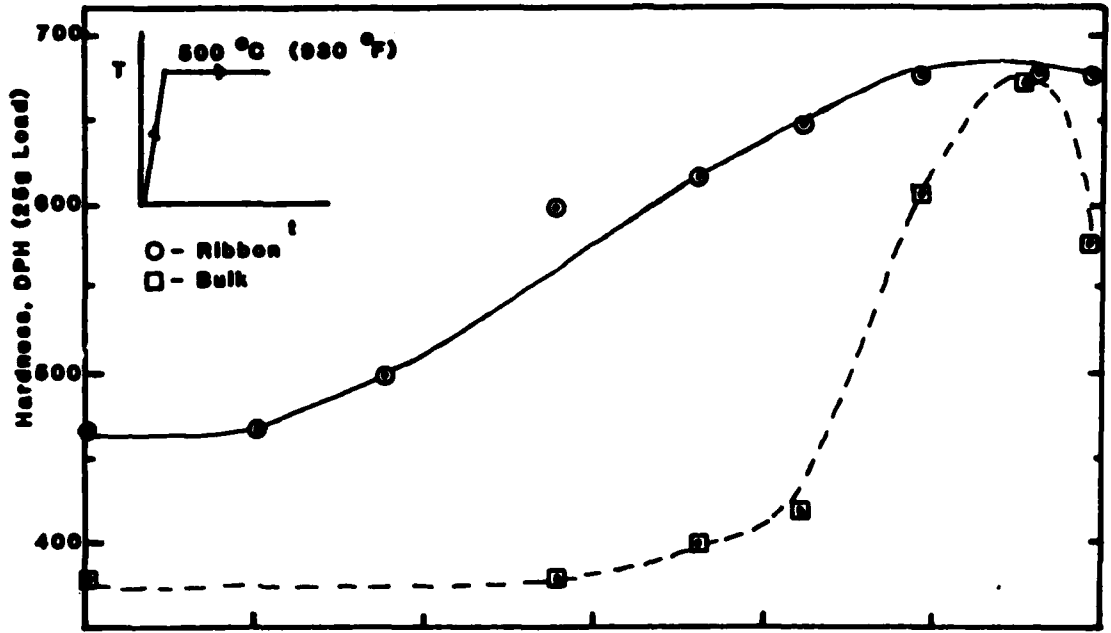


Figure 7

### Age Hardening Response of Ti-15Cr-4Al



1984 USAF-SCEEE GRADUATE STUDENT SUMMER SUPPORT PROGRAM

Sponsored by the

AIR FORCE OFFICE OF SCIENTIFIC RESEARCH

Conducted by the

SOUTHEASTERN CENTER FOR ELECTRICAL ENGINEERING EDUCATION

FINAL REPORT

NEW PHENOXY SUBSTITUTED DIANHYDRIDES

Prepared by:	Donna Brandelik
Academic Rank:	Graduate Teaching Assistant
Department and University:	Department of Chemistry Wright State University
Research Location:	Air Force Wright Aeronautical Laboratories, Materials Laboratory, Polymer Branch
USAF Research Contract:	Dr. Fred Arnold
SFRP Supervising Faculty Member:	Dr. William A. Feld
Date:	August 25, 1984
Contract No:	F49620-82-C-0035

New Phenoxy Substituted Dianhydrides

by

Donna Brandelik

ABSTRACT

Synthesis of 3-phenoxyphthalic dianhydride from durene was initiated and the intermediate compounds were fully characterized. The results showed that these intermediates were very soluble in common solvents. The final product is still under investigation. A model compound, 9-oxo-xanthene-1-carboxylic acid, was synthesized and partially characterized. The final product needs further analysis. Suggestions for future research are outlined to further advance this project.

### Acknowledgement

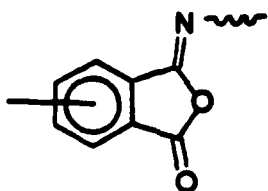
The author would like to thank the Air Force Systems Command, the Air Force Office of Scientific Research and the Southeastern Center for Electrical Engineering Education for providing the opportunity to spend a very interesting and productive summer at the Materials Laboratory, Wright-Patterson AFB, Ohio. The equipment and personnel at the Polymer Branch were especially appreciated.

The cooperation of Dr. Fred Arnold as research contact, the collaboration and guidance of Dr. William A. Feld in suggesting this area of research, and many helpful discussions with Mr. Bruce Reinhardt are gratefully acknowledged.

## I. INTRODUCTION:

Polyimides are known to have excellent thermal and thermo-oxidative stability, and for this reason can be used as part of a composite polymer system that must withstand high temperatures. Some polyimides form a rigid rod polymer chain that can give internal strength to the composite structure. One of the problems encountered with this system is developing a polyimide which is soluble in common solvents, such that it is readily incorporated into the composite matrix.

In general, polyimides tend to be insoluble and intractable. An isomeric form of an imide, commonly known as an isoimide (1) can be used to enhance processibility without compromising the ultimate thermal and thermo-oxidative stability.

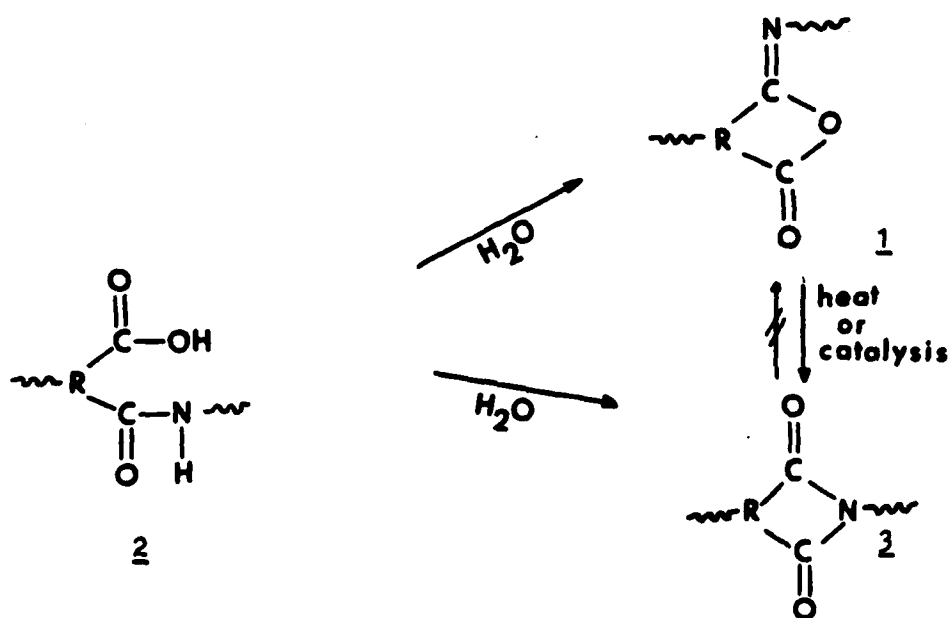


1

The isoimide, when compared to the imide, was generally found to have a much lower melting point and was much more soluble in a variety of solvents. The isoimide can readily be converted irreversibly to the imide form, either thermally or catalytically. The catalysis uses

nucleophilic catalysts such as acetic anhydride, to promote the isoimide-to-imide conversion.

The formation of the cyclic isoimide structure is through the cyclodehydration of the amic acid precursor by selected chemical reagents. Generally chemical dehydration of N-substituted amic acids (2) gives varying ratios of isoimide (1) and imide (3), depending on the reaction conditions deployed, the nature of the amic acid and the chemical reagent used. Thermal cyclodehydration invariably yields the imide structure.



Polyimides with no pendent groups show low solubility in common solvents. The purpose of this research is to investigate the effects of the dianhydride monomer pendent groups on the solubility of the polyimide or a precursor polyisoimide.

## II. OBJECTIVES:

The main objectives of this research were to:

- 1) synthesize 3-phenoxyphthalic dianhydride,
- 2) compare it to 3,6-diphenoxyphthalic dianhydride for solubility in common solvents,
- 3) and synthesize a xanthone model compound to show that byproducts can be formed by internal cyclization.

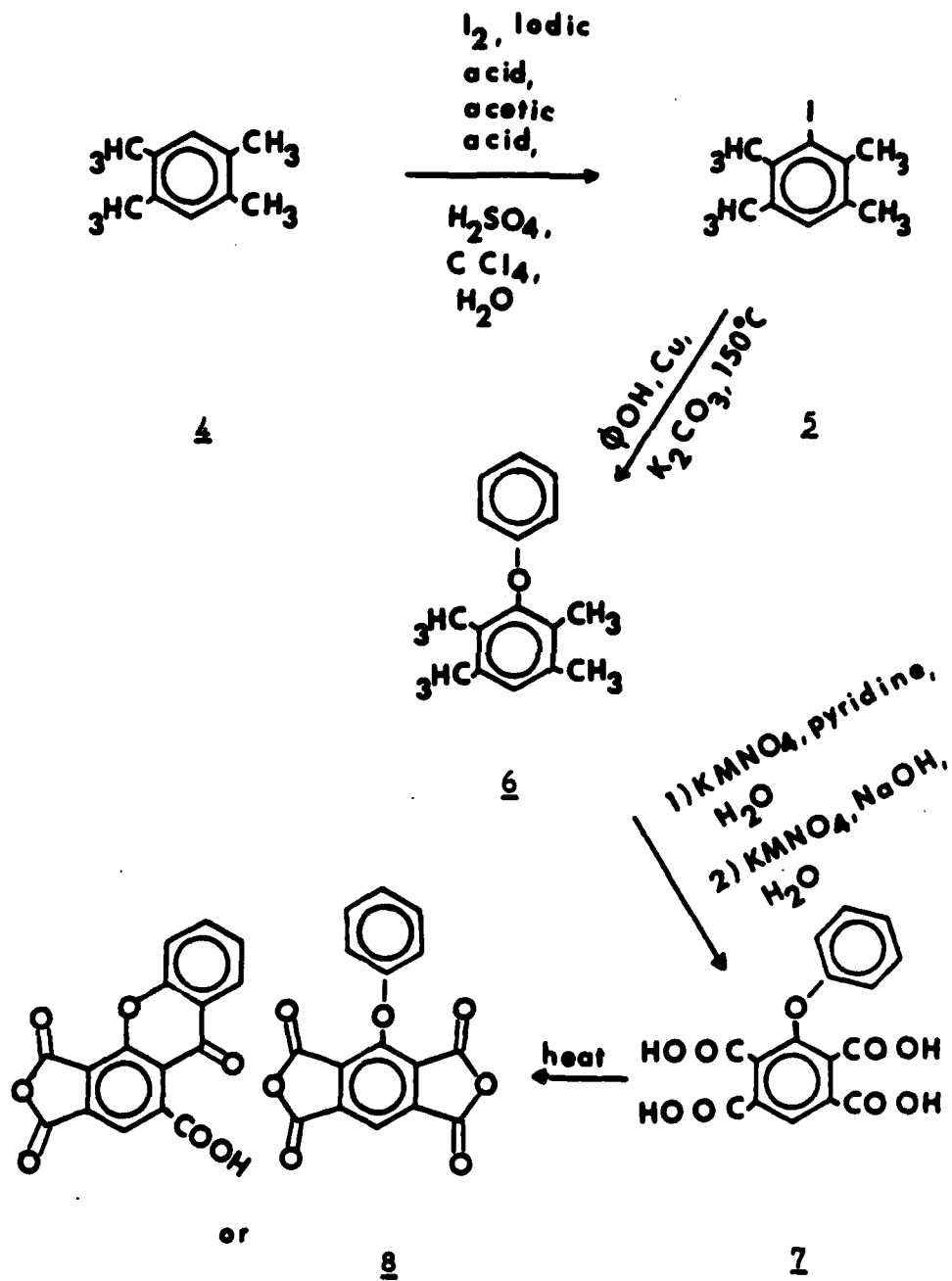
## III. OVERVIEW OF THE SYNTHESIS:

The preparation of a monophenoxydianhydride was begun because the diphenoxydianhydride intermediate compound, diphenoxydurene, was found to have low solubility in ethanol; and due to its decreased symmetry, a monophenoxy compound would likely have an increased solubility. The results indicate that the intermediate monophenoxy compounds do have increased solubility in common solvents.

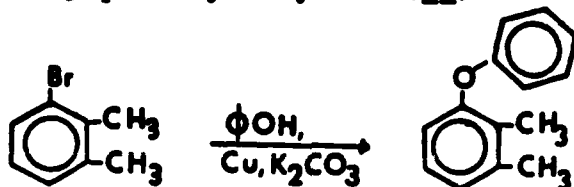
Durene was used in a five step synthesis to produce 3,6-diphenoxyphthalic dianhydride. Steps one through four produced the desired product, but the last step produced several products, as evidenced by a thin layer chromatograph of this material. A model compound, 3-bromo-o-xylene, was then investigated to determine whether a second product was forming through an internal cyclization of a phenolic pendent group and an acid function in the

ortho position. This product is called a xanthone and has a bright yellow irridescent color, making it difficult to ascertain whether a dianhydride was forming in the last step of the synthesis, since the dianhydride was also a bright lemon yellow color, but not irridescent.

Using durene (4) as a parent compound, 3-iododurene (5) was formed. This compound had excellent solubility in ethanol, and produced a white, fluffy, crystalline product, which was used to prepare 3-phenoxydurene (6). The compound 3-phenoxydurene was obtained as a white, electrostatic, crystalline product. Oxidation of this compound produced a tetraacid, 3-phenoxyphromellitic acid (7). Pyrolysis of this compound yielded a compound (8), which was recrystallized from toluene and is currently being identified.



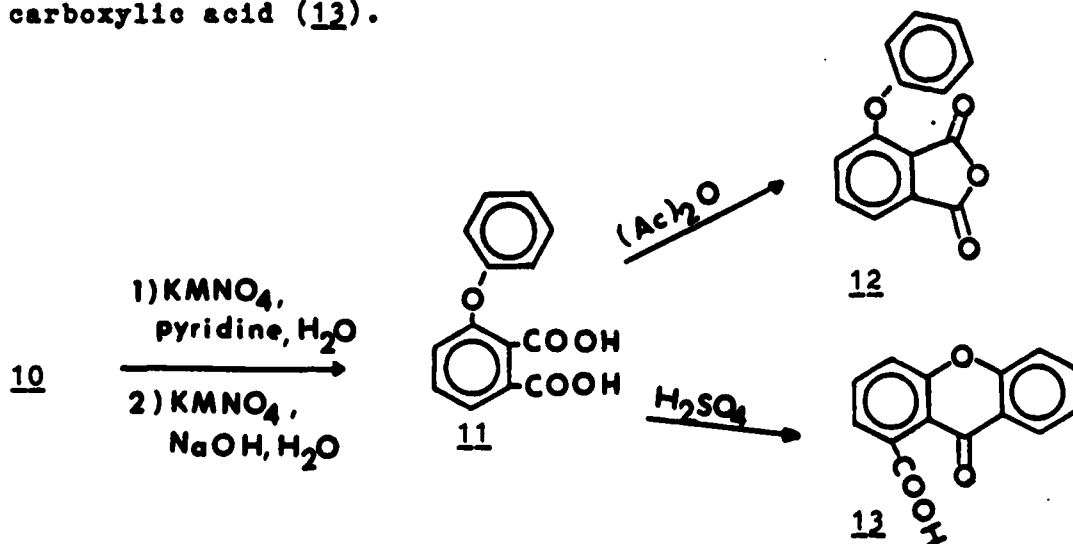
The model compound was prepared by the reaction of 3-bromo-o-xylene (9) with phenol, copper and potassium carbonate to yield 3-phenoxy-o-xylene (10).



9

10

Oxidation of this compound produced 3-phenoxyphthalic acid (11), which forms 3-phenoxyphthalic anhydride (12) when reacted with acetic anhydride. The xanthone product, which was anticipated did not form. This may be due to the lack of steric hindrance like that found in 3,6-diphenoxydurene. The reaction of 3-phenoxyphthalic acid (11) and concentrated sulfuric acid produced a white precipitate, which by infrared analysis appears to be 9-oxo-xanthene-1-carboxylic acid (13).



## V. INSTRUMENTATION:

Nuclear Magnetic Resonance (NMR) spectra were obtained employing a Varian EM-360-A spectrometer, and all samples were run in deuterated chloroform. Tetramethylsilane was used as an internal standard and sample concentrations were approximately 10% w/v. Infrared spectra (IR) were recorded with a Beckman Model 33 spectrometer using KBr discs. Elemental analysis were performed by AFWAL/MLSA on the base complex. All results are listed in the experimental section.

## V. EXPERIMENTAL:

### Preparation of 3-iododurene

In a three-necked flask (500 ml), fitted with an air condenser, were placed durene (50.0 g, 0.373 mol), iodine (38.0g, 0.150 mol), iodic acid (14.5 g, 0.082 mol), acetic acid (120 ml), sulfuric acid (4 ml), water (20 ml), and carbon tetrachloride (10 ml). The purple-brown mixture was heated on an oil bath with stirring at 75°C for twelve hours. The hot solution was then poured into an aqueous (150 ml) sodium bisulfite solution, (10.0 g, 0.096 mol) and stirred to destroy the excess iodine. The yellow precipitate was collected by vacuum filtration and steam distilled at 140 to 150°C. About 500 ml of the distillate was collected and contained the excess unreacted durene.

The remaining solution was allowed to evaporate leaving crude crystals of 3-iododurene which were recrystallized from ethanol yielding pure, white, fluffy needles (90.86 g, 94%): mp = 80-81°C (Lit. mp = 80°C); IR (KBr) 2980-2825, 1595, 1450, 1375, 1000, 860, 770, 690  $\text{cm}^{-1}$ . NMR ( $\text{CDCl}_3$ )  $\delta$  2.2(s,6H), 2.4(s,6H), 6.7(s,1H).

#### Preparation of 3-Phenoxydurene

A three-necked flask (500 ml) fitted with an air condenser was charged with 3-iododurene (20.8 g, 0.080 mol), potassium carbonate (12.0 g, 0.080 mol), phenol (80.0 g, 0.850 mol), and copper bronze (8.0 g). The maroon mixture was heated on an oil bath for twelve hours at 160°C. The hot solution was poured into a sodium hydroxide (34.0 g, 0.850 mol) solution (500 ml) to remove the excess phenol. Vacuum filtration produced a tan powdery product, mixed with copper. Extraction with ethanol produced white crystals which were very electrostatic (10.8 g, 60%): mp = 109-110°C; IR (KBr) 2950-2850, 1590-1575, 1475, 1375  $\text{cm}^{-1}$ . NMR ( $\text{CDCl}_3$ )  $\delta$  1.9(s,6H), 2.2(s,6H), 6.5-7.3(m,5H). Anal. Calcd for  $\text{C}_{16}\text{H}_{18}\text{O}$ : C, 84.91; H, 8.02. Found: C, 84.71; H, 8.02.

#### Preparation of 3-phenoxydurene

In a three-necked flask (1000 ml), fitted with a reflux condenser, were placed 3-phenoxydurene (9.21 g, 0.035 mol),

pyridine (360 ml), and water (150 ml). This mixture was heated to 100°C and potassium permanganate (32.22 g, 0.204 mol) was added slowly. The solution was refluxed at 110-120°C for three and one half hours. Vacuum filtration through celite gave a clear, pale yellow filtrate which was vacuum evaporated. The residue was treated with a sodium hydroxide (12.0 g, 0.300 mol) solution (220 ml). The mixture was heated to 100°C and potassium permanganate (19.3 g, 0.122 mol) was added slowly. After refluxing for one and one half hours, ethanol (15 ml) was added to remove the the excess potassium permanganate. Vacuum filtration through celite yeilded a pale yellow solution which was vacuum evaporated to reduce the volume to about 75 milliliters. The concentrated solution was cooled in an ice bath and stirred while cold concentrated hydrochloric acid (24 ml), was added dropwise to produce a white precipitate. Effervescence was observed as the pH went from 14 to 2. The precipitate was vacuum filtered to yeild 3-phenoxypropionellitic acid (9.78 g, 70%): IR (KBr) 3600-2400, 1725-1675, 1475, 1375, 1300  $\text{cm}^{-1}$ .

#### Preparation of 3-phenoxypropionellitic dianhydride

In a flask (50 ml) was placed 3-phenoxypropionellitic acid (2.0 g, 0.0028mol). The flask was heated under vacuum at 190-210°C whereby the dianhydride sublimed on the flask

walls. After two hours the dianhydride was removed from the flask and recrystallised from toluene yielding yellow needles (1.25 g, 63%): IR (KBr) 3000-2500, 1840-1800, 1700, 1300, 900  $\text{cm}^{-1}$ .

#### Preparation of 3-phenoxy-o-xylene

In a three-necked flask (250 ml) fitted with an air condenser were placed 3-bromo-o-xylene (10.2 ml, 0.075 mol), potassium carbonate (18.0 g, 0.130 mol), phenol (120.0 g, 1.28 mol), and copper bronze (12.0 g). The mixture was heated to 160°C for twelve hours. The hot maroon solution was poured into a sodium hydroxide (51.0 g, 1.28 mol) solution (780 ml) and stirred to wash the copper and remove the excess phenol. The product was extracted with ether which was dried with magnesium sulfate to yield a clear yellow filtrate. Recrystallisation from methanol yielded pale yellow shiny crystals of pure 3-phenoxy-o-xylene (9.26 g, 62%): mp = 56-57°C; IR (KBr) 3000-2900, 1600, 1500-1450  $\text{cm}^{-1}$ ; NMR ( $\text{CDCl}_3$ )  $\delta$  1.9(s,6H), 2.1(s,6H), 6.7(m,5H). Anal. Calcd for  $\text{C}_{14}\text{H}_{14}\text{O}$ : C, 84.81; H, 7.12. Found: C, 84.68; H, 7.12.

#### Preparation of 3-phenoxyphthalic acid

A three-necked flask (250 ml) equipped with an air condenser was charged with 3-phenoxy-o-xylene (4.5 g, 0.0227 mol), pyridine (100 ml), and water (40 ml). When

heated to a temperature of 100°C, potassium permanganate (8.96 g, 0.057 mol) was added slowly to oxidize the compound. The solution was refluxed for three and one half hours at 110-120°C and vacuum filtered through celite to yield a clear yellow solution, which was vacuum evaporated to give a yellow solid. The residue was mixed with a sodium hydroxide (4.0 g, 0.100 mol) solution (73 ml) and potassium permanganate (6.45 g, 0.041 mol) was added slowly. After refluxing for one and one half hours, ethanol (10 ml) was added to destroy the excess potassium permanganate. A nearly clear filtrate was obtained by vacuum filtration through celite. The filtrate was vacuum evaporated to reduce the volume to 100 ml. This solution was cooled in ice and stirred while cold concentrated hydrochloric acid (12.5 ml) was added dropwise to change the acid salt to the acid form. The pH went from 14 to 2, yielding a white precipitate, which when filtered and dried gave 3-phenoxyphthalic acid (2.67 g, 46%): mp = 202-203°C (Lit. mp = 204°C); IR (KBr) 3400-2400, 1700, 1600, 1300  $\text{cm}^{-1}$ .

#### Preparation of 3-phenoxyphthalic anhydride

In a flask (50 ml) fitted with an air condenser were placed 3-phenoxyphthalic acid (0.5 g, 0.0019 mol), and acetic anhydride (25 ml). The mixture was refluxed for one

hour at 120-130°C, and then placed in an evaporating dish. Recrystallisation from hexane yielded white crystals of 3-phenoxyphthalic anhydride (0.34 g, 73%): mp = 106-107°C (Lit.mp = 106-108°C); IR (KBr) 1850, 1790, 1625-1580, 1475, 1275  $\text{cm}^{-1}$ .

#### Preparation of 9-oxo-xanthene-1-carboxylic acid<sup>3</sup>

A flask (50 ml) was charged with 3-phenoxyphthalic acid (0.5 g, 0.0019 mol), and concentrated sulfuric acid (20 ml) and heated on an oil bath to 90°C for two hours. The yellow solution was poured into water (60 ml), forming a white precipitate. Vacuum drying yielded a powdery product (0.29 g, 31%): IR (KBr) 3000, 1700, 1625, 1600, 1300, 1075  $\text{cm}^{-1}$ .

#### VI. RECOMMENDATIONS:

Intermediates of 3-phenoxyphthalic dianhydride were found to have increased solubility in common solvents. The recommendations for further research include:

- 1) further characterization of the "monophenoxydianhydride",
- 2) investigation of the effect of longer pendent groups,
- 3) and polymerization of existing dianhydrides to test for increased solubility.

## REFERENCES

1. H. O. Winth, F. U. Herrmann, and W. Kern, Makromol. Chem., 1964, 80, 120.
2. D. H. R. Barton, J. C. Blazejewski, B. Charkiot and W. B. Motherwell, J. Chem. Soc. Chem. Comm., 1981, 503.
3. A. A. Goldberg, A. H. Wragg, J. Chem. Soc., 1958, 4227.
4. F. J. Williams, H. M. Relles, P. E. Donahue, and J. S. Manello, J. Org. Chem., 1977, 42, 3425.
5. AFWAL-TR-83-4079 Technical report.

**1984 USAF GRADUATE STUDENT SUMMER SUPPORT PROGRAM**

**Sponsored by the**

**AIR FORCE OFFICE OF SCIENTIFIC RESEARCH**

**Conducted by the**

**SOUTHEASTERN CENTER FOR ELECTRICAL ENGINEERING EDUCATION**

**FINAL REPORT**

**STOCHASTIC BEHAVIOR OF RANDOM LAY CABLES**

**Prepared by: Frederick C. Breslin**

**Academic Department: Mathematics and Statistics**

**University: University of New Mexico**

**Research Location: Air Force Weapons Laboratory, NTATT,**

**Kirtland Air Force Base, Albuquerque, NM 87117**

**USAF Research Contact: Dr. Carl E. Baum**

**SFRP Supervising**

**Faculty Member: Professor Alexander P. Stone**

**Date: July 27, 1984**

**Contract No: F49620-82-C-0035**

# STOCHASTIC BEHAVIOR OF RANDOM LAY CABLES

By

Frederick C. Breslin

## ABSTRACT

The analysis of EMP effects depends on parameters which in effect may be random variables. One such example is the physical orientation of a cable within a structure. Further there are situations where a parameter may be deterministic, e.g., terminal impedance, but to investigate system behavior over a broad range of possible terminations one is forced to treat terminal impedance as a random variable. In this report we develop a model for a random lay cable with random termination and derive the stochastic properties of the associated electromagnetic matrices of interest.

## ACKNOWLEDGEMENT

The author thanks the Air Force Systems Command, the Air Force Office of Scientific Research and the Southeastern Center for Electrical Engineering Education for providing the support that made this effort possible.

Particular thanks are due to Dr. Carl E. Baum, Air Force Weapons Laboratory, for suggesting the problem, and to him and to Professor Alexander P. Stone, University of New Mexico for many helpful contributions.

## 1. INTRODUCTION

Given a particular visualization of a cable and its terminations such parameters of interest as the scattering matrix can be calculated and the system's response to EMP determined for that particular visualization. However, there are other visualizations that might be encountered. For example, one may find pin #2 in the uppermost position of a connector rather than pin #1 as was assumed. Will the EMP response of this second visualization differ significantly from that of the first? This question can in principle be answered by a recalculation of all parameters for this second visualization. But the number of possible visualizations that need to be calculated can get rapidly out of hand even for relatively simple systems. This direct calculation approach fails even more rapidly when one extends his area of inquiry beyond a specific cable to a generic type of cable, e.g., aircraft communications cables in general.

The approach we will take in this effort is to treat the parameters of the cable and its terminations as random variables. We will develop a stochastic model for a random lay cable. Based on this model, the question: "Will the EMP response of this second visualization differ significantly from that of the first?" will be answered probabilistically.

## 2. OBJECTIVES OF THE RESEARCH EFFORT

The first goal of this effort is to develop a stochastic model that describes a random lay cable. Clearly there are as many random lay cable models as there are possible definitions for what constitutes a random lay. In this study we adopt the approach that the parameters of the cable elements are fixed and that it is their spatial orientation and terminal impedances that are random.

Having defined our model, our next goal is to develop the stochastic properties of the model. Finally, we derive the distribution theory for scattered current in a random lay cable.

### 3. PERMUTATION MATRICES

In constructing our model of the random lay cable we will make extensive use of the concept of a permutation matrix. It is therefore appropriate at this point to review the properties of such matrices.

#### A. ALGEBRAIC PROPERTIES

**Property 1:**

Let  $\Pi_{ij}$  be an identity matrix with its  $i$ th and  $j$ th rows interchanged. Then  $\Pi_{ij}M$  is the matrix  $M$  with its  $i$ th and  $j$ th rows interchanged.

**Property 2:**

$M\Pi_{ij}$  is the matrix  $M$  with its  $i$ th and  $j$ th columns interchanged.

**Property 3:**

$\Pi_{ij}M\Pi_{ij}$  is the matrix  $M$  with its  $i$ th and  $j$ th rows and columns interchanged.

**Property 4:**

The  $\Pi_{ij}$ 's are symmetric, orthogonal matrices.

**Property 5:**

Define a permutation matrix  $P$ :

$$P = \Pi_{ij} \cdot \Pi_M \cdot \dots \cdot \Pi_{yz} .$$

Then  $P$  is an orthogonal matrix.

**Property 6:**

$P' MP$  is the matrix  $M$  with a sequence of row and column interchanges.

**Property 7:**

$P$  is of the form that each column (row) contains one 1. The rest of the elements in the column (row) are 0.

**Property 8:**

$P$  is of full rank.

**Property 9:**

$$[P' MP]^{-1} = P' M^{-1} P$$

**Property 10:**

$$(P' MP)(P' NP) = P' MNP$$

**Property 11:**

The effect of  $P' MP$  is to relocate diagonal elements of  $M$  onto the diagonal of  $P' MP$  and to relocate off diagonal elements of  $M$  onto off diagonal elements of  $P' MP$ .

**B. STOCHASTIC PROPERTIES**

**Stochastic Property 1:**

The expected value of the permutation matrix  $P$  is

$$E[P] = \frac{1}{N} J,$$

where  $J$  is an  $N \times N$  matrix all of whose elements are 1.

### Stochastic Property 2:

The expected value of the matrix  $P' MP$  is

$$E[P' MP] = \begin{cases} \bar{m}_d & \text{on diagonal} \\ \bar{m}_o & \text{off diagonal} \end{cases}$$

where  $\bar{m}_d$  is the average of the diagonal element of  $M$  and  $\bar{m}_o$  is the average of the off diagonal elements of  $M$ .

### Stochastic Property 3

The expected value of the matrix  $(P' MP)^2 = P' M^2 P$  is

$$E[(P' MP)^2] = \begin{cases} \frac{1}{N} \sum_{i^h} m_{i^h} m_{i^h} & \text{on diagonal} \\ \frac{1}{N^2 - N} \sum_{ijk} m_{k_i} m_{k_j} & \text{off diagonal} \end{cases}$$

### Stochastic Property 4

The variance of  $P' MP$  is

$$\text{Var}[P' MP] = \begin{cases} \frac{1}{N} \sum_{i^h} m_{i^h}^2 - (\bar{m}_d)^2 & \text{on diagonal} \\ \frac{1}{N^2 - N} \sum_{ijk} m_{k_i} m_{k_j} - (\bar{m}_o)^2 & \text{off diagonal} \end{cases}$$

## 4. THE RANDOM LAY CABLE MODEL

Consider a cable consisting of  $N$  parallel conductors and an infinite ground plane. The  $i$ th conductor is characterized by

$r_{wi} \equiv$  the radius of the wire

$t_i \equiv$  the thickness of the insulation

$d_{ij} \equiv$  the distance from the center of the  $i$ th wire to the center of the  $j$ th wire

$h_i \equiv$  the distance of the center of the  $i$ th wire above the ground plane.

Paul and Feather [1] show that the per unit length capacitance matrix is of the form

$$c_{ij} = k_1(ij)r_{wi} + k_2(ij)(r_{wi} + t_i) \quad (1)$$

where  $k_1(ij)$  and  $k_2(ij)$  are constants which are functions of the Displacement matrix. They show further that when the wires are separated sufficiently from each other and the ground plane, an approximate per unit length inductance matrix is of the form

$$l_{ii} = k_3 \ln \left( \frac{2h_i}{r_{wi}} \right) \quad (2)$$

$$l_{ij} = k_3 \ln \left( \frac{\sqrt{d_{ij}^2 + 4h_i h_j}}{d_{ij}} \right) \quad (3)$$

Let  $L$  and  $C$  be respectively the per unit length inductance and capacitance matrices associated with some reference cable orientation. Then from (1), (2), (3) and Property 3 it follows that  ${}_k L$  and  ${}_k C$ , for the  $k$ th permutation  $({}_k P)$ , can be written as

$${}_k C = ({}_k P') (C) ({}_k P) \quad (4)$$

$${}_k L = ({}_k P') (L) ({}_k P)$$

Having modeled the capacitance and inductance matrix associated with an arbitrary cable lay in terms of a permutation matrix, we now apply our knowledge of the properties of such matrices to derive the stochastic properties of the random lay cable.

**A. EXPECTED VALUE OF INDUCTANCE, CAPACITANCE AND IMPEDANCE MATRICES FOR A RANDOM LAY CABLE:**

From (4), the  $k$ th permutation of the cable will result in capacitance and inductance matrices of the form

$$({}_k C) = ({}_k P') (C) ({}_k P)$$

$$({}_k L) = ({}_k P') (L) ({}_k P)$$

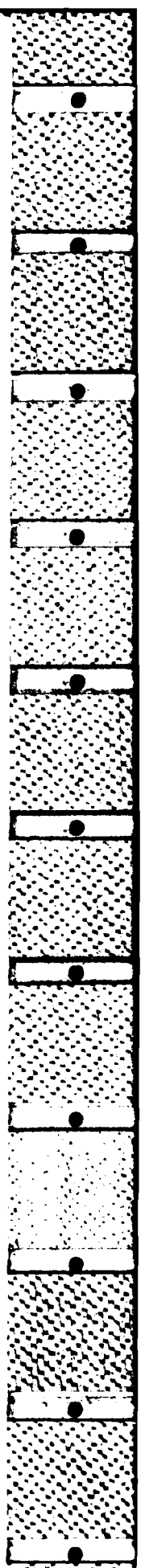
Since every permutation is considered equally likely, the expected value of the  $L$  and  $C$  matrices of a random lay cable comes directly from Stochastic Property 2.

$$E[C] = \begin{aligned} & \frac{1}{N} \sum c_{ii} && \text{on diagonal} \\ & \frac{1}{N^2-N} \sum c_{ij} && \text{off diagonal} \end{aligned}$$

$$E[L] = \begin{aligned} & \frac{1}{N} \sum l_{ii} && \text{on diagonal} \\ & \frac{1}{N^2-N} \sum l_{ij} && \text{off diagonal} \end{aligned}$$

where  $N$  is the number of conductors in the cable and  $c_{ij}$  and  $l_{ij}$  are the elements of the capacitance and inductance matrix for the arbitrarily selected reference orientation of the cable.

The expected value of the characteristic impedance and admittance matrices follow in a similar manner. Defining the characteristic impedance matrix  $Z_c$  as [2]



$$Z_c = C^{-1}T[\lambda]^{1/2}T^{-1}$$

where

$$[\lambda] = T^{-1}CLT$$

then the characteristic impedance matrix for the  $k$ th permutation is

$${}_kZ_c = {}_kC^{-1}T[\lambda_k]^{1/2}T^{-1}$$

By Properties 3 and 10

$$[\lambda_k] = T^{-1}(P' CLP)T$$

Since  $CL = T^{-1}[\lambda]T$

$$[\lambda_k] = T^{-1}P' T^{-1}[\lambda]TPT$$

$${}_kZ_c = [P' CP]^{-1}T \cdot T^{-1}P' T^{-1}[\lambda^{1/2}]TPTT^{-1}$$

By Property 9

$${}_kZ_c = P' C^{-1}PP' T^{-1}[\lambda^{1/2}]TP$$

$${}_kZ_c = P' C^{-1}T^{-1}[\lambda^{1/2}]TP$$

$${}_kZ_c = P' Z_c P$$

Further

$${}_kY_c = {}_kZ_c^{-1} = [P' Z_c P]^{-1}$$

$${}_kY_c = P' Z_c^{-1}P$$

$${}_kY_c = P' Y_c P$$

By Stochastic Property 2 the expected value of the impedance matrix is

$$E[Z] = \begin{cases} \frac{1}{N} \sum z_{ii} & \text{on diagonal} \\ \frac{1}{N^2-N} \sum z_{ij} & \text{off diagonal} \end{cases}$$

and the expected value of the admittance matrix is

$$E[Y] = \begin{cases} \frac{1}{N} \sum y_{ii} & \text{on diagonal} \\ \frac{1}{N^2-N} \sum y_{ij} & \text{off diagonal} \end{cases}$$

## B. THE EXPECTED VALUE OF THE SCATTERING MATRIX

Let the terminal admittance of the random lay cable be  $Y_T$ . Assume that the elements of  $Y_T$  are fixed. Then [3]

$$\begin{aligned} {}_k S &= [I - ({}_k Z)({}_k Y_T)][I + ({}_k Z)({}_k Y_T)]^{-1} \\ {}_k S &= [P' (I - Z_{ref} Y_{T_{ref}})P][P' (I + Z_{ref} Y_{T_{ref}})P]^{-1} \\ {}_k S &= [P' (I - Z_{ref} Y_{T_{ref}})P]P' (I + Z_{ref} Y_{T_{ref}})^{-1}P \end{aligned}$$

Since  $P' P = I$  (Property 5)

$$\begin{aligned} {}_k S &= P' (I - Z_{ref} Y_{T_{ref}})(I + Z_{ref} Y_{T_{ref}})^{-1}P \\ {}_k S &= P' S P \end{aligned}$$

Using Stochastic Property 2, the expected value of the scattering matrix is

$$E[S] = \begin{aligned} & \frac{1}{N} \sum s_{ii} = \bar{s}_{ii} && \text{on diagonal} \\ & \frac{1}{N^2-N} \sum s_{ij} = \bar{s}_{ij} && \text{off diagonal} \end{aligned}$$

### C. VARIABILITY OF EM MATRICES:

So far we have looked at the expected value of some matrices of interest under our random lay cable model. We have found that they all have essentially the same form of expected value. While the values of the elements of the matrix will tend to have the expected value, any one visualization of a random cable is likely to produce different results. The question to be addressed now is the extent to which the elements of an EM matrix are likely to vary from their expected value.

Worst case variability is of interest. Clearly the maximum possible variation in any of the electromagnetic matrices considered is simply the difference between the largest and smallest on (off) diagonal elements of the reference matrix for diagonal (off diagonal) terms. In addition we will find a measure of the average expected variation of matrix elements.

A common measure of variability is the Coefficient of Variation defined as

$$\nu = \frac{\text{standard deviation of } y}{\text{expected value of } y} \quad (5)$$

Clearly  $\nu = 0$  implies no variability what so ever. Hence the expected value of  $y$  is a perfect description of  $y$ . While on the other hand,  $\nu = \infty$  implies that the random variable  $y$  is so variable that its expected value is of little use in describing the variable. In our treatment we will use a form equivalent to (5)

$$\nu = \left[ \frac{E\{Y^2\}}{(E\{Y\})^2} - 1 \right]^{1/2} \quad (6)$$

The electromagnetic matrices of interest have all been representable in the form  ${}_k M = P' M P$  and their expected values have had the form

$$E\{M\} = \begin{bmatrix} a & b & \cdots & b \\ b & a & & \\ \vdots & & & \\ b & & & a \end{bmatrix}$$

We will find the same true for variation. Therefore, we will develop the variation only for the scattering matrix since these results are immediately transferable to any other matrix of interest.

From Stochastic Property 3 we have the expected value of the  $ij$ th element of the matrix  $S^2 = S' S$  as

$$E\{S^2\} = \begin{aligned} & \frac{1}{N} \sum_i \sum_k s_{ki}^2 \quad \text{diag.} \\ & \frac{1}{N^2 - N} \sum_i \sum_{\substack{k \\ i \neq j}} \sum_j s_{ki}, \quad \text{off diag.} \end{aligned}$$

Then by (4) and (5) the coefficient of variation for on diagonal elements is

$$\nu = \left[ \frac{\frac{1}{N} \sum_k s_{ki}^2}{\left(\frac{1}{N} \sum_i s_{ii}\right)^2} - 1 \right]^{1/2}$$

For the off diagonal elements the coefficient of variation is from (5) and (6)

$$\nu = \left[ \frac{\frac{1}{N^2 - N} \sum_{i, n} s_{ki} s_{nj}}{\left( \frac{1}{N} \sum_i s_{ii} \right)^2} - 1 \right]^{1/2} \quad (7)$$

### 5. PROPERTIES OF A RANDOM LAY CABLE WITH STOCHASTIC RESISTIVE TERMINATION

Consider a random lay cable of  $N$  conductors with a ground plane. Assume that its characteristic impedance is of the form

$$Z_c = \begin{bmatrix} c & b & \cdots & b \\ b & a & & \\ \vdots & & & \vdots \\ b & & & a \end{bmatrix}. \quad (8)$$

Let the  $i$ th conductor be terminated with a resistance  $r_i$  which is an independent random variable taking on values zero to infinity with a probability density  $f(r_i)$ . Then

$$Z_T = \begin{bmatrix} r_1 & & & \\ & r_2 & & \\ & & & \\ & & & r_N \end{bmatrix}. \quad (9)$$

Consider the Scattering Matrix in the form [3]

$$S = [Z_T - Z_c] \cdot [Z_T + Z_c]^{-1}$$

An invigorating exercise in matrix algebra using (8) and (9) yields for the  $i$ th row and  $j$ th column of the scattering matrix  $S$

$$\frac{-kb(r_i - a)}{(r_i + a - b)(r_i + a - b)} - \frac{(r_j + a - b - bk)b}{(r_j + a - b)^2} + W(i, j) \quad i \neq j$$

$$\frac{(r_i + a - b - bk)(r_i - a)}{(r_i + a - b)^2} + W(i, j) \quad i = j \quad (10)$$

where

$$k = 1 - b \sum_i \frac{1}{(r_i + a - b)}$$

$$W(i, j) = \sum_{l \neq i, j} \frac{kb^2}{(r_i + a - b)(r_l + a - b)}$$

#### Example Calculation

Let  $I$  be the current vector at the termination. Then from [4]

$$I = \frac{1}{2} Y_c [V_+ - V_-]$$

Taking

$$V_+ = \left( 2 \frac{I_0}{N} \right) S \cdot Z_c \cdot \mathbf{1}$$

$$V_- = \left( 2 \frac{I_0}{N} \right) Z_c \cdot \mathbf{1}$$

where  $\mathbf{1}$  is a column of 1's. It follows that

$$I = \left( \frac{I_0}{N} \right) \left[ \mathbf{1} - Z_c^{-1} \cdot S \cdot Z_c \cdot \mathbf{1} \right]$$

We wish to find the probability that

$$1 - Z_c^{-1} \cdot S \cdot Z_c \cdot 1 > N. \quad (11)$$

For the  $N = 2$  case, take  $Z_c$  as in (7) and from (10)

$$\mathfrak{S} = \begin{bmatrix} \frac{(r_1-a)(r_2+a) + b^2}{(r_1+a)(r_2+a) - b^2} & \frac{-2b(r_1-a)}{(r_1+a)(r_2+a) - b^2} \\ \frac{-2b(r_2-a)}{(r_1+a)(r_2+a) - b^2} & \frac{(r_2-a)(r_1+a) + b^2}{(r_1+a)(r_2+a) - b^2} \end{bmatrix} \quad (12)$$

Simplifying notation

$$\mathfrak{S} = \begin{bmatrix} s_{11} & s_{12} \\ s_{21} & s_{22} \end{bmatrix}$$

Then condition (11) is equivalent to

$$-(a-b) > a(s_{11}+s_{12}) - b(s_{21}+s_{22}) \quad (13)$$

where it has been assumed that  $a - b > 0$ . If not, reverse the inequality.

Assume that  $s_{11} + s_{12}$  and  $s_{21} + s_{22}$  are independent random variables distributed uniform  $[-1,1]$ . Then, with  $u = a(s_{11}+s_{12}) - b(s_{21}+s_{22})$ ,

$$f(u) = \begin{cases} \frac{1}{4ab}(a+b-u) & a-b \leq u \leq a+b \\ \frac{1}{2a} & -a+b \leq u \leq a-b \\ \frac{1}{4ab}(a+b+u) & -a-b \leq u \leq -a+b \end{cases}$$

Integrating

$$P_r(u < t) = \frac{a+b}{4ab} + \frac{1}{4ab}(t-a-b)$$

Setting  $t = -(a-b)$  we get

$$P_r(u < -(a-b)) = \frac{-a+b}{4ab}$$

note that our assumption that  $a - b > 0$  implies that if  $a > 0$  ( $a < 0$ ) then  $b < 0$  ( $b > 0$ ) must hold for (13) to occur.

## 6. RECOMMENDATIONS

I believe that there are two areas for further research and at least one immediate application for these results.

1. Intuitively it appears that the random lay cable results will be applicable far beyond the simplistic assumptions of the model. Indeed any equally probable random perturbations which can be expressed as  $ij$  interactions should produce Stochastic Property 2. This assertion needs proof.
2. The treatment of random resistive termination can be extended to random impedance in a straightforward manner. However, in general, the resulting probability integrals will require numerical techniques for solution. This is fine for a specific calculation but hinders development of the distribution theory.

In approaching the general distribution theory one can perhaps identify assumptions about the distributions of the  $Z_T$  and  $Z_C$  matrices that lead to tractable probability integrals. The preferred approach, however, is to identify probability distributions for  $Z_T$  and  $Z_C$  that in some sense agree with the real world and then do battle with  $\mathcal{S}$ . This will almost certainly

produce an intractable result. But, since the result must be a probability distribution function it can almost certainly be approximated with a tractable expression. Such a result would not only further development of the general distribution theory but knowledge of the behavior of the functions is likely to yield physical insight into the random lay cable problem.

Finally, even in this rudimentary form the random lay cable model has an immediate practical application to EMP experiments. The model can at least give an indication whether in a particular experiment "random lay" will be an important factor that might alter results.

## REFERENCES

1. C.R. Paul and A.E. Feather, "Computation of the transmission line inductance and capacitance matrix from the generalized capacitance matrix", *IEEE Transactions Volume EMC-18, No. 4*, November 1976, pp. 175-183.
2. F.M. Tesche and T.K. Liu, "Selected topics in transmission-line theory for EMP internal interaction problems", *AWFL TR-77-73*, Air Force Weapons Laboratory, Kirtland Air Force Base, Albuquerque, NM 87117, August 1977, pp. 68-69.
3. C.E. Baum, "Bounds on norms of scattering matrices", *Interaction Note 432*, Air Force Weapons Laboratory, Kirtland Air Force Base, Albuquerque, NM 87117, June 1983, pg. 10.
4. C.E. Baum, T.K. Liu and F.M. Tesche, "On the analysis of general multiconductor transmission-line networks" *Interaction Note 350*, Air Force Weapons Laboratory, Kirtland Air Force Base, Albuquerque, NM 87117, November 1978, pg. 58.

1984 USAF-SCEEE GRADUATE STUDENT SUMMER SUPPORT PROGRAM

Sponsored by the

AIR FORCE OFFICE OF SCIENTIFIC RESEARCH

Conducted by the

SOUTHEASTERN CENTER FOR ELECTRICAL ENGINEERING EDUCATION

FINAL REPORT

THE USAF ORGANIZATIONAL ASSESSMENT PACKAGE:

FOUR CRITICAL DECISIONS

Prepared by: Jan Leeman Brooks

Academic Department: Department of Management & Marketing

University: The University of Alabama

Research Location: Directorate of Research and Analysis,  
Leadership and Management Development Center,  
Maxwell AFB, Montgomery, AL

USAF Research Contact: Capt. James K. Lowe, Ph.D.

Date: September 21, 1984

Contract No.: F49620-82-C-0035

THE USAF ORGANIZATIONAL ASSESSMENT PACKAGE:

FOUR CRITICAL DECISIONS

by

Jan Leeman Brooks

ABSTRACT

Choices at four major decision points faced by researchers using factor analysis were compared first through a review of their theoretical bases and second through application of methods to a set of data. The purpose of the study was to determine what choices would be most suitable for use with the proposed revision to the Organizational Assessment Package used by the Leadership and Management Development Center. The decision points include: extraction technique, rotation criterion, number of factors rule, and the procedure for estimating scores, including the technique for weighting, and the technique for computing composites. Only the first comparison, the theoretical bases, is reported here; a more comprehensive version of this report will appear as one section of a technical report to be published by the Leadership and Management Development Center. That report will include the second comparison, the application of methods to a set of data. Recommendations regarding each of the four decisions are made.

### ACKNOWLEDGEMENT

The author expresses appreciation and gratitude to the Air Force Systems Command, the Air Force Office of Scientific Research and the Southeastern Center for Electrical Engineering for a summer of hard, rewarding work at the Leadership and Management Development Center at Maxwell AFB.

She owes the greatest measure of thanks to the personnel of the Directorate of Management Strategies and Education and the Directorate of Research and Analysis and is particularly indebted to Sgt. John Kopek, CMSgt. Judy Vermilya, Capt. Michael Cox, Lt. Karl Ibsen, Maj. Mickey Dansby, Lt. Col. Jerry Snow, and Lt. Col. Lloyd Woodman for helpful, stimulating, often humorous discussions.

The author was incredibly fortunate in having the collaboration of Lt. Richard Brown, who patiently explained abstruse statistical issues, and of Capt. James K. Lowe, who persistently offered curiosity, focus, and encouragement.

## I. INTRODUCTION

Factor analysis allows social scientists to bring many interesting constructs down to the empirical arena by measuring them in an adequate way, or -- better -- in a way that may be adequate if the [process] is fed with accurately chosen and measured data, and the [technical] phases are steered by a combination of semantic competence, experience with empirical research, familiarity with the substantive domain, solid [theoretical] foundations, and a good deal of common sense . . . (Marradi, 1981, p. 12).

The major decisions faced by researchers using factor analysis, "a set of multivariate statistical techniques" (Cooper, 1983, p. 141), appear to be four. If one chooses to view them as sequential then they may occur in an order something like this:

1. the technique for extraction;
2. the criterion for rotation;
3. the rule for number of factors to retain; and,
4. the procedure for estimating scores, including,
  - a. the technique for weighting, and
  - b. the technique for computing composites.

Although presented here as separately defined and progressive, the decisions are not so clearly delineated during the actual research process. As work on the Organizational Assessment Package (OAP)

approached its tenth year, those four decisions were examined in the light of the latest research on factor analysis to determine their suitability for a proposed revision to the OAP. At the same time, considerable effort was made to identify any changes in the "substantive domain" or "theoretical foundations" of the research program. For instance, in the early days stress was not included as a formal variable or factor of interest; yet in later years, as the organizational theory knowledge base expanded, stress became relevant in organizational assessment. Considerable thought also was given to isolating transitions in objectives that may have transpired over the duration of the program. Early in the research, for example, "valid" and "reliable" individual factors were of primary importance. As responsible parties grew more experienced, both in measurement and instrumentation and in consultation, theoretical relationships among the factors emerged as important. This type transition naturally leads to reconsideration of data analysis methods, more specifically, to reconsideration of the four decisions listed above.

The first decision facing users of factor analysis is what type extraction technique to use. During the developmental work done on the OAP, principal components analyses was the chosen method for extracting factors. That original decision apparently was based primarily on that method's utility in discovering interpretable factors (Guilford & Lacey, 1947) and secondarily on its utility in extracting replicable factors (Hightower, 1982; Hightower & Short, 1982; Short

& Hamilton, 1981). Guilford (1981, p. 411) states that "replications are essential for credibility and for scientific respectability."

The other three decisions related to factor analytical techniques for the OAP included the use of orthogonal rotation-varimax technique; the Kaiser-Guttman "K1" (Guttman, 1954; Kaiser, 1960; Kaiser & Caffrey, 1965) and Cattell (1966) scree rules for number of factors to retain; and a "factor-based" (Alwin, 1973) procedure for weighting scores for truncated composites.

## II. OBJECTIVES

Each of these four decisions was re-considered in the study reported here; an effort was made to obtain at least one comparison of techniques for each decision. In some cases, the choice of alternatives was made difficult by their sheer numbers. The plenitude of options for each decision required that their examination here be somewhat cursory. However, although options may not be discussed here in sufficient detail for the reader's own purposes, references are cited so that the curious may pursue their specific interests.

Table 1 is a simplified chart of the four factor analysis decisions of interest here.

TABLE 1. Four Critical Decisions in Factor Analysis

<u>DECISION</u>	<u>OAP</u>	<u>COMPARISON</u>
1) Extraction	PCA	FA
2) Rotation	Orthogonal	Oblique
3) Number	K1 Scree	Residuals Strength
4) Estimation	Truncated Composite	Truncated Composite
Weighting	All-or- None	All-or- None
Computing	Means	Sum

In column two are the choices made by the early OAP researchers. In column three are the techniques chosen for comparison by current researchers. Section III of this paper discusses the theoretical differences among available choices for each of the four decisions. Section IV presents recommendations based upon implications from theory. (NOTE: The abbreviated literature review in Section III forms the basis of the SCEEE report; more comprehensive versions of Sections III and IV are included in a technical report to be published by LMDC.)

### III. IMPLICATIONS FROM THEORY

#### A. First Decision: Technique for Extraction of Factors.

Two of the more popular factor analysis techniques are principal components analysis (PCA) and common factor analysis (FA). The researcher who chooses to use either PCA or FA most likely has one of two purposes in mind (Everett & Entekin, 1980). Basically, either the goal is to reduce a large number of variables to a smaller number, that is, to furnish a linear composite as a summary measure; or the goal is to identify patterns of intercorrelations, that is, to analyze the underlying structure of observed variables. Tabachnick and Fidell (1983) expand these two major goals into four, and Rummel (1967) into a description of ten overlapping uses of factor analysis.

Principal components analysis produces components (Hotelling, 1933); factor analysis produces factors (Spearman, 1904, 1927; Thurstone, 1935, 1947). For ease of usage the term factor will be used here to refer to both except where distinction is necessary. The term "factor"

has long been used by the OAP researchers for convenience even though accuracy would demand the use of the term "component" (Lowe et al., 1984) given their choice of extraction techniques. The primary differences between the two procedures are the goal of the analysis and the variance that is analyzed.

The goal of PCA is to extract maximum variance from the data set with each component. PCA is the solution of choice for the researcher who is primarily interested in reducing a large number of variables down to a smaller number. PCA is also recommended as the first step toward a more detailed factor analysis (FA) (Tabachnick & Fidell, 1983).

Principal factors extraction (FA) differs from PCA in that its goal is to identify underlying dimensions not easily recognized or observed. Mathematically, the difference involves the contents of the principal diagonal in the correlation matrix. In PCA the correlation matrix which is factored has unities in the diagonal, and in FA there are communality estimates in the principal diagonal (Rummel, 1970; Hair et al., 1979).

Comparison of these models suggests that factor analysis, with its concern for hypothetical underlying observed behavior, will please those concerned with behavioral theory, while components analysis may be regarded as a data analysis and reduction technique (Farr, 1971). This differentiation in applications was of interest to the OAP researchers as they sought to recognize transitions in objectives that have occurred over the years of the program.

Specifically, if one considers goals as ends, and objectives as means to those ends, then one can see that means may change frequently while the ends (goals) remain the same, that is, organizational assessment and development remain the goals while the means to achieve the goal are modified by advances in statistical theory as well as organizational theory. (For a thorough description of such changing objectives, see "The Establishment and Growth of the Leadership and Management Development Center, 1975-1980").

B. Second Decision: Criterion for Rotation of Factors.

After extraction, rotation is used to improve the interpretability and scientific utility of the solution. Immediately the researcher encounters a problem because there are such a large number of rotation criteria available, all accounting for the same amount of variance in the original data (Tabachnick & Fidell, 1983). Each represents factors defined slightly differently; and since each is mathematically equivalent to the others, each can be advanced as "best."

A fundamental decision is required between orthogonal and oblique rotation techniques. In orthogonal rotation, the factors are uncorrelated with one another. Results involving uncorrelated patterns are easier to communicate, and the loadings can be interpreted as correlations (Rummel, 1967). Thus, when the original OAP researchers chose orthogonal rotation, they chose ease of description and interpretation. Also, since they intended using factor score estimates (actually "factor-based" estimates), for comparing factor structure among groups, orthogonal rotation proved advantageous.

The specific orthogonal rotation technique chosen by the early researchers was varimax rotation. The goal of varimax rotation is to make the factors as simple as possible by maximizing the variance of the loadings across variables within factors, that is, to maximize the variance of the square of the loading in each column of the factor matrix (Cooper, 1983). More simply, varimax rotation maximizes the variance of the factor loadings for each factor by making high loadings higher and low ones lower.

However, for all its conceptual simplicity, orthogonal rotation is not an advantage if it distorts the true relationships among factors by imposing independence on correlated dimensions. In most factor analytic situations, it seems more likely that factors are correlated than that they are not, since clusters of variables in the "real world" are more likely than not related to one another (Rummel, 1967). As the current OAP researchers and consultants delved into the subject matter, theories of organizational behavior, they began to recognize the interrelatedness of the factors with which they work and to scrutinize the decisions of their predecessors. In other words, they began to speculate that, besides yielding more information, oblique rotation appears justified on theoretical grounds; the underlying structures producing the results -- the factors -- do not operate independently of one another in reality (Tabachnick & Fidell, 1983). In theoretical terms, that would be like proposing that perception of job stress is not correlated with perception of availability of organizational support (i.e., materials, tools,

etcetra, necessary to do the job).

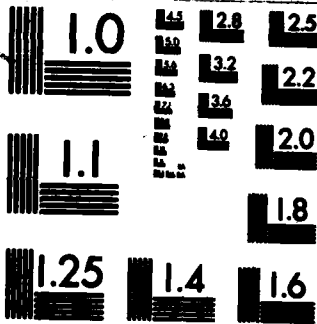
The specific oblique rotation technique chosen for comparison with varimax was direct quartimin. Actually, both direct quartimin and direct oblimin were used, but for reasons discussed elsewhere, direct oblimin was discontinued early in the analysis. The goal of both oblique techniques developed by Jennrich and Sampson (1966) is to simplify loadings. Other oblique rotation schemes proceed by optimizing a simplicity function applied to the reference structure; they are plagued with the problem of rotating to singularity. The algorithm derived by Jennrich and Sampson avoids this problem.

Oblique rotation, then, seems more desirable because it is theoretically and empirically more realistic (Hair et al., 1979). Recognizing correlations between factors means that the search for meaning can be carried to the second order using factor analysis or other analysis of covariance techniques. The general hypothesis given by Joreskog (1970) for the analysis of covariance structures corresponds to a second-order factor model (McDonald, 1979). The factor correlations themselves may be factor-analyzed to determine the more general, the more abstract, the comprehensive relationships and the more pervasive influences underlying phenomena (Rummel, 1967).

C. Third Decision: Rule for Determining the Number of Factors to Retain.

Determining the number of components or factors to retain is usually the third major decision to be made; it is complicated when





MICROCOPY RESOLUTION TEST CHART  
 NATIONAL BUREAU OF STANDARDS-1963-A

some method of rotation has been performed. The number of factors problem has no general solution even though it is more important than selection of extraction and rotation techniques (Tabachnick & Fidell, 1983). "The" appropriate rule apparently is still waiting to be discovered. According to Horn and Engstrom (1979) fifty years of research have offered 50 rules, none of which is considered "the" solution to the number of factors problem.

In examining the decision about the number of factors to retain four of Rummel's "rules of thumb" were chosen for consideration. Two, the "K1" and Cattell's scree are used by the OAP researchers; two additional rules were chosen for comparison in this study.

In their 1982 article, Zwick and Velicer give a brief but excellent description of several rules, including two of interest here. The following discussion relies heavily upon their introduction and upon that of Rummel (1970). The appropriate rule for PCA is considered by some (Lee & Comrey, 1979) to be Kaiser-Guttman rule but by others to be Bartlett's chi-square (Zwick & Velicer, 1982). The Kaiser-Guttman procedure is to extract all factors with eigenvalues of 1.0 or greater.

Cattell's scree test as originally proposed (Cattell, 1966) is to plot the number of factors against the proportion of variance each extracts and then, beginning at the low end of the plot, work upwards looking for flatness (Hakstian, Rogers & Cattell, 1982). After fitting a straight line through the break, retain those eigenvalues above the line. The scree test resulted from the

practical observation that the factor variance levels off when the factors are largely measuring random error. The strengths of this technique are its apparent simplicity and reported validity, the ease of plotting eigenvalues for visual inspection, and its effectiveness when strong components are present.

Examining the matrix of residual correlations is another practical criterion for solving the number of factors problem. If all the residuals are less than an arbitrary number (say, .10) then the reproduced correlation matrix is very similar to the original correlation matrix and extraction is adequate (Tabachnick & Fidell, 1983). Practical experience will suggest a cutoff for those residuals not high enough to be considered meaningful (Rummel, 1970).

The fourth criterion, strength of relations, depends on the size of the factor loadings. In the case of orthogonal factors, the factor loading squared is the proportion of variance of a variable explained by the factor. Factors may be excluded as "trivial" if their highest loadings account for no more than 5 or 10 per cent of the variance of any one variable" (Rummel, 1970, p. 362).

D. Fourth Decision: Procedures for Estimating Scores and Creating Composites.

When principal components analysis (PCA) is the multivariate technique chosen, "true" scores are computed. When factor analysis is chosen, scores are "estimated." The preceding statements are insidiously simple. One must not accept them at face value. The issue of factor scores is complicated by various approaches and familiarity with them is necessary in order to avoid making mistakes.

The term "exact scores" or "true scores" often is understood and used, if not erroneously, at least somewhat carelessly. A true score is associated with principal components analysis, and is a linear combination of the variables. For an exact and unique solution to be possible, the number of factors must equal the number of variables (Rummel, 1970). If the researcher decides to extract only factors with eigenvalues greater than one, subjective and arbitrary judgment enters the scene, and a "true score" thus receives its first modification, its first shift away from "truth."

Complicating the issue is the fact that exact solutions exist for these shifts, these truncated composites, and can be derived (Rummel, 1970; Kaiser, 1962). These "shifts" are then easily taken for and presented as original "truth." (For a comprehensive discussion of the subjective nature of factor analysis, see Marradi, 1979).

Factor scores or factor score estimates thus must involve consideration of the related issues of weighting and of truncated composite computation. The last two decades have seen considerable attention devoted to the problems of estimating composite scores for unmeasured variables with multiple indicators. According to Saris et al. (1978) factor analytic models have received the bulk of the attention. There appear to be three primary approaches to scores: exact, regression estimates, and composite estimates (Rummel, 1970).

Subtypes of the composite estimate approach are of interest here.

The estimation technique that the OAP researchers utilize for scores is "factor-based" all-or-none weighting for truncated composites. To explain, the first modification of the "true" score is made when the number of components, or factors, is determined. The second shift, moving further from "true" scores, occurs when the weighting decision is made; in the instance of all-or-none weighting (Cattell, 1978), the process which actually occurs is item selection for the composite, or truncation of the "true" score.

Weighting. Items with high loadings in the factor pattern matrix are weighted as 1's and items with low loadings are weighted as 0's; the item is either in or out, all-or-none. The definition of "high" is arbitrary; most frequently .30 is the standard (Hunter, 1980; Harris, 1967). Marradi (1981) argues that "a sharp drop in the loadings' magnitude is a better cutting point than any predetermined numerical threshold. Semantic differences between the discarded and the retained indicators should also be evaluated." With the OAP, the definition of high is .40, with the corollary that the item is not to be loaded above .30 by any other factor.

Alwin (1973) investigated five of Horn's (1965) procedures for estimation, for differentially weighting variables, comparing them to what he called the "factor-based" estimation procedure. He concludes: "While the methods of factor score estimation are perhaps quite sophisticated from a mathematical point of view, there may be little defense for them in practice . . . even under the best of circumstances, there may be little gained by way of predictive and

theoretical power by the use of [differential weighting] methods. Susmilch and Johnson (1976) extended the study of scores for composites and concluded that differential weighting can in some instances be superior to "factor-based" scoring but that whether the techniques generally make a difference is as yet undetermined.

Computation of the composite. Calculation of the factor score estimate can be accomplished by summing the scores on the items which were selected through weighting or by calculating the mean of the composite (Cattell, 1957; Guilford, , Ghiselli et al., 1981). The OAP researchers use the mean; their truncated composite is calculated by summing the means of the items which make up the factor.

In this study the composite was compared to a simple sum of the items included in the truncated composite. The weighting procedure was the same, all-or-none. Not only is summing the simplest procedure for obtaining a factor score estimate, but evidence indicates it is the only one necessary (Ghiselli et al., 1981). Comrey (1973) states his preference for "using variables that are total scores summed over several homogeneous items that have been shown to be measuring the same variables. These total scores have many more possible data points than [those] associated with a single item. Such scores are more continuous, tend to be more normally distributed, and are almost always more reliable than individual item scores."

#### IV. RECOMMENDATIONS

##### A. Specific

###### First Decision: Technique for Extraction of Factors.

Based on findings in the literature reviewed here, and assuming that the Organizational Assessment Package (OAP) will continue to be revised and updated to reflect expanding knowledge of organizational behavior, principal factor analysis (FA) appears to be the appropriate technique for extracting factors. Two corollary recommendations are: (1) that "test" or "embryo" factors be determined first through principal components analysis and then through principal factor analysis. To add two new factors, stress and influence tactic, to the assessment package, one could generate 10-12 items that appear to cover their domains, use PCA to identify those items which best reflect the constructs (in an idealized world) and then use PFA to observe how the factors act in the "real world" with their correlated cousins; and, (2) that "test" factors be added to a model of organizational effectiveness after testing of the factor has been completed, after the embryo has become an adult. (See recommendations under "General").

Second Decision: Technique for Rotation of Factors. The appropriate technique for data reduction appears to be orthogonal and for determining underlying structure or relationships it appears to be oblique. Two corollary recommendations, based on the same assumption in the previous section, are: (1) that "test" factors be identified, tested, and refined by using orthogonal rotation-

varimax technique; and, (2) that "adult" factors, added to the model, be determined using oblique rotation-direct quartimin technique.

Third Decision: Rule for Number of Factors to Retain. In determining the number of factors to retain, the researchers can easily use each of the methods described here; they are available in computer packages and are an efficient way of double-checking results. Since this issue is more critical than extraction or rotation, using several techniques greatly strengthens confidence in the findings.

Fourth Decision: Procedures for Estimating Scores and Creating Composites. According to most recent knowledge and practice in the field, the all-or-none weighting of truncated composites, currently in use by OAP researchers, seems to be the most widely accepted technique for weighting, especially in the behavioral sciences. Its continued use is recommended along with a change in the computation of the composites. The OAP researchers use the sum of the means of the items to estimate factor scores. A simpler procedure is to use a simple sum of the scores on the items.

#### B. General

In addition to recommendations made about each of the decisions studied here, several other relevant issues emerged during the course of the study. First, during the ten-year period of OAP research, the theoretical model on which the measurement is based has been revised many, many times. From a leadership effectiveness model, it became an organizational effectiveness model, then an open systems

model; informally, it has been seen as a communication process model, a motivation model, and a group dynamics model.

The confusion seems to have arisen partly from the fact that uncorrelated factors (principal components) while unrelated in the statistical world, are related in the real world. There is a direct correlation between job autonomy and job satisfaction, whether negative or positive. In explaining results to supervisors, one has a tendency to use correlated items, items one knows are related, items the supervisor knows are related, instead of these theoretical "uncorrelated factors." Principal factor analysis (FA) would help to alleviate this problematic tendency of offering single items as valid and reliable information when in fact they contain a high proportion of measurement error.

A second issue related to the use of single items as feedback material is the combining of several items, each developed to measure one and only one construct, into a new and separate construct. This questionable practice might be avoided if the measurement instrument were flexible enough for developing new factors, for instance, stress, influence tactics, delegation, among others. The model, as well as the measurement instrument, should allow for revisions, additions, substitutions.

As one might imagine, a model of organizational effectiveness which includes thirteen factors already and provides for additions and revisions, could get fairly complicated fairly quickly. Therefore, use of an additional statistical technique is recommended for testing hypotheses about relationships among factors and for testing the fit of submodels.

LISREL (linear structural relationships) is a general statistical model which allows for testing, first, whether the factors are in fact captured by the items used and, second, whether those factors account for organizational effectiveness. If the theoretical model (or submodel) in use does not contribute to an understanding of organizational structure, processes, or behavior, then it is of little value to the ultimate "users," the supervisors.

#### REFERENCES

Due to limitations of space, the references are not listed here; however, copies of the reference list as well as each of the articles cited are available from Capt. J. Lowe, LMDC/AN, Maxwell AFB, Montgomery, AL 36 .

**1984 USAF-SCEEE GRADUATE STUDENT SUMMER SUPPORT PROGRAM**

**Sponsored by the  
AIR FORCE OFFICE OF SCIENTIFIC RESEARCH**

**Conducted by the  
SOUTHEASTERN CENTER FOR ELECTRICAL ENGINEERING EDUCATION**

**FINAL REPORT**

**THE UNIQUENESS OF PHASE RETRIEVAL FROM INTENSITY MEASUREMENTS**

<b>Prepared by:</b>	<b>Howard W. Brown</b>
<b>Academic Rank:</b>	<b>Graduate Researcher</b>
<b>Department and University:</b>	<b>Department of Civil Engineering The Ohio State University</b>
<b>Research Location:</b>	<b>Materials Laboratory Wright-Patterson AFB, Ohio 45433</b>
<b>USAF Research:</b>	<b>Dr. James M. Whitney</b>
<b>Date:</b>	<b>September 24, 1984</b>
<b>Contract No.:</b>	<b>F49620-82-C-0035</b>

THE CALCULATION OF MODE II ENERGY RELEASE RATE  
IN THE DELAMINATION OF COMPOSITE MATERIALS

by

Howard W. Brown

ABSTRACT

An approximate method for the evaluation of mode II energy release rate in the delamination of composite materials is investigated. The model is a cantilever beam consisting of a unidirectional composite material with a midplane starter crack at the free edge. A modified method of a theory developed by Whitney and Sun is used to evaluate the displacement field and the distribution of interlaminar stresses caused by the loading at the free edge. The results of this modified theory indicate pure mode II delamination of the cantilever. Suggestions for future research in this area are offered.

### Acknowledgement

I would like to thank the Air Force Systems Command, the Air Force Office of Scientific Research and the Southeastern Center for Electrical Engineering Education for providing me with the opportunity to work with and learn from the people of the Air Force Materials Laboratory, Wright-Patterson AFB, Ohio.

I would like to thank Dr. James M. Whitney for suggesting the area of research and his assistance in the execution of that research, and I would like to thank Drs. Ranbir S. Sandhu and Robert Sierakowski of The Ohio State University for making me aware of this opportunity and for their recommendations which enabled me to obtain this appointment.

## I. INTRODUCTION:

The unseen delamination of composite materials is a major problem. When an interlaminar crack occurs it may grow in size by three different modes which are dependent upon the stress fields surrounding the crack tip. If delamination becomes extensive the strength of the composite material becomes impaired and the structure is subject to catastrophic failure.

The first mode of fracture, mode I, is an opening mode caused by in plane , normal, interlaminar stress. The second mode of fracture, mode II, is a slipping mode caused by in plane, shear, interlaminar stress. And, the third mode of fracture, mode III, is a tearing mode caused by out of plane, shear, interlaminar stress. These modes of fracture can be predicted by determining the energy release rates for mode I, mode II and mode III fractures. It is thought that the energy release rate is a material property of linear elastic materials. Thus knowing the energy release rate is important in the designing of structures made of composite materials.

Methods for calculating the mode I energy release rate,  $G_I$ , have been examined. Whitney, Browning & Hoogsteden [1], used a double cantilever beam to calculate  $G_I$  and O'Brien [2] used a free delamination specimen which has been modified by Whitney and Knight [3]. Methods to calculate the

mode II energy release rate,  $G_{II}$ , are now being explored. The short beam test has been shown to fail with the breakdown of beam theory due to the shortness and large width to depth ratio of a short beam. The method explored in this work is a cantilever beam with a starter crack.

## II. OBJECTIVES OF THE RESEARCH EFFORT

The subject that is being researched is the energy release rate for delaminating composites materials. I am attempting to derive a method for analytically determining the mode II energy release rates of delaminating composites.

## III. STATEMENT OF PROBLEM

The cantilever beam is unidirectional,  $[0^0]_s$ , with a starter crack at the midplane of the free edge. An unattached spacer is inserted in the crack at the free edge so as to allow equal distribution of load on each cantilever formed by the crack and to remove stresses along the free surfaces of the crack surface.

The energy release rate is defined as follows:

$$G = \frac{\partial U^*}{\partial a} \quad (1)$$

where  $G = G_I = G_{II} + G_{III}$ .

$$U^* = P\Delta/2,$$

$P$  is the loading and is constant,

$\Delta$  is the displacement, and

a is the crack length.

To calculate the deflection as a function of crack length the higher order laminated plate theory set forth by Whitney and Sun[4] and modified by Pagano[5] is used. The beam is divided into four sections as shown in figure 1.

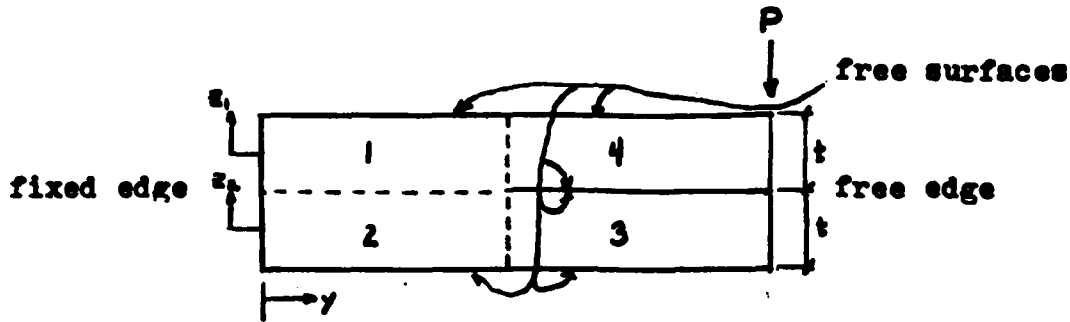


figure 1. Model for plate theory

The constitutive equations for a unidirectional composite is written as follows:

$$\begin{bmatrix} \sigma_x \\ \sigma_y \\ \sigma_z \\ \tau_{yz} \\ \tau_{xz} \\ \tau_{xy} \end{bmatrix} = \begin{bmatrix} C_{11} & C_{12} & C_{13} \\ C_{12} & C_{22} & C_{23} \\ C_{13} & C_{23} & C_{33} \\ & & & C_{44} \\ & & & & C_{55} \\ & & & & & C_{66} \end{bmatrix} \begin{bmatrix} \epsilon_x \\ \epsilon_y \\ \epsilon_z \\ \gamma_{yz} \\ \gamma_{xz} \\ \gamma_{xy} \end{bmatrix} \quad (2)$$

where  $C_{ij}$  are components of the stiffness matrix,  
 $\sigma_x$  are normal stresses,  
 $\tau_{xy}$  are shear stresses,  
 $\epsilon_x$  are normal strains and  
 $\gamma_{xy}$  are shear strains.

The displacements are assumed to be of the forms

$$\begin{aligned} u &= U + z \psi \\ v &= V + z \Omega \\ w &= W + z \phi \end{aligned} \quad (3)$$

The displacement equations as set forth in [4] are written as follows

$$\begin{bmatrix} L_{11} & 0 & 0 \\ 0 & L_{22} & L_{26} \\ 0 & L_{26} & L_{66} \end{bmatrix} \begin{bmatrix} U \\ V \\ \phi \end{bmatrix} = \begin{bmatrix} -q_x \\ -q_y \\ m \end{bmatrix} \quad (4)$$

$$\begin{bmatrix} L_{33} & 0 & L_{35} \\ 0 & L_{44} & 0 \\ L_{35} & 0 & L_{55} \end{bmatrix} \begin{bmatrix} W \\ \psi \\ \Omega \end{bmatrix} = \begin{bmatrix} q \\ m_x \\ m_y \end{bmatrix} \quad (5)$$

where  $L_{11} = tC_{66} ( )_{,yy}$ ,

$L_{22} = tC_{22} ( )_{,yy}$ ,

$L_{26} = k_1 tC_{23} ( )_{,y}$ ,

$L_{33} = -k^2 tC_{44} ( )_{,yy}$ ,

$$L_{35} = -k^2_1 t C_{44} ( )_{,y} ,$$

$$L_{44} = t^3 C_{66} ( )_{,yy} / 12 - k^2_1 t C_{55} ,$$

$$L_{55} = t^3 C_{22} ( )_{,yy} / 12 - k^2_1 t C_{44} ,$$

$$L_{66} = -k^2_4 t^3 C_{44} ( )_{,yy} / 12 ,$$

$$q_x = \tau_{xz}(t/2) - \tau_{xz}(-t/2) ,$$

$$q_y = \tau_{yz}(t/2) - \tau_{yz}(-t/2) ,$$

$$q = \sigma_z(t/2) - \sigma_z(-t/2) ,$$

$$m_x = [ \tau_{xz}(t/2) + \tau_{xz}(-t/2) ] t/2 ,$$

$$m_y = [ \tau_{yz}(t/2) + \tau_{yz}(-t/2) ] t/2 , \text{ and}$$

$$m = [ \sigma_z(t/2) + \sigma_z(-t/2) ] t/2 .$$

$k$  and  $k_4$  are correction factors as in [4].

The laminate constitutive relations are given by

$$N_y = t C_{22} V_{,y}$$

$$N_{xy} = t C_{66} U_{,y}$$

$$M_y = t^3 C_{22} \Omega_{,y} / 3$$

$$M_{xy} = t^3 C_{66} \psi_{,y} / 3$$

$$Q_y = k^2_1 t C_{44} (\Omega + W_{,y})$$

(6)

$$R_y = k_4^2 t^3 C_{44} \phi_{,y} / 3$$

The boundary conditions for section 1 are

$V = 0$	at $y = 0$	and	$N_y = a$	at $y = L-a$
$U = 0$			$N_{xy} = b$	
$\Omega = 0$			$M_y = c$	
$\psi = 0$			$M_{xy} = d$	
$W = 0$			$Q_y = e$	
$\phi = 0$			$R_y = f$	

The boundary conditions for section 2 are

$V = 0$	at $y = 0$	and	$N = \alpha$	at $y = L-a$
$U = 0$			$N = \beta$	
$\Omega = 0$			$M = \gamma$	
$\psi = 0$			$M = \delta$	
$W = 0$			$Q_y = \epsilon$	
$\phi = 0$			$R_y = \zeta$	

The boundary conditions for section 3 are

$N_y = \alpha$	at $y = L-a$	and	$N_y = 0$	at $y = L$
$N_{xy} = \beta$			$N_{xy} = 0$	
$M_y = \gamma$			$M_y = 0$	
$M_{xy} = \delta$			$M_{xy} = 0$	
$Q_y = \epsilon$			$Q_y = P/2$	
$R_y = \zeta$			$R_y = 0$	

And the boundary conditions for section 4 are

$N_y = a$	at $y=L-a$	and	$N_y = 0$	at $y = L$
$N_{xy} = b$			$N_{xy} = 0$	
$M_y = c$			$M_y = 0$	
$M_{xy} = d$			$M_{xy} = 0$	
$Q_y = e$			$Q_y = P/2$	
$R_y = f$			$R_y = 0$	

#### IV. SOLUTION TO PROBLEM

Since section 1 and 2 are connected, interlaminar stresses may exist and the displacements  $u$ ,  $v$  and  $w$  are continuous across the boundary. The equations (4) and (5) for sections 1 and 2 and the continuity equations (7) and (8) are combined to yield equations (9) and (10).

$$u_1 - \psi_1 t/2 = u_2 + \psi_2 t/2 \quad (7)$$

$$v_1 - \Omega_1 t/2 = v_2 + \Omega_2 t/2 \quad (8)$$

$$w_1 - \phi_1 t/2 = w_2 + \phi_2 t/2$$

$$\begin{bmatrix} L_{11} & 0 & 0 & 0 & -1 \\ 0 & -L_{11} & 0 & 0 & -1 \\ 0 & 0 & -2I_{44}/t & 0 & -1 \\ 0 & 0 & 0 & -2I_{44}/t & -1 \\ 1 & -1 & -t/2 & -t/2 & 0 \end{bmatrix} \begin{bmatrix} u_1 \\ u_2 \\ 1 \\ 2 \end{bmatrix} = \{0\} \quad (9)$$



Equations (7) and (10) can be solved to obtain the following solutions.

$$\begin{bmatrix} v_1 \\ \phi_1 \\ v_2 \\ \phi_2 \\ w_1 \\ \Omega_1 \\ w_2 \\ \Omega_2 \\ \tau_{yz} \\ \sigma_z \end{bmatrix} = C_1 \begin{bmatrix} 0 \\ 1 \\ 0 \\ -1 \\ 0 \\ 0 \\ 0 \\ 0 \\ 0 \\ 0 \end{bmatrix} + C_2 \begin{bmatrix} 0 \\ 1 \\ 0 \\ 0 \\ t/a \\ 0 \\ 0 \\ 0 \\ 0 \\ 0 \end{bmatrix} + C_3 \begin{bmatrix} 0 \\ 0 \\ 0 \\ 0 \\ 1 \\ 0 \\ 1 \\ 0 \\ 0 \\ 0 \end{bmatrix} + C_4 \begin{bmatrix} 0 \\ 0 \\ 0 \\ 0 \\ 0 \\ 0 \\ 0 \\ 0 \\ 0 \\ 0 \end{bmatrix} + C_5 \begin{bmatrix} 1 \\ 0 \\ 1 \\ 0 \\ 0 \\ 0 \\ 0 \\ 0 \\ 0 \\ 0 \end{bmatrix} \begin{bmatrix} t \\ 0 \\ 0 \\ 0 \\ -y \\ 1 \\ -y \\ 1 \\ 0 \\ 0 \end{bmatrix}$$

$$\begin{bmatrix} t/(2k_1^2 C_{44}) \\ -y/(k_2 t C_{23}) \\ 0 \\ y/(k_2 t C_{23}) \\ 0 \\ 1/(2k_1^2 C_{44}) \\ 0 \\ 1/(2k_1^2 C_{44}) \\ 1 \\ 0 \end{bmatrix} + C_6 \begin{bmatrix} A \\ B \\ A \\ B \\ E \\ F \\ E \\ F \\ O \\ J \end{bmatrix} (C_7 e^{\lambda y} + C_8 e^{-\lambda y} + C_9 e^{2\lambda y} + C_{10} e^{-2\lambda y}) + \begin{bmatrix} A \\ B \\ -A \\ -B \\ E \\ F \\ E \\ F \\ I \\ O \end{bmatrix} (C_{11} e^{\lambda y} + C_{12} e^{-\lambda y})$$

where

$$\lambda_{1,2} = \left[ \left( \frac{k_1^2 t c_{44} - k_1^2 t c_{23}^2}{k_4^2 c_{44}} \right) + \left( \frac{k_1^2 t c_{44} + k_1^2 t c_{23}^2}{k_4^2 c_{44}} \right)^2 + 12 k_1^6 t^2 c_{23}^2 / k_4^{-2} \right]^{\frac{1}{2}} / \left( \frac{1}{6} + k_1^2 / (2 k_4^2) \right) t^3 c_{22} \quad \text{and}$$

$$\lambda_3 = 3 k_1 c_{23} \left( -1 / (c_{22} c_{44}) \right)^{\frac{1}{2}} / k_4 t$$

## V. RECOMMENDATIONS

The solution to the problem has not been completed at this point due to the complexity of the problem and the limited time to solve it. It needs to be completed.

The results although not completed well enough indicate that the  $\lambda_{1,2}$  does not appear in the final solution whereas  $\lambda_3$  does. This indicates that the deflection depends on sine and cosine functions. It does not seem likely that this is the case but no error has been found to account for it. This problem needs to be addressed.

Finally, experiments need to be done to check the validity of the analysis.

## REFERENCES

1. J. M. Whitney, C. E. Browning and W. Hoogsteden, "A Double Cantilever Beam Test for Characterizing Mode I Delamination of Composite Materials," J. Reinforced Plastics and Composites, Oct. 1982.
2. T. K. O'Brien, "Characterization of Delamination Onset and Growth in a Composite Laminate," Damage in Composite Materials, ASTM STP 775, K. L. Reifsnider, Ed., American Society for Testing and Materials, 1982. pp 140-167.
3. James M. Whitney and Marvin Knight, "A Modified Free-Edge Specimen," yet to be published.
4. J. M. Whitney and C. T. Sun, "A Higher Order Theory for Extensional Motion of Laminated Composites," J of Sound and Vibration, (1973) 30 (1), pp 85 - 97
5. N. J. Pagano, "On the Calculation of Interlaminar Normal Stress in Composite Laminate," J. Composite Materials, Vol 3 (January 1974), p. 65.

1984 USAF-SCEE SUMMER GRADUATE RESEARCH PROGRAM

Sponsored by the

AIR FORCE OFFICE OF SCIENTIFIC RESEARCH

Conducted by the

SOUTHEASTERN CENTER FOR ELECTRICAL ENGINEERING EDUCATION

FINAL REPORT

INFRARED MEASUREMENTS OF DISILANE PRODUCTION FROM

A D.C. DISCHARGE IN SILANE

Prepared by: Robert F. Cheney and Randall Schadt  
Academic Department: Physics  
University: University of Missouri-Rolla  
Research Location: Air Force Wright Aeronautical Laboratories,  
Aero Propulsion Laboratory, Energy Conversion  
Branch, Plasma Physics Group  
USAF Research Contact: Charles A. DeJoseph  
SFRP Supervising  
Faculty Member: Dr. Richard Anderson  
Date: Sept. 10, 1984  
Contract No.: F49620-82-C-0035

INFRARED ABSORPTION MEASUREMENTS OF THE  $\nu_4$  BAND  
OF SILANE IN A HEATED CELL

by

Randall J. Schadt

and

Robert F. Cheney

ABSTRACT

Absorption spectra of the  $\nu_4$  band of silane were measured with a Fourier spectrometer at a resolution of  $0.06 \text{ cm}^{-1}$ . Measurements were accomplished after the silane (1% in Argon) was thermally excited to  $250^\circ\text{C}$  in a 31 cm. pathlength, Pyrex cell at a pressure of 133 Torr. The region for which absorption was measured covered  $850$  to  $1000 \text{ cm}^{-1}$ . Comparison between spectra at a temperature of  $250^\circ\text{C}$  to that of  $21^\circ\text{C}$  revealed the enhancement of some lines. These enhanced absorption lines either resulted from the excitation of higher rotational levels of the ground state or from the excitation of the first excited vibrational level. For this reason, this experiment is not definitive in identifying which line results from which of the two possible excitations. Therefore, the present study serves the purpose of providing initial identification of candidate lines for the transition from the first excited vibrational level of the  $\nu_4$  band of silane.

## I. INTRODUCTION

The deposition of an amorphous silicon thin film is vitally important to the making of all semiconductor devices. To a wide extent, this process is accomplished by plasma decomposition of monosilane ( $\text{SiH}_4$ ). As yet, the depositing mechanisms and depositing species are not fully known. Many deposition models have been proposed, but not enough is known about the deposition process to give any model a high degree of predictability. This report is concerned with one part of the complex silane chemistry which takes place in a low pressure discharge similar to those used in deposition.

It has been suggested that neutral species, primarily  $\text{SiH}_3$ , are responsible for most of the deposition of the silicon film.<sup>1</sup> It is possible that large amounts of disilane ( $\text{Si}_2\text{H}_6$ ), formed by an associative process of silane ( $\text{SiH}_4$ ), can breakdown to  $\text{SiH}_3$ . Both this radical and disilane have been detected mass spectrographically,<sup>1</sup> but it is not certain whether the disilane was actually formed in the discharge or in the ionizer of the mass spectrograph. Therefore, this project is concerned with detecting disilane in the discharge using infrared absorption spectroscopy. This would remove whatever uncertainty exists concerning the production of disilane in a d.c. discharge of silane. It is hoped that this study will clarify deposition models and thereby help to predict what techniques and experimental conditions can produce a more uniform film with greater purity and less substrate stress.

## II. OBJECTIVES

The objective of this experiment was to determine under what total pressures and discharge currents, if any, is disilane ( $\text{Si}_2\text{H}_6$ ) formed in a d.c. gas discharge of silane ( $\text{SiH}_4$ ). If it is formed, what is the relationship between the loss of silane and the formation of disilane?

### III. APPARATUS AND CALIBRATION

Figure 1 gives a pictorial representation of the apparatus. Gas flow was through the discharge tube, through a 20.25m "White" type absorption cell, and into a roughing pump. Regulating the flow was accomplished with a flow meter and needle valve. A glass tube of length 21 cm between electrodes and inner diameter of 2.2 cm was used as a discharge tube. A baratron capacitance manometer monitored the pressure of the gas in the discharge tube. An ammeter monitored the current in the discharge which was maintained by a current regulated power supply. The infrared beam, provided by a glow bar, passed through the spectrometer, through the discharge tube and absorption cell, then onto a liquid-nitrogen cooled Hg-Cd-Te detector. The detector was interfaced with a computer which collected, processed, and plotted the spectra which were then inspected for the characteristic spectra of disilane.

Calibration runs of silane and disilane were made by taking spectra with no discharge. Transmission spectra were calculated by ratioing measured spectra against background spectra with the cell evacuated. This ratioing removed system influence on the collected spectra.

Figures 2 and 3 show typical calibration spectra at 2.0 Torr for silane and disilane respectively. The path length of the "White" type cell was set at its maximum, 20.25m, for these runs. Figure 2 shows that silane does not have a definite peak at  $1 \text{ cm}^{-1}$  resolution, but it does exhibit a broad absorption band from  $869\text{-}913 \text{ cm}^{-1}$ . Figure 3 shows that disilane has a classic P-Q-R band shape with a width of  $50 \text{ cm}^{-1}$  and centered at  $843 \text{ cm}^{-1}$ . A resolution of  $1 \text{ cm}^{-1}$  will clearly resolve this band shape if it is present in spectra obtained during a discharge run.

#### IV. CALIBRATION CURVES

Beer's Law states that the intensity of radiation passing through an absorbing gas decays exponentially,

$$I(\nu, p) = I_0(\nu) e^{-k(\nu, p)nx} \quad (1)$$

where  $I$  is the intensity of the radiation,  $I_0$  the incident intensity,  $\nu$  the frequency of the radiation,  $p$  the total pressure of the gas,  $n$  the partial pressure of the absorbing species,  $x$  the path length into the gas, and  $k(\nu, p)$  the absorption coefficient.

If the radiation has been passed through a spectrometer before the absorbing gas, then the measured signal at a detector placed in the beam path is;

$$S(\nu, p) = \int_{-\infty}^{+\infty} \phi(\nu-\nu') \mathcal{T}(\nu') I_0(\nu') e^{-k(\nu', p)nx} d\nu' \quad (2)$$

where  $\phi(\nu-\nu')$  is the spectrometer instrumental line shape (ILS) function and  $\mathcal{T}(\nu')$  is the spectrometer/detector transfer function which reflects the efficiency of the system. With no absorbing species present in the gas (i.e. background spectra) the signal is;

$$S'(\nu) = \int_{-\infty}^{+\infty} \phi(\nu-\nu') \mathcal{T}(\nu') I_0(\nu') d\nu' \quad (3)$$

Since  $\mathcal{T}(\nu')$  and  $I_0(\nu')$  change very slowly with respect to the spectrometer ILS, they can be pulled out of the integral,

$$S(\nu, p) = \mathcal{T}(\nu) I_0(\nu) \int_{-\infty}^{+\infty} \phi(\nu-\nu') e^{-k(\nu-\nu', p)nx} d\nu' \quad (4)$$

$$S'(\nu) = \mathcal{T}(\nu) I_0(\nu) \int_{-\infty}^{+\infty} \phi(\nu-\nu') d\nu' \quad (5)$$

The ILS is a normalized function, so,

$$S'(\nu) = \mathcal{T}(\nu) I_0(\nu) \quad (6)$$

and,

$$\frac{S(\nu, p)}{S'(\nu)} = \int_{-\infty}^{+\infty} \phi(\nu-\nu') e^{-k(\nu-\nu', p)nx} d\nu' \quad (7)$$

Since  $k(\nu-\nu', p)$  is not known (in general) it is difficult to calculate the partial pressure of the absorbing species. The following is

a method for circumventing this problem.

Calibration curves of path length versus absorbance obtained at constant  $n$  and  $p$  were used to determine the partial pressure of the absorbing species in the discharge. From equation 7 it can be seen that the transmittance has the same dependence on both path length and partial pressure. Hence, fixing the path length and allowing the partial pressure to change (such as in discharges) has the same effect on the transmittance as fixing the partial pressure and varying the path length. Mathematically, this is stated as,

$$n_c x_c = n_d x_d \text{ or } n_d = n_c \frac{x_c}{x_d} \quad (8)$$

where the  $c$  and  $d$  subscripts refer to calibration and discharge runs respectively. The partial pressure of the absorbing species in the calibration runs,  $n_c$ , and the path length in the discharge runs,  $x_d$ , can be set by the experimenter. Therefore, only  $x_c$  for a given absorbance need be known to calculate the partial pressure of the absorbing species in the discharge,  $n_d$ . (Note: It must be remembered that equation 8 is valid only at a given absorbance.)

To determine the correct  $x_c$  to be used in equation 8 for any given discharge run, calibration runs were made at different path lengths and fixed total and partial pressures. The quantity  $x_c/x_d$  was then plotted against the absorbance obtained in the runs. A polynomial curve fit to this calibration data was then used to find  $x_c/x_d$  for discharge data. This ratio was then inserted into equation 8 to calculate the partial pressure of the absorbing species in the discharge,  $n_d$ .

As mentioned earlier, silane does not exhibit a definite peak at  $1 \text{ cm}^{-1}$  resolution. Therefore, an integrated absorbance over part of the silane band which did not overlap the disilane spectrum ( $869-913 \text{ cm}^{-1}$ )

past .6 mA. At that point the production of disilane falls off. Figure 9 shows that the disilane production from the dissociated silane falls off with increased current. These facts could be due to one or both of the following reasons:

1. Dissociation of the disilane due to increased collisions with the electrons of the discharge.
2. Further dissociation of the silane so that less radicals are present to form disilane.

The ratio used in Figure 9 is somewhat misleading because it is a ratio of the partial pressure of silane, containing one silicon atom, to that of disilane, containing two silicon atoms. From a silicon accountability standpoint, the relevant ratio is twice that used in Figure 9. In other words, 4 to 34% of the silicon in the loss of silane went into the formation of disilane.

The conclusion of this report is that up to 34% of the silicon from dissociated silane in a d.c. discharge of 1% silane in argon forms disilane under the following experimental conditions:

Pressure: 1.0 to 2.0 Torr

Flow Rate: 35 to 118 sccm

Residence Times: 7.1 to 12.0 msec.

Discharge Current: .1 to 1.5 mA

It is hoped that this conclusion will aid in the understanding of the silicon deposition process.

## VI. RECOMMENDATIONS

It is recommended that further studies of discharge products in a d.c. gas discharge of silane be carried out in order to obtain better understanding of the silicon deposition process. One possible study could deal with finding  $\text{SiH}_3$  in the discharge. Another study could deal with the rate of  $\text{SiH}_3$  formation from disilane in a d.c. gas discharge.

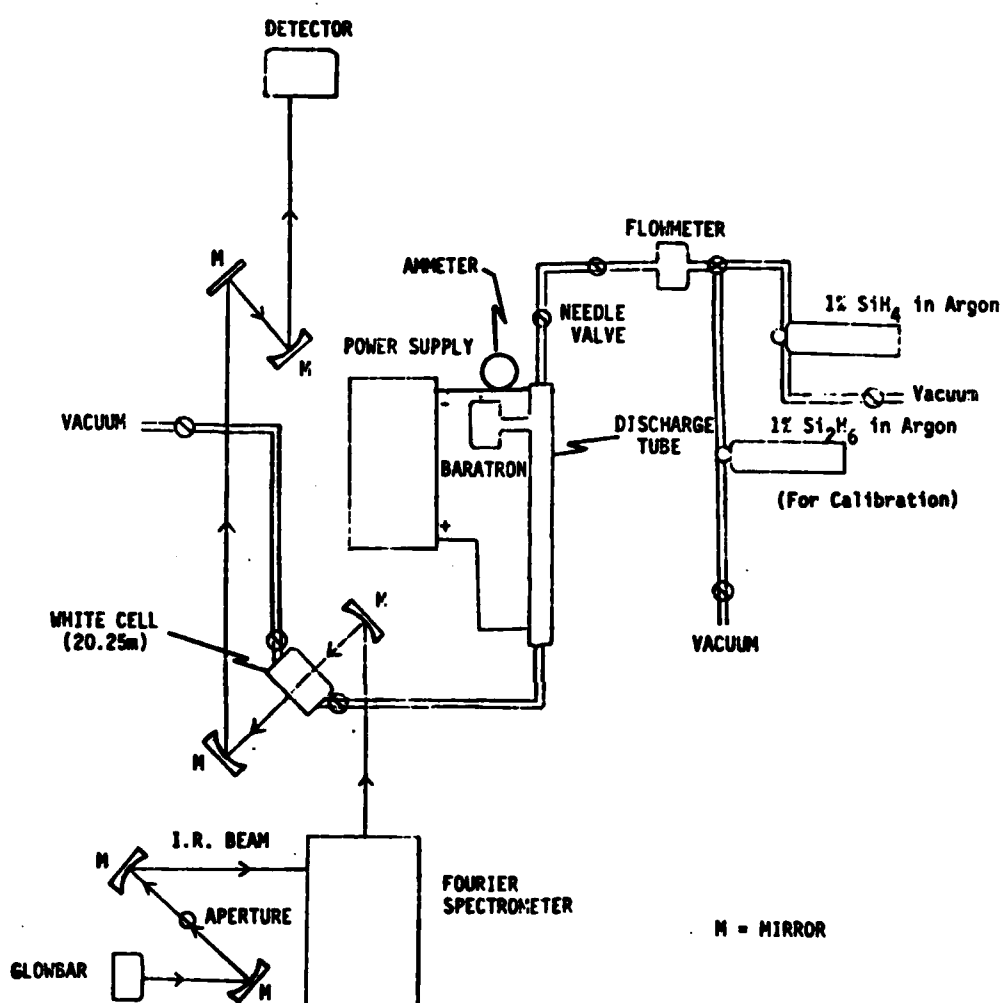


FIGURE 1  
 SCHEMATIC DIAGRAM OF APPARATUS TO DETECT  $\text{Si}_2\text{H}_6$   
 IN A D.C. DISCHARGE OF 1%  $\text{SiH}_4$  IN ARGON

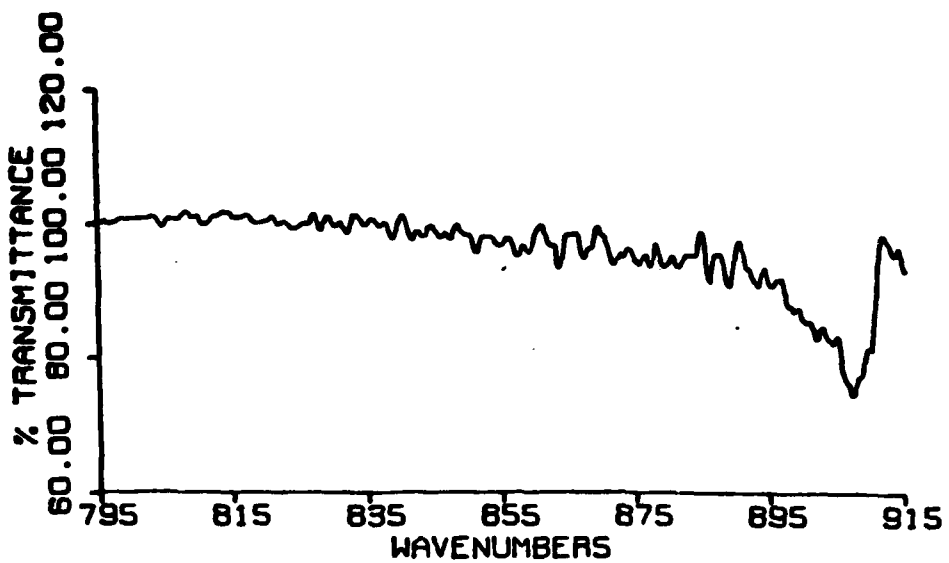


Figure 2 - Silane Calibration

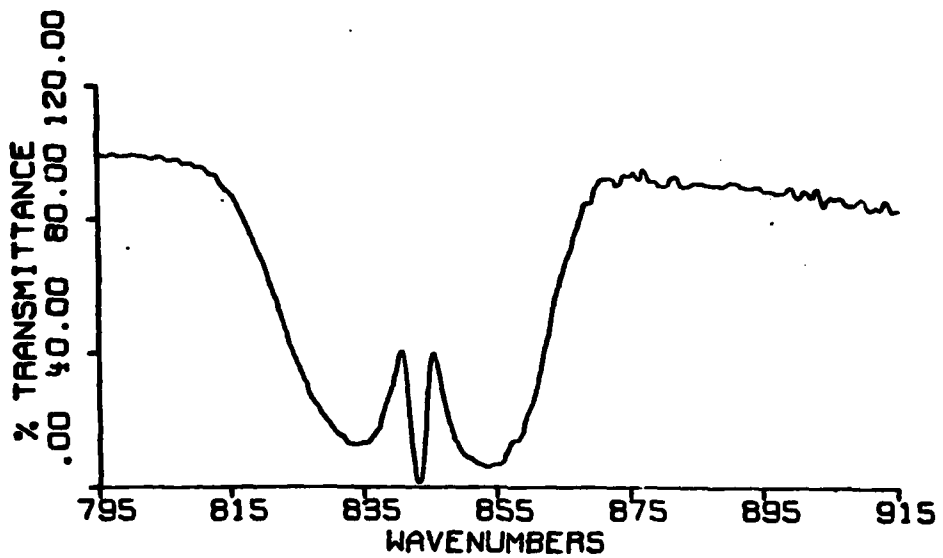


Figure 3 - Disilane Calibration

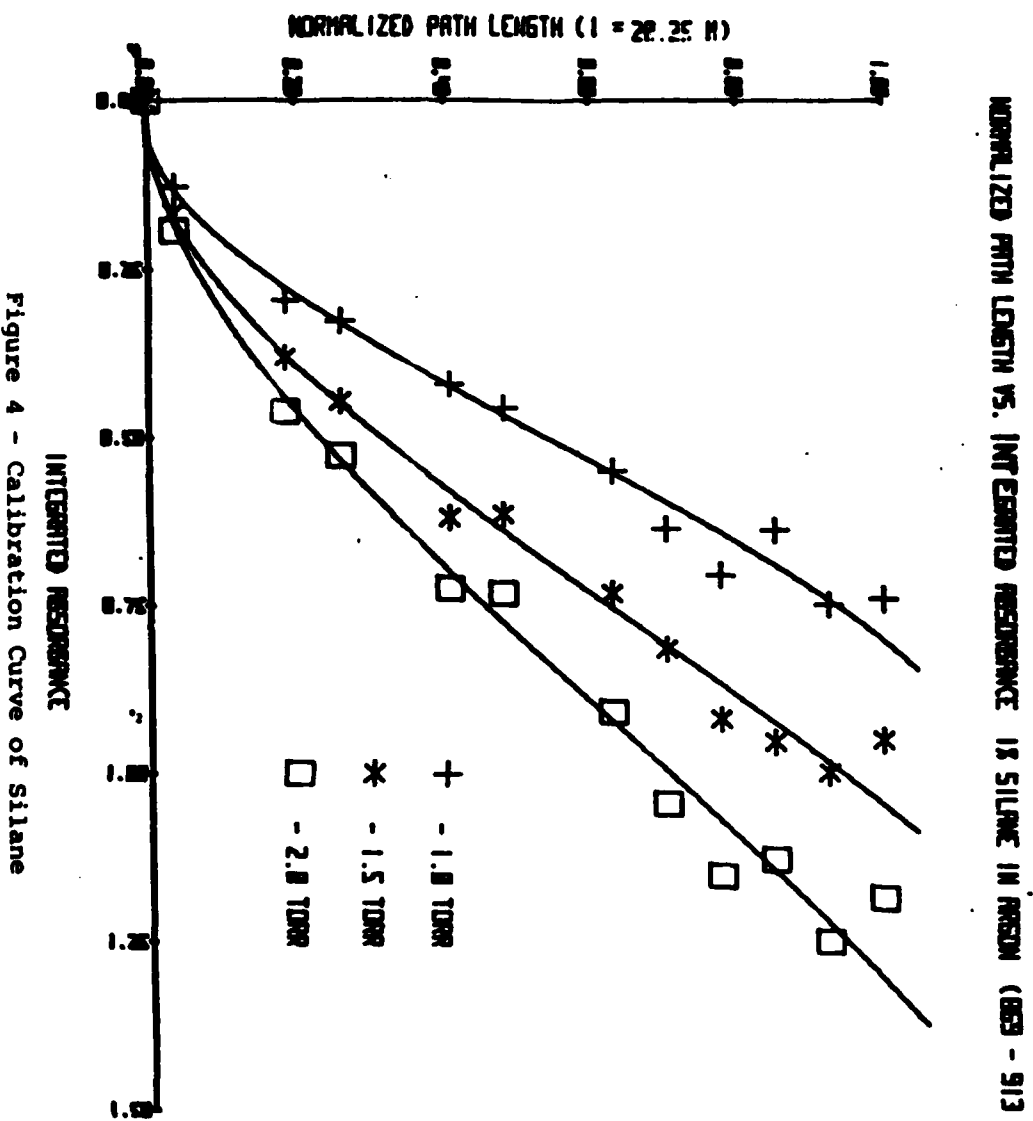


Figure 4 - Calibration Curve of Silane

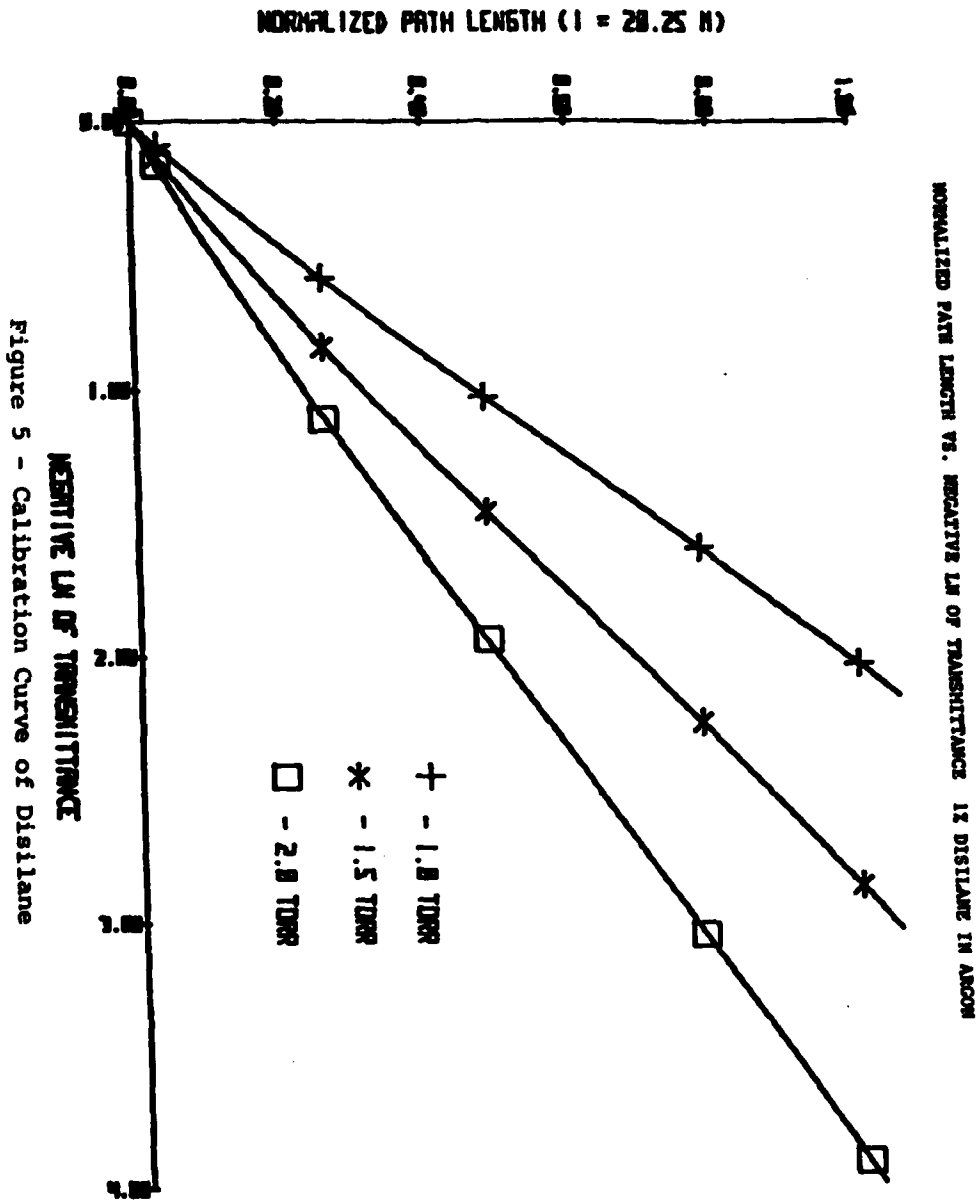


Figure 5 - Calibration Curve of Disilane

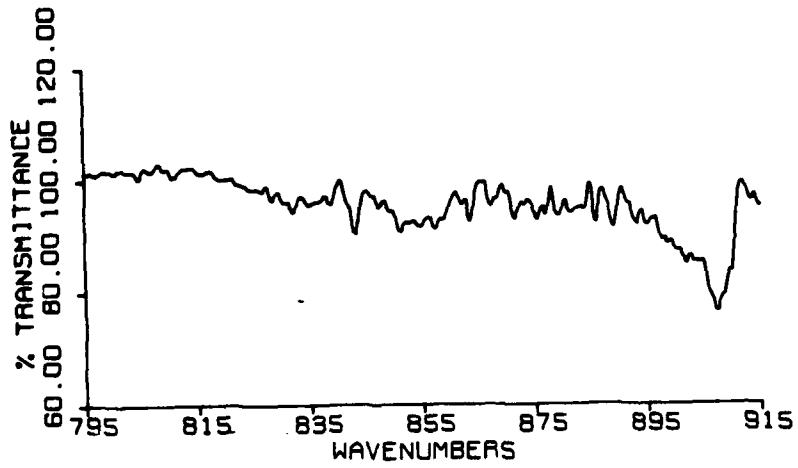


Figure 6 - Spectra at .2mA Discharge Current

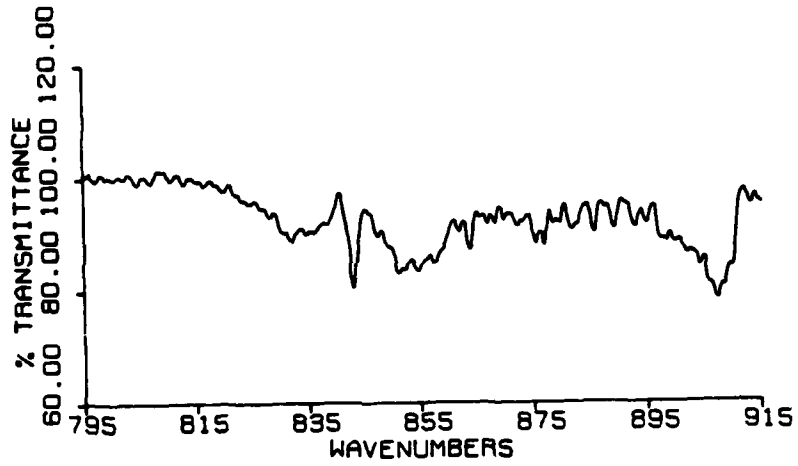


Figure 7 - Spectra at .6mA Discharge Current

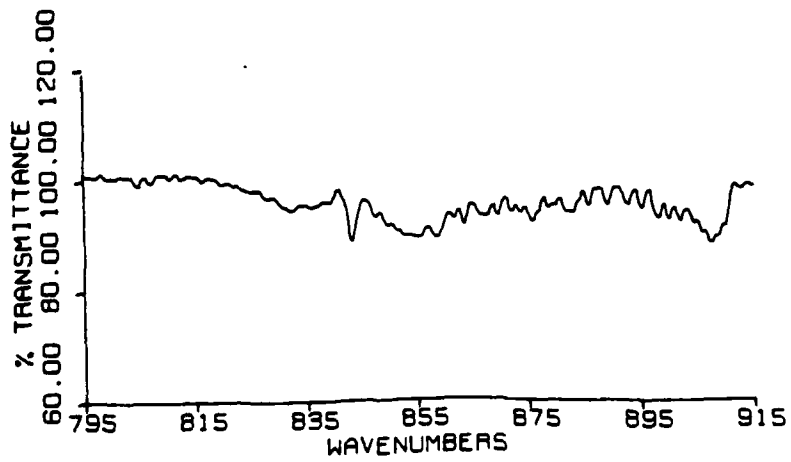


Figure 8 - Spectra at 1.5mA Discharge Current

Formation of  $\text{Si}_2\text{H}_6$  to Loss of  $\text{SiH}_4$

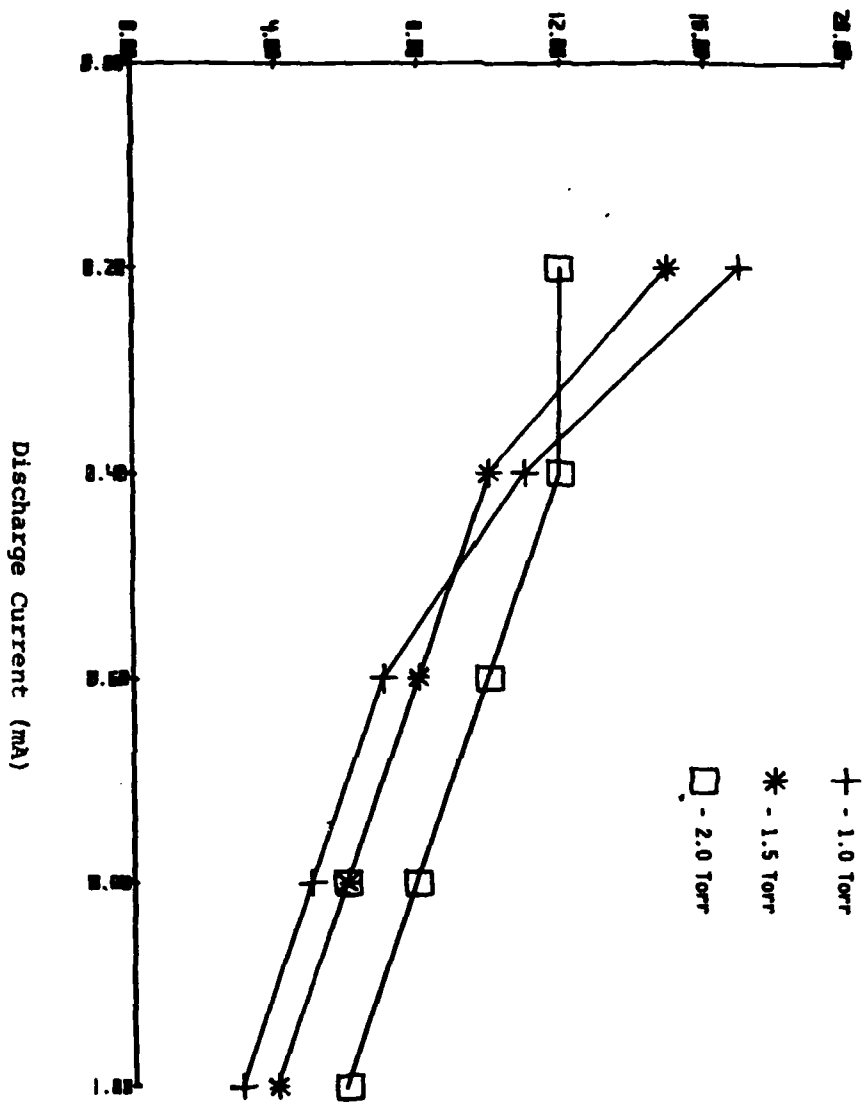


Figure 9  
Formation of  $\text{Si}_2\text{H}_6$  to Loss of  $\text{SiH}_4$  versus Discharge Current

Table 1  
Silane

3<sup>rd</sup> Order Polynomial Curve Fit Correlation Coefficient = .999

Order \ Pressure	1.0 Torr	1.5 Torr	2.0 Torr
0th	$-8.5884 \times 10^{-4}$	$1.3439 \times 10^{-3}$	$-3.0339 \times 10^{-3}$
1st	$-1.6108 \times 10^{-1}$	$-7.704 \times 10^{-2}$	$3.882 \times 10^{-2}$
2nd	3.6748	1.7820	1.0431
3rd	-2.3791	$-7.5417 \times 10^{-1}$	$-3.6834 \times 10^{-1}$

Table 2  
Disilane

3<sup>rd</sup> Order Polynomial Curve Fit Correlation Coefficient = .999

Order \ Pressure	1.0 Torr	1.5 Torr	2.0 Torr
0th	$6.7817 \times 10^{-4}$	$1.5492 \times 10^{-4}$	$1.2020 \times 10^{-3}$
1st	$3.9267 \times 10^{-1}$	$2.6724 \times 10^{-1}$	$2.1072 \times 10^{-1}$
2nd	$9.6604 \times 10^{-2}$	$5.6648 \times 10^{-2}$	$2.4886 \times 10^{-2}$
3rd	$-2.4097 \times 10^{-2}$	$-1.0014 \times 10^{-2}$	$-3.4888 \times 10^{-3}$

Table 3  
Residence Times and Flow Rates

Pressure	1.0 Torr	1.5 Torr	2.0 Torr
Flow Rate (sccm)	35	70	118
Residence Time (msec)	12.0	9.0	7.1

Table 4  
 Silane Discharge  
 Partial Pressure of Silane ( $10^{-3}$  Torr)

Pressure Current	1.0 Torr	1.5 Torr	2.0 Torr
.2mA	8.1	12.5	15.9
.4mA	6.7	9.2	12.6
.6mA	4.9	7.7	10.4
.8mA	4.3	5.6	8.1
1.0mA	2.9	4.1	5.7

Table 5  
 Silane Discharge  
 Partial Pressure of Disilane ( $10^{-3}$  Torr)

Pressure Current	1.0 Torr	1.5 Torr	2.0 Torr
.2mA	.33	.39	.51
.4mA	.37	.58	.87
.6mA	.35	.57	.94
.8mA	.27	.53	.95
1.0mA	.20	.40	.82

REFERENCES

1. R. Robertson, D. Hils, H. Chatham, and A. Gallagher, "Radical species in argon-silane discharges," Applied Physics Letters 43(6), pp. 544-546, 1983.

### Acknowledgement

The authors would like to thank the Air Force Systems Command, the Air Force Office of Scientific Research and the Southeastern Center for Electrical Engineering Education for providing them with the opportunity to spend a very worthwhile and interesting summer at the Air Force Aero Propulsion Laboratory, Wright-Patterson AFB, OH. They would like to acknowledge the laboratory, in particular the Plasma Physics group, for its hospitality and excellent working conditions.

Finally, they would like to make special thanks to Charles A. DeJoseph for his excellent guidance and supervision throughout the research project.

1984 USAF-SCEEE GRADUATE STUDENT SUMMER SUPPORT PROGRAM

Sponsored by the

AIR FORCE OFFICE OF SCIENTIFIC RESEARCH

Conducted by the

SOUTHEASTERN CENTER FOR ELECTRICAL ENGINEERING EDUCATION

FINAL REPORT

FINITE ELEMENT MODELING OF A WALL UNDER BLAST LOADS

Prepared by: Susan M. Cheney  
Academic Department: Civil Engineering  
University: The Ohio State University  
Research Location: Air Force Engineering and Services  
Center, Engineering Research Division,  
Air Base Survivability Branch  
USAF Research Contact: Walter Buchholtz  
Date: 21 Sept. 1984  
Contract No.: F49620-82-C-0035

# FINITE ELEMENT MODELING OF A WALL UNDER BLAST LOADS

by

Susan M. Cheney

## ABSTRACT

The results of several blast tests on reinforced concrete boxes are attempted to be duplicated by a finite element model using the computer code Abaqus. Half of the front wall of the box is modeled. Loading data is drawn from the results of the blast tests. Two models are developed, a larger one where the properties of the steel and concrete are smeared together, and a smaller one where the horizontal and vertical steel rebars are modeled. The concrete material model available with Abaqus is used. Preliminary results were obtained by the end of the research period, and a description of the further work to be done is included.

### ACKNOWLEDGEMENT

The author would like to thank the Air Force Systems Command, the Air Force Office of Scientific Research and the Southeastern Center for Electrical Engineering Education for providing her with the opportunity to spend a very educational and worthwhile summer at the Air Force Engineering and Services Center, Tyndall AFB, Fl. She would like to thank the Center and especially the Air Base Survivability branch for providing both an excellent place to live and an excellent place to work. In particular, she would like to thank Lt. Tom Hilferty for the data from the blast tests, Capt. Paul Rosengren for the help in formulating the model and using Abaqus, Ken Williams for his help in using the computer, and Walt Buchholtz for sponsoring her.

## I. INTRODUCTION:

NATO has established certain design standards for reinforced concrete hardened shelters. Recently the Air Force Engineering and Services Center conducted a series of blasts designed to examine the NATO design standards with respect to the percentage of steel required and the type of shear reinforcement used. These tests are very expensive to conduct and require much time to set up. A finite element model which can predict the response of the structure would aid in getting the most from the limited number of tests that can be run and also might be used to predict results when tests can not be run.

The finite element code Abaqus was chosen to test the model because it was the most sophisticated finite element code available at the Engineering and Services Center and few people at the Center had tested Abaqus to its fullest capabilities. Abaqus contained a concrete material model and rebar elements which would make it especially suited to this problem. Also, Abaqus uses a wavefront solver which permits large problems to be run.

To prevent any complications with security and classification of research materials, data obtained from the blast tests was used to determine the loading on the structure instead of the standard formulas which relate the weight of the explosive and the distance from the wall to the center of the blast.

## II. OBJECTIVES:

The main objective of this project was to use the finite element code Abaqus to model the effects of a blast loading on a

reinforced concrete wall. The attempt to model the difference between stirrups and dowel rods was not to be made. It is intended to model the different percentages of steel reinforcement in the walls. The author did not expect to be completely finished at the end of the research period.

### III. TEST SERIES:

Starting in August 1982 the Air Force Engineering and Services Center conducted a series of blast tests on NATO standard concrete walls under the direction of Lt. Tom Hilferty. All information on the tests and the illustration were provided by Lt. Hilferty. The first series was to test the effect on the strength of the wall of the percentage of steel in the concrete, and to determine the relative value of the use of stirrups over the use of dowels. The tests were intended to simulate in halfscale the effects on a two foot thick wall of a near miss of a thousand pound bomb exploding on the ground surface. Therefore the actual thickness of the wall was approximately 1 ft. and the weight of the explosive charge was half that in a thousand lb. bomb. The actual dimensions of the concrete boxes tested are shown in Fig. 1. The boxes were bolted to a large angle-shaped concrete reaction block to keep them in place during the tests. The reaction block had a sand berm behind it to keep it in place. Each of the boxes carried instrumentation to measure the pressure exerted on the wall by the blast, the strain in the rebars, the deflection of the midpoint of the wall, and the acceleration of various points in the box. The typical instrumentation layout is shown in Fig. 2. The explosive was placed on the ground surface a short distance away

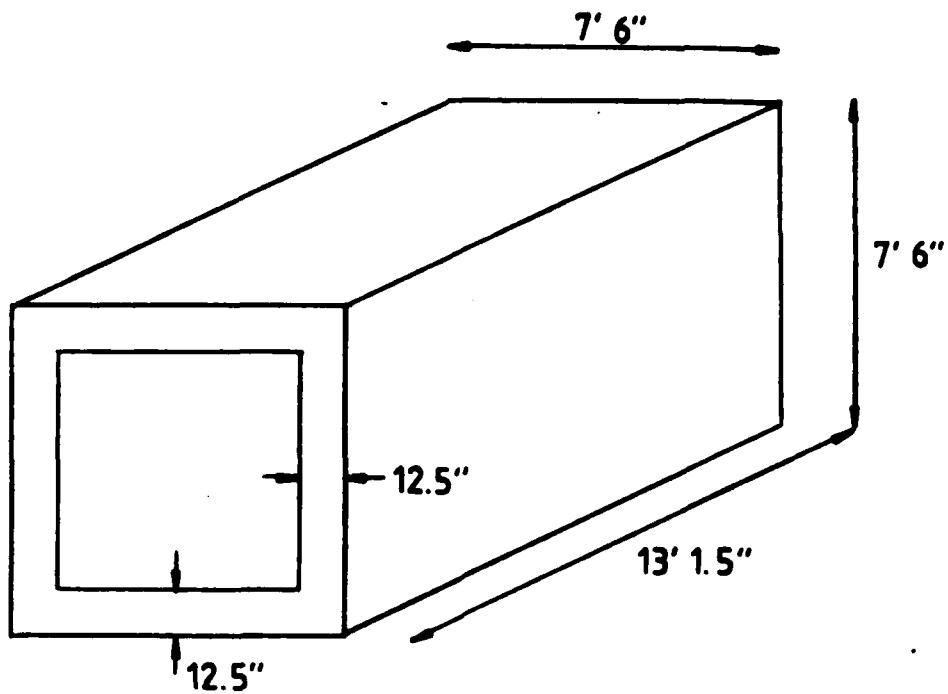


**FIG.1 Test Specimen**

**Table 1 Test Parameters**

Test	Percent Steel	Shear Reinforcement
SWT-1	1%	Stirrups
SWT-2	0.5%	Stirrups
SWT-3	0.5%	Dowels
SWT-4	0.25%	Dowels
SWT-5	2%	Stirrups
SWT-6	0.25%	Stirrups

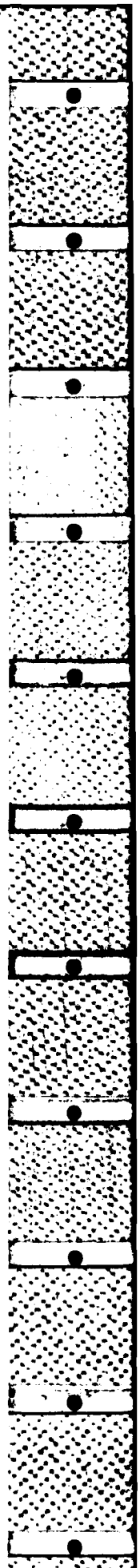
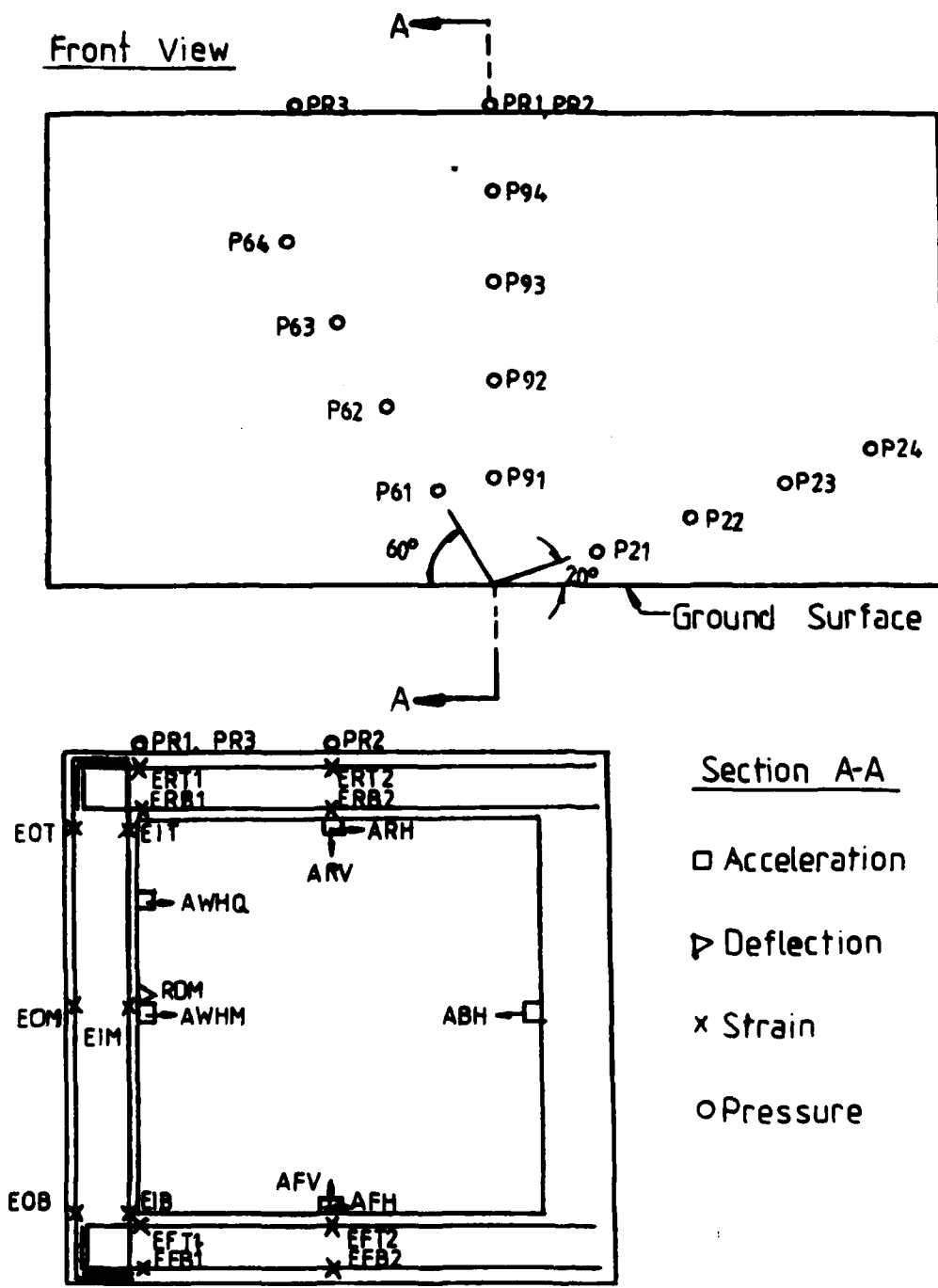


**FIG.2 Typical Instrumentation Layout**

from the center of the wall. A total of six tests were run, with the percentage of vertical steel varying from 2% to 0.25% and using either stirrups or dowel rods. The design strength of the concrete was 5000 psi, and 36 ksi steel was used as reinforcement. Percentages of steel and shear reinforcement used are shown in Table 1.

The instrumentation yielded a large amount of data, although the data varied considerably from test to test. The pressure gauges closest to the center of the blast were frequently destroyed by the blast and there was little good data obtained on the pressures at the bottom center of the wall. The data as increasingly better the further away from the bottom center of the wall. However, in every case there was considerable variation in the pressures recorded in each test. The data from the accelerometers was used to obtain deflection data. The deflections recorded by the accelerometers differed significantly from those obtained by the scratch test. Of the two, the scratch test data was considered more reliable because it gave the kind of decaying sinusoidal wave that was expected, while the accelerometer usually gave a gradually increasing curve. The data on the strains in the rebars was not used in this project.

#### IV. MODEL:

Much time was wasted in attempting to find a model which would fit in the computer. There was no sizing routine for Abaqus, so finding a model small enough to fit in the computer yet large enough to give good accuracy was a matter of trial and error. A

number of different models were tried before a satisfactory one was found. It was decided to model only the front wall of the box, and since that was half-symmetric, only half of the front wall was modeled. The 0.25% steel wall was chosen to be modeled. The first model, which was the larger of the two, did not contain any rebar elements, while the second model used rebar elements to model both the vertical and horizontal steel reinforcement in both the inside and outside faces.

The first model was three elements (4 nodes) deep through the thickness of the wall, 12 elements (13 nodes) deep along the length, and 23 elements (24 nodes) high. The second model was two elements deep (3 nodes) through the thickness, 12 elements (13 nodes) deep along the length, and 23 elements (24 nodes) high. In the second model rebars were defined running horizontally and vertically through the center of each element. The stirrups or dowels were not modeled, although they could have been modeled but with some difficulty. The nodal and element data for both meshes were generated in a short Fortran routine written by Ken Williams of the Engineering and Services Center and input directly into Abaqus.

A small amount of difficulty was encountered with attempting to define only one rebar per element. The Abaqus version 4-4-62 would not accept the SINGLE parameter to define only one rebar per element. However, this difficulty was overcome by using the default option to define a row of rebars in each element, but setting the rebar spacing to be larger than the length of the element. This produced only one rebar per element in the direction desired.

The model was considered to be fixed along the bottom to the concrete reaction block. Also, the model was considered to be fixed along the back face where the roof and floor joined the wall. This meant that the back of the wall had to be fixed for a distance of 12.5 inches below the top and above the bottom of the wall. The elements in the very top and bottom of the mesh were made slightly larger to be as tall as they were deep. Thus in the case of the larger mesh, the very bottom and top three elements together were exactly 12.5 inches high. In the smaller mesh, the very top and bottom two elements together were exactly 12.5 inches high. Fig. 3 shows the smaller mesh. The larger size of the elements in the bottom and top layers is noticeable.

Also, since the wall was assumed to be half-symmetric and only one half of the wall was modeled, certain boundary conditions must be imposed to maintain half-symmetry. Namely, the side of the model that is at the center of the wall must be restrained in the X direction as shown in Fig.3.

In the first model, which contained no rebar elements, the value of Young's modulus chosen was the recommended value for  $f'_c = 5000$  psi concrete,  $3.84 \times 10^6$  psi, increased by the rule of mixtures to account for the 0.25% steel. This was figured to be  $3.95 \times 10^6$  psi and the material was considered to be isotropic since the steel ratio was approximately the same in the X and Z directions, although the steel ratio in the Y direction was much less. Poisson's ratio for concrete, 0.2, was increased according

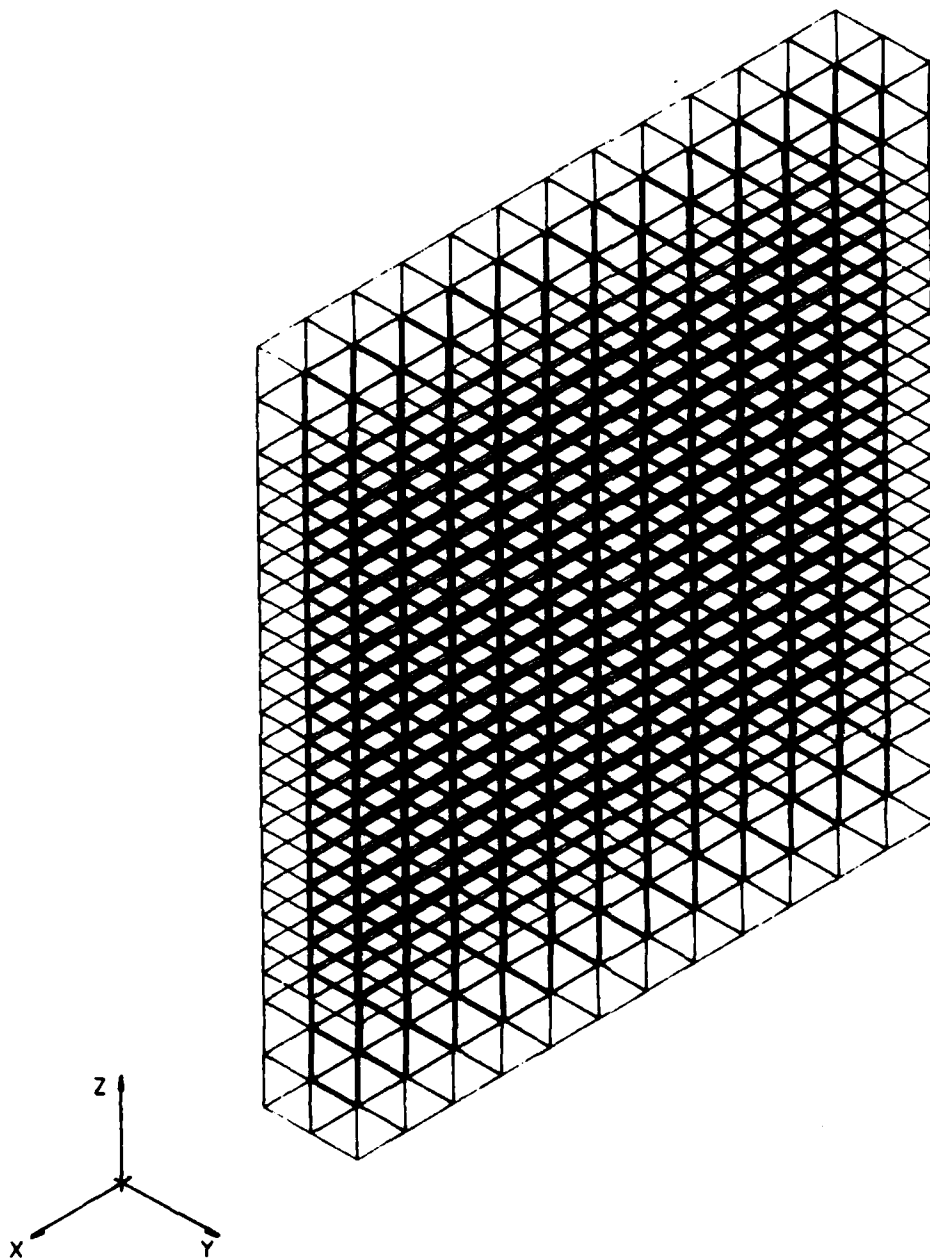
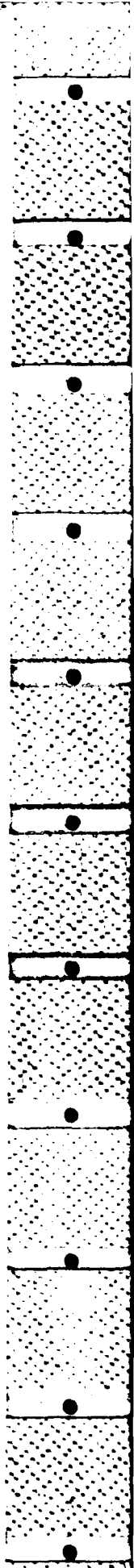


FIG.3 Smaller Mesh



to a formula derived by Capt. Paul Rosengren of the Engineering and Services Center based on energy methods. This was calculated to be 0.20255.

In the second model, which contained rebar elements, there was no need to smear the material properties of the steel and concrete. Thus the value of Young's modulus for concrete was the value used in the first model before smearing,  $3.84 \times 10^6$  psi. Poisson's ratio for concrete was considered to be 0.2. Both the concrete and the steel were considered to be isotropic. The steel was considered to be an elastic-perfectly plastic material. For the steel, Young's modulus was taken as  $29 \times 10^6$  psi and Poisson's ratio was taken as 0.3. Yield stress was considered to be 36,000 psi.

Both models used the concrete material option contained in Abaqus. This material option uses the Chen and Chen failure surface. The yield stress was taken to be 3000 psi and the ultimate stress was taken to be 5000 psi.

Loading information was taken from the data provided by the pressure gauges in the six wall tests. The pressure-time history of the blast was modeled as a double triangle, as shown in Fig. 4. The five items of data that were taken from each pressure gauge on each test are also shown in Fig. 4. These items of data are the peak pressure, the time of arrival of the blast wave, the time of the peak pressure, the intermediate time, and the end time. The intermediate time is the time where the slope of the pressure time history is discontinuous after the peak, and

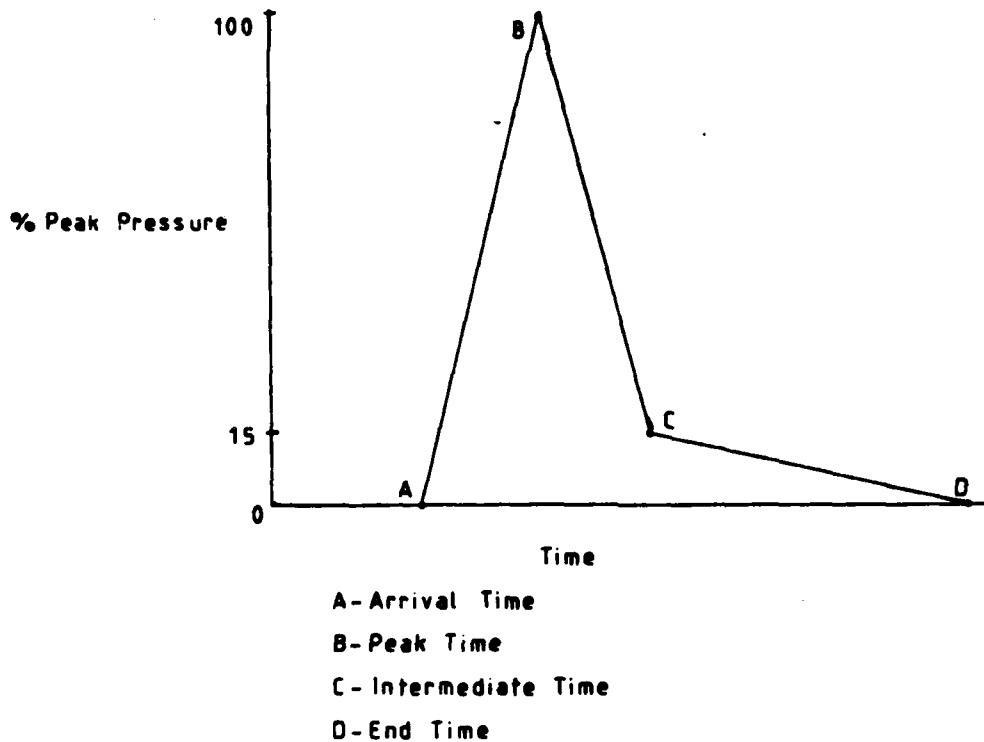


**FIG.4 Percent Pressure-Time History Curve**

Zone	Arrival Time	Peak Time	Intermediate Time	End Time
TH1	0.6 msec	0.7 msec	1.0 msec	1.62 msec
TH2	0.8 msec	0.92 msec	1.27 msec	2.3 msec
TH3	1.0 msec	1.075 msec	1.43 msec	3.25 msec
TH4	1.2 msec	1.245 msec	1.72 msec	4.0 msec

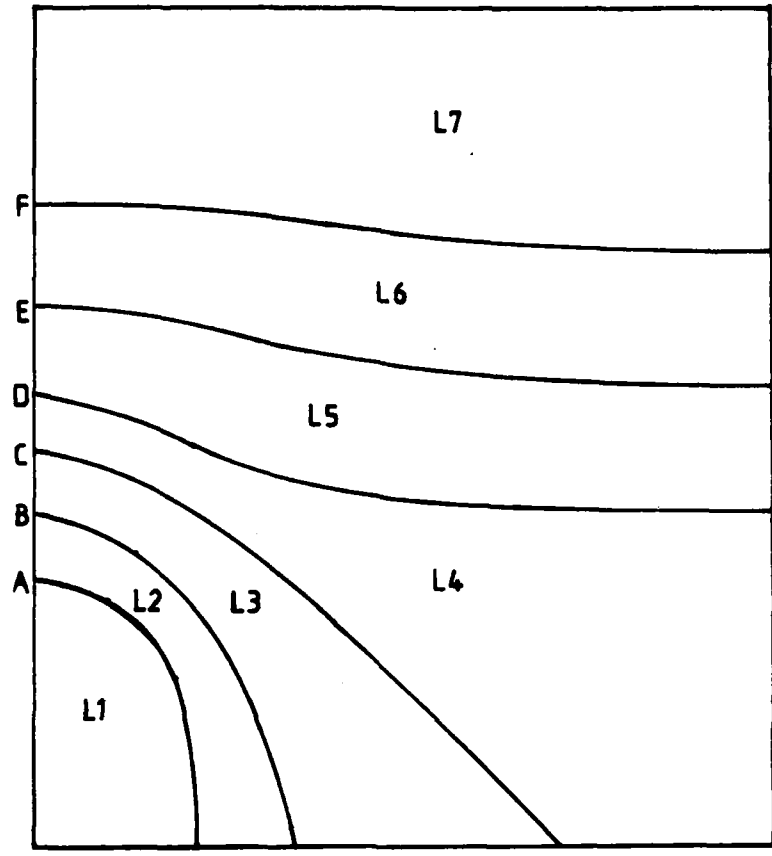
**Table 2 Pressure-Time History Zones**  
 14-13

the end time is the time where the blast pressure finally fades to zero.

The data for each pressure guage was averaged among the six tests, except in the case of the pressure guages closest to the center of the blast, P91, P61, and P21. These three guages were destroyed in most of the tests. So little information was obtained for these guages that the data for the three guages for all six tests was averaged together to produce one value for the three guages. With these averaged values, three graphs were drawn showing the peak pressure distribution along the three lines of guages. From these plots, data was taken to obtain the equipressure curves shown in Fig. 5. Equipressure lines are labeled A-H. These equipressure lines were used to break the front face elements up into equipressure element groups. The average pressure values used as the loads on the element groups are labeled as L1-L7.

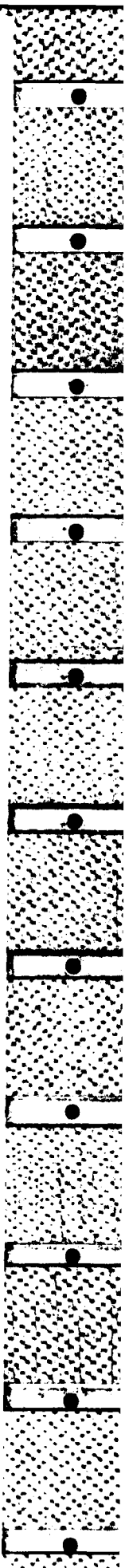
A similar process of data averaging, graph plotting and plotting of equipressure lines across the front face of the model was followed for the four times of interest. However, the four times were found to vary independantly of each other across the face of the model. In other words, two points that had the same arrival time might not have the same peak, intermediate, and end times. Therefore it was decided to divide the front face of the model up into four equal percent pressure-time history zones. These zones were based on the arrival time of the blast, because the arrival time was the most easily distinguishable time point, and also because there was more arrival time data.

Front  
View



- |              |               |
|--------------|---------------|
| A = 7000 psi | L1 = 7900 psi |
| B = 5000 psi | L2 = 6000 psi |
| C = 3000 psi | L3 = 4000 psi |
| D = 2000 psi | L4 = 2500 psi |
| E = 1000 psi | L5 = 1500 psi |
| F = 500 psi  | L6 = 750 psi  |
|              | L7 = 300 psi  |

**FIG.5 Blast Pressure Distribution**

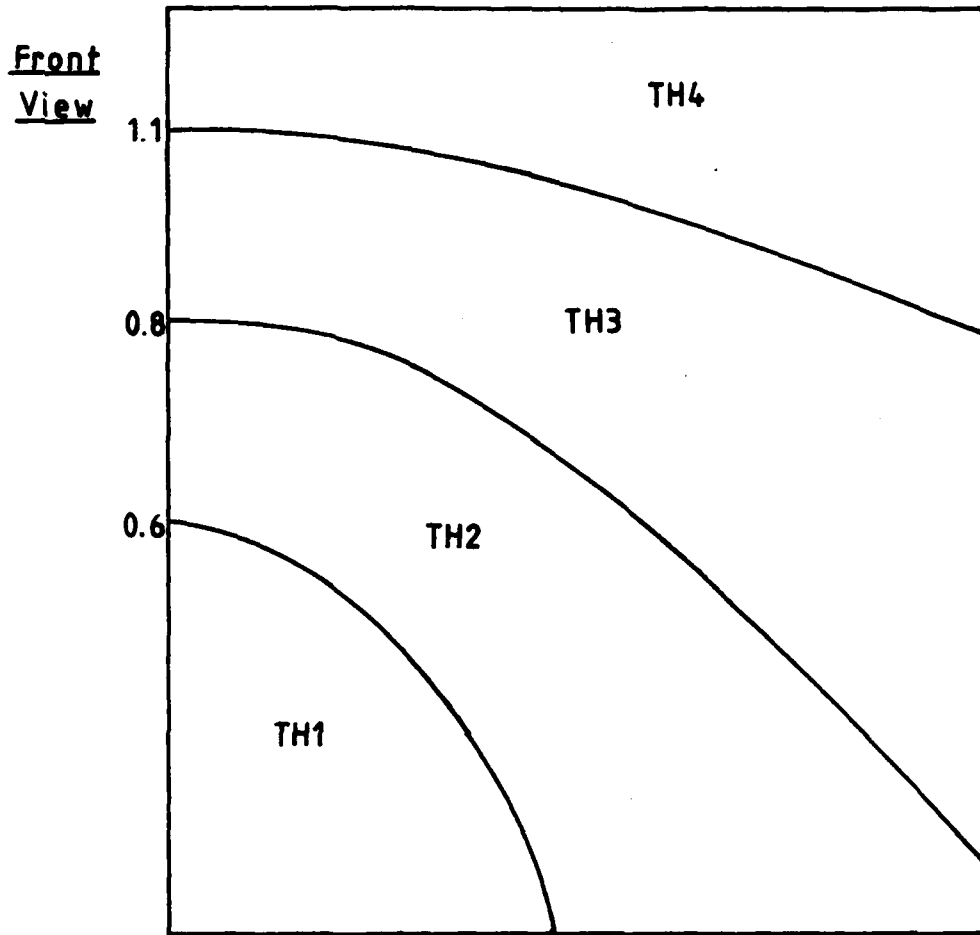


Even when the pressure gauge would fail under the blast, the arrival time of the blast was still recorded. The peak, intermediate and end times were averaged for each zone. The arrival time distribution and the equal percent pressure-time history zones are shown in Fig. 6. Equal pressure lines are labeled A-C, and equal percent pressure-time history zones are labeled TH1-TH4. Information on the peak, intermediate, and end times for each of the zones is given in Table 2.

Abaqus allows the user to input the peak load and pressure-time history independently, so that the peak load and pressure-time zones did not have to coincide, and they do not, as shown in Fig. 5 and Fig. 6. Also a maximum time step of 0.2 msec was chosen for the first 5 msec, which completely covered the time of loading for all of the elements, and a maximum time step of 1 msec was chosen for the next 20 msec, for a total analysis time of 25 msec. Abaqus uses a modified Newmark method. The default damping coefficient was used.

#### V. RESULTS:

The data obtained from Abaqus was much too extensive to permit all but a very general description of the results. Both models were producing preliminary results at the end of the ten week program. Fig. 7 shows the displaced shape of the back face of the wall shortly after the blast hit the bottom of the wall. While results were obtained only for the first five msec, it seems that both models were considerably stiffer than necessary.



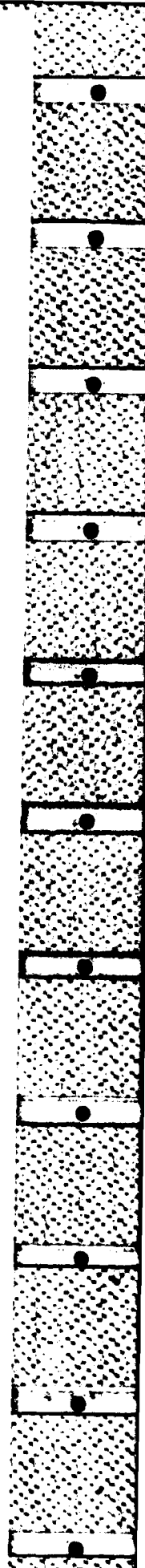
TH1- 0.6 msec

TH2- 0.7 msec

TH3- 1.0 msec

TH4- 1.2 msec

**FIG.6 Arrival Time Distribution**



DISPL  
MAG. FACTOR =  $+4.7E+19$   
SOLID LINES - DISPLACED MESH  
DASHED LINES - ORIGINAL MESH

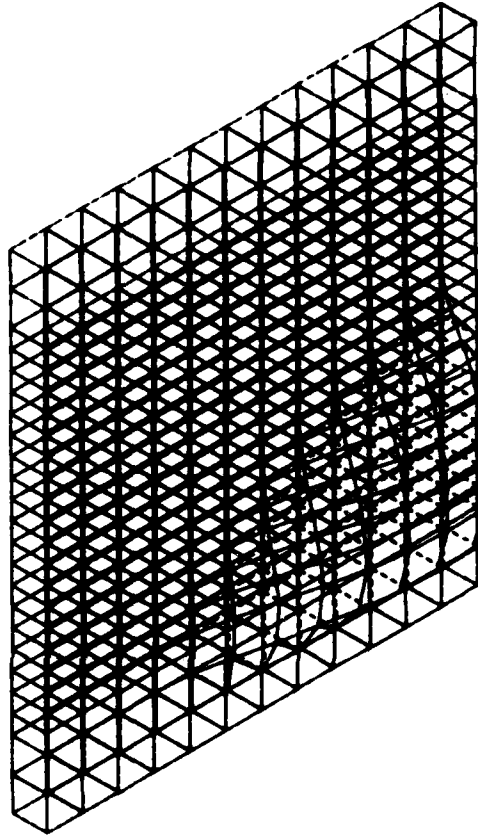


FIG.7 Back Layer of Elements at 0.65 msec

Displacements were approximately a tenth of what was expected from the results of the blast tests, and the period of the vibrations was smaller as well. This could be due to several reasons. The maximum time increment used in Abaqus, 0.2 msec, would have allowed the program to miss the peak pressures applied on the wall. Missing the peak by even a short time drastically reduces the loading. To correct this, a maximum time increment of 0.1 msec for the first 1.8 msec should be tried, followed by another step with a maximum time increment of 0.2 msec until approximately 5 msec, which more than covers the time of loading in all of the pressure-time history curves. Lastly, a final step should be added, one with a maximum time increment of 1 msec for the next 20 msec. This would make a final analysis time of 25 msec, half the time for which data is recorded in the blast tests. Also, since the period appeared to be shorter than expected, a reduction factor might be applied to the Young's modulus of both the concrete and the steel. A series of runs might be made to determine if an appropriate correction factor is the same for all percentages of steel used.

However, some conclusions can be drawn from the preliminary data supplied by Abaqus. First of all, it seems reasonable to predict that some cracking would occur at the wall-roof joint. This prediction is based on a much enlarged computer drawing (too large to include in this paper) of the displaced structure showing a marked tendency of the joint to rotate, even though

the back face was fixed. Also, it seems reasonable to predict interior spalling at the bottom of the wall, based on the displacement pattern which showed much greater displacements at the bottom of the wall. More work needs to be done in determining a good method of predicting spalling.

VI. RECOMMENDATIONS:

First of all the author would recommend that the Engineering and Services Center check with either Control Data or Hibbet, Karlsson and Sorensen, the developers of Abaqus, for a sizing routine so that in the future the routine could be used to aid in sizing a problem to fit the computer. Secondly, the author would recommend not attempting to use the SINGLE parameter in defining rebars since the program did not want to accept the parameter. Instead the default parameter should be used. While this defines a layer of rebars, a single rebar may be defined with this option by setting the spacing to be larger than the size of the element.

**1984 USAF-SCEEE GRADUATE STUDENT SUMMER SUPPORT PROGRAM**

**Sponsored by the**

**AIR FORCE OFFICE OF SCIENTIFIC RESEARCH**

**Conducted by the**

**SOUTHEASTERN CENTER FOR ELECTRICAL ENGINEERING EDUCATION**

**FINAL REPORT**

**ANALYSIS OF THE J-79, J-57, AND TF-33 JOB ANALYSIS  
QUESTIONNAIRE ASSESSING TASK DIFFICULTY**

<b>Prepared by:</b>	<b>Michael D. Covert</b>
<b>Academic Department:</b>	<b>Psychology</b>
<b>University:</b>	<b>The Ohio State University</b>
<b>Research Location:</b>	<b>Air Force Human Resources Laboratory</b>
<b>USAF Research Contact:</b>	<b>LTC Rodger Ballentine</b>
<b>SFRP Supervising Faculty Member:</b>	<b>Dr Robert Vance, Assistant Professor</b>
<b>Date:</b>	<b>28 September, 1984</b>
<b>Contract No:</b>	<b>F49620-82-C-0035</b>

ANALYSIS OF J-79, J-57, AND TF-33 JOB ANALYSIS  
QUESTIONNAIRE ASSESSING TASK DIFFICULTY

by

Michael D. Coovert

Abstract

A very specific job analysis questionnaire was developed in order to measure relative difficulty of specific tasks on three different engines. Descriptive statistics were run comparing specific items with their more general item form found on the CODAP surveys. A between engine difference was found on phase two tasks, with J-79 tasks being rated more difficult than the tasks for the J-57 and the TF-33. Additionally, descriptive statistics were utilized to compare the specific tasks to the more generalized form found on the CODAP Surveys. There appears to be only small differences between the specific versus the more general item forms.

Acknowledgement

The author would like to thank the Air Force Systems Command, the Air Force Office of Scientific Research and the Southeastern Center for Electrical Engineering Education for providing him with an opportunity to spend a very beneficial and enjoyable summer at the Air Force Human Resources Laboratory, Brooks AFB, TX. He would like to thank LTC Rodger Ballentine, Dr Bruce Gould, Lt Joe Taylor, Capt Jack Blackhurst, and Dr Bob Vance for their suggestions and guidance.

Special thanks go to Joe Taylor and Bob Vance for the many enjoyable lunch hours which truly aided this project.

## I. Introduction

This study is a very small piece of a much larger Air Force project that calls for the development of measurement techniques which will allow for the collection of valid, accurate, and reliable hands-on performance information that can be related to recruit capabilities. Of the jet engine mechanics in the Air Force, a good portion work with one of three specific engines, the J-79, J-57, or the TF-33. General task data describing the Jet Engine Mechanic is maintained in the Occupational Survey Research data base.

The purpose of this project was to discern the answer to a couple of different questions. First, are the tasks in the Occupational Survey Research data base too general to be of use in developing specific measures of performance? Second, is there a great enough variation between the specific engine types to warrant developing specific tests for each engine type?

## II. Objectives of the Research Effort

The primary objectives of the research effort were to provide descriptive statistics assessing the similarity between: (1) the task difficulty survey items and the CODAP survey items and (2) the engine specific items and the general or "mother" items from the CODAP survey. A third objective was to assess the specific differences between the engines in terms of task difficulty ratings.

## III. Comparison of Task Difficulty with CODAP

The scale used in this study is the same scale used for collecting occupational data. Task difficulty is defined in terms of the amount of time required to learn to do the task satisfactorily. The scale point anchors are as follows: 1=extremely low, 2=very low, 3=low, 4=below average, 5=average, 6=above average, 7=high, 8=very high, 9=extremely high.

One purpose of the study was to examine the relationship of the engine specific task statement on the task difficulty survey, with the more general task statement ("mother" item) from the original CODAP data base. Table 1 below presents a side by side comparison of the task difficulty survey means and CODAP means, standard deviations, and rank-order within phases. The task statements are clustered according to phase as they appeared on the task difficulty survey. The general task statements are identical to the task statements that appeared on the original CODAP survey. Phase one tasks are also tasks performed on all three engines, yet more specific than the general CODAP task statements. Phase two and phase three tasks are engine specific. Phase three tasks are also clustered by functional area, that is, if they are performed in the shop or out on the flightline.

GENERAL

CODAP	T.D.		T.D.			CODAP		
			MEAN	S.D.	RANK	MEAN	S.D.	RANK
159	4	Align installed engine	5.29	1.38	15	5.23	1.33	15
194	5	Apply protective coatings to engines or engine parts	3.43	1.52	32	3.50	1.49	33
196	6	Assemble or disassemble turbine units	6.27	1.39	2	5.68	1.30	4
199	10	Blend compressor or turbine blades	5.07	1.53	18.5	5.03	1.37	19
288	11	Blend inlet blades	5.07	1.53	18.5	5.10	1.48	17
290	14	Clean engines	3.65	1.45	31	3.97	1.38	29
206	23	Inspect fuel manifolds or nozzles	5.85	1.32	10	5.16	1.27	16
296	41	Inspect combustion chambers	5.41	1.05	13	5.08	1.31	18
299	42	Inspect engine exhaust cones	4.74	1.14	21	4.58	1.32	22
203	43	Inspect engine oil seals	5.15	1.41	17	4.78	1.38	21
270	46	Inspect test cells not equipped with noise suppressor	6.29	1.11	1	5.56	1.31	6
167	47	Inspect screens on aircraft engines	5.05	1.36	20	4.56	1.48	24
211	48	Inspect turbine rotors	5.64	1.21	11	5.37	1.49	11
311	49	Inspect vibration analyzers	5.92	1.56	9	5.28	1.25	14
322	98	Isolate malfunctions in engine inlet guide vane (IGV) systems	6.15	1.33	5	6.11	1.33	2
314	99	Isolate malfunctions in engine afterburner systems	6.26	1.25	3	6.19	1.56	1
316	100	Isolate malfunctions in engine bleed air systems	6.07	1.21	7	5.51	1.38	7
321	101	Isolate malfunctions in engine ignition systems	5.49	1.36	12	5.66	1.12	5
327	102	Isolate malfunctions in engine RPM indicating system	4.69	1.31	23	5.36	1.40	12

339	103	Maintain special tools	4.22	1.44	27	4.57	1.15	23
131	105	Make entries on oil analysis request forms (DD Form 2026)	4.11	1.62	28	4.48	1.42	25
135	106	Make entries on Servicable Tag or Servicable Label forms (DD Form 1574 or DD Form 1574-1)	3.89	1.27	30	4.35	1.50	27
142	107	Make entries on Unservicable (Reparable) Tag or Label forms (DD Form 1577-2 or DD Form 1577-3)	3.98	1.34	29	4.31	1.53	28
223	108	Mark engine containers	3.20	1.26	34	3.36	1.60	34
177	109	Perform home station checks on installed engines	4.72	1.03	22	5.47	1.44	9
274	114	Preserve or depreserve engine fuel systems	4.58	1.49	25	4.94	1.22	20
344	115	Pressure check engines prior to operation	4.64	1.27	24	3.59	1.48	30
345	116	Read or record engine operation data	5.22	1.25	16	3.57	1.45	31
364	125	Remove or install Inlet Guide Vane (IGV) system components	5.32	1.17	14	5.40	1.29	10
354	126	Remove or install engine bleed valve seals	4.47	1.29	26	4.42	1.19	26
186	127	Remove or install engines in aircraft	6.13	1.33	6	5.82	1.23	3
356	128	Remove or install fuel system components	6.00	1.41	8	5.50	1.10	8
382	129	Remove or install variable nozzle system components	6.17	1.27	4	5.31	1.24	13
391	132	Seal engine openings	3.11	1.52	35	3.52	1.58	32
395	139	Take spectrometric oil analysis samples	3.30	1.36	33	3.14	1.55	35

PHASE I

CODAP	T.D.		T.D.		CODAP	
			MEAN	S.D.	MEAN	S.D.
302	15	Conduct operator serviceability inspections on 4100A trailers	4.64	1.54	4.27	1.37
145	40	Inspect areas for foreign object damage (FOD) matter	4.78	1.67	4.92	1.56
300	44	Inspect engine or accessory spines	5.26	1.26	4.69	1.39
301	45	Inspect engine plumbing	4.96	1.25	4.75	1.38
373	88	Install lockwire	3.24	1.40	4.30	1.48
343	110	Place protective covers on engines	2.50	1.31	2.89	1.64
397	142	Transport engines to work sections	3.00	1.28	3.31	1.52
130	104	Make entries on AFTO Forms 349 (Maintenance Data			4.54	1.55
134		Collection Record) AFTO Forms 350 (Reparable Item			4.45	1.49
127		Processing Tag), or AFTO Forms 781 A (Maintenance			4.59	1.42
		Discrepancy and Work Document)	4.31	1.80	4.53	1.49
394	136	Service J-79 engine starters	3.12	1.40	3.59	
394	134	Service J-57 engine starters	3.09	1.38		1.43
394	137	Service TF-33 (P7) engine starters	3.05	1.43		
375	73	Install J-79 engine tachometer generators	3.68	1.29	3.97	
375	61	Install J-57 engine tachometer generators	3.64	1.31		1.41
375	80	Install TF-33 (P7) engine tachometer generators	3.56	1.37		
352	71	Install J-79 engine starters	4.43	1.13		
352	60	Install J-57 engine starters	4.47	.99	4.68	1.21

352	79	Install TF-33 (P7) engine starters	4.58	.98	8
297	31	Inspect J-79 engine first stage compressors	5.29	1.26	1
297	25	Inspect J-57 engine first stage compressors	4.8	1.33	5
297	36	Inspect TF-33 (P7) engine first stage compressors	5.18	1.13	3

PHASE II - J-79

CODAP	T.D.		T.D.			CODAP		
			MEAN	S.D.	RANK	MEAN	S.D.	RANK
363	69	Install J-79 engine ignition exciter boxes	4.64	1.25	7	4.66	1.06	6
360	66	Install J-79 engine exhaust gas temperature thermocouple harnesses	5.40	1.11	5	4.47	1.19	5
353	68	Install J-79 engine forward top anti-icing ducts	4.80	1.03	6	4.65	1.21	7
374	72	Install J-79 engine starter adapter pads	3.83	1.41	8	4.53	1.45	8
351	65	Install J-79 engine constant speed drives (CSD)	6.22	1.11	3	5.31	1.22	3
387	131	Rig J-79 engine inlet guide vane systems	6.86	1.41	1	6.09	1.16	1
385	130	Rig J-79 afterburner components	6.59	1.30	2	5.80	1.17	2
348	63	Install J-79 engine afterburner secondary flaps	5.81	1.10	4	5.16	1.01	4

PHASE II - J-57

<u>CODAP</u>	<u>I.D.</u>		<u>I.D.</u>		<u>CODAP</u>	
			<u>MEAN</u>	<u>S.D.</u>	<u>MEAN</u>	<u>S.D.</u>
363	56	Install J-57 engine ignition exciter boxes	4.53	1.31	4.66	1.06
360	53	Install J-57 engine exhaust gas temperature thermocouple harnesses	4.73	1.00	4.79	1.19
353	50	Install J-57 engine anti-icing valves	4.89	1.23	4.65	1.21
374	59	Install J-57 engine starter control valves	4.67	1.00	4.53	1.15
359	58	Install J-57 engine pressure ratio probes	4.43	1.02	4.88	1.18
396	10	Transfer J-57 engines from 4100 stands to 3010 trailers	3.64	1.46	3.66	1.52
208	27	Inspect J-57 engine oil cooler and tab assemblies	5.18	1.17	5.42	1.34
351	119	Remove J-57 engine oil coolers	5.38	1.40	5.31	1.22

15-10

PHASE II - TF-33

<u>CODAP</u>	<u>I.D.</u>		<u>I.D.</u>		<u>CODAP</u>	
			<u>MEAN</u>	<u>S.D.</u>	<u>MEAN</u>	<u>S.D.</u>
363	75	Install TF-33 (P7) engine ignition exciter boxes	4.13	1.16	4.66	1.06
360	76	Install TF-33 (P7) engine exhaust gas temperature thermocouple harnesses	4.43	1.04	4.79	1.19

353	84	Install TF-33 (P7) engine nacelle anti-icing control valves	4.75	1.13	1.5	4.65	1.21	5
374	78	Install TF-33 (P7) engine starter control valves	4.58	.98	3	4.53	1.15	6
359	77	Install TF-33 (P7) engine pressure ratio probes	4.21	1.11	5	4.88	1.18	2
396	141	Transfer TF-33 (P7) engines from 4100 stands to 3000 trailers	3.73	1.50	8	3.66	1.52	8
351	74	Install TF-33 (P7) constant speed drive (CSD) oil tanks	4.75	1.19	1.5	5.31	1.22	1
393	138	Service TF-33 (P7) engine constant speed drive (CSD) oil tanks	3.05	1.39	9	3.56	1.41	9
370	124	Remove TF-33 (P7) engine forward cowl doors	3.90	1.23	7	4.12	1.44	7

PHASE III - J-79/SHOP

CODAP	I.D.		T.D.			CODAP		
			MEAN	S.D.	RANK	MEAN	S.D.	RANK
210	32	Inspect J-79 engine first stage turbine nozzle vanes	5.64	1.42	7	5.21	1.33	8
229	143	Wrap engines for shipment by air	3.72	1.49	11	4.54	1.24	11
239	67	Install J-79 engine forward and rear number 3 oil seals	6.11	1.02	1.5	5.72	1.37	3.5
238	70	Install J-79 engine number 3 bearings	6.11	1.21	1.5	6.26	1.31	1.5
349	64	Install J-79 engine bleed air system collector bowls	5.50	1.37	8.5	4.98	1.03	9
234	62	Install J-79 engine afterburners	5.50	1.25	8.5	4.82	1.17	10
208	33	Inspect J-79 engine starters, oil lines, and oil coolers	5.00	.99	10	5.42	1.34	6
201	30	Inspect J-79 engine bearings	5.93	1.31	6	5.27	1.44	7

235	120	Remove J-79 engine front gear boxes	5.98	1.39	4	5.53	1.16	5
238	121	Remove J-79 engine number 3 bearings	5.97	1.13	5	6.26	1.31	1.5
247	122	Remove J-79 engine turbine rotors	6.00	1.03	3	5.72	1.33	3.5

PHASE III - J-57/SHOP

CODAP	T.D.		T.D.			CODAP		
			MEAN	S.D.	RANK	MEAN	S.D.	RANK
210	26	Inspect J-57 engine first stage turbine nozzle vanes	5.41	1.52	6	5.21	1.33	6
229	143	Wrap engines for shipment by air	3.72	1.49	8	4.54	1.24	7
289	12	Clean J-57 engine parts using cleaners other than ultrasonic cleaners	3.82	1.26	7	4.19	1.43	8
238	57	Install J-57 engine number 4 1/2 inner races and bearings	6.15	1.20	2	6.26	1.31	1.5
247	54	Install J-57 engine front compressor drive turbines	6.15	1.20	2	5.72	1.33	3.5
346	55	Install J-57 engine fuel pumps	5.84	1.19	5	5.43	1.24	5
247	117	Remove J-57 engine front compressor drive turbines	6.15	1.12	2	5.72	1.53	3.5
238	118	Remove J-57 engine number 4 1/2 inner bearings and races	5.90	1.03	4	6.26	1.31	1.5

PHASE III - TF-33/SHOP

CODAP	T.D.		T.D.		CODAP	
			MEAN	S.D.	MEAN	S.D.
210	38	Inspect TF-33 (P7) engine first stage turbine nozzle vanes	5.43	1.30	5.21	1.33
229	143	Wrap engines for shipment by air	3.72	1.49	4.54	1.24
289	13	Clean TF-33 (P7) engine parts using cleaners other than ultra-sonic cleaners	3.68	1.25	4.19	1.43
238	83	Install TF-33 (P7) engine inner races and number 4 1/2 bearings	6.03	1.36	6.26	1.31
239	85	Install TF-33 (P7) engine number 6 oil seals	5.66	.97	5.72	1.37
346	86	Install TF-33 (P7) engine thrust reversal pumps	5.00	1.32	5.43	1.24
247	87	Install TF-33 (P7) engine turbine rotors	6.26	1.34	5.72	1.33
349	81	Install TF-33 (P7) engine bleed air system actuator and control assemblies	5.21	.98	4.98	1.03
240	82	Install TF-33 (P7) engine first stage fan sections	6.11	1.26	5.90	1.35
208	39	Inspect TF-33 (P7) engine nose cowls and hydraulic pumps	5.08	.84	5.42	1.34
247	123	Remove TF-33 (P7) engine turbine rotors	5.94	1.14	5.72	1.33

PHASE III - J-79/FLIGHTLINE

CODAP	I.D.		I.D.			CODAP		
			MEAN	S.D.	RANK	MEAN	S.D.	RANK
286	2	Adjust operating J-79 engines	4.54	1.64	9	5.66	1.44	4
292	17	Connect JET CAL test equipment to J-79 engines	5.15	1.46	8	4.34	1.36	10
325	20	Determine source of high oil consumption on J-79 engines	6.12	1.38	3	5.87	1.42	3
165	29	Inspect J-79 aircraft throttle controls for freedom of movement	5.46	1.50	6	5.10	1.31	7
303	34	Inspect J-79 engines before or after operation	5.44	1.28	7	5.05	1.36	8
328	94	Isolate J-79 engine starter system malfunctions when engine fails to rotate	5.48	1.41	5	5.25	1.25	6
181	111	Position 4000A stands for J-79 engine removals or installations	4.45	1.64	10	4.02	1.47	11
393	135	Service J-79 engine oil systems	3.49	1.44	12	4.56	1.41	12
162	7	Attach J-79 engines to 4000A trailers	4.14	1.22	11	5.47	1.44	5
319	93	Isolate J-79 engine fuel system malfunctions when there is low fuel flow and the starting speed is reached but there is no start	6.42	1.47	1	6.44	1.20	1
349	64	Install J-79 engine bleed air system collector bowls	5.50	1.37	4	4.98	1.03	9
318	92	Isolate J-79 engine exhaust gas temperature malfunctions	6.37	1.22	2	6.03	1.41	2

PHASE III - J-57/FLIGHTLINE

CODAP	T.D.		T.D.			CODAP		
			MEAN	S.D.	RANK	MEAN	S.D.	RANK
286	1	Adjust operating J-57 engines using a screwdriver	3.81	1.44	12	5.66	1.44	4
292	16	Connect JET CAL test equipment to J-57 engines	5.05	1.34	9	4.34	1.36	11
325	19	Determine source of high oil consumption on J-57 engines	6.16	1.38	1	5.84	1.42	3
165	24	Inspect J-57 aircraft throttle controls for freedom of movement	5.25	1.26	8	5.10	1.31	7
303	28	Inspect J-57 engines before or after operation	5.33	1.36	5.5	5.05	1.36	8
328	90	Isolate J-57 engine starter system malfunctions when the engine fails to rotate	5.33	1.04	5.5	5.25	1.25	6
181	112	Position 4100 stands for J-57 engine removals or installations	4.00	1.47	11	4.02	1.47	12
171	91	Isolate J-57 engine-to-aircraft throttle rigging system malfunctions when throttle is out of alignment	6.12	1.23	3	6.30	1.28	2
349	51	Install J-57 engine bleed air system actuator and control assemblies	5.27	1.36	7	4.98	1.03	9.5
393	133	Service J-57 engine oil systems	3.02	1.39	14	3.56	1.41	14
319	89	Isolate J-57 engine fuel system malfunctions when the engine fails to obtain combustion	6.14	1.28	2	6.44	1.20	1
293	22	Drain J-57 fuel filters	3.44	1.35	13	3.58	1.45	13

349	52	Install J-57 engine bleed air system governors	5.53	1.24	4	4.98	1.03	9.5
162	9	Attach a sling and hoist to J-57 engines on a B52G aircraft	4.30	1.35	10	5.47	1.45	5

PHASE III - TF-33/FLIGHTLINE

CODAP	T.D.		T.D.			CODAP		
			MEAN	S.D.	RANK	MEAN	S.D.	RANK
286	3	Adjust operating TF-33 (P7) engines using a screwdriver	4.24	1.58	9	5.66	1.44	4
292	18	Connect JET CAL test equipment to TF-33 (P7) engines	5.05	1.35	8	4.34	1.36	10
325	21	Determine source of high oil consumption on TF-33 (P7) engines	6.13	1.36	2	5.87	1.42	3
165	35	Inspect TF-33 (P7) aircraft throttle controls for freedom of movement	5.08	1.32	7	5.10	1.31	7
303	37	Inspect TF-33 (P7) engines before or after operation	5.26	1.23	4	5.05	1.36	8
328	96	Isolate TF-33 (P7) engine starter system malfunctions when engine fails to rotate	5.18	1.33	6	5.25	1.25	6
181	113	Position 4100 stands for TF-33 (P7) engine removals or installations	3.95	1.55	11	4.02	1.47	11
171	97	Isolate TF-33 (P7) engine-to-aircraft throttle rigging system malfunctions when throttle is out of alignment	5.92	1.26	3	6.30	1.28	2

349	81	Install TF-33 (P7) engine bleed air system actuator and control assemblies	5.21	.98	5	4.98	1.03	9
162	8	Attach TF-33 engines to 4100 trailers	4.15	1.04	10	5.47	1.44	5
319	95	Isolate TF-33 (P7) engine fuel system malfunctions when engine fails to obtain combustion and there is an indication of fuel flow	6.17	1.37	1	6.44	1.20	1

Table 1. Means, standard deviations, and rank-orders of the task difficulty ratings and the original CODAP ratings.

Examination of Table 1 reveals that with few exceptions there does not appear to be large differences between the original CODAP rating of a task and the task difficulty level reported on this survey. Likewise, with few exceptions, the rank-order of items between the two forms is preserved.

Another useful way to examine the relative difficulty of groups of tasks is to collapse over individual items and obtain an average difficulty level for a group of items.

Table 2 presents the mean task difficulty of tasks in a phase as well as the standard deviations of those means.

	MEAN							
			J-79		J-57		TF-33	
	T.D.	CODAP	T.D.	CODAP	T.D.	CODAP	T.D.	CODAP
GENERAL	4.99	4.84						
PHASE I	4.08	4.31						
PHASE 2			5.52	5.12	4.68	4.73	4.17	4.46
PHASE 3/SHOP			5.59	5.43	5.39	5.42	5.28	5.37
PHASE 3/FLIGHTLINE			5.21	5.15	4.91	5.04	5.12	5.32
S.D.								
	.97	.82						
	.88	.66						
			1.05	.58	.53	.54	.55	.58
			.71	.55	1.03	.75	.89	.61
			.91	.84	1.03	.91	.77	.74

Table 2. Means and standard deviations by phase and engine type of the task difficulty survey and the original CODAP survey.

IV. Differential Difficulty according to engine type.

As can be seen from inspection of the above means, the J-79 appears to be a more difficult engine in terms of the amount of time it takes

to learn the tasks. To explore this question empirically, the average of all the tasks for each engine type within a phase was computed for each of the 46 jet engine mechanics who completed the task difficulty survey.

Three within subjects one-way analysis of variances were performed for phase two, phase three/shop, and phase three/flightline tasks. The ANOVA's were 1 (phase) X 3 (engine type: J-79, J-57, and TF-33). Table 3 presents the summary tables for each of the three ANOVA's.

ANOVA Summary table on averaged task means across engine types for phase two tasks.

<u>Source</u>	<u>SS</u>	<u>DF</u>	<u>MS</u>	<u>F</u>	<u>p</u>
Phase II	44.07	2	22.03	11.47	.0001
Error	172.90	90	1.92		
Mean	2728.85	1	2728.85		
Error	121.13	45	2.69		

ANOVA Summary table on averaged task means across engine types for phase three shop tasks.

<u>Source</u>	<u>SS</u>	<u>DF</u>	<u>MS</u>	<u>F</u>	<u>p</u>
Phase 3-Shop	2.07	2	1.03	2.14	N.S.
Error	43.52	90	.48		
Mean	3749.92	1	3749.92		
Error	101.92	45	2.26		

ANOVA Summary table on averaged task means across engine types for phase three flightline tasks.

<u>Source</u>	<u>SS</u>	<u>DF</u>	<u>MS</u>	<u>F</u>	<u>p</u>
Phase					
3-Flightline	3.08	2	1.54	.83	N.S.

Error	166.55	90	1.85
Mean	3125.90	1	3125.90
Error	108.81	45	2.42

Table 3. ANOVA summary tables for each of the 1 (phase) X 3 (engine type) ANOVA's which were performed.

The only significant ANOVA was for the phase two tasks. This indicates that learning to perform the phase two tasks are significantly more difficult for the J-79 than for either the J-57 or the TF-33 jet engine (refer again to table 2 for the means).

V. Comparison with 'mother' task statements.

Another major focus of this project was to compare the more specific task difficulty task statements with the more general 'mother' task statement as it appears in the CODAP data base. This is done in order to help determine if it is worthwhile to develop the more specific task difficulty surveys for other AFSC's. Table 4 presents the 'mother' task statements along with their task statement number, mean, and rank ordering. Also presented are the task statement number, mean, and rank order of the tasks by engine types as they appeared on the task difficulty survey.

**TASK STATEMENT**

**MOTHER**

**J-79**

**J-57**

**TF-33**

Install engine ignition exciter boxes	363	4.66	22	69	4.68	18	56	4.53	18	75	4.13	24
Install engine exhaust gas temperature thermocouple harness	360	4.79	20	66	5.40	14	53	4.73	16	76	4.43	20
Install anti-icing equipment	353	4.65	23	68	4.80	17	50	4.89	14	84	4.75	16.5
Install engine starter equipment	374	4.53	24	72	3.83	23	59	4.67	17	78	4.58	18.5
Install engine pressure ratio probes	359	4.88	10				58	4.43	20	77	4.21	22
Transfer engine from 4100 stands to 3000 series trailers	396	3.66	28				140	3.64	24.2	141	3.73	26
Install constant speed drives	351	5.31	11	65	6.22	2				74	4.74	16.5
Inspect first stage turbine nozzle vane	210	5.21	14	32	5.64	8	26	5.41	8	38	5.43	7
Install engine bearings	238	6.26	2.5	70	6.11	4.5	57	6.15	3	83	6.03	4
Install engine oil seals	239	5.72	6	67	6.11	4.5				85	5.66	6
Install fuel pumps	346	5.43	10				55	5.84	7	86	5.00	15
Install turbine rotors	247	5.72	6				54	6.15	3	87	6.26	1
Install bleed air system	349	4.98	17.5	64	5.50	9.5				81	5.21	9.5
Remove turbine rotors	247	5.72	6	122	6.00	6	117	6.15	3	123	5.94	5
Remove engine bearings	238	6.26	2.5	121	5.97	7	118	5.90	6			
Adjust operating engine	286	5.66	8	2	4.54	19	1	3.81	23	3	4.24	21
Connect JET CAL test equipment	292	4.34	25	17	5.15	16	16	5.05	13	18	5.05	14
Determine source of high oil consumption	325	5.87	4	20	6.12	3	19	6.16	1	21	6.13	3
Inspect throttle controls for freedom of movement	165	5.10	15	29	5.46	12	24	5.25	12	35	5.08	13
Inspect engines before or after operation	303	5.05	16	34	5.44	13	28	5.33	9.5	37	5.26	8



'mother' task

J-79 specific	.811
J-57 specific	.830
TF-33 specific	.800

Table 5. Correlations between the engine specific tasks and the more general 'mother' task.

A final correlation which is of interest is one between the 35 items that are identical on both the original CODAP survey and the specific task difficulty survey (the general items listed in table 1). The correlation is .851. Given the different populations surveyed and the different instructions on the two surveys, this is a very high correlation.

VI. Recommendations

Generally, there are only minor differences between the ratings provided on the task difficulty survey and the original survey items. The mean differences and rank order of items fluxuated very little with additional support being provided by the high correlations between the 'mother' task items and the engine specific task items. There are between engine differences with the J-79 being more difficult than either the J-57 or the TF-33. This difference is significant, however, only on the phase two tasks.

Given the results of these analyses, this author recommends that tasks should be selected to be as comparable as possible across engines, with the slight increase in difficulty of the J-79 tasks being allowed to propagate through to the actual performance test. This ensures the performance measurement tasks will be as face valid as possible across engines, yet will still reflect the real world differences between the engines.

A final recommendation for further work is to artificially constrain parts of the data set and then try to predict both the task

difficulty ratings of general items and the differential difficulty of the task between engine types. This would allow preliminary inferences to be made regarding the utility of the more specific task difficulty data versus the more general CODAP data.

1984 USAF-SCEEE GRADUATE STUDENT SUMMER SUPPORT PROGRAM

Sponsored by the

AIR FORCE OFFICE OF SCIENTIFIC RESEARCH

Conducted by the

SOUTHEASTERN CENTER FOR ELECTRICAL ENGINEERING EDUCATION

FINAL REPORT

THE PHYSIOLOGIC CHARACTERIZATION, PREDICTION, AND BIOFEEDBACK  
TREATMENT OF MOTION SICKNESS

Prepared by:	William E. Czelen, M.D.
Academic Rank:	Asst. Resident Instructor/Physician
Department and University:	Department of Community/Aerospace Medicine Wright State University School of Medicine
Research Location:	USAF School of Aerospace Medicine/ Brooks AFB/AFIT/WPAFB
USAF Research Contact:	Col. David R. Jones/SAM
SFRP Supervising Faculty Member:	Dr. Matthew Kabrisky/Prof./AFIT
Date:	September 6, 1984
Contract No.	F49620-82-C-0035

THE PHYSIOLOGIC CHARACTERIZATION, PREDICTION, AND BIOFEEDBACK

TREATMENT OF MOTION SICKNESS

by

William E. Czelen, M.D.

ABSTRACT

This report describes an effort to more fully characterize the physiologic manifestations and variation induced by motion and motion sickness and is directed at providing an automated biofeedback system to treat the disorder in aircrew.

Work is underway on several facets of a multidisciplinary effort directed to medical considerations, biomedical design, engineering, computer hardware design, component interfacing, and software development. These energies are directed toward the acquisition and analysis of physiologic data to more effectively describe, predict, treat, and ultimately obviate motion sickness with biofeedback techniques.

The areas to be discussed in this report include:

1. ) A review of the general descriptors of motion sickness
2. ) Discussion of the incidence and susceptibility factors
3. ) The anatomical correlates of motion sickness
4. ) Overview of the motions causing the disorder
5. ) Current state of theories of motion sickness etiology
6. ) Current status of treatment/prevention regimens
7. ) Background of biofeedback applications
8. ) Biophysical, instrumentation and engineering considerations
9. ) System organization
- 10.) Current system status and required future effort

#### ACKNOWLEDGEMENT

The author would like to thank the Air Force Systems Command, the Air Force Office of Scientific Research and the Southeastern Center for Electrical Engineering Education for providing him the opportunity to have worked with an outstanding group of scientists, engineers, and physicians both at Brooks Air Force Base, San Antonio, Texas, and at Wright Patterson Air Force Base/Air Force Institute of Technology, Dayton, Ohio.

The author would also especially like to thank Dr. Matthew Kabrisky for generously sharing his laboratory and for his encouragement and collaboration.

## I INTRODUCTION

In the last few years, energy has been directed at an alternative approach to restore airsick aircrew to flight status. Researchers at Brooks AFB have successfully treated a group of motion-sick personnel with basic biofeedback techniques. Recently, work was begun by Brooks/AFIT on the implimentation of an automated version of a biofeedback/motion-sickness trainer. This research is an extension of that initial effort.

## II OBJECTIVES

The principal objective of this project is to develop the integrated hardware of an automated biofeedback trainer. This is to be done by 1.) identifying and studying the relevant physiologic parameters seen to be modulated by motion sickness, 2.) developing the transducers and signal precessing hardware to permit analysis of these signals, and 3.) combining these developments into a usable display and analysis system that would enable standardized operation of a patient-responsive therapeutic device.

## III REVIEW OF MOTION SICKNESS

Motion sickness, or motion maladaptation syndrome (11), a generic term describing sea sickness, air sickness, car sickness, or swing, camel, elevator, horse, simulator, cinerama and space sickness, is characterized by the symptom/sign complex of malaise, pallor, cold sweats, nausea and vomiting.

The onset and development typically follows a regular sequence beginning with stomach awareness. With the continuation of an unfamiliar motion stimulus, increasing nausea results, with the concomitant development of circumoral or facial pallor and cold sweats (in the anatomical regions usually concerned with thermoregulatory perspiration).

An accelerated period of advanced symptoms follows continued motion stimulation, the "avalanche phenomenon", with increased salivation, a feeling of warmth, lightheadedness, apathy, malaise, and depression, then finally retching and vomiting.

Many additional signs and symptoms of motion sickness have been reported and are more variably manifested. The signs include:

1. Cardiovascular manifestations of increase or decrease of pulse rate, rise or fall of blood pressure (BP), reduced peripheral blood circulation in the extremities, fingers, and skin of the head, and an increase of muscle blood flow. (Graybiel & Lackner felt there was no consistent relationship between BP and heart rate but nonetheless confirmed a lability in the BP )(19).

2. Respiratory changes of increased or slowed respiration and shallow breathing, with potential sighing or yawning, and violent diaphragmatic contractions with retching.

3. Gastrointestinal signs including inhibition of stomach motility and tone, duodenal spasm, inhibition of intestinal tone, salivation, swallowing, diarrhea or constipation, and passage of flatus or belching.

4. Hematologic signs which are numerous and variable and usually secondary or responses to other generalized or systemic changes.

5. Thermal signs that have included a fall in body temperature, and a fall of skin, mouth, and extremity temperature.

6. Ocular changes such as ocular imbalance, miosis, mydriasis during emesis, and prolonged nystagmus (in rotation induced motion sickness) (12).

7. An increase in skeletal muscle tension generally as a function of stress and tension. (2)

The spectrum of GI symptoms beyond nausea have included moist or dry mouth, epigastric discomfort or awareness, anorexia, and abdominal cramps. Vestibular symptoms include dizziness, disorientation, and vertigo. Central nervous system symptoms also seen are lethargy, somnolence, headache (particularly frontal), anxiety, a desire for fresh air, feelings of isolation, mental confusion, a desire for solitude, social indifference, and excessive sensitivity to sensations as sight, odors, temperature, and touch by clothing.

The bewildering array of signs and symptoms of vestibular disturbance has been divided into two categories by Graybiel. The first, of a reflex nature included: 1. tumbling sensation with coriolis stimulation, 2. coriolis oculogyral illusion (apparent motion sensed during head flexion out of a rotational plane), 3. coriolis nystagmus, 4. ataxia (as onboard a ship), and 5. dizziness.

The second category contained the symptoms or 'epiphenomena', superimposed

upon the first, due to unusual vestibular activity that "through a facilitory-inhibitory process, irradiates to cells not normally stimulated (17) (the chemoreceptor trigger zone or CTZ, the emetic center, area postrema, and hypothalamus). These are the symptoms that are absurd in terms of the organisms need; they make no contribution to restoring homeostasis.

The important implication of the preceding array of manifestations is the impact on performance and behavior. These complications include inactivity, being quiet and subdued, carelessness even in routine activities, measurable physical performance decrement in reflex tasks or interaction, poor time estimation, and reduced computational/mathematical performance.

#### INCIDENCE/SUSCEPTIBILITY TO MOTION SICKNESS

Motion sickness, the term used first by Irwin in 1881, is inducible in most normal subjects with sufficiently intense or prolonged stimulation.

Some examples of its incidence are 25-30% on Atlantic Ocean crossings, a .5-1% incidence in commercial airline travel, and up to an 8-10% incidence during 'moderately heavy' turbulence.

The incidence on trains has been .13% versus a greater than 3-4% estimate for automobile transportation.

Military trainees experience an incidence from 18% (pilots), and from 39% (in the United Kingdom) (11), to between 60 (20) and 66% (41) in student navigators. In current mission profiles at low altitude, the incidence of motion sickness in the increased turbulence is high among non-pilot crew members.

Motion sickness has resulted in an attrition rate of about 1% for pilots and 5% for navigators.

Motion sickness susceptibility is widely variable between individuals and species. Man is far from unique in his susceptibility to motion sickness. While dogs appear of similar susceptibility to man, a lesser but substantial degree is found in horses, cows, monkeys, chimpanzees, sheep, cats, seals, various birds such as chickens, and even codfish. Apparently immune, in spite of their highly developed vestibular organs, are most birds; as hens, pigeons, ducks and geese, as well as rabbits, guinea pigs, and hogs (41) (59).

It appears that children under 2 years of age and elderly people show lesser susceptibility than average. Also, from near 2 years old to adolescence, susceptibility seems increased. From age 17 to 39, susceptibility progressively falls. Females generally are more susceptible than males, even prior to menarche.

Time of day, interval since the last meal, and ambient air temperature have been found to have no influence on susceptibility (41).

Individual human susceptibility can be reliably predicted from experience based questionnaires and so be used as a screen to aircrew trainee selection (53). Recent studies of personality correlation with susceptibility, while showing no relation to introversion/extroversion on the Eysenck's Personality Inventory (EPI), did show a positive correlation with the neuroticism scale (61). Mirabile and Ford state that: "generally, individuals resistant to motion sickness are more involved in and determined by their immediate environment, while susceptible individuals are more autonomous and self contained" (39).

Reason suggests that motion sickness susceptibles may have a nervous system more 'receptive' to stimulation. He found that those reporting more past motion sickness experiences have a more prolonged after-effect to rotation after cessation of motion. He also found a consistently exaggerated estimate of loudness of tones, at a rate faster than the stimulus intensity increased (50).

#### MOTIONS RESPONSIBLE FOR MOTION SICKNESS

The variety of basic motions capable of causing motion sickness include vertical oscillation, rotation (particularly effective), counter-rotating room and slow-rotation room, all of which have been employed in studies on motion sickness induction.

Experiments with swings and vertical oscillators have demonstrated an optimal motion sickness induction at frequencies of from 15 to 22 cycles per minute, at an acceleration level of from .2 to .4 G with .36 G at the peak level of activity.

While McCauley and O'Hanlon (43) and others have found a peak incidence of motion sickness susceptibility at .17 Hz. (6 cycles/min.), Guinard and McCauley demonstrated a statistical increase in incidence with the addition of 2nd and 3rd (12 cycles/min & 18 cycles/min) harmonic elements to the motion environment.

Animal and human experiments have confirmed that complex motions combining

vertical and angular accelerations, linear accelerations in several planes simultaneously, or linear plus angular accelerations, are more effective than single component stimulation.

Interestingly, some changing accelerations do not cause motion sickness; horseback riding, sinusoidal angular rotations and simple violent accelerations. Guignard (21) states that oscillation above 1 Hz., even at severe intensities is not associated with motion sickness in man.

#### ANATOMICAL CORRELATES OF MOTION SICKNESS

Prior to discussion of the explanation and theories of motion sickness, the anatomically relevant organs in the syndrome will be reviewed.

Those organs, regions, and associations known or believed to play a role in motion sickness include 1.) the vestibular apparatus, its neural connections and associated nuclei, 2.) the cerebellum, 3.) the eyes and their associated motor nuclei, 4.) the brainstem centers related to emesis, 5.) well defined pathways from these regions and nuclei to all spinal segments, and even 6.) vague connections with the hypothalamus and cerebral cortex.

The components of the vestibular apparatus of interest are 1.) the three pairs of semicircular canals, 2.) the chambers of the utriculae and sacculae, and 3.) the eighth cranial (vestibular) nerve (with its bipolar cells derived from Scarpa's ganglion).

The semicircular canals consist of 2 sets of 3 mutually orthogonal lightly viscous endolymph filled canals, approximately in the basic planes of the extrinsic eye muscles. The sensory regions of the canals are called cristae ampullaris and gelatinous cupulae which project into the endolymph and are stimulated by angular acceleration motions. The endolymph deflects the cristae because, due to its inertial lag with a head rotation, it flows in a direction opposite to the head motion and bends the structure. The deflection of the cupula reaches an equilibrium after a change in stimulation within 20-30 seconds.

Under appropriate conditions, stimulation of each semicircular canal results in binocular movements of the eyes complimentary to apparent head movement. Also,

rightward accelerations result in leftward eye movements coupled with clockwise rotation, leftward accelerations produce eye movement to the right and counterclockwise rotation.

The second and third components, the utriculae and sacculae, each contain a 2 mm diameter region called the macula. This area in the utricle detects the orientation of the head with respect to gravity or inertial forces while the saccule may in addition be a sensor for vibration. The four maculae, in alternate planes, are composed of calcium carbonate crystals, the otoconia (with a specific gravity of 3), imbedded in a mucilagenous mass covering thousands of hair cells which connect to the vestibular nerve (1) (25). These nerve cells, firing at a baseline rate of about 15 Hz., change their 'firing' frequency, up or down with hair cell bending in response to an inertial force (25). The composite pattern of discharge forms the basis of the brain's perception of orientation. Otolith stimulation by forward or upward acceleration causes reflex downward eye movement (7).

The vestibular nerve terminates largely in the vestibular nuclei, located in the brainstem near the floor of the fourth ventricle. The labyrinth also appears to receive afferent fibers, which may play a similar role to the gamma efferents of the neuromuscular spindle (participating in control of tonus and reflex) (7). A notable portion of the fibers alternatively pass to the cerebellum and terminate in the flocculo-nodular lobe and adjacent vermian cortex. The cerebellum reciprocally connects to many vestibular components, the labyrinth, and vestibular nuclei, bilaterally.

The vestibular nuclei transmit to the spinal cord via the vestibulo-spinal tracts and assist in local myotactic reflexes to reinforce the tone of limb and trunk extensor muscles. They connect to the nuclei of cranial nerves III, IV, and VI (the cranial nerves controlling the eyes) via the MLF (medial longitudinal fasciculus) which enables eye fixation on stationary objects when the body turns. And finally, the vestibular nuclei connect to the pontine and brainstem reticular formation; very near the loci of the vomiting center and chemoreceptive trigger zone, and to the cerebral cortex through ill-defined pathways.

## THEORIES OF MOTION SICKNESS ETIOLOGY

Theories that attempt to explain the etiology of motion sickness must take into account the structures known to be vital in the production of the syndrome. The components are the peripheral vestibular organs and the vestibular nerve (individuals without intact vestibular apparatus or bilateral 8th nerve sectioning are immune to motion sickness), the vestibular nuclei, the nodulus and uvula of the cerebellum (75% of dogs with surgical extirpation of these components lost their vomiting response to motion) (15), the emetic center and CTZ (chemoreceptive trigger zone) of the brainstem, and the effector nerves and organs of the emetic response. The higher brain centers—the cerebral cortex, are not essential to the development of motion sickness, as decerebrate patients have developed the syndrome.

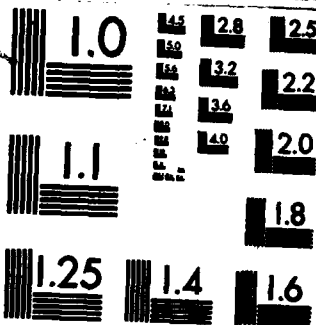
Also important to consider are those structures that are contributory but not essential to induce the syndrome. Significant here is the visual system. While blind subjects are equally susceptible to motion sickness (17), motion sickness may be induced solely through visual field movement as in cinerama sickness.

Adaptation must also be a primary element in the theory, since learned tolerance to motion is well established, as is symptom recurrence after cessation of stimulation (returning to land after a sea voyage (mal de demarqement) or earth sickness upon return from earth orbit).

The overstimulation concept does not account for the absence of motion sickness with some strong motion stimuli; nor the ready inducibility with head movement during rotation or simple caloric stimulation. The overstimulation theory also does not account for visual-field motion induced sickness.

The current theory which most comprehensively combines the above elements is the 'Neural Mismatch Theory'. Here, vestibular, visual, and proprioceptive information, at variance with what is expected from past experience, leads to symptoms. This mismatch is a function of 'sensory rearrangement', the term used by experimental psychologists to describe situations in which "information arriving at one set of sense receptors is systematically distorted to render it incompatible





MICROCOPY RESOLUTION TEST CHART  
 NATIONAL BUREAU OF STANDARDS-1963-A

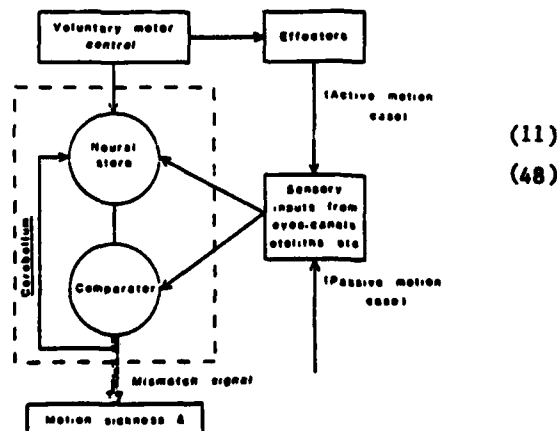
with that arriving at functionally related receptors" (49). The theory suggests that current sensory information is combined with a central memory or neural store in a comparator. When the compared signals are similar, all is well. In the presence of discoordinate information, an error or mismatch signal is generated.

There are six classical categories of sensory conflict in the sensory rearrangement schema capable of inducing motion sickness (49):

- a.) visual vs. vestibular rearrangement: as in looking out of the side window of a car or watching waves over the side of a ship
- b.) visual without vestibular stimulation: as in motion picture movement/acceleration or in vehicle simulators with a dynamic visual display
- c.) vestibular without visual stimulation: as in riding in an enclosed vehicle without external visual reference
- d.) canal/otolith rearrangement: as in exposure to cross coupled (coriolis) acceleration, or with rapid head movements in zero G
- e.) canal without otolith stimulation: as in caloric stimulation or pressure vertigo from ambient pressure change
- f.) otolith without canal stimulation: as in low frequency, < .5 Hz., vertical stimulation, or rotation about an earth horizontal axis at constant angular velocity (as on a barbecue spit).

The adaptive function of this signal is to reprogram the neural store, while the by-product of the error signal is the complex of neurovegetative responses of motion sickness. This error signal appears to initiate a stress-like response of the autonomic nervous system and leads to patterns, largely maladaptive, of somatic, visceral and sensory activity.

A graphical model of the components of the neural mismatch model follow:



Oman (44) has combined the prior concepts and temporal data to provide a mathematical model that accounts for the time course of evolution of motion sickness symptomatology, the slow and fast aspects of averaging dynamics, the concepts of delay and threshold, and the exponential response (the avalanche phenomenon) seen with protracted stimulation.

#### STATUS OF TREATMENT/PREVENTION REGIMENS

The current state of theory, prevention, recommendations and treatment for motion sickness revolve around experimental knowledge on the dynamics of adverse motion environments, and knowledge of the efficacy of anticholinergic and sympathomimetic drugs (63). (There is also experimental evidence demonstrating the existence in the vestibular nuclei of some neurons responsive only to acetylcholine and others responsive only to norepinephrine. (16) )

The pharmacologic therapies include prophylactic antihistamines such as promethazine and dimenhydrinate, parasympatholytics such as scopolamine, and sympathomimetics such as ephedrine and amphetamine. The combination of scopolamine and amphetamine, being synergistic (64), provide the greatest objective efficacy and increased tolerance to motion (63).

The most popularly promoted, and singularly effective, pharmacologic treatment/prevention for motion sickness currently is scopolamine administered transdermally prophylactically. Efficacy rates range from 67 to 75% (18) (47) (10), while the incidence of side effects (blurred vision and decreased alertness) is nearly as great, progressing over time to greater than 50% overall. (27) It has also been anecdotally reported that a high frequency of disorientation, memory loss and hallucinations is associated with transdermal scopolamine. (32) There is however, in addition to the anti-motion sickness activity of sympathomimetics, ephedrine and amphetamine, a beneficial reduction of the side effects of scopolamine-most notably the weariness.

The major complications of drug therapy are the side effects affecting performance and alertness and the severe impairment of higher mental functions (41).

The remaining, only partially effective, and sometimes impractical suggestions for prevention and therapy include positioning oneself amidships while on board

ship, or over the wings in an airplane. Also, recumbent, or semi-recumbent positions, with head bracing to minimize motion, and avoidance of reading are also suggested, as are avoidance of alcohol, consumption of small amounts of fluid and simple foods, or avoidance of oral intake if the sojourn is brief (3). Seasickness victims are aided by being out on deck and as in most vehicles, to have in their visual field a horizon or similar inertial space reference, while if below deck, to close the eyes to reduce symptomatology (41).

If time permits, or if of necessity the motion stimulation is recurrent over prolonged periods, adaptation is the most common and most effective, side-effect free, defence against motion sickness (35).

Unfortunately, currently the only completely effective way to avoid motion sickness, short of labyrinthectomy, is avoidance of motion.

#### BACKGROUND ON BIOFEEDBACK APPLICATIONS

With a consideration of the composite effectiveness and complications of the current armamentarium against motion sickness, it becomes quite obvious that much room remains for alternative treatments or prevention. The following relates to the individual refractory to conventional therapies, particularly the crewmember whose loss from flying status would also entail loss of an extensive training investment.

The techniques and principles to be discussed relate to the detailed multi-dimensional physiologic variation in the motion sick environment. Through the detection, measurement, analysis, and sensory feedback of relevant biophysical data, it is proposed that an effective form of advanced automated autogenic biofeedback can be applied to the learned prevention of motion sickness.

The premise for the efficacy of autogenic biofeedback is that motion sickness is an autonomic nervous system response that can be interrupted by voluntary control of the nervous system (42) (34).

The precedent for effective forms of biofeedback treatment for several diverse physiological problems exists.

Levy, Jones, and Carlson (34) reported in 1961, the successful rehabilitation

of aircrew who developed motion sickness either during training or after beginning active duty. They used coriolis stimulation by chair rotation and head movements to evoke changes in GSR (galvanic skin response), skin surface temperature, and EMG (electromyograph) activities.

By detecting and signaling to the crewmember the early autonomic changes that occur 'prior' to the perception of adverse subjective symptoms, the subjects actively learned to react to these changes and obviate symptomatology.

Their program is labor intensive in that it required the efforts of two flight surgeon psychiatrists and one biofeedback technician to train the patient and control the instrumentation. The reported success rate for their subjects refractory to drug therapy was 84%, vs. 48% for prior techniques of adaptation/desensitization training.

Toscano and Cowings (58) monitored heart rate, respiration rate, face and blood volume, GSR, and intercostal muscle activity during coriolis stimulation also in a rotating chair apparatus. They compared feedback training to an alternate unrelated task and demonstrated an objective ability to maintain autonomic baseline levels under stressful motion sickness inducing conditions. With the use of autogenic biofeedback, they trained their subjects to tolerate a 2 to 3 time increase in nauseogenic head movements.

Also, Cowings and Toscano (9) demonstrated that both highly and moderately motion sick susceptible subjects adjusted to nauseogenic stimulation with biofeedback at similar rates.

They suggest that autogenic feedback training appears to increase the threshold of the 'facultative linkage' of Graybiel (the linkage to the autonomic symptom centers), and thus the threshold of the autonomic symptomatology without affecting the perception, vestibular, and sensory responses to nauseogenic stimuli or the contents of the neural store.

Nicogossian (42) also cites Levy where, as an example of the ability of biofeedback, the motion induced fall in skin temperature of 8-10 degrees F can be reduced to 1-2 degrees or even reversed.

Rebman (51) has even demonstrated the use of non instrumented behaviorally trained muscle relaxation to successfully treat nausea and vomiting associated with air travel.

#### IV BIOPHYSICAL CONSIDERATIONS, INSTRUMENTATION AND ENGINEERING CONSIDERATIONS

The approach being taken on this system of biophysical monitoring and biofeedback revolves around a consideration of the significant systems and measurable parameters known and previously mentioned to experience modulation by the motion sickness syndrome.

In addition to the 1.) heart rate, 2.) respiration rate, 3.) intercostal muscle activity, 4.) blood pulse volume, 5.) skin temperature, and 6.) GSR, of prior investigators, an attempt is being made to evaluate the contribution of all parameters having a recognized correlate in symptoms and signs.

We will ultimately measure variables related to:

- 1.) Heart Rate
- 2.) Peripheral Pulse Blood Volume/Vascular Tone
- 3.) Facial Pulse Volume/Vascular Tone
- 4.) Thoracic Respiration (rate and character)
- 5.) Abdominal (diaphragmatic) Respiration
- 6.) GSR
- 7.) Salivation
- 8.) Gastric Tone and Activity
- 9.) Intestinal Tone and Activity
- 10.) Ocular Movement/Nystagmus (ENG)
- 11.) Peripheral Temperature
- 12.) EMG (skeletal muscle tone)
- 13.) EEG (electroencephalogram)
- 14.) Subjective Subject Input (as a measure of the cardinal symptom, nausea)

Discussion of the individual parameters follows with analysis of the physiologic relevance, implications and biomedical and engineering considerations.

A few initial considerations apply to all instrumentation amplifiers to be used as bioelectric potential sensors with direct electrical connection to a subject's skin. Precautions were taken in the basic design of all amplifiers to provide a very high impedance path through the electrodes to obviate an application of greater than several microamperes of current through a subject and endangering the heart or brain. All amplifiers are additionally safeguarded by using battery power.

Secondly, in order to block the DC offset potential generated by signal acquisition electrodes, most amplifier designs will incorporate a low frequency cutoff in the region of .005 Hz.

Differential input instrumentation FET op-amps are used in most designs to provide the high impedance required in the presence of skin impedances from 10K to 500K ohms. Where possible, when dealing with very low physiologic signal levels, a chopper-stabilized amplifier system is used to minimize DC drift and to provide maximal noise, common mode, and half-cell potential signal rejection.

The electrodes to acquire the bioelectric potentials are of the silver/silver chloride variety because of their stable half-cell potentials and low noise characteristics ( 5) (45).

The electrocardiogram or cardiograph, a well established motion influenced physiologic variable, is being obtained through two precordial electrodes. The signal parameters consist of a frequency range of from .05 Hz. to 80 Hz. with an amplitude in the range of a few millivolts. (55)

Vascular tone and pulse volume are being measured with dual photoplethysmograph sensors to detect changes in peripheral blood flow of the face and finger. The system being used is similar to the Tektronix type 410 where the intensity of a reflected light source on the face, or the reduced intensity of a light transmitted through a finger, provides a measure of the change of periodic blood flow associated with the pallor of motion sickness. The frequency response of the system is from .05 to 10 Hz. with a fundamental of 1.3 Hz. (=pulse of 78/min) (56).

Respiration is being measured with dual circumferential pneumogram sensors. As an alternative to the strain gauge type of transducer, variable capacitors are being used to provide a changing capacitance as an analog to respiratory torso excursion. Respiration manifests changes in rate, depth, as well as a shift from diaphragmatic to thoracic breathing as motion sickness symptomatology develops. The biomedical considerations are a fundamental frequency of .25 Hz. for a respiratory rate of 15/min., and due to the need to measure baseline variations in respiratory excursions, a frequency response of from DC to 2 Hz.

The GSR or galvanic skin response, is a well studied parameter included in most prior studies and therapies of biofeedback control of physiologic parameters. It's measurement is facilitated with the use of commercially available instruments—here the Autogen 3000. The study of GSR extends back to 1878 with Fere (14). The change in resistance of the GSR is called the Fere effect and is a consistently influenced parameter during motion sickness sweating symptomatology. It is determined by measuring the impedance change to a 2 or 3 Hz. low level AC signal applied to 3 finger electrodes (2).

Gastrointestinal function receives special emphasis, with consideration of multiple anatomic regions. At the proximal end is the variable salivation rate. The well known phenomenon of motion sickness associated dry mouth or salivation will be measured with a technique analogous to the GSR measurement but will employ one electrode in the mouth and one outside. The slow changes in salivation rates require an amplifier response of from 0 to 3 Hz. and can use the Autogen 3000 GSR instrumentation.

The electrical activity of the stomach, a function of its contractile state, is measured by the electrogastrogram or EGG. The stomach is well known to become atonic with the experience of nausea, while during retching, the distal stomach contracts and the proximal stomach relaxes (54).

Cowings & Toscano and Earl & Peterson (13) have employed a random peri-umbilical application of abdominal electrodes for gastric signal

acquisition. The design of EGG being used here is directed to selective frequency study of the stomach based upon its general mixing contractions, the 'Basic Electrical Rhythm' or BER of approximately 1/min. to as high as 3/min. (.016 to .05 Hz.) measurable surface smooth muscle potentials of from .5 to 80 mV (23) (56).

The EGG in this system was designed and constructed around FET chopper stabilized op-amp active filters with a frequency response providing a sharp cutoff at .1 Hz. and having a gain from 60 to 80 db. (30). Electrode placement involves an active electrode over the stomach in the left upper abdominal quadrant and a reference electrode several inches away (56).

The final gastrointestinal tract region of concern is the small intestine. It is well established also that the tone of at least the duodenum increases with the early motion sickness symptoms, eg, nausea (24) (54). The small intestine additionally is characterized by its BER of 12/min. (.2 Hz.) at the duodenum with a frequency decreasing distally to the ileum to a rate of 7-9/min. (.12 Hz.) (23).

The 'Electrointestinogram', to provide a specific indicator of intestinal versus gastric GI tract activity, was designed and built around the same format as the EGG (IC choice, etc.). It was designed with a frequency response of from .1 to .24 Hz., with third and fourth order active filters to have a band pass gain of approximately 80 db. (4) (5) (30) (33). Electrode placement is directly over the organ mass of choice, the duodenum/jejunum region, the mid abdominal area with a reference electrode at the periphery of the abdomen.

The numerous connections and associations between the vestibular and ocular systems, as well as the phenomenon of optokinetic nystagmus associated motion sickness, necessitates a consideration and measurement of the predictive/therapeutic features of nystagmus in motion sickness.

Electronystagmography (ENG) is the technique of monitoring ocular movement by measuring the change in the potential seen across both eyes. The eyeball is polarized, negative to positive, from the retina to the cornea. Electrodes placed lateral to each eye will measure a rightward glance as a right to left positive potential proportional to the magnitude of the rightward angle and a

similar potential to a vertical glance if electrodes are placed above and below the eye.

Mathog & Cramer stated that motion sickness susceptibility can be estimated from the rate and decay of nystagmus (36). Guedry (20) showed a correlation between a learned reduction in nystagmographic responses to rotation and a reduction in motion sickness symptomatology. Collins (8) also demonstrated the association of nystagmus with rotation induced motion symptomatology in skaters. The skaters normally suppress their nystagmus, but with eyes closed experience vertigo, dizziness and motion sickness symptoms. Also, Dowd (12) showed that the rapid rate of recovery from the slow phase of nystagmus correlated with resistance or delay of motion sickness symptoms.

On the basis of this evidence, an ENG acquisition system was designed with an amplifier system similar to the aforementioned ones. Designed and built was an active filter amplifier with a frequency response of from DC to 30 Hz. (35 Hz. response is cited by Jantti as the response of some commercial amps) (0 to 20 Hz. cited by Strong) (29) (55) and a gain of approx. 85 db to respond the signal levels of from 5 to 10 microvolts per degree of eye movement (62).

For the parameters of 1) peripheral body temperature, which has been demonstrated to fall with vasoconstriction associated with stress, and 2) EMG, electromyography, measuring muscle tension which notably increases with stress, commercial Autogen Corp. models 60 and 1100, are employed.

Finally, an attempt is being made to quantify the subjective, imprecise descriptors of higher brain disfunction, embodied in the terms of fatigue, lethargy, depression, apathy, reduced motivation, or sleepiness that have been noted with motion sickness.

The EEG, electroencephalogram, with a signal level of from 0 to 300 microvolts, will be monitored during the presymptomatic stages of motion in the well established brain wave bands that are associated with different levels of arousal.

Alpha waves, 8-13 Hz., are found in normal awake subjects when in a quiet resting state, and disappear when attention is directed to some conscious type of mental activity. Beta waves, from 14-50 Hz., most frequently recorded from parietal and frontal regions of the scalp, are associated on the higher end of their spectrum with intense activation of the CNS or during tension. Theta waves, from 4-7 Hz., occur during emotional stress in adults, particularly during dissatisfaction and frustration or sudden removal of pleasure.

It is anticipated that, through the selective measurement of these EEG bands, and comparison of various band ratios such as Beta (arousal)/Theta (stress), an additional parameter applicable to interactive modifiable biofeedback will be generated to modify the motion sickness response.

The final input to the composite monitoring system is a subjective well-being parameter which relates to the subject's moment to moment self perception of symptomatology.

#### V SYSTEM ORGANIZATION

The instrumented subject is seated in a rotating chair apparatus (13) and executes a programmed set of head movements out of the Z axis (vertical plane) to induce coriolis stimulation.

The analog data from the subjects transducer/amplifiers are processed on board the chair by a CIM-800 micro computer, analog to digital converter, and parallel output to transmit the 16 bit data (4 bits of channel identification and a 12 bit datum value) (13) through the slip rings of the rotating chair.

Data so processed, digitized, are more immune to noise generated by the slip rings and also is in a form ready to be processed by the next stage of the

system. That is the MASSCOMP minicomputer, which is being configured by project associates to receive, process, store and display up to 12 channels of physiologic data in a real time, adjustably updated video display screen format. This will permit variable selection of the most relevant of several channels to present to the rotating subject to act upon in his biofeedback exercises.

#### VI RECOMMENDATIONS: CURRENT SYSTEM STATUS AND REQUIRED EFFORT

The required effort remaining on the system involves 2 or 3 levels. Required at the signal acquisition level are 1.) efforts at calibration, 2.) reconfiguration of transducer systems as for the pneumograph, 3.) reorganization of transducer and electrode hardware to provide a more rapid and efficient installation procedure, 4.) system hardware documentation (electrical parameters and circuits), and 5.) final design/modification work on the data channels newly implemented for this project (ENG, modified EGG, EIG, GSR2 (salivation response), and EEG (filter and ratio circuits).

As important, remain the selection, development, and evaluation of feedback data configuration for both operator and patient consoles.

Remaining is the development of the algorithm which selects the more useful physiologic variables appropriate to an individual subject.

Lastly, work remains on the current effort to design a more effective video/audio feedback display for on chair interaction, one which permits subject concentration upon individual variables or a comprehensive system state variable.

It is expected also, as a byproduct of this first comprehensive measurement system, that a more complete qualitative/quantitative description of the motion sickness syndrome will evolve.

#### REFERENCES

- 1.) Adams, V.: Deafness, Dizziness and Disorders of Equilibrium. PRINCIPLES OF NEUROLOGY. 2nd. Ed. 1981
- 2.) Autogenic Systems: INSTRUCTION MANUALS FOR THE AUTOGEN 60, 1100, 3000 Berkeley, CA. 1975
- 3.) Berkow, R. (Ed.): Motion Sickness. Chap 252:2135-2136. MERCK MANUAL. 14th Ed. 1982
- 4.) Buchsbaum, W. H.: BUCHSBAUMS COMPLETE HANDBOOK OF PRACTICAL ELECTRONIC REFERENCE DATA. 2nd Ed. Prentice-Hall Inc, NJ. July, 1980
- 5.) Carr, J. J., Brown, J. M.: INTRODUCTION TO BIOMEDICAL EQUIPMENT TECHNOLOGY. John Wiley & Sons. 1981
- 6.) Clark, R. G.: Chap. 14. ESSENTIALS OF CLINICAL NEUROANATOMY & NEUROPHYSIOLOGY. 5th Ed. Manter & Gatz. 1975
- 7.) Cohen, M. M.: Visual-Proprioceptive Interactions. INTERSENSORY PERCEPTION AND SENSORY INTEGRATION. Plenum Press, NY. 1981
- 8.) Collins, W. F.: Problems in Spatial Orientation: Vestibular Studies of Figure Skaters. TRANS. AMM. ACAD. OF OPHTHAL. AND OTOLARYNG. 70:575-578. 1966
- 9.) Cowings, P. S., Toscano, W. B.: The Relationship of Motion Sickness Susceptibility to Learned Autonomic Control for Symptom Suppression. AV. SPACE ENVIR. MED. 53(6):570-575. 1982
- 10.) Dahl, E., Offer-Ohlson, D., Lillevold, P. E., Sandvick, L.: Transdermal Scopolamine, Oral Meclizine, and Placebo in Motion Sickness. CLINICAL PHARM. THER. 36(1):116-120. July, 1984
- 11.) Dhenin, G.: Motion Sickness. Chap. 22:468-493. AVIATION MEDICINE. 1978
- 12.) Dowd, P. J., Moore, E. W., Cramer, R. L.: Relationships of Fatigue and Motion Sickness to Vestibulo-Ocular Responses to Coriolis Stimulation. HUMAN FACTORS. 17(1):98-105. 1975
- 13.) Earl, O. A, Peterson, C. N.: PHYSIOLOGIC DATA ACQUISITION SYSTEM AND MOTION SICKNESS PREVENTION TRAINER, AFIT/GE/EE. 1983
- 14.) Fere, C.: Note Sur Les Modifications de la Tension Electrique dans la Corps Humain. COMPTES RENDUS DES SEANCES DE LA SOCIETE DE BIOLOGIE. Vol. 5:28-33. 1888
- 15.) Graybiel, A.: The Vestibular System. Chap. 12. BIOASTRONAUTICS DATA BOOK. 2nd Ed. 1973
- 16.) Graybiel, A.: Susceptibility to Acute Motion Sickness in Blind Persons. AEROSPACE MED. 41(6):650-653. 1970

- 17.) Graybiel, A.: Structural Elements in the Concept of Motion Sickness. AEROSPACE MED. 40(4):351-367. 1968
- 18.) Graybiel, A., Cramer, D. B., Wood, C. D.: Antimotion sickness Efficacy of Scopolamine 12 & 72 Hours After Transdermal Administration. AV. SPACE. ENVIR. MED. 53(8):770-772. 1982
- 19.) Graybiel, A., Lackner, J. R.: Evaluation of the Relationship Between Motion Sickness Symptomatology and BP, HR, & Body Temp. AV. SPACE. ENVIR. MED. 51(3):211-214. 1980
- 20.) Guedry, F. E.: Visual Control of Habituation to Complex Vestibular Stimulation in Man. ACTA OTOLARYNG. 58:377-389. 1964
- 21.) Guinard, J. C., McCauley, M. E.: Motion Sickness Incidence Induced by Complex Periodic Waveforms. AV. SP. ENVIR. MED. 53(6):554-563. 1982
- 22.) Guyton, A. C.: The Reticular Activating System, Wakefulness, Sleep, Attention, Brain Waves, & Epilepsy. Chap. 54. TEXTBOOK OF PHYSIOLOGY. 6th Ed. 1981
- 23.) Guyton, A. C.: Movement of Food Through the Alimentary Tract. Chap 63. TEXTBOOK OF MEDICAL PHYSIOLOGY. 6th Ed. 1981
- 24.) Guyton, A. C.: Physiology of GI Disorders. Chap. 66. MEDICAL PHYSIOLOGY. 6th Ed. 1981
- 25.) Guyton, A. C.: Motor Function of the Brain Stem and Basal Ganglia. Chap. 52. MEDICAL PHYSIOLOGY. 6th Ed.:640-651. 1981
- 26.) Harding, R., Mills, F. J.: Function of the Special Senses in Flight. BRITISH MEDICAL JOURNAL. Vol. 286. 4 June, 1983
- 27.) Homick, J. L., Kohl, R. L., Reschke, M. F., Degioanni, J., Cintron-Trevino, N. M.: Transdermal Scopolamine in the Prevention of Motion Sickness: Evaluation of the Time Course of Efficacy. AV. SPACE. ENVIR. MED. 54(11):994-1000. 1983
- 28.) Irwin, J. A.: The Pathology of Seasickness. LANCET. Vol. 2:907-909. 1881
- 29.) Jantti, V.: Spike Artifact Associated with Fast Eye Movement in Electronystagmography and its Importance in the Automatic Analysis of Saccades. ORL. 44:216-225. 1982
- 30.) Johnson, D. E., Johnson, J.R., Moore H.D.: A HANDBOOK OF ACTIVE FILTERS Prentice Hall, Englewood Cliffs, N.J.
- 31.) Johnson, P.: Transderm Scop Patches for Prevention of Motion Sickness. NEJM. 31(7):468. Aug., 1984
- 32.) Kohl, R. L., Homick, J. L.: Motion Sickness: A Modulatory Role for the Central Cholinergic Nervous System. NEUROSCI. & BEHAV. REVIEWS. vol. 7:73-85. May, 1982
- 33.) Lancaster, D.: ACTIVE FILTER COOKBOOK. H. W. Sams & Co. Ind, Ind.

1975

- 34.) Levy, R. A., Jones, D. R., Carlson, E. H.: Biofeedback Rehabilitation of Airsick Aircrew. AV. SPACE ENVIR. MED. 52(2):118-121. 1981
- 35.) Lovan, W. D.: Motion Sickness. AFP Vol. 29:6. June, 1974
- 36.) Mathog, R. H., Cramer, R. L.: Testing of the Vestibular System. AEROSPACE MED. 42(7):741-745. 1971
- 37.) Matz, G. J., Wolfe, J. W.: Comparison of Nystagmic Responses in Basic Airmen, Grounded Pilots, and Active Pilots. AEROSPACE MED. 42(6):627-629. 1971
- 38.) McEachern, D., Morton, G., Lehman, P.: Seasickness and Other Forms of Motion Sickness. WAR MEDICINE. Vol. 2, No. 5. Sept., 1942
- 39.) Mirabile, C. S., Ford, M.R.: A Clinically Useful Polling Technique for Assessing Susceptibility to Motion Sickness. PERCEPTUAL & MOTOR SKILLS. 54:987-991. 1982
- 40.) Mohler, S.: Motion Sickness and Problems of Air Travel. TEXTBOOK OF MEDICINE. Beeson-McDermott. Chap. 29.1. 15th Ed. 1979
- 41.) Money, K. E.: Motion Sickness. PHYSIOLOGICAL REVIEWS. Vol. 50, No. 1. Jan., 1970
- 42.) Nicogossian, A. E., Parker, J. F.: The Neurovestibular System. Chap. 8. SPACE PHYSIOLOGY AND MEDICINE. NASA SP-447. Sept., 1982
- 43.) O'Hanlon, J. F., McCauley, M. E.: Motion Sickness Incidence as a Function of the Frequency of Acceleration of Vertical Sinusoidal Motion. AEROSPACE MED. 45:366-369. 1974
- 44.) Oman, C. M.: A Heuristic Mathematical Model for the Dynamics of Sensory Conflict and Motion Sickness. ACTA OTOLARYNG. (suppl.). No. 392:1-44. 1982
- 45.) Outerbridge, J. S., Jones, G. M.: Reflex Vestibular Control of Head Movement in Man. AEROSPACE MED. 42(9):935-940. 1971
- 46.) Pitman, J. R., Yolton, R. L.: Etiology and Treatment of Motion Sickness: A Review. J. AMER. OPTOMET. ASSN. Vol. 54(1):31-38. 1983
- 47.) Price, N. M., Schmitt, L. G., McGuire, J., Shaw, J. E., Trobough, G.: Transdermal Scopolamine in the Prevention of Motion Sickness at Sea. CLINICAL PHARM. AND THERAPEUTICS. Vol. 29(3):414-419. Mar., 1981
- 48.) Reason, J. T.: Motion Sickness Adaptation: A Neural Mismatch Model. JOURNAL OF THE ROYAL SOCIETY OF MEDICINE. VOL. 71:819-829. Nov., 1978
- 49.) Reason, J. T.: Motion Sickness: A Special Case of Sensory Rearrangement. ADVANCEMENT OF SCIENCE. Vol. 26(130):386-393. 1970
- 50.) Reason, J. T.: Relations Between Motion Sickness Susceptibility, the Spiral Effect and Loudness Estimation. BR. J. PSYCHOL.

- 51.) Reiman, V. L.: Self Controlled Desensitization With Cue-Controlled Relaxation for Treatment of a Conditioned Response to Air Travel. J. BEHAV. THER. & EXP PSYCHIAT. Vol. 14, No. 2:161-164. 1983
- 52.) Royal, L., Jessen, B., Wilkins, M.: Motion Sickness Susceptibility in Student Navigators. AV. SP. ENVIR. MED. 55(4):227-80 1983
- 53.) Ryback, R. S., Rudd, R. E., Matz, G. J., Jennings, C. L.: Motion Sickness in USAF Flying Personnel. AEROSPACE MED. 41(6):672-677. 1970
- 54.) Schuster, M. M.: Disorders of Motility. TEXTBOOK OF MEDICINE. 15th Ed. p1475-79. Beeson-McDermott. 1979
- 55.) Strong, P.: Respiration and Temperature. Chap. 9. BIOPHYSICAL MEASUREMENTS. Tektronix. 1st Ed. 1973
- 56.) Strong, P.: BIOPHYSICAL MEASUREMENTS. Tektronix. 1st Ed. June, 1973
- 57.) Tokola, O., Laitinen, L. A., Aho, J., Gothoni, G., Vapaatolo, H.: Drug Treatment of Motion Sickness: Scopolamine Alone and Combined With Ephedrine in Teal and Simulated Situations. AV. SPACE. ENVIR. MED. 55:636-41. 1984
- 58.) Toscano, W. B., Cowings, P. S.: Reducing Motion Sickness: A Comparison of Autogenic Feedback Training and an Alternative Cognitive Task. AV. SPACE ENVIR. MED. 53(5):449-453. 1982
- 59.) Tyler, D. B., Bard, P.: Motion Sickness. PHYSIOLOGICAL REVIEWS. Vol. 29:311-369. 1949
- 60.) Watanabe, I., Ikeda, M.: Electronystagmography Outside the Hospital Using a Pocket Sized Electrocardiograph. ACTA OTOLARYNG. (Suppl. 393:49-57). 1983
- 61.) Wilding, J. M., Meddis, R: A Note on Personality Correlates of Motion Sickness. BR. J. PSYCHOL. 63,4:619-620. 1972
- 62.) Wolff, H. S.: Chap. 3. BIOMEDICAL ENGINEERING. McGraw Hill. 1970
- 63.) Wood, C. D., Graybiel, A.: A Theory of Motion Sickness Based on Pharmacological Reactions. CLINICAL PHARM. AND THERAPEUTICS. Vol. 11:5. Sept.-Oct., 1970
- 64.) Wood, C. D., Graybiel, A.: Theory of Antimotion Sickness Drug Mechanisms. AEROSPACE MED. 43(3):249-252. 1972

1984 USAF-SCEEE GRADUATE STUDENT SUMMER SUPPORT PROGRAM

Sponsored by the

AIR FORCE OFFICE OF SCIENTIFIC RESEARCH

Conducted by the

SOUTHEASTERN CENTER FOR ELECTRICAL ENGINEERING EDUCATION

FINAL REPORT

AN ALGORITHM FOR SEGMENTING FLIR IMAGERY CONTAINING BRIDGES

Prepared by: Jennifer Davidson

Academic Department: Department of Mathematics

University: University of Florida

Research Location: Air Force Armament Laboratory  
Guided Weapons Division  
Electro-Optical Terminal Guidance Branch

USAF Research Contact: Mr. Neal Urquhart

SFRP Supervising  
Faculty Member: Dr. Sam Lambert

Date: July 20, 1982

Jennifer Davidson

ABSTRACT

This report presents an algorithm for segmenting FLIR imagery which contain bridges. The algorithm uses edge based segmentation and the concept of reverse-parallel line segmentation to isolate target-like regions.

The algorithm is coded in Fortran and is available along with a users guide at the Image Processing Lab at Air Force Armament Laboratory, Eglin AFB.

### Acknowledgements

The author would like to express her appreciation and gratitude to the Air Force Systems Command, the Air Force Office of Scientific Research, and the Southeastern Center for Electrical Engineering Education for providing the opportunity to spend a very interesting and valuable summer at the Air Force Armament Laboratory, Eglin AFB, FL. In particular, she would like to acknowledge the staff of the Electro-Optical Terminal Guidance Branch of the Guided Weapons Division. Their hospitality and support made this summer research a very pleasant experience. Special thanks and sincere gratitude are due Lt Col Lawrence Ankeney, PHD, Mr Neal Urquhart, and Dr. Gerhard Ritter for their continued encouragement and for their guidance and suggestions that made this project a successful one. Also, appreciation is extended to the personnel in the Image Processing Lab who were extremely generous with their time and expertise, and who provided solutions to seemingly unsolvable problems which inevitably arise from using computers.

Finally, the author would like to acknowledge the assistance of Mrs. Merlynn Bath in the preparation of this manuscript.

## Introduction

The solution of the problem of automatic recognition of high value targets in FLIR images is of obvious importance to the USAF. The ability of a seeker to "lock on after launch" would help to ensure the safety of American pilots. An automatic target recognition system must use scene content to classify objects. Using contextual information serves to localize the target search area, therefore decreasing the number of pixels to be processed. Thus, techniques need to be developed to extract and utilize contextual information. (1)

Generally the first step in extracting information is that of segmenting the image into subregions. The real time benefit of scene segmentation is that certain uninteresting subregions of the image can be discarded while the remaining interesting subregions can then be examined more closely, but requiring much less computation. Artificial intelligence techniques can then be used to decide which features should be computed for a given subregion and how to interpret the interaction of specific measurements for the computed features.

Many types of segmentation techniques exist. Edge-based segmentation is one common type. The basic idea of edge-based segmentation is to outline the objects in the image and then use shape information and/or information available in the "neighborhood" of an edge to classify objects. Some examples of edge based segmentation can be found in (2). Region based segmentation is another type. This technique groups pixels into regions which are homogeneous with respect to some measure. Examples of region based segmentation can be found in the extended bibliography. After segmentation, either the target should be contained in one of the remaining subregions, or the remaining subregions should include sufficient contextual information so that further relationship analysis will permit potential target subregions to be identified. In either case, further analysis is generally required before a final decision is made as to which subregions are most target-like. The problem now is to determine which type of segmentation technique best applies to segment a large variety of images containing

high value targets.

### RESEARCH GOALS AND OBJECTIVES

The research objectives for the Summer Research period are:

- 1) To investigate existing segmentation techniques related to the automatic recognition of bridges in FLIR imagery;
- 2) To determine features that can be used to characterize bridges in FLIR imagery;
- 3) To modify existing algorithms or develop new algorithms for segmentation and feature extraction to make them particularly applicable to bridge recognition;
- 4) To implement the algorithms in 3) on the computer and test them. This software will be modular so that it can be changed and/or expanded.

### III. General Outline of the Approach

This section presents a general outline of the algorithm which was implemented. The details of each part of the algorithm will be presented in sections IV-VI.

Edge-based segmentation is used rather than region-based segmentation because:

- 1) Bridges do not generally constitute large regions in an image.
- 2) The fact that the edges of a bridge have opposite change in contrast can be exploited.

The first stage of the algorithm is convolution with a set of six edge masks, each mask having two directions associated with it. The resulting edge image is thinned and thresholded using both magnitude and directional information. The thinned edges are then approximated piecewise by directed line segments. Next, the directed line segments are grouped in pairs, each pair consisting of directed line segments whose directions differ by approximately  $180^\circ$  (called "Revpars") and are "close" to each other. In the case of a  $0^\circ/180^\circ$  pair the region outside the pair of line segments is checked for the existence of water.

The output of the algorithm is a collection of pairs of directed line segments which satisfy certain contextual relationships. These

pairs of line segments represent possible bridges.

#### IV. The Edge Detection and Thinning

##### A. The Edge Masks

The algorithm originally used the set of six 5x5 masks as shown in Figure 1a. The original image is convolved with each mask yielding six possible edge values for each pixel. Each resultant pixel for the convolved image is assigned the value with the largest magnitude and either assigned the direction 0 associated with that mask if the value is positive, or  $(0+180^\circ)$  (modulo  $360^\circ$ ) if the value is negative. Thus, at the end of the convolution stage each pixel of the original image has both a magnitude and direction associated with it.

The reason the 5x5 masks were used was that they offered twelve possible directions. The other edge masks that were investigated offered only eight:  $0^\circ, 45^\circ, \dots, 345^\circ$ . Eight directions did not result in enough directional sensitivity. Consider the following: A bridge is oriented in an image at approximately 60-65 degrees. The top edge is labelled as a  $90^\circ$  edge and the bottom edge is labelled as a  $225^\circ$  edge (as opposed to a  $270^\circ$  edge). In order to classify the pair as a possible bridge one would have to define line segments whose directions differ by  $180^\circ \pm 45^\circ$  as reverse parallel line segments. But then an actual  $110^\circ$  edge and an actual  $210^\circ$  edge would be considered as reverse parallel line segments, which is absurd. Therefore, the use of an 8 direction mask does not provide the required directional sensitivity.

The 5x5 masks have the disadvantage of being insensitive to fine detail. Detail is important in bridge classification because:

- 1) Bridges from long range (3-6 miles) comprise a very small percentage of the total image but it is highly desirable to isolate subregions of the original image which may contain bridges at this range. There would then be time for more intense localized processing on each of the smaller subregions.

- 2) Many bridges have superstructures and substructures which can be used as features for classification. The structures appear as fine details in FLIR images.

The 3x3 edge masks have much more sensitivity to detail than the 5x5

1	1	1	1	1
1	1	1	1	1
0	0	0	0	0
-1	-1	-1	-1	-1
-1	-1	-1	-1	-1

180°

-1	-1	0	1	1
-1	-1	0	1	1
-1	-1	0	1	1
-1	-1	0	1	1
-1	-1	0	1	1

90°

1	1	1	1	1
-0.3	.7	1	1	1
-1	-0.8	0	.8	1
-1	-1	-1	-.7	.3
-1	-1	-1	-1	-1

150°

1	1	1	1	1
1	1	1	.7	-.3
1	.8	0	-.8	-1
.3	-.7	-1	-1	-1
-1	-1	-1	-1	-1

210°

-1	.3	1	1	1
-1	-.7	.8	1	1
-1	-1	0	1	1
-1	-1	-.8	.7	1
-1	-1	-1	-.3	1

120°

1	1	1	.3	-1
1	1	.8	-.7	-1
1	1	0	-1	-1
1	.7	-.8	-1	-1
1	-.3	-1	-1	-1

240°

Figure 1.a

1	1	1
1	1	1
0	0	0

180°

-1	0	1
-1	0	1
-1	0	1

90°

.7	1	1
-.8	0	.8
-1	-1	-.7

150°

1	1	.7
.8	0	-.8
-.7	-1	-1

210°

-.7	.8	1
-1	0	1
-1	-.8	.7

120°

1	.8	-.7
1	0	-1
.7	-.8	-1

240°

Figure 1.b

edge masks. By simply "peeling off" the outside layers of the 5x5 masks (see figure 1.b) we obtained a set of 3x3 edge masks which were satisfactory in the following sense:

- 1) Edges that were picked up by the 5x5 masks were picked up by the 3x3 masks.
- 2) More details were picked up than with the 5x5 masks.
- 3) The masks were tested on synthetic data and were able to detect 12 directions in a consistent fashion. For example, on a 120° line, convolution with the 120° mask produced a larger magnitude than convolution with the other masks.

Thus the 3x3 edge masks were implemented also. The user can choose either the 5x5 or 3x3 masks.

#### B. Thinning and Thresholding

The convolved image is thresholded with the threshold level, T, being determined by

$$T = X + \alpha S$$

where X is the mean of the edge magnitudes, S is the standard deviation, and  $\alpha$  is a parameter which can be set by the user. Experimental results indicate that the bridge pixels at medium and long range, or about 13,000-30,000 feet, have low to medium edge magnitudes. Therefore, the threshold could not be set very high. The low threshold resulted in a large number of "noise" edge pixels (see figure 2), many of which had roughly the same edge magnitudes as the bridge pixels. The difference between the bridge pixels and the noise pixels is that the bridge pixels form connected component edges. Thus, the average edge magnitude in a 3x3 window of a bridge pixel tends to be significantly higher than that of a "noise" pixel. For this reason, a local averaging operation was performed on the convolved, thresholded edge image, while retaining the original edge magnitudes to prevent blurring. The averaged edge image is then thresholded again at the same threshold. The thresholded averaged edge image is then reduced to a binary image by setting the nonzero elements equal to one. The resulting binary image is then multiplied by the convolved thresholded binary edge image. The user of

the program has the option of thresholding, setting the parameter , performing the local averaging, and setting the threshold parameter for the second threshold independently of the first. Notice that the local averaging operation could be performed before the first threshold is applied, but this may cause pixels "close" to an edge to have artificially high edge magnitudes.

The original thinning algorithm used was that of Nevatia and Babu (2). Experimental results indicated that these thinning conditions were too harsh for our purposes. In particular, bridge pilings and bridges from long and medium range are sometimes two pixels wide and edges which are side by side cannot be retained with the original thinning algorithm. Therefore, Nevatia and Babu's original decision rules were modified and new decision rules were added. The final version of the thinning algorithm declares an edge element to be present at a pixel if:

- 1) The edge directions of the two neighbors which are in a position normal to the direction of the center edge pixel under consideration are within  $30^\circ$  of this center pixel under consideration or the magnitudes of these neighbors are both zero, and

- 2) The output edge magnitude at the center pixel is greater than the edge magnitudes of the two neighbors. (The normal to a  $30^\circ$  direction is approximated by the diagonals on a 3x3 grid.)

or

- 1) One of the previously mentioned neighboring pixels is within  $30^\circ$  of the opposite direction of the center pixel and the other neighbor is within  $30^\circ$  of the center pixel under consideration and

- 2) The center edge pixel is a local maximum with respect to its neighbor in the same direction.

In addition, a smoothing operation performed on the direction array. The smoothing operation is performed before thinning. The following illustrates the implementation of the smoothing operation. If a  $30^\circ$  direction potential edge element has neighbors in positions 1 and 5 (see Figure 5) whose directions are both  $0^\circ$ , then the  $30^\circ$  potential edge element is changed to a  $0^\circ$  direction. This procedure is used to

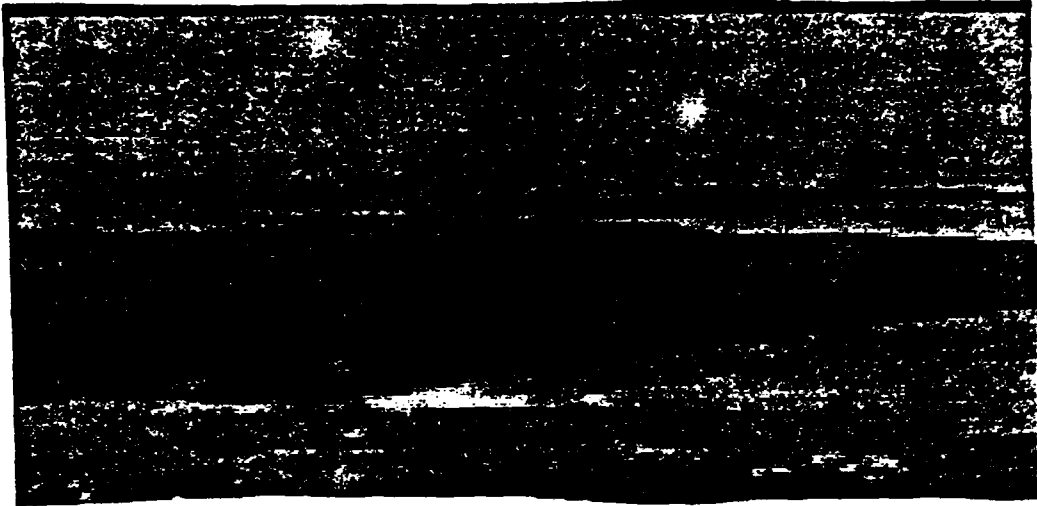


Figure 2a. original image.



Figure 2b. thinned image using 5x5 masks.

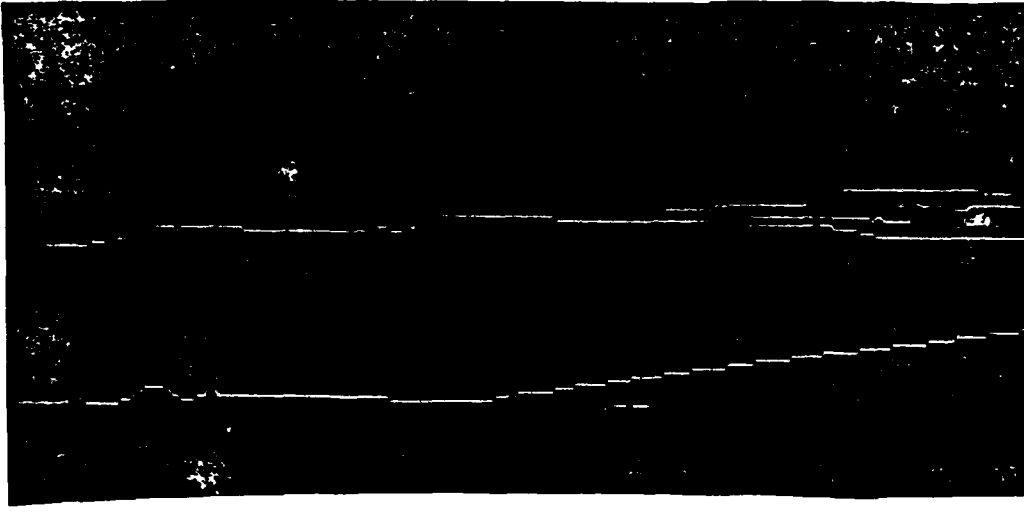


Figure 2c. Thinned image using 3x3 masks

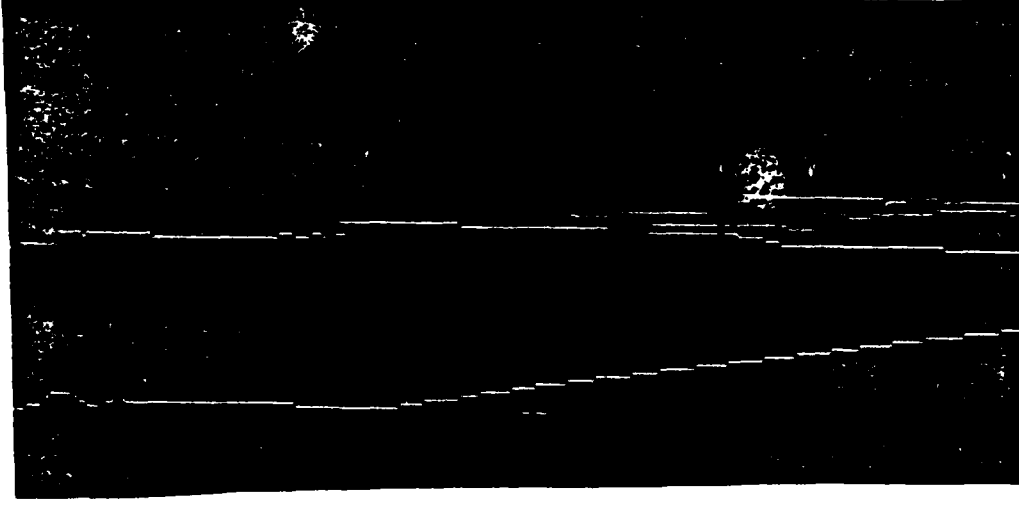


Figure 2d. local averaged thinned image.

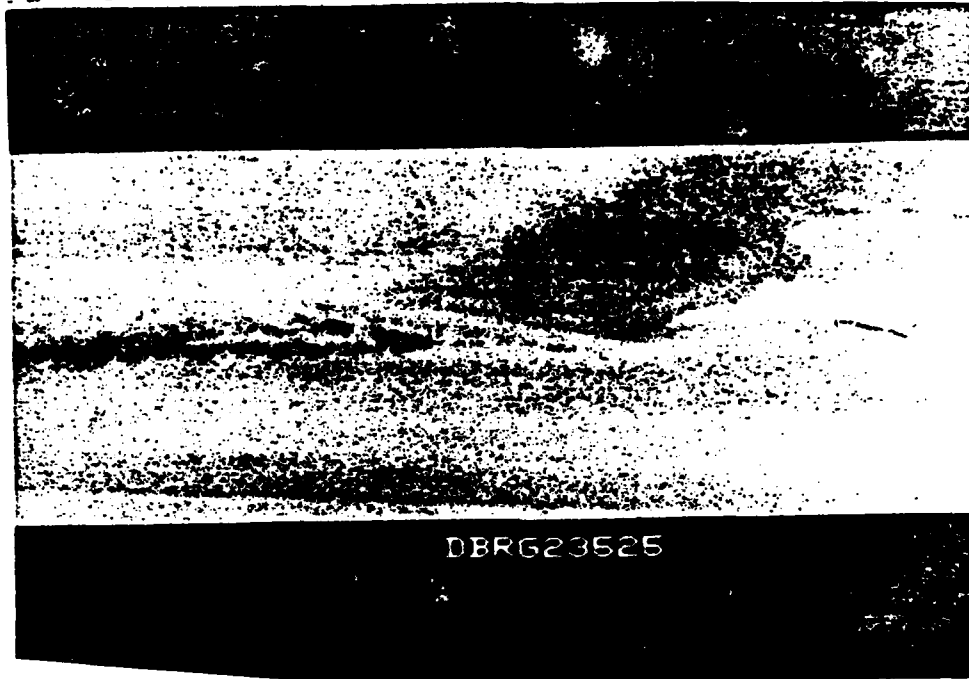


Figure 3a. Original image.

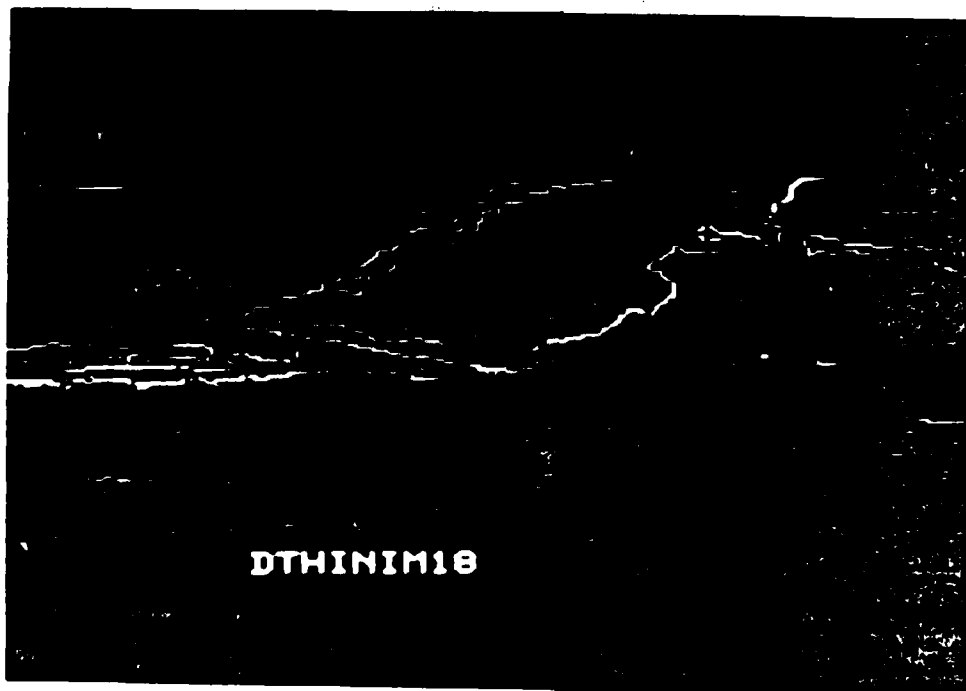


Figure 3b. Thinned image using 3x3 masks.

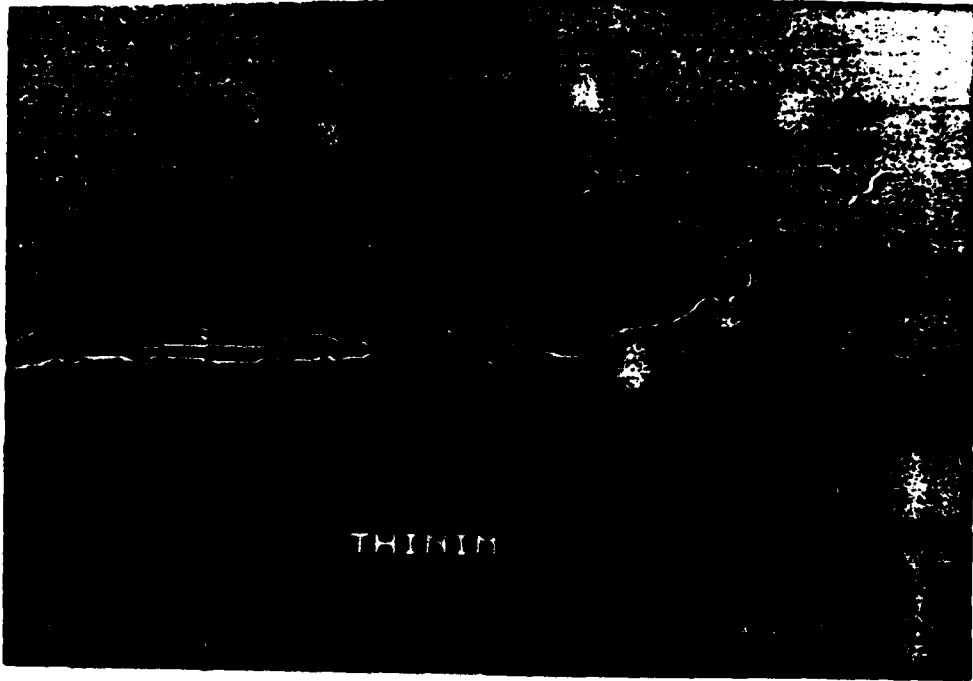


Figure 3c. Thinned image using 3x3's and local average.



Figure 4a. Original image

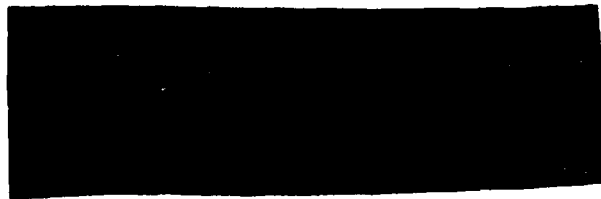


Figure 4b. Thinned image with 3x3 masks.

prevent gaps in edges due to variation in edge magnitudes.

Results of different combinations of masks and thinning techniques are shown in figures 2 through 4.

#### V. Determination of Line Segments

The extraction of line segments from the thinned image is accomplished in two stages. The first step chooses neighbors preceding and following an edge pixel, and the second step links pixels sequentially in line segments, labelling the line segments by their end points. The method is a slight variation from the line linking routine in (2).

First, the neighboring edge pixels preceding and following a given edge pixel are determined, called predecessors and successors, respectively. Two pixels are labelled as successors and two as predecessors for a given pixel. The neighbors lie in one of eight positions relative to the edge pixel, as labelled below:

4	3	2
5	X	1
6	7	8

Figure 5

One step of the thinning process possibly eliminates the two pixels in the direction perpendicular to the edge pixel direction. Thus, an edge pixel looks for possible successors in the remaining three positions, which point in the general direction of the edge pixel direction. For example, if the edge pixel has  $30^\circ$  direction, then possible successors lie in positions 1, 2, and 3.

A pixel is retained initially as a possible successor if the following two conditions are met:

- 1) Its magnitude is not equal to zero;
- 2) Its direction lies within  $30^\circ$  of the direction of the edge pixel.

If only one pixel satisfies these conditions, then there is only one successor. If there are two such pixels, then the pixel with the greater magnitude is the primary successor and the remaining one is the secondary successor. If there are three pixels satisfying these conditions, then the primary successor is the one whose Euclidean distance to the edge pixel is a minimum. In this case, the second successor is the one whose direction is different from the primary successor's direction.

Predecessors are chosen by the same method as for successors. For example, in the case where the edge pixel has  $0^\circ$  direction, its successors would be located in positions 8, 1, or 2 and its predecessors located in position 4, 5 or 6. Note also that if a pixel A has a successor B, then A is a predecessor of B.

The output from this subroutine is four arrays, each of whose dimension is the same as the original image, and whose entries are numbers from 0 to 8 representing that pixel's successors and predecessors. Zero designates that a pixel has no predecessor/successor.

It was discovered, at too late a date to rewrite the code, that the predecessor array could be generated almost directly from the successor array. This would approximately cut in half the amount of code needed for this subroutine.

The second step uses the successor and predecessor arrays to link the pixels sequentially in line segments. The output from this subroutine is two arrays, one containing the X coordinates of the endpoints of the line segments, and the other containing the Y coordinates of the endpoints of the line segments. The line segments are directed, as the masks that determine the pixels' directions have twelve possible directions.

Starting from the top left-hand corner, an edge pixel that has no predecessor is found. The primary successors are followed from this initial pixel. If the initial pixel has more than two successors, then a line segment is constructed, with the initial pixel being one end point and the third successor being the other end point. For each

successor that lies between the two end points, the distance between it and the line segment is checked. If each intermediate successor has a distance to the line segment of one unit or less, then the next successor of the present endpoint is located. This successor becomes the end point of an extended line segment whose other end point is still the initial pixel. Again, the distances of each intermediate successor to the newly constructed line segment is checked, and if each distance is less than or equal to one unit, then the process continues to find the next successor, create a new line segment, check distances of the intermediate successors, etc. If at any time the distance from an intermediate successor to the present line segment is greater than one unit, the process stops. The end points of a line segment are output, with the starting point having the coordinates of the initial pixel, and the terminal point having the coordinates of the next to the last successor checked. This terminal point becomes the initial pixel of a new line segment, and successors are traced from it as described above, until a pixel with no successors is reached. This pixel is always the last of the successors of our initial pixel. Overlapping the endpoints of the line segments in this manner will avoid creating gaps in otherwise continuous boundaries.

If two pixels have the same point as a primary predecessor, then there exists a "fork" in the line segment being traced. Since only the first successors are traced, the line segments described by following the second successor would be omitted by the above line tracing algorithm. This situation is avoided by making a first pass at the data and changing the primary predecessor array as follows: Let A and B denote the two pixels with C as a common predecessor, and let the arrows in Figure (6) denote the direction of the respective pixels. The second successor of C is found; suppose it is B. The predecessor of B (namely C) is changed to zero, that is, B is no longer considered to have a predecessor. Thus, when the pixel B is checked to see if it has a predecessor, it will not, and thus a line segment will be initialized at pixel B.

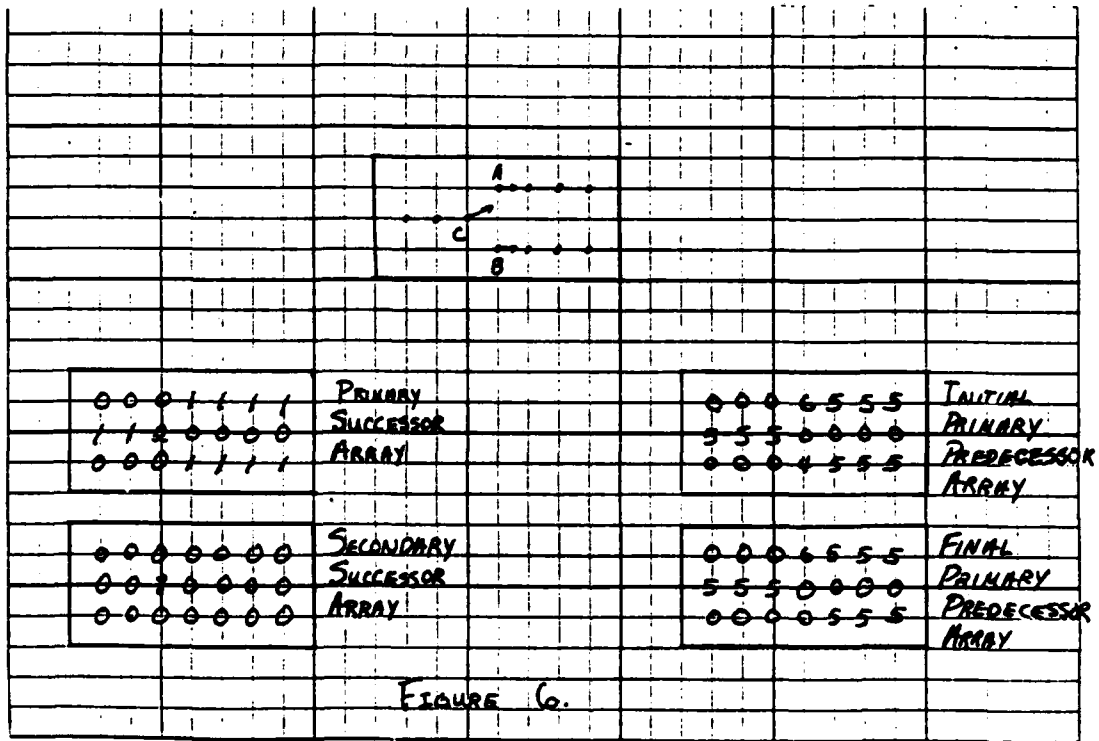


FIGURE 6.

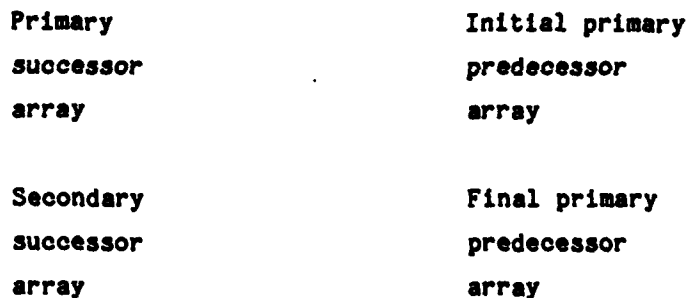


Figure 6

After the last pixel in a sequence of successors is reached, i.e., the pixel has no successor, the search resumes for the next pixel that has no predecessor. The output is arranged in the following manner:

X(1)	Y(1)	X(2)	Y(2)
X(3)	Y(3)	X(4)	Y(4)
.	.	.	.
.	.	.	.
.	.	.	.
X(2n-1)	Y(2n-1)	X(2n)	Y(2n)

where  $(X(2i-1), Y(2i-1))$  are coordinates of the initial pixel of the  $i$ th line segment, and  $(X(2i), Y(2i))$  are the coordinates of the terminal pixel of the  $i$ th line segment, for  $i = 1, \dots, n$ , where  $n$  equals the number of line segments in the image.

VI. Finding Reverse Parallel Line Segments.

This stage of the algorithm groups the directed line segments into pairs. Two directed line segments will be grouped into a pair, or labelled a Revpar, if the following conditions are satisfied:

- 1) They have approximately opposite directions.
- 2) The "distance" between them is less than a parameter BW

which can be set by the user.

3) They overlap.

Before explaining how the conditions are checked it is important to point out that the  $(x,y)$  coordinates of a point denote the position of the point in an array, which is not the usual  $x,y$  coordinate system (figure 7). Therefore, if orientation is to be measured from the horizontal, many familiar formulas appear different. For example the slope of the line passing through the points  $(x_1, y_1)$ ,  $(x_2, y_2)$  is given by

$$\text{Slope} = \frac{x^1 - x^2}{y^2 - y^1}$$

The change from the usual coordinate system into the new coordinate system is accomplished by the transformation  $(x,y) \rightarrow (y,-x)$ . Thus a formula in the new coordinate system can be found by applying the above transformation to the familiar formulas.

Condition 1) is checked by first computing the slopes of the directed line segments. The arctangent of the slope is computed. If the result,  $W$ , is negative then  $180^\circ$  is added to  $W$  so that  $w$  will be between  $0^\circ$  and  $180^\circ$ . Let  $D$  be the direction associated with the initial point of the line segment. Then if

$$|D - W| \geq 30^\circ$$

then  $W' = W + 180^\circ$ , otherwise  $W' = W$ . This procedure preserves reverse orientations. At this point in the algorithm the  $n$ th line segment has a direction  $W'_2$  associated with it. The algorithm then labels two line segments,  $L_n$  and  $L_m$ , as a Revpar if

$$165^\circ \leq |W'_n - W'_m| \leq 195^\circ.$$

Condition 2) is checked only if condition 1) is satisfied. The "distance" between two directed line segments,  $L_n$  and  $L_m$ , is actually the distance between the line determined by  $L_n$  (for example) and the initial point,  $(X_{2m-1}, Y_{2m-1})$ , of  $L_m$ .

Condition 3) is checked only if condition 2) is satisfied. The  $0^\circ/180^\circ$  and  $90^\circ/270^\circ$  degree cases are straightforward. The  $30^\circ/210^\circ$  will be presented here, the other cases being similar. Figure 8 shows what is meant by a pair of overlapping directed line segments. The

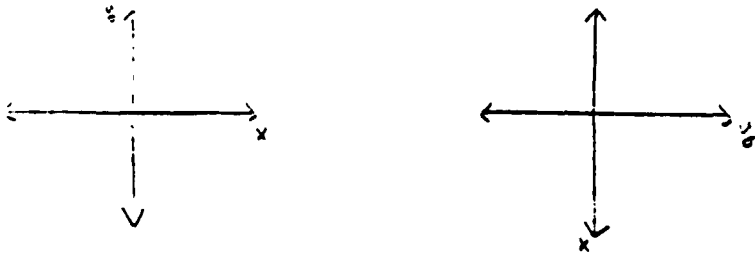


Figure 7.

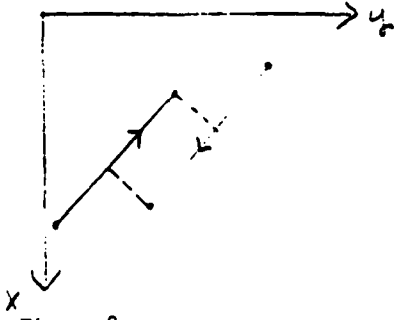
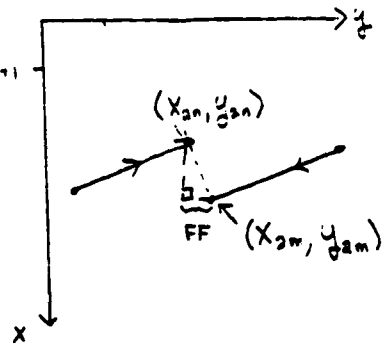
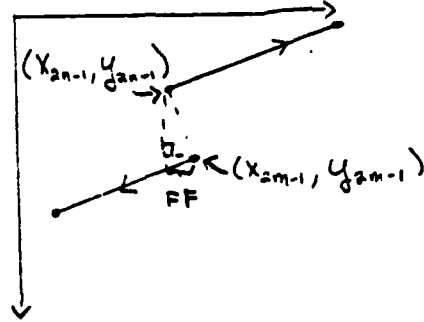


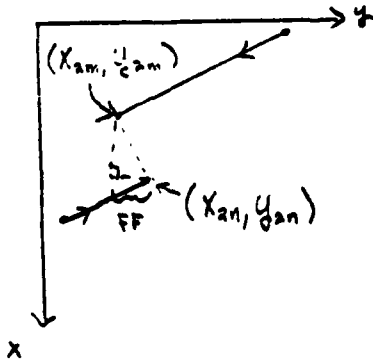
Figure 8.



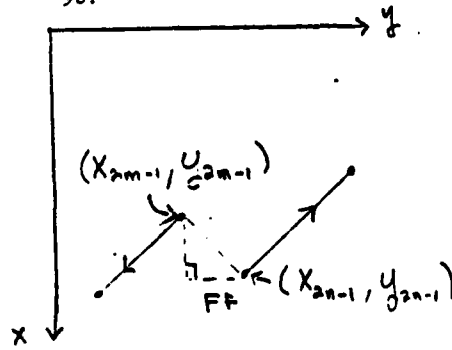
9a.



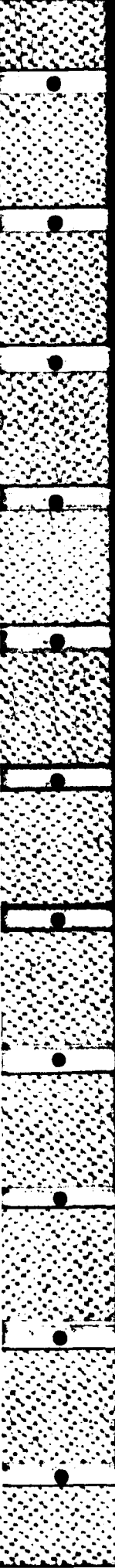
9b.



9c.



9d.



30°/210°, 60°/240°, 120°/300°, and 150°/330° cases require four checks to determine if they do not overlap. Let  $L_n$  be a directed line segment with endpoints  $(X_{2n-1}, Y_{2n-1})$ ,  $(X_{2n}, Y_{2n})$  and  $L_m$  be a directed line segment with endpoints  $(X_{2m-1}, Y_{2m-1})$ ,  $(X_{2m}, Y_{2m})$ . Assume that  $W_n$  is approximately 30° and that the pair  $(L_n, L_m)$  satisfy conditions 1) and 2). Also, let DBL be the "distance" between them. Then  $(L_n, L_m)$  will be said to overlap if the following four conditions are false.

VI. A. Figure 9a.

$$Y_{2n} + FF \leq Y_{2m} \text{ and } X_{2n} < X_{2m}$$

or

B. Figure 9b.

$$Y_{2n-1} + FF \geq Y_{2m-1} \text{ and } X_{2n-1} < X_{2m-1}$$

or

C. Figure 9c.

$$Y_{2m} + FF \geq Y_{2n} \text{ and } X_{2m} < X_{2n}$$

or

D. Figure 9d.

$$Y_{2m-1} + FF \leq Y_{2n-1} \text{ and } X_{2m-1} < X_{2n-1}$$

The outputs at this stage of the algorithm are:

1) An  $n \times n$  binary array, where  $n$  is the number of line segments detected. If  $(L_i, L_j)$  is a Revpar then the  $ij$ th entry of the array is a one,

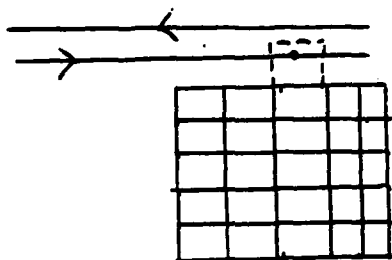
2) The original image with the pixels that are part of a Revpar highlighted. This image can be displayed on the Deanza and hardcopy produced (see Figurea 2-4).

#### VII. Labelling Line Segments as Bridge Edges

The final step of the algorithm is to use contextual information to determine if any of the reverse parallel lines are possible bridges. Many bridges pass over water, so the presence of water around a Revpar would increase the confidence that a Revpar represents a bridge. The mean and standard deviation are used as features to classify water. Presently, this statistical data is gathered by processing the picture separately with a statistical processing package available from the Image Processing Lab. It is feasible that the statistical data could be

generated from an internal subroutine; however, our ten-week appointment this summer was too short to permit us to do so.

A pair of reverse parallel lines are inspected to determine where they "overlap," in the sense of the previous chapters. Then one or both lines are traced, on the portions where they overlap, by following successors. At each edge pixel, the mean average and standard deviation for a given neighborhood are calculated, with the neighbor array values taken from the original image and the neighborhood on the outside of the lines. If the results are within certain tolerances previously determined by the user, the edge pixel is declared to be a bridge pixel. For the case where the pair of reverse parallel lines are  $0^\circ$  and  $180^\circ$ , the only edge pixels checked are those that are along the lower line, the line segment closest to the bottom edge of the image. See Figure (10) for the  $0^\circ$  neighborhood. The assumption made here is that if a bridge over water is approached so it appears to be parallel to the horizon, then there most probably will be water "in front of" the bridge, relative to the viewer. It was observed that sometimes the contour of the land directly "behind" the bridge (relative to the viewer) was



Neighborhood for edge pixel on a  $0^\circ/180^\circ$  line segment  
Figure (8)

"close" to the bridge so that neighborhoods on the region of the upper line edge pixels would overlap on what was land, and thus the statistics would be outside the set tolerances. A suggestion for a future improvement might be to check for water next to both lines, with the upper line increasing the confidence it is a bridge if those edge pixels are declared bridge pixels in addition to the edge pixels on the lower line.

This is the only case coded at the present time. The remaining

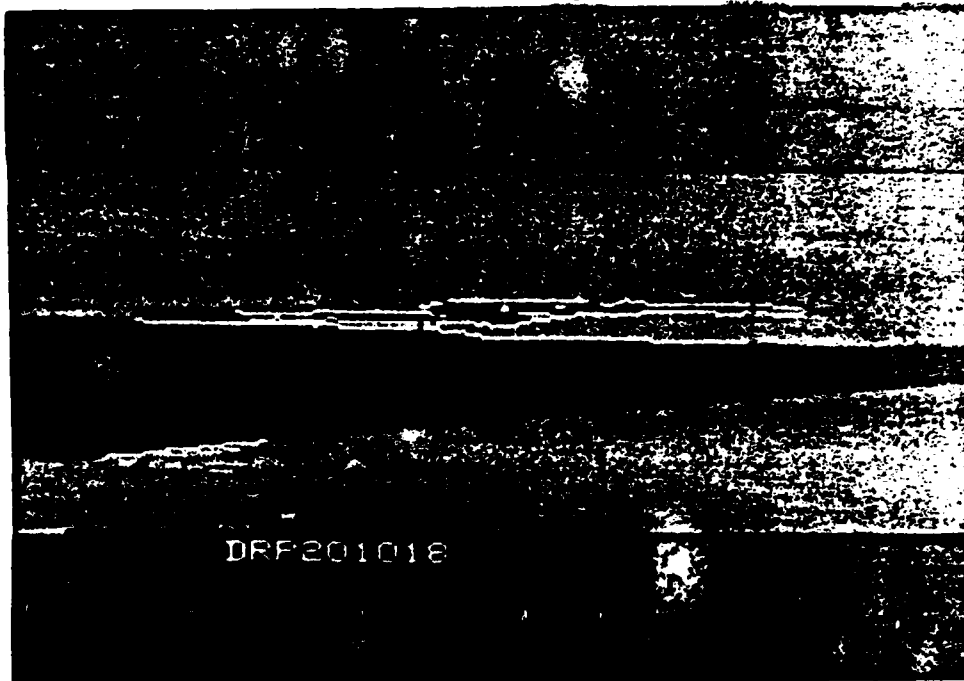


Figure 10a. Original image with Revpars highlighted.(see Fig 2a for original)

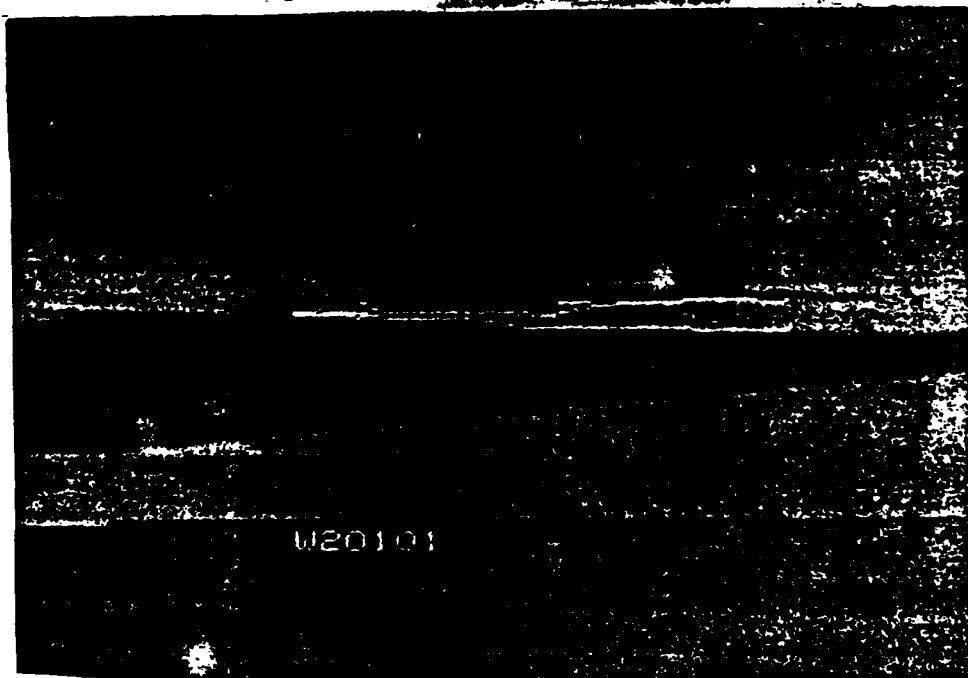


Figure 10b. Original image with only Revpars close to water highlighted.

five cases, for the reverse parallel lines  $30^\circ - 210^\circ$ ,  $60^\circ - 240^\circ$ , etc., are similar to the  $0^\circ/180^\circ$  case. Unfortunately, time ran short to code and debug these last cases.

#### VIII. Recommendations.

The Fortran program that implements the algorithms developed to detect bridges on data gathered by Texas Instruments, Inc., (TI), is located in the Image Processing Lab (IPL) at Eglin AFB. A user's guide is available which will help the user to set parameters for the purpose of experimentation. The program was designed to operate specifically on TI images as provided by the IPL; however, with only slight modifications, it will process other imagery whose dimensions are less than or equal to  $120 \times 360$ .

Bridges in FLIR images appear to have intensities which are local maximums in the direction orthogonal to the edges of the bridge. A simple procedure could be used to check if a Revpar has this property. A line segment, L, can be constructed which passes through the midpoints of the overlapping parts of the Revpar. The midpoint of L would be halfway between the line segments which make up the Revpar. The endpoints can be chosen outside of the bridge. A parabola can then be fit through the intensity values of these three points. Only the leading coefficient of the interpolating polynomial needs to be checked. If the coefficient is positive then the Revpar is probably not a bridge, if the coefficient is negative then the Revpar could be a bridge.

The line segment approximation subroutine could be simplified. Presently the algorithm approximates the edges by extending a line segment to the successor of an endpoint and then checking the distances of all the points that are already on the line segment to the new line segment. This procedure involves many computations of distance, which is inefficient. If a characterization of what is considered a line segment by the algorithm could be found using the octal chain code, then the computation time may possibly be decreased significantly.

It would be desirable to be able to extend the program to include locating bridges over other terrain. This is feasible due to the modular structure of the program. Up through finding reverse parallel

line segments, the algorithm does not use contextual information concerning the immediate surroundings of the Revpar. Subroutines could be added so that if certain conditions were satisfied, the appropriate subroutine would be called to use contextual information to determine if the line segments constitute a bridge over a specific terrain, as for example, over railroad tracks.

Other contextual and geometric information can be utilized to increase the confidence a bridge is located. Super- and substructures can be classified. The periodicity of bridge pilings which occur at regular intervals may be able to be utilized.

The fact that bridges usually connect homogeneous regions may be utilized. For example, narrow peninsulas in bodies of water are often detected as possible bridges, which is undesirable. Bridges also result in discontinuities of the objects they cross. This is taken advantage of as in the case of bridges over water. Another example is a bridge over a road disconnects the roads it crosses over. Thus, examining scene content and geometric details in the area of the reverse parallel lines will aid in detecting bridges in various contexts.

The algorithm could be applied to other fixed high value targets. Immediately before the algorithm looks for REVPAR's the image has been segmented into directed line segments. These directed line segments could be used as "primitives" for further analysis. A runway could be described in terms of directed line segments. In fact, any object whose shape can be approximated by a polygon can be described in terms of directed line segments. Thus the possibilities for other applications of modifications of the algorithm are good.

## IX. Results

The algorithm processed 60 images, 37 of which were inspected closely. For each input image, the output was two images, one image containing the thinned edges and the other image containing the reverse parallel lines. These images were hardcopied and put in a large binder, available from the IPL. Of the 37 thinned images, 17 retained 90% or more of the target edge pixels. Eighteen retained partial edges of the target. Partial edges are any edges up to 90% of the total target edge pixels. Of the 37 revpar images, 14 retained 90% or more of the target edge pixels, and 20 retained partial edges of the target. Of the 35 thinned images that retained any target edge pixels, nearly all (90%) of the detected target edges were present in the corresponding revpar images. The results are contained in the table below:

	No. of Images/35	Percent
Whole edge of target in		
Thinned Image	17	49%
Partial edge of target in		
thinned image	18	51%
Total	35	100%
Whole edge of target in		
revpar image	14	40%
Partial edge of target		
in revpar image	18	51%
Total	32	91%

The algorithm seemed to detect targets at long range where there is less detail. This is probably partially due to the line segmentation subroutine, which kept line segments from 2 pixels in length and longer. Therefore, closer to the target where edges are likely to have more detail, short line segments describing these edges were numerous and seemed to "clutter" the image.

Of the four images where the water checking subroutine was run, the

revars kept did include target pixels. See Figures for these results.

The algorithm does an excellent job of detecting edges where there is a reasonable amount of contrast. The reverse parallel lines are also fairly well detected. Hopefully, these two procedures provide much information which can be utilized to continue development on a fairly high confidence bridge detection algorithm.

## Appendix A - Program Users Guide

This appendix has four parts; how to run the program, a flow chart of the program, and a list of subroutines with a brief description of what each subroutine does, and an indexed list of images.

Anyone wishing to use the program is advised to read the main body of the report and then examine the flow chart (Figure A). The program is designed to be experimental, and therefore there are parameters which the user can set and subroutines which the user can choose to use or not use. In order to set the parameters and choose the routines to use one should have a clear idea of how the program works.

### 1. How to Run the Program

The program is designed to operate on the bridge images (DBRG) in the TI database. (Changing to other IRHVTA images would be a matter of minor revisions of the READ and WRITE statements).

You must have the following things available in your account:

- i) The programs DATAIN.EXE  
BRBATC/FOR  
BCOMLINK.COM  
BRUN.COM

- ii) The file NAME.DAT

- iii) A directory to store the output images.

The first thing you must do is create a directory to store the output images. For example if you want to create the directory [DOE.IMAGES] simply type

```
CREATE/DIR [DOE.IMAGES]
```

on the CRT.

Next thing to do is change the name of the output files in the code itself must be changed. This can be done by the following steps:

- i) type EDIT BRBATC.FOR return
- ii) type C return

You are now in the edit mode

- iii) Use the FIND command to look for NAME1.

NAME 1 occurs three times, one for each output image. When you find it, simply replace the existing directory and subdirectory with your directory and subdirectory [DOE.IMAGES]. DO THIS IN ALL THREE CASES.

iv) type CTRLZ

v) type EXIT

Now you must compile and link the program which can be done by typing SUBMIT BCOMLINK. The job is run by batch mode.

The above steps only need only be done once. At this point you will have the executable program BRBATCH.EXE which is what you will use to run the program.

Now you type RUN DATAIN. The questions shown in Figures 2 will appear on the screen sequentially. The indented questions will be asked only if the preceding question was answered Y.

To answer question number 2 you must enter the index numbers of the images you want to process. The index numbers are given on the last 3 pages of this appendix. For example, if you want to process DBRG 20126.IMG you would enter 6. Questions 5 and 6 offer room for experimentation. You may answer N to 5 and Y to 6. The program will then do the local average and then threshold. You may answer Y to 5 and N to 6. The program will then simply threshold. You may answer Y to both or N to both. To answer 8-10 you must know that:

AVI:= mean intensity of water

ALPH:= standard deviation of ALPH

G:= mean standard deviation of water

BETA:= standard deviation of G.

There is room for experiment here also. For example, if the user wanted to use only the standard deviation of water as a feature the user could set AVI and ALPH equal to zero.

If the user answers Y to 12 then the parameters, the bridge file name, and the number of Revpars will be written to a file PARJOBNO.DAT.

## 2. SUBROUTINES

This section lists the subroutines in the order that they are

called. A brief description of what they do is given, and the user supplied parameters they use are listed.

CONV

Parameters: MSIZE

This is a subroutine to convolve an image with a mask. The mask can be 3x3, or 5x5. MSIZE is the size of the mask.

APRUNE

This subroutine smooths the direction array using a variable window.

THRESHOLD

Parameters: ALPHA:

This subroutine computes the mean M and standard deviation S of an array. Zero values are not used in the computation. The array is then thresholded at

$$T = M + \text{ALPHAXS.}$$

LOCAVE

This subroutine uses 3x3 windows to perform a local averaging operation on an array.

THIN

This subroutine thins the convolved image according to the conditions listed in Section IV.

SCALE

This subroutine linearly scales an array so that its entries will have values between 0 and 255.

RERITVIM

This subroutine puts an image into the proper format for display on the Deanza. RERITVIM calls the library routines VIMALL and VIMPOT. The formatted image is written to a file.

CHANGE

This subroutine changes the subscripts from (Column, Row) to (Row, Column).

PRELINK

This subroutine generates the successor-predecessor files used to later approximate the edges by linear segment.

PIXLINK

This subroutine generates the endpoints of the line segments which approximate the edges. The number of line segments is computed here.

REVPAR

Parameters BW

This subroutine establishes pairs of reverse parallel line segments. BW is an upper bound on the distance between the segments of a REVPAR.

SUCCESS

This subroutine computes the coordinates of the successor of a pixel.

CHANGE2

This subroutine changes the subscripts from (Row, Column) to (Column, Row).

WATERCK

This subroutine checks for water below a horizontal Revpar.

STARTI

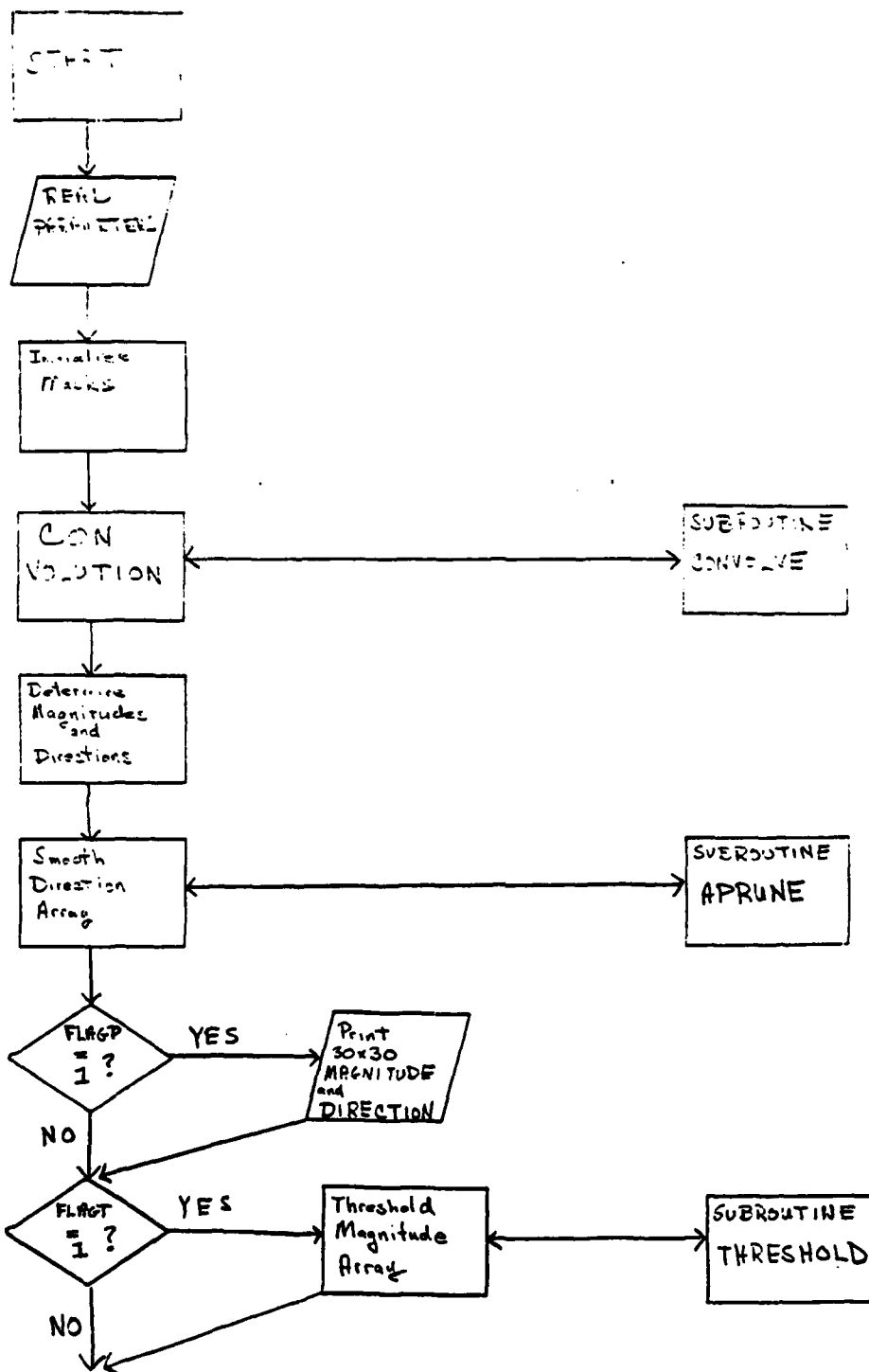
This subroutine is used to determine to initial and endpoints of the overlapping parts of a Revpar if the  $0^\circ$  line is on the bottom.

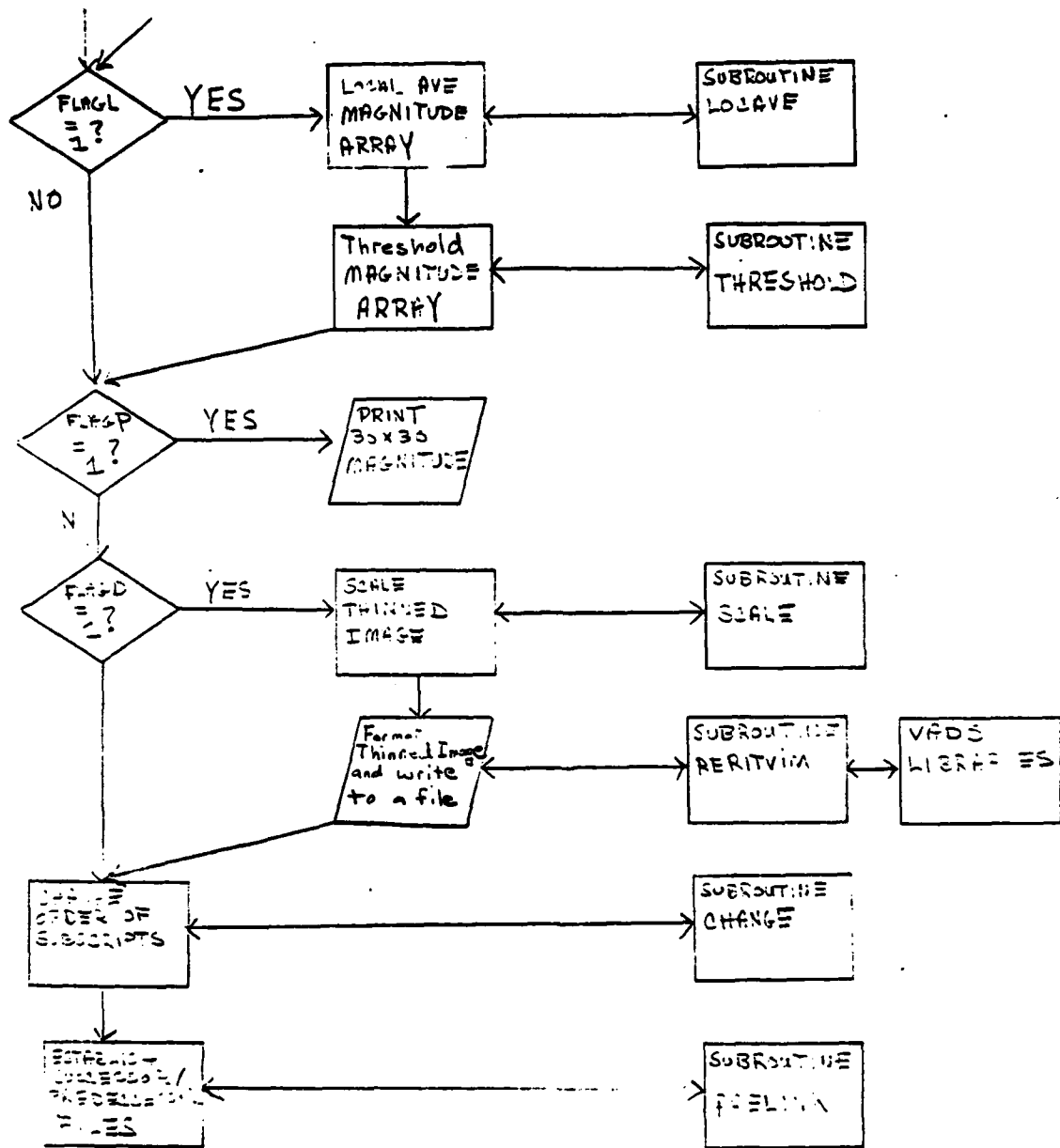
STARTJ

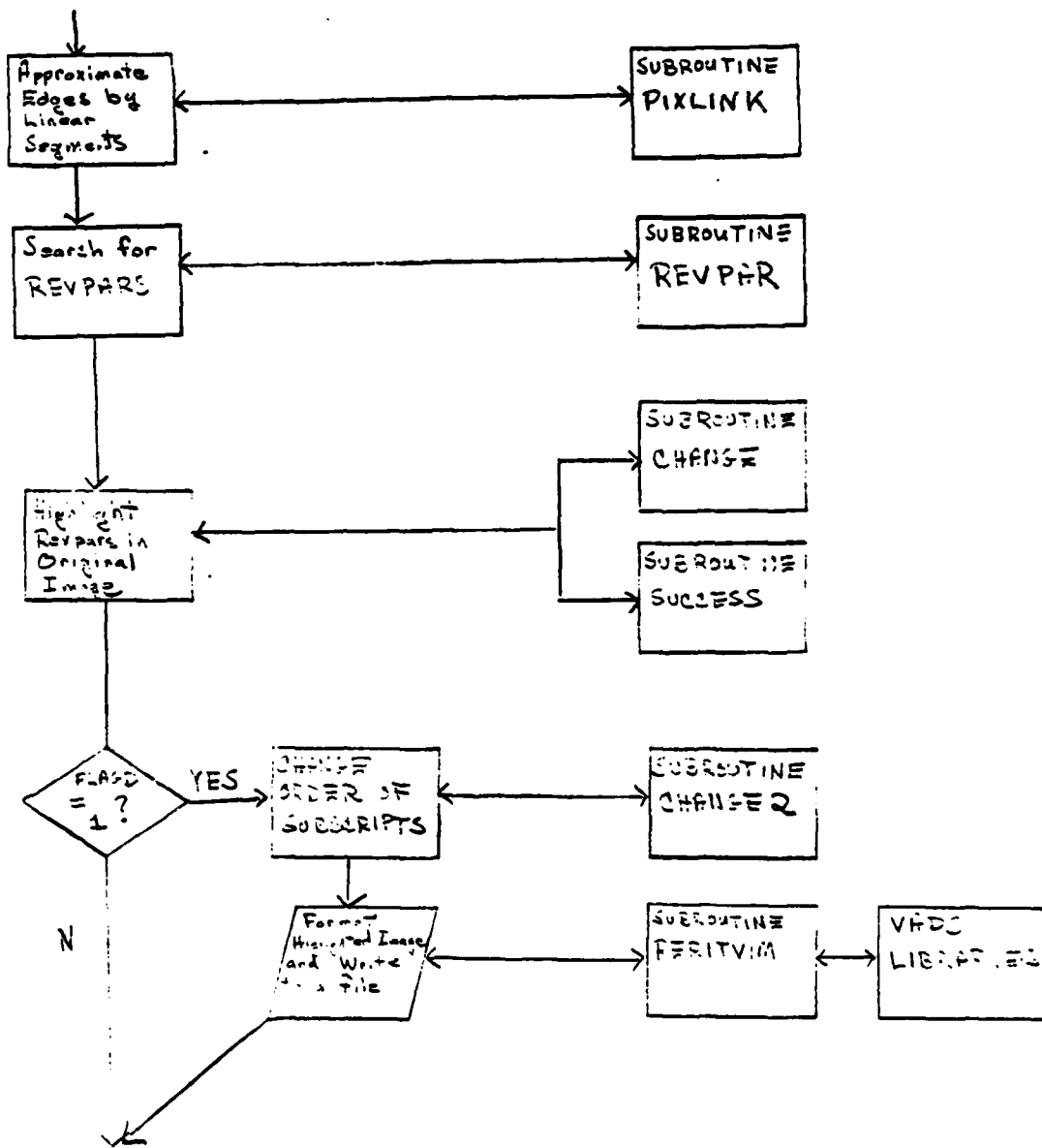
Same as STARTI except if  $180^\circ$  line is on the bottom.

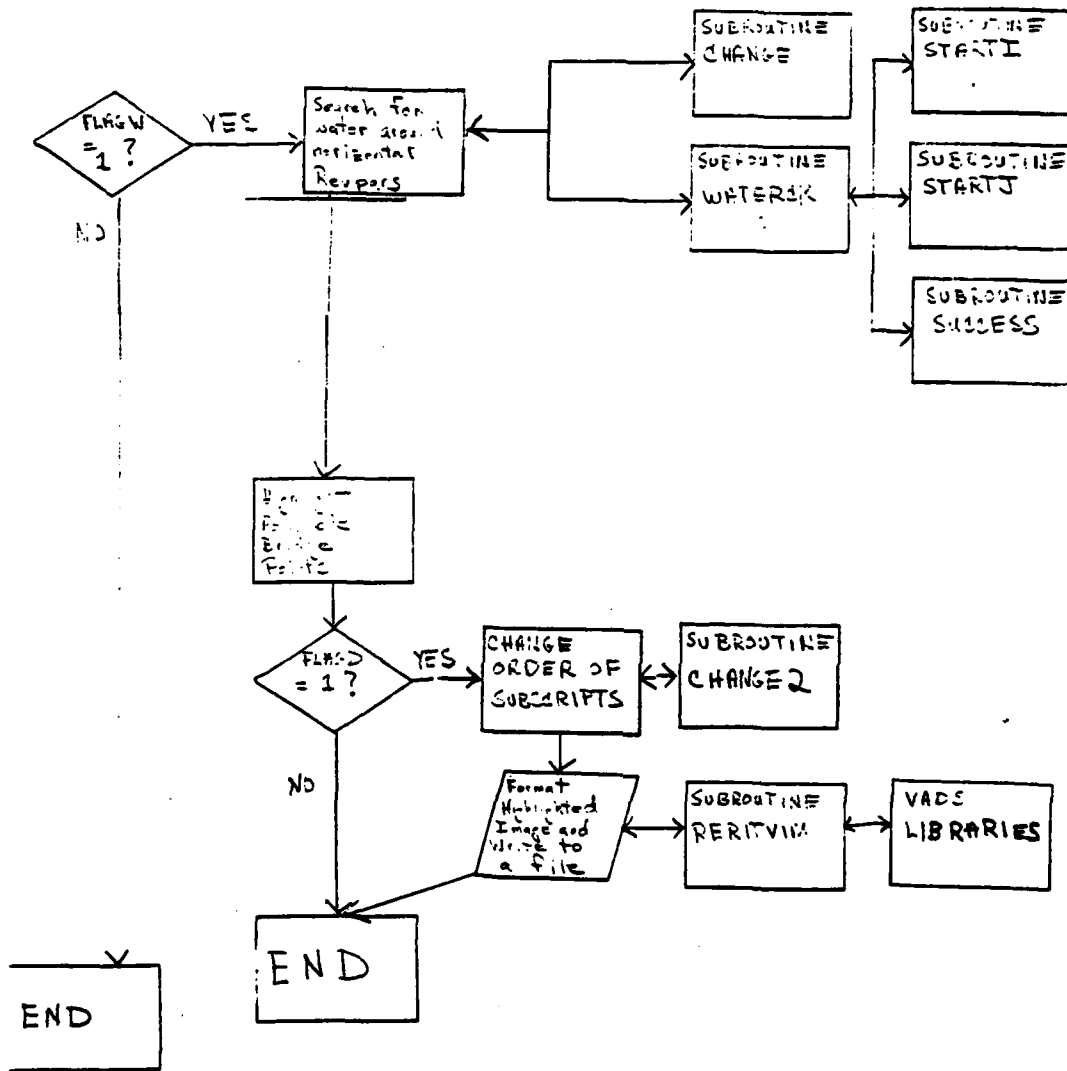
3. The next four pages contain the flowchart of the program. The left most column contains processing steps done by the main routine. The middle column contains optional processing steps. The rightmost column contains subroutines.

4. The pages after that contain the indexed listing of the bridges. This is the listing you must use to run the program.









1. ENTER THE NUMBER OF IMAGES YOU ARE PROCESSING IN YOUR JGB (UP TO 50)
2. ENTER THE FILE NUMBERS IN THE USERS GUIDE THAT YOU WISH TO PROCESS. TYPE THEM IN ONE AT A TIME.
3. THE MASK SIZE DEFAULT IS FOR THE 3X3 MASKS. DO YOU WISH TO CHANGE IT TO THE 5X5 MASKS? (Y OR N)
4. THERE ARE TWO OPTIONS FOR OUTPUT FROM THIS PROGRAM. ONE IS TO GET IMAGE TYPE FILES AND DISPLAY THEM ON THE DE ANZA, AND THE OTHER IS TO HAVE A 30X30 SUBARRAY OUTPUT IN A FILE WHICH YOU CAN PRINT OUT ON THE PRINTER. IF YOU WOULD LIKE THE 30X30 PRINTOUT ON THE PRINTER OPTION, PLEASE TYPE Y. TYPING N WILL CREATE FILES TO BE DISPLAYED ON THE DE ANZA.
  - 4.1 PLEASE ENTER THE UPPER LEFT HAND COORDINATES OF THE 30X30 SUBARRAY. (ROW, COLUMN).
5. DO YOU WISH TO THRESHOLD? (Y OR N)
  - 5.1 THE FIRST THRESHOLD PARAMETER IS ALPHA= ,ALPHA, . DO YOU WISH TO CHANGE IT? (Y OR N)
    - 5.2 YOU MUST ENTER A DECIMAL POINT IN YOUR ANSWER. PLEASE ENTER THE NEW ALPHA PARAMETER:
6. THE LOCAL AVERAGE WILL BE COMPUTED ON THE IMAGE IF YOU TYPE IN A Y. IT WILL NOT BE COMPUTED IF YOU TYPE IN A N.
  - 6.1 THE SECOND THRESHOLD PARAMETER IS ALPHA1= ,ALPHA1, . DO YOU WISH TO CHANGE IT? (Y OR N)
    - 6.2 YOU MUST ENTER A DECIMAL POINT IN YOUR ANSWER. PLEASE ENTER THE NEW ALPHA1 PARAMETER:
7. THE DEFAULT FOR THE BRIDGE WIDTH IS 8 PIXELS. DO YOU WISH TO CHANGE IT? (Y OR N)
  - 7.1 PLEASE TYPE IN THE NUMBER OF PIXELS YOU WANT FOR THE BRIDGE WIDTH. IT CAN BE ANY REAL NUMBER, UP TO 7 DIGITS LONG. YOU MUST TYPE A DECIMAL IN YOUR NUMBER.

THE WATER STATISTICS ARE SET AS FOLLOWS:

AVI= ,AVI,

ALPH= ,ALPH,

G= ,G,

BETA= ,BETA,

8. DO YOU WISH TO CHANGE AVI? (Y OR N)?

8.1 YOU MUST TYPE A DECIMAL IN YOUR NUMBER. PLEASE ENTER THE NEW  
VALUE FOR AVI:

9. DO YOU WISH TO CHANGE ALPH? (Y OR N)?

9.1 YOU MUST TYPE A DECIMAL IN YOUR NUMBER. PLEASE ENTER THE NEW  
VALUE FOR ALPH:

10. DO YOU WISH TO CHANGE G? (Y OR N)?

10.1 YOU MUST TYPE A DECIMAL IN YOUR NUMBER. PLEASE ENTER THE NEW  
VALUE FOR G:

11. DO YOU WISH TO CHANGE BETA? (Y OR N)?

11.1 YOU MUST TYPE A DECIMAL IN YOUR NUMBER. PLEASE ENTER THE NEW  
VALUE FOR BETA:

12. DO YOU WISH A PRINTOUT OF ALL THE PARAMETERS? (Y OR N)

THE PRINTOUT IS BOTH ON THE SCREEN AND IN THE FILE <sup>PARJEN.DAT</sup> ~~PAR.DAT~~.

13. THE DEFAULT IS TO CHECK FOR WATER. TYPE Y IF YOU WISH TO DO THIS.  
TYPE N IF YOU DON'T.

Appendix B  
Extended Bibliography  
Books

- Duda, R. Pattern Recognition and Scene Analysis, (J. Wiley and Sons, Inc., New York, 1973).
- Grasselli, A. Automatic Interpolation and Classification of Images, (Academic Press, New York, 1969).
- Mott - Smith, J. C. Picture Processing and Psychopictorics, (Academic Press, New York, 2970).
- Pavlidis, T. Structural Pattern Recognition, (Springer - Verlag, Berlin, 1977).
- Pratt, W. K. Digital Image Processing, (J. Wiley and Sons, New York, 1978).
- Rosenfeld, A. Picture Processing by Computer, (Academic Press, New York, 1969).

Extended Bibliography

Articles

- Barnard, S. "Disparity Analysis of Images," IEEE Transactions, PAMI, July 1980.
- Calabi, L. "Shape Recognition, Prairie Fires, Convex Deficiencies and Skeletons," American Mathematical Monthly, April 1968
- Delp, E. "Edge Detection Using Contour Tracing," Center for Robotics and Integrated Manufacturing, College of Engineering, University of Michigan, August 1983.
- Dudani, S. "Locating Straight-Line Edge Segments on Outdoor Scenes," Pattern Recognition, 1978, Vol. 10.
- Elliott, F. "Segments Wobble on Infrared Images," SPIE Proceedings, Vol. 359, August 1982.
- Frei, W. "Fast Boundary Detection: A Generalization and a New Algorithm," IEEE Transactions on Computers, October 1977.
- Hamadini, N. "Automatic Target Cueing in IR Imagery," AFITAU Thesis, December 1981
- Kestner, W. "Object Guided Segmentation of Aerial Images," IEEE Publication. March 1980.
- Kim, J. "A Context Dependent Automatic Target Recognition System," SPIE Conference, May 1984.
- Levialdi, S. "On Shrinking Binary Picture Patterns," Communications of the ACM, January 1972.
- Lineberry, M. "Image Segmentation by Edge Tracing," SPIE Proceedings, Vol. 359, August 1982.
- Rosenfeld, A. "Edge and Curve Detection for Visual Scene Analysis," IEEE Transactions on Computers, May 1971.
- Smith, M. "A New Algorithm for Edge Detection," Proceedings of the Third International Conference on Pattern Recognition, 1974.
- Velasco, F. "Some Methods for the Analysis of Sharply Bounded Clusters," IEEE Transactions on Systems, Man and Cybernetics, August 1980.

**1984 USAF-SCEEE SUMMER FACULTY-GRADUATE STUDENT SUMMER  
SUPPORT PROGRAM**

**Sponsored by the**

**AIR FORCE OFFICE OF SCIENTIFIC RESEARCH**

**Conducted by the**

**SOUTHEASTERN CENTER FOR ELECTRICAL ENGINEERING EDUCATION**

**Final Report**

**Computer-Based Optimization Algorithm  
for LOGAIR Cargo Allocation**

**Prepared by:** Dr. Kendall E. Nygard, Associate Professor  
and Director of Operations Research  
Timothy R. Downes, Graduate Student  
Researcher

**Department and  
University:** Division of Mathematical Sciences,  
North Dakota State University

**Research Location:** Air Force Logistics Command, Directorate  
of Management Sciences (XRS)  
Wright-Patterson AFB, Ohio

**USAF Research  
Contact:** Mr John Madden

**Date:** August 10, 1984

**Contract No.:** F49620-82-C-0035

**Computer-Based Optimization Algorithms  
for LOGAIR Cargo Allocation**

by

**Dr. Kendall E. Nygard  
Timothy R. Downes**

**Abstract**

This report describes a mathematical formulation for modeling the LOGAIR system. It also discusses other contributions made during the summer research program.

The LOGAIR system is a privately contracted airlift system providing daily air cargo service to 56 bases in the continental United States (COMUS). The Air Force manages and controls the operation which uses 16 separate routes. Allocation of cargo to system capacity is presently handled manually by controllers stationed at WPAFB and various Air Logistics Centers located elsewhere.

Because of the limited efficiency of manually allocating cargo, and the great potential for human error, a way of mathematically modeling the allocation process and incorporating this model into a computer-based allocation system is investigated. The discussion centers on how certain aspects of the allocation process can be modeled as a multi-period generalized assignment problem, while other aspects could be modeled as a multicommodity capacitated transshipment problem.

Although the above formulations are difficult combinatorial optimization problems, recent studies suggest that the allocation models could be solved daily on a microcomputer. The mathematical models developed to date are presented and suggestions made for further research in development of the model and for implementing this model as the basis of a computer-based allocation system.

### Acknowledgements

The authors would like to thank the Air Force Office of Scientific Research, the Air Force Logistics Command and the Southeastern Center for Electrical Engineering Education for providing us with the opportunity to spend a worthwhile summer becoming familiar with the operations of the Air Force Logistics Command. We would particularly like to thank Mr Vic Presutti and Mr John Madden of the Directorate of Management Sciences for their hospitality and valuable assistance throughout the summer. We would also like to thank the personnel of AFLC/AFOCO and AFLC/DS for all the time they gave us while we gathered the necessary information on the LOGAIR system.

## I. INTRODUCTION

Many problems of both practical and theoretical importance involve finding combinations of variables which provide optimal or near optimal solutions given an objective function and a specific set of constraints. For the Air Force in particular, one such problem is the daily task of allocating cargo to available airlift capacity in the LOGAIR (Logistics Airlift) system.

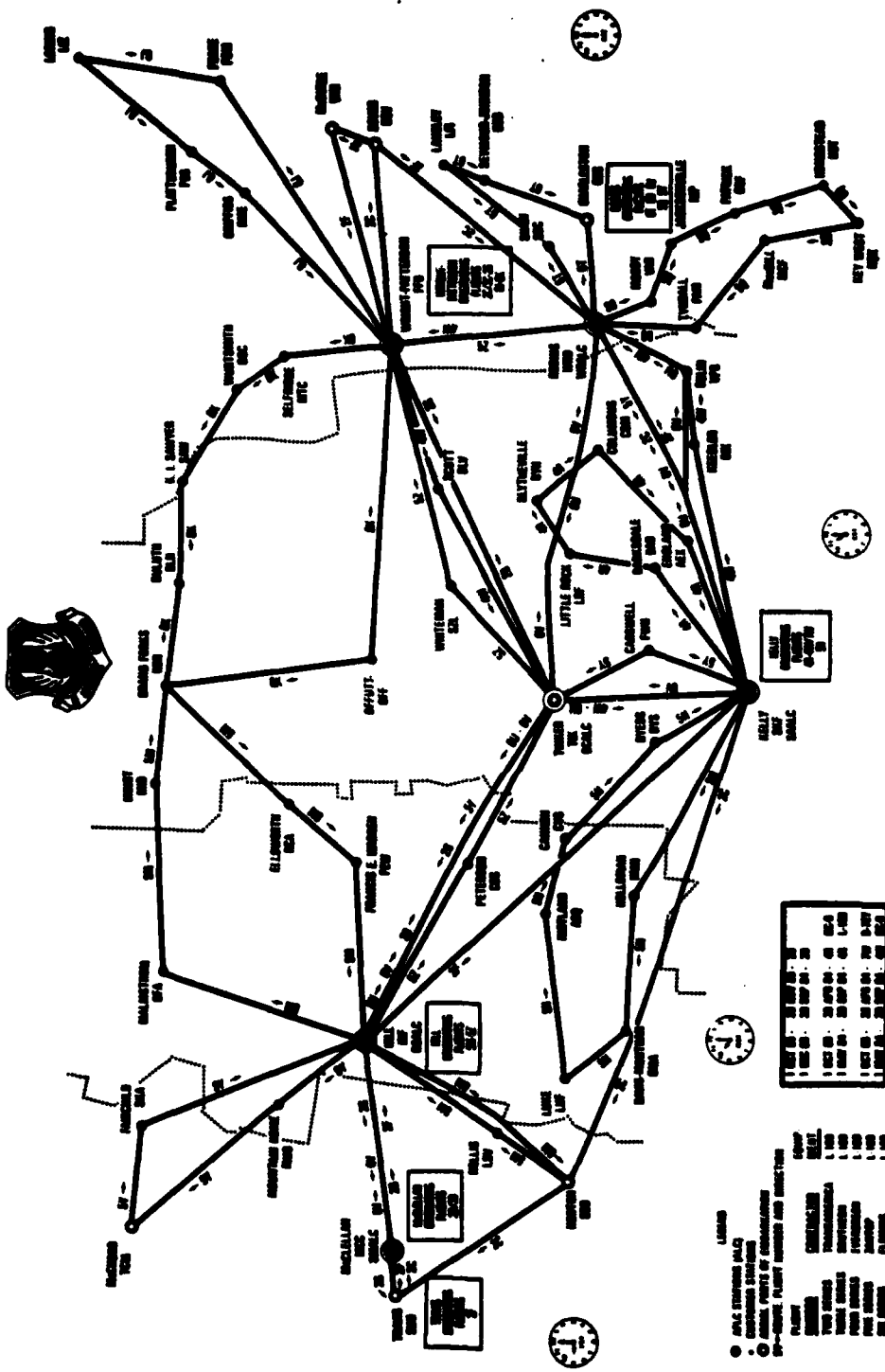
LOGAIR exists to provide fast transportation of high priority cargo among 56 Air Force bases in the Continental United States (CONUS). As shown in Figure 1, five Air Logistics Centers (ALC's) located at the Kelly, Tinker, Hill, McClellan and Warner-Robbins Air Force Bases as well as Wright-Patterson AFB (WPAFB) serve as cargo interchange points with feeder routes emanating from each location. Trunk routes connect the ALCs, WPAFB and points of embarkation at McGuire, Dover and Travis Air Force Bases. Allocation to these routes is made manually by controllers at WPAFB and some of the ALCs.

As Figure 1 suggests, allocation of cargo to the LOGAIR system is a complex task due to the enormous number of ways that pallets can be assigned to aircraft. The problem is complicated by multiple types and priorities of cargo pallets and types of aircraft. In addition, all bases must be adequately serviced and transit times must meet Air Force requirements. The complexity of the problem limits the efficiency of a manual allocation system, but lends itself to some degree of mathematical modeling and automation.

In an effort to model the more complex combinatorial characteristics of the cargo allocation problem, the authors have spent 10 weeks learning much of the operation of the LOGAIR system and developing preliminary models which reflect particular aspects of the allocation process. This paper describes these preliminary models, their use in a computer-based allocation system and the potential benefits of such a system. In addition, other contributions made to the AFLC during the same 10 week period are briefly discussed.

# UNITED STATES AIR FORCE LOGISTIC AIRLIFT ROUTE STRUCTURE

EFFECTIVE 1 OCTOBER 1963



- LEGEND**
- MILITARY STATION (MIL)
  - COMMERCIAL STATION
  - AIRPORT (A)
  - AIRCRAFT PLANT (PLANT)
  - AIRCRAFT PLANT NUMBER AND DIRECTION
- | PLANT | NUMBER | DIRECTION |
|-------|--------|-----------|
| 1     | 100    | 100       |
| 2     | 200    | 200       |
| 3     | 300    | 300       |
| 4     | 400    | 400       |
| 5     | 500    | 500       |
| 6     | 600    | 600       |
| 7     | 700    | 700       |
| 8     | 800    | 800       |
| 9     | 900    | 900       |
| 10    | 1000   | 1000      |

FIGURE 1

## II. OBJECTIVES

The objective of this study was to develop a mathematical model for the LOGAIR cargo allocation process. This model would be the basis for a computer-based on-line allocation system.

### III. EVALUATION of PRESENT MANUAL ALLOCATION PROCESS

Because of the complexity of the cargo allocation process, the efficiency of a manual allocation system is limited. There are three basic reasons for this.

First, even the most experienced human controllers cannot simultaneously consider the enormous number of ways that the pallets could be assigned on a given day. As a result, it is frequently the case that allocations which move more cargo exist, but are overlooked by the controller. An underlying mathematical model could identify allocations which improve aircraft utilization and move more cargo.

Second, under the present entirely human allocation process, arithmetic errors tend to occur, necessitating backtracking and double checking at times when their human skills need to be more creatively used. A computer-based system would eliminate much of this error.

Finally, the ten LOGAIR controllers tend to use personalized allocation schemes, which produce a variety of final allocations. A mathematical model would add consistency to the process, making all persons involved more comfortable with the allocations, making it easier for supervisors to review allocations and to train new controllers.

#### IV. THE MATHEMATICAL MODEL

During the Summer of 1984, preliminary work on the mathematical model was carried out by the authors. Several characteristics of the problem appear in models which have been recently described in the literature by the author of this proposal and other researchers. These include the multi-period and multiple-choice knapsack problems (Faaland, 1981; Sinha and Zoltner, 1979), the generalized assignment problem (Nygard et al, 1984; Nygard and Nelson, 1983; Fisher and Jaikumar, 1981); and the multicommodity network flow problem (Kennington and Helgason, 1980, Rosenthal, 1983). We now present some of our progress on the mathematical model. The following notation is adopted:

### Indices and Index Sets

$i$  = index of a base served by LOGAIR.  $i = 1, 2, \dots, n$ , where  $n$  is the total number of bases in the entire LOGAIR System. For a particular flight  $f$ ,  $n_f$  is the index set of bases served by flight  $f$ .

$p$  = index of a priority class for airlift available cargo.

$p \in P = \{s, 1, 2\}$ , where  $s$  is special high priority (MICAP and 999 cargo), 1 and 2 are military standard transportation priorities 1 and 2.

$f$  = index of a LOGAIR route.  $f \in F$ , where  $F$  is the set of all routes.

$k$  = pallet index.  $k \in K_{ij}^p$ , where  $K_{ij}^p$  is the set of priority  $p$  pallets at base  $i$  destined for base  $j$ .

### Constants

$NUM_{ij}^p$  = Number of priority  $p$  pallets at base  $i$  destined for base  $j$ .

$CAP_f$  = Pallet capacity of the aircraft type which flies route  $f$ .

$d_{ij}$  = Distance from base  $i$  to base  $j$ .

$W_{ij}^{pk}$  = Weight of the  $k^{\text{th}}$  pallet of priority  $p$  at base  $i$  destined for base  $j$ .

$PR_p$  = Mathematical "weight" associated with priority  $p$  (chosen so that higher priority cargo is allocated first)

$C_{ij}^{pk} = d_{ij} * W_{ij}^{pk} * PR_p$  = Benefit of Shipping the  $k^{\text{th}}$  pallet of priority  $p$  from base  $i$  to base  $j$ .

### Variables

$$X_{ij}^{pk} = \begin{cases} 1 & , \text{ if the } k^{\text{th}} \text{ pallet of priority } p \\ & \text{ at base } i \text{ destined for base } j \\ & \text{ is allocated to flight } f \\ 0 & , \text{ Otherwise} \end{cases}$$

For a particular fixed route index  $f$ , consider the following mathematical model:

$$\text{Max} \quad \sum_{i=1}^n \sum_{j=1}^n \sum_{p \in P} \sum_{k \in K_{ij}^p} C_{ij}^{pk} * X_{ij}^{pkf}$$

Subject to:

$$\sum_{j=2}^n \sum_{p \in P} \sum_{k \in K_{1j}^p} X_{1j}^{pkf} \leq \text{CAP}_f$$

$$\sum_{j=3}^n \sum_{p \in P} \sum_{k \in K_{1j}^p} X_{1j}^{pkf} + \sum_{j=3}^n \sum_{p \in P} \sum_{k \in K_{2j}^p} X_{2j}^{pkf} \leq \text{CAP}_f \quad (1)$$

⋮

$$\sum_{j=n}^n \sum_{p \in P} \sum_{k \in K_{1j}^p} X_{1j}^{pkf} + \sum_{j=n}^n \sum_{p \in P} \sum_{k \in K_{2j}^p} X_{2j}^{pkf} +$$

$$+ \dots + \sum_{j=n}^n \sum_{p \in P} \sum_{k \in K_{n-1,j}^p} X_{n-1,j}^{pkf} \leq \text{CAP}_f$$

$$\sum_{k \in K_{ij}^p} X_{ij}^{pkf} \leq \text{NUM}_{ij}^p \quad (2)$$

$i, j = 1, 2, \dots, n; p \in P$

Each constraint in set (1) represents a leg of the flight, and ensures that aircraft pallet capacity is not exceeded. Note that the constraints model off-loading along the route as appropriate, so that the constraints are not fully cumulative as they are in a multi-period knapsack problem (Faaland, 1981). An additional constraint set similar to (1) is needed to ensure that the total weight the aircraft is allowed to carry is not exceeded.

Constraint set (2) ensures that the model allocates only pallets which are actually available for shipment. In practice, this model must be expanded to accommodate the two different sizes of pallets in use, and the regularly occurring need to link two or more pallets together in a train. Constraint set (2) can be modified and written with equations by adding a dummy flight which can absorb all excess pallets from each leg at an artificially high cost. The new constraints would be:

$$X_{ij}^{pkd} + X_{ij}^{pkf} = 1 \quad i, j = 1, 2, \dots, n_f; k \in K_{ij}^r; p \in P$$

where d is the index of the dummy flight. The resultant model might then be called a multi-period generalized assignment model. The model extends the generalized assignment model because the pallet allocations use aircraft capacity on flight legs beyond the leg on which they are first allocated. The author of this proposal has implemented two state-of-the-art generalized assignment codes for use in vehicle routing (Nygard et al, 1984; Nygard and Nelson, 1983).

The above model could only handle a few of the existing LOGAIR routes, since most of the routes have flight legs in common and tradeoffs among flights need to be accommodated. An extension of the above model could simultaneously allocate a collection of flights with common legs.

To accomplish the extension, a network can be defined, with a node for each base, and arcs for the flight legs. Assume that common flight legs are coalesced into a single arc, with a capacity equal to the sum of all the component flight leg capacities. The cargo allocation problem can then be modeled as an integer multi-commodity capacitated transshipment problem on this network. In this formulation, adopt the following notation:

$b_{iq}$  = Supply of pallets of type q at base i, where  $q \in Q$ , an index set of all pallet types. In this model, there is a pallet type for each origin-destination pair (i,j) and priority p. Negative supply values are used for demands at destination bases.

$U_h$  = Joint capacity over all commodities of network arc h, where  $h \in H$ , an index set of arcs in the network.

$F_i$  = Forward star of node i (Collection of all arcs which originate at node i).

$R_i$  = Reverse star of node i (Collection of all arcs which terminate at node i).

$D_{hq}$  = Disutility associated with a pallet of type q being transported over arc h (This is the negative of the aircraft utilization measure used in the first model).

With this notation, the following optimization problem can be written:

$$\begin{aligned} & \text{Min } \sum_{h \in H} \sum_{q \in Q} C_{hq} X_{hq} \\ \text{Subject to: } & \sum_{h \in F_i} X_{hq} - \sum_{h \in R_i} X_{hq} = b_{iq} \quad h \in H, q \in Q \\ & \sum_{q \in Q} X_{hq} \leq U_h \quad h \in H \\ & X_{hq} \geq 0 \text{ and integer} \quad h \in H, q \in Q \end{aligned}$$

The solution to this optimization problem yields a set of integer cargo movements (flows) which maximize aircraft utilization. If there is surplus capacity on a common flight leg, the existing LOGAIR preferred flight list would be used to choose among the aircraft. A dummy node and dummy arcs leading to it from supply nodes would absorb excess supply and ensure feasible allocations when aircraft capacity cannot handle all cargo waiting to be moved. Like the first model, this formulation requires refinement to handle weight as well as pallet count capacity, and additional variables to model alternative pallet sizes and trains.

Both of the above formulations are difficult combinatorial optimization problems. However, very recent progress on the generalized assignment problem carried out by the author (Nygard et al 1984, Nygard and Nelson, 1983) and on the continuous version of the multi-commodity capacitated transshipment problem by others (Rosenthal, 1983) suggest that this cargo allocation problem can be solved to optimality on a microcomputer on a daily basis. Under this proposal, the basic research needed to fully develop these models would be carried out. The study will be complete with actual coding and experiments carried out.

## V. RECOMMENDATIONS

Both of the above formulations are difficult combinatorial optimization problems. However, very recent progress on the generalized assignment problem carried out by one of the authors (Nygard et al 1984, Nygard and Nelson, 1983) and on the continuous version of the multi-commodity capacitated transshipment problem by others (Rosenthal, 1983) suggest that this cargo allocation problem can be solved to optimality on a microcomputer on a daily basis.

The authors have submitted a proposal to conduct the research that is needed to fully develop these models and to implement them as part of a computer-based allocation system. We feel that, aside from benefits realized from standardizing allocation procedures, expediting the allocation process and reducing arithmetic errors, the proposed system could result in the following three basic types of benefits:

1. Decreased Need to Invest in Spares. Lower Order and Ship Times (OST) and retrograde time (DRT) can allow a reduction in the investment for spares needed to maintain the same level of readiness. A recent study carried out by Gambill of AFLC/XRS (Gambill, 1984) calculated potential cost savings in inventory investment for a range of OST and DRT values and an 80% availability level. This study indicates that a decrease of one day in OST and DRT corresponds to a cost decrease of about \$34.9 million, or about 2.3 percent.

2. Increased Readiness. Assuming system costs are held constant, reductions in OST and DRT can help increase readiness. Even though readiness is a function of many factors and MICAP items are typically shipped within DoD standards for transit time (Van Valkenburgh, 1980; Wasem, 1983), some calculations which relate to readiness improvement are still possible. One part of the Gambill Study (Gambill, 1984) assumed constant costs and calculated increases in the availability of weapon systems which result from OST and DRT decreases. For example, with a one day decrease in OST and DRT, weighted total availability over all weapon systems increased from a baseline of 80% to a new level of 81.95%.

3. Decreased Direct Costs. When major cargo backlogs occur, additional flights called extra sections are employed to move the cargo. Use of the proposed mathematical model may occasionally eliminate the need for extra sections, saving the direct costs of fuel, contractor payments, and landing fees. These annual operating costs for the entire LOGAIR system are presently about \$100 million per year. Eliminating, for example, a 2000 mile flight which costs \$7.5/mi to operate would save \$15,000 in operating costs.

## VI. OTHER CONTRIBUTIONS

In addition to researching a cargo allocation model formulation, the authors also presented several technical reports discussing alternative approach to problems of immediate concern for AFLC personnel.

One report suggests improvements to the Logistics Management Institute (LMI) Aircraft Availability Model used by AFLC/XRS. This report recommends several computational techniques which can potentially decrease run-times of the model by taking advantage of structure occurring naturally in the data and by replacing a sequential search by a binary search.

A second report discusses a program designed and coded this summer. The purpose of the program was to compare two files created by the same model on two separate computer systems to see if both files contain identical data. A copy of the program along with appropriate documentation was submitted to AFLC personnel for review.

A third report proposed a generalized network model to simulate how aircraft availability relates to maintenance, distribution and procurement systems. A scaled-down model was presented to appropriate AFLC personnel along with a description of how this approach might be applied on a larger scale.

A final report addressed the Air Force Program Objective Memorandum (POM) assessment. The POM involves the need to relate the funding of different categories of support to warfare capability of specific weapons systems. The approach suggested in this report modeled, in a macro way, how various support activities result in levels of weapons systems, and the way levels of weapon systems combine to result in general wartime capability. The technique used was the analytic hierarchy process developed primarily by Thomas Saaty (Saaty, 1982).

The suggestions made in the first two reports will likely be implemented. The latter two reports were presented to help AFLC personnel maintain an awareness of techniques in the forefront of current research. Copies of these reports may be obtained from HQ AFLC/XRS.

## REFERENCES

- (1) Faaland, B., "The Multiperiod Knapsack Problem," *Operations Research* 29(3), 1981 pp 612-616.
- (2) Fisher, M., "The Lagrangian Relaxation Method for Solving Integer Programming Problems," *Management Science* 27(1), 1981.
- (3) Fisher, M., R. Jaikumar, and L. Van Wassenhove, "A Multiplier Adjustment Method for the Generalized Assignment Problem," preprint to appear in *Management Science*, 1984.
- (4) Gambill, J. "Study for LOGAIR Hub Return on Investment" AFLC/XRS document, June, 1984.
- (5) Kennington, J. and R. Helgason, Algorithms for Network Programming New York: Wiley, 1980
- (6) Nelson, M., K. Nygard, J. Griffin and W. Shreve, "Implementation Techniques for the Vehicle Routing Problem," *Computers and Operations Research*, in press, 1984.
- (7) Nygard, K., R. Walker and P. Greenberg, "Computational Experience with a Generalized Assignment-based Algorithm for Vehicle Routing," technical report presented at the TMS/CRSA National Meeting, San Francisco, May, 1984.
- (8) Rosenthal, R. "Resource Directive Multicommodity Flows Algorithms," talk presented at North Dakota State University under the Operations research visiting scholar series, November, 1983.
- (9) Saaty, T. and L. Vargas, The Logic of Priorities, Boston: Kluwer-Nijhoff, 1982.
- (10) Sinha, P. and Z. Zoltners, "The Multiple Choice Knapsack Problem," *Operations Research* 27(3), 1983 pp 503-515.
- (11) Van Valkenburg, N. "LOGAIR Mark 2: An Alternative Logistics Airlift System," *Air Force Journal of Logistics*, Spring, 1980, pp 25-29.
- (12) Wasem, V., LOGAIR: A Study to Determine the Feasibility of Implementing a Hub and Spoke Distribution Network for LOGAIR AFLC document, October, 1983.

1984 USAF-SCEEE SUMMER FACULTY RESEARCH PROGRAM

Sponsored by the

AIR FORCE OFFICE OF SCIENTIFIC RESEARCH

Conducted by the

SOUTHEASTERN CENTER FOR ELECTRICAL ENGINEERING EDUCATION

FINAL REPORT

CALCULATION OF ENHANCED HEATING IN TURBULENT BOUNDARY  
LAYERS INFLUENCED BY FREE STREAM TURBULENCE

Prepared by: Dr. Paavo Sepri  
and Mr. Jon L. Ebert

Academic Ranks: Associate Professor  
and Graduate Student

Department and University: School of A.M.N.E.  
University of Oklahoma

Research Location: Air Force Wright Aeronautical Laboratories  
Aero-Propulsion Laboratory  
Turbine Engine Division  
Components Branch

USAF Research Contact: Mr. Charles D. MacArthur

Date: 27 August 1984

Contract No.: F49620-82-C-0035

CALCULATION OF ENHANCED HEATING IN TURBULENT  
BOUNDARY LAYERS INFLUENCED BY FREE STREAM TURBULENCE

by

Paavo Sepri and Jon L. Ebert

ABSTRACT

A preliminary phenomenological computational model has been formulated and implemented for the purpose of predicting increased heating in boundary layer environments which are influenced by free stream turbulence. The model has been constructed primarily by scrutiny of recently published extensive flow measurements over heated flat plates, and it is also supported partially by analytical considerations. The mixing length model existing in the code STANCOOL has been modified to incorporate these free stream turbulence effects. The comparisons between measurements and calculations generally show improvement, but certain discrepancies are noted which require further investigation. An apparently novel observation is made concerning the structure of much of the outer region of a turbulent boundary layer in the presence of higher levels of free stream turbulence. Several variables follow a simple exponential character which may be of fundamental importance. This observation is used to lend credence to the computational model, but it also raises an apparent dilemma involving the energy equation. A central role in these calculations is played by the turbulent Prandtl number profile, the modeling of which determines quantitatively the heating of a surface. Comments are offered in connection with possible channel flow effects on measurements of  $Pr_t$  which indicate large decreases towards the free stream.

### ACKNOWLEDGEMENTS

The authors gratefully acknowledge the opportunity and support extended to them by the Air Force Systems Command, the Air Force Office of Scientific Research, and The Southeastern Center for Electrical Engineering Education during the course of this investigation. The effort was conducted at the AFWAL Aero-Propulsion Laboratory, Wright-Patterson AFB, Ohio. The hospitality of the personnel of the Components Branch of the Turbine Engine Division remains greatly appreciated.

Mr. Charles MacArthur and Dr. Richard Rivir are particularly deserving of our thanks for their interest in the project and for their guidance, suggestions, and joint discussions. The computer support and fellowship of Lieutenants Mike Stanek and Tom Currie are also gratefully acknowledged.

539

## I. INTRODUCTION

In the design of modern turbines it is becoming increasingly important to have a computational tool which can predict blade heating environments accurately and cost-effectively. The subject is sensitive owing to conflicting requirements; namely, improved engine performance is connected with increased gas temperature, whereas increased blade lifetime requires a lowered blade temperature. Since a blade typically operates near its structural limit, it is estimated that a decrease of only 30° F could double its lifetime<sup>1</sup>. Current methods of blade cooling, such as transpiration and/or internal flow, are also limited by their adverse effects on overall engine efficiency. Coolant flow rates are essentially limited by the allowable pressure differential along the passages. In view of these restrictions in design, it is important to have accurate means of calculating the associated blade heat transfers.

Any attempt to calculate the flow environment around the blades is hindered by the compounded complexity of the actual case, and also by the fact that turbulence remains an unsolved problem in general. Therefore, for this short investigation, an attempt is made to focus on a simplified problem, which retains some of the essential phenomena of the actual problem. The investigation is thus restricted to turbulent flow over a 2D flat plate which is heated so as to yield heat flux information. This restriction is particularly relevant from the computational viewpoint, owing to the recent publication of extensive experimental results for this case by Blair<sup>2-8</sup>.

One of the important effects, which influence heat transfer to a surface, is the presence of free stream turbulence (FST) external to the boundary layer. Although this subject has received considerable attention

in the past<sup>9-15</sup>, there appear to be conflicting claims<sup>11</sup> and an incomplete understanding, especially for the regime of higher FST levels encountered by turbine blades. It has been one of the goals of the recent investigations by Blair<sup>2</sup>, Bradshaw<sup>11</sup>, and Hancock<sup>16</sup> to clarify experimentally the extent of augmented heating in the presence of increased FST.

In an investigation prior to the present one, MacArthur<sup>1</sup> has applied a recent version of the widely used code STANS<sup>17</sup> to assess the extent of predictability of FST effects in turbulent heating, as compared with the measurements of Blair. The results were mixed: although some cases agreed well, and several trends were generally followed, it was apparent that the code neither reliably nor accurately predicted the location and extent of transition nor the observed increase in heating in a fully turbulent boundary layer modified by increased FST levels. This code, named STANCOOL, has several model options for calculating transition and also the structure of a turbulent boundary layer. Although one might have expected the inclusion of a turbulence kinetic energy equation into the model to have produced better results than the simpler mixing length model, both calculations agreed with each other better than with the data in several cases. These results have pointed to the need for improved computational capability.

The present investigation is meant to be in continuation of the effort by MacArthur, with the overall aim of understanding the effect of FST in the augmentation of turbulent heat transfer. This investigation focuses on the case of turbulent flow over a flat plate and the method of modifying STANCOOL so as to produce better agreement with the recent measurements by Blair.

## II. OBJECTIVES

It is appropriate to make a distinction between two types of objectives: long range and immediate. Clearly, the long range objectives are beyond the scope of the present investigation because the actual problems of interest are exceedingly complex, with various aspects having been subjected to considerable attention for several decades. Nevertheless for the sake of perspective, one might nominate two long range objectives. The practical objective involves the attainment of a computational capability which predicts heating and flow conditions in the real turbine blade environment both accurately and cost-effectively. An objective from the more philosophical viewpoint, but with practical consequences, is the increased understanding of the mechanisms and structure of turbulent shear flows.

For the present investigation the immediate objectives are restricted to the following:

- (1) To achieve a working understanding of the existing code, STANCOOL, which is meant to calculate boundary layer development and heating in flow situations similar to those in turbine blade environments.
- (2) To become familiar with literature pertaining to the effects of free stream turbulence on heating augmentation, in particular the recent extensive experimental works by Blair.
- (3) To formulate a preliminary turbulence model which incorporates the effects of FST into STANCOOL in an improved fashion.
- (4) To compare results of the modified code with Blair's data.
- (5) To recommend continued investigations in light of the present findings.

By means of these fundamental investigations, it is anticipated that

more accurate and reliable codes will eventually be at hand.

### III. PROBLEM DESCRIPTION

In order to meet the objectives listed in the previous section, the method of attack has consisted of four phases. First, Blair's data have been logged into computer storage for the purposes of plotting, scrutiny, and eventual comparison with computations. Second, detailed profile data have been compared with corresponding profiles obtained from STANCOOL, utilizing the mixing length model for computations. These comparisons have revealed possible causes for the earlier discrepancies<sup>1</sup> noted for Stanton number, which may be viewed as an integrated effect. Third, a modification of the turbulence model is being proposed on the basis of these comparisons and on the basis of earlier observations by Miyazaki and Sparrow<sup>9</sup> and Belov et al.<sup>10</sup>. Last, a comparison is made between Blair's data and the results of the new model.

A full description of the configuration and the physical parameters is given in Blair's reports<sup>2-8</sup>, and earlier computations using STANCOOL have been described by MacArthur<sup>1</sup>. The latest documentation available for the use of STANCOOL is given in Reference 17. Briefly, the measurements were made in a recirculating wind tunnel over a heated flat plate with a mean external velocity of 100 ft/sec. Typical mean temperature differences between the wall and the free stream were in the range 10°F to 40°F. The free stream turbulence level was varied by means of insertion of 5 different grid configurations upstream of the tunnel contraction section. The streamwise decay of FST intensity was in accord with those of previous grid generated experiments, and the intensity ranged approximately from 0.25% to 7%. Measurements included wall temperature distributions, wall heat fluxes, profiles of mean velocity and mean temperature, and profiles

of various turbulence correlations at selected downstream locations.

In Figure 1 are illustrated the variations of Stanton number and skin friction coefficient with changes in Reynolds number and FST parametrically. FST is seen to influence the results in two ways: (1) the location of transition moves upstream dramatically with increasing FST, and (2) both  $S_t$  and  $C_f$  increase in the fully turbulent boundary layer as FST increases. In fact, the results have shown<sup>4</sup> that the Reynolds analogy factor,  $2S_t/C_f$ , increases with FST, indicating that the heating is proportionately more sensitive to FST than is the skin friction coefficient. This observation is particularly important for turbine blade cases because these may occur at higher levels of FST (perhaps 20%) than have been measured in simulations. Blair's data for  $S_t$  are more extensive and exhibit less scatter than those for  $C_f$ . Therefore, the  $S_t$  data provide a better basis for comparison with computations. The solid lines in Figure 1 represent results from STANCOOL utilizing the pre-existing mixing length model. The predictions of transition location are not adequate, although it is important to note<sup>4</sup> that the experimental transition for grid configuration 0 (least FST) was prematurely effected owing to 3D corner flow effects, and that the extreme mismatch with calculations in this case should be discounted. Since the pre-existing mixing length model provides no mechanism for FST effects, the increase of  $S_t$  and  $C_f$  in the fully turbulent region is clearly not followed by the computations. During the ten week summer period of investigation, the focus has been restricted to the structure of the fully turbulent boundary layer.

Since  $S_t$  and  $C_f$  are evaluated at the solid boundary only, they possibly represent symptoms of more pervasive phenomena occurring throughout the

— STANCOOL Computations  
(Previous Mixing Length Model)

Blair Data<sup>4</sup>

FST(Nom.%)

- 0.25
- + 1.0
- 2.0
- γ 4.4
- △ 5.3

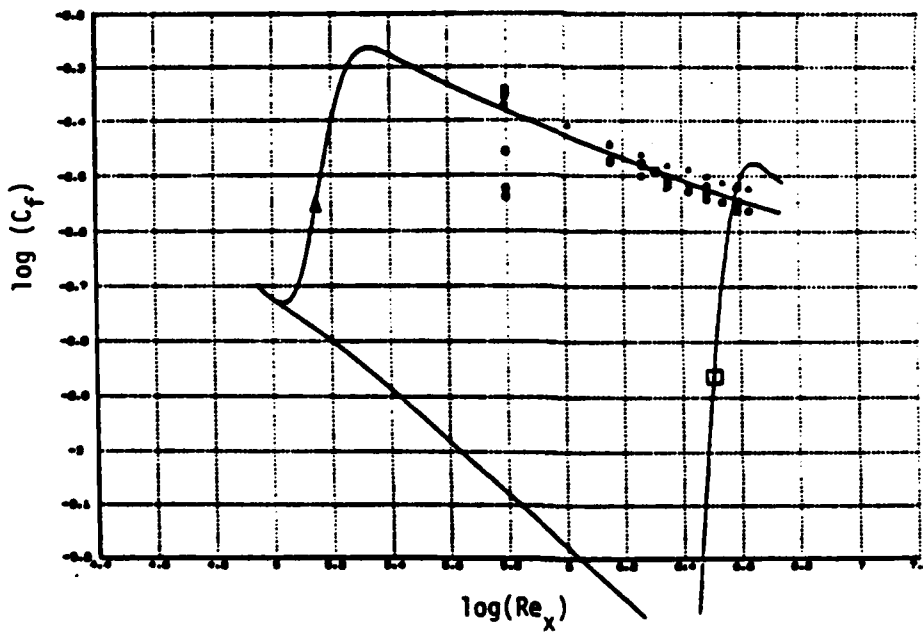
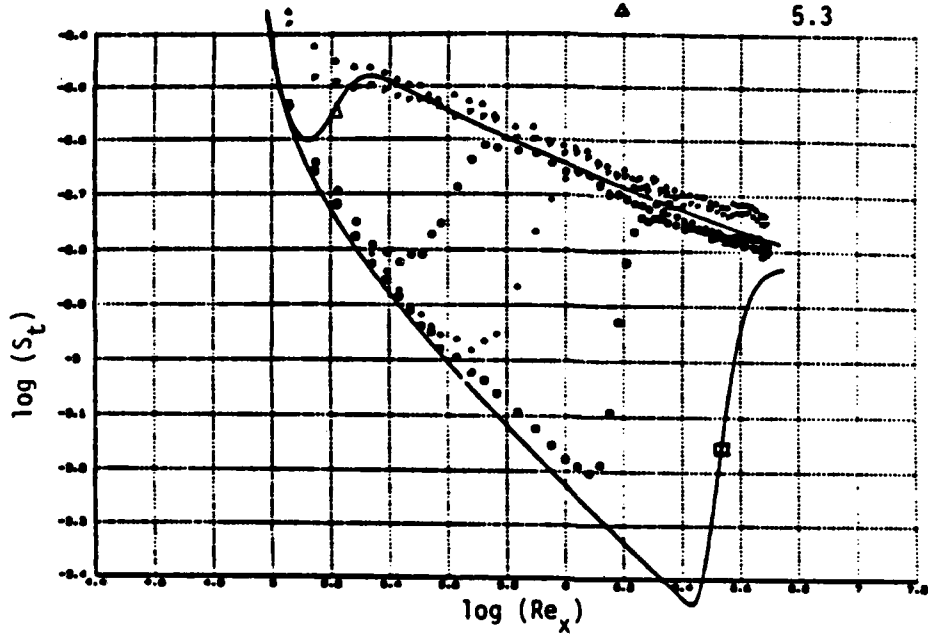


Figure 1: Comparisons of  $\log(S_t)$  and  $\log(C_f)$  vs.  $\log(Re_x)$  for various levels of FST.

boundary layer structure. In an effort to improve the understanding of underlying causes, a comparison of mean profiles was made. In Figure 2 are sample comparisons between computed and measured mean profiles at downstream location  $x = 84$  in. with grid configuration 4 (greatest FST). For this extreme case it is evident that the existing mixing length model does not match the  $\bar{u}$  profile in the center of the boundary layer, although the match near the wall appears to be better. However, the wall region is better shown in a logarithmic format since the variations there are extremely rapid. Similar comparisons of  $\bar{u}$  in cases of weaker FST show much better agreement, indicating that FST has a marked effect on boundary layer structure.

Lastly, in the comparison of profiles, it is important to illustrate the effect of FST on the Reynolds stress term  $\overline{u'v'}$ , and on the turbulent heat transfer term,  $\overline{v'T'}$ . These terms need to be modeled correctly, so that the ensuing computations of  $\bar{u}$  and  $T$  produce the correct results for skin friction and wall heating respectively. In Figure 2 it is seen that the mixing length hypothesis does not produce an adequate characterization of the Reynolds stress profile. In fact, the mismatch becomes worse as the FST increases. The experiments clearly indicate that values for  $\overline{u'v'}$  and  $\overline{v'T'}$  are increased towards the boundary layer edge and are decreased towards the wall in comparison to the model. Later results herein will show that the characteristics of turbulence decay into the free stream are severely altered by the presence of FST.

The avenue for an improved computation scheme then becomes more apparent. FST effects need to be accurately incorporated into the  $\overline{u'v'}$  and  $\overline{v'T'}$  descriptions. Subsequent computations of  $\bar{u}$ ,  $T$ ,  $S_t$  and  $C_f$  should then reflect better matches with the corresponding data. This point should

— STANCOOL  
(Previous Mixing Length Model)

□ Blair Data<sup>4</sup>  
5.3% FST (Nom.)

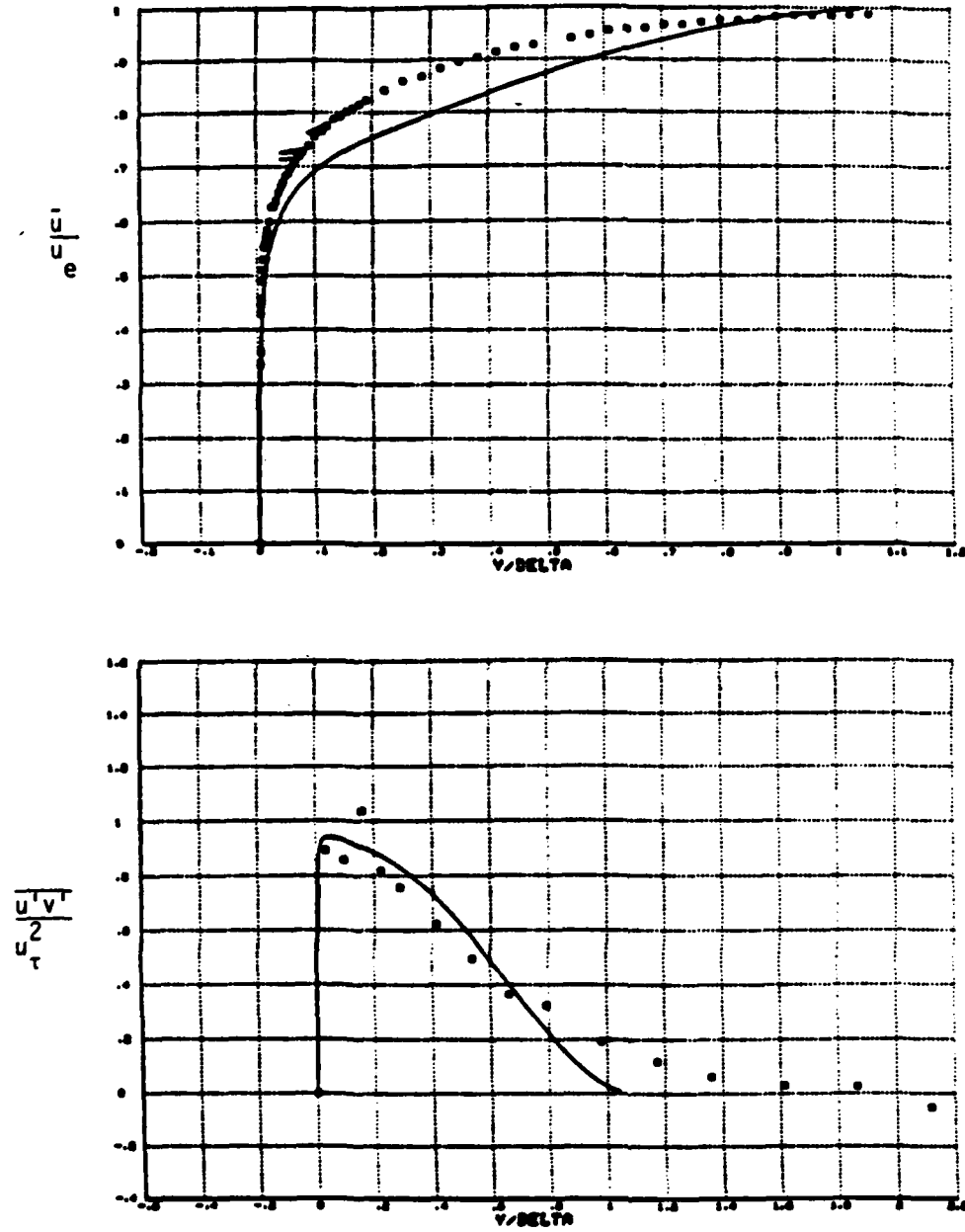


Figure 2: Mean velocity and Reynolds stress profiles.

be valid regardless of the complexity of the computational method, such as inclusion of higher order turbulence equations. An improvement in terms of a modified mixing length model is attempted in the next section.

#### IV. MODELING OF FREE STREAM TURBULENCE

A rational and consistent model for  $\overline{u'v'}$  and  $\overline{v'T'}$  is difficult to construct. Every model based on the equations of motion, regardless of complexity, requires a set of closure assumptions. In past investigations it has occurred that even the most refined and time consuming approaches have lead to results that have failed to produce improved predictions. The approach taken here has been to scrutinize Blair's data in order to appreciate the actual effects of FST, and then to formulate a simple model which contains the observed effects. By variations of the model parameters, important interplays in the equations of motion are highlighted, thereby indicating directions for continued and more accurate modeling.

The initial observation has been that the mixing length model fails to capture the essence of Coles' wake region<sup>18</sup> as the FST increases. Furthermore, as is evident from Figure 2, the turbulence structure extends into the free stream far beyond the usual definition of the boundary layer edge,  $\delta$ . This observation has also been made in References 19-22. However the extent to which the outer structure influences the wall region is not clear, and needs to be assessed. In studying the effect of FST on heating at the stagnation point of a cylinder, Miyazaki and Sparrow<sup>9</sup> proposed the following extension to the mixing length model:

$$\overline{u'v'} = \epsilon^2 \left| \frac{\partial \bar{u}}{\partial y} \right| \frac{\partial \bar{u}}{\partial y} + A \epsilon u_e I_e \left( \frac{y}{\delta} \right) \frac{\partial \bar{u}}{\partial y} - \overline{u'_e v'_e} (y/\delta)^2 \quad (1)$$

where the first term on the right is the usual mixing length model<sup>9</sup> and the second two terms represent the additional effects of FST. Here,  $I_e$  is the turbulence intensity external to the boundary layer. The coefficient,  $A$ , is the sole parameter that may be adjusted to match data. Miyazaki and Sparrow claim that the inspiration for their model originated from the experimental work of Belov et al.<sup>10</sup>, who observed that the r.m.s. fluctuation profile in the absence of FST was augmented in a linear fashion by the presence of FST.

Equation (1) appeared to be a reasonable starting point for the present investigation, especially since the measurements of Belov et al. were conducted over a flat plate, and also because the modification of STANCOOL would be particularly simple. The mixing length model was changed to:

$$\overline{-u'v'} = \epsilon_M \frac{\partial \bar{u}}{\partial y} \quad (2)$$

where  $\epsilon_M = \lambda^2 \left| \frac{\partial \bar{u}}{\partial y} \right| + A \lambda u_e I_e (y/\delta)$

This change in the code produced a significant, but limited, improvement. Now, several correct trends were introduced which were absent earlier:  $S_t$  and  $C_f$  increased with  $I_e$ ; the  $\bar{u}$  and  $\bar{T}$  profiles became fuller and matched Blair's data better; and the  $\overline{u'v'}$  and  $\overline{v'T'}$  profiles extended into the free stream at an improved rate. However, inconsistencies also appeared. With only one free parameter,  $A$ , it was not possible to match the variety of comparisons simultaneously. In particular:

- (1) With a good  $\overline{u'v'}$  match, the  $\bar{u}$  comparison with data was noticeably inadequate, although improved over the previous model; and vice-versa.

- (2) The  $S_t$  and  $C_f$  predictions required different values for  $A$  than did the mean profiles.
- (3) The slope of  $S_t$  and  $C_f$  vs.  $Re_x$  did not agree with the data for a constant value for  $A$ .

In an attempt to improve the Miyazaki and Sparrow model, Blair's data were replotted in several variations, one of which was a semilogarithmic version of the velocity defect, as exemplified in Figure 3. It is striking that the mean velocity defect appears to be well characterized by an exponential behavior for approximately the outer 80% of the boundary layer. Since this observation appears to be new in the literature, and since profound deductions might be connected with it, the issue was pursued further. The present conclusions are summarized as follows:

- (1) The exponential character does not occur for lower levels of FST ( $\leq 3\%$ ) as seen from Blair's data, in which cases the free stream levels are approached more rapidly.
- (2) It is suspected that the exponential character is approached as a limiting form for sufficiently high FST ( $> 4\%$  here), and that this form may hold for all higher levels of FST.
- (3) The mean temperature behavior has an exponential character which appears identical to that of the mean velocity.
- (4) A short distance downstream of the leading edge ( $\sim 2$  ft), the velocity and temperature profiles become self-preserving to an excellent degree, as described by the subsequent equations.
- (5) The  $\overline{v^2 T^2}$  profile also has a limiting exponential character as seen in Figure 3. However, the corresponding  $\overline{u^2 v^2}$  profile appears not to have such a form, either owing to experimental scatter or to a fundamental

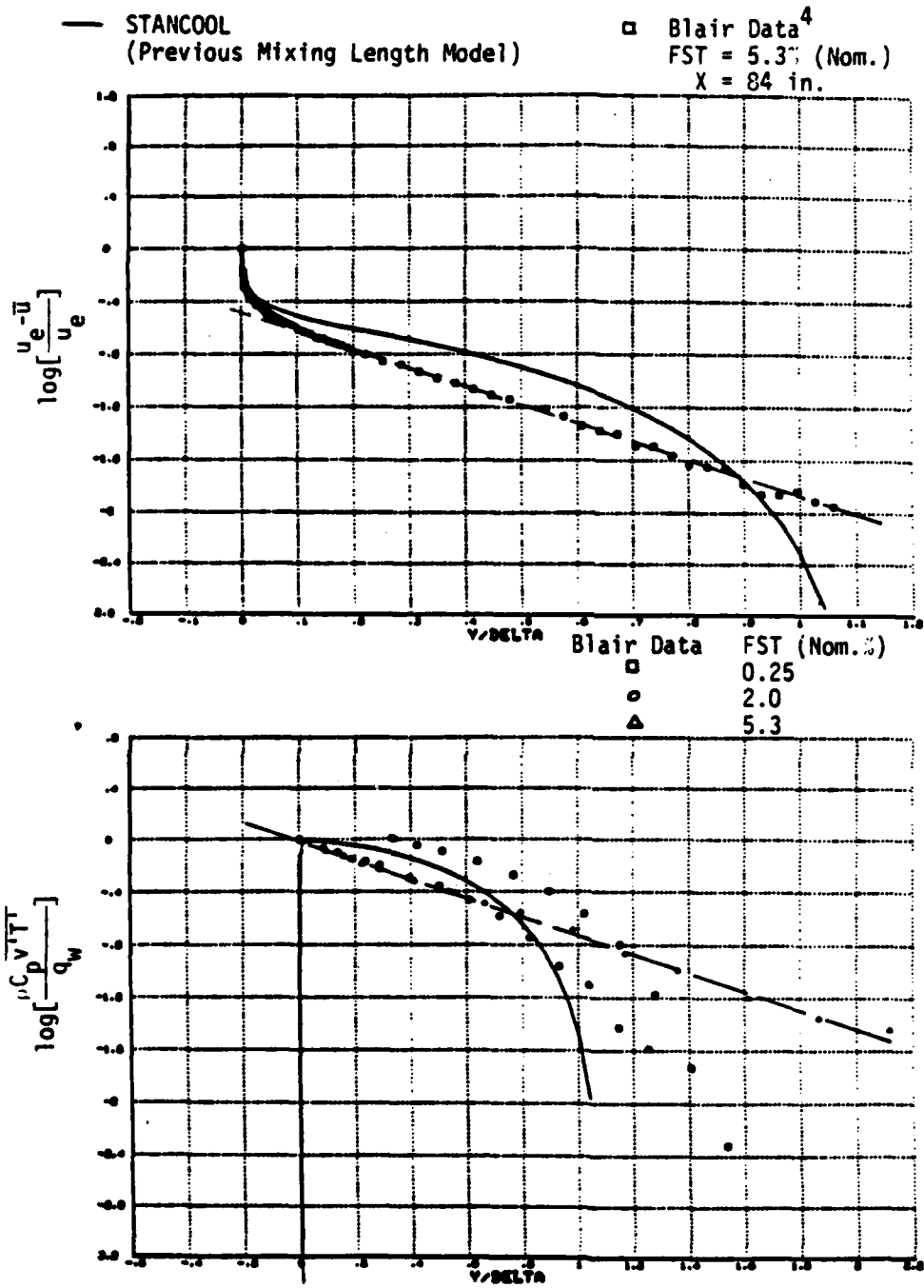


Figure 3: Boundary layer wake region characterized by exponential decay for cases of high FST levels.

difference in its nature. It is extremely interesting to note that the exponential decay rate of  $\sqrt{v''}$  appears to be exactly one half of the corresponding rates for  $T$  and  $\bar{u}$ . This point will resurface in what follows.

Given the observed exponential character of the outer region, it is possible to utilize the mean fluids equations to deduce explicit functional forms for  $\bar{u}''v''$  and  $\sqrt{v''}T''$  as applicable. The argument is summarized as follows:

(1) From experimental observation:

$$\frac{\bar{u}}{u_e} = 1 - \frac{1}{\beta} \exp[-\alpha \frac{y}{\delta}] \quad ; \quad \frac{\bar{T} - T_e}{T_w - T_e} = \frac{1}{\beta} \exp[-\alpha y/\delta] \quad (3)$$

where  $\alpha, \beta \equiv \sqrt{10}$

(2) From the ideal gas equation ( $\bar{p} \equiv \text{constant}$ ):

$$\frac{\bar{p}_e}{\bar{p}} = 1 + [\frac{T_w}{T_e} - 1] \frac{\exp[-\sqrt{10} y/\delta]}{\sqrt{10}} \quad (4)$$

(3) By integration of the conservation of mass equation:

$$\frac{\bar{p}v''}{\bar{p}_e u_e} = - [\frac{1}{T_e} \frac{dT_w}{dx} + \frac{T_w}{T_e} \frac{1}{\delta} \frac{d\delta}{dx} (1 + \sqrt{10} \frac{y}{\delta})] \frac{\delta \exp[-\sqrt{10}y/\delta]}{10} \quad (5)$$

(4) By integration of the momentum equation:

$$-(\frac{\bar{p}}{\bar{p}_e}) \frac{\bar{u}''v''}{u_e^2} = \{c(x) \frac{\partial \bar{u}''/u_e}{\partial y/\delta} + [\frac{1}{Re\delta} + \frac{1}{10} \frac{d\delta}{dx} (1 + \sqrt{10} \frac{y}{\delta})]\} \frac{\partial u''/u_e}{\partial y/\delta} \quad (6)$$

(5) By integration of the energy equation:

$$-(\frac{\bar{p}}{\bar{p}_e}) \frac{\sqrt{v''}T''}{u_e^3} = \{A_T(x) + yB_T(x)\} \exp[-\sqrt{10} y/\delta] \quad (7)$$

+ higher order exponentials

Several observations are made concerning these equations. First, the form obtained for  $\overline{u'v'}$  in Equation (6) is strikingly similar to the Miyazaki and Sparrow model given in Equation (2), and therefore this model appears to have further support. It should be emphasized that Equation (6) is not meant to be applicable in the wall region in which the exponential behavior is not observed. However, the term which includes the coefficient,  $c(x)$ , is very similar in form to the usual mixing length hypothesis. This leads to the speculation that FST may influence the wall region directly through this non-linear term. Second, there are two additional terms appearing in Equation (6) which do not appear in the earlier model. In comparison to the other terms,  $Re\delta^{-1}$  is negligible for the fully turbulent boundary layer, and it is therefore discarded below. The constant term is comparable to the  $y/\delta$  term and is therefore retained below. Third, the coefficient of the  $y/\delta$  term explicitly depends on  $x$ , whereas in the initial model based on Equation (2) the factor,  $A$ , was considered to be constant.

The deduction following from the energy equation leads to a noteworthy dilemma. For the high FST cases the experimental results for  $\overline{v'T'}$  consistently follow the form shown in Figure 3, in which the decay rate is one half that of the mean velocity and mean temperature. However, these assumptions lead to Equation (7), which indicates that the slowest decay is identical to that of  $\bar{u}$  and  $\bar{T}$ , not the half power. Furthermore, the appearance of the  $y/\delta$  factor in Equation (7) suggests that the semilogarithmic plot should not yield a straight line, in contradiction to experimental observation. Such a mismatch in form cannot be reconciled by adjusting the magnitudes of the coefficients; and therefore, there appears to be a fundamental inconsistency, which may have profound consequences. It is

necessary to reconsider the assumptions leading to Equation (7). Such an effort is beyond the present scope and is recommended for continued investigation. In brief, however, the mean energy equation leading to Equation (7) is the one utilized in STANCOOL, and it is commonly assumed to apply<sup>17</sup> in these cases. By cursory inspection and by an order of magnitude analysis, it appears that certain correlation functions involving density fluctuations ought not be neglected, and inclusion of these may resolve the dilemma.

In light of the previous discussion, the turbulence model formulated for the present study has evolved to the following:

Eddy viscosity:

$$c_M = \lambda^2 \left| \frac{\partial \bar{u}}{\partial y} \right| + A u_e I_e(x) \lambda \delta^m(x) D^n u_\tau^2(x) [1 + B(y/\delta)] \quad (8)$$

Turbulent Prandtl number:

$$Pr_t = \frac{c_M}{c_H} = \frac{\lambda^2 \left| \frac{\partial \bar{u}}{\partial y} \right| + [C_1 I_e + C_2] u_e \lambda \delta^m D^n u_\tau^2 [1 + B \frac{y}{\delta}]}{\lambda^2 \left| \frac{\partial \bar{u}}{\partial y} \right| + C_3 u_e \lambda \delta^m D^n u_\tau^2 [1 + B \frac{y}{\delta}] \exp[\frac{B}{4} \frac{y}{\delta}]} \quad (9)$$

where

$D$  is the van Driest damping factor<sup>17</sup>,

and

$$u_\tau^2 = \tau_w(x) = \frac{d\delta}{dx}$$

In Equation (8) the damping factor is included so that the FST addition vanishes in the wall region in comparison to the mixing length model. Furthermore, the streamwise dependence of the FST effect may be adjusted via the power of  $\delta(x)$ . The form chosen for  $Pr_t$  requires further comment, as it is clearly a compromise utilized solely for the sake of computation in

STANCOOL. In STANCOOL the turbulence effect on heating is modeled directly through  $Pr_t$ , and use of any other method would require extensive alterations of the code. In the spirit of the Reynolds analogy, it is assumed that the forms of  $\overline{u'v'}$  and  $\overline{v'T'}$  are similar, and this leads to the ratio expressed in Equation (9). The added modifications are introduced primarily in an effort to fit Blair's measurements of  $Pr_t$ . The exponential factor is added in compensation for the observed decay rate of  $\overline{v'T'}$  and also to produce the large decrease of  $Pr_t$  with increasing  $y$  that has been observed by several investigators <sup>4, 9</sup>. The constant,  $a$ , is included in an effort to vary  $Pr_t$  in the near wall region, and the constants  $C_1, C_2, C_3$  are chosen to match the observed increase of  $Pr_t$  with increasing  $I_e$ .

#### V. RESULTS

It is shown in this section that typical computations utilizing the model described by Equations (8) and (9) can produce results which are in better agreement with Blair's data than was the case with the original STANCOOL options. However, it is not claimed that the new model is free of inconsistencies, nor that it may be used with confidence in extrapolation to other flow regimes. The model is intended to highlight some of the new observations concerning the effects of FST, and also to be a vehicle for continued improvements.

Figures 4, 5, and 6 are intended to parallel the earlier discussions, with the inclusion of the results of the latest computations. In Figure 4 the computed boundary layer has been forced to undergo transition near the experimentally observed locations, with the objective of removing this added uncertainty from the comparisons. In contrast to Figure 1, the Stanton number now increases in the turbulent boundary layer as the FST

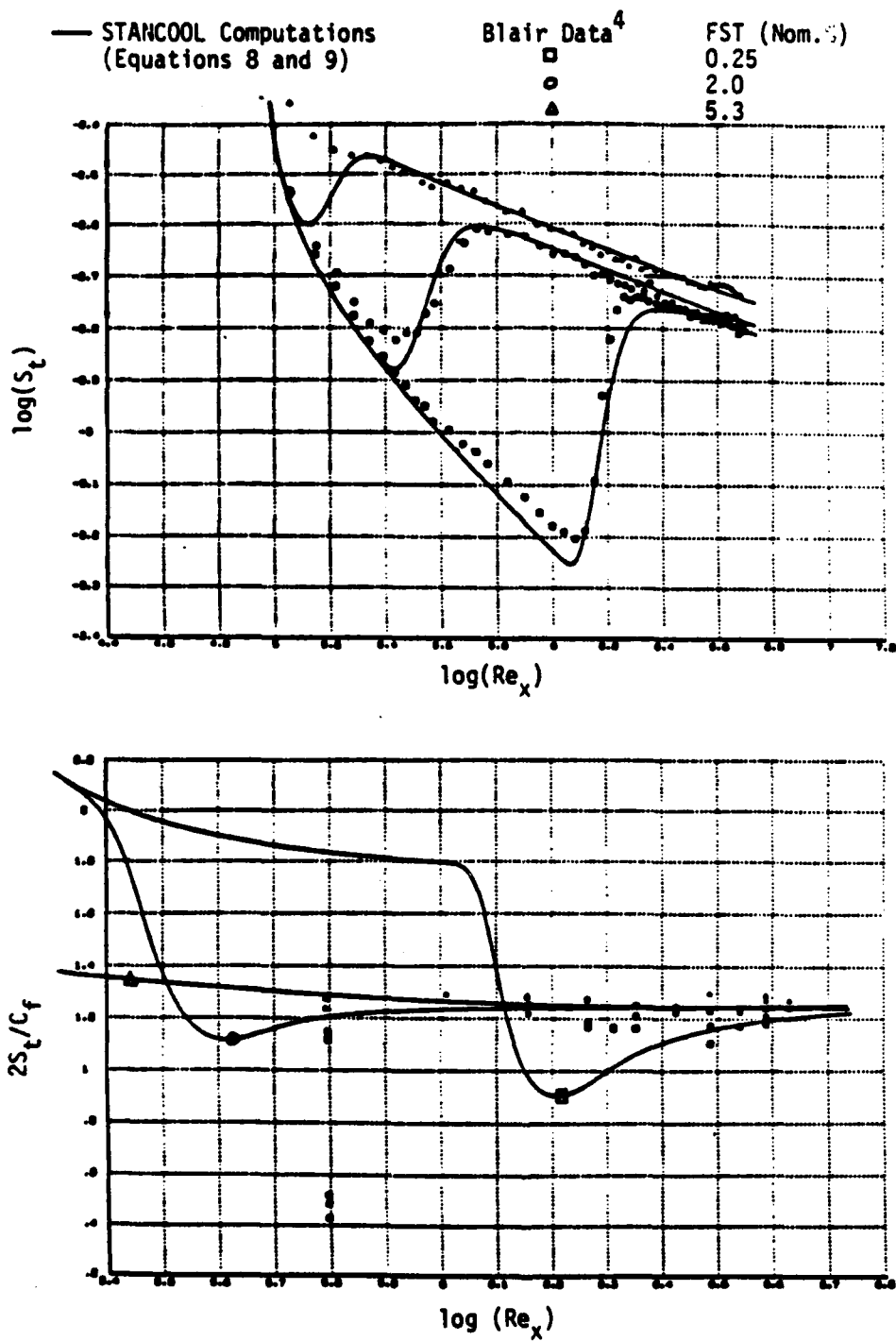


Figure 4: New mixing length model. Comparisons of Stanton number and Reynolds analogy factor with Blair's data.

level increases, and the comparison is good. In order to achieve these computations, the parametric values chosen in the model are as follows:

$$\begin{aligned} A &= 0.013 \\ m &= 1 \\ n &= 4 \\ B &= \sqrt{10} \\ C_1 &= 3 \\ C_2 &= 0.2 \\ C_3 &= 0.2 \\ a &= 1.18, 1.20, 1.50 \quad (\text{as FST increases}) \end{aligned} \quad (10)$$

In addition, the exponential coefficient in the van Driest damping factor<sup>17</sup> was chosen to be:  $A^+ = 35$ . During the search for these values, several other observations emerged. As might have been anticipated, significant changes in the outer portions of the  $\overline{u^*v^*}$  and  $Pr_t$  modeling had minor effects on  $C_f$  and  $S_t$ , unless the exponent of the damping factor,  $n$ , was chosen small enough so that the usual mixing length did not dominate the wall region. Although it has been claimed<sup>11</sup> that the wall region is rather insensitive to external changes, it is evident from Figure 3 that FST influences not only the wake but also that the law of the wall region is greatly reduced in size, perhaps disappears totally for high FST levels. It is vitally important to have measurements to small values of  $y^+(-5)$ , because the character of the damping factor cannot be inferred from the logarithmic region. In the present computations, the FST influence on  $C_f$  and  $S_t$  required an independent adjustment of  $A^+$  in order to effect correct trends. In addition, the near wall region of  $Pr_t$  required adjustment via the parameter,  $a$ , in order to model FST effects on  $S_t$ .

Although the arguments leading to Equation (6) prescribe a specific  $x$  dependence for the turbulence model, this dependence had to be slightly altered by the exponent,  $m$ , in Equation (8) in order to match the observed  $x$  variation of  $C_f$  and  $S_t$ .

In the lower half of Figure 4 are shown the variations of the Reynolds

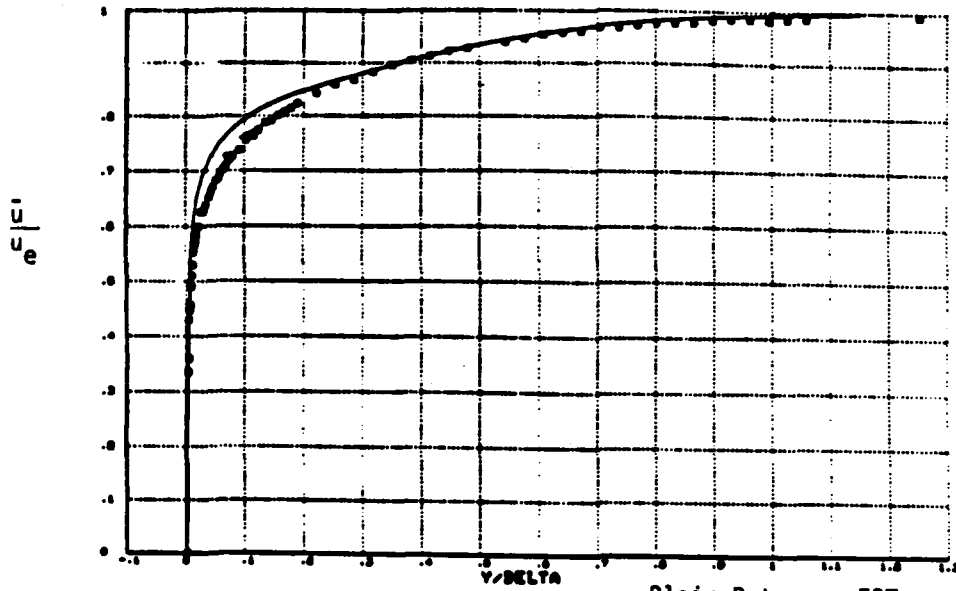
analogy factor,  $2S_t/C_f$ , with changes in  $R_{ex}$  and FST. At several downstream stations the scatter in the data provides an indication of three dimensional flow effects, since these differences arise from variations in spanwise location.<sup>4</sup> Nevertheless, as the FST increases from 0.25% to 5%, it appears that  $2S_t/C_f$  increases from 1.15 to 1.25 approximately. The present  $Pr_t$  model is seen to yield a computational result that is similar qualitatively. It should be noted that the laminar computation of the Reynolds analogy factor is high owing to the experimental staggering of heating onset with respect to the leading edge<sup>4</sup>.

In Figure 5 is exhibited an improved overall calculation of  $\bar{u}$  as compared with Figure 2. By further adjustment of the parameters it is possible to decrease the mismatch near the wall. A similar improvement occurs for  $\bar{T}$ . However acceptable this plot may seem in the wake region, a detailed scrutiny in semilogarithmic form reveals that the measured exponential decay of the corresponding deficits (cf. Figure 3) is not reproduced by the computations. Therefore, a fundamentally correct nature is absent from the modeling. However, this difference may be important only in principle. Further comparisons of velocity profiles are shown in law of the wall coordinates in the lower half of Figure 5. There is an important mismatch in the logarithmic region between the computations and the data, and this corresponds to the mismatch in the upper half of the figure. Although further adjustments of the parameters could decrease the mismatch, it is clear that further investigation is required. It is seen that an increase of FST has a pronounced effect in decreasing Coles' wake region<sup>18</sup>.

Another deficiency is revealed in Figure 6 in regard to the  $\overline{v'T}$  comparison. In spite of the fact that  $S_t$  and  $\bar{T}$  have been well calculated

— STANCOOL Computations  
(Equations 8 and 9)

□ Blair Data<sup>4</sup>  
FST = 5.3% (Nom.)  
X = 84 in.



Blair Data  
□ 0.25  
○ 2.0  
△ 5.3

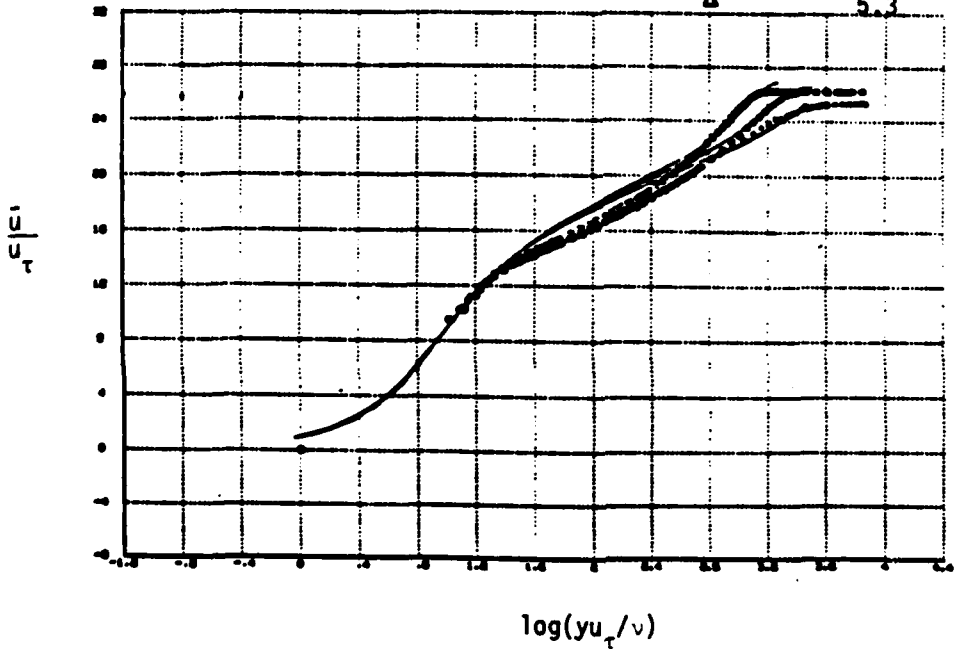


Figure 5: Velocity profile comparisons with new mixing length model.

(in comparison), the corresponding calculation for  $\overline{v'T'}$  has not matched the data, although a correct trend has been established with increasing FST. None of the parametric variations in the modeling seem to have produced the exponential character of the measured  $\overline{v'T'}$ , and this issue remains perplexing.

Lastly, in Figure 6, the comparisons of  $Pr_t$  are shown. The main observations are that the near wall modeling influences  $S_t$ , whereas the bulk of the  $Pr_t$  shape influences the  $T$  profile only slightly in the wake region. During scrutiny of Blair's data, it was noticed that outside of the boundary layer  $Pr_t$  passed through zero and became negative in some cases. Since the downward trends were too consistent to be attributed to experimental scatter, an explanation was sought. It was already noted earlier that the turbulence clearly extends beyond the usual boundary layer edge. In fact, towards the most downstream stations of measurement, the data indicate that the structure is still non-uniform even at the channel centerline, whereas the boundary layer thickness is roughly of half that length. Therefore, it is very likely that channel flow effects have influenced the  $Pr_t$  measurements. Since only the upper wall is heated, the  $\overline{v'T'}$  profile has the same sign throughout the channel height, while  $\overline{u'v'}$  must change sign near the tunnel centerline by symmetry. Since the upper and lower boundary layers are not matched in thickness, it is probable that  $\overline{u'v'}$  and  $\frac{\partial u}{\partial y}$  have zero crossings at different  $y$  locations, thereby invalidating the usual mixing length approach. Such circumstances could lead to negative values for  $Pr_t$ . It is therefore conjectured that true boundary layer measurements, uncontaminated by channel effects, would not contain such large decreases in  $Pr_t$  in the wake region as were observed here. It would be of interest to reconsider previous  $Pr_t$  measurements (and the wide



scatter in results) more systematically in light of this channel flow observation. A further question arises as to which case is closer to the actual turbine blade situation. These issues remain for continued investigation.

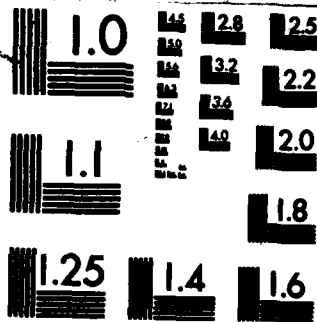
#### VI. SUMMARY OF ACCOMPLISHMENTS

- (1) A working knowledge of the code STANCOOL has been attained.
- (2) An extension of the Miyazaki and Sparrow model for FST effects has been incorporated into STANCOOL.
- (3) The extensive measurements of Blair have been studied and compared with sample calculations using the modified code. Results have shown a significant improvement, but several discrepancies have been identified.
- (4) A fundamental exponential behavior in the wake region of a turbulent boundary layer for cases of high FST has been noted, apparently for the first time.
- (5) An explanation is proposed for the observed large drop in  $Pr_t$  in the wake region. It is conjectured that this behavior is symptomatic of channel flow effects in such experiments.
- (6) Deductions from the observed exponential behavior reveal a logical dilemma concerning the energy equation. This dilemma may be of fundamental importance and requires further investigation.

#### VII. RECOMMENDATIONS:

Several issues require further investigation experimentally, theoretically and computationally. In order of increasing difficulty in each category these are:





MICROCOPY RESOLUTION TEST CHART  
NATIONAL BUREAU OF STANDARDS-1963-A

### Experimental

- (1) Exploration of the outer boundary layer with hot wires for cases of higher FST to determine the extent of the exponential character noted for the first time herein.
- (2) Measurements of  $Pr_t$  designed to assess the extent of channel flow influence on this variable.
- (3) Variation of FST scale size.
- (4) Measurements in thicker boundary layers to determine heat transfer and the damping factor very close to the surface.
- (5) Experiments to include measured density fluctuations in environments of higher levels of FST.

### Theoretical

- (1) Further deductions concerning the exponential wake region.
- (2) Formulation of an FST model which includes the influence of scale sizes and phase lags throughout the boundary layer.
- (3) Further refinements to the theory of transition onset and extent in the presence of FST.
- (4) Resolution of the observed heat transfer dilemma involving the energy equation. Assessment and inclusion of additional correlation terms involving density and perhaps pressure fluctuations.

### Computational

- (1) Continuation of the present modeling. Inclusion of further data comparisons.
- (2) Extension of the current modeling to include the TKE equation and higher order equations.

- (3) Further modeling of FST effects on transition.
- (4) Calculations including pressure gradient and non-equilibrium cases.  
Extensions to higher FST calculations.

### VIII. REFERENCES:

1. MacArthur, C. D., "Prediction of Free-Stream Turbulence Effects on Boundary Layer Heat Transfer - An Evaluation of the Heat Transfer Code STANS", 1983 USAF-SCEEE Graduate Student Summer Support Program, Contact No: F49620-82-0035, 16 September 1983.
2. Blair, M. F., "Influence of Free-Stream Turbulence on Turbulent Boundary Layer Heat Transfer and Mean Profile Development, Parts I & II", ASME Journal of Heat Transfer, Vol. 105, February 1983, pp. 33-47.
3. Blair, M. F., "Influence of Free-Stream Turbulence on Boundary Layer Transition in Favorable Pressure Gradients", ASME Journal of Engineering for Power, Vol. 104, October 1982, pp. 743-750.
4. Blair, M. F., "The Effect of Free-Stream Turbulence on the Turbulence Structure and Heat Transfer in Zero Pressure Gradient Boundary Layers", United Technologies Research Center Report: R82-915634-2, East Hartford, Conn., November 1982.
5. Blair, M. F., "Final Data Report-Vol. I-Velocity and Temperature Profile Data for Zero Pressure Gradient, Fully Turbulent Boundary Layers", UTRC Report R81-914388-15, E. Hartford, Conn., January 1981.
6. Blair, M. F., "Final Data Report-Vol. II-Velocity and Temperature Profile Data for Accelerating, Transitional Boundary Layers", UTRC Report R81-914388-16, E. Hartford, Conn., January 1981.
7. Blair, M. F., "Combined Influence of Free-Stream Turbulence and Favorable Pressure Gradients on Boundary Layer Transition and Heat Transfer", UTRC Report R81-914388-17, E. Hartford, Conn., March 1981.
8. Blair, M. F., "The Influence of Free-Stream Turbulence on the Zero Pressure Gradient Fully Turbulent Boundary Layer", UTRC Report R80-914388-12, E. Hartford, Conn. September 1980.
9. Miyazaki, H. and E. M. Sparrow, "Analysis of Effects of Free-Stream Turbulence on Heat Transfer and Skin Friction", ASME Journal of Heat Transfer, Vol. 99, November 1977, pp. 614-619.
10. Belov, I. A., Gorshkov, G. F., Komarov, V. S., and V. S. Terpigor'ev, "Influence of Jet Turbulence on Flow in the Boundary Layer Near the Wall", Translated from Zhurnal Prikladnoi Mekhaniki i Tekhnicheskoi Fiziki, No. 6, November-December 1982, pp. 77-82.
11. Simonich, J. C., and P. Bradshaw, "Effect of Free-Stream Turbulence on Heat Transfer through a Turbulent Boundary Layer", ASME Journal of Heat Transfer, Vol. 100, November 1978, pp. 671-677.
12. Bayley, F. J. and W. J. Priddy, "Effects of Free-Stream Turbulence Intensity and Frequency on Heat Transfer to Turbine Blading", ASME Journal of Engineering for Power, Vol. 103, January 1981, pp. 60-64.

13. McDonald, H., and J. P. Kreskovsky, "Effect of Free Steam Turbulence on the Boundary Layer", Int. J. Heat Mass Transfer, Vol. 17, 1974, pp. 705-716.
14. Junkhan, G. H., and G. K. Serovy, "Effects of Free-Stream Turbulence and Pressure Gradient on Flat-Plate Boundary-Layer Velocity Profiles and on Heat Transfer," ASME Journal of Heat Transfer, Vol. 89, May 1967, pp. 169-176.
15. Hall, D. J., and J. C. Gibbings, "Influence of Stream Turbulence and Pressure Gradient upon Boundary Layer Transition", Journal of Mechanical Engineering Science, Vol. 14, No. 2, 1972, pp. 134-146.
16. Hancock, P. E., and P. Bradshaw, "The Effect of Free-Stream Turbulence on Turbulent Boundary Layers", Dept. of Aeronautics, Imperial College, London, England, Report in Progress - Private Communication.
17. Crawford, M. E., and W. M. Kays, "STANS - A Program for Numerical Computation of Two-Dimensional Internal and External Boundary Layer Flows", NASA CR-2742, November 1976.
18. Coles, D. E., "Turbulent Boundary Layers in Pressure Gradients: A Survey Lecture Prepared for the 1968 AFOSR-IFP-Stanford Conference on Computation of Turbulent Boundary Layers", Rand Corp. Memorandum RM-6142-PK, October 1969.
19. Charnay, G., G. Comte-Bellot, and J. Mathieu, "Development of a Turbulent Boundary Layer on a Flat Plate in an External Turbulent Flow", AGARD CP93, Paper No. 27, 1971.
20. Huffman, F. D., D. R. Zimmerman, and W. A. Bennet, "The Effect of Free-Stream Turbulence Level in Turbulent Boundary Layer Behavior", AGARD AG164, 1972, pp. 91-115.
21. Hancock, P. D., "Effect of Free-Stream Turbulence in Turbulent Boundary Layers", Ph.D. Thesis, Imperial College, London Univ., 1980.
22. Evans, R. L., "Free-Stream Turbulence Effects on the Turbulent Boundary Layer," A.R.C. C.P. 1282, 1974.

**1984 USAF-SCEEE SUMMER FACULTY RESEARCH PROGRAM**

**Sponsored by the**

**AIR FORCE OFFICE OF SCIENTIFIC RESEARCH**

**Conducted by the**

**SOUTHEASTERN CENTER FOR ELECTRICAL ENGINEERING EDUCATION**

**FINAL REPORT**

**MULTIPLE TURBINE DISK SIMULATION USING ALPID**

**Prepared by:** James R. Farmer  
**Academic Rank:** Graduate Student  
**Department and University:** Civil/Mechanical Engineering Department  
University of Vermont  
**Research Location:** AFNAL/MLLM  
Wright Patterson Air Force Base  
**USAF Research:** Dr. Harold L. Gegel  
**Date:** 19 September 1984  
**Contract No:** F49620-82-C-0035

MULTIPLE TURBINE DISK SIMULATION USING ALPID

by

James R. Farmer

ABSTRACT

This report discusses the results of a first stage in computer modelling of a three dimensional multiple turbine disk forging using the two dimensional finite element code ALPID (Analysis of Large Plastic Incremental Deformation). Contained is a brief mathematical overview of the theory behind ALPID and the results of a pseudo-symmetric plane of the forging. The direction of further work is suggested.

## I. INTRODUCTION

The simulation of complex forging geometries is valuable in many aspects. Usually the die geometry is determined from the finished part specifications and can't be altered significantly. On the other hand the forging preform may be changed to accommodate the desired stress field, effective strain history, and developed strain rate effects in the final forged part. By simulating a forging process using various preforms and die velocities an indication of the behavior of material flow, internal stresses, die forces required, along with other parameters may be found. More importantly the cost of physical modelling using different preforms is greatly reduced by narrowing the number of preform candidates to those who yield acceptable results from the computer simulation.

Additionally the cost of performing three dimensional computer simulations as well as the complexity involved with their formulation is at present prohibitive. It is therefore beneficial to look at various areas or symmetric planes of the forging and model them in a two dimensional sense. From this an approximation to the three dimensional simulation is obtained. Using ALPID in this manner provides a rough approximation of material behavior within the forging.

## II. OBJECTIVES

The main objective of this project was to develop using ALPID a forging process for the manufacture of a multiple (seven) turbine disk forging in a single isothermal operation. Emphasis is placed on property/microstructure control and material conservation through near net shape design.

The two dimensional code ALPID was to be used in an attempt to simulate this inherently three dimensional forging.

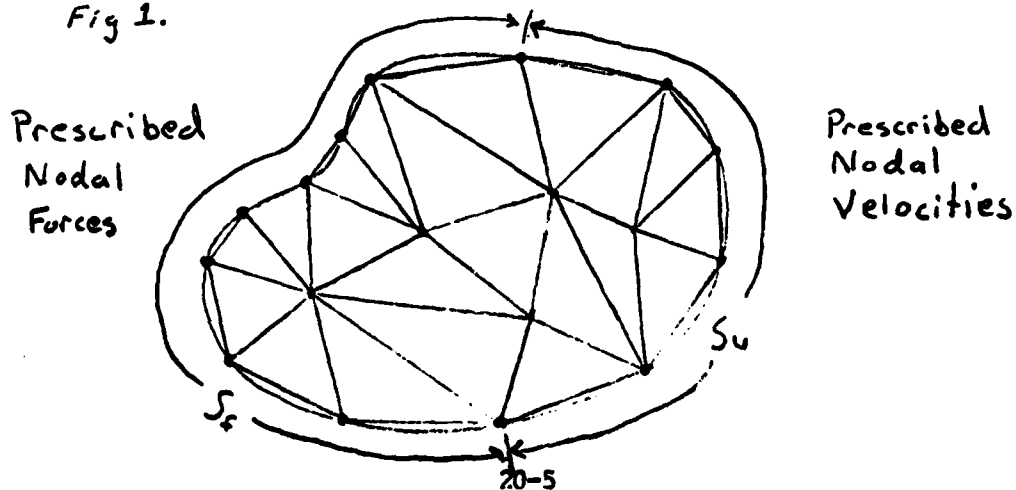
### III. ALPID THEORY AND USE

The finite element code is based, (1,2) on solving for the velocity field which provides a stationary value for the following functional.

$$\Phi = \int_{\text{Volume}} \bar{\sigma} \dot{\bar{\epsilon}} dV + \int_{\text{Volume}} \frac{\lambda}{2} \dot{\epsilon}_v^2 dV - \int_{S_F} F \cdot v dS$$

The functional is derived from a virtual work principle and the integrals represent distortional, dilatational, and input energies respectively.  $\bar{\sigma}$  and  $\dot{\bar{\epsilon}}$  are the effective stress and strain rate respectively and are derived from the velocity field,  $v$ .  $F$  represents the surface force supplied to the boundary  $S_F$  and  $\lambda$  is a large positive constant for the penalty constraint on the volumetric strain rate,  $\dot{\epsilon}_v$ . The remainder of the boundary not included in  $S_F$  is  $S_u$  and encompasses all prescribed surface velocities (Fig. 1).

Fig 1.



The velocity field which satisfies the functional statement is that which satisfies the following discrete system of equations.

$$\frac{\partial \Phi(w_i)}{\partial w_j} = 0, \quad (j=1, \dots, N \times p)$$

$N$  is the number of nodal points and  $p$  is the number of degrees of freedom per node. Due to the inherent non-linearity from work hardening in plastic flow the system of equations is solved using a standard Newton-Raphson iterative technique. Convergence requirements are placed on the unbalanced force vector as well as on the velocity solution vector.

For a complete development of ALPID theory as well as matrix formulation see reference (2).

In using two dimensional ALPID one generates a mesh describing the workpiece under axisymmetric or plane strain loading conditions. Care must be taken in ensuring that areas of high stress and strain rates contain a refined mesh and other areas a relatively coarse mesh. On the mesh boundaries  $S_u$  and  $S_f$ , nodal velocities and forces respectively are prescribed. In most cases one need only define nodes which are initially in contact with a die or may come in contact during deformation. ALPID converts the die velocity to nodal velocities and in addition

computes the normal and traction nodal forces as a function of the nodal velocity relative to the die surface. A prescribed constant friction factor is used in this computation. All nodes not initially in contact with a die are prescribed to have zero forces acting on them. If during simulation a node comes in contact or breaks contact with a die, ALPID prescribes velocities or forces on that node respectively.

At each time step during a deformation simulation ALPID computes all nodal velocities not prescribed using the Newton-Raphson method mentioned previously. When a velocity field is found which satisfies the convergence requirements, all stress and strain rate tensor components as well as total effective strain and effective strain rate are available as output. Additionally nodal and die force components are computed and available.

When using ALPID one should have available a method of mapping a new grid mesh on a previously deformed mesh. During deformation a grid mesh may become severely distorted and at some point element Jacobian determinants may become  $\leq 0$ . Before this occurs the remeshing process is performed by transforming the stress-strain field from the old mesh to a new undistorted mesh. The simulation then proceeds.

One final note on ALPID use is that an appropriate material property subroutine, (3) must be supplied. This subroutine contains the constitutive relation  $\bar{\sigma} = \bar{\sigma}(\bar{\epsilon}, \dot{\bar{\epsilon}}, T)$

required for the distortion integral in the functional statement. This relation which is obtained from isothermal compression testing within a range of strain rates, is addressed for each element at each time step to establish the flow stress under the particular conditions of strain rate, temperature, and strain.

#### IV. RESULTS

Two simulations are presented. The first is one half of plane A (see figs. 2,3-5). All nodes except those on the top surface are constrained to move in either the horizontal or vertical directions. As the die is pushed down into the material the portion of the material not in contact with the die is forced upward while the rest is forced down. Results of effective strain rate and total effective strain are given along with the deformed grid mesh. The simulation proceeded through 90% of the total reduction in height required for this process.

The second simulation (figs. 6-9) is more representative of the actual forging process. The die configuration allows flashing to occur at the upper right hand corner as well as having a draft angle built in to facilitate workpiece removal from an actual forge. This simulation uses a variable die velocity (fig. 10) in an attempt to cause a near constant strain rate within the material. As can be seen in comparison between the two simulations

a near constant strain rate does occur in this simulation while in the first, the strain rate increases quickly due to the constant die velocity as the simulation proceeds. Effective strain rate, total effective strain, and grid distortions are presented.

As can be seen in the figures the regions where material is being forced away by the die display high total effective strain. Regions toward the center of the disk are strained much less. The flash region as expected is an area of high strain which also appears to propagate through the material in the flash vicinity.

The simulations present an initial attempt to analyze the three dimensional problem in a two dimensional sense. Deformation modelling in a plane parallel to the horizontal axis was attempted, but problems arose in incorporating metal addition to the section, or in assigning appropriate boundary conditions to accommodate an equivalent deformation.

Due to computer system time constraints the second simulation could not proceed past 50% reduction. This problem is being resolved so that the complete simulation may be carried through.

The simulations result in evaluating all components of stress and strain rate tensors as well as computing effective strain rate and total effective strain. The results of effective strain rate may be compared with material processing maps currently being developed at

W.P.A.F.B. (3). The processing maps dictate the optimal processing parameters ( $\dot{\epsilon}$ , T) required to obtain a desired internal material microstructure. One goal of these simulations is to determine the die velocity and preform shape, which will force the majority of the workpiece to lie in these optimal regions hence producing a forging with the desired property/microstructure characteristics.

#### V. DISCUSSION AND RECOMMENDATIONS

The idea of modelling a three dimensional forging with a two dimensional code might seem a waste of effort and resources. How could anything useful come out of such an analysis ?

One must realize that the time, effort, and expense of development as well as the cost involved in just a two dimensional analysis of this type is substantial. The storage requirements are massive and the CPU time is exceedingly long. When extrapolating the problems associated with two dimensional analysis to three dimensions, the proposition of obtaining cost effective solutions becomes minute. This is not to say that three dimensional analysis in the area of solid mechanics is impossible, but at the present time, impractical. Only the latest generation of super computers can handle the analysis and even they are operating at their limits with a complex three dimensional deformation simulation. The development of pre and post processors for the three dimensional code as well as

remeshing techniques pose additional large scale tasks. Granted for a not too complex three dimensional problem, a specialized code could be formulated (and has been (4)) but the prospect of developing a code to handle arbitrary three dimensional preform/die shapes is at present inconceivable. It is therefore beneficial to analyze three dimensional deformation with a two dimensional code.

At present one must analyze each simulation to check for the desired processing parameters and make adjustments accordingly for the following run. Future work to modify ALPID to automatically compute the desired velocity profile would significantly improve the development of an optimal forging process given arbitrary preform, die configuration, and desired final microstructure.

Also of value in running ALPID would be an automatic remeshing scheme. As stated before, during large deformation the grid mesh tends to break down. Work on an algorithm to detect approaching grid failure and correct it automatically by an appropriate remeshing would reduce the required user/code interaction immensely.

Physical modelling with plasticine and/or lead should be conducted (and to date has been started) to investigate the accuracy of the simulations. So far the simulations are qualitatively consistent with the initial plasticine modelling. With follow up work in this area and on other three dimensional deformations one should soon be able to

confidently analyze such problems in this manner until three dimensional deformation codes are available and their use practical.

### REFERENCES

- 1) Kobayashi, S., Lee, C.H., and Oh, S.I., "Workability Theory of Materials in Plastic Deformation Processes," USAF Technical Report AFML-TR-73-192, 1973.
- 2) Kobayashi, S., Chen, C.C., "Rigid-Plastic Finite Element Analysis of Plastic Deformation in Metal Forming Processes," USAF Technical Report AFML-TR-79-4105, 1979.
- 3) Prasad, Y.V.R.K., Gegel, H.L., Morgan, J.T., Malas, J.C., Doraivelu, S.M., and Barker, D.R., "A New Systems Approach To Dynamic Modelling of Material Behavior In Metal Working Processes," Proceedings of AIME Special Session Titanium Net Shape Technologies, F.H.Froes, D.Eylon, C.C.Chen, eds., AIME, L.A., Ca. Febuary, 1984.
- 4) Semiatin, S.L., Oh, S.I., and Altan, T., "Processing Science Research To Develop Scientific Methods For Controlling Metal Flow, Microstructures, and Properties in Three Dimensional Metal Forming Processes," USAF Technical Report AFWAL-TR-83-4109, 1983.

### ACKNOWLEDGMENTS

The author wishes to thank the Air Force Systems Command and the Air Force Office of Scientific Research for making possible the ten week effort at W.P.A.F.B. I would also like to thank Dr. Delcie Durham for her support in making the effort possible and Dr. Ragu Srinivasan for his endless assistance and guidance with the computer systems at W.P.A.F.B.

Fig 2.

Multiple  
Disk  
(Top View)

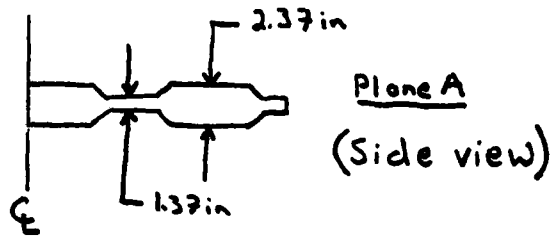
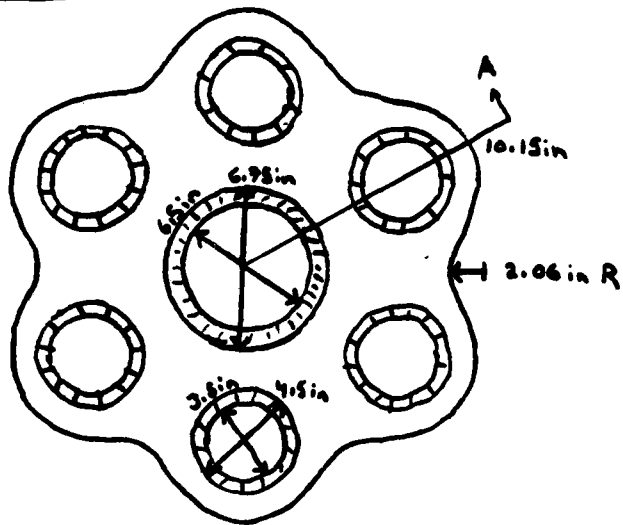


Fig 10.

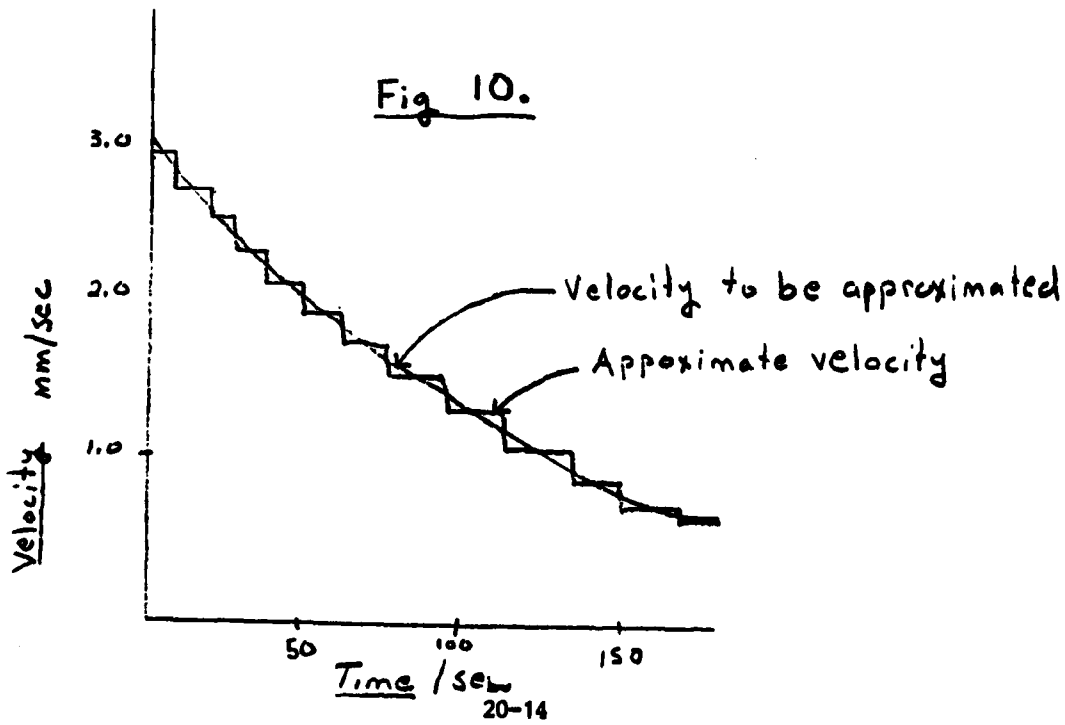
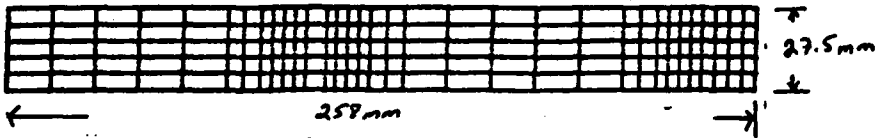
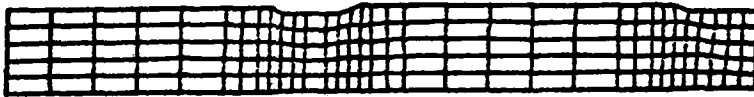


Fig 3

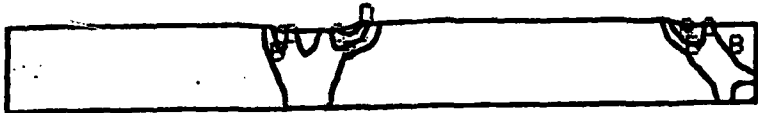
Undeformed Grid Mesh



STEP #5: 22.5% REDUCTION  
Deformed Grid Mesh



Effective Strain Rate



+<A =	0.000>
+<B =	0.065>
+<C =	0.130>
+<D =	0.195>
+<E =	0.260>
+>>	

Total Effective Strain



+<A =	0.000>
+<B =	0.029>
+<C =	0.056>
+<D =	0.087>
+<E =	0.116>
+<F =	0.144>
+<G =	0.173>
+<H =	0.202>
+<I =	0.231>
+<J =	0.260>
+>>	

Fig 4.

STEP #10  
45% REDUCTION



+X A	0.000
+X B	0.175
+X C	0.350
+X D	0.525
+X E	0.700
+>>	



+X A	0.000
+X B	0.078
+X C	0.156
+X D	0.233
+X E	0.311
+X F	0.389
+X G	0.467
+X H	0.544
+X I	0.622
+X J	0.700
+>>	

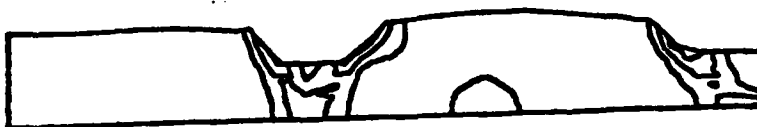


Fig 5

STEP #20  
90% REDUCTION



+X A	0.000>
+X B	0.265>
+X C	0.530>
+X D	0.795>
+X E	1.060>
+>>	



+X A	0.000>
+X B	0.118>
+X C	0.236>
+X D	0.353>
+X E	0.471>
+X F	0.589>
+X G	0.707>
+X H	0.824>
+X I	0.942>
+X J	1.060>
+>>	

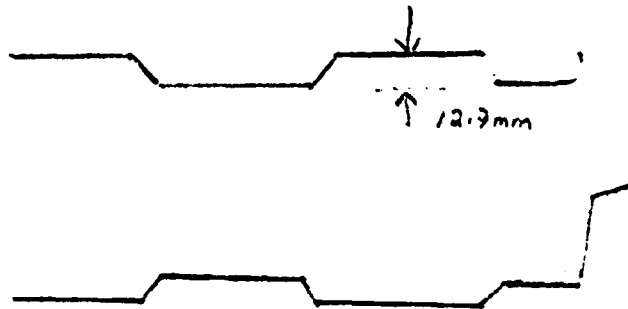


Fig 6

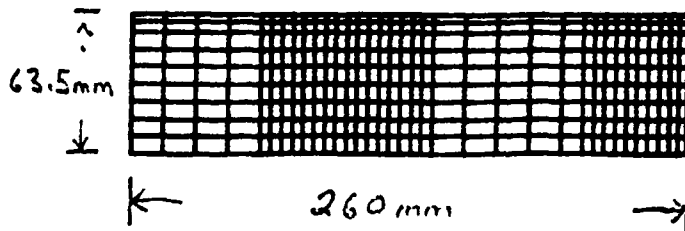
MULTIPLE TURBINE DISK SIMULATION USING ALPID (PHASE 1)

Fifty percent reduction from pancake preform.  
25 seconds elapsed time.

Die Configuration



Undeformed Grid Mesh



401

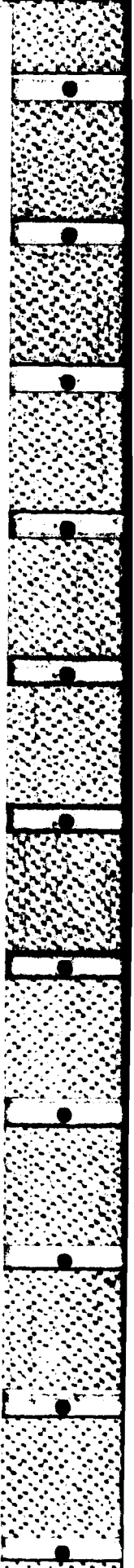
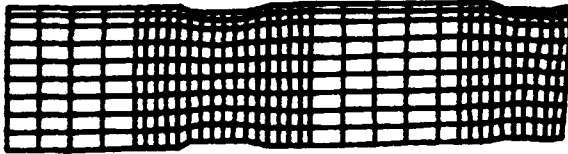


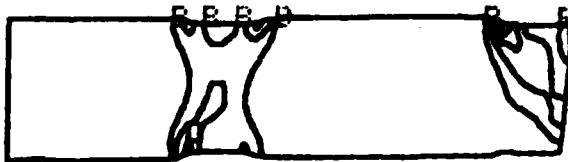
Fig 7

STEP #10  
20% REDUCTION

Grid Distortion



Effective Strain Rate



+<A> =	0.000
+<B> =	0.036
+<C> =	0.012
+<D> =	0.019
+<E> =	0.027
+<F> =	0.023

Total Effective Strain

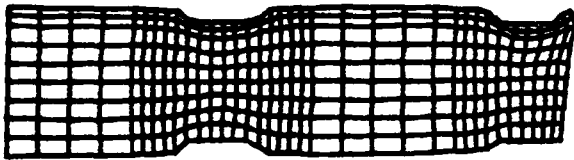


+<A> =	0.000
+<B> =	0.036
+<C> =	0.112
+<D> =	0.169
+<E> =	0.224
+<F> =	0.230

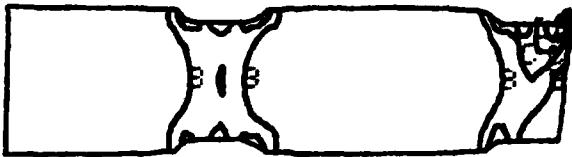
Fig 8

STEP #20  
40% REDUCTION

Grid Distortion

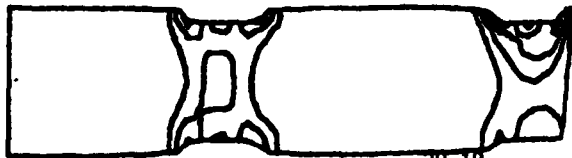


Effective Strain Rate



+<A =	0.000>
+<B =	0.007>
+<C =	0.014>
+<D =	0.021>
+<E =	0.028>
+<F =	0.034>

Total Effective Strain

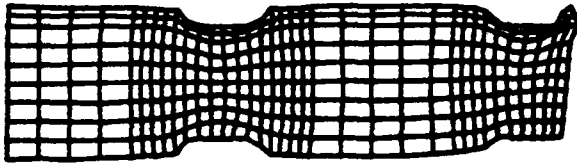


+<A =	0.000>
+<B =	0.195>
+<C =	0.213>
+<D =	0.319>
+<E =	0.426>
+<F =	0.532>

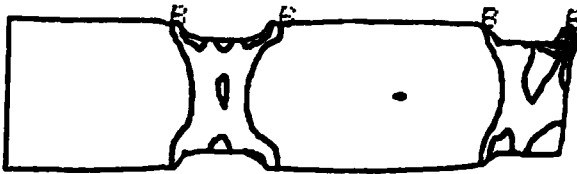
Fig 9

STEP #30  
50% REDUCTION

Grid Distortion

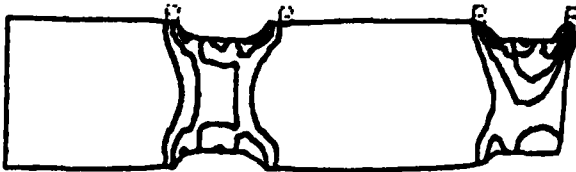


Effective Strain Rate



+<A =	0.000
+<B =	0.007
+<C =	0.014
+<D =	0.022
+<E =	0.029
+<F =	0.036

Total Effective Strain



+<A =	0.000
+<B =	0.187
+<C =	0.254
+<D =	0.381
+<E =	0.507
+<F =	0.634

1984 USAF-SCEEE GRADUATE STUDENT SUMMER SUPPORT PROGRAM

Sponsored by the

AIR FORCE OFFICE OF SCIENTIFIC RESEARCH

Conducted by the

SOUTHEASTERN CENTER FOR ELECTRICAL ENGINEERING EDUCATION

FINAL REPORT

THE EFFECTS OF NUCLEAR RADIATION ON THE OPTICAL  
CHARACTERISTICS OF (SiO<sub>2</sub>-ZrO<sub>2</sub> on Si SUBSTRATE) MIRRORS

Prepared by: Mark A. Ferrel

Academic Department: Department of Nuclear Engineering

University: Kansas State University

Research Location: Frank J. Seiler Research Laboratory  
Directorate of Lasers and Aero-Mechanics

USAF Research Contact: Dr. Albert J. Alexander, Major, USAF

SFRP Supervising  
Faculty Member: Dr. Hermann J. Donnert, Professor

Date: 17 August 1984

Contract No: F49620-82-C-0035

THE EFFECTS OF NUCLEAR RADIATION ON THE OPTICAL  
CHARACTERISTICS OF (SiO<sub>2</sub>-ZrO<sub>2</sub> on Si SUBSTRATE) MIRRORS

by

Mark A. Ferrel

ABSTRACT

The military has a lot of interest in the effects of nuclear radiation on the optical characteristics of laser components for future weapons systems. If the radiation effects can be modeled, then the amount of damage in a given situation could be predicted.

The mirrors (which were SiO<sub>2</sub>-ZrO<sub>2</sub> on a Si substrate deposited for maximized reflectivity at a wave length of 1.315 μm) have a 50% Iodine laser damage threshold of 36.11 J/cm<sup>2</sup>. The mirrors were exposed to no irradiation. The equation which best fit the data is below. D is the percent damage at a given laser pulse energy level and P is the laser pulse energy level in mJ.

$$D = \frac{100}{\pi} \arctan \left[ .565(P-10.78) + .0038(P-10.78)^3 + .000096(P-10.75)^5 \right] + 50$$

A least squares fit was used fit the function to the data. The standard deviation for this fit is  $\pm 10.51\%$  damage.

It was also found that given a constant laser power as mirror reflectivity decreases the amount of damage increases. This is expected since the mirror is absorbing more of the laser energy at low reflectivities. A mirror with 83% reflectivity had a 50% laser damage threshold of 27.81 J/cm<sup>2</sup>, while the mirrors with 98% reflectivity had a 50% damage threshold of 36.11 J/cm<sup>2</sup>.

As soon as the data is available from the irradiated mirrors, the data will be similarly analyzed and modeled.

## I. INTRODUCTION:

Determination of nuclear-radiation effects on the optical characteristics of laser components, such as mirrors, windows, and Q switches, has recently become a matter of vital interest with the scope of several projects under the auspices of the Strategic Defense Initiative (SDI). Such knowledge, at least of a phenomenological nature, is of utmost and urgent importance for the design of laser systems for anti-missile defense applications. In the long run, basic understanding of response kinetics and the concomitant ability to formulate theoretical models will be essential to harden these systems and reduce their vulnerability to hostile actions.

Based on the common knowledge of solid-state physics, energy deposition from absorption of nuclear radiation changes the microstructure of the crystal lattice and the distribution of the electrons and holes in quantum - mechanically available energy states; to complicate matters, inevitable impurities and dislocation defects are generally of profound importance. Such changes impact a variety of physical properties of the solid material, such as electrical conductivity and optical absorbance. Thus, the essential question to be answered is not whether germane effects will actually occur, but as to what their magnitude and the associated practical significance for the military systems design might be.

Except for very preliminary efforts by the author, Dr. Donnert<sup>1</sup> and Kevin Zook at FJSRL<sup>2</sup> and by researchers at Sandia National Laboratory (SNL)<sup>3</sup>, virtually no research to explore this vital problem area has been reported. Published observations of nuclear-irradiation effects on the performance of fiber optics<sup>4</sup>, although in themselves certainly interesting, are of exceedingly limited value in addressing the laser-component problem because the vagaries in solid-state behavior and the lack of a sound theoretical understanding preclude any quantitatively credible scientific inference. Simply speaking, the state of the art is on square one.

## II. OBJECTIVES OF THE RESEARCH EFFORT:

The objectives of the research effort are:

- a) To determine the 50% Iodine Laser damage threshold of the mirrors ( $\text{SiO}_2\text{-ZrO}_2$  on a Si substrate deposited for maximized reflectivity at  $\lambda = 1.315 \mu\text{m}$ ).
- b) To model the mirror damage data and then accurately be able to predict the amount of damage given initial conditions.
- c) To determine how the laser damage to the mirrors changes as the reflectivity of the mirrors changes.
- d) To determine how the 50% laser damage threshold changes when the mirrors have been exposed to nuclear irradiation.
- e) To model the nuclear irradiated mirror laser damage data and then be able to predict the amount of damage to the mirrors, given initial conditions.
- f) To correlate the micro-structure damage with the observed macro damage to the mirrors.

## III. PROCEDURE TO MEET OBJECTIVES:

In order to accomplish the first objective, mirrors #1,2,6 and 7 were shot with the Sandia National Laboratories Iodine Atomic Laser (#T763607 913) which used a Lambda Regulated Power Supply (Model #LM D28R and Serial #099240) over a range of Laser Pulse Energies. The iodine laser had a wavelength of  $1.315 \mu\text{m}$  and a pulse length of 10 microseconds. Mirrors #1,2, and 7 had a reflectivity of 98% while Mirror #6 had a reflectivity of 83%. By comparing the damage results from mirrors #1, 2, and 7 with the damage results from mirror #6, objective 3 could be met.

The criteria used for "laser damage" was any detectable circular pattern that could be seen by the eye using a Leitz Wetzlar microscope with a magnification of 20 x. If the mirror's damage was due to the laser, a near perfect circular pattern was formed. The diameter of the circular pattern varied from about .042 microns to .216 microns, but the circular pattern was always present. This circular pattern makes it easy to distinguish the laser induced damage from natural defects which are rarely circular in shape.

Each mirror was shot with the iodine laser at site locations .15 inches apart to prevent overlap of laser damage sites. After all

possible sites were shot on each mirror, the mirrors were examined under the Leitz Wetzlar microscope at 20x power to verify whether each site damaged or not.

#### IV. GRAPHICAL ANALYSIS:

Once the laser damage data was taken and verified, the data was graphed using several different data groupings. A model was fit to each graph which will be discussed later. Since the laser pulse energy was over a range of 8.0 mJ to about 21 mJ, this pulse energy was divided into evenly spaced increments (See Table 1). The average fluence ( $J/cm^2$ ) can be calculated by multiplying the laser pulse energy by 3.35. There were a few shots at laser pulse energized at greater than 21 mJ, but they were spaced very far apart. These points were used in the analysis but all the points about 21 mJ were treated as two groups.

#### V. MODELING DATA:

From the graphs made of the laser damage data, it was apparent that some type of arctan function would work best. After trying several different arctan fits the function below was arrived upon as the best.

$$D = A \arctan \left[ C_1(P-K) + C_3(P-K)^3 + C_5(P-K)^5 \right] + B \quad (1)$$

where A and B = Parameter Constants

$C_{1,3,5}$  = Constants to be determined

K = Laser pulse energy that causes damage 50% of the time

P = Laser pulse energy (mJ)

D = % of time sample will damage at P.

A least squares fit along with a bisection<sup>6</sup> routine was used to determine  $C_1$ ,  $C_3$ ,  $C_5$  and K. The actual values for the constants for each model along with the standard deviations are in Table 2.

#### VI. STATISCAL ANALYSIS:

F-tests were performed on all the models<sup>7</sup>. In all but a couple of exceptions, the F-tests verified that the different models are of the same damage data.

Figure 3 shows model 1 which was the best fit to the data. All six models are reported in Figure 1. It is evident from Figure 1 that as the power groupings of each model changed, the functions changed (also see Table 2).

The statistics could be improved with more damage testing of the mirrors. This is not possible, however, due to the small quantity of mirrors available.

#### VII. RESULTS OF LOWER REFLECTIVITY:

It is apparent from Figure 3 that as the reflectivity decreases the 50% laser damage threshold also decreases. This would be expected since the less laser energy a mirror reflects, the more laser energy is absorbed. Given as constant laser pulse energy, the smaller the mirror reflectivity the more it will damage.

The reflectivity of mirror #6 is about 15% less than that of mirror #1, 2, and 7 (83% compared to 98%). The drop in the 50% laser damage threshold was 23% ( $36.11 \text{ J/cm}^2$  to  $27.81 \text{ J/cm}^2$ ). Although there is not enough data at the lower reflectivities to draw any conclusive conclusions it appears that the 50% laser damage threshold will drop rapidly for small changes in mirror reflectivity.

The mirrors which have been fast-neutron irradiated in the beam-stop at Los Alamos Mason Physics Facility (LAMPF) have not yet been received. Other materials in the same sample box have fairly high levels of neutron induced radiation. Once the radiation levels are below safety limits the mirrors will be removed. The irradiated mirrors will then be tested as mirrors #1, 2, 6, and 7 were.

The micro-structure damage will then be correlated to the observed macro damage.

#### VII. RECOMMENDATIONS:

Because of the great importance optical equipment will have with respect to military application in the future, the research of the effects of nuclear radiation on the optical characteristics of laser components should be continued and expanded. Since very little research has been done in this area the research area can easily be expanded to cover many of the topics pertinent to military needs.

### VIII. FIGURES AND TABLES

- Table 1 - Shows each model and the increments the laser pulse energy was broken into along with the data points used in the least squares fit of each model. To convert laser pulse energy (mJ) to fluence ( $J/cm^2$ ), multiply by 3.35.
- Table 2 - Shows the parameter values for each model and the standard deviation of each model.
- Figure 1 - Graphical comparison of the six models for the mirrors with 98% reflectivity (mirrors 1,2, and 7).
- Figure 2 - Graph shows how the laser damage curve changes for a mirror with 83% reflectivity (mirror 6).
- Figure 3 - Graph of best fit model to data from mirrors with 98% reflectivity (mirros 1,2, and 7).

Table 1.

Model 1

<u>Laser Pulse Energy Increments (mJ)</u>	<u>Average Pulse Energy within Laser Pulse Energy Increment</u>	<u>% Damage</u>
7.5 - 10.4	9.43	29.4
10.5 - 13.4	11.66	65.4
13.5 - 16.4	15.15	80.0
16.5 - 19.4	18.02	100.0
19.5 - 22.4	20.08*	60.0*
22.5 - 25.4	23.9	100.0
25.5 - ↑	36.7	100.0

Model 2

7.1 - 10.0	9.22	35.7
10.1 - 13.0	11.39	57.0
13.1 - 16.0	14.69	61.0
16.1 - 19.0	17.0	77.8
19.1 - 22.0	19.93*	67.0*
22.1 - 25.0	23.9	100.0
25.1 - ↑	36.7	100.0

Model 3

7.5 - 9.4	8.26	0.0
9.5 - 11.4	10.55	52.0
11.5 - 13.4	12.53	80.0
13.5 - 15.4	14.65	85.0
15.5 - 17.4	16.38	80.0
17.5 - 19.4	18.27	100.0
19.5 - 21.4	20.08*	60.0*
21.5 - 25.4	23.9	100.0
25.5 - ↑	36.7	100.0

Table 1 Continued:

<u>Laser Pulse Energy Increments (mJ)</u>	<u>Average Pulse Energy within Laser Pulse Energy Increment</u>	<u>% Damage</u>
Model 4		
7.1 - 9.0	8.26	0.0
9.1 - 11.0	10.39	55.0
11.1 - 13.0	11.88	60.0
13.1 - 15.0	14.34	77.0
15.1 - 17.0	16.11	73.0
17.1 - 19.0	17.93	100.0
19.1 - 21.0	19.93*	67.0*
21.1 - 25.0	23.9	100.0
25.1 - ↑	36.7	100.0
Model 5		
7.5 - 8.4	8.26	0.0
8.5 - 9.4	-	-
9.5 - 10.4	9.92	42.0
10.5 - 11.4	11.06	62.5
11.5 - 12.4	11.97	67.0
12.5 - 13.4	13.08	80.0
13.5 - 14.4	14.10	100.0
14.5 - 15.4	14.89	78.0
15.5 - 16.4	16.09	67.0
16.5 - 17.4	17.07	100.0
17.5 - 18.4	18.3	100.0
18.5 - 19.4	-	-
19.5 - 20.4	19.95*	50.0*
20.5 - 21.4	-	-
25.5 - ↑	36.7	100.0

Table 1 Continued:

<u>Laser Pulse Energy Increments (mJ)</u>	<u>Average Pulse Energy within Laser Pulse Energy Increment</u>	<u>% Damage</u>
Model 6		
7.1 - 8.0	8.26	0.0
8.1 - 9.0	-	-
9.1 - 10.0	9.76	55.0
10.1 - 11.0	10.82	53.8
11.1 - 12.0	11.48	60.0
12.1 - 13.0	12.68	60.0
13.1 - 14.0	13.4	67.0
14.1 - 15.0	14.62	80.0
15.1 - 16.0	15.60	80.0
16.1 - 17.0	16.53	67.0
17.1 - 18.0	-	-
18.1 - 19.0	18.30	100.0
19.1 - 20.0	19.65*	50.0*
20.1 - 21.0	20.05	100.0
21.1 - 25.0	23.9	100.0
25.1 - ↑	36.7	100.0

Model for Mirror #6 (83% Reflectivity)

<u>Laser Pulse Energy Increments (mJ)</u>	<u>Average Pulse Energy within Laser Pulse Energy Increment</u>	<u>% Damage</u>
7.1 - 9.0	8.50	54.0
9.1 - 11.0	9.62	73.0
11.1 - 13.0	11.6	100.0

\* Data points not used in least squares fit modeling.

Table 2.

Model	C1	C3	C5	K	Std. Dev.
1	.565	.0038	.000096	10.78	+ 10.51
2	.219	.0012	.000014	11.23	+ 14.07
3	.931	.0003	.000020	10.62	+ 22.08
4	.301	.0029	.000014	10.28	+ 36.84
5	.678	.0008	.000026	10.66	+ 37.05
6	.360	.0026	.000022	10.94	+ 40.65
Mirror #6 (83% Reflectivity)	.925	.077	.012	8.3	+ 8.52

Function fit to data is below.

$$D = \frac{100}{\pi} \text{Arctan} \left[ C_1(P-K) + C_3(P-K)^3 + C_5(P-K)^5 \right] + 50$$

where D is % Damage

P is Pulse energy of the laser

K is 50% laser damage threshold

FIGURE 1

COMPARISON OF LASER DAMAGE MODELS

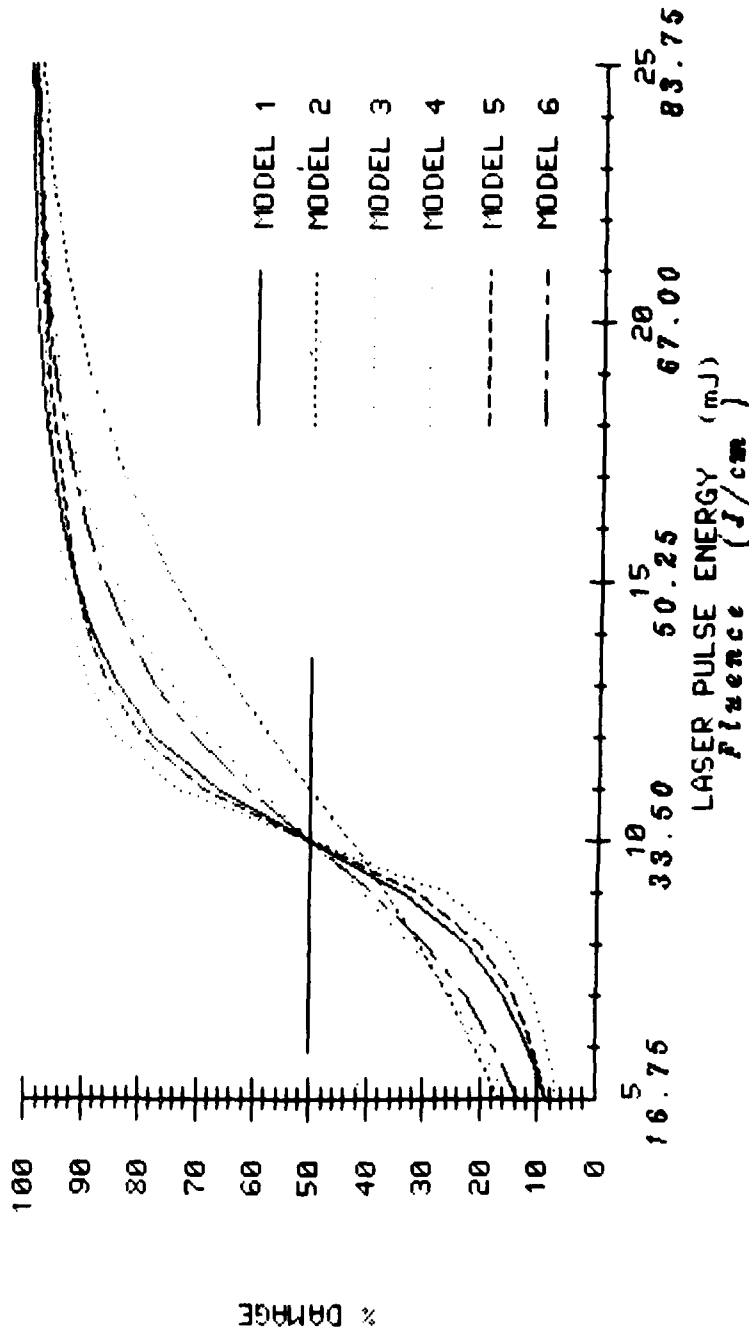


FIGURE 2

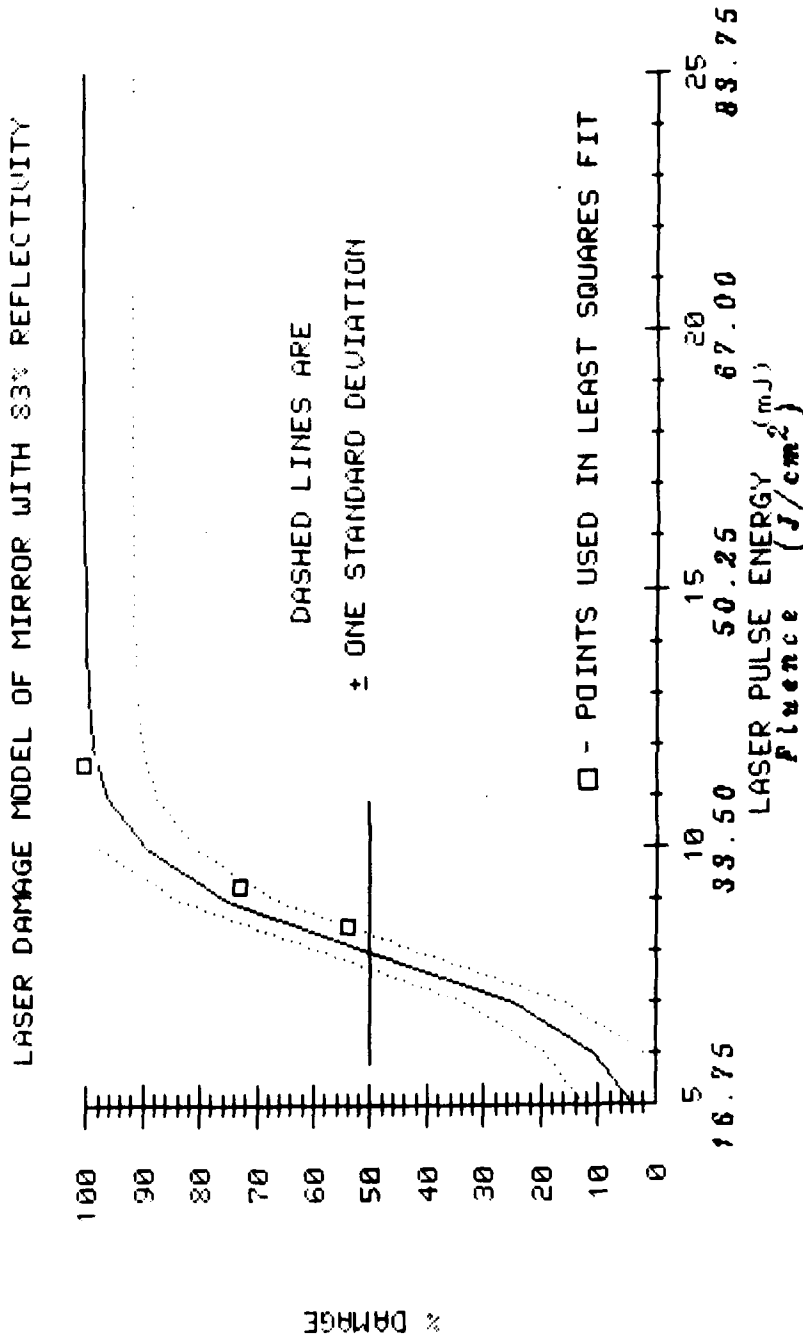
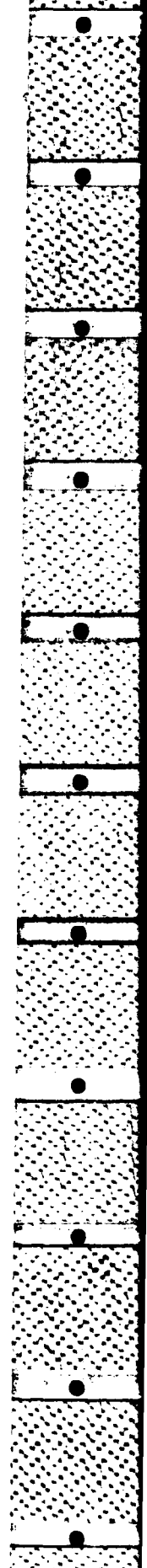
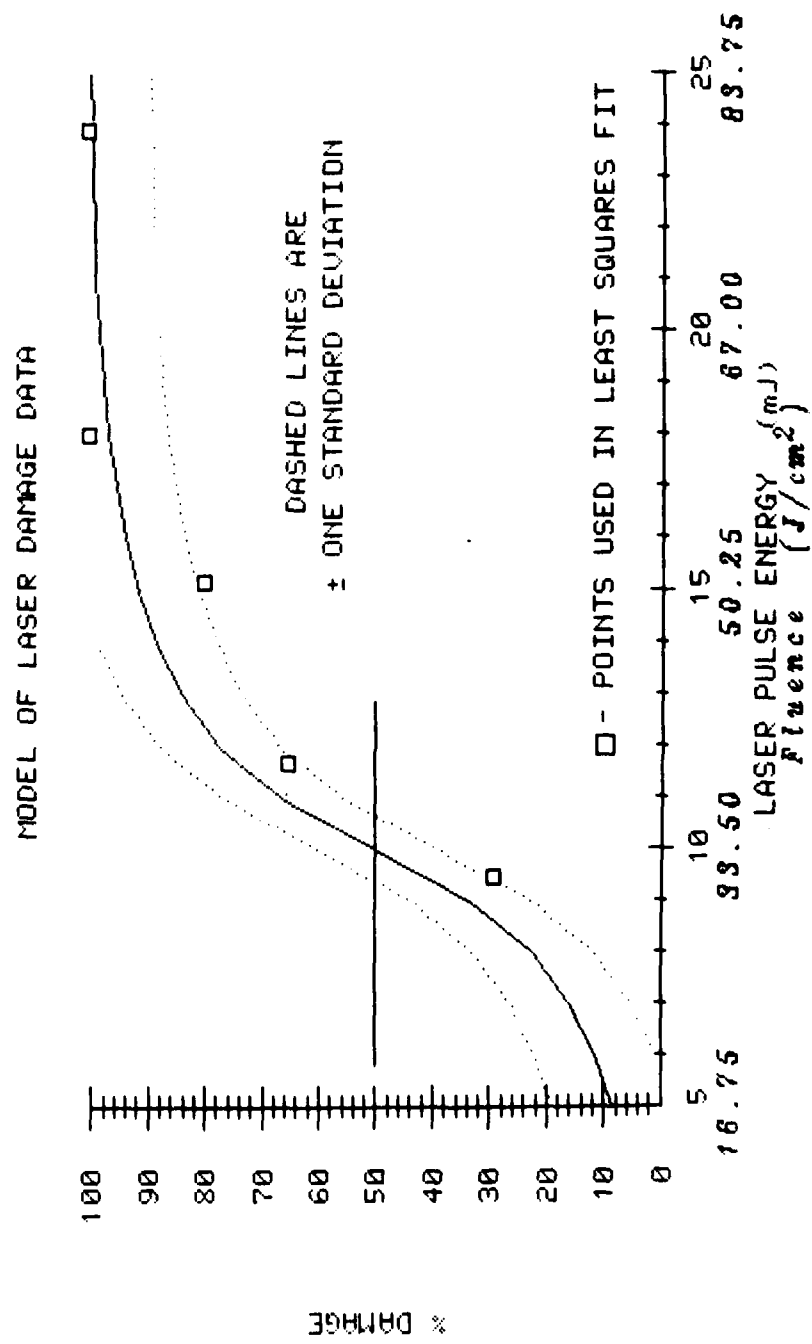


FIGURE 3



ACKNOWLEDGEMENTS

The author would like to thank the Air Force Systems Command, the Air Force Office of Scientific Research, and the Southeastern Center for Electrical Engineering Education for providing him with a very good learning experience at the Frank J. Seiler Research Laboratory, U.S. Air Force Academy, Colorado Springs, Colorado. He would also like to thank Mr. Lee Burton for his help in the laboratory which was invaluable. Captain Vic Villhard's aid with the computer system was greatly appreciated. The many helpful discussions with Dr. O'Connell, Dr. Glasgow, Dr. Romberger, and Mr. Kevin Zook were greatly appreciated.

The author would like to thank Lt Col T. Saito and Major A. Alexander for their hospitality and making the laboratories at FJSRL available to the author.

The assistance given to the author by Ms Leah Kelly has been very helpful.

A special thanks to Dr. H. Donnert for his help throughout the summer and for involving the author in some very interesting research.

## REFERENCES

1. Dr. H. Donnert, FJSRL and KSU Professor, Private Communication.
2. K.D. Zook, FJSRL and KSU, Private Communication.
3. P.J. Bramou and R.A. Hamil, SNL, Private Communication.
4. D. Boucher, ed., "Optical Fibers in Adverse Environments," SPIE Report, Volume 404, 1983.
5. Dr. H. Donnert, Final Report, 1984 USAF-SCEEE FSRP.
6. Hornbeck, W. Robert, Numerical Methods, New York, Quantum Publishers, Inc. (1975).
7. Chatfield, Christopher, Statistics for Technology, Great Britain, J.W. Arrowsmith, Ltd. (1978).

1984 USAF-SCEEE GRADUATE STUDENT SUMMER SUPPORT PROGRAM

Sponsored by the

AIR FORCE OFFICE OF SCIENTIFIC RESEARCH

Conducted by the

SOUTHEASTERN CENTER FOR ELECTRICAL ENGINEERING EDUCATION

FINAL REPORT

THE EFFECTS OF PSYCHOPHYSICAL MATCHING ON THE TRANSFER OF  
TRAINING BETWEEN ALTERNATIVE MOTION SIMULATORS

Prepared by: John M. Flach

Academic Department: Experimental Psychology

University: The Ohio State University

Research Location: Aerospace Medical Research Laboratory,  
Human Engineering Division

USAF Research Contact: Dr. Rik Warren & Dr. Grant McMillan

SFRP Supervising  
Faculty Member: Dr. Rik Warren

Date: September 10, 1984

Contract No: F49620-82-C-0035

THE EFFECTS OF PSYCHOPHYSICAL MATCHING ON THE TRANSFER OF  
TRAINING BETWEEN ALTERNATIVE MOTION SIMULATORS

by

John M. Flach

ABSTRACT

In this study psychophysical matching techniques were employed to equate the subjective experience of motion between two alternative motion simulation devices--the RATS, a full-body motion environment and the ALCOGS, which presented motion cues through a moving seat pan. The psychophysical matching technique, designated SIGMA, for Subjective Interactive Gain Measurement Analysis, resulted in equivalent roll-axis tracking performance between the two simulators. However, training subjects in the ALCOGS using the motion drive algorithm derived using the SIGMA technique did not result in better transfer between simulators than training with no motion cues.

## I. INTRODUCTION

The Advanced Low Cost G-Cuing System (ALCOGS) was developed to fulfill the need for a "highly responsive and flexible research G-cuing system for tactical aircraft simulation" (Kleinwaks, 1980). This system includes hydraulically-actuated seat-pan, backrest, and seatbelt elements mounted in an aircraft seat frame. The Air Force Aerospace Medical Research Laboratory has recently been investigating the feasibility of using the ALCOGS to provide motion information in simulated flight environments (McMillan, Levison, & Martin, 1984; Levison, McMillan, & Martin, 1984). The results from these investigations have been mixed. On the one hand, performance in a roll-axis tracking task showed significant improvement when rotational information was provided using the one-piece seat-pan of the ALCOGS. Yet, on the other hand, this improved performance did not transfer to a similar roll-axis tracking task performed in a whole-body motion simulation environment provided by the Roll-Axis Tracking Simulator (RATS). That is, subjects trained with motion cues provided through the seat pan of the ALCOGS did no better when transferred to a whole-body motion environment than subject trained in a static (no motion) environment. The present investigation was initiated to study ways for improving the transfer of training between the moving seat-pan of the ALCOGS and the whole-body motion of the RATS for a roll-axis tracking task. Two factors were chosen for examination: 1) the algorithm used to drive the ALCOGS' seat-pan, and 2) the compatibility between simulator motion and visually presented information.

### A. The Roll-Axis Drive Algorithm

McMillan, Levison, and Martin (1984) investigated the effects of four

different algorithms for driving the seat-pan of the ALCOGS in a roll-axis tracking task. These algorithms were:

$$\theta_{\text{ALCOGS}} = -.32 \theta_{\text{RATS}} + .02 \ddot{\theta}_{\text{RATS}} \quad (1)$$

$$\theta_{\text{ALCOGS}} = -.32 \theta_{\text{RATS}} \quad (2)$$

$$\theta_{\text{ALCOGS}} = .02 \ddot{\theta}_{\text{RATS}} \quad (3)$$

$$\theta_{\text{ALCOGS}} = -.23 \dot{\theta}_{\text{RATS}} \quad (4)$$

The algorithm represented in Equation 1 equates the seat-pan angle in the ALCOGS to a combination of angular position and acceleration in the RATS. This algorithm was chosen in an attempt to equate the two simulators for buttocks pressure. McMillan et al. (1984) found that performance in a roll-axis tracking task (RMS error) was slightly improved relative to performance under static conditions when this "pressure matching" algorithm was used to drive the seat-pan. However, the amount of improvement was small relative to the improvement seen when whole-body motion cues (RATS) were provided to trackers in a previous study (Levison, Lancraft, & Junker, 1979).

McMillan et al. (1984) next tested performance (RMS error) in a roll-axis tracking task using the algorithms of Equations 2 and 3 to drive the seat-pan of the ALCOGS. These equations were derived by setting either the position or the acceleration terms of Equation 1 to zero. Thus, Equation 2 represents a position algorithm in which the angular position of the seat-pan is proportional to the angular position of the RATS. Equation 3 represents an acceleration algorithm in which the angular position of the seat-pan is proportional to the angular acceleration of the RATS. The roll-axis tracking performance obtained using these algorithms seemed to indicate that the position component of Equation 1 was "providing much more

useful information than the acceleration component" (McMillan et al., 1984). In fact, asymptotic performance using the position algorithm to drive the seat-pan was equivalent to asymptotic performance in the whole-body motion environment of the RATS.

Finally, to complete the picture, McMillan et al. (1984) tested performance (RMS error) using the velocity algorithm shown in Equation 4. In this algorithm, angular position of the seat-pan is made proportional to angular velocity in the RATS. The asymptotic roll-axis tracking performance obtained using the velocity algorithm to drive the seat-pan exceeded asymptotic performance in the RATS.

Thus, two of the four seat-pan drive algorithms tested (position or velocity) resulted in performance which equaled or exceeded the performance obtained in the whole-body motion environment of the RATS. This is the positive aspect of the mixed results alluded to in the opening paragraph. The negative aspect is that training subjects with the seat-pan being driven by either the position or velocity algorithms resulted in no better transfer to the whole-body motion environment (RATS) than did training subjects with a static seat. This suggests that experience in using the motion cues provided by the ALCOGS' seat-pan does not result in an enhanced ability to pick-up motion cues in the whole-body motion environment. One possible explanation for this lack of positive transfer between the two motion cuing devices is that the motion doesn't "feel" the same. The present study will employ psychophysical matching techniques in an attempt to equate the two-motion devices in terms of their subjective "feel." If the algorithm which results as a function of this psychophysical matching proves to be different in form from the previously tested algorithms (e.g.,

a first-order lead or a first-order lag), then it is hoped that training subjects with this new algorithm will result in greater positive transfer between the two-motion cuing systems.

#### B. Visual Motion Display Compatibility

A second factor which might contribute to the lack of positive transfer between the ALCOGS and the RATS is a possible conflict in the way visual information is presented in the two simulation devices. Figure 1 shows three alternative visual displays. Each visual display is composed of two symbols: a schematic plane ( $\perp$ ) and a dotted reference line (---). Angular position error is represented by the angular difference between the schematic plane and the dotted reference line.

Figure 1(c) represents the visual display used in the RATS. In this configuration the schematic plane moves with respect to the display screen, and the dotted reference line is stationary with respect to the display screen. However, the entire visual display is moving with the RATS. Further, simulator motion and motion of the schematic plane are coupled such that the schematic plane is always perpendicular to gravity. This coupling of motion within the visual display and motion of the display itself could result in one of two possible perceptions on the part of the tracker. If the human tracker adopts the screen as her reference frame, then the plane symbol should appear to be moving with respect to the stationary dotted reference line when tracking in the RATS. Given this perspective, the displays shown in Figure 1(a) would be appropriate for use in the ALCOGS. However, the human tracker could also adopt the force of gravity as her reference frame. In this case, the dotted reference line should be perceived as moving with respect to the stationary plane symbol.

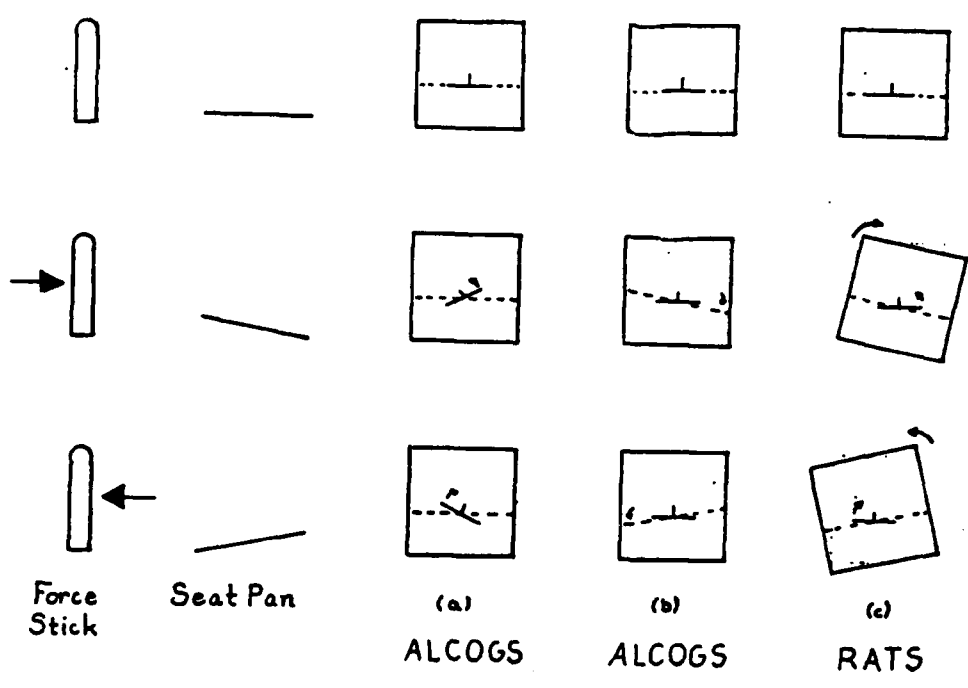


Figure 1: Alternative visual displays of roll-axis tracking information.

when tracking in the RATS. In this case, Figure 1(b) would be more appropriate for use in the ALCOGS.

The previous roll-axis tracking tasks performed using the ALCOGS have all used the visual display shown in Figure 1(a). These studies have assumed the visual display as the reference frame. However, if the trackers are actually orienting to gravity, then the displays seen in the ALCOGS and in the RATS may have appeared to be very different. This difference may have resulted in negative transfer which masked any positive transfer due to the motion cues provided by the moving seat-pan. This hypothesis will be tested by including the two ALCOGS' display alternatives shown in Figure 1 as a between-subjects factor in the present study.

## II. OBJECTIVES OF THE RESEARCH EFFORT

The primary objective of this research effort was to improve the amount of positive transfer between the ALCOGS and the RATS in a roll-axis tracking task. This objective is a small part of a larger effort on the part of the Air Force Aerospace Medical Research Laboratory to evaluate the value of the ALCOGS, both as a research tool for studying the role of motion information in flight control tasks and as an alternative to larger, more expensive motion base simulators for training tactical aircraft skills.

A secondary objective of this project was to examine a new methodology for psychophysically matching displays for continuous control tasks. This new methodology has been designated SIGMA for Subjective Interactive Gain Measurement Analysis. SIGMA provides a methodology for collecting magnitude estimations across a range of frequencies and then combining these estimates into an approximate operator describing function for

equating two displays. SIGMA may prove to be a valuable tool for psychologically equating displays for dynamic tasks that differ along any physical dimension (e.g., modality, lag, etc.)

### III. EXPERIMENT

#### A. Equipment

Two simulation devices were used in this study. The dynamic seat, a subsystem of the ALCOGS, was used to provide dynamic cuing and the RATS was used to provide whole-body motion cuing.

The dynamic seat is a hydraulically accuated seat-pan which can be driven in four degrees of freedom: longitudinal, heave, pitch, and roll. For this study, only the seat-pan roll was used.

The RATS consists of a rotating frame, drive train, and control console. It is capable of 360 degree rolls. The axis of rotation is through the subject's buttocks.

Both simulators were driven with an EAI 580 analog computer and a PDP 11/60 digital computer. The dynamics were representative of the roll response of a fighter-type aircraft. This simulation operated at 100 Hz and included delays of only 75 msec in the visual and motion loops.

A small TV monitor mounted at the subject's eye level displayed tracking error. The reference line subtended a visual angle of less than 9 degrees. The display configurations are shown in Figure 1.

#### B. Subjects

Six naive subjects, three male and three female, participated in the early phases of this study. Four of these subjects, two male and two female, continued into the final tracking phase of the study.

### C. Procedure

The investigation consisted of four phases. Phase I investigated the subjects' ability to match motion amplitudes within the same simulator (ALCOGS). This phase involved two 1-hour sessions per subject. During a session a subject was presented with six different reference signals (two amplitudes ( $\pm 5$  degrees,  $\pm 2$  degrees) at each of three frequencies (0.08 Hz, 0.25 Hz, 0.80 Hz)). A single presentation lasted for 120 seconds. During this time a subject was seated in the ALCOGS while seat-pan roll was driven at a particular amplitude-frequency combination. After this reference presentation there was a break of approximately 5 minutes during which the subject was removed from the simulator. Following the break, subjects were returned to the ALCOGS. A signal at the same frequency as the reference signal was then presented to the subject and he/she was asked to adjust the signal amplitude until the seat motion was equivalent to the previously presented reference motion. Adjustments were made using a force stick mounted on the right-hand side of the ALCOGS. The initial amplitude was always zero. The order in which reference signals were presented to subjects was counterbalanced across the six subjects.

Phase I was included to provide a baseline from which to assess later judgments. That is, it was intended to provide an index of the variability to be expected for matching judgments and also provide an index for any consistent distortions in this judgment which might be attributed to memory.

Phase II was similar to Phase I, with the exception that reference signals were presented using the RATS, and matches were made in the ALCOGS. Like Phase I, Phase II also consisted of two 1-hour session in which six

reference signals were presented to the subjects. The same reference signals used in Phase I were used in Phase II. The goal of Phase II was to generate a pattern of amplitude ratios across frequencies. This pattern could then be used to generate an approximate describing function for relating perceived motion in the RATS to perceived motion in the ALCOGS. Using this describing function an optimal algorithm for driving the dynamic seat could then be derived.

In Phase III, reference signals were presented using a visually displayed line pivoting about its center and matches were made by adjusting the amplitude of roll motion in the simulator. Thus, visual roll motion amplitude at a particular frequency was matched to simulator roll motion amplitude at the same frequency. This phase consisted of four sessions--two sessions in the RATS and two sessions in the ALCOGS. The same six reference signals as were used in Phase I and II were used in Phase III. Adjustments of simulator motion were made using a force stick.

The goal of Phase III was the same as for Phase II. That is, to derive a describing function for subjectively equating motion in the two simulators. Whereas, Phase II used direct comparisons between the two simulators, Phase III employed a visual referent as a mediator between the two devices. Thus, Phase III resulted in two describing functions-- $H_R$  maps from the visual referent to RATS motion and  $H_A$  maps from the visual referent to ALCOGS motion as shown in Equations 5 and 6.

$$\phi_{\text{RATS}} (H_R) = \phi_{\text{VISUAL}} \quad (5)$$

$$\phi_{\text{ALCOGS}} (H_A) = \phi_{\text{VISUAL}} \quad (6)$$

$$\phi_{\text{RATS}} (H_R) = \phi_{\text{ALCOGS}} (H_A) \quad (7)$$

$$\phi_{\text{RATS}} = (H_A/H_R) \phi_{\text{ALCOGS}} \quad (8)$$

These two equations (5 and 6) can then be combined as shown in Equations 7 to yield a transfer function for equating the RATS and the ALCOGS as shown in Equation 8. An advantage of using the visual referent as a mediator is that it eliminates the delays involved with switching from one simulator to the other as in Phase II.

In the final phase, Phase IV, four subjects performed a roll-axis tracking task. This task entailed maintaining wings-level flight in the presence of a roll disturbance, which appeared random, but was actually generated by a sum-of-sines procedure to simplify analysis. Subjects were trained to asymptote in the ALCOGS, with the seat-pan being driven with an algorithm chosen on the basis of the previous phases. Two of the four subjects used the visual display shown in Figure 1(a) and four subjects used the visual display shown in Figure 1(b). Following training, subjects were transferred to a similar roll-axis tracking task in the RATS to assess the training benefit of experience with motion in the ALCOGS.

#### D. Results and Discussion

The results from Phase I are shown in Figure 2(a). Plotted in Figure 2(a) are the mean magnitude estimations in decibels, averaged across the six subjects and the two amplitudes for each of the three frequencies presented. The mean magnitude estimates for the lower two frequencies were close to 0 db indicating fairly good matches to the reference signal. The mean magnitude estimate for the higher frequency was slightly more than 2 db indicating a tendency to over estimate the amplitude of signals at this frequency. The range of magnitudes is indicated by the bars on the graph in Figure 2(a). Variability of the estimates tended to be high.

The results from Phase II showed a pattern very similar to that

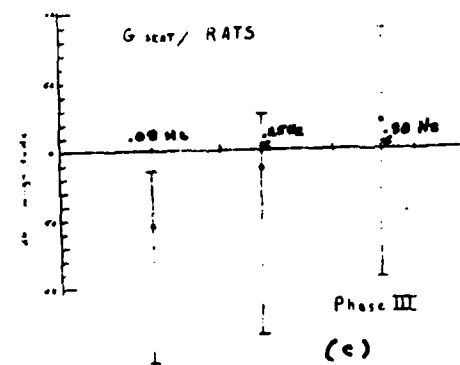
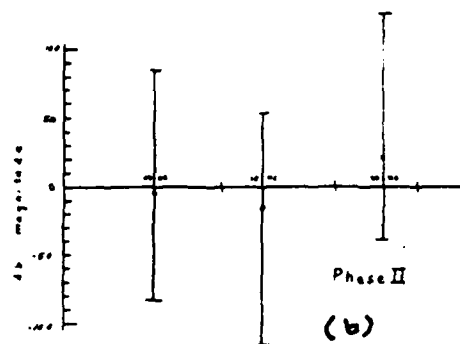
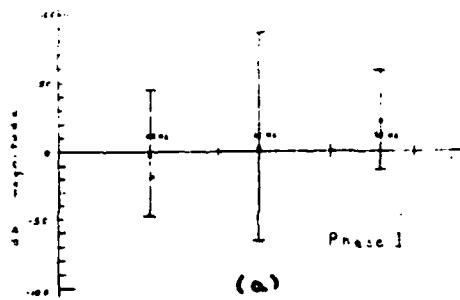


Figure 2: Magnitude estimates at three frequencies (.08 Hz, .25 Hz, and .80 Hz) obtained for Phase I, II, and III.

obtained for Phase I as can be seen in Figure 2(b). The fact that the magnitude estimates obtained between simulators in Phase II are similar to the magnitude estimates obtained in a single simulator in Phase I suggest that a 1 to 1 position match between motion in the two simulators would be the most subjectively similar. That is, the optimal drive algorithm should be obtained from subtracting the magnitude estimates (in decibels) obtained in Phase I from those obtained in Phase II. Doing this results in a describing function which can best be modelled as a gain of 1--a position drive algorithm. This is consistent with the data reported by McMillan, Levison, and Martin (1984) which showed equal asymptotic performance for subjects in the RATS and in the ALCOGS with a position drive algorithm. However, this does not solve the problem of transfer between simulators. As previously noted, subjects trained with a position algorithm in the ALCOGS did no better than subjects trained under static conditions when transferred to the whole-body motion environment of the RATS.

The results obtained for Phase III showed a different pattern. Figure 2(c) shows the magnitude ratios between the G-seat (ALCOGS) and the RATS obtained in Phase III. This pattern, in which the gain increases across frequency at less than 20 db per decade, suggests that the optimal algorithm for driving the ALCOGS should be a combination of position and velocity. Although the range of magnitudes at each frequency was large, the pattern of increasing gain with increasing frequency was consistent across subjects. For six out of six subjects the gain for the second frequency (.25 Hz) was higher than the first (.08 Hz), and for five of six subjects the gain for the third frequency (.80 Hz) was higher than the second.

In order that the relative proportion of position to velocity information could better be determined Phase III was repeated with three additional frequencies being tested. Figure 3 shows the results of this replication. The opened circles in Figure 3(a) show the mean ratio of G-seat (ALCOGS) motion to visual motion at each frequency. The filled circles in Figure 3(a) show the mean ratio of RATS motion to visual motion. The ratio of the mean for the G-seat (ALCOGS) to that for the RATS at each frequency is shown by the diamonds in Figure 3(a). Figure 3(b) shows the same data, however, the ratio of G-seat (ALCOGS) to RATS was calculated for each subject individually and then the resulting ratios were averaged across subjects. The pattern of results is similar in either case. This pattern suggests that the optimal algorithm for driving the ALCOGS is the combination of position and velocity shown in Equation 9:

$$\theta_{\text{RATS}} = .67 \theta_{\text{ALCOGS}} + .11 \dot{\theta}_{\text{ALCOGS}} \quad (9)$$

This algorithm was used to drive the ALCOGS seat-pan in the training part of Phase IV of this study. Figure 4 compares the RMS error across trials for subjects using the new algorithm (solid lines) against results from previous studies (dotted lines) in which subjects were trained using either a static display (S), a position drive algorithm (P) in the ALCOGS, a velocity drive algorithm (V) in the ALCOGS, or the whole-motion environment of the RATS (R). The first 20 sessions shown in Figure 4 represent the training phase and sessions 21-30 represent the transfer phase. All subjects were in the whole-body motion environment of the RATS for the transfer phase. As can be seen from Figure 4, the new algorithm resulted in training performance which was more similar to performance in the RATS than either of the other drive algorithms (position or velocity).

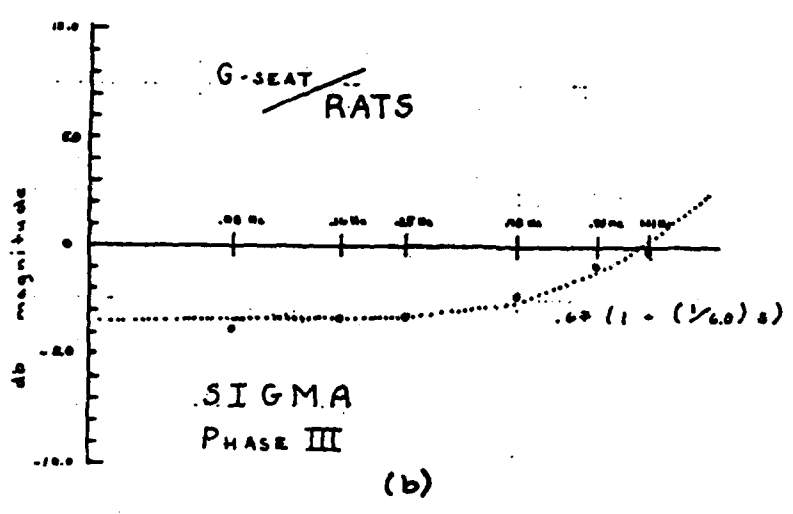
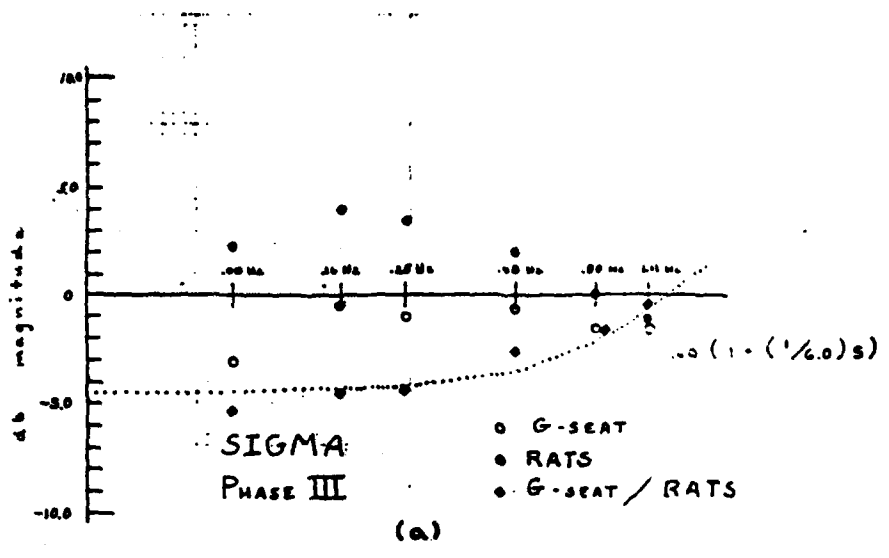


Figure 3: Magnitude estimates obtained at six frequencies (0.08 Hz, 0.16 Hz, 0.25 Hz, 0.48 Hz, 0.96 Hz, and 1.1 Hz) in replication of Phase III.

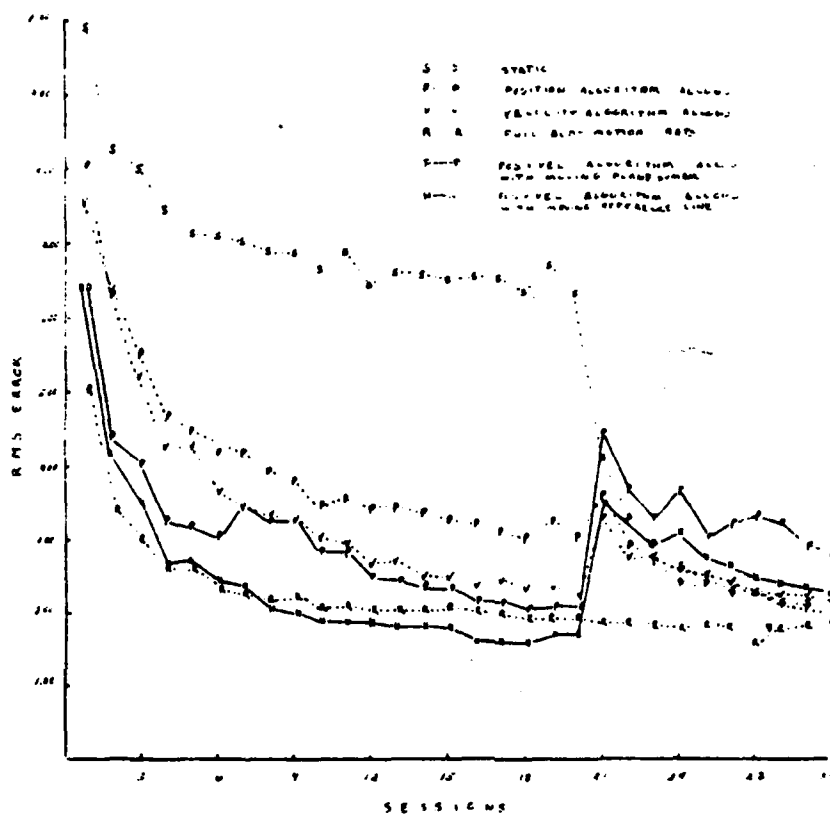


Figure 4: Comparison of tracking performance in a roll-axis tracking task as a function of style of motion presentation.

However, transfer to the RATS was no better with the new algorithm than with any of the previous algorithms or even than with a static visual presentation (no motion).

The difference in performance between the subjects who used the display shown in Figure 1(a) (moving plane---P) and those who used the display shown in Figure 1(b) (moving reference line---H) may be indicative of individual differences rather than any real superiority of one display over the other. Because of the small sample size (2 subjects per condition), these differences may not be reliable. Surprisingly, the two alternative visual displays did not seem to differentially affect the transition between simulators.

#### IV. RECOMMENDATIONS

It appears that the type of motion cues presented in the ALCOGS and interestingly, the type of visual cues presented in the ALCOGS have little consequence for latter performance in the RATS. This suggests that there may be another factor whose effect masks any benefits resulting from training in the ALCOGS. This other factor may be an increase in anxiety in the RATS due to the relative severity of large errors in this simulator as compared to the ALCOGS. The range of movement and the amount of jostling the subject can potentially receive is much greater for the RATS than for the ALCOGS. To test whether this hypothesis is correct, it is recommended that subjects should be trained in the RATS and then transferred to the ALCOGS. Transfer in this direction should not be contaminated by increased subject anxiety. Transfer to the ALCOGS should be best with the motion algorithm and the visual display which are most similar to the subject's perceptions in the RATS.

The relatively close match between performance with the algorithm derived using the SIGMA technique and the performance in the RATS suggests that this technique may be a useful tool for matching information displays in continuous control tasks. However, it is possible that similar performance matches might be achieved by increasing the gain on the position or velocity algorithms. Additional testing is necessary using other types of displays before a confident verdict can be made as to the usefulness of this procedure.

In conclusion, there are three recommendations for continuing this research effort.

- 1) Repeat the tracking phase of the study reported here including four more subjects in each of the two visual display conditions. This is needed so that reliable comparisons can be made with previous studies and between the two visual displays.

- 2) Conduct an additional study reversing the order of tasks. That is, train subjects in the RATS and transfer them to the ALCOGS. Different subjects should receive different motion algorithms and visual displays in the ALCOGS. Subjects with the motion algorithm and visual display most similar to perceptions in the RATS should show the smoothest transition between simulators.

- 3) Test the SIGMA procedure in another domain with different types of cross-modality displays.

#### REFERENCES

1. Levison, W.H., Lancraft, R.E., and Junker, A.M., "Effects of Simulator Delays on Performance and Learning in a Roll-Axis Tracking Task," Fifteenth Annual Conference on Manual Control, Wright State University, Dayton, Ohio, March 1979, pp. 168-186.
2. Levison, W.H., McMillan, G.R., and Martin, E.A., "Models for G-Seat Cuing on Roll-Axis Tracking Performance," Twentieth Annual Conference on Manual Control, NASA-ARC, California, June 1984.
3. McMillan, G.R., Levison, W.H., and Martin, E.A., "Motion Simulation with a G-seat System: Sensory and Performance Mechanisms," Ninth Psychology in DOD Symposium, U.S. Air Force Academy, April 1984.

### ACKNOWLEDGMENTS

The author wishes to acknowledge the sponsorship of the Air Force Systems Command, Air Force Office of Scientific Research and the Aerospace Medical Research Laboratory. Special thanks go to Dr. Rik Warren and Dr. Grant McMillan. Dr. Warren acted as my supervising faculty advisor and was instrumental in my receiving the opportunity to work in an Air Force laboratory. Dr. McMillan was closely involved in the development and implementation of the research project reported in this paper. Not only did Dr. McMillan make many valuable suggestions for the design of the experiment, but he provided the laboratory facilities necessary to implement this project. Both, Dr. Warren and Dr. McMillan were excellent hosts. I had a very enjoyable and interesting summer as a guest in their laboratory.

Thanks also go to Matt Mittendorf and Melody Snell. Matt Mittendorf supervised the development and maintenance of the software and hardware required for the experiments reported here. He was instrumental in translating my often vague ideas into concrete realities. Melody Snell acted as a research assistant on this project. She was responsible for scheduling everything from subjects to maintenance. She was the experimenter who had direct contact with subjects in all phases of this project. Ms. Snell also graciously shared her office with me during my visit.

Finally, I wish to thank Dr. Bob Shaw and Joe Solomon for their time and patience in interchanging ideas throughout the summer.

1984 USAF-SCEEE GRADUATE STUDENT SUMMER SUPPORT PROGRAM  
Sponsored by the  
AIR FORCE OFFICE OF SCIENTIFIC RESEARCH  
Conducted by the  
SOUTHEASTERN CENTER FOR ELECTRICAL ENGINEERING EDUCATION  
FINAL REPORT

AN ALGORITHM FOR SEGMENTING FLIR IMAGERY CONTAINING BRIDGES

Prepared by: Paul Gader

Academic Department: Department of Mathematics

University: University of Florida

Research Location: Air Force Armament Laboratory  
Guided Weapons Division  
Electro-Optical Terminal Guidance Branch

USAF Research Contact: Mr. Neal Urquhart

SFRP Supervising  
Faculty Member: Dr. Sam Lambert

Date: July 20, 1982

Paul Gader

ABSTRACT

This report presents an algorithm for segmenting FLIR imagery which contain bridges. The algorithm uses edge based segmentation and the concept of reverse-parallel line segmentation to isolate target-like regions.

The algorithm is coded in Fortran and is available along with a users guide at the Image Processing Lab at Air Force Armament Laboratory, Eglin AFB.

### Acknowledgements

The author would like to express his appreciation and gratitude to the Air Force Systems Command, the Air Force Office of Scientific Research, and the Southeastern Center for Electrical Engineering Education for providing the opportunity to spend a very interesting and valuable summer at the Air Force Armament Laboratory, Eglin AFB, FL. In particular, he would like to acknowledge the staff of the Electro-Optical Terminal Guidance Branch of the Guided Weapons Division. Their hospitality and support made this summer research a very pleasant experience. Special thanks and sincere gratitude are due Lt Col Lawrence Ankeney, PHD, Mr Neal Urquhart, and Dr. Gerhard Ritter for their continued encouragement and for their guidance and suggestions that made this project a successful one. Also, appreciation is extended to the personnel in the Image Processing Lab who were extremely generous with their time and expertise, and who provided solutions to seemingly unsolvable problems which inevitably arise from using computers.

Finally, the author would like to acknowledge the assistance of Mrs. Merlynn Bath in the preparation of this manuscript.

## Introduction

The solution of the problem of automatic recognition of high value targets in FLIR images is of obvious importance to the USAF. The ability of a seeker to "lock on after launch" would help to ensure the safety of American pilots. An automatic target recognition system must use scene content to classify objects. Using contextual information serves to localize the target search area, therefore decreasing the number of pixels to be processed. Thus, techniques need to be developed to extract and utilize contextual information. (1)

Generally the first step in extracting information is that of segmenting the image into subregions. The real time benefit of scene segmentation is that certain uninteresting subregions of the image can be discarded while the remaining interesting subregions can then be examined more closely, but requiring much less computation. Artificial intelligence techniques can then be used to decide which features should be computed for a given subregion and how to interpret the interaction of specific measurements for the computed features.

Many types of segmentation techniques exist. Edge-based segmentation is one common type. The basic idea of edge-based segmentation is to outline the objects in the image and then use shape information and/or information available in the "neighborhood" of an edge to classify objects. Some examples of edge based segmentation can be found in (2). Region based segmentation is another type. This technique groups pixels into regions which are homogeneous with respect to some measure. Examples of region based segmentation can be found in the extended bibliography. After segmentation, either the target should be contained in one of the remaining subregions, or the remaining subregions should include sufficient contextual information so that further relationship analysis will permit potential target subregions to be identified. In either case, further analysis is generally required before a final decision is made as to which subregions are most target-like. The problem now is to determine which type of segmentation technique best applies to segment a large variety of images containing

high value targets.

### RESEARCH GOALS AND OBJECTIVES

The research objectives for the Summer Research period are:

- 1) To investigate existing segmentation techniques related to the automatic recognition of bridges in FLIR imagery;
- 2) To determine features that can be used to characterize bridges in FLIR imagery;
- 3) To modify existing algorithms or develop new algorithms for segmentation and feature extraction to make them particularly applicable to bridge recognition;
- 4) To implement the algorithms in 3) on the computer and test them. This software will be modular so that it can be changed and/or expanded.

### III. General Outline of the Approach

This section presents a general outline of the algorithm which was implemented. The details of each part of the algorithm will be presented in sections IV-VI.

Edge-based segmentation is used rather than region-based segmentation because:

- 1) Bridges do not generally constitute large regions in an image.
- 2) The fact that the edges of a bridge have opposite change in contrast can be exploited.

The first stage of the algorithm is convolution with a set of six edge masks, each mask having two directions associated with it. The resulting edge image is thinned and thresholded using both magnitude and directional information. The thinned edges are then approximated piecewise by directed line segments. Next, the directed line segments are grouped in pairs, each pair consisting of directed line segments whose directions differ by approximately  $180^\circ$  (called "Revpars") and are "close" to each other. In the case of a  $0^\circ/180^\circ$  pair the region outside the pair of line segments is checked for the existence of water.

The output of the algorithm is a collection of pairs of directed line segments which satisfy certain contextual relationships. These

pairs of line segments represent possible bridges.

#### IV. The Edge Detection and Thinning

##### A. The Edge Masks

The algorithm originally used the set of six 5x5 masks as shown in Figure 1a. The original image is convolved with each mask yielding six possible edge values for each pixel. Each resultant pixel for the convolved image is assigned the value with the largest magnitude and either assigned the direction 0 associated with that mask if the value is positive, or  $(0+180^\circ)$  (modulo  $360^\circ$ ) if the value is negative. Thus, at the end of the convolution stage each pixel of the original image has both a magnitude and direction associated with it.

The reason the 5x5 masks were used was that they offered twelve possible directions. The other edge masks that were investigated offered only eight:  $0^\circ, 45^\circ, \dots, 345^\circ$ . Eight directions did not result in enough directional sensitivity. Consider the following: A bridge is oriented in an image at approximately 60-65 degrees. The top edge is labelled as a  $90^\circ$  edge and the bottom edge is labelled as a  $225^\circ$  edge (as opposed to a  $270^\circ$  edge). In order to classify the pair as a possible bridge one would have to define line segments whose directions differ by  $180^\circ \pm 45^\circ$  as reverse parallel line segments. But then an actual  $110^\circ$  edge and an actual  $210^\circ$  edge would be considered as reverse parallel line segments, which is absurd. Therefore, the use of an 8 direction mask does not provide the required directional sensitivity.

The 5x5 masks have the disadvantage of being insensitive to fine detail. Detail is important in bridge classification because:

- 1) Bridges from long range (3-6 miles) comprise a very small percentage of the total image but it is highly desirable to isolate subregions of the original image which may contain bridges at this range. There would then be time for more intense localized processing on each of the smaller subregions.

- 2) Many bridges have superstructures and substructures which can be used as features for classification. The structures appear as fine details in FLIR images.

The 3x3 edge masks have much more sensitivity to detail than the 5x5

1	1	1	1	1
1	1	1	1	1
0	0	0	0	0
-1	-1	-1	-1	-1
-1	-1	-1	-1	-1

180°

1	1	1	1	1
-.3	.7	1	1	1
-1	-.8	0	.8	1
-1	-1	-1	-.7	.3
-1	-1	-1	-1	-1

150°

-1	.3	1	1	1
-1	-.7	.8	1	1
-1	-1	0	1	1
-1	-1	-.8	.7	1
-1	-1	-1	-.3	1

120°

-1	-1	0	1	1
-1	-1	0	1	1
-1	-1	0	1	1
-1	-1	0	1	1
-1	-1	0	1	1

90°

1	1	1	1	1
1	1	1	.7	-.3
1	.8	0	-.8	-1
.3	-.7	-1	-1	-1
-1	-1	-1	-1	-1

210°

1	1	1	.3	-1
1	1	.8	-.7	-1
1	1	0	-1	-1
1	.7	-.8	-1	-1
1	-.3	-1	-1	-1

240°

Figure 1.a

1	1	1
1	1	1
0	0	0

180°

-1	0	1
-1	0	1
-1	0	1

90°

.7	1	1
-.8	0	.8
-1	-1	-.7

150°

1	1	.7
.8	0	-.8
-.7	-1	-1

210°

-.7	.8	1
-1	0	1
-1	-.8	.7

120°

1	.8	-.7
1	0	-1
.7	-.8	-1

240°

Figure 1.b

edge masks. By simply "peeling off" the outside layers of the 5x5 masks (see figure 1.b) we obtained a set of 3x3 edge masks which were satisfactory in the following sense:

- 1) Edges that were picked up by the 5x5 masks were picked up by the 3x3 masks.
- 2) More details were picked up than with the 5x5 masks.
- 3) The masks were tested on synthetic data and were able to detect 12 directions in a consistent fashion. For example, on a  $120^\circ$  line, convolution with the  $120^\circ$  mask produced a larger magnitude than convolution with the other masks.

Thus the 3x3 edge masks were implemented also. The user can choose either the 5x5 or 3x3 masks.

#### B. Thinning and Thresholding

The convolved image is thresholded with the threshold level,  $T$ , being determined by

$$T = X + \alpha S$$

where  $X$  is the mean of the edge magnitudes,  $S$  is the standard deviation, and  $\alpha$  is a parameter which can be set by the user. Experimental results indicate that the bridge pixels at medium and long range, or about 13,000-30,000 feet, have low to medium edge magnitudes. Therefore, the threshold could not be set very high. The low threshold resulted in a large number of "noise" edge pixels (see figure 2), many of which had roughly the same edge magnitudes as the bridge pixels. The difference between the bridge pixels and the noise pixels is that the bridge pixels form connected component edges. Thus, the average edge magnitude in a 3x3 window of a bridge pixel tends to be significantly higher than that of a "noise" pixel. For this reason, a local averaging operation was performed on the convolved, thresholded edge image, while retaining the original edge magnitudes to prevent blurring. The averaged edge image is then thresholded again at the same threshold. The thresholded averaged edge image is then reduced to a binary image by setting the nonzero elements equal to one. The resulting binary image is then multiplied by the convolved thresholded binary edge image. The user of

the program has the option of thresholding, setting the parameter , performing the local averaging, and setting the threshold parameter for the second threshold independently of the first. Notice that the local averaging operation could be performed before the first threshold is applied, but this may cause pixels "close" to an edge to have artificially high edge magnitudes.

The original thinning algorithm used was that of Nevatia and Babu (2). Experimental results indicated that these thinning conditions were too harsh for our purposes. In particular, bridge pilings and bridges from long and medium range are sometimes two pixels wide and edges which are side by side cannot be retained with the original thinning algorithm. Therefore, Nevatia and Babu's original decision rules were modified and new decision rules were added. The final version of the thinning algorithm declares an edge element to be present at a pixel if:

- 1) The edge directions of the two neighbors which are in a position normal to the direction of the center edge pixel under consideration are within  $30^\circ$  of this center pixel under consideration or the magnitudes of these neighbors are both zero, and

- 2) The output edge magnitude at the center pixel is greater than the edge magnitudes of the two neighbors. (The normal to a  $30^\circ$  direction is approximated by the diagonals on a 3x3 grid.)

or

- 1) One of the previously mentioned neighboring pixels is within  $30^\circ$  of the opposite direction of the center pixel and the other neighbor is within  $30^\circ$  of the center pixel under consideration and

- 2) The center edge pixel is a local maximum with respect to its neighbor in the same direction.

In addition, a smoothing operation performed on the direction array. The smoothing operation is performed before thinning. The following illustrates the implementation of the smoothing operation. If a  $30^\circ$  direction potential edge element has neighbors in positions 1 and 5 (see Figure 5) whose directions are both  $0^\circ$ , then the  $30^\circ$  potential edge element is changed to a  $0^\circ$  direction. This procedure is used to



Figure 2a. original image.

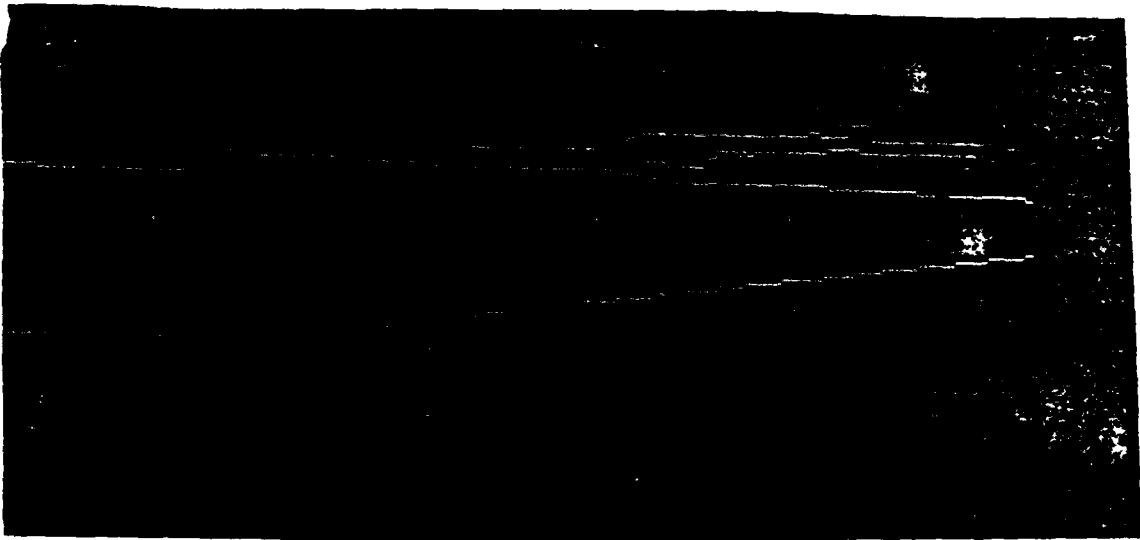


Figure 2b. thinned image using 5x5 masks.



Figure 2c. Thinned image using 3x3 masks

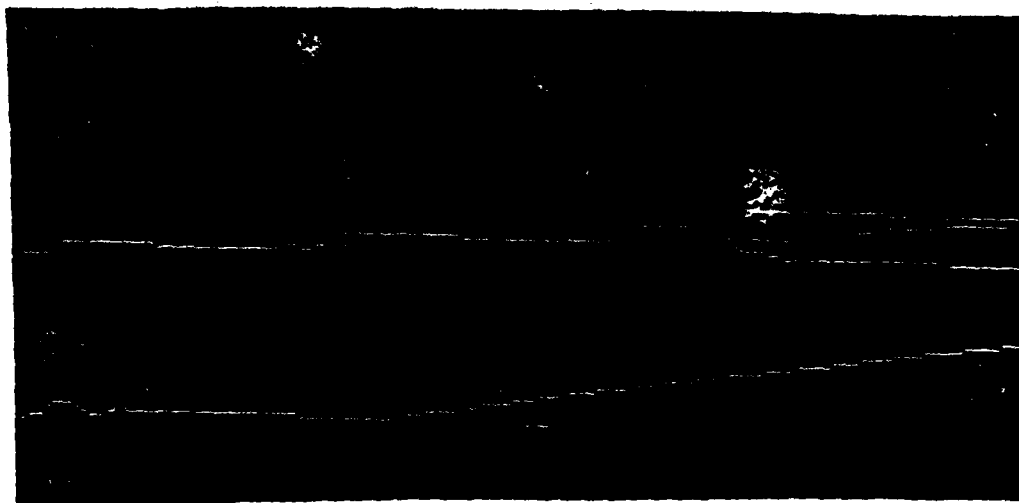


Figure 2d. local averaged thinned image.

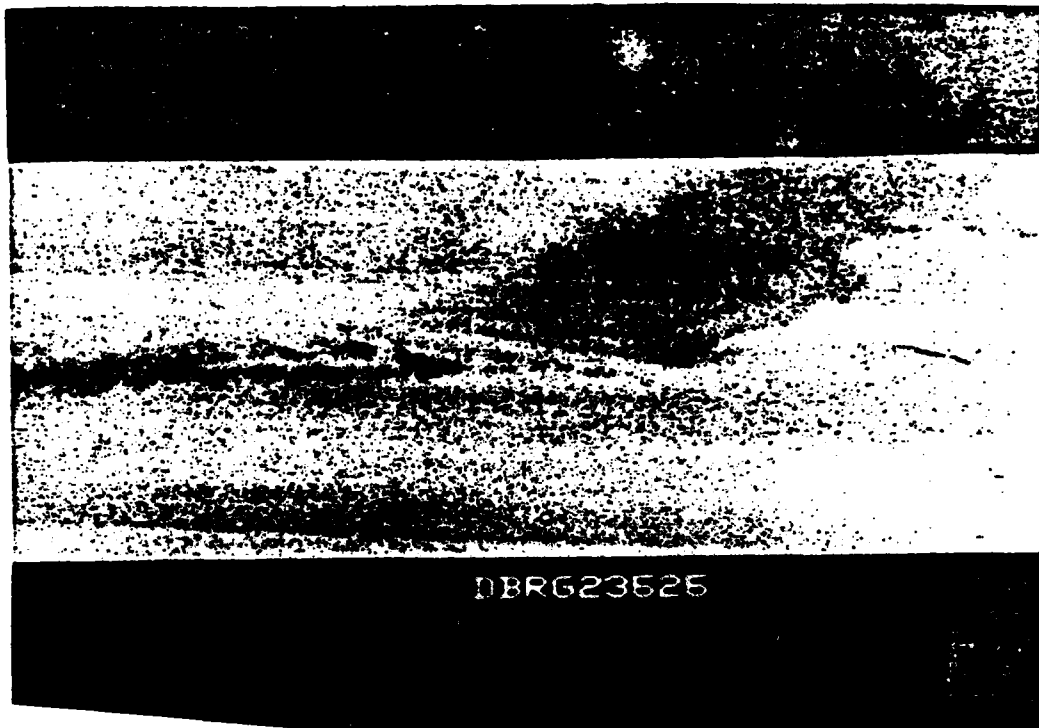


Figure 3a. Original image.



Figure 3b. Thinned image using 3x3 masks.

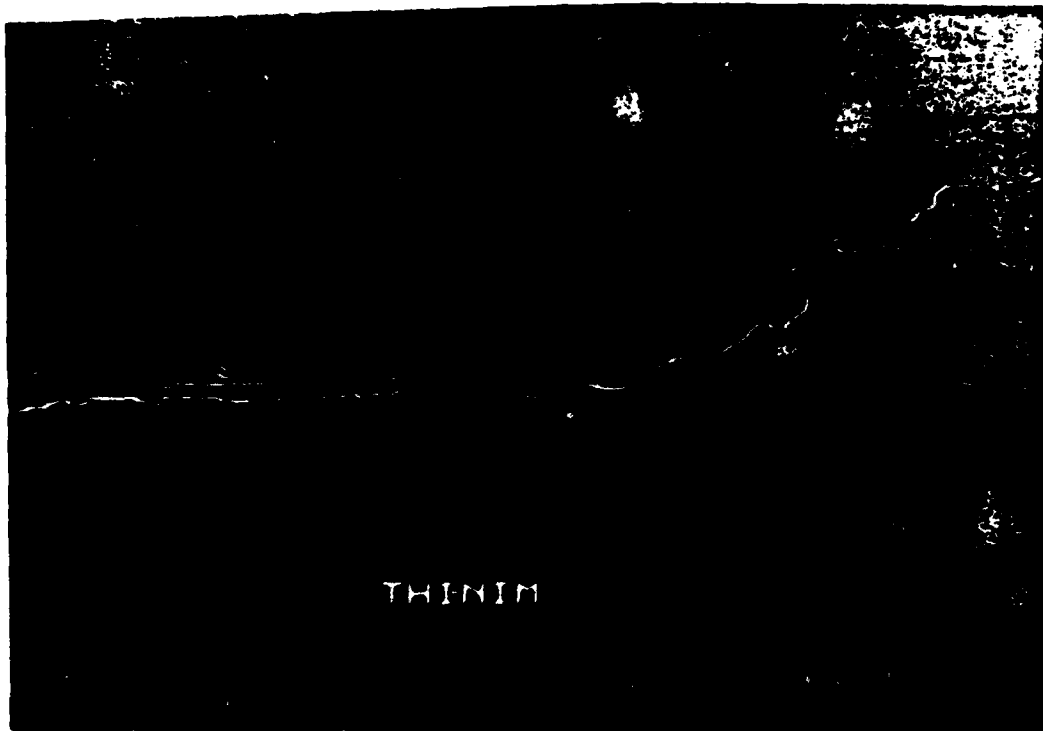


Figure 3c. Thinned image using 3x3's and local average.

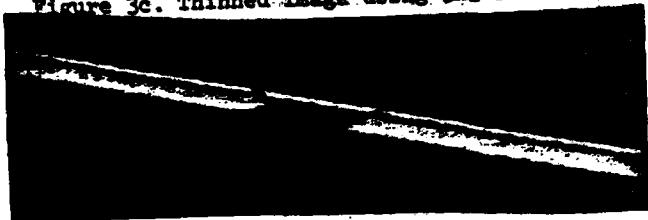


Figure 4a. Original image



Figure 4b. Thinned image with 3x3 masks.

prevent gaps in edges due to variation in edge magnitudes.

Results of different combinations of masks and thinning techniques are shown in figures 2 through 4.

#### V. Determination of Line Segments

The extraction of line segments from the thinned image is accomplished in two stages. The first step chooses neighbors preceding and following an edge pixel, and the second step links pixels sequentially in line segments, labelling the line segments by their end points. The method is a slight variation from the line linking routine in (2).

First, the neighboring edge pixels preceding and following a given edge pixel are determined, called predecessors and successors, respectively. Two pixels are labelled as successors and two as predecessors for a given pixel. The neighbors lie in one of eight positions relative to the edge pixel, as labelled below:

4	3	2
5	X	1
6	7	8

Figure 5

One step of the thinning process possibly eliminates the two pixels in the direction perpendicular to the edge pixel direction. Thus, an edge pixel looks for possible successors in the remaining three positions, which point in the general direction of the edge pixel direction. For example, if the edge pixel has  $30^\circ$  direction, then possible successors lie in positions 1, 2, and 3.

A pixel is retained initially as a possible successor if the following two conditions are met:

- 1) Its magnitude is not equal to zero;
- 2) Its direction lies within  $30^\circ$  of the direction of the edge pixel.

If only one pixel satisfies these conditions, then there is only one successor. If there are two such pixels, then the pixel with the greater magnitude is the primary successor and the remaining one is the secondary successor. If there are three pixels satisfying these conditions, then the primary successor is the one whose Euclidean distance to the edge pixel is a minimum. In this case, the second successor is the one whose direction is different from the primary successor's direction.

Predecessors are chosen by the same method as for successors. For example, in the case where the edge pixel has  $0^\circ$  direction, its successors would be located in positions 8, 1, or 2 and its predecessors located in position 4, 5 or 6. Note also that if a pixel A has a successor B, then A is a predecessor of B.

The output from this subroutine is four arrays, each of whose dimension is the same as the original image, and whose entries are numbers from 0 to 8 representing that pixel's successors and predecessors. Zero designates that a pixel has no predecessor/successor.

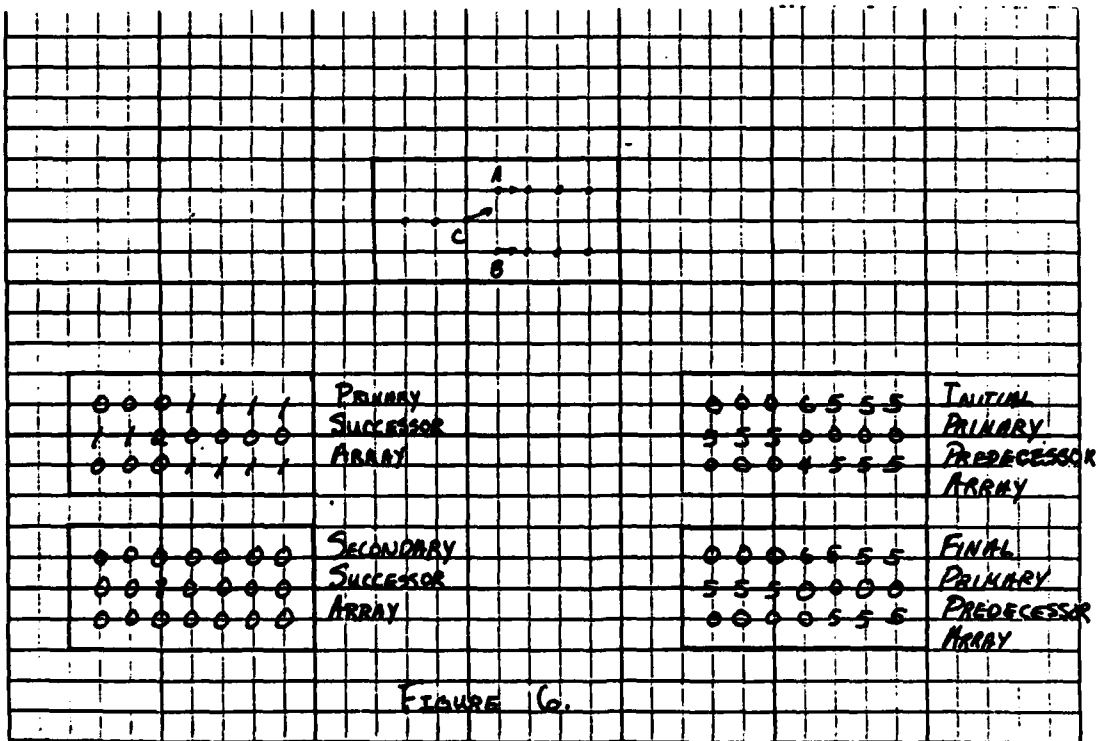
It was discovered, at too late a date to rewrite the code, that the predecessor array could be generated almost directly from the successor array. This would approximately cut in half the amount of code needed for this subroutine.

The second step uses the successor and predecessor arrays to link the pixels sequentially in line segments. The output from this subroutine is two arrays, one containing the X coordinates of the endpoints of the line segments, and the other containing the Y coordinates of the endpoints of the line segments. The line segments are directed, as the masks that determine the pixels' directions have twelve possible directions.

Starting from the top left-hand corner, an edge pixel that has no predecessor is found. The primary successors are followed from this initial pixel. If the initial pixel has more than two successors, then a line segment is constructed, with the initial pixel being one end point and the third successor being the other end point. For each

successor that lies between the two end points, the distance between it and the line segment is checked. If each intermediate successor has a distance to the line segment of one unit or less, then the next successor of the present endpoint is located. This successor becomes the end point of an extended line segment whose other end point is still the initial pixel. Again, the distances of each intermediate successor to the newly constructed line segment is checked, and if each distance is less than or equal to one unit, then the process continues to find the next successor, create a new line segment, check distances of the intermediate successors, etc. If at any time the distance from an intermediate successor to the present line segment is greater than one unit, the process stops. The end points of a line segment are output, with the starting point having the coordinates of the initial pixel, and the terminal point having the coordinates of the next to the last successor checked. This terminal point becomes the initial pixel of a new line segment, and successors are traced from it as described above, until a pixel with no successors is reached. This pixel is always the last of the successors of our initial pixel. Overlapping the endpoints of the line segments in this manner will avoid creating gaps in otherwise continuous boundaries.

If two pixels have the same point as a primary predecessor, then there exists a "fork" in the line segment being traced. Since only the first successors are traced, the line segments described by following the second successor would be omitted by the above line tracing algorithm. This situation is avoided by making a first pass at the data and changing the primary predecessor array as follows: Let A and B denote the two pixels with C as a common predecessor, and let the arrows in Figure (6) denote the direction of the respective pixels. The second successor of C is found; suppose it is B. The predecessor of B (namely C) is changed to zero, that is, B is no longer considered to have a predecessor. Thus, when the pixel B is checked to see if it has a predecessor, it will not, and thus a line segment will be initialized at pixel B.



Primary  
successor  
array

Initial primary  
predecessor  
array

Secondary  
successor  
array

Final primary  
predecessor  
array

Figure 6

After the last pixel in a sequence of successors is reached, i.e., the pixel has no successor, the search resumes for the next pixel that has no predecessor. The output is arranged in the following manner:

X(1)	Y(1)	X(2)	Y(2)
X(3)	Y(3)	X(4)	Y(4)
.	.	.	.
.	.	.	.
.	.	.	.
X(2n-1)	Y(2n-1)	X(2n)	Y(2n)

where  $(X(2i-1), Y(2i-1))$  are coordinates of the initial pixel of the  $i$ th line segment, and  $(X(2i), Y(2i))$  are the coordinates of the terminal pixel of the  $i$ th line segment, for  $i = 1, \dots, n$ , where  $n$  equals the number of line segments in the image.

#### VI. Finding Reverse Parallel Line Segments.

This stage of the algorithm groups the directed line segments into pairs. Two directed line segments will be grouped into a pair, or labelled a Revpar, if the following conditions are satisfied:

- 1) They have approximately opposite directions.
- 2) The "distance" between them is less than a parameter BW

which can be set by the user.

3) They overlap.

Before explaining how the conditions are checked it is important to point out that the  $(x,y)$  coordinates of a point denote the position of the point in an array, which is not the usual  $x,y$  coordinate system (figure 7). Therefore, if orientation is to be measured from the horizontal, many familiar formulas appear different. For example the slope of the line passing through the points  $(x_1, y_1)$ ,  $(x_2, y_2)$  is given by

$$\text{Slope} = \frac{x_1 - x_2}{y_2 - y_1}$$

The change from the usual coordinate system into the new coordinate system is accomplished by the transformation  $(x,y) \rightarrow (y,-x)$ . Thus a formula in the new coordinate system can be found by applying the above transformation to the familiar formulas.

Condition 1) is checked by first computing the slopes of the directed line segments. The arctangent of the slope is computed. If the result,  $W$ , is negative then  $180^\circ$  is added to  $W$  so that  $w$  will be between  $0^\circ$  and  $180^\circ$ . Let  $D$  be the direction associated with the initial point of the line segment. Then if

$$|D - W| \geq 30^\circ$$

then  $W' = W + 180^\circ$ , otherwise  $W' = W$ . This procedure preserves reverse orientations. At this point in the algorithm the  $n$ th line segment has a direction  $W'_n$  associated with it. The algorithm then labels two line segments,  $L_n$  and  $L_m$ , as a Revpar if

$$165^\circ \leq |W'_n - W'_m| \leq 195^\circ.$$

Condition 2) is checked only if condition 1) is satisfied. The "distance" between two directed line segments,  $L_n$  and  $L_m$ , is actually the distance between the line determined by  $L_n$  (for example) and the initial point,  $(X_{2m-1}, Y_{2m-1})$ , of  $L_m$ .

Condition 3) is checked only if condition 2) is satisfied. The  $0^\circ/180^\circ$  and  $90^\circ/270^\circ$  degree cases are straightforward. The  $30^\circ/210^\circ$  will be presented here, the other cases being similar. Figure 8 shows what is meant by a pair of overlapping directed line segments. The

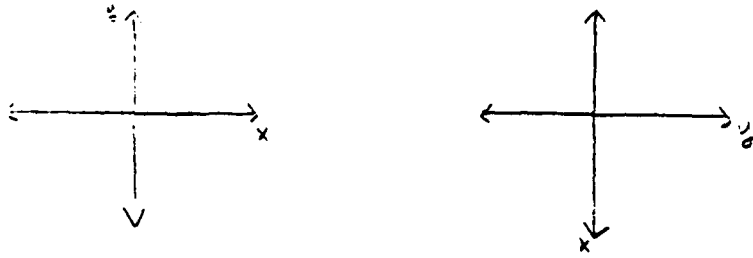


Figure 7.

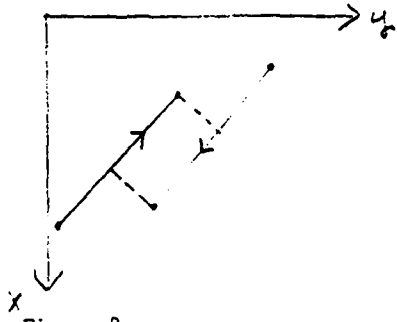
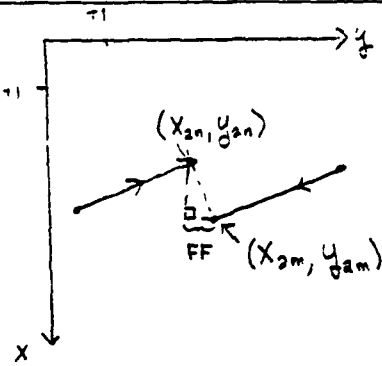
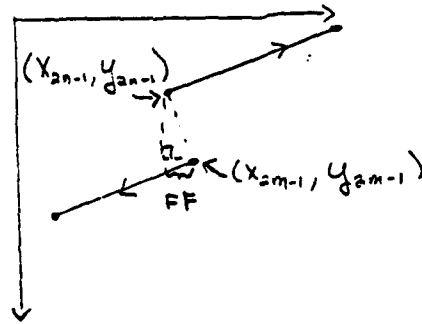


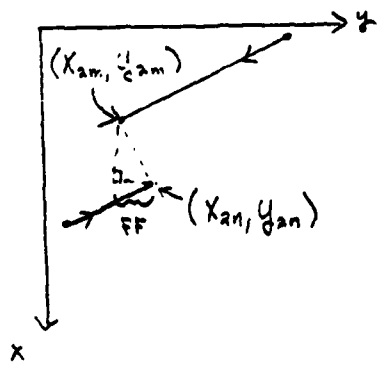
Figure 8.



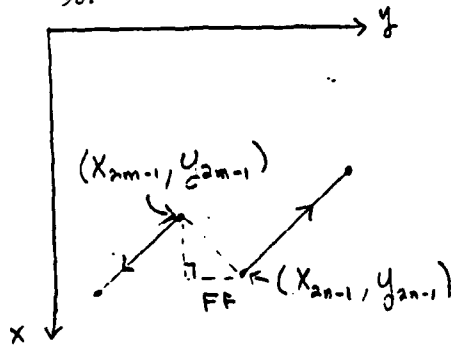
9a.



9b.



9c.



9d.

30°/210°, 60°/240°, 120°/300°, and 150°/330° cases require four checks to determine if they do not overlap. Let  $L_n$  be a directed line segment with endpoints  $(X_{2n-1}, Y_{2n-1})$ ,  $(X_{2n}, Y_{2n})$  and  $L_m$  be a directed line segment with endpoints  $(X_{2m-1}, Y_{2m-1})$ ,  $(X_{2m}, Y_{2m})$ . Assume that  $W_n'$  is approximately 30° and that the pair  $(L_n, L_m)$  satisfy conditions 1) and 2). Also, let DBL be the "distance" between them. Then  $(L_n, L_m)$  will be said to overlap if the following four conditions are false.

VI. A. Figure 9a.

$$Y_{2n} + FF \leq Y_{2m} \text{ and } X_{2n} < X_{2m}$$

or

B. Figure 9b.

$$Y_{2n-1} + FF \geq Y_{2m-1} \text{ and } X_{2n-1} < X_{2m-1}$$

or

C. Figure 9c.

$$Y_{2m} + FF \geq Y_{2n} \text{ and } X_{2m} < X_{2n}$$

or

D. Figure 9d.

$$Y_{2m-1} + FF \leq Y_{2n-1} \text{ and } X_{2m-1} < X_{2n-1}$$

The outputs at this stage of the algorithm are:

1) An  $n \times n$  binary array, where  $n$  is the number of line segments detected. If  $(L_i, L_j)$  is a Revpar then the  $ij$ th entry of the array is a one,

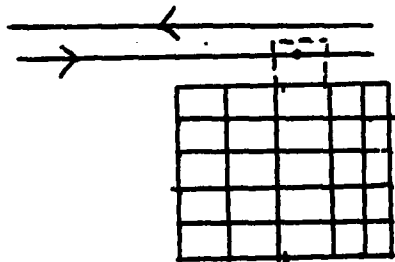
2) The original image with the pixels that are part of a Revpar highlighted. This image can be displayed on the Deanza and hardcopy produced (see Figurea 2-4).

#### VII. Labelling Line Segments as Bridge Edges

The final step of the algorithm is to use contextual information to determine if any of the reverse parallel lines are possible bridges. Many bridges pass over water, so the presence of water around a Revpar would increase the confidence that a Revpar represents a bridge. The mean and standard deviation are used as features to classify water. Presently, this statistical data is gathered by processing the picture separately with a statistical processing package available from the Image Processing Lab. It is feasible that the statistical data could be

generated from an internal subroutine; however, our ten-week appointment this summer was too short to permit us to do so.

A pair of reverse parallel lines are inspected to determine where they "overlap," in the sense of the previous chapters. Then one or both lines are traced, on the portions where they overlap, by following successors. At each edge pixel, the mean average and standard deviation for a given neighborhood are calculated, with the neighbor array values taken from the original image and the neighborhood on the outside of the lines. If the results are within certain tolerances previously determined by the user, the edge pixel is declared to be a bridge pixel. For the case where the pair of reverse parallel lines are  $0^\circ$  and  $180^\circ$ , the only edge pixels checked are those that are along the lower line, the line segment closest to the bottom edge of the image. See Figure (10) for the  $0^\circ$  neighborhood. The assumption made here is that if a bridge over water is approached so it appears to be parallel to the horizon, then there most probably will be water "in front of" the bridge, relative to the viewer. It was observed that sometimes the contour of the land directly "behind" the bridge (relative to the viewer) was



Neighborhood for edge pixel on a  $0^\circ/180^\circ$  line segment

Figure (8)

"close" to the bridge so that neighborhoods on the region of the upper line edge pixels would overlap on what was land, and thus the statistics would be outside the set tolerances. A suggestion for a future improvement might be to check for water next to both lines, with the upper line increasing the confidence it is a bridge if those edge pixels are declared bridge pixels in addition to the edge pixels on the lower line.

This is the only case coded at the present time. The remaining

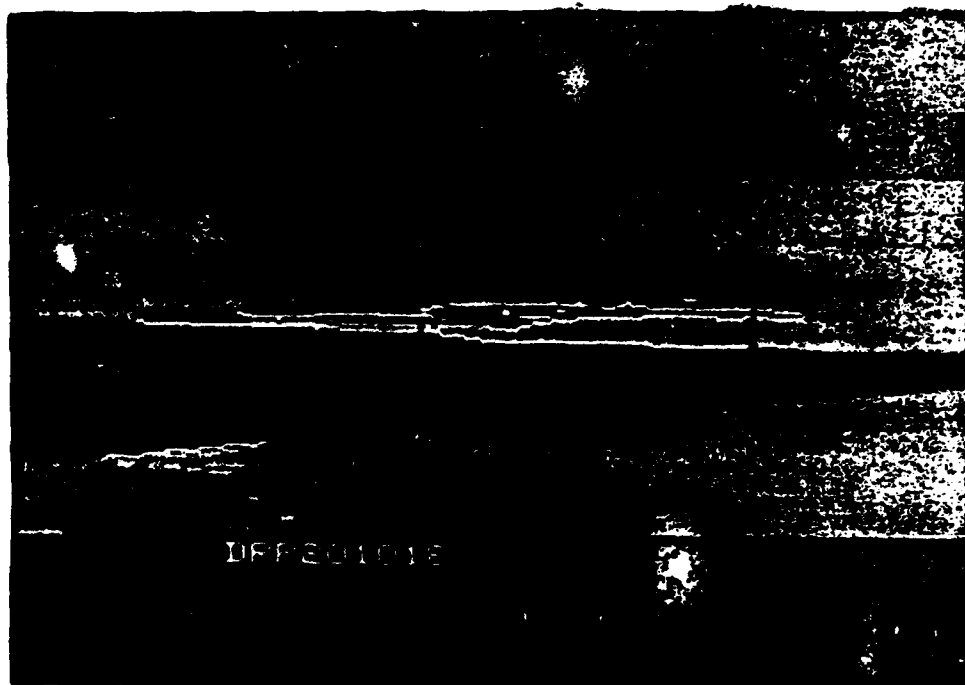


Figure 10a. Original image with Revpars highlighted. (see Fig 2a for original)

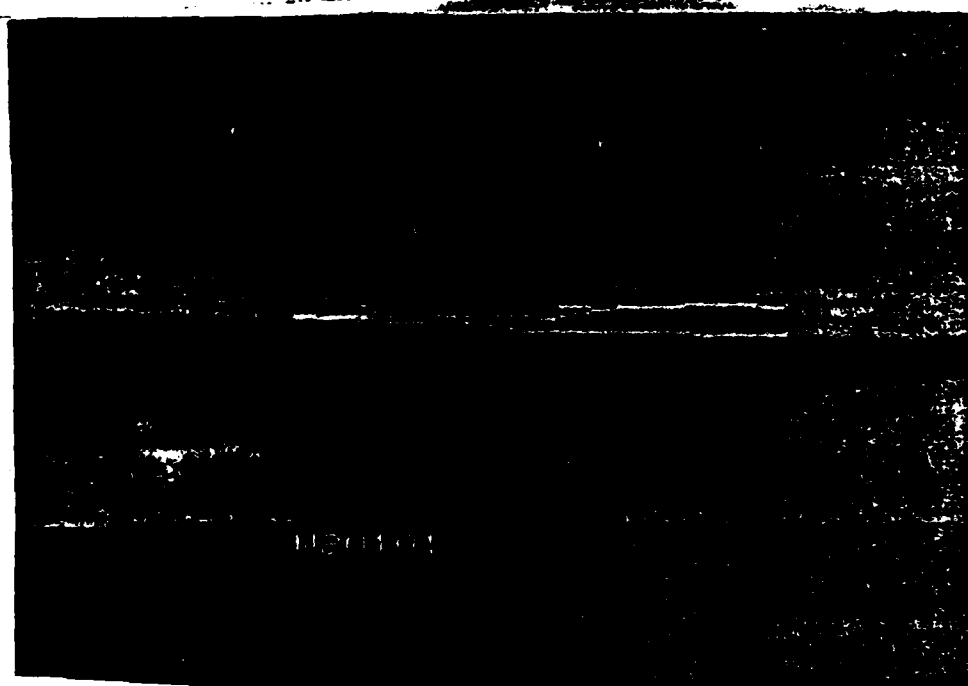


Figure 10b. Original image with only Revpars close to water highlighted.

five cases, for the reverse parallel lines  $30^\circ - 210^\circ$ ,  $60^\circ - 240^\circ$ , etc., are similar to the  $0^\circ/180^\circ$  case. Unfortunately, time ran short to code and debug these last cases.

#### VIII. Recommendations.

The Fortran program that implements the algorithms developed to detect bridges on data gathered by Texas Instruments, Inc., (TI), is located in the Image Processing Lab (IPL) at Eglin AFB. A user's guide is available which will help the user to set parameters for the purpose of experimentation. The program was designed to operate specifically on TI images as provided by the IPL; however, with only slight modifications, it will process other imagery whose dimensions are less than or equal to  $120 \times 360$ .

Bridges in FLIR images appear to have intensities which are local maximums in the direction orthogonal to the edges of the bridge. A simple procedure could be used to check if a Revpar has this property. A line segment, L, can be constructed which passes through the midpoints of the overlapping parts of the Revpar. The midpoint of L would be halfway between the line segments which make up the Revpar. The endpoints can be chosen outside of the bridge. A parabola can then be fit through the intensity values of these three points. Only the leading coefficient of the interpolating polynomial needs to be checked. If the coefficient is positive then the Revpar is probably not a bridge, if the coefficient is negative then the Revpar could be a bridge.

The line segment approximation subroutine could be simplified. Presently the algorithm approximates the edges by extending a line segment to the successor of an endpoint and then checking the distances of all the points that are already on the line segment to the new line segment. This procedure involves many computations of distance, which is inefficient. If a characterization of what is considered a line segment by the algorithm could be found using the octal chain code, then the computation time may possibly be decreased significantly.

It would be desirable to be able to extend the program to include locating bridges over other terrain. This is feasible due to the modular structure of the program. Up through finding reverse parallel

line segments, the algorithm does not use contextual information concerning the immediate surroundings of the Revpar. Subroutines could be added so that if certain conditions were satisfied, the appropriate subroutine would be called to use contextual information to determine if the line segments constitute a bridge over a specific terrain, as for example, over railroad tracks.

Other contextual and geometric information can be utilized to increase the confidence a bridge is located. Super- and substructures can be classified. The periodicity of bridge pilings which occur at regular intervals may be able to be utilized.

The fact that bridges usually connect homogeneous regions may be utilized. For example, narrow peninsulas in bodies of water are often detected as possible bridges, which is undesirable. Bridges also result in discontinuities of the objects they cross. This is taken advantage of as in the case of bridges over water. Another example is a bridge over a road disconnects the roads it crosses over. Thus, examining scene content and geometric details in the area of the reverse parallel lines will aid in detecting bridges in various contexts.

The algorithm could be applied to other fixed high value targets. Immediately before the algorithm looks for REVPAR's the image has been segmented into directed line segments. These directed line segments could be used as "primitives" for further analysis. A runway could be described in terms of directed line segments. In fact, any object whose shape can be approximated by a polygon can be described in terms of directed line segments. Thus the possibilities for other applications of modifications of the algorithm are good.

## IX. Results

The algorithm processed 60 images, 37 of which were inspected closely. For each input image, the output was two images, one image containing the thinned edges and the other image containing the reverse parallel lines. These images were hardcopied and put in a large binder, available from the IPL. Of the 37 thinned images, 17 retained 90% or more of the target edge pixels. Eighteen retained partial edges of the target. Partial edges are any edges up to 90% of the total target edge pixels. Of the 37 revpar images, 14 retained 90% or more of the target edge pixels, and 20 retained partial edges of the target. Of the 35 thinned images that retained any target edge pixels, nearly all (90%) of the detected target edges were present in the corresponding revpar images. The results are contained in the table below:

	No. of Images/35	Percent
Whole edge of target in		
Thinned Image	17	49%
Partial edge of target in		
thinned image	18	51%
Total	35	100%
Whole edge of target in		
revpar image	14	40%
Partial edge of target		
in revpar image	18	51%
Total	32	91%

The algorithm seemed to detect targets at long range where there is less detail. This is probably partially due to the line segmentation subroutine, which kept line segments from 2 pixels in length and longer. Therefore, closer to the target where edges are likely to have more detail, short line segments describing these edges were numerous and seemed to "clutter" the image.

Of the four images where the water checking subroutine was run, the

revpars kept did include target pixels. See Figures for these results.

The algorithm does an excellent job of detecting edges where there is a reasonable amount of contrast. The reverse parallel lines are also fairly well detected. Hopefully, these two procedures provide much information which can be utilized to continue development on a fairly high confidence bridge detection algorithm.

## Appendix A - Program Users Guide

This appendix has four parts; how to run the program, a flow chart of the program, and a list of subroutines with a brief description of what each subroutine does, and an indexed list of images.

Anyone wishing to use the program is advised to read the main body of the report and then examine the flow chart (Figure A). The program is designed to be experimental, and therefore there are parameters which the user can set and subroutines which the user can choose to use or not use. In order to set the parameters and choose the routines to use one should have a clear idea of how the program works.

### 1. How to Run the Program

The program is designed to operate on the bridge images (DBRG) in the TI database. (Changing to other IRHVTA images would be a matter of minor revisions of the READ and WRITE statements).

You must have the following things available in your account:

- i) The programs DATAIN.EXE  
BRBATCH/FOR  
BCOMLINK.COM  
BRUN.COM
- ii) The file NAME.DAT
- iii) A directory to store the output images.

The first thing you must do is create a directory to store the output images. For example if you want to create the directory [DOE.IMAGES] simply type

```
CREATE/DIR [DOE.IMAGES]
```

on the CRT.

Next thing to do is change the name of the output files in the code itself must be changed. This can be done by the following steps:

- 1) type EDIT BRBATCH.FOR return
- ii) type C return

You are now in the edit mode

- iii) Use the FIND command to look for NAME1.

NAME 1 occurs three times, one for each output image.  
When you find it, simply replace the existing  
directory and subdirectory with your directory  
and subdirectory [DOE.IMAGES]. DO THIS  
IN ALL THREE CASES.

- iv) type CTRLZ
- v) type EXIT

Now you must compile and link the program which can be done by  
typing SUBMIT BCOMLINK. The job is run by batch mode.

The above steps only need only be done once. At this point you  
will have the executable program BRBATCH.EXE which is what you will use  
to run the program.

Now you type RUN DATAIN. The questions shown in Figures 2 will  
appear on the screen sequentially. The indented questions will be asked  
only if the preceding question was answered Y.

To answer question number 2 you must enter the index numbers of  
the images you want to process. The index numbers are given on the last  
3 pages of this appendix. For example, if you want to process DBRG  
20126.IMG you would enter 6. Questions 5 and 6 offer room for  
experimentation. You may answer N to 5 and Y to 6. The program will  
then do the local average and then threshold. You may answer Y to 5 and  
N to 6. The program will then simply threshold. You may answer Y to  
both or N to both. To answer 8-10 you must know that:

- AVI:= mean intensity of water
- ALPH:= standard deviation of ALPH
- G:= mean standard deviation of water
- BETA:= standard deviation of G.

There is room for experiment here also. For example, if the user wanted  
to use only the standard deviation of water as a feature the user could  
set AVI and ALPH equal to zero.

If the user answers Y to 12 then the parameters, the bridge file name,  
and the number of Revpars will be written to a file PARJOBNO.DAT.

## 2. SUBROUTINES

This section lists the subroutines in the order that they are

called. A brief description of what they do is given, and the user supplied parameters they use are listed.

CONV

Parameters: MSIZE

This is a subroutine to convolve an image with a mask. The mask can be 3x3, or 5x5. MSIZE is the size of the mask.

APRUNE

This subroutine smooths the direction array using a variable window.

THRESHOLD

Parameters: ALPHA:

This subroutine computes the mean M and standard deviation S of an array. Zero values are not used in the computation. The array is then thresholded at

$$T = M + \text{ALPHAXS}.$$

LOCAVE

This subroutine uses 3x3 windows to perform a local averaging operation on an array.

THIN

This subroutine thins the convolved image according to the conditions listed in Section IV.

SCALE

This subroutine linearly scales an array so that its entries will have values between 0 and 255.

RERITVIM

This subroutine puts an image into the proper format for display on the Deanza. RERITVIM calls the library routines VIMALL and VIMPOT. The formatted image is written to a file.

CHANGE

This subroutine changes the subscripts from (Column, Row) to (Row, Column).

PRELINK

This subroutine generates the successor-predecessor files used to later approximate the edges by linear segment.

PIXLINK

This subroutine generates the endpoints of the line segments which approximate the edges. The number of line segments is computed here.

REVPAR

Parameters BW

This subroutine establishes pairs of reverse parallel line segments. BW is an upper bound on the distance between the segments of a REVPAR.

SUCCESS

This subroutine computes the coordinates of the successor of a pixel.

CHANGE2

This subroutine changes the subscripts from (Row, Column) to (Column, Row).

WATERCK

This subroutine checks for water below a horizontal Revpar.

STARTI

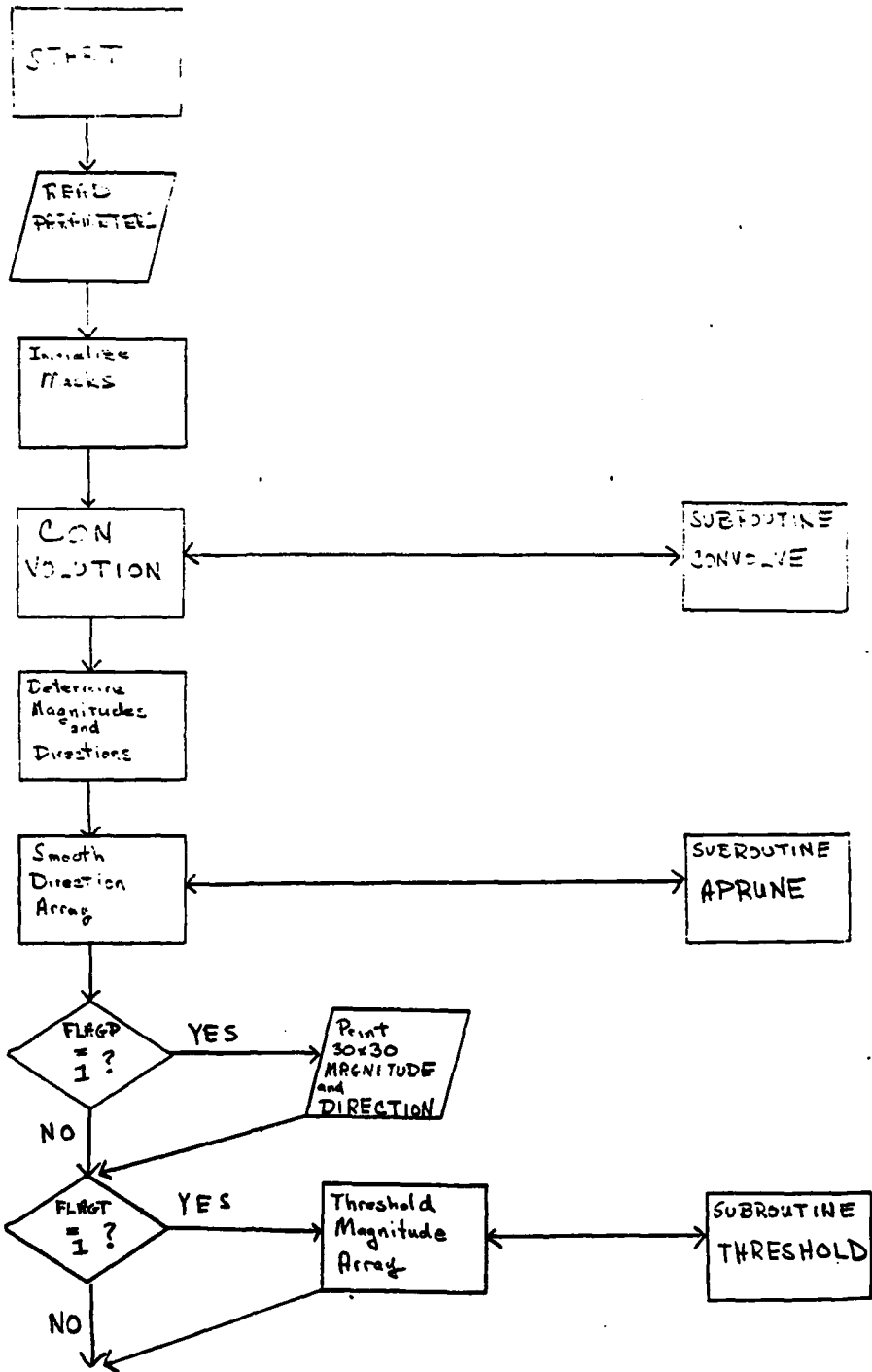
This subroutine is used to determine to initial and endpoints of the overlapping parts of a Revpar if the  $0^\circ$  line is on the bottom.

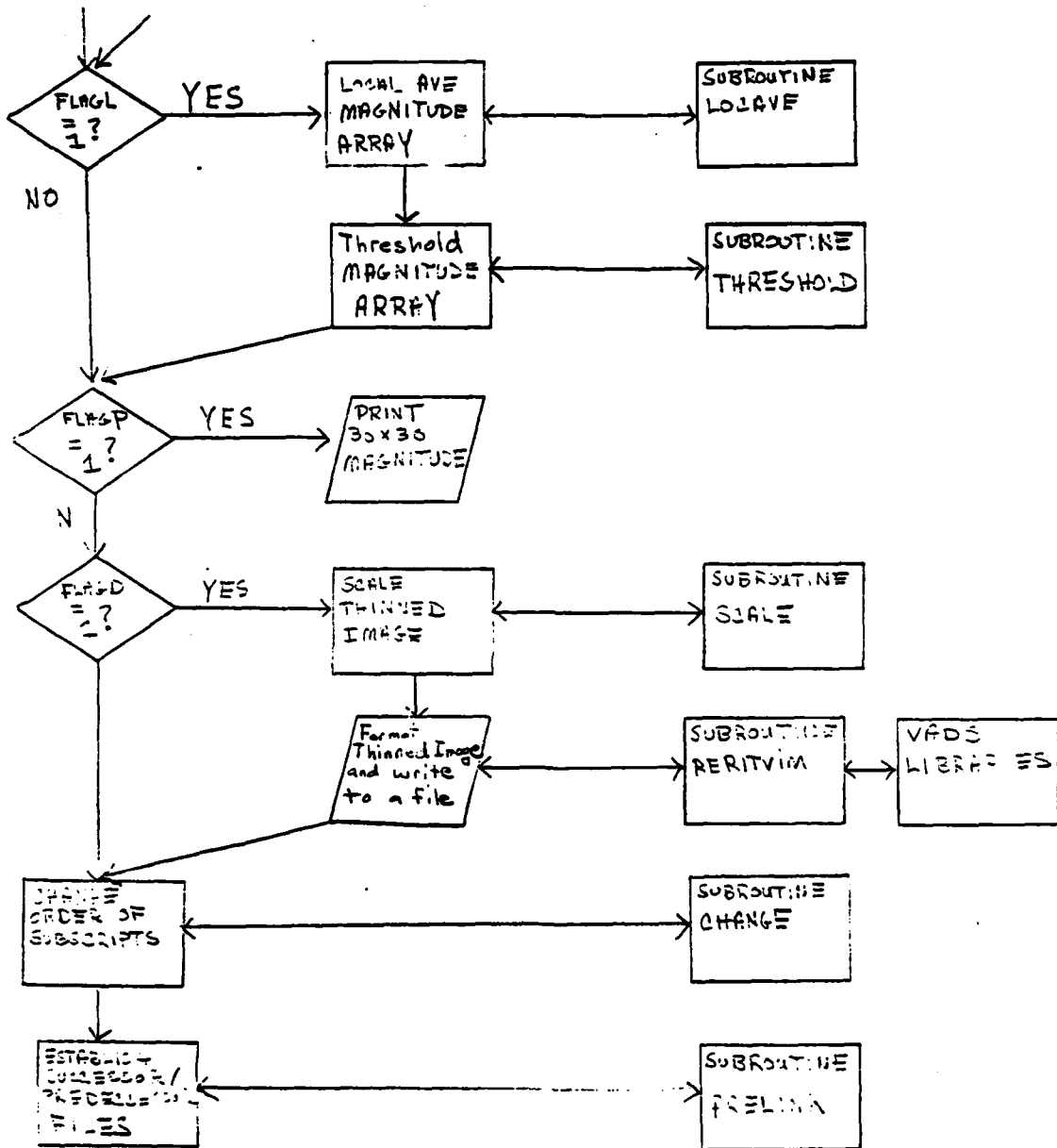
STARTJ

Same as STARTI except if  $180^\circ$  line is on the bottom.

3. The next four pages contain the flowchart of the program. The left most column contains processing steps done by the main routine. The middle column contains optional processing steps. The rightmost column contains subroutines.

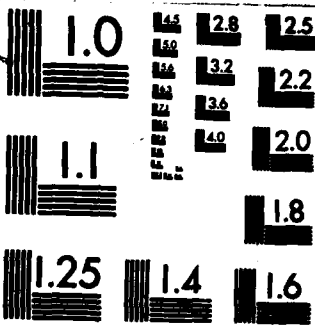
4. The pages after that contain the indexed listing of the bridges. This is the listing you must use to run the program.



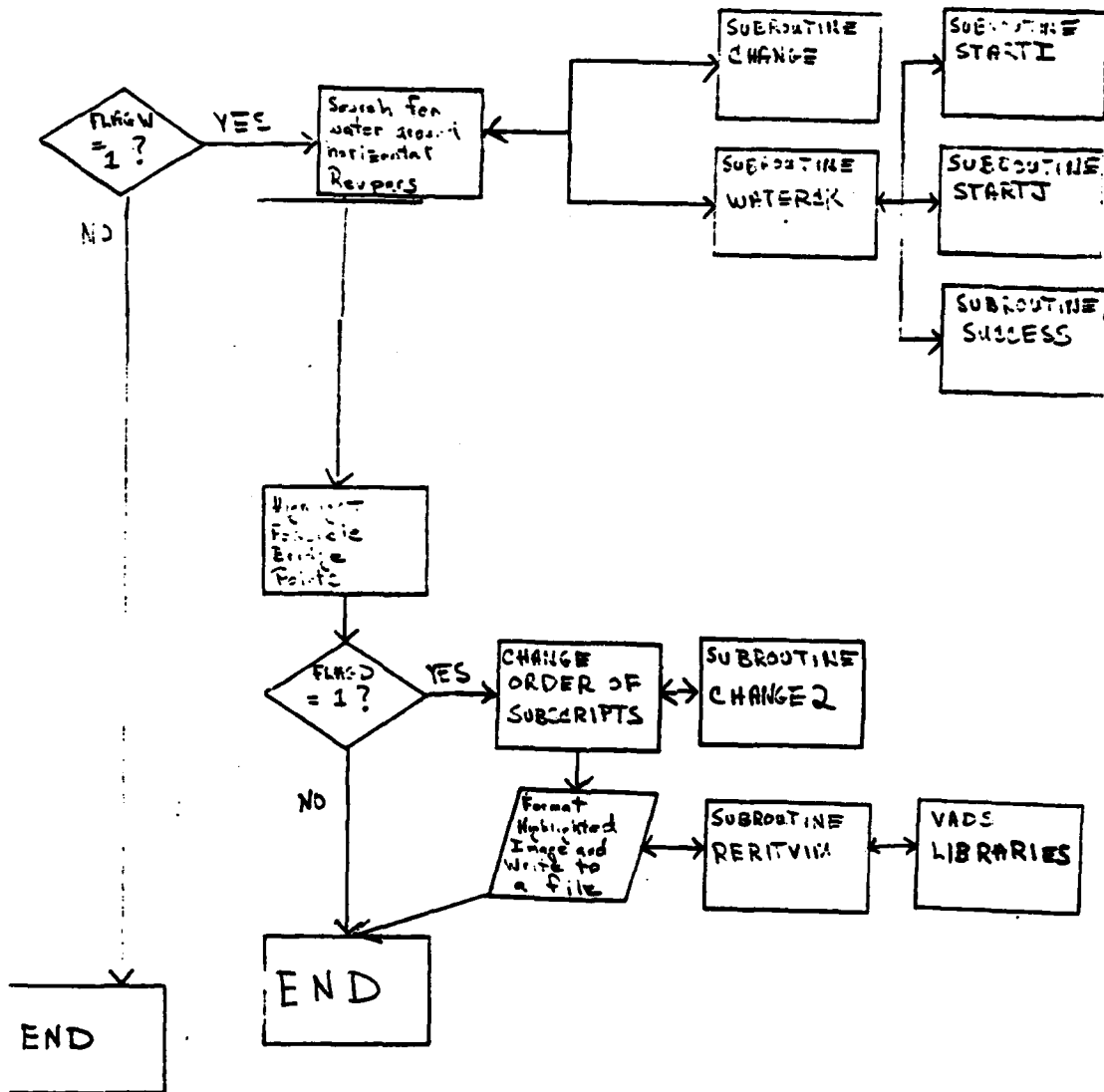








MICROCOPY RESOLUTION TEST CHART  
NATIONAL BUREAU OF STANDARDS-1963-A



1. ENTER THE NUMBER OF IMAGES YOU ARE PROCESSING IN YOUR JOB (UP TO 50).
2. ENTER THE FILE NUMBERS IN THE USERS GUIDE THAT YOU WISH TO PROCESS. TYPE THEM IN ONE AT A TIME.
3. THE MASK SIZE DEFAULT IS FOR THE 3X3 MASKS. DO YOU WISH TO CHANGE IT TO THE 5X5 MASKS? (Y OR N)
4. THERE ARE TWO OPTIONS FOR OUTPUT FROM THIS PROGRAM. ONE IS TO GET IMAGE TYPE FILES AND DISPLAY THEM ON THE DE ANZA, AND THE OTHER IS TO HAVE A 30X30 SUBARRAY OUTPUT IN A FILE WHICH YOU CAN PRINT OUT ON THE PRINTER. IF YOU WOULD LIKE THE 30X30 PRINTOUT ON THE PRINTER OPTION, PLEASE TYPE Y. TYPING N WILL CREATE FILES TO BE DISPLAYED ON THE DE ANZA.
  - 4.1 PLEASE ENTER THE UPPER LEFT HAND COORDINATES OF THE 30X30 SUBARRAY. (ROW, COLUMN).
5. DO YOU WISH TO THRESHOLD? (Y OR N)
  - 5.1 THE FIRST THRESHOLD PARAMETER IS ALPHA= , ALPHA. DO YOU WISH TO CHANGE IT? (Y OR N)
  - 5.2 YOU MUST ENTER A DECIMAL POINT IN YOUR ANSWER. PLEASE ENTER THE NEW ALPHA PARAMETER:
6. THE LOCAL AVERAGE WILL BE COMPUTED ON THE IMAGE IF YOU TYPE IN A Y. IT WILL NOT BE COMPUTED IF YOU TYPE IN A N.
  - 6.1 THE SECOND THRESHOLD PARAMETER IS ALPHA1= , ALPHA1. DO YOU WISH TO CHANGE IT? (Y OR N)
  - 6.2 YOU MUST ENTER A DECIMAL POINT IN YOUR ANSWER. PLEASE ENTER THE NEW ALPHA1 PARAMETER:
7. THE DEFAULT FOR THE BRIDGE WIDTH IS 8 PIXELS. DO YOU WISH TO CHANGE IT? (Y OR N)
  - 7.1 PLEASE TYPE IN THE NUMBER OF PIXELS YOU WANT FOR THE BRIDGE WIDTH. IT CAN BE ANY REAL NUMBER, UP TO 7 DIGITS LONG. YOU MUST TYPE A DECIMAL IN YOUR NUMBER.

THE WATER STATISTICS ARE SET AS FOLLOWS:

AVI= ,AVI.  
ALPH= ,ALPH.  
G= ,G.  
BETA= ,BETA.

8. DO YOU WISH TO CHANGE AVI? (Y OR N)?  
8.1 YOU MUST TYPE A DECIMAL IN YOUR NUMBER. PLEASE ENTER THE NEW  
VALUE FOR AVI:
9. DO YOU WISH TO CHANGE ALPH? (Y OR N)?  
9.1 YOU MUST TYPE A DECIMAL IN YOUR NUMBER. PLEASE ENTER THE NEW  
VALUE FOR ALPH:
- 10 DO YOU WISH TO CHANGE G? (Y OR N)?  
10.1 YOU MUST TYPE A DECIMAL IN YOUR NUMBER. PLEASE ENTER THE NEW  
VALUE FOR G:
- 11 DO YOU WISH TO CHANGE BETA? (Y OR N)?  
11.1 YOU MUST TYPE A DECIMAL IN YOUR NUMBER. PLEASE ENTER THE NEW  
VALUE FOR BETA:
- 12 DO YOU WISH A PRINTOUT OF ALL THE PARAMETERS? (Y OR N)

THE PRINTOUT IS BOTH ON THE SCREEN AND IN THE FILE ~~PAR.DAT~~ <sup>PARJOEN.CAT.</sup>

- 13 THE DEFAULT IS TO CHECK FOR WATER TYPE Y IF YOU WISH TO DO THIS.  
TYPE N IF YOU DON'T.

Appendix B  
Extended Bibliography  
Books

- Duda, R. Pattern Recognition and Scene Analysis, (J. Wiley and Sons, Inc., New York, 1973).
- Grasselli, A. Automatic Interpolation and Classification of Images, (Academic Press, New York, 1969).
- Mott - Smith, J. C. Picture Processing and Psychopictorics, (Academic Press, New York, 1970).
- Pavlidis, T. Structural Pattern Recognition, (Springer - Verlag, Berlin, 1977).
- Pratt, W. K. Digital Image Processing, (J. Wiley and Sons, New York, 1978).
- Rosenfeld, A. Picture Processing by Computer, (Academic Press, New York, 1969).

## Extended Bibliography

### Articles

- Barnard, S. "Disparity Analysis of Images," IEEE Transactions, PAMI, July 1980.
- Calabi, L. "Shape Recognition, Prairie Fires, Convex Deficiencies and Skeletons," American Mathematical Monthly, April 1968
- Delp, E. "Edge Detection Using Contour Tracing," Center for Robotics and Integrated Manufacturing, College of Engineering, University of Michigan, August 1983.
- Dudani, S. "Locating Straight-Line Edge Segments on Outdoor Scenes," Pattern Recognition, 1978, Vol. 10.
- Elliott, F. "Segments Wobble on Infrared Images," SPIE Proceedings, Vol. 359, August 1982.
- Frei, W. "Fast Boundary Detection: A Generalization and a New Algorithm," IEEE Transactions on Computers, October 1977.
- Hamadini, N. "Automatic Target Cueing in IR Imagery," AFITAU Thesis, December 1981
- Kestner, W. "Object Guided Segmentation of Aerial Images," IEEE Publication. March 1980.
- Kim, J. "A Context Dependent Automatic Target Recognition System," SPIE Conference, May 1984.
- Levialdi, S. "On Shrinking Binary Picture Patterns," Communications of the ACM, January 1972.
- Lineberry, M. "Image Segmentation by Edge Tracing," SPIE Proceedings, Vol. 359, August 1982.
- Rosenfeld, A. "Edge and Curve Detection for Visual Scene Analysis," IEEE Transactions on Computers, May 1971.
- Smith, M. "A New Algorithm for Edge Detection," Proceedings of the Third International Conference on Pattern Recognition, 1974.
- Velasco, F. "Some Methods for the Analysis of Sharply Bounded Clusters," IEEE Transactions on Systems, Man and Cybernetics, August 1980.

1984 USAF-SCEEE GRADUATE STUDENT SUMMER SUPPORT PROGRAM

Sponsored by the

AIR FORCE OFFICE OF SCIENTIFIC RESEARCH

Conducted by the

SOUTHEASTERN CENTER FOR ELECTRICAL ENGINEERING EDUCATION

FINAL REPORT

NEUROTRANSMITTER SYSTEMS IN THE CEREBELLAR GLOMERULUS:

ANALYSIS OF GABA UPTAKE, EXCHANGE, AND RELEASE

Prepared by:	Carolyn L. Green
Academic Department:	School of Medicine Student
University:	Wayne State University
Research Location:	USAF School of Aerospace Medicine Clinical Sciences Division Neuropsychiatry Branch Brooks AFB, TX
USAF Research Contact and Co-Author:	David M. Terrian, Ph.D.
Date:	September 28, 1984
Contract Number:	F49620-82-C-0035

NEUROTRANSMITTER SYSTEMS IN THE CEREBELLAR GLOMERULUS:

ANALYSIS OF GABA UPTAKE, EXCHANGE, AND RELEASE

by

Carolyn L. Green  
David M. Terrian, Ph.D.

ABSTRACT

The cerebellar glomerulus is being utilized by this laboratory as a model for investigating chemical integrative processes in local neuronal circuits. In this report, we give evidence to support the suggestion that 4-Aminobutyric acid (GABA) functions as an inhibitory neurotransmitter in this synaptic complex. Cerebellar glomeruli were isolated from the bovine cerebellar vermis in high purity (93%) and subjected to an extensive series of in vitro biochemical analyses. These experiments revealed that glomerular particles release [<sup>3</sup>H] GABA, in a Ca<sup>2+</sup>-dependent manner, in response to membrane depolarization and are endowed with a high affinity uptake system capable of rapidly terminating the inhibitory action of this amino acid. However, the functional implications of these findings could not be clearly interpreted until the relative contribution of GABA exchange had been quantitatively examined and controlled for.

Kinetic analysis indicated that cerebellar glomeruli accumulate [<sup>3</sup>H] GABA at two different high affinity sites, their affinities (K<sub>m</sub>) were calculated to be 2.2 x 10<sup>-6</sup>M and 3 x 10<sup>-5</sup>M. Although an exchange of [<sup>3</sup>H] GABA with the endogenous pool of GABA clearly contributed to the uptake measured in these experiments, at least 50% of the [<sup>3</sup>H] GABA accumulated by glomerular particles is stored in an osmotically-sensitive, nonexchangeable pool. These transport sites were not further distinguished from one another in experiments which measured their temperature sensitivity, sodium dependency, responsiveness to metabolic inhibitors, or substrate specificity. These results suggest that a heterogeneous population of interactive neuronal uptake sites comprise a single transport system responsible for the net accumulation of GABA in cerebellar glomeruli.

Glomerular particles preloaded with [<sup>3</sup>H] GABA exhibited a Ca<sup>2+</sup>-independent release of this amino acid in response to membrane depolarization. However, the depolarizing agents (K<sup>+</sup> and veratridine) used in these experiments are known to increase the inward transport of Na<sup>+</sup> which, in turn, would stimulate the Na<sup>+</sup>-dependent homoexchange of GABA. It is demonstrated that, when one displaces [<sup>3</sup>H] GABA from this exchange pool, a K<sup>+</sup>-evoked and Ca<sup>2+</sup>-dependent release of [<sup>3</sup>H] GABA occurs. The observed net uptake of GABA together with the depolarization-induced, Ca<sup>2+</sup>-dependent release of GABA from glomerular particles strongly indicates that functionally active GABAergic synapses are present in this structure.

Acknowledgement

I would like to thank the Air Force Systems Command, Air Force Office of Scientific Research, and the Southeastern Center for Electrical Engineering Education for the opportunity to participate in research at the USAF School of Aerospace Medicine, Branch of Neurosciences in the Clinical Sciences Division at Brooks AFB, TX. Many thanks to Betsy Hofstetter for her technical assistance and to Drs. S.H. Enna and P. Krogsgaard-Larsen for gifts of chemicals.

I am very grateful to Dr. David Terrian for his instruction and guidance, with special gratitude for sharing with me the enthusiasm and quality of research which I hope to someday achieve.

## I. INTRODUCTION

An impressive body of evidence supports the conclusion that GABA functions as an inhibitory neurotransmitter in the mammalian central nervous system. Perhaps the most convincing evidence has come from studies of the cerebellum, where the Purkinje cells have been shown to act by releasing GABA from their terminals (3,6). It has long been suspected that the inhibitory interneurons of the cerebellar cortex are also GABAergic in nature. But until recently, it had not been possible to identify the actual site(s) of release within these local neuronal circuits. The ability to isolate cerebellar glomeruli, and perform in vitro analyses of this structure (4,5,23), has greatly enhanced our ability to relate such biochemical responses to their proper morphological substrate. These glomerular synaptic complexes can now be isolated as structurally-intact entities which are thought to contain a single population of inhibitory nerve terminals, e.g., the Golgi axon terminals (4). Electrophysiological and anatomical studies clearly support this supposition (15,21). More recently, a series of biochemical investigations have demonstrated that these glomerular particles possess high affinity transport sites for [<sup>3</sup>H] GABA which, based upon electron microscopic autoradiography, are almost exclusively located over the axo-dendritic synapses formed by the juxtaposition of Golgi axon terminals and granule cell dendrites (5,7,22,23). Autoradiographic studies have also demonstrated that [<sup>3</sup>H] muscimol binding sites are more densely distributed within the cerebellar glomerulus than in other relevant parts of this brain region, including the deep cerebellar nuclei (8).

In this paper, we confirm previous reports that cerebellar glomeruli are endowed with high affinity transport sites for [<sup>3</sup>H] GABA. At variance with these reports, however, is our finding that these transport sites do not have

a common affinity for [<sup>3</sup>H] GABA. In an additional series of experiments we also demonstrate the stimulation-coupled release of [<sup>3</sup>H] GABA from superfused glomerular particles. Taken together, these findings argue in favor of the suggestion that GABA is utilized as a neurotransmitter in the local inhibitory pathway formed by Golgi cells in the cerebellar cortex.

## II. OBJECTIVES

The experiments conducted this summer were part of an ongoing study intended to identify the neurotransmitter systems endogenous to cerebellar glomeruli and to characterize interactions among these systems. This research program is currently being supported by AFOSR Task 2312V4.

Two major criteria have proven useful in screening amino acid neurotransmitter candidates. First, the amino acid must be accumulated by a high-affinity transport mechanism which is thought to limit its postsynaptic action. Second, a decrease in the transmembrane potential should stimulate the graded release of the amino acid and this response should be calcium ( $Ca^{2+}$ ) dependent.

Using the above criteria, our summer objective was to determine if 4-aminobutyric acid (GABA) functions as a neurotransmitter in the cerebellar glomerulus.

## III. HIGH AFFINITY TRANSPORT OF [<sup>3</sup>H] GABA IN CEREBELLAR GLOMERULI

### Introduction:

Kinetic analysis clearly demonstrates that the uptake of GABA is mediated by systems of "high affinity" ( $K_m$ s of approximately  $5 \times 10^{-5}M$  or lower) and "low affinity" ( $K_m$ s of the order of  $10^{-4}M$  or higher). These transport systems are further distinguished by the observation that only the high affinity

system has an absolute requirement for sodium ions, a high degree of structural specificity, and is localized to synaptic terminals. A popular interpretation of these findings has been that high affinity uptake functions to limit the postsynaptic action of GABA and, therefore, may be useful in identifying GABAergic pathways in the CNS (20). Low affinity uptake, on the other hand, is thought to replenish intracellular amino acid pools involved in intermediary metabolism. A number of methodological considerations must be taken into account before an accurate measure of GABA can be made (13). Recently, the criticism has been raised that an exchange of [<sup>3</sup>H] GABA with endogenous GABA could account for much of the observed radiolabel accumulation seen in synaptosomal fractions (14) and glial cells (18). This exchange process has been termed "homoexchange" and has stimulated a number of investigators to re-evaluate the utility of high affinity uptake sites in identifying GABAergic synapses. Before one may conclude that a true net accumulation of GABA has indeed been observed, it is essential that the contribution of homoexchange be subtracted from the total [<sup>3</sup>H] GABA uptake measured.

As mentioned previously, it has been demonstrated that glomerular particles isolated from rat cerebelli possess high affinity transport sites for [<sup>3</sup>H] GABA (5,22). Unfortunately, no attempt was made in these experiments to assess the extent to which an exchange process might account for the observed uptake of [<sup>3</sup>H] GABA. We have addressed this issue and find evidence of an exchange process for [<sup>3</sup>H] GABA in glomerular particles which, although quantitatively significant, does not account for more than 50% of the [<sup>3</sup>H] GABA uptake measured. The most striking finding of this study, however, emerged when our kinetic analysis revealed that [<sup>3</sup>H] GABA was being taken up by two distinct high affinity transport sites. To characterize the functional

properties of these transport mechanisms, a further series of biochemical experiments were conducted. Glomerular particles for the above studies were isolated from the bovine cerebellar vermis by a method recently developed in this laboratory (manuscript in preparation).

**Methods and Results:**

(a) Isolation of cerebellar glomeruli from bovine cerebellar vermis. Bovine cerebellum was obtained in the slaughter house from recently killed animals, within 15 min of death, and immediately placed on ice. Less than 20 min later the vermis was removed by dissection and manually homogenized in 9 volumes of 0.3M sucrose. Magnesium ions (1mM  $MgSO_4$ ) were included in all media used throughout the procedure to preserve the structural integrity of the glomerular particles, as suggested by Hajos et al. (4). Homogenization conditions were such that the shear stresses approximated those reported previously by Coakley (2). The homogenate was passed through a series of nylon filters (111 $\mu$ /70 $\mu$ /52 $\mu$ ) to remove debris and centrifuged at 900 g for 10 minutes. The resultant pellet was washed once with the same volume and centrifuged again. This procedure yielded a pellet ( $P_1$ ) which was resuspended in an 18% (w/v) Ficoll- $Mg^{2+}$  solution, dissolved in 0.3M sucrose, and was centrifuged at 7,500 g for 40 minutes using an SW28 rotor and Beckman L5-50B Ultracentrifuge (total accumulated centrifugal effect,  $w^2t$ , equal to 175  $rad^2/sec \times 10^7$ ). Electron microscopic examination of the resultant pellet (crude nuclear fraction, N) shows it to primarily consist of intact granule cells and cell debris. The combined supernatants were diluted 50% (v/v) in 0.3M sucrose and centrifuged at 20,000 g for 20 minutes. This pellet (crude glomerular fraction, CGF) was resuspended in 30ml of 0.3M sucrose and 5ml aliquots were layered onto 25ml of 1.2M sucrose. The final pellet (purified glomerular fraction, PGF) was obtained by centrifuging this suspension at

53,000 g for 60 minutes ( $w^2t = 158 \text{ rad}^2/\text{sec} \times 10^8$ ). The PGF was resuspended in 0.32M glucose to give a final protein concentration of  $13.25 \pm 1.30 \text{ mg/ml}$  ( $\pm$  S.E.M.). The final preparation was typically obtained within 4.5 hours. The purity of the preparation was determined to be  $92.6 \pm 3.9\%$  ( $\pm$  S.E.M.) by graphic digitization of random electron micrographs ( $n = 27$ ).

(b) Measurement of [ $^3\text{H}$ ] GABA Uptake. The general method of Levi and Raiteri (12) was used in these experiments. Aliquots of the PGF suspension (50  $\mu\text{l}$ ) were diluted to a final volume of 1.0 ml with oxygenated incubation medium (12) containing [ $^3\text{H}$ ] GABA at the concentrations indicated, 16 mM glucose, and  $10^{-5}\text{M}$  amino-oxyacetic acid. The final protein concentration of this suspension usually ranged between 0.4 and 0.7 mg/ml. Incubations were carried out at  $37^\circ\text{C}$  for 10 minutes in an open microfuge tube. Preliminary experiments confirmed that [ $^3\text{H}$ ] GABA uptake proceeded in a linear fashion under these conditions. Immediately following incubation the tubes were centrifuged for 45 seconds at 13,500 g in an Eppendorf Microfuge 5414. Where indicated, samples of the supernatant were taken for measurement of radioactivity and calculation of [ $^3\text{H}$ ] GABA accumulation according to the method of Kuriyama et al. (11). The pellets were then washed twice with ice-cold incubation medium and recentrifuged before digestion in 0.5 ml of 1N NaOH overnight. The radioactivity of each pellet was estimated by scintillation counting after addition of 0.5 ml glc HAc and 10 ml of Aquasol II scintillant. Control tubes were preincubated in the presence of [ $^3\text{H}$ ] GABA for 10 minutes, at  $0^\circ\text{C}$ . The radioactivity in these control samples was subtracted from their corresponding experimental sample, prior to any further calculations, to correct for passive uptake and nonspecific binding of the

radioisotope to glomerular particles. Trichloroacetic acid precipitates of the PGF suspensions were assayed for protein according to the method of Lowry (16).

(c) Calculation of transport kinetic constants. The affinity ( $K_m$ ) and maximal velocity ( $V_{max}$ ) for [ $^3H$ ] GABA uptake were calculated using a weighted nonlinear regression analysis (9). A conventional Lineweaver-Burk plots of the data appeared to be nonlinear and concave downward, indicating the uptake may have been mediated by more than one transport system. Table I lists the kinetic constants ( $K_m$  and  $V_{max}$ ) which were derived from our analysis of the data. A low affinity uptake process, characterized by a  $K_m$  of 920 $\mu$ M, was identified but not studied further. Uptake rates for the remaining two

TABLE I: KINETIC PARAMETERS FOR ACTIVE  $^3H$ -GABA UPTAKE SYSTEMS IN BOVINE CEREBELLAR GLOMERULI\*

	$K_m$ ( $\mu$ M)	$V_{max}$ (nmol·mg Protein·10 min $^{-1}$ )	nH
Low Affinity	918.5	32.4	
High Affinity 2	30.1	4.0	0.88
High Affinity 1	2.2	1.0	1.02

\* All values calculated using a weighted nonlinear regression analysis of Lineweaver-Burk plots, according to the method of Kohn et al.(9).

transport systems are plotted according to the Lineweaver-Burk format in Figure 1. These uptake systems clearly possess a high affinity (HA) for [ $^3H$ ] GABA, one system displayed a  $K_m$  of  $2.2 \times 10^{-6}M$  (HA1) while the other displayed a  $K_m$  of  $3.0 \times 10^{-5}M$  (HA2). In previous studies a single high affinity system has been described with intermediate  $K_m$  values of  $9.5 \times 10^{-6}M$  (22) and  $15 \times 10^{-6}M$  (5). Since these values lie between those reported here, it seems possible that they represent a mixture of HA1 and HA2 affinities which are not distinguishable without more detailed analysis. In the present experiments we

have extended the range of GABA concentrations down from  $1.0\mu\text{M}$  to  $0.2\mu\text{M}$  and doubled the number of experimental points between  $0.2$  and  $50\mu\text{M}$ . This suggestion is supported by the fact that when these additional values are omitted from the graphic analysis a single line is obtained with an x-intercept ( $K_m$ ) equivalent to  $11.1\mu\text{M}$  (graph not shown). The maximum transport velocities ( $V_{max}$ ) calculated for both HA1 and HA2 (Table I) are similar to that reported by Wilkin et al. (22) for uptake of [ $^3\text{H}$ ] GABA into cerebellar glomerulus particles.

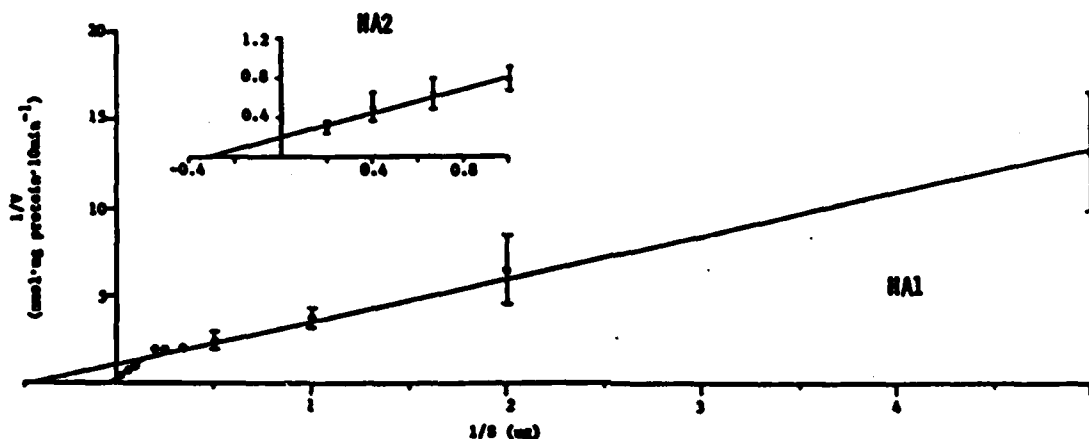
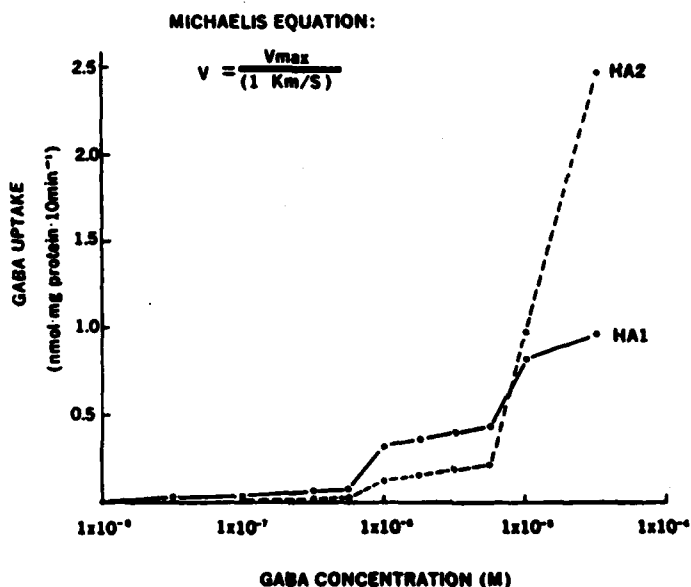


Fig. 1. Lineweaver-Burk plots of data from 5 experiments show that two high affinity (HA)  $^3\text{H}$ -GABA uptake systems are present in cerebellar glomerulus particles; HA1 and HA2. Experimental points (s.e.) for both lines were plotted by computer analysis.

Using the Michaelis-Menten equation, we obtained an estimate of what the relative contributions of HA1 and HA2 would be to net GABA accumulation over a given range of substrate concentrations (Fig. 2). This analysis suggests that at a concentration of  $10^{-6}\text{M}$  the velocity of GABA uptake by HA1 would be twice that attributable to HA2. At  $10^{-5}\text{M}$  GABA, the velocities of the two systems are roughly equivalent and at  $10^{-4}\text{M}$  HA2 would account for more than 75% of the total GABA transported. Interpreting the physiological significance of these two transport systems is difficult, at best, without an estimate of the endogenous concentration of GABA within the synaptic cleft. Nevertheless, our

data clearly show that [<sup>3</sup>H] GABA is actively and efficiently accumulated by glomerular particles. An additional series of experiments were conducted, therefore, in order to further investigate the possibility that either, or both, of these transport sites are specifically related to a GABAergic pathway in cerebellar glomeruli.

Fig. 2. RELATIVE CONTRIBUTION OF HIGH AFFINITY GABA UPTAKE SYSTEMS AT VARYING SUBSTRATE CONCENTRATIONS



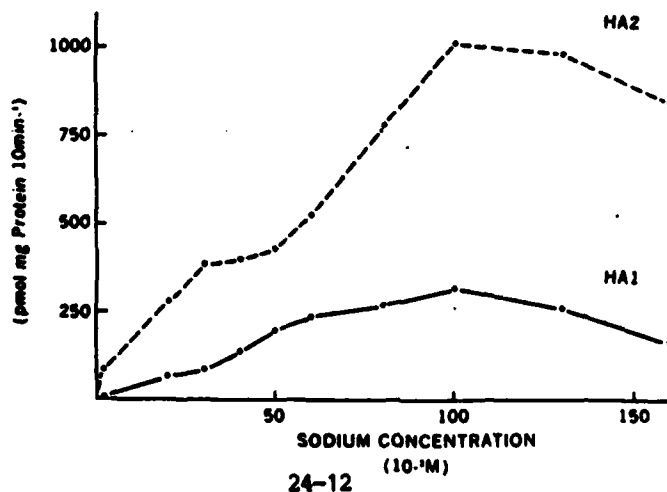
(d) Sodium and energy dependencies of [<sup>3</sup>H] GABA uptake. Most of the high affinity transport systems characterized thus far seem to share the following properties: they are highly sodium-dependent; temperature-sensitive; and are inhibited by 2,4-dinitrophenol and other metabolic inhibitors. To compare the functional properties of HA1 and HA2 transport systems we measured [<sup>3</sup>H] GABA uptake in the presence of either 0.5 $\mu$ M or 30 $\mu$ M [<sup>3</sup>H] GABA, respectively. Uptake of [<sup>3</sup>H] GABA at either of these substrate concentrations was greatly reduced by incubating glomerular particles at 0-4°C or in a sodium-free medium (Table

II and Fig. 3). Uptake was maximal at a sodium concentration of 100mM (Fig. 3) and the Hill coefficients ( $n_H$ ) for HA1 and HA2 were 1.02 and 0.88 (Table I), respectively. A significant decrease in uptake also occurred when metabolic activity was inhibited by incubating the glomerulus particles in the presence of 2,4-dinitrophenol or ouabain (Table II). While equimolar substitution of sucrose for glucose in the incubation medium did inhibit uptake (Table II), it was much less effective than either of the metabolic inhibitors tested. This would seem to indicate that [ $^3$ H] GABA transport in glomerular particles is not strongly dependent on glycolysis.

TABLE II. INHIBITION OF [ $^3$ H]-GABA UPTAKE INTO GLOMERULAR PARTICLES

METABOLIC INHIBITORS	TEST CONC. ( $10^{-3}M$ )	% CONTROL UPTAKE	
		HA 1	HA 2
0°C Incubation	N/A	4	8
2,4-Dinitrophenol	0.5	25	40
Sucrose (Equimolar)	N/A	74	77
Ouabain	1.0	28	69
Low Sodium	2:0	10	18

Fig. 3. SODIUM DEPENDENCE OF  $^3$ H-GABA UPTAKE SYSTEMS IN CEREBELLAR GLOMERULI



(e) Relative importance of net uptake and exchange. Osmotically shocking the glomeruli after they have been preloaded with [ $^3\text{H}$ ] GABA results in a loss of greater than 95% of the radioactivity, regardless of the substrate concentration used (data not shown). This demonstrates that [ $^3\text{H}$ ] GABA is being transported into osmotically-sensitive, membrane bound, pools of this fraction. These vesicular structures appear to have an enormous ability to accumulate GABA, in fact [ $^3\text{H}$ ] GABA is concentrated over 300-fold from the medium by both the HA1 and HA2 uptake systems (Table III). However, these results do not rule out the possibility that a net accumulation of GABA is being simulated by the exchange of radiolabeled for unlabeled GABA molecules. In order to determine the contribution of homoexchange to the observed uptake, glomerular particles were preloaded with [ $^3\text{H}$ ] GABA (0.5 $\mu\text{M}$  or 30 $\mu\text{M}$ ) and incubated for 7 minutes at 37°C. Aliquots (50 $\mu\text{l}$ ) of different cold GABA solutions were then added to the medium to give final concentrations ranging from 0 to 1,000  $\mu\text{M}$  and the glomeruli were incubated an additional 3 minutes (total incubation time was 10 minutes). Under these conditions, any [ $^3\text{H}$ ] GABA which had been accumulated by an exchange process would be released back into the medium and provide an indication of the relative importance of net uptake and exchange. Roughly 50% of the [ $^3\text{H}$ ] GABA accumulated under these conditions was displaced by the addition of cold GABA to the medium (Table IV). This response was maximal at the lowest concentration tested (100 $\mu\text{M}$ ). Therefore, the remaining [ $^3\text{H}$ ] GABA appears to have been transported into amino acid "pools" which actively accumulate endogenous GABA. The observation that similar results were obtained regardless of which transport system (HA1 or HA2) was the primary contributor to uptake (Table IV) suggests that both HA1 and HA2 are capable of accumulating GABA in osmotically-sensitive compartments of the cerebellar glomeruli.

TABLE III. ACTIVE ACCUMULATION OF [<sup>3</sup>H]-GABA BY GLOMERULAR PARTICLES\*

<u>[<sup>3</sup>H]-GABA CONC.</u>		<u>pmol·mg Protein<sup>-1</sup></u>
<u>(<math>\mu</math>M)</u>		<u>pmol·mg Medium<sup>-1</sup></u>
HA1	0.5	385 $\pm$ 19
HA2	30	369 $\pm$ 19

\* Accumulation was shown to be temperature-dependent and osmotic shock decreased the above values ( $\bar{X} \pm$  S.E.M.) by greater than 95%.

TABLE IV. HOMOEXCHANGE OF [<sup>3</sup>H]-GABA IN GLOMERULAR PARTICLES

CONC. OF UNLABELED GABA IN THE INCUBATION MEDIUM ( $\mu$ M)	% COUNTS BOUND/mg. PROTEIN *	
	( $\bar{X} \pm$ S.E.M.)	
	HA1	HA2
0	28 $\pm$ 4	57 $\pm$ 8
100	13 $\pm$ 2	31 $\pm$ 7
200	13 $\pm$ 2	29 $\pm$ 3
400	14 $\pm$ 1	32 $\pm$ 7
600	14 $\pm$ 1	27 $\pm$ 3
1000	12 $\pm$ 1	29 $\pm$ 4

\* Calculated as:

$$\frac{\text{Pellet (CPM)} \times 100}{\text{Total (CPM)} \times \text{mg Protein}}$$

$$\text{Total} = \text{Pellet} + \text{Supernatant}$$

(f) Inhibitors of GABA uptake. Both glial and neuronal elements have been shown to accumulate GABA via high affinity uptake systems in various regions of the central nervous system. Cerebellar synaptosomes, granule cells, and astrocytes have all recently been shown to possess GABA transport systems with  $K_m$  values of less than  $10^{-5}$ M (19). Autoradiographic studies indicate that the glial cells associated with cerebellar glomeruli do not transport GABA at low ( $10^{-6}$ M) substrate concentrations (7,22), and suggest that the Golgi axon terminals account for virtually all GABA uptake in this synaptic complex. However, the distribution of uptake sites was not examined at

substrate concentrations which would preferentially label the HA2 sites we have reported ( $> 10^{-5}M$ , see Fig. 2). The possibility must be considered, therefore, that the HA1 and HA2 transport systems are associated with these two cellular entities. To address this issue, we screened a number of structural analogues for GABA which are known to inhibit glial and neuronal uptake of GABA with varying degrees of selectivity and potency (10). These experiments revealed that those GABA analogues which have been shown to either be potent inhibitors of both neuronal and glial transport carriers (GABA, Guvacine, trans-4-Aminocrotonic acid), or relatively selective inhibitors of neuronal uptake (Nipecotic acid, Diaminobutyric acid), were clearly the strongest inhibitors of [ $^3H$ ] GABA uptake in cerebellar glomeruli (Table V). The  $IC_{50}$  values (the inhibitor concentration producing 50% inhibition of uptake) for these compounds ranged from approximately 1 to  $10\mu M$ . In contrast, those substances which inhibit glial uptake in a reasonably specific manner ( $\beta$ -Alanine, THAO, THPO) were found to be relatively weak inhibitors of glomerular GABA uptake,  $IC_{50}$  values ranging from 130 to  $600\mu M$  (Table V). Although the ratio of  $IC_{50}$  values for HA2/HA1 exceeded a value of 1.0 for all analogues tested, none of the HA2/HA1 ratios were greater than 4.0. These apparent discrepancies in potency can easily be explained by the differences in HA1 and HA2 substrate affinities. These results, therefore, indicate that both the HA1 and HA2 transport sites for [ $^3H$ ] GABA in cerebellar glomeruli are neuronal. Moreover, these uptake systems appear to accumulate GABA by a structurally specific mechanism since uptake was not inhibited by a variety of different amino acids (Table V). The observation that muscimol ( $5 \times 10^{-5}M$ ) did not influence our measurements of [ $^3H$ ] GABA uptake (Table V) further suggests that artifacts due to a surface exchange, rather than inward transport, of [ $^3H$ ] GABA may be disregarded.

TABLE V. INHIBITION OF [<sup>3</sup>H] GABA UPTAKE IN CEREBELLAR GLOMERULI BY STRUCTURAL ANALOGUES OF GABA

Analogue	IC <sub>50</sub> (μM)	
	HA1	HA2
GABA	0.7	1.6
(R,S) Nipecotic acid	1:1	1:4
trans-4-Aminocrotonic acid	1.4	6.0
Guvacine	2.8	9.6
L-2,4-Diaminobutyric acid	7.0	8.0
B-Alanine	130.0	260.0
THAO <sup>a</sup>	190.0	600.0
THPO <sup>b</sup>	200.0	290.0

The following produced no significant inhibition at a concentration of  $5 \times 10^{-4}$ M: muscimol, glutamate, glutamine, glycine, phenylalanine, serine.

IC<sub>50</sub> values for inhibitors of [<sup>3</sup>H] GABA uptake were determined by incubating glomerular particles in a Krebs-Ringer medium containing either 0.5μM (HA1) or 50μM (HA2) - [<sup>3</sup>H] GABA and the inhibitor at different concentrations (0-5,000μM). Results are means of triplicate determinations and S.E.M.s were less than 10%. The IC<sub>50</sub> values were determined by the method of Beart et al. (1). Glomerular particles were not preincubated in the presence of inhibitor.

<sup>a</sup> 5,6,7,8-tetrahydro-4H-isoxazolo[4,5c]azepin-3-01

<sup>b</sup> 4,5,6,7-tetrahydroisoxazolo[4,5c]pyridin-3-01

(g) General discussion and summary. Cerebellar glomeruli appear to accumulate [<sup>3</sup>H] GABA by two distinct high affinity transport mechanisms. Although an exchange process clearly contributes to the uptake measured in these experiments, at least half of the [<sup>3</sup>H] GABA accumulated by glomerular particles appears to represent a net uptake and not homoexchange with the endogenous pool of GABA. This conclusion is supported by both a high tissue/medium ratio for [<sup>3</sup>H] GABA and the fact that neither 100 nor 1,000μM nonradioactive GABA could displace any more than 50% of the [<sup>3</sup>H] GABA accumulated by this tissue preparation.

Kinetic analysis provided the only evidence to support the suggestion that two classes of GABA transport systems are present in the cerebellar glomeruli. These systems could not be distinguished from one another on the basis of their temperature sensitivity, sodium dependency, responsiveness to metabolic inhibitors, or substrate specificity. A one-to-one relationship between GABA transport and sodium transport was indicated by Hill plot analysis, suggesting that these carriers both require the binding of one sodium ion for each molecule of GABA transported. It has not yet been unequivocally established that structural analogues of GABA can distinguish neuronal from glial uptake sites. However, pronounced differences in the sensitivity of glomerular transport systems to these inhibitors were noted and argue strongly in favor of the interpretation that neuronal, rather than glial, elements are primarily responsible for [ $^3\text{H}$ ] GABA uptake in this fraction. These results are supported by autoradiographic studies which indicate that GABA transport sites in cerebellar glomeruli are associated with the Golgi axon terminals (7,22).

Clearly both GABA uptake sites have a high enough affinity and transport capacity to conceivably play some physiological role. The similarities in their functional properties suggests that these are not independent, or distinct, classes of transport systems. It is hypothesized that the nonlinear relationship between uptake velocity and substrate concentration (Fig. 1) reflects the interaction of two negatively cooperative sites in a single transport system. Such a microheterogeneity of neuronal GABA uptake sites has previously been proposed (12) based upon studies of neurons cultured from cerebral cortex. If this is the case, one would predict that the subcellular distribution of these neuronal uptake sites (HA1 and HA2) would be similar. The accuracy of this prediction could be easily tested by autoradiographic

localization of uptake sites following incubation with 0.5 and 30 $\mu$ M [ $^3$ H] GABA. The ability to clearly distinguish neuronal processes in isolated cerebellar glomeruli makes it an ideal model for testing this hypothesis.

#### IV. DEPOLARIZATION-INDUCED RELEASE OF [ $^3$ H] GABA

##### **Introduction:**

The ability to isolate a reasonably pure fraction of cerebellar glomeruli provides an almost unique opportunity for correlating biochemical observations with specific neuronal elements. Thus far, work on this preparation has been limited to investigations of amino acid transport and receptor binding. In establishing a neurotransmitter role for a substance, however, it is usually considered important to show that it is released from nerve terminals as a result of presynaptic stimulation. Here we report a systematic analysis of the depolarization-induced release of [ $^3$ H] GABA from cerebellar glomeruli and the ionic requirements for this response.

##### **Methods and Results:**

(a) Measurement of [ $^3$ H] GABA release. Glomerular particles were prepared from bovine cerebellar vermis as described in Section III(a). Glomeruli were preloaded with [ $^3$ H] GABA using the incubation conditions described previously (see uptake studies) except that incubations were performed in 5 ml of medium containing protein at a concentration of 3.5 - 5.0 mg/ml and [ $^3$ H] GABA at a final concentration of 0.2  $\mu$ M (10  $\mu$ Ci). Aliquots (1.0 ml) of this PGF suspension were transferred to parallel perfusion chambers similar to those described by Raiteri et al. (17), collected on Whatman GF/B filters, and washed with 15 ml of Krebs-Ringer medium (13). The glomerular particles were then perfused at a rate of 4.0 - 4.6 ml/min and fractions were collected every 10 seconds directly into liquid scintillation vials. After the spontaneous

release of [ $^3\text{H}$ ] GABA had reached a steady baseline, the standard medium was replaced by a medium containing the test substance(s). All solutions contained 0.1 mM amino-oxyacetic acid, 11.0 mM glucose, 1.2 mM  $\text{MgSO}_4$ , and 20.0 mM Hepes buffered at pH 7.35. Additional details for each experiment are given below the appropriate Figure. The percentage of total radioactivity release per 10 sec interval was calculated according to the method of Levi and Raiteri (13) and represents the average of at least 3 experimental determinations.

(b) Depolarization-induced release in response to  $\text{K}^+$ . A baseline for the spontaneous efflux of [ $^3\text{H}$ ] GABA was established by perfusing glomeruli with a "low"  $\text{K}^+$  medium (5 mM KCl) throughout the experiment (Fig. 4). After a relatively stable baseline was reached, the glomeruli were exposed to a media containing depolarizing concentrations of KCl (37-90 mM). The data in Figure 4 demonstrate that [ $^3\text{H}$ ] GABA is rapidly released in response to K-induced depolarization and that this response is dose-dependent. That is, the amount of [ $^3\text{H}$ ] GABA released is directly related to the concentration of  $\text{K}^+$  and, therefore, the degree of membrane depolarization.

(c) Depolarization-induced release in response to veratridine. Veratridine was also shown to stimulate the release of [ $^3\text{H}$ ] GABA from glomerular particles in a graded manner (Fig. 5) and with a potency which was an order of magnitude greater than  $\text{K}^+$  ( $10^{-6}$  versus  $10^{-5}\text{M}$ ). This difference in potency may be explained by the fact that veratridine selectively depolarizes neuronal, rather than glial, membranes by locking open the voltage-sensitive  $\text{Na}^+$ -channels which are unique to this type of membrane. The discrepancy in potency between these depolarizing agents, therefore, strongly suggests that [ $^3\text{H}$ ] GABA is released from neuronal elements intrinsic to cerebellar glomeruli.

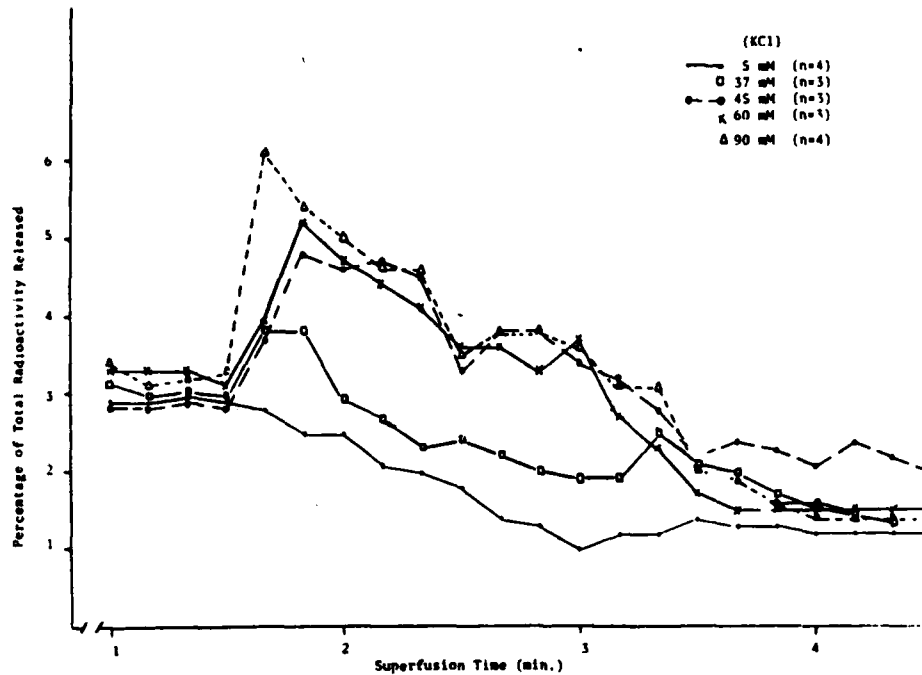


Fig. 4. Release of  $[^3\text{H}]\text{GABA}$  from glomerular particles depolarized with different  $\text{K}^+$  concentrations. Glomeruli were perfused with 15 ml medium, containing 2.7 mM  $\text{CaCl}_2$ , prior to depolarization.

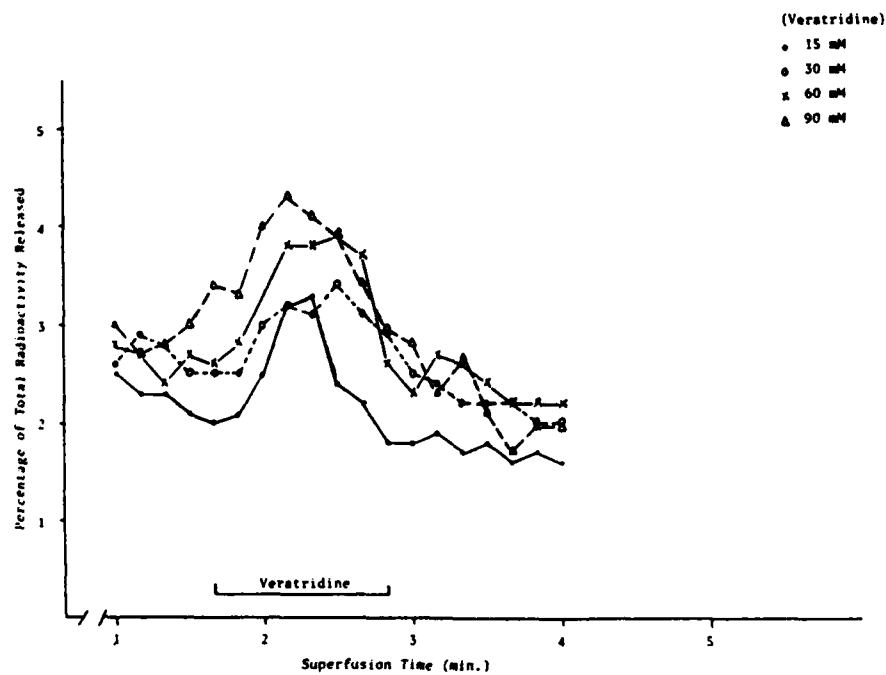


Fig. 5. Release of  $[^3\text{H}]\text{GABA}$  from glomerular particles depolarized with different concentrations of Veratridine (15-90 mM). Glomeruli were perfused with 10 ml medium, containing 2.7 mM  $\text{CaCl}_2$ , prior to depolarization. Each curve is the average of three separate determinations.

(d) Calcium dependence of depolarization-induced release. High  $[K^+]$  has been shown to stimulate the release of radiolabeled amino acids from both neuronal and glial structures. However, only the  $K^+$ -induced release from neuronal structures is  $Ca^{2+}$ -dependent. In this series of experiments, an attempt was made to further characterize the stimulus-evoked release of  $[^3H]$  GABA and to identify the structures responsible for this release. On the basis of our earlier results (Fig. 4), 42 mM KCl was chosen as an appropriate stimulus since, at this concentration, an increase or decrease in the amount of  $[^3H]$  GABA release could be noted. Veratridine was also used at a concentration which had been shown to produce an intermediate response (45  $\mu M$ ). Figures 6 and 7 show that, although a modest degree of  $Ca^{2+}$ -dependence was detectable, the majority of  $[^3H]$  GABA efflux was  $Ca^{2+}$ -independent, regardless of which depolarizing agent was used.

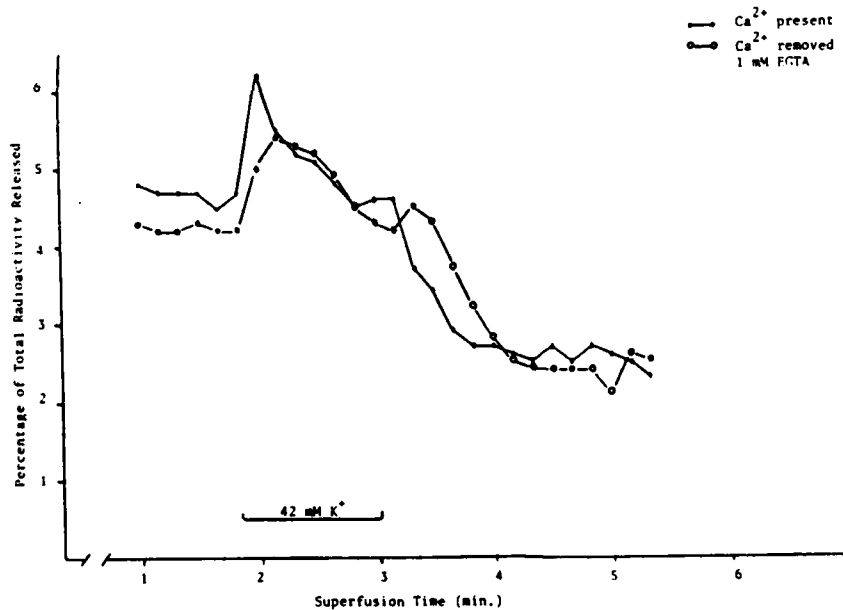


Fig. 6. Effect of  $Ca^{2+}$  on the  $K^+$ -evoked release of  $[^3H]$ GABA from cerebellar glomeruli. Each curve represents the average of three separate determinations.

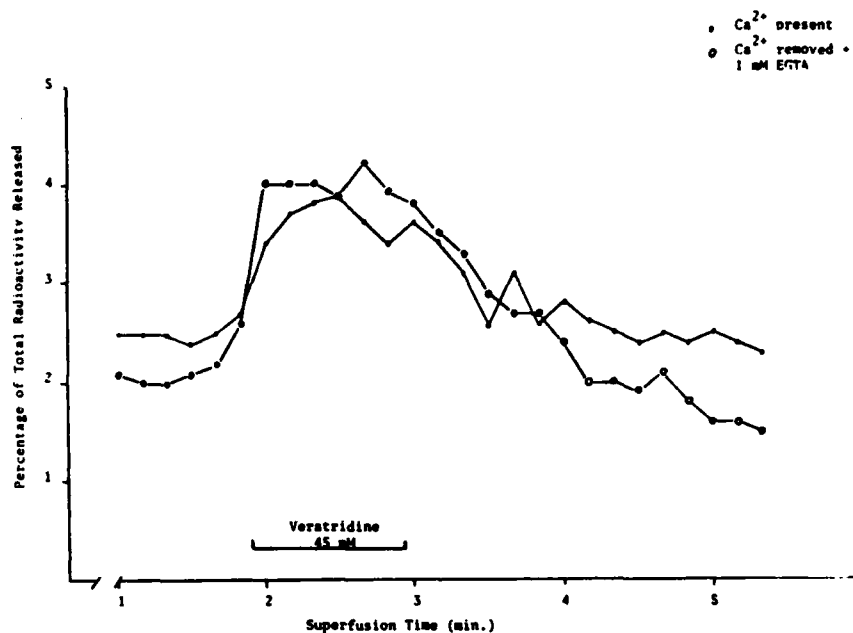


Fig. 7. The effect of Ca<sup>2+</sup> on the Veratridine-evoked release of [<sup>3</sup>H]GABA from cerebellar glomeruli. Each curve represents the average of three separate determinations.

The failure to detect a larger Ca<sup>2+</sup>-dependent component of [<sup>3</sup>H] GABA release prompted us to re-evaluate the possibility that glial structures contribute to the release being measured under these conditions. Glomerular particles were preloaded with [<sup>3</sup>H] GABA as described above, except that β-Alanine (2.5 x 10<sup>-3</sup>M) was added to the incubation medium. At this concentration, β-Alanine would be expected to inhibit the glial uptake of [<sup>3</sup>H] GABA and, thus allow one to minimize the glial contribution to the observed release. Should the Ca<sup>2+</sup>-dependent component of [<sup>3</sup>H] GABA release become more pronounced under these conditions, it would indicate that both glial and neuronal structures were contributing to release. Figure 8 shows that [<sup>3</sup>H] GABA release is essentially the same for glomeruli incubated in the

presence and absence of  $\beta$ -Alanine and that the removal of  $\text{Ca}^{2+}$  did not effect the baseline efflux of this amino acid. Thus, the  $\text{Ca}^{2+}$ -independent component of [ $^3\text{H}$ ] GABA release appears to be neuronal in nature.

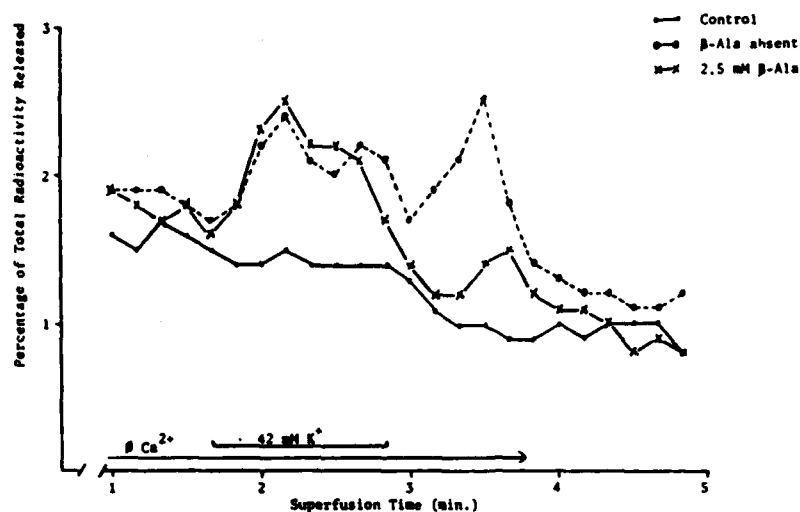


Fig. 8. Effect of  $\beta$ -Alanine (2.5 mM) on the  $\text{Ca}^{2+}$ -independent release of [ $^3\text{H}$ ]GABA. Glomerular particles were preloaded with [ $^3\text{H}$ ]GABA, with or without  $\beta$ -Alanine present, and then perfused with a  $\text{Ca}^{2+}$ -free medium containing a high (42 mM) or low (5 mM, Control) concentration of KCl.

(e) Contribution of homoexchange to the observed release of [ $^3\text{H}$ ] GABA. Depolarizing agents, such as  $\text{K}^+$  and veratridine, stimulate the inward transport of  $\text{Na}^+$  and, therefore, are also capable of enhancing  $\text{Na}^+$ -dependent amino acid homoexchange (14). We have demonstrated that roughly 50% of the [ $^3\text{H}$ ] GABA accumulated by glomerular particles can be attributed to an exchange of radioactive for nonradioactive GABA (Table IV) which is  $\text{Ca}^{2+}$ -independent. These observations suggested a mechanism which may well account for the large  $\text{Ca}^{2+}$ -independent component of [ $^3\text{H}$ ] GABA release measured in our earlier experiments. To explore this possibility, we conducted the following series of experiments. Glomerular particles were preloaded with [ $^3\text{H}$ ] GABA as described above (Section IVa) and spontaneous release (baseline control) was

124

measured by perfusing with a  $\text{Ca}^{2+}$ -free, low  $\text{K}^+$  (5 mM), medium. Homoexchange of recently accumulated [ $^3\text{H}$ ] GABA was maximally stimulated by adding cold GABA (25  $\mu\text{M}$ ) to this perfusing medium. The  $\text{Na}^+$  dependence of GABA homoexchange, stimulated in this manner, was tested by perfusing with a  $\text{Na}^+$ -free medium to which GABA (25  $\mu\text{M}$ ) had been added (NaCl was replaced by an equimolar concentration of choline chloride and  $\text{K}_2\text{HPO}_4$  was substituted for  $\text{Na}_2\text{HPO}_4$ ). Finally, glomerular particles were depolarized (42 mM  $\text{K}^+$ ) in the presence of GABA (25  $\mu\text{M}$ ) in order to determine whether homoexchange and neurosecretion are additive under these conditions, or if [ $^3\text{H}$ ] GABA efflux can be explained solely on the basis of a homoexchange process.

Figure 9 shows that GABA has an extremely potent stimulatory effect on [ $^3\text{H}$ ] GABA efflux which is absolutely dependent on  $\text{Na}^+$  ions. The magnitude of GABA-evoked release is greater than that produced by a maximally-stimulating dose of either  $\text{K}^+$  (Fig. 4) or veratridine (Fig. 5). This appears to be consistent with the suggestion that these depolarizing agents indirectly stimulate [ $^3\text{H}$ ] GABA release by enhancing the activity of a  $\text{Na}^+$ -dependent exchange of GABA. Since GABA acts more directly on this exchange mechanism, it would be expected to have a more potent influence. However, homoexchange can not account for all of the [ $^3\text{H}$ ] GABA released in response to membrane depolarization. This conclusion is supported by the fact that [ $^3\text{H}$ ] GABA release is slightly increased when  $\text{K}^+$  (42 mM) is added to a GABA containing perfusion medium (Fig. 9). These experiments provide a dramatic example of how misleading the results of such release studies can be when one fails to take into account the contribution made by homoexchange, particularly when complex neuronal preparations (i.e., brain slices, prisms) are utilized.

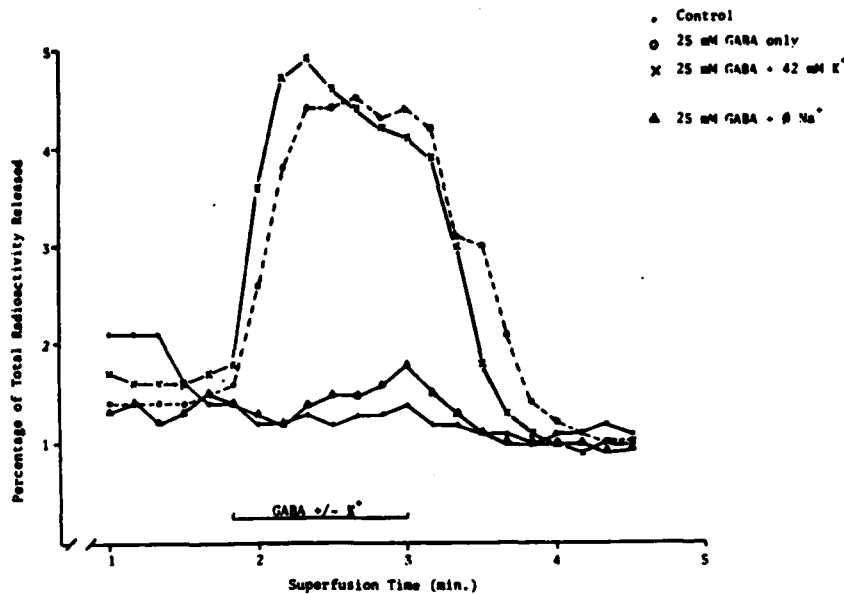


Fig. 9. Effect of external GABA on depolarization-induced release of recently accumulated (<sup>3</sup>H)GABA. Glomerular particles were perfused with 10 ml of a Ca<sup>2+</sup>-free, low  $\text{K}^+$  medium and then exposed to GABA (25  $\mu\text{M}$ ) with or without high  $\text{K}^+$  (42  $\text{mM}$ ) or  $\text{Na}^+$ . Each curve is the average of three separate determinations.

(f) Neurosecretion of [<sup>3</sup>H] GABA from cerebellar glomeruli. Having demonstrated the importance of controlling for homoexchange when measuring depolarization-induced release of amino acids, we endeavored to establish such a control procedure. We were able to accomplish this by perfusing the glomerular particles with 10 ml of a medium containing cold GABA (25  $\mu\text{M}$ ) prior to depolarization. Pretreating the glomeruli in this fashion insured that the exchangeable pool of GABA had equilibrated prior to further experimentation, thus eliminating homoexchange as a contributing factor. Figure 10 shows that this is indeed the case, since the spontaneous efflux of [<sup>3</sup>H] GABA is no longer stimulated by perfusing glomeruli with an additional 10 ml of medium containing GABA. Under these conditions, if one now depolarizes the glomerular particles with a high concentration of  $\text{K}^+$  (50  $\text{mM}$ ), and [<sup>3</sup>H] GABA efflux occurs, it may be assumed to represent a neurosecretion of the amino

acid. Indeed, such a response was elicited under these conditions (Fig. 10). This finding prompted us to re-evaluate the  $\text{Ca}^{2+}$ -dependence of  $[^3\text{H}]$  GABA release, since in our earlier experiments homoexchange had been a major contributor to  $[^3\text{H}]$  GABA efflux and is  $\text{Ca}^{2+}$ -independent. As Figure 10 demonstrates, the high  $[\text{K}^+]$ -evoked release of  $[^3\text{H}]$  GABA displayed a marked dependence upon  $\text{Ca}^{2+}$ . Thus, it would appear that the modest  $\text{Ca}^{2+}$  dependence of  $\text{K}^+$ -evoked release noted in our earlier experiments was probably due to the existence of a substantial non $\text{Ca}^{2+}$ -dependent release of  $[^3\text{H}]$  GABA from a homoexchange pool.

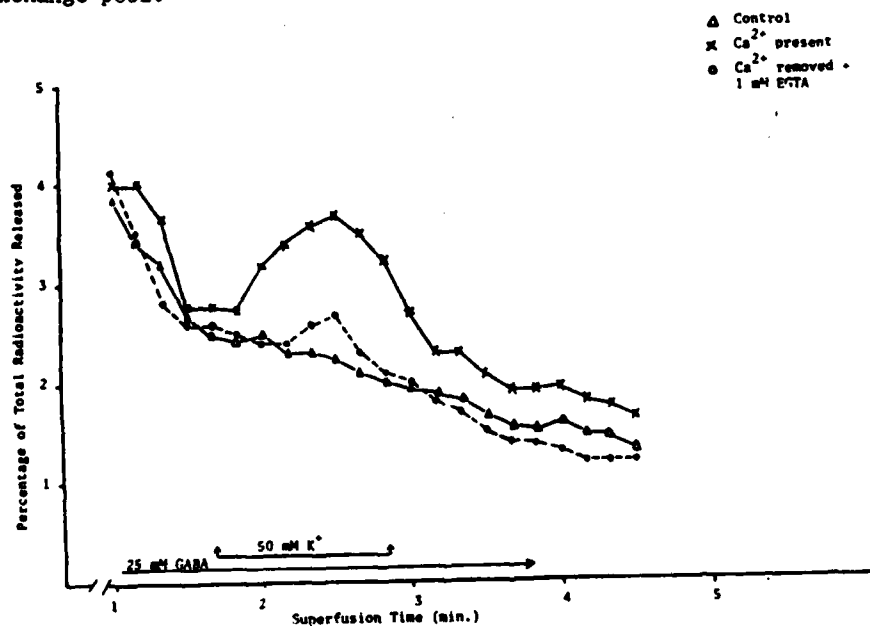


Fig. 10. Calcium dependence of  $\text{K}^+$ -evoked  $[^3\text{H}]$ GABA release from cerebellar glomeruli following equilibration of the exchangeable GABA pool. Each curve represents the average of duplicate determinations.

#### V. RECOMMENDATIONS

The overall objective of this project is to determine whether sensory integration within the cerebellar glomerulus occurs via multiple neurotransmitters, the presynaptic modulation of neurotransmitter release, or

both. The release studies described above are to first be used to determine which neurotransmitters are released in the glomeruli. Candidates include acetylcholine, glutamate, glycine, aspartate, and as discussed here, GABA. The criteria used to identify any candidate as a glomerular transmitter are the same as those described previously for GABA and thus the same uptake and release studies should be repeated for each.

In order to complete the GABA release studies begun this summer, the  $K^+$  and veratridine depolarization, and calcium dependence studies described in Part IV should be repeated. In this way, it will be possible to observe any true calcium-dependent release separately from the transport contribution. In addition, release should be observed in the presence of the voltage-sensitive  $Na^+$  channel blocker, tetrodotoxin. A high-performance liquid chromatography separation should be carried out on the release product to establish what percentage of radioactivity represents nonspecifically labelled metabolites rather than GABA.

Finally, the following should be done to verify and characterize the  $Ca^{++}$ -dependence of release. Inhibition of release by  $Ca^{++}$  channel blocker verapamil in the presence of calcium and a depolarizing solution should be demonstrated. Conversely, GABA release in the presence of  $Ca$ -ionophore A23187, calcium, and nondepolarizing solution should occur. Saturability should be investigated by varying  $Ca^{++}$  concentration at a given depolarizing concentration of  $K^+$  or veratridine.

Once the glomerular neurotransmitters have been tentatively identified, presynaptic modulators of their release can be studied. A variety of neuromodulators with a corresponding variety of presynaptic receptors have been shown to modulate transmission patterns. Such modulators may originate

in the same neuron as the presynaptic receptor, or in adjacent nerve terminals. Of specific note here will be the action of nucleoside neuromodulators and their interactions of neurotransmitters.

The nucleoside adenosine has been demonstrated to restrict  $Ca^{2+}$  entry and thus inhibit  $Ca^{2+}$ -dependent transmitter release. A high density of adenosine receptors has been demonstrated in the granule cell layer, and thus may be present in the glomerulus. Since the criteria to identify a substance as neuromodulator include the presence of metabolizing enzymes for that substance, it would be useful to assay for the presence of adenosine deaminase and nucleosidase in the glomerulus. These enzymes catalyze the breakdown of adenosine to inosine and hypoxanthine. Their presence would suggest that adenosine is normally present in vivo in the cerebellar glomerulus.

If adenosine is indicated as a glomerular neuromodulator, it will then be appropriate to measure variation of  $K^+$ -induced release of a given neurotransmitter in the presence and absence of adenosine receptor agonists. A dose response curve could then be correlated to the known affinity of the agonist for the adenosine receptor. In addition, specific binding may be determined using displacement techniques. It would be of interest to test the effects of other nucleosides such as guanosine, cytidine, and uridine in the glomerular preparation.

The simplicity of neural components in the glomerular preparation is an advantage over the often used tissue slices to study the nature of neurotransmitter interaction. Superfusion is also advantageous over other release methods in that endogenously produced substances are rapidly cleared, and the results of added antagonists only are observed. With this method, the

variation in release of a specific labelled neurotransmitter in response to another neurotransmitter agonist, or antagonist, may be studied to give some insight into polysynaptic communication in a multi-transmitter environment.

The possibilities for neurotransmitter and neuromodulator interactions are many. Therefore, the results of each study will determine the next most appropriate direction for research. The prospect that interactions within the cerebellus can be elucidated is exciting since the glomerulus promises to be a simple prototype for multisensory integration leading to response. A complex and intriguing extension of this concept of chemical integrative processes in local neuronal circuits is the suggestion that each neuron may have a unique set of membrane conductances determined by its type and environment.

#### REFERENCES

1. Beart, P.M., G.A.R. Johnston, and M.L. Uhr (1972). Competitive inhibition of GABA uptake in rat brain slices by some GABA analogues of restricted conformation. *J Neurochem*, 19:1855-1861.
2. Coakley, W.T. (1974). Comparison of conditions of tissue fragmentation. *Brain Res*, 70:281-284.
3. Curtis, D.R., A.W. Duggan, and D. Felix (1970). GABA and inhibition of Deiter's neurones. *Brain Res*, 23:117-120.
4. Hajos, F., G. Wilkin, J. Wilson, and R. Balazs (1975). A rapid procedure for obtaining a preparation of large fragments of the cerebellar glomeruli in high purity. *J Neurochem*, 24:1277-1278.
5. Hamberger, A., H.A. Hansson, J.W. Lazarewicz, T. Lundh, and A. Sellstrom (1976). The cerebellar glomerulus: isolation and metabolic properties of a purified fraction. *J Neurochem*, 27:267-272.
6. Ito, M. (1972). Cerebellar control of the vestibular neurons. *Prog Brain Res*, 37:387-390.
7. Kelly, J.S., D. Fabienne, and F. Schon (1975). The autoradiographic localization of the GABA-releasing nerve terminals in cerebellar glomeruli. *Brain Res*, 85:255-259.
8. Kingsbury, A.E., G.P. Wilkin, A.J. Patel, and R. Balazs (1980). Distribution of GABA receptors in the rat cerebellum. *J Neurochem*, 35:739-742.
9. Kohn, M.C., L.E. Menten, and D. Garfinkel (1979). A convenient computer program for fitting enzymatic rate laws to steady state data. *Comput Biomed Res*, 12:461-469.
10. Krogsgaard-Larsen, P. (1980). Inhibitors of the GABA uptake systems. *Molec Cell Biochem*, 31:105-121.
11. Kuriyama, K., H. Weinstein, and E. Roberts (1969). Uptake of GABA by mitochondrial and synaptosomal fractions from mouse brain. *Brain Res*, 16:479-492.
12. Larsson, O.M., J. Drejer, L. Hertz, and A. Schousboe (1983). Ion dependency of uptake and release of GABA and (RS)-nipecotic acid studied in cultured mouse brain cortex neurons. *J Neurosci Res*, 9:291-302.
13. Levi, G. and M. Raiteri (1973). GABA and glutamate uptake by subcellular fractions enriched in synaptosomes: critical evaluation of some methodological aspects. *Brain Res*, 57:165-185.
14. Levi, G. and M. Raiteri (1974). Exchange of neurotransmitter amino acid at nerve endings can simulate high affinity uptake. *Nature*, 250:735-737.

15. Llinas, R.R. (1981). Electrophysiology of the cerebellar networks. In: Handbook of Physiology. Vol. II: The Nervous System, pp. 831-875.
16. Lowry, O.H., N.J. Rosebrough, A.L. Farr, and R.J. Randall (1951). Protein measurement with Folin phenol reagent. J Biol Chem, 193:265-275.
17. Raiteri, M., F. Angelini, and G. Levi (1974). A simple apparatus for studying the release of neurotransmitters from synaptosomes. Eur J Pharmacol, 25:411-414.
18. Sellstrom, A. and A. Hamberger (1976). GABA release from neurons and glia. Acta Physiol Scand, 98:94-102.
19. Shank, R.P. and G. Campbell (1984). Amino acid uptake, content, and metabolism by neuronal and glial enriched cellular fractions from mouse cerebellum. J Neuroscience, 4:58-69.
20. Snyder, S.H., A.B. Young, J.P. Bennett, and A.H. Mulder (1973). Synaptic biochemistry of amino acids. Fed Proc, 32:2039-2047.
21. Szentagothai, J. (1970). Glomerular synapses, complex synaptic arrangements and their operational significance. In: Handbook of Physiology. Vol. III: The Nervous System, pp. 427-443.
22. Wilkin, G., J.E. Wilson, R. Balazs, F. Schon, and J.S. Kelly (1974). How selective is high affinity uptake of GABA into inhibitory nerve terminals. Nature, 252:397-399.
23. Wilson, J.E., G.P. Wilkin, and R. Balazs (1976). Metabolic properties of large fragments of the cerebellar glomeruli: glucose metabolism and amino acid uptake. J Neurochem, 26:957-965.

1984 USAF-SCEE GRADUATE STUDENT SUMMER SUPPORT PROGRAM

Sponsored by the

AIR FORCE OFFICE OF SCIENTIFIC RESEARCH

Conducted by the

SOUTHEASTERN CENTER FOR ELECTRICAL ENGINEERING EDUCATION

FINAL REPORT

A DYNAMIC APPROACH TO AIRFRAME COST ESTIMATION

Prepared by                    Bruce Harmon  
Academic Department        Economics  
University:                    University of Cincinnati  
Research Location:          Business Research Management Center AFBMRC/RDCB  
USAF Research Contact:     T. R. Gullledge, Jr.  
   Assistant Professor  
Date:                             September 14, 1984  
Contract No:                  F49620-82-C-0035

A Dynamic Approach to Airframe Cost Estimation

by

Bruce R. Harmon

ABSTRACT

Traditionally cost estimation for military airframe programs has ignored important aspects of economic theory. The progress function has been the dominant analytical tool used in relating production quantities to airframe cost. Efforts have been made to synthesize the progress function with neoclassical economic production and cost theory. The most promising of these efforts posits a dynamic cost function where the production process is modeled taking into account the effects of learning and production rate. This research examines this approach and provides an empirical test of its validity. To do this a dynamic cost model is applied to the F-4 airframe program and parameters are estimated using historical production data.

## I. INTRODUCTION

In the realm of cost estimation for military airframe production programs "learning curves" or "progress functions" hold an important role. Traditional neoclassical economic cost theory has more often than not been ignored as a tool in cost estimation; conversely the concept of learning by doing has not drawn much attention in the economics literature.

Historically cost estimating in the military environment has been achieved through the use of a variety of techniques:

- 1) Industrial engineering time standards,
- 2) Parametric cost estimating models,
- 3) Learning curves.

These methods and combinations of methods have been used with varying degrees of success throughout the post WWII period. The general orientation of these approaches has been toward cost estimation in the program planning stages of a weapons system prior to the start-up of actual production.

This study does not concern itself with industrial engineering time standards or parametric cost models. The problems in disaggregating the production process and trying to judge cost by engineering time standards flow from the perverse incentives endemic to the political and contracting peculiarities of government weapons procurement, i.e there is a tendency to be over-optimistic when estimating costs through industrial engineering time standards. Parametric cost models are less subjective; they are based upon cross-sectional regression models in which the dependent variable is specified as the cost of the  $i$ th aircraft while the independent variables are the aircraft's physical and performance characteristics. As parametric models are estimated using historical data, and the technological volatility of the aerospace industry must be taken as a given, this approach has obvious flaws. However, parametric cost models have proven to be more accurate than the industrial engineering approach and thus are important tools in the cost estimators' repertoire.

Both of these methods are geared toward producing cost estimates in the planning stages of the weapons procurement process and thus are not well suited to providing cost updates once production has started. These cost updates are important because of the special nature of the funding process for military airframe programs. Before production commences on a given weapons system a tentative monthly production schedule is negotiated

between the government and arms contractor for the life of that program. This schedule is then used by the contractor for production planning purposes. This tentative schedule however is contingent upon annual appropriations from Congress which are then formalized through annual contractual agreements between the Department of Defense and the contractor. Thus there is a need to estimate cost changes arising from changes in production schedules after production is started.<sup>13</sup>

At first glance learning curve analysis seems to hold much promise in coming to terms with the cost updating problem. The learning curve or progress function is based upon the observed decrease in per-unit production costs as cumulative output increases. Many reasons for this phenomena have been suggested; a good summary can be found in Asher<sup>3</sup>:

1. Job familiarization by workers,
2. General improvement in tool coordination, shop organization, and engineering liason,
3. Development of more efficiently produced sub-assemblies,
4. Development of more efficient parts supply systems,
5. Development of more efficient tools.

It can be seen that a change in contracted orders for a given year will change the manufacturer's relative position on the learning curve and thereby change the average per unit cost of airframes procured in that year. However, learning curves are still deficient for the cost updating problem because they ignore all facets of microeconomic cost theory which impact program costs. Specifically, changes in contracted orders will change production rate and thus unit cost; this relationship between production rate and unit cost is familiar to economists as the U shaped average cost curve. It has only been recently that researchers in the cost estimation field have attempted to integrate economic theory with traditional learning curve analysis. These attempts at integration (e.g., Smith<sup>13</sup>, Large, et al.<sup>9</sup>, Bemis<sup>5</sup>, Cox and Gansler<sup>6</sup>, Crouch<sup>7</sup>) have generally been unsatisfactory; they have either found production rate to be a statistically unimportant variable or have been riddled with statistical problems (i.e. multicollinearity) associated with the elementary log-linear specification of their models (Gulledge<sup>8</sup>).

More recently promising attempts at integration have been made in the economics and management science literature. These efforts have centered

around the specifications of learning augmented dynamic cost and production functions (e.g., Rosen<sup>12</sup>, Washburn<sup>14</sup>, Womer<sup>15</sup>, and Gullledge<sup>16</sup>).

## II. OBJECTIVES

The purpose of this research is to provide insight into these new developments by empirically testing the robustness of a learning augmented dynamic cost function. The hope is that validation or rejection of such a model will add to research efforts aimed at integrating traditional economic theory with the learning by doing hypothesis. The point of departure for this study can be found in the work of Womer and Gullledge<sup>16</sup>. Their approach to the problem is to specify a homogeneous production function in which a learning hypothesis is explicitly included. This production function is restated as a constraint to an optimization problem where the discounted costs of production are minimized. The first order conditions are then solved for the optimal time paths of resource use rate and discounted cost. The solution to the optimization problem can be reformulated in such a way as to allow the estimation of the model parameters using historical airframe production and cost data. In this effort the Womer-Gullledge model is restated so that application of a richer and more disaggregated data series is feasible. Parameter estimation is achieved using nonlinear least squares.

## III. WOMER AND GULLEDGE<sup>16</sup>

Womer and Gullledge<sup>16</sup> take into account four "cost drivers" when they specify their learning augmented production function. Two of these cost drivers are related to the learning by doing hypothesis while two others are associated with production rate effects more familiar to neoclassical economic theory. All of these cost drivers are drawn from the frame of reference of a conceptual production line.

The first learning effect influences efficiency at each station on the production line; as the cumulative number of airframes which has gone through a given work station increases, that work station becomes more efficient. This is the effect which is most often associated with the learning by doing concept.

The second learning effect deals with learning over time which takes place independently of activity at a given work station. Womer and Gulledge clarify this point: "a position late in the production line may benefit from the experience of earlier positions, thus work at later positions proceeds more efficiently than work at early positions on the same airframe".

The first rate effect relates costs to the speed of the production line. To increase the speed of the production line more labor must be applied to each position on the line; as each position is crowded diminishing returns to labor are expected.

A second way to increase production rate is to increase the length of the production line. Specifically, this means adding more stations to the production line, which in turn requires having more airframes in the production facility at a given time and a more intensive use of tools and other equipment. This general crowding of fixed resources adversely affects production efficiency and unit costs may increase.

Womer and Gulledge attempt to capture these four cost drivers in an estimable analytic model. This model is geared to the application of data from the C141 transport airframe production program. This data consists of 91 quarterly observations applicable to airframes aggregated into batches and lots respectively. The next sections will present the model in a form applicable to a richer and more extensive data series describing the production history of the F-4 fighter program.

#### IV. THE F-4 PHANTOM II PROGRAM

The F-4 or Phantom II was designed and built by the McDonnell Aircraft Corporation of St. Louis Missouri. As a multirole fighter the F-4 operates from carrier decks or 5000 foot runways; it has prodigious ground attack capabilities yet is still an effective air superiority fighter. The first F-4 was flown on May 27, 1958 and deliveries continued until 1979. The Phantom II is operational within the U.S. Air Force and Navy as well as numerous foreign air forces. The F-4 program was initiated by the U.S. Navy and the first production series were flown by the Navy in an interceptor/attack role. However, later versions were built to suit the needs of the U.S. Air Force and foreign air forces as well as the Navy's own reconnaissance fleet; an updated model of the Navy's original design was also built incorporating extensive airframe modifications. In all, 10 distinct models of the F-4 were produced.

As can be imagined this heterogeneity could greatly complicate the task of data analysis. This is particularly true when we are trying to estimate learning effects: there is always a question of the applicability of learning gained from the production of an airframe dissimilar to the subject airframe. This is not an insurmountable problem but the researcher felt it's defeat was beyond the scope of this project. Because of this problem and the massiveness of the data collected over the span of F-4 production it was decided that only those observations associated with the original Navy model would be used. This however still leaves a very extensive data series intact.

Data for this study is drawn from two sources. Direct man hours per month by block of airframes are reported in the McDonnell Aircraft Company document "Report 7290-F-4 Cost Data".<sup>10</sup> Aircraft delivery dates by aircraft are taken from the Office of Assistant Secretary of Defense (Program Analysis and Evaluation) publication "Acceptance Rates and Tooling Capacity for selected Military Aircraft."<sup>11</sup> The original Navy production run consisted of 634 airframes built over a 110 month period beginning January 1958. These 634 airframes were produced in 31 blocks which in turn comprised 9 production contracts or job orders. In all 617 observations are relevant to the first F-4 A/B version of the Phantom II.

Other data problems were also encountered. Each contract had a small amount of manhours expended on work deemed common to all the blocks within that contract. These manhours had to be distributed over all the blocks within the subject contract to insure consistency. Some blocks showed a small amount of manhours expended in months after all of the airframes within that block were delivered. These hours were aggregated into the last month consistent with the delivery schedule. Two observations indicated the unlikely occurrence of negative labor hours expended. It was assumed that these negative hours represented effort expended in earlier months on an assembly which was subsequently withdrawn from that block of airframes. These negative hours were redistributed over months preceding their occurrence in the data.

#### V. THE MODEL

The model specifies a production function which attempts to capture the four cost drivers exposted by Womer and Gullledge. Also included is a

term which tries to explain why production activity trails off as a block of airframes approaches completion. The discounted costs of production are minimized subject to this production function, and the optimal time path of resource use is derived. Cost here is measured in units of the variable resource, in this case, labor hours. This practice of counting costs in terms of labor hours is considered a superior method within military cost analysis circles. The variables used when applying this model to the F-4 data are as follows:

- $i$  = an index for a block of airframes in the same contract  $j$ , all of which are delivered by time  $t_{ij}$ ,
- $n_j$  = the number of blocks in contract  $j$ ,
- $m$  = the total number of contracts in the production program,
- $D_{ij}$  = the total number of airframes in block  $i$  of contract  $j$ ,
- $E_{ij}$  = a measure of experience prior to the midpoint of block  $i$ ,
- $E_{ij}$  =
- $V$  = the number of airframes in production in the facility at time  $t$ ,
- $t^{b_{ij}}$  = the date the work begins for block  $i$  of contract  $j$ ,
- $t^{e_{ij}}$  = the date the work ends for block  $i$  of contract  $j$ ,
- $q_{ij}(t)$  = production rate at time  $t$  on block  $i$  of contract  $j$ ,
- $Q_{ij}(t)$  = cumulative production on block  $i$  of contract  $j$  at time  $t$ , i.e.,
- $x_{ij}(t)$  = the rate of resource use at time  $t$  of block  $i$  of contract  $j$ ,
- $\delta$  = a parameter describing learning prior to block  $i$ .

- $\epsilon$  = a parameter describing learning on block  $i$ ,
- $\gamma$  = a parameter describing returns to the variable resources,
- $\alpha$  = a parameter associated with decreasing returns in labor productivity as a block of airframes nears completion,
- $\nu$  = a parameter describing returns to the length of the production line,
- $\eta$  = a parameter describing returns to the size of the batch,
- $r$  = the discount rate,
- $C$  = discounted program cost,
- $C'$  = discounted variable cost for a single batch of airframes.

The production function is;

$$q_{ij}(t) = AV^{\eta} D_{ij}^{\gamma} E_{ij}^{\epsilon} Q_{ij}(t)^{\alpha} (t_{ij} - t)^{\nu} x_{ij}^{\nu}(t). \quad (1)$$

Although this function attempts to capture all the forementioned cost drivers as well as accommodate economic theory it must be recognized that it is still a very simple representation of a very complicated process.

The  $(t_{ij} - t)^{\alpha}$  term attempts to depict decreases in labor productivity which would account for the observed drop-off in production activity as a block of airframes nears completion. The a priori explanation is that as an airframe is readied for delivery the final detail work and testing procedures cannot be compressed over time because of crowding; it becomes increasingly difficult to substitute labor for time. Also implicit in this term is the second learning effect, i.e., learning may occur over time on a given block of airframes. This phenomena is more explicitly treated in the  $Q_{ij}$  argument. Both  $\alpha$  and  $\epsilon$  are expected to be between 0 and 1. The  $E_{ij}^{\epsilon}$  term describes the more conventional learning effect where the relevant

learning is assumed to have occurred while producing previously delivered airframes.

The first rate effect, the speed of the production line, is captured in the  $x_{ij}^{1/\gamma}(t)$  and  $D_{ij}^n$  terms. The  $D_{ij}^n$  term represents the number of airframes in the Block, an indication of how many positions on the line are occupied by that Block.  $n$  is expected to be between 0 and 1.  $x_{ij}^{1/\gamma}(t)$  captures the effect of applying more labor to a fixed number of positions. Since the a priori assumption is that there are diminishing returns to the variable resource, we expect  $\gamma$  to be greater than 1. The second rate effect, the length of the production line, is carried by the  $V^r$  term. The expectation is that as more airframes are under construction in the facility fixed resources are crowded and a small loss in efficiency results. Thus  $r$  is expected to be negative and of a small magnitude.

Here the objective of the firm is assumed to be cost minimization. This may seem somewhat unrealistic in the military procurement environment, but efforts have been made since World War II to write cost minimization incentives into arms contracts.

Thus the firm's optimal behavior can be derived from the following problem:

$$\begin{aligned} \text{Min } C &= \sum_{j=1}^m \sum_{i=1}^{n_i} \int_{t_{ij}}^{t_{ij}^e} x_{ij}(t) e^{-rt} dt \\ \text{Subject to: } q_{ij}(t) &= AV^n D_{ij}^n E_{ij}^b Q_{ij}^e(t) (t_{ij} - t)^e x_{ij}^{1/\gamma}(t) \\ Q_{ij}(t_{ij}^e) &= D_{ij} \\ Q_{ij}(t_{ij}) &= 0. \end{aligned} \quad (2)$$

This is an optimal control problem which may be transformed into a problem of Lagrange. This can then be solved using classical variational techniques. Due to space limitations we will sidestep the rather lengthy and involved mathematical exposition of this solution. (Womer and Gullledge<sup>16</sup> provide a thorough mathematical discourse on an almost identical problem). Instead, we will go directly to the optimum time path of resource use:

$$x_{ij}(t) = BV^{r\gamma} D^{\gamma(1-\gamma)} E^{-r\delta} \Gamma^{-\gamma} \left[ \rho (t_{ij}^e - t_{ij}) / (\gamma - 1), \right. \quad (3)$$

$$\left. \alpha \gamma / (\gamma - 1) + 1 \right] \times (t_{ij}^e - t)^{\alpha \gamma / (\gamma - 1)} e^{-r\rho (t_{ij}^e - t) / (\gamma - 1)}$$

Where  $\Gamma[\rho (t_{ij}^e - t_{ij}) / (\gamma - 1), \alpha \gamma / (\gamma - 1) + 1]$  is the incomplete gamma function.

As the data for the F-4 program is monthly data, the subject of interest is the resource use over a monthly period. Where  $T_k$  and  $T_L$  represent the beginning and ending dates for a given month, the procedure is to integrate (3) with  $T_k$  and  $T_L$  as the limits of integration, i.e.

$$X(T_k) - X(T_L) = \int_{T_L}^{T_k} x(t) dt$$

This yields: (4)

$$\begin{aligned} X_{ij}(T_k) - X_{ij}(T_L) = & B' E_{ij}^{-\lambda} D_{ij}^{\gamma(1-\epsilon-n)} \\ & \times \Gamma^{-\gamma} [\rho(t_{ij} - t_j) / (\gamma - 1), \alpha\gamma / (\gamma - 1) + 1] V^{-\gamma} \\ & \times \{ \Gamma[\gamma\rho(t_{ij} - T_L) / (\gamma - 1), \alpha\gamma / (\gamma - 1) + 1] - \\ & \Gamma[\gamma\rho(t_{ij} - T_k) / (\gamma - 1), \alpha\gamma / (\gamma - 1) + 1] \}. \end{aligned}$$

## VI. EMPIRICAL INVESTIGATION

To apply the F-4 data to this theoretical specification we must restate the problem. Let  $B_0 = B'$  and  $B_1 = \alpha\gamma / (\gamma - 1) + 1$ . As it is impossible to estimate and independently, let  $\lambda = \epsilon + \nu$ . The relevant expression is:

$$\begin{aligned} X_{ij}(t_k) - X_{ij}(T_L) = & \beta_0 E_{ij}^{-\lambda} D_{ij}^{\gamma(1-\lambda)} V^{\gamma} \\ & \times \Gamma^{-\gamma} [\rho(t_{ij} - t_j) / (\gamma - 1), \beta_1] \\ & \times \{ \Gamma[\gamma\rho(t_{ij} - T_L) / (\gamma - 1), \beta_1] \\ & - \Gamma[\gamma\rho(t_{ij} - T_k) / (\gamma - 1), \beta_1] \}. \end{aligned}$$

(5)

It is possible to estimate the parameters in (5) using Marquardt's compromise. In accordance with military practice the discount rate  $\rho$  is set at 10% per year.

The parameter estimates and asymptotic standard errors are as follows:

Parameters	Estimates	Standard Error
$\beta_0$	182.62	41.10
$\beta_1$	4.66	0.26
$\delta$	0.467	0.022
$\gamma$	1.017	0.0012
$\nu$	- 0.262	0.057

$\lambda$  was not significantly different from zero. When  $\lambda$  is set to 0, i.e. the effects of the  $Q_{ij}^{\epsilon}$  and  $D_{ij}^{\nu}$  terms are ignored, negligible increases are observed in the residual sum of squares. As can be seen all of the other parameters are significantly different from zero. All of the significant

parameters are consistent with a priori expectations and the values previously estimated using C141 data. The value of  $\gamma$  is significantly different from 1 indicating that there are decreasing returns to labor in the production process. The estimate for  $\delta$ , 0.467, indicates a 72% learning curve which is within the historically observed range of learning curve values. The small negative value for  $\nu$  confirms expectations about the effects of facility crowding. The interpretation of  $\lambda$  is ambiguous. On reflection the sign of the a priori value of  $\tau$  is not so clear-cut.  $D_{ij}$  could be another proxy for facility crowding, indicating a negative value for  $\tau$ . On the other hand Block size could be analogous to planned production volume; Alchian<sup>2</sup> postulates that as planned volume increases unit cost decreases. The parameter measuring learning on a given block of airframes,  $\epsilon$ , should unambiguously carry a value greater than zero, however, this value could be very small. It should be noted that when estimation was performed using C141 data  $\lambda$  was not significantly different from zero. Overall, the model fits<sup>2</sup> the data very well. The non-linear least squares estimation yields an  $R^2$  of 0.79.

#### VII. RECOMMENDATIONS

The main obstacle to using this model for day-to-day cost estimation is its large data requirements. However the Contractor Cost Data Reporting System may be a source of appropriate data. Progress curve reports (DD Form 1921-2) supply labor hours by logical group, but on inspection of some "completed" forms it seems that percentage completion data is not given where it is specified. For the progress curve reports to be potentially useful for this analysis the percentage completion numbers must be supplied.

Another drawback to this model is that it deals only with variable costs. A comprehensive approach to the cost updating problem must also grapple with the distribution of fixed overhead costs. Balut<sup>4</sup> presents a methodology for doing just that, and Gullede<sup>8</sup> attempts to test this approach using data from the F-16 program.

Research aimed at solving the cost updating problem should follow three different paths:

1. The Womer-Gullede approach should be explored further. Emphasis should be placed on reparameterizing the model in such a way as

to allow its application to complete production programs where multiple iterations of the original model are produced. This would allow estimation to be performed using the whole of the F-4 data series. Also important in this reparameterization would be the clarification of the role which the  $Q_{ij}$  and  $D_{ij}$  terms play.

2. Further exploration of the overhead distribution problem should be made. Balut's approach seems to be a suitable point of departure.
3. A synthesis of these two approaches should be attempted.

## REFERENCES

1. Aeronautical Systems Division Cost Library. Program and Cost Data Notebook, F-4. Wright-Patterson Air Force Base, OH.
2. Alchian, A.. "Costs and Outputs" In Economic Forces at Work. Indianapolis: Liberty Press, 1977.
3. Asher, H. Cost-Quantity Relationships in the Airframe Industry. R-291, Santa Monica: The RAND Corporation, 1956.
4. Balut, S.J. "Redistributing Fixed Overhead Costs". Concepts, Vol. 4, No. 2 (1980), 63-76.
5. Bemis, J.C. "A Model For Examining the Cost Implications of Production Rate". Concepts, Vol. 4, No. 2 (1981), 84-94.
6. Cox, L.W. and J.S. Gansler. "Evaluating the Impact of Quantity, Rate and Competition". Concepts, Vol. 4, No. 2 (1981), pp. 29-53.
7. Crouch, R. "Avoiding Bias in Progress Functions". Defense Management Journal, Vol. 16 (1980), 40-5.
8. Gullede, T.R. "Production Rate Variations Cost Models". Final Report, USAF-SCEEE Summer Faculty Research Program, St. Cloud, Florida, 1984.
9. Large, J.P., K. Hoffman, and F. Kontrovich. Production rate and Production Costs, R-1609-PA-E Santa Monica: The RAND Corporation, 1956.
10. McDonnell Aircraft Company. F-4 Cost Data. Report 7290, St. Louis, Mo, 1972.
11. Office of Assistant Secretary of Defense (Program and Evaluation). Acceptance Rate and Tooling Capacity for Selected Military Aircraft, Washington, D.C., 1974.
12. Rosen, S. "Learning by Experience as Joint Production". Quarterly Journal of Economics, Vol. 86 (1972), 366-382.
13. Smith, L.L. An Investigation of Changes in Direct Labor Requirements Resulting From Changes in Airframe Production Rate, Ph.D. Dissertation, University of Oregon, Eugene, OR, 1976.
14. Washburn, A.R. "The Effects of Discounting Profits in the Presence of Learning in the Optimization of Production Rates," AIIE Transactions, Vol. 4 (1972), 205-213.
15. Womer, N.K. "Learning Curves, Production Rate, and Program Costs," Management Science, Vol. 23 (1979), 312-319.
16. Womer, N.K. and T.R. Gullede. "A Dynamic Cost Function for an Airframe Production Program". Engineering Costs and Production Economics (September, 1983), 213-227.

### ACKNOWLEDGMENTS

This Research was sponsored by the Air Force Office of Scientific Research/AFSC, United States Air Force. Research was conducted through the Air Force Business Research Management Center, Wright-Patterson AFB. Great assistance was also provided by the Aeronautical Systems Division Cost Library, the ASD cost research branch - ASD/ACCR, and the Faculty of the Air Force Institute of Technology. Special thanks is accorded Dr. Thomas Gullledge who thoughtfully guided this research effort.

1984 USAF-SCEEE GRADUATE STUDENT SUMMER SUPPORT PROGRAM

Sponsored by the

AIR FORCE OFFICE OF SCIENTIFIC RESEARCH

Conducted by the

SOUTHEASTERN CENTER FOR ELECTRICAL ENGINEERING EDUCATION

FINAL REPORT

A READOUT ELECTRONICS DESIGN FOR AN INFRARED ARRAY

Prepared by: Thomas L. Hayward  
Academic Department: Physics and Astronomy  
University: University of Wyoming  
Research Location: Air Force Geophysics Laboratory,  
Optical Physics Division, Infrared  
Branch  
USAF Research Contact: Dr. Paul D. LeVan  
SFRP Supervising  
Faculty Member: Dr. Alan F. Bentley, Asst. Professor  
Eastern Montana College  
Date: August 27, 1984  
Contract No: F49620-82-C-0035

A READOUT ELECTRONICS DESIGN FOR  
AN INFRARED ARRAY

by

Thomas L. Hayward

ABSTRACT

The Air Force Geophysics Laboratory (AFGL) has obtained a 58x62 gallium-doped silicon DR0 array from Santa Barbara Research Center. This array will be used for ground-based infrared astronomical observations in the 10 micron band on the Wyoming Infrared Observatory (WIRO) 2.3-meter telescope. The estimated infrared background radiation from the telescope and the earth's atmosphere requires very fast readout electronics for this device. A preliminary design, based on Motorola MC68010 microprocessors running at 10 MHz, is presented in this report. Two 68010's will handle preliminary co-adding of data as they come from the array, dumping the co-added data to the WIRO PDP-11/34 minicomputer at regular intervals. Other elements of the system, including a preliminary co-adding routine for the 68010, are discussed briefly. A discussion of the work yet to be done concludes the report.

### Acknowledgement

I would like to thank the Air Force Systems Command, the Air Force Office of Scientific Research, and the Southeastern Center for Electrical Engineering Education for the opportunity to spend a very enjoyable summer at the Air Force Geophysics Laboratory, Hanscom AFB, Ma. I would like to thank Dr. Thomas L. Murdock and Dr. Paul D. LeVan for suggesting this project and for much valuable assistance. I am also indebted to Dr. Alan F. Bentley, Dr. Stephen J. Little, Peter Tandy, and Paul Cucchiaro for many useful discussions.

## I. INTRODUCTION:

Until recently, the only way to map a celestial object at infrared wavelengths ( $\lambda \approx 1 - 100$  microns) was to place a single detector at the telescope focus and scan across the object in two dimensions on a point-by-point basis. This 'raster scanning' technique has produced impressive results, both from ground-based telescopes (eg.: ref. 1), and from the Infrared Astronomy Satellite (IRAS)<sup>2</sup>, but it is relatively slow and requires exceptional pointing control. The past few years, however, have seen the development of infrared array detectors which have many unit cells (detector elements) on a single semiconductor chip. These arrays promise great increases in the efficiency of infrared observations both from the ground and from space, and several groups in the United States are developing systems that interface various types of arrays to telescopes and computers.<sup>3,4</sup>

To implement this new array technology in space, the Air Force Geophysics Laboratory (AFGL) is planning to fly LAIRTS, a 0.6-meter class cryogenic telescope, on the Space Shuttle at the end of this decade. LAIRTS will use a set of four 64x64 arrays, making up a 128x128 unit cell focal plane instrument, to image infrared sources at wavelengths of up to 25 microns. The LAIRTS array employs a relatively new method of reading out the data known as direct readout (DRO). To evaluate DRU technology, AFGL has obtained a 58x62 gallium-doped silicon DRO array, on loan from Santa Barbara Research Center, for

laboratory testing, followed by observing on the Wyoming Infrared Observatory (WIRO) 2.3-meter telescope.

The present array actually consists of two arrays: a 58x62 unit cell, gallium-doped silicon photoconductive detector array mated to a readout multiplexer. Photons incident on a detector array unit cell lead to current at the semiconductor junction which is integrated in the corresponding unit cell of the multiplexer array. Because the 'wells' in the readout multiplexer array hold a limited number of electrons (about  $10^6$  before nonlinearities become important) the array must be read out periodically. In a DRO device, each unit cell has its own output MOSFET. The voltage at the MOSFET's output is proportional to the charge stored in the readout array well. When a unit cell is addressed (in an X-Y coordinate manner), its MOSFET's output line is switched to one of the array output lines. The voltage is converted to a digital signal which is added by a computer to the sum of the previous readouts of that unit cell. The unit cell is then reset (by zeroing the charge in the well), and another integration cycle begins. No transfer of charge takes place, as in a CCD or CID, hence the name Direct Readout.

The gallium-doped silicon detector array is sensitive to radiation at wavelengths of up to about 18 microns. Because of absorption by the earth's atmosphere, use of this array will be limited to the 8-12 micron band. Since the atmosphere emits very strongly at these wavelengths, the wells fill up very quickly, and very short readout intervals are required. The high background radiation problem is even worse with the

AFGL array because only two output lines are available. This allows only two unit cells to be read out at once, which limits the total number of unit cells that can be read out before they fill up. Chopping techniques, in which the detector alternately looks at blank sky and the IR source of interest, must be used to subtract the background from the desired signal.

## II. OBJECTIVES:

The main objective of this project was to develop an electronics design to handle the very high data rate from this array. In the design discussed below, this problem is met by using 10 MHz Motorola MC68010 microprocessors to do much of the co-adding of array unit cells before sending the data to the Wyoming PDP-11 minicomputer for more complicated data processing and storage. This design is based on that used by Arens, Lamb, and Peck<sup>3</sup> to read out a CID array with similar background problems.

## III. THE ATMOSPHERIC BACKGROUND:

The intensity of the atmospheric background may be estimated by treating the atmosphere as a blackbody with a temperature of 295 K and an emissivity of 0.1.<sup>5</sup> The intensity at the detector is then:

$$I_{\lambda} = B_{\lambda} \epsilon A \quad (1)$$

$$\text{where } B_{\lambda} = (2hc^2/\lambda^5) (\exp (hc/\lambda kT) - 1)^{-1} \quad (2)$$

= brightness of thermal blackbody radiation

$\epsilon$  = emissivity of atmosphere  $\approx 0.1$

A = area of telescope primary mirror

At  $\lambda = 10$  microns,  $T = 295$  K, and  $A = 4.2 \times 10^4 \text{ cm}^2$  for the WIRO 2.3-meter telescope, we have:

$$I_{\lambda} = 8.9 \times 10^{-4} \text{ erg.s}^{-1}.\mu\text{m}^{-1}.\text{arcsec}^{-2} \quad (3)$$

The energy of a 10 micron photon is  $2 \times 10^{-13}$  ergs, so the photon flux is  $4.5 \times 10^9 \text{ s}^{-1}.\mu\text{m}^{-1}.\text{arcsec}^{-2}$ . Since the telescope is also emitting with approximately the same temperature and emissivity, the background is about:

$$I_{\lambda} = 10^{10} \text{ photons.s}^{-1}.\mu\text{m}^{-1}.\text{arcsec}^{-2}. \quad (4)$$

For a given number of photons incident on the detector, only a fraction of them are converted to electrons which are stored in the readout array wells. The detector quantum efficiency (DQE) is the number of electrons created in the detector array per incident photon. The photoconductive gain is the number of electrons stored in the readout array wells per electron created in the detector array. While the exact specifications for the present AFGL array are not yet available, both the DQE and photoconductive gain typically equal about 0.5. Therefore, for every electron stored in the readout array wells, approximately four photons interact with the detector array, and the expected 'fill rate per micron per square arcsec.' for the readout wells is approximately  $2.5 \times 10^9 \text{ electrons.s}^{-1}.\mu\text{m}^{-1}.\text{arcsec}^{-2}$ .

The rate at which the wells fill with electrons depends on two more parameters: the solid angle of sky viewed by a single unit cell, and the bandwidth of any filters in the

optical path. The optics for this array will be designed so that 2x2 unit cells will fit within the Airy diffraction disk of the 2.3-meter telescope at 10 microns. The diameter of this disk is 2.2 arcseconds, requiring a unit cell size of 0.78 arcseconds. Each unit cell therefore will view an area of about 0.6 square arcseconds on the sky (the exact area will depend on the spacing between the unit cells. Finally, to reduce the incident background radiation at the detector, filters with relatively narrow bandwidths of about 0.5 microns will be placed just above the detector.

In the above case, the fill rate becomes about  $7.5 \times 10^8$  electrons/sec. The well depth of the AFGL array is about  $10^6$  electrons, so the array must be read out about 750 times per second to prevent well overflows, implying a readout interval of only 1.3 milliseconds. In other words, if 100 unit cells are to be read out, then 50 read cycles must be executed in 1.3 ms (two unit cells are read out simultaneously, one for each output line). At the end of 1.3 ms, the first unit cell pair, which by now is almost full of electrons, is again read out, starting another 50 read cycles. While these calculations should be considered only approximate, the readout interval is of the same order of magnitude as that given for an array-telescope system with similar characteristics.<sup>4</sup>

#### IV. THE ELECTRONICS DESIGN:

Figure 1 shows a block diagram of the proposed system to handle the above data rate, which is so high that the PDP-11 alone would be able to process only a few unit cells in the

1.3 ms readout interval. Even the system discussed here will not be fast enough to process data from the entire array in this interval; only a subset of the array can be read out. The major components in the block diagram are summarized below. Note that the components on the 'even column' array output line are duplicated on the 'odd column' line.

PDP-11 : Will have overall control of entire system, including start and stop of integrations and final data processing and storage.

Timing Unit: Upon receipt of a PDP-11 command to commence an integration, the timing unit will control the more detailed steps of the integration process.

Amp : One preamplifier for each line amplifies the signal from the array.

CDS : Correlated Double Sampler. This is a circuit which samples the preamp's output just before and just after a unit cell's signal appears on the output line, and outputs the difference between the two readings. Acts as a filter of  $1/f$  noise in the output signal. The primary source of  $1/f$  noise is the output MOSFET's of the array.

S/H : Sample/Hold circuit. Samples the CDS output and holds it steady over the interval required for the A/D conversion.

ADC : Analog-to-Digital Converter. Converts the analog

output signal to a digital signal. A Burr-Brown model ADC 803CM with a 1.5 microsecond conversion time is recommended.

Dual Parallel Port Module : This is a Motorola model MVME 410 I/O board which allows communications between peripherals and the microcomputer board. Will be used both for input of unit cell data from the ADC and for output of co-added frame data to the PDP-11.

I/O Channel Interface : A Motorola model MVME 316 board which interfaces the I/O channel of the DPP module to the VME bus of the 68010 microcomputer board.

MC68010 Microcomputer Board : A Motorola model MVME 120 microcomputer module based on the MC68010 microprocessor. This board handles the co-adding of data as it comes through the DPP module from the ADC, and stores data temporarily until called upon to transfer the co-added frames to the PDP-11.\*

Because the timing unit, preamplifier, correlated double sampler, and sample/hold hardware has not yet been selected, only the general design of these components is discussed here.

The DRO array requires some rather complicated signals from the timing unit to address the unit cells.<sup>6</sup> To address

\* For detailed specifications of the ADC and these three Motorola boards, see the Burr-Brown ADC 803 data sheet and the appropriate Motorola user's manuals.

one of the 58 rows, two groups of seven lines each are provided. Setting three out of the seven lines in a group (allowing 35 combinations) to a high level instructs a decoder to address a certain row in that group. Only one group of seven lines is needed for the columns; a three out of seven input is decoded as for the rows, but a pair of adjacent columns is addressed. Therefore, by addressing both a row and a pair of columns, the signals of the two unit cells at the intersection appear on the two output lines; the signal of the odd-column unit cell appears on one line, and that of the even cell on the other. In addition to the 21 clock lines needed for the addressing, at least one line will be needed to reset the addressed pair of unit cells. The timing unit must be able to provide these clock and reset signals at precise time intervals. A good choice for the timing unit may be a third microcomputer board-Dual Parallel Port system. The DPP, as will be discussed later, has 32 data lines of which 21 could easily run the clocks. The microprocessor could simply step through the on-board memory, placing the clock codes stored in memory on the appropriate clock lines. Since the readout interval determined above is highly uncertain and may vary with changing atmospheric conditions, it will be desirable to adjust the size of the array subset actually in use in order to read out the maximum number of unit cells possible in the actual readout interval. This could be easily accomplished with a microcomputer timing unit by changing a few parameters in the software. Such a timing unit could also handle rela-

tively easily the other control lines traveling to and from it as shown in figure 1.

The operation of the correlated double sampler has been summarized above. More specifically, the CDS will first sample the preamplifier's output just after a unit cell is addressed. The unit cell will then be reset, and after an appropriate time interval the signal again will be sampled, and the voltage difference between the two samples will appear at the CDS output. A HOLD command to the sample/hold circuit then will clamp the voltage at the ADC input while the CDS circuit is reset and another unit cell is addressed. This CDS scenario is based on that given in White *et al.*<sup>7</sup> for a charge coupled device (CCD), but has been modified due to the difference in CCD and DRO readout steps. White *et al.* presents a circuit schematic which could be the basis for the present system.

The interval between the two CDS samplings will be dependent on the noise spectra of the output MOSFET's of the array. A sampling interval of time  $t$  will generally filter  $1/f$  noise with periods much longer than  $t$ . While the actual MOSFET noise spectra are not yet available, the interval for other systems is about 8 microseconds.<sup>3,6</sup> When the unit cell address time, amplifier settling time, reset time, and sample/hold acquisition time are added on, the total time to read a unit cell could be as long as 15 microseconds. These estimates are highly speculative, but it appears that this phase of the readout process will be about two times slower than the 68010 coadding phase. At 15 microseconds per unit cell pair, almost

174 unit cells (three rows) could be read out in the 1.3 millisecond time available. While this is only a fraction of the array, the system will still be 174 times faster than raster scanning with a single detector at similar resolution if this data rate can be achieved.

Once the sample/hold circuit has clamped its output voltage, the timing unit sends a short (about 100 nanosecond) CONVERT pulse to the ADC, then will go on to address the next unit cell. While the next cell is being read out, the ADC converts the analog input to a 12-bit digital output, and the 68010 adds this to the previous data from that unit cell. The proposed Burr-Brown ADC 803CM will perform the conversion in 1.5 microseconds. During the conversion, the status line of the ADC is high, and when it goes low the DPP module reads the transition as an End of Conversion (EOC) signal, and reads the data from the ADC.

The DPP module contains two MC6821 Peripheral Interface Adapter (PIA) IC's (no. 1 and no. 2). Each chip has two 8-bit ports and accompanying data registers (A and B), for a total of 32 data lines on the DPP. Each of the four data registers of the DPP is seen by the 68010 microprocessor as a memory location with a distinct address. Therefore, it is a simple matter for the 68010 to move data from the DPP ports to an internal data register and add it to data already stored in memory.

Each of the four ports also contains an 8-bit data direction register, an 8-bit control register, and two control

lines.<sup>8</sup> In this design, ports 1A and 1B are configured as input ports (by the software presented below), and ports 2A and 2B are output ports. The control register for port 1A is configured so that a high-to-low transition on C1A1 (port 1A, control line 1) will set bit 7 of control register 1A to a value of 1, and so that C1A2 is high when bit 7 is set. Bit 7 is cleared when data register 1A is read by the 68010.

As shown in figure 1, the ADC status line is connected to C1A1, and C1A2 leads to the timing unit. When the 68010 has finished the previous addition, it will poll bit 7 of control register 1A. The high-to-low transition of the ADC status line (the EOC signal) will set bit 7 and cause control line C1A2 to go high. The timing unit should be programmed not to send a new convert pulse to the ADC while C1A2 is high; this helps to prevent missing data, which would ruin an integration. When the 68010 finds bit 7 set, it reads the data registers 1A and 1B. Bit 7 is cleared after the data is read, which tells the timing unit that the data is safely within the microprocessor and the DPP is ready to accept more data from the ADC.

The data entering the 68010 from the DPP is a 16-bit word. The four most significant bits (MSB) are all zeroes; the twelve least significant bits (LSB) are ADC input. The co-added data stored in memory, however, will be 32-bit words, allowing  $2^{20} = 1,048,576$  additions of 12-bit ADC data. At 1.3 milliseconds per readout, integrations of over 200 minutes will be possible before longer words are required. In practice, most integrations will be only a few minutes long. The 68010 will add the new data to the proper memory location,

then will resume polling of bit 7 of control register 1A, as described above, until new data become available.

#### V. SOFTWARE AND OPERATING MODES:

A preliminary software subroutine to execute the basic co-adding operations is presented in table 1. This subroutine is written in M68000 assembly language code. The five columns are: (1) Line number; (2) Label; (3) Instruction Mnemonic; (4) Instruction operand; (5) Comment. (Please refer to one of the many M68000 programming books for the details of M68000 instructions and the assembly language format.) In summary, lines 1-10 set various labels equal to hexadecimal constants. Lines 12 and 13 reserve locations in memory for the size of the array to be read out and the start address of the co-added memory block. Lines 15-24 begin the actual program by initializing data and address registers of the 68010, and initializing the data direction and control registers of the DPP so that they will function as described above. Lines 25-29 compose the actual loop that the 68010 executes once per unit cell readout. At 10 MHz clock frequency, the 68010 will require 6 microseconds to execute this loop. Adding the 1.5 microseconds required for the A/D conversion shows that this phase will run faster than readout phase time of about 15 microseconds.

This program was written to estimate the time involved in the co-adding phase, and will require considerable modification before it can be implemented. Lines 1-23 will probably

be part of a master program which calls the loop of lines 25-30. The master program will determine the starting address of the memory block that stores the co-adding results, and will interpret information from the PDP-11 to determine when to begin and end the co-adding to a certain block of memory (see below).

The timing unit and the 68010 will have to keep track of the chopping from source to background. Chopping is accomplished by wobbling the secondary mirror of the telescope. The PDP-11, which controls the chopping, will have to tell the timing unit to stop integrating while the mirror is in motion, then to resume integrating when finished. The PDP-11 will also have to tell the 68010 whether the detector is looking at the source or the background. These connections, while they have not yet been worked out in detail, could probably be accomplished with two lines as shown in figure 2. The INTEGRATE line would be high when the detector is supposed to be taking data and low when it is not. The CHOP line would be high when on the source and low when on the background. The 68010 then would be programmed to co-add to a different block of memory for source and background data.

In normal use, the 68010 memory will probably consist of two blocks; a block for source data and a block for background data. The 68010 will alternate between the two blocks depending on the chop position as the integration progresses. At the end of an integration, the data contained in each block would be placed on the output lines to be read by the PDP-11. Several other operating modes are possible, however. For

example, instead of alternating between two blocks of memory, the 68010 could write the data from each chop into a different block. This way the data from a 'bad' chop cycle (say, one in which unusual noise is present), could be removed from the good data before the individual chops are co-added. This may be a useful mode in the testing phase of the program. The length of an integration would be limited, by the amount of memory present on the board, to a few seconds, however, so more frequent data dumps to the PDP-11 would be required.

The co-added frame data will be transferred to the PDP-11 over two standard 16-bit I/O buses, one for each of the two 68010 boards. One 68010 could write 16 bits of a 32-bit word into one PDP-11 data buffer while the PDP-11 reads the data in its other buffer. The PDP-11 could recombine the data into 32-bit words for storage and processing.

## VI. RECOMMENDATIONS:

The next step in designing this system is to determine the timing requirements of the CDS, which will drive the overall speed of the entire system. The timing signals necessary to run the CDS, sample/hold circuit, and ADC will determine if a standard microcomputer board will serve as a timing unit, or if the timing unit will have to be custom built. The 68010-to-PDP-11 interface needs to be more fully developed; and, lastly, the software to run the timing unit, 68010 microprocessors, and the PDP-11 needs to be written and tested.

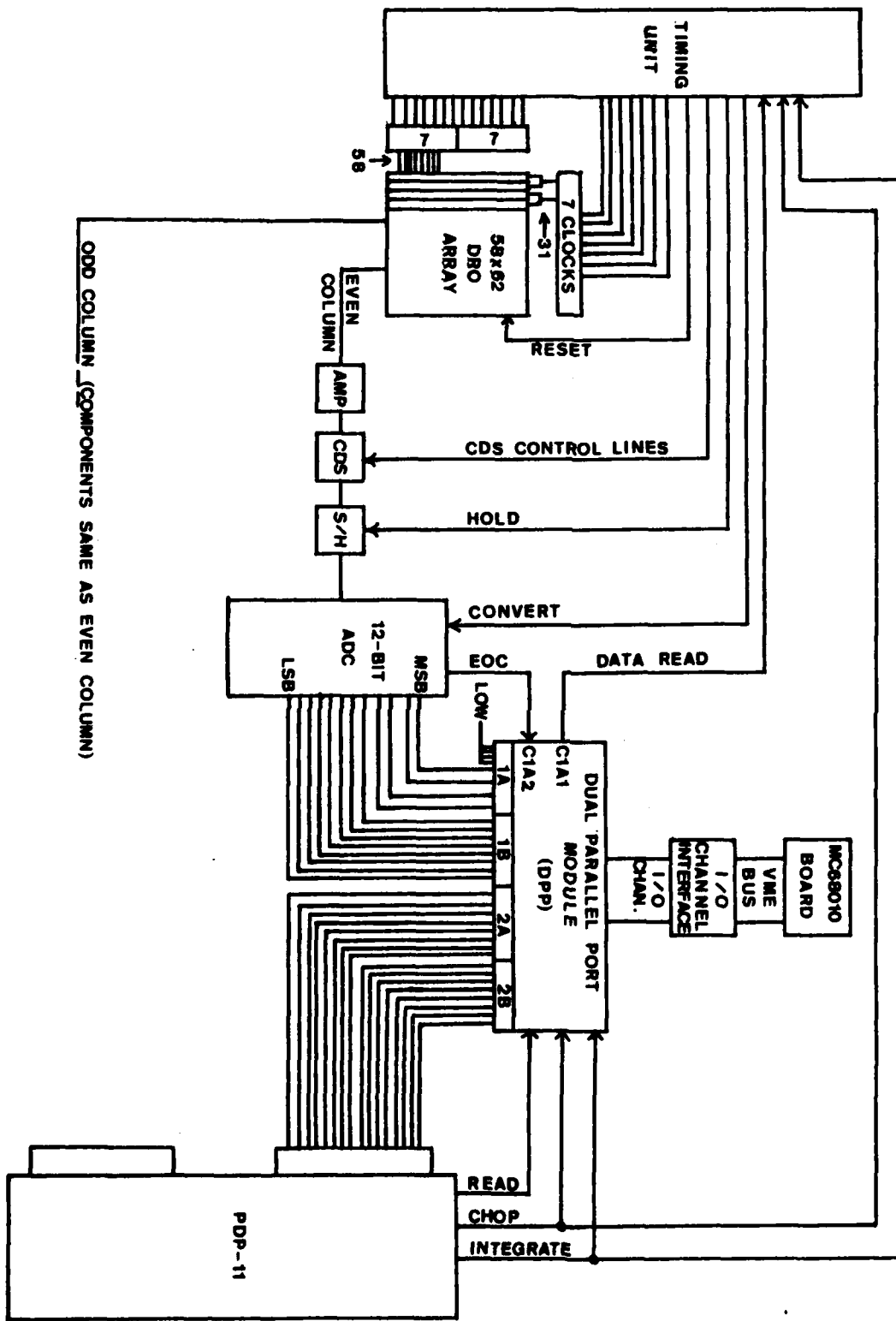


Fig. 1: Electronics Block Diagram  
26-18

Table 1: Co-adding Subroutine

1	DATA	EQU	\$4000	
2	PROGRAM	EQU	\$6000	
3	DPP	EQU	\$0	Dual Parallel Port Base Address
4	DD1A	EQU	\$0	Offset port 1A data dir. register
5	DR1A	EQU	\$0	Offset port 1A data register
6	CR1A	EQU	\$1	Offset port 1A control register
7	DD1B	EQU	\$2	Offset port 1B data dir. register
8	DR1B	EQU	\$2	Offset port 1B data register
9	CR1B	EQU	\$3	Offset port 1B control register
10	CREG	EQU	\$24	High-to-low on C1A1 sets CR1A bit 7 and C1A2 until data read
11		ORG	DATA	
12	LENGTH	DSW	1	No. of pixel pairs to add
13	STADDR	DSL	1	Start address of co-added memory
14		ORG	PROGRAM	
15	PGM COADD	MOVEA.L	#DPP,A0	Get DPP base address
16		MOVE.W	LENGTH,D0	Init. pixel count
17		SUB.W	#1,D0	Branch on -1
18		MOVE.B	#7,D1	Init. for BTST
19		CLR.B	CR1A(A0)	Init. control reg. 1A
20		CLR.B	CR1B(A0)	Init. control reg. 1B
21		CLR.B	DD1A(A0)	Port 1A is an input
22		CLR.B	DD1B(A0)	Port 1B is an input
23		MOVE.B	#CREG,CR1A(A0)	Configure control reg. 1A
24		MOVEA.L	STADDR,A1	Get addr. of first memory location
25	LOOP	BTST.B	D1,CR1A(A0)	Has A/D conv. been completed? (8)*
26		BEQ	LOOP	If not then loop (6)
27		MOVEP.W	DR1A(A0),D2	Else move 16-bit A/D data to D1 (16)
28		ADD.L	D2,(A1)+	Add D1,(A1),store in (A1), increment (20)
29		DBF	D0,LOOP	If count = -1, LOOP(10)
30		RTS		Else end subroutine
31		END	PGM COADD	

\* Numerals in parentheses are the number of clock cycles required to execute the instruction on the 68010, taken from the M68000 Programmer's Reference Manual, fourth edition, which is available from Motorola. The co-adding loop (lines 25-29) requires 60 clock cycles to execute, or 6 microseconds if the 68010 is running at 10 MHz.

## REFERENCES

1. John A. Hackwell, Gary L. Grasdalen, and Robert D. Gehrz, "10 and 20 Micron Images of Regions of Star Formation," Astrophys. J., Vol. 252, pp. 250-268, 1982.
2. Astrophys. J. (Letters) special issue of IRAS results, Vol. 278, pp. L1-L85, 1984.
3. John F. Arens, Gerald M. Lamb, and Michael C. Peck, "Infrared Camera for Ten Micrometer Astronomy," Optical Engineering, Vol. 22, pp. 267-268, 1983.
4. John F. Arens, G. M. Lamb, M. C. Peck, H. Moseley, W. Hoffmann, R. Tresch-Fienberg, and G. G. Fazio, "High Spatial Resolution Observations of NGC 7027 with a 10 Micron Array Camera," Astrophys. J., Vol. 279, pp. 685-693, 1984.
5. John A. Hackwell, private communication.
6. Donald C. Campbell, SBRC private communication.
7. Marvin H. White, Donald R. Lampe, Franklyn C. Blaha, and Ingham A. Mack, "Characterization of Surface Channel CCD Image Arrays at Low Light Levels," IEEE Journal of Solid-State Circuits, Vol. SC-9, pp. 1-12, 1974.
8. Gerry Kane, Doug Hawkins, and Lance Leventhal, 68000 Assembly Language Programming, (Osborne/McGraw-Hill, Berkeley, Ca., 1981), chapter 13.

**1984 USAF-SCEEE GRADUATE STUDENT SUMMER SUPPORT PROGRAM**

Sponsored by the

**AIR FORCE OFFICE OF SCIENTIFIC RESEARCH**

Conducted by the

**SOUTHEASTERN CENTER FOR ELECTRICAL ENGINEERING EDUCATION**

**FINAL REPORT**

**THE FACTOR ANALYSIS METHODOLOGY**  
**APPLIED TO MOE CATEGORIZATION AND EVALUATION**

Prepared by: ron r. hightower  
Academic Department: Electrical Engineering  
University: Kansas State University  
Research Location: Air Force Weapons Laboratory, Advanced  
Control Division, Advanced Laser Optics  
Branch  
USAF Research Contact: Dr. Al Davenport  
SFRP Supervising  
Faculty Member: Dr. Eddie Fowler  
Date: August 1, 1984  
Contract No: F49620-82-C-0035

The Factor Analysis Methodology  
Applied to MOE Categorization and Evaluation

by

Ron Hightower

ABSTRACT

An introductory discourse on network MOEs (measures of effectiveness) provides the reader with a brief background and comments on some of the problems associated with MOEs. Following this the methodology of factor analysis is outlined and its applicability to MOE analysis is explained. The three phases of the method are demonstrated using actual MOEs. First the intercorrelation coefficients of the MOEs are calculated. This is followed by the actual factor analysis which in this paper was done using the Principal Axis Method. The results of the analysis are interpreted and the method as a whole is evaluated. Recommendations are made as to improvements of the method.

ACKNOWLEDGEMENTS

This is just a note of thanks to the Air Force Systems Command, the Air Force Office of Scientific Research, and the South Eastern Center for Electrical Engineering Education. I would like to also acknowledge the weapons laboratory for allowing us access to their computing facilities at various times of the day and night and for providing an excellent work environment which made this research possible.

Thanks also to fellow researchers Russ Thomas and Kurt Ziegler, whose help and involvement provided the basis of this report. And also Dr. Eddie R. Fowler, my SRRP supervisor, without whom this paper might never have happened.

## I. Introduction

Communications networks are used in many ways by the armed forces. Old networks are constantly being updated and new networks are being designed. When designing or updating networks it is necessary to evaluate the old ones with respect to some criteria in order to discover their flaws. New networks must be evaluated to justify their construction.

It is difficult to determine if a network is good because the term 'good' may refer to many characteristics and is very subjective. A network may be good with respect to how many users are serviced, what percentage of the time a message will complete its intended path, how susceptible the network is to wartime degradation, how well information travels through the system during various times of use, and how much the network will cost to build and maintain.

The above list of characteristics provides an idea as to what is important in evaluating communications networks. The concepts of susceptibility and information flow are not well defined and can only be evaluated subjectively. A subjective evaluation of these characteristics would provide answers such as 'very susceptible' or 'not good flow' which are of limited usefulness.

To avoid subjective evaluation, network characteristics are quantified through the use of an equation. By using an equation to evaluate a network a well-defined answer is produced that is consistent irregardless of who calculated it. Any number that quantifies evaluation can be called a measure of effectiveness (NOE). A network NOE uses the basic, defining qualities of a network and provides a number which can be used objectively to discuss a network's worth.

A communications network can be represented with a small set of numbers which reflect all the network's characteristics. All real world qualities can be combined into the numbers of this list:

- (1) Probability that a message will traverse a given link.
  - (2) Maximum amount of information flow possible through a link.
  - (3) The probability that a message will traverse a node.
  - (4) Maximum amount of flow possible through a given node.
  - (5) Some numbers which represent the shape (topology) of the network.
- The cost of building a network is not considered in this paper.

Some MOEs that are commonly referred to in the literature are connectivity, path reliability, shortest path from source node to destination node, maximum flow from a source node to destination node.

Connectivity is defined as the ratio of node pairs that can communicate after network disruption to the number of node pairs that could communicate originally.

Path Reliability is the probability that a given source node can talk to a given destination node.

Shortest Path between nodes does not always refer to physical distance. In communications networks the shortest path often means the fastest path from node to node and total distance means the total time of message travel.

Maximum Flow is a measure of how much information traffic can flow from a source node to a destination node. Since every link can only handle a limited amount of traffic then there exists some upper limit on the total amount of information traffic from node to node and this MOE is that limit.

## II. Objectives

The objective of this research was to learn factor analysis, a powerful mathematical tool, and apply it to the analysis of networks. Originally the factor analysis method was also to be applied to network simulation computer programs but this proved to be a fruitless pursuit as will be briefly explained later.

After the initial learning stage was underway it became apparent that the factor analysis method could be of great use in evaluating and categorizing MOEs. Depending on the results of the analysis it might be possible to replace the large number of MOEs with a few representative MOEs which would still provide the same ability in evaluating networks.

## III. MOEs, MODs, CMOEs, and Degrees of Meaningfulness

A lengthy list of MOEs was developed and eventually it was noticed that some of the MOEs had a different flavor than the others. The distinction became apparent when computing the MOEs for a small set of example networks. It proved very difficult to evaluate all the MOEs in a consistent manner and still use the original definitions.

The MOEs were divided into three classes: Network Measures of Effectiveness, Measures of Degradation, and Component Measures of Effectiveness. Although related they differ in usage.

A Network MOE is any numerical quantity that refers to the overall performance of the network. An example of this is the probability that the network is connected (PC). Since every link has a certain probability of being able to pass messages, then there is a certain probability that one or more nodes will be completely separated from the network. PC is the probability that every node can talk to every other node through some path. It is an MOE that evaluates the network as one whole entity.

In contrast to Network MOEs there exist Component MOEs which refer to only a part of the network. A network can be subdivided in several ways and the subdivisions can be evaluated separately. The separate values can then be combined in various ways to produce Network MOEs. Hofstadter referred to this type of analysis as Reductionism, where the whole system is evaluated by examining its parts, as opposed to Holism where the system is evaluated as one entity. Examples of network subdivisions are links, nodes, source-destination node pairs, and local neighborhoods within the network. Examples of these MOEs respectively are link redundancy, flow per node, maximum flow from source to destination, and link connectivity which evaluates a small neighborhood with respect to a given link usefulness.

In addition to MOEs and CMOEs a class of quantification was derived which measured, directly or inversely, the amount of degradation that a network had sustained. These were called Measures of Degradation (MODs). An example MOD is connectivity. Because connectivity is a ratio of node pairs before and after degradation, it will always be exactly one unless some degradation occurs. Another example of MOD type values is the percentage of links down, i.e. the percentage of links in the network that are unable to pass messages.

There are two kinds of MODs; directly and inversely related MODs. Links Down is a direct MOD because as the number of links down increases the amount of degradation increases. Connectivity is an inverse MOD because of connectivity decreases (from 1.0 to 0.0) the amount of degradation increases. They are inversely related.

The distinction between MOEs and MODs will become important later.

MOEs have different degrees of meaningfulness and this corresponds to different amounts of resolution. An MOE with high resolution will have a low degree of meaningfulness and vice versa.

In the introduction a list of characteristics was presented which included, for example, susceptibility to wartime degradation. If an MOE existed which directly quantized susceptibility then this MOE would have a high degree of meaningfulness because it would quantize a high level concept. This same MOE would have low resolution for the same reason. By quantizing a high level concept this MOE would be ignoring the details of the network being evaluated. This is analogous to viewing an oil painting from so far away that the fine brush strokes used by the artist can no longer be seen but only the picture itself is visible.

Other MOEs exist which have low degrees of meaningfulness and therefore high resolution. An example of a high resolution MOE is the number found by averaging the link probabilities of the network together. Average Link Probability is somewhat useful in evaluating a network because it reflects the basic robustness of the network's links. At the same time it ignores the topology of the network and the information flow associated with the links. A lot of information is being ignored when this MOE is calculated and so it is said to have a low degree of meaningfulness. This is analogous to viewing the oil painting from so close that it is impossible to discern the features of the actual picture.

This is a list of MOEs discussed in this paper and their approximate meaningfulness:

HIGH	WNR.....NR weighted for all network degradation configurations.
HIGH	LC.....Link Connectedness rates all links for redundancy and loading.
HIGH	AVEREL...The average probability that node pairs are connected.
HIGH	PC.....The probability that all node pairs are connected.
MED	CON.....The ratio of connected node pairs after and before degradation.
MED	NODPRB...Average probability that node has at least one link up.
MED	AVESP....Average length of all shortest paths between node pairs.
MED	AVEMAX...Average of maximum flow possible between node pairs.
MED	AVENIP...Average number of independent paths between node pairs.
LOW	NODFLO...Average amount of incident flow per node.
LOW	AVEPRB...The average of all link probabilities.

MOEs with high meaningfulness are usually difficult to validate because they quantify high level concepts which are not well defined. No objective standard exists for testing the MOE against. For example, if an MOE supposedly quantified the susceptibility of a network to wartime degradation there would be no good number to test it with. If a number already existed with quantified the network susceptibility then where did it come from? and how was its validity checked? It is possible that if several MOEs existed that were supposed to quantify the same characteristic, like susceptibility, then they could all be tested against each other and some sort of consensus could be derived. (This is basically what Factor Analysis achieves.) But the consensus would not necessarily equate with susceptibility because there is no guarantee that the entire set of MOEs is not also quantifying some other characteristic. There might be a hidden characteristic which all the MOEs have in common, that is not related to susceptibility. This is a problem with Factor Analysis in that when a common factor is mathematically produced there is nothing which explicitly says what that factor is. It must be interpreted and the results are then somewhat subjective.

Low level concepts are easier to validate because the answer is known intuitively. If an MOE quantifies a low level concept, such as average link probabilities, then the answer is easy to check by hand. Low level MOEs tend to be used more widely because they are easier to accept. Connectivity is a straight forward MOE, for example, which is easy to validate and it is very widespread in the literature. MOEs which try to evaluate many concepts at the same time, such as link connectivity, will not enjoy very widespread popularity.

The remainder of the paper outlines the Factor Analysis methodology and its implementation. An actual MOE analysis is used as an example of the process and the results are interpreted as the final step. Some recommendations for the improved use of this methodology follow that.

#### IV. Factor Analysis

Factor Analysis takes a set of tests, such as MOEs, and attempts to find a reduced set of tests which still provide the same power in testing subjects. Typically, Factor Analysis has been applied to psychological tests and most of the literature deals with that aspect of its use. A set of tests is applied to some group of people and the results are factor analyzed. The results would provide the researcher with a reduced set of tests or perhaps an idea for new, more useful tests. It depends of whether the researcher is looking for the common factors that his group of people share or if he is trying to find a small set of tests to use in further experiments. In this paper the emphasis was on finding a reduced number of tests for deciding the 'goodness' of future networks, although there was some interest in finding any factors that networks share other than the self-evident ones.

(Just as a side note. The Factor Analysis Method had been suggested as a way to analyze computer simulations and determine which of the inputs were less important than others. The idea was to factor analyze the inputs and the outputs together and if any of the inputs were close to the outputs then they were 'important'. The problem was that a correlation coefficient, explained in the next paragraph, determines how linear a relationship is and not how sensitive one variable is to a second. An attempt was made to replace the correlation matrix with a 'sensitivity matrix' but it was decided that if a sensitivity matrix could be somehow be produced then that would be the answer and factor analysis wouldn't be necessary. QED)

The correlation coefficient measures to what extent two tests, two MOEs for example, are testing a common characteristic. A coefficient of .75 means that the two MOEs share just enough in common to be worth mentioning. Anything below .7 is only correlated a little. Two MOEs which are correlated better than .9 are quantifying a shared factor, although each has some specific characteristic that the other is not. Above .98 the two MOEs are evaluating the same characteristic.

Although Fruchter<sup>1</sup> mentions several different types of correlation coefficients he disclaims most of them as being unsuitable for factor analysis. Rummel<sup>2</sup> gives an interesting discourse on intervariable relationships and gives an equation for calculating the product moment correlation coefficient (to which Fruchter had given his blessing). Lipson and Sheth<sup>3</sup> reduced this same product moment equation into a more useful form, given below:

$$r = \frac{n\sum xy - \sum x \sum y}{\text{SQRT}((n\sum x^2 - (\sum x)^2)(n\sum y^2 - (\sum y)^2))} \quad (1)$$

The coefficient,  $r$ , can be from 1.0 (perfect correlation) to 0.0 (no correlation) to -1.0 (inversely perfect correlation). To convey an idea about how closely related variables have to be to produce certain values of correlation, the plots in figure 1 were drawn out. Normally these plots would not need to be drawn but they do provide an idea about how the variables are interrelated.

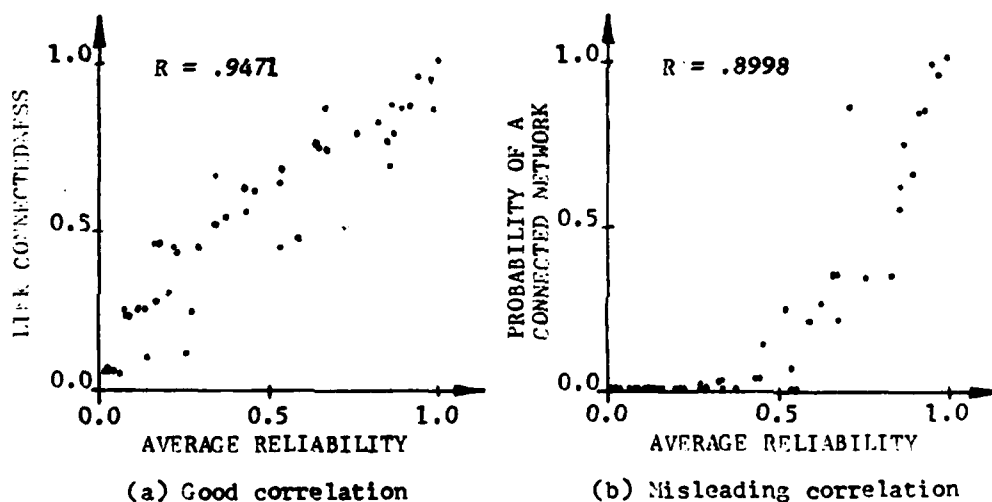


Figure 1. Illustration of correlations between variables.

Figure 1 shows a problem with the moment-product correlation coefficient. The data points in figure 1a lie roughly along a line from the lower left corner to the upper right corner. The r-coefficient in this case is measuring how far the points are spread away from the imaginary line that passes through them. In figure 1b this is not the case exactly. It can be seen that two distinct parts exist in this plot. On the left there is a portion where all the data points lie next to the lower axis. This means that the vertical value is very close to zero, independent of the horizontal values. The correlation coefficient for just this portion of the graph would be very low. The right half of the graph, however, brings this number up in value and actually makes it fairly high. The correlation between these variables is at the same time good and bad. Because the correlation coefficient is a single number there is only so much information that it can reflect. According to Fruchter, Rummel, Lipson, and Sheth; the moment-product correlation coefficient does all right.

The correlation coefficient must be calculated between every two NOEs and the values are then put into a symmetrical matrix. An example correlation matrix is shown in table 1a. It was calculated from the data in table 2. There are a number of methods used in Factor Analysis which convert the correlation matrix into a set of factors and these different methods really form the basis of Factor Analysis.

Before continuing with the Factor Analysis process, the method of computing the correlation matrix should be expounded upon.

The first step was to choose a list of NOEs to evaluate. Factor Analysis is rather sensitive to the list of tests being analyzed. If two tests share some sort of mathematical dependence then it is possible for new factors to be introduced that do not actually exist.<sup>2</sup> This was a difficult restriction to observe because network NOEs are by nature mathematical entities, unlike the psychological tests that Factor Analysis is usually applied to. Two NOEs may be mathematically related through some hidden process and this could influence the results harmfully.

An example of a hidden mathematical dependence was provided when a new MOE was being developed. The idea was to take a given network and calculate connectivity for all the possible ways that the network could be degraded. Each possible network degradation would have a certain probability of occurring and this number would be multiplied by the connectivity calculated for that configuration. This WC MOE, unfortunately, turned out to be the exact same test as Average Reliability. But that fact was not discovered until the correlation matrix was calculated and a 1.000 was found in the appropriate place. WC is calculated in a similar way as WC (weighted connectivity) and it is possible that the high correlation between the two is due to this mathematical relationship.

In addition to WC, connectivity and average degree were left out of the MOE list. Also average-number-of-independent-paths. With all the flow-per-link values set equal to 1.0, some of these MOEs became the same test. When all flows equal one the maximum flow between a source node and destination node is the same value as the number of independent paths so AVEMAX is the same as AVENIP. The same is true for AVEDEC and NODFLO. Degree is the number of links incident to a given node and flow-per-node is the sum of flows incident to a given node and with all the flows equal to one these are the same.

Having carefully picked a list of MOEs to evaluate it became time to choose a set of subject networks to use the MOEs upon. Because some of the MOEs took a very long time to compute for networks with lots of links it was necessary to limit the networks to only ten links. If time had permitted then larger networks would have been used but time was a limited quantity. Ten representative networks were chosen for some particular qualities that needed to be tested. The maximally connected network (see figure 2a) is the best network known to modern networkology. On the other hand, the straight-line network is the very worst in some respects (2c). The basis for picking these particular networks was to find the boundaries of all possible networks and then all other networks would have to fall within that envelope.

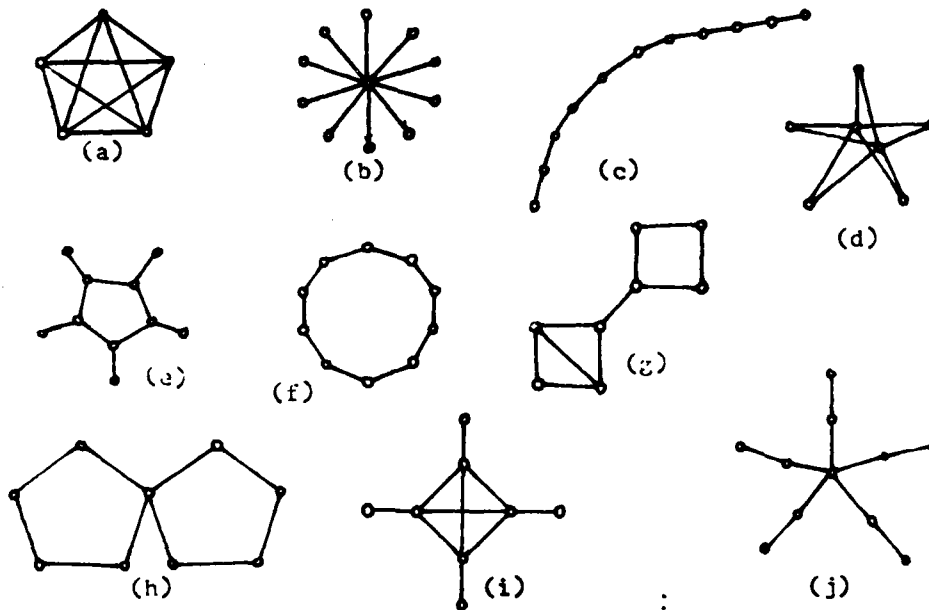


Figure 2. Networks used in analysis.

Each of the ten networks above was used five times; once with all link probabilities equal to 0.1, once with all link probabilities equal to 0.3, 0.5, 0.7, and 0.9. This provided a sample of 50 networks.

Principal Axis Method

There is not space here to outline the principal axis method. It is well defined in Fruchter's book<sup>1</sup>. Briefly, the correlation matrix is tested to see if the sum of the columns is equal to the sum of the dot-products of the rows with the column-sum vector. If they are not equal then the matrix is squared and the test is made again. When the test finally succeeds then the factor loadings are derived from the column sums. These factor loadings are used to calculate the residual matrix. This residual matrix is in then tested and squared like the original matrix until the test passes. The factor loadings derived from the columns sums this time belong to the second factor. This continues until all the meaningful factors are determined. Table 1b shows the factor loadings derived from the correlation matrix above it.

	WNR	LC	AVEREL	PC	NODPRB	AVESP	AVEMAX	NODFLO	AVEPRB
WNR	0.0000	0.9351	0.9723	0.8964	0.8514	-0.2040	0.1961	0.2178	0.9235
LC	0.9351	0.0000	0.9471	0.7931	0.9585	-0.1195	0.1716	0.1860	0.9698
AVEREL	0.9723	0.9471	0.0000	0.8998	0.8955	-0.3204	0.3250	0.3611	0.8963
PC	0.8964	0.7931	0.8998	0.0000	0.6996	-0.3390	0.4636	0.4748	0.7117
NODPRB	0.8514	0.9585	0.8955	0.6996	0.0000	-0.1024	0.2103	0.2131	0.9366
AVESP	-0.2040	-0.1195	-0.3204	-0.3390	-0.1024	0.0000	-0.6216	-0.7208	0.0000
AVEMAX	0.1961	0.1716	0.3250	0.4636	0.2103	-0.6216	0.0000	0.9137	0.0000
NODFLO	0.2178	0.1860	0.3611	0.4748	0.2131	-0.7208	0.9137	0.0000	0.0000
AVEPRB	0.9235	0.9698	0.8963	0.7117	0.9366	0.0000	0.0000	0.0000	0.0000

Table 1a. Correlation matrix for nine measures of effectiveness.

	WNR	LC	AVEREL	PC	NODPRB	AVESP	AVEMAX	NODFLO	AVEPRB
FACTOR 1	0.8697	0.8647	0.8987	0.8252	0.8286	0.3047	0.3625	0.3813	0.8099
FACTOR 2	0.3972	0.5003	0.2453	-0.0382	0.4314	-0.5054	-0.5735	-0.5980	0.6349
FACTOR 3	0.3326	0.2971	0.4634	0.4293	0.2570	0.4116	0.5058	0.5428	0.1093
FACTOR 4	-0.3917	0.1457	-0.2904	-0.4375	0.3101	0.1034	0.2425	0.2686	0.0444

Table 1b. Significant factors calculated from table 1a.

WNR	LC	AVEREL	PC	MODPRB	AVESP	AVEMAX	MODFLO	AVEPRB
0.0277	0.1141	0.1313	0.0081	0.3439	1.0000	4.0000	4.0000	0.1000
0.2005	0.4367	0.5253	0.2563	0.7599	1.0000	4.0000	4.0000	0.3000
0.4549	0.7538	0.8535	0.7109	0.9375	1.0000	4.0000	4.0000	0.5000
0.6924	0.9396	0.9814	0.9575	0.9919	1.0000	4.0000	4.0000	0.7000
0.8999	0.9933	0.9998	0.9995	0.9999	1.0000	4.0000	4.0000	0.9000
0.0057	0.0833	0.0264	0.0000	0.1501	1.8182	1.0000	1.8182	0.1000
0.0526	0.2581	0.1282	0.0000	0.3611	1.8182	1.0000	1.8182	0.3000
0.1727	0.4422	0.2955	0.0010	0.5454	1.8182	1.0000	1.8182	0.5000
0.3976	0.6271	0.5282	0.0282	0.7273	1.8182	1.0000	1.8182	0.7000
0.7586	0.8122	0.8264	0.3487	0.9091	1.8182	1.0000	1.8182	0.9000
0.0040	0.0875	0.0200	0.0000	0.1736	4.0000	1.0000	1.8182	0.1000
0.0295	0.2727	0.0746	0.0000	0.4718	4.0000	1.0000	1.8182	0.3000
0.0964	0.4673	0.1637	0.0010	0.7045	4.0000	1.0000	1.8182	0.5000
0.2537	0.6627	0.3280	0.0282	0.8718	4.0000	1.0000	1.8182	0.7000
0.6326	0.8583	0.6771	0.3487	0.9736	4.0000	1.0000	1.8182	0.9000
0.0086	0.0871	0.0419	0.0000	0.2305	2.2500	1.4643	2.5000	0.1000
0.0688	0.2938	0.1715	0.0034	0.5835	2.2500	1.4643	2.5000	0.3000
0.2196	0.5239	0.3776	0.0684	0.8125	2.2500	1.4643	2.5000	0.5000
0.4869	0.7332	0.6521	0.3536	0.9415	2.2500	1.4643	2.5000	0.7000
0.8345	0.8742	0.9166	0.8332	0.9945	2.2500	1.4643	2.5000	0.9000
0.0049	0.0800	0.0247	0.0000	0.1900	2.7778	2.0000	2.0000	0.1000
0.0381	0.2480	0.0952	0.0001	0.5100	2.7778	2.0000	2.0000	0.3000
0.1319	0.4248	0.2208	0.0107	0.7500	2.7778	2.0000	2.0000	0.5000
0.3642	0.6025	0.4693	0.1493	0.9100	2.7778	2.0000	2.0000	0.7000
0.8067	0.7802	0.8765	0.7361	0.9900	2.7778	2.0000	2.0000	0.9000
0.0053	0.0856	0.0260	0.0000	0.1855	2.3333	1.2222	2.0000	0.1000
0.0460	0.2677	0.1122	0.0001	0.4785	2.3333	1.2222	2.0000	0.3000
0.1636	0.4681	0.2743	0.0059	0.6875	2.3333	1.2222	2.0000	0.5000
0.4103	0.6769	0.5392	0.0888	0.8365	2.3333	1.2222	2.0000	0.7000
0.7950	0.8661	0.8678	0.5424	0.9495	2.3333	1.2222	2.0000	0.9000
0.0044	0.0819	0.0213	0.0000	0.1690	2.5455	1.0000	1.8182	0.1000
0.0368	0.2568	0.0904	0.0000	0.4438	2.5455	1.0000	1.8182	0.3000
0.1284	0.4418	0.2159	0.0010	0.6563	2.5455	1.0000	1.8182	0.5000
0.3288	0.6244	0.4293	0.0282	0.8225	2.5455	1.0000	1.8182	0.7000
0.7108	0.7992	0.7689	0.3487	0.9500	2.5455	1.0000	1.8182	0.9000
0.0066	0.0912	0.0322	0.0000	0.2071	2.1667	2.0000	2.2222	0.1000
0.0557	0.2876	0.1364	0.0009	0.5378	2.1667	2.0000	2.2222	0.3000
0.1951	0.5128	0.3281	0.0352	0.7708	2.1667	2.0000	2.2222	0.5000
0.4756	0.7547	0.6286	0.2790	0.9191	2.1667	2.0000	2.2222	0.7000
0.8549	0.9552	0.9388	0.8437	0.9911	2.1667	2.0000	2.2222	0.9000
0.0130	0.0817	0.0613	0.0001	0.2527	1.5238	2.1429	2.8571	0.1000
0.1155	0.2663	0.2844	0.0214	0.6020	1.5238	2.1429	2.8571	0.3000
0.3384	0.4820	0.5985	0.2061	0.8125	1.5238	2.1429	2.8571	0.5000
0.6235	0.6982	0.8613	0.6110	0.9350	1.5238	2.1429	2.8571	0.7000
0.8897	0.8574	0.9856	0.9508	0.9929	1.5238	2.1429	2.8571	0.9000
0.0095	0.0906	0.0452	0.0000	0.2220	1.8571	1.4286	2.5000	0.1000
0.0816	0.3152	0.2018	0.0018	0.5300	1.8571	1.4286	2.5000	0.3000
0.2480	0.5512	0.4330	0.0371	0.7188	1.8571	1.4286	2.5000	0.5000
0.5027	0.7393	0.6824	0.2143	0.8459	1.8571	1.4286	2.5000	0.7000
0.8195	0.8564	0.9005	0.6534	0.9499	1.8571	1.4286	2.5000	0.9000

Table 2. 50 networks tested for 9 measures of effectiveness.

## RESULTS

The factor loadings in table 1b. are graphically reproduced in figure 3. The principal axis method of deriving factors finds a least squares solution<sup>1</sup> which extracts the maximum amount of variance from each factor. It also produces a unique solution which is a main advantage of the principal axis method. What it does not do is align factors so that they pass through clusters of MOEs.

Fruchter describes a mathematical definition for clusters which involved the calculation of a 'B-coefficient'. The B-coefficient gives the ratio of the average intercorrelation of the variables in a cluster to their average correlation with the variables not included in the cluster<sup>1</sup>. Fruchter mentions an arbitrary threshold of 1.3 for the B-coefficient but then says that the goal is to find the highest possible value.

For the cluster of points (1,2,3,4,5,9) the B-coefficient was found to be 4.0838 and that was the highest value calculated. Since the factors are by no means fixed in place, Factor 1 was rotated until it passed through the center of the cluster. (note that factors 1 and 2 were rotated together to preserve orthogonality.) The center of the cluster was found by averaging all the factor loadings of the MOEs within the cluster. The center was: F1=.85, F2=.36 which is just below MOE number 1 in the figure (WNR).

## INTERPRETATIONS

What has occurred, then, is the appearance of two MOE clusters which are almost perfectly orthogonal. In Factor Analysis if two vectors are orthogonal then there is zero correlation between the two. The results here are not at all surprising, but they are revealing. The cluster of 6,7, and 8 (average shortest path, average maximum flow, and average flow incident per node) are all MOEs based on the link-flow values and the general topology of the network. On the other hand, the cluster of 1,2,3,4,5, and 9 dealt with the link probabilities mostly, the general topology in a most cases, and the link-flow values not at all.

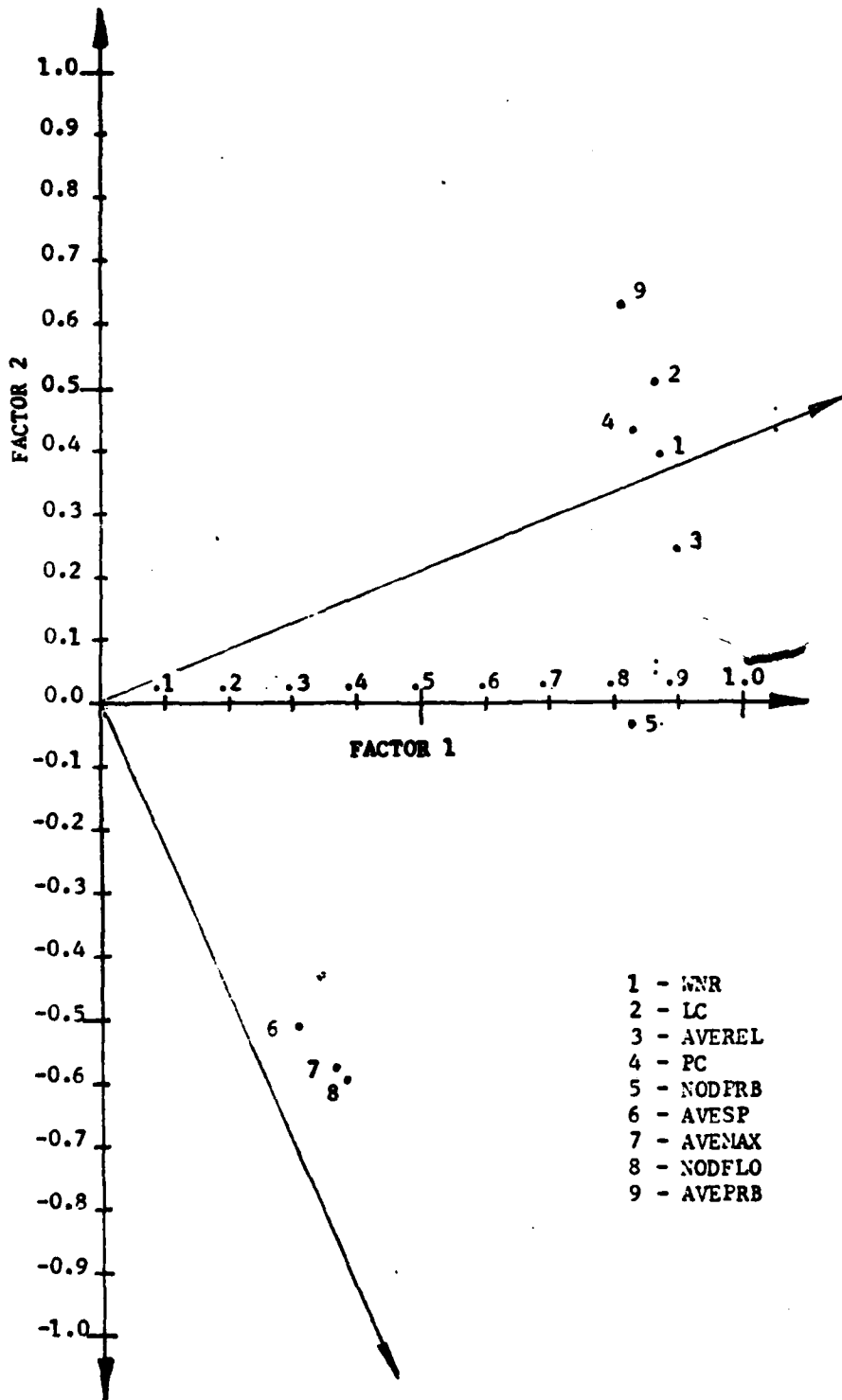


Figure 3. Vectorial representation of correlation coefficients in table 1a.

562

Note in table 1a that MOE 9 (average probability of links) has zero correlation with all the MOEs in cluster (6,7,8). This was because MOE 9 dealt only with link probabilities and MOEs 6,7, and 8 completely ignored link probabilities. Note also that MOE 9 is at the far end of the main cluster away from the 'flow cluster'.

Note however that none of the other MOEs in the main cluster used link-flow values in their calculations, yet they all had some correlation with the flow cluster. It would seem possible that there is some small characteristic of networks which gets evaluated by all the MOEs except AVEPRB. This researcher suspects that this small common characteristic is the undefined concept of 'good topology'. Perhaps with more networks and more MOEs and more time this abstract concept could be gleaned out.

#### V. Recommendations

That is exactly what this researcher recommends. Now that the process has been sketched out it needs to be refined, validated, and used on a more extensive and well thought out data base. Some of the more powerful methods available in Factor Analysis could be used such as the diagonal and centroid methods of factoring and such concepts as oblique factors if it proves necessary.

A list of better defined and more designed MOEs could replace the current list. The method of creating ad hoc MOEs plays havoc with the Factor Analysis method and should be avoided.

Also it would be good to find somebody who really wants the results of this research.

REFERENCES

1. Fruchter, Benjamin, Introduction to Factor Analysis, Princeton, New Jersey, D. Van Nostrand Company, INC., 1954.
2. Rummel, R.J., Applied Factor Analysis, Evanston, Northwestern University Press, 1970.
3. Lipson, Charles and Sheth, Narendra, Statistical Design and Analysis of Engineering Experiments, St. Louis, McGraw Hill Book Company, 1973.
4. Hofstadter, Douglas R., Godel, Escher, Bach: An Eternal Golden Braid, New York, Vintage Books, 1979.

**Specifically:**

Fruchter pages 99-104, 201  
Rummel pages 38, 213-215  
Lipson pages 372-373

**1984 USAF-SCEEE GRADUATE STUDENT SUMMER SUPPORT PROGRAM**

**Sponcered by the**

**AIR FORCE OFFICE OF SCIENTIFIC RESEARCH**

**Conducted by the**

**SOUTHEASTERN CENTER FOR ELECTRICAL ENGINEERING EDUCATION**

**FINAL REPORT**

**THE "PROCESSING WINDOW" FOR THE NEAR BETA**

**Ti-10V-2Fe-3Al ALLOY**

**Prepared by:** Joseph M. Hjelm

**Academic Department:** Materials Science and Engineering

**University:** Wright State University

**Research Location:** Air Force Materials Laboratory, Metals  
and Ceramics Division, Structural  
Metals Branch

**USAF Research Contact:** Dr. F.H. Froes

**SFRP Supervising  
Faculty Member:** Dr. I. Weiss

**Date:** 25 September, 1984

**Contract No:** F49620-82-C-0035

THE "PROCESSING WINDOW" FOR THE NEAR BETA

Ti-10V-2Fe-3Al ALLOY

by

Joseph M. Hjelm

ABSTRACT

The effect of hot deformation and post deformation heat treatment on the development of grain structure in the Ti-10V-2Fe-3Al alloy was studied in this project. It has been shown that a combination of deformation temperature, total strain, and post deformation heat treatment can provide a "processing window" yielding an equiaxed recrystallized grain structure.

The determination of the "processing window" of commercial Ti-10V-2Fe-3Al was the object of this project. Test coupons, taken from the ingot, were forged to a 30% (36% true strain) reduction at die temperatures ranging from 815°C (1500°F) to 1230°C (2200°F). These were then annealed for 1 hr in vacuum at temperatures between 870°C (1600°F) and 1343°C (2450°F). From these tests we found that a "processing window" does exist, with the lowest minimum annealing temperature being 1175°C (2150°F) at a forging temperature of 980°C (1800°F). Suggestions for further research in this area are also offered.

### ACKNOWLEDGEMENTS

The author would like to thank the Air Force Systems Command, the Air Force Office of Scientific Research and the Southeastern Center for Electrical Engineering Education for giving him the opportunity to do this research at the Air Force Materials Laboratory, Wright Patterson AFB, OH. He would like to thank the Structural Metals branch for use of its laboratory facilities.

Also, he would like to thank Dr. I. Weiss, for getting him involved in the SCEEE program to begin with. And the people from METCUT and Systems Research Laboratory, without whose help this project would never have been finished.

## I. INTRODUCTION:

Processing beta titanium alloys can lead to the formation of a mixed grain size structure containing both large and small grains (1,2). During deformation of beta titanium (which has high stacking fault energy) dynamic recovery occurs so rapidly that dynamic recrystallization is suppressed and consequently, static recrystallization is also slowed down, leading to the formation of a partially recrystallized structure.(3). It was found, that heat treatment alone will not remove this mixed grain size structure (2). Thus, processing from the ingot in order to obtain the desired room temperature mechanical properties, requires the control of grain size, grain shape, and uniformity. The combination of deformation temperature, total strain and post deformation heat treatment can describe the conditions to produce a "processing window" yielding a uniform grain size.

## II. OBJECTIVES:

The purpose of this study was to investigate the effect of hot deformation, post deformation heat treatment, and initial grain size and shape (equiaxed or columnar) on the development of grain structure in the Ti-10V-2Fe-3Al alloy. And determine whether a "processing window" can be found for this alloy.

### III. MATERIALS AND EXPERIMENTAL PROCEDURE:

Forging blanks (75.5mm diameter x 127mm) were taken from a 305mm cast ingot with a nominal composition of Ti-10V-2Fe-3Al. These blanks were sectioned from the ingot in the location as shown in figure 1, with the structure of the as cast ingot given in figure 2. These were then hot die forged to 30% (36% true strain) reduction at temperature ranging from 815°C (1500°F) to 1225°C (2235°F) as shown in Table 1. A 1000 ton hydraulic press was used at a

TABLE 1:  
THERMOMECHANICAL VARIABLES USED TO PROCESS  
THE Ti-10V-2Fe-3Al ALLOY INGOT PREFORMS

SERIAL #	FIRST UPSET		ANNEALING			SERIAL #
	TEMPERATURE °C/(°F)	REDUCTION %	TEMPERATURE °C/(°F)	TIME (HR)	COOLING	
A	815 (1500)	30	871-1343 (1600-2450)	1	oil-Q	A
B	982 (1800)	30	1037-1343 (1900-2450)	1	oil-Q	B
C	1149 (2100)	30	1135-1343 (2075-2450)	1	oil-Q	C
D	1232 (2250)	30	1121-1343 (2050-1343)	1	oil-Q	D

ram speed of 12.5 cm/min (5 in/min) with the above die temperatures. Deformed specimens were polished and then macro etched in Kroll solution to deeply groove the deformed grain boundaries. The etched specimens were then vacuum annealed for 1 hr at the above temperatures and oil quenched. After quenching the specimens show on their polished surface the recrystallized grains (thermally etched) and the prior de-

formed grain boundaries ("ghost boundaries") simultaneously. This procedure was used to determine the progress of recrystallization during annealing (4).

### FORGING BLANKS LOCATION

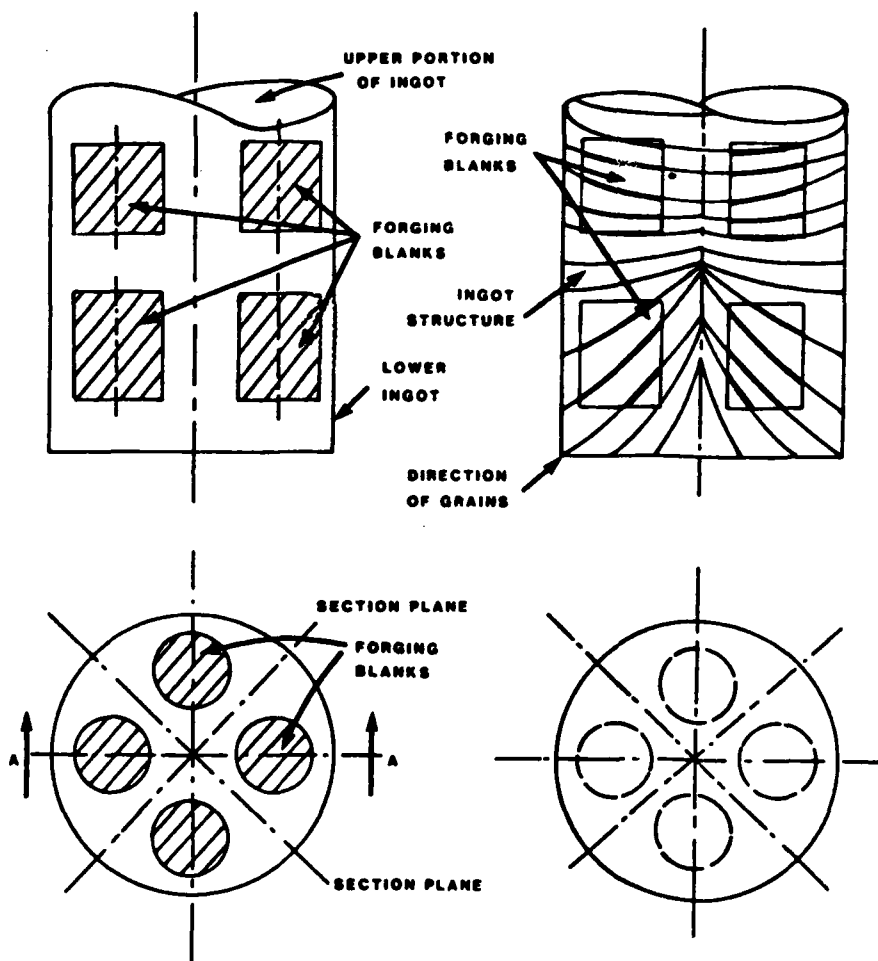


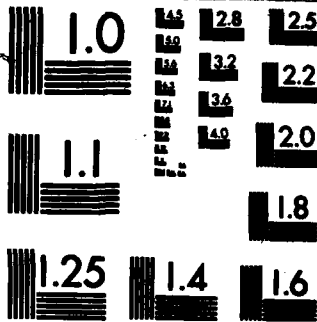
FIGURE 1

FORGING BLANKS LOCATION

FIGURE 2

INGOT STRUCTURE





MICROCOPY RESOLUTION TEST CHART  
NATIONAL BUREAU OF STANDARDS-1963-A

#### IV. INITIAL MICROSTRUCTURE:

The initial microstructure of the forging blanks, as shown in Figure 3, are different due to the location of the blank in the original ingot (refer to the ingot structure given in Fig. 2). Samples A and D show a columnar grain structure, with some grains exceeding 50mm in length. While samples B and C have an equiaxed grain structure, with most grains being smaller than 25mm. A deformation substructure is seen in the equiaxed grains when deformed in excess of 1150°C (2100°F) as shown in Figure 3c.

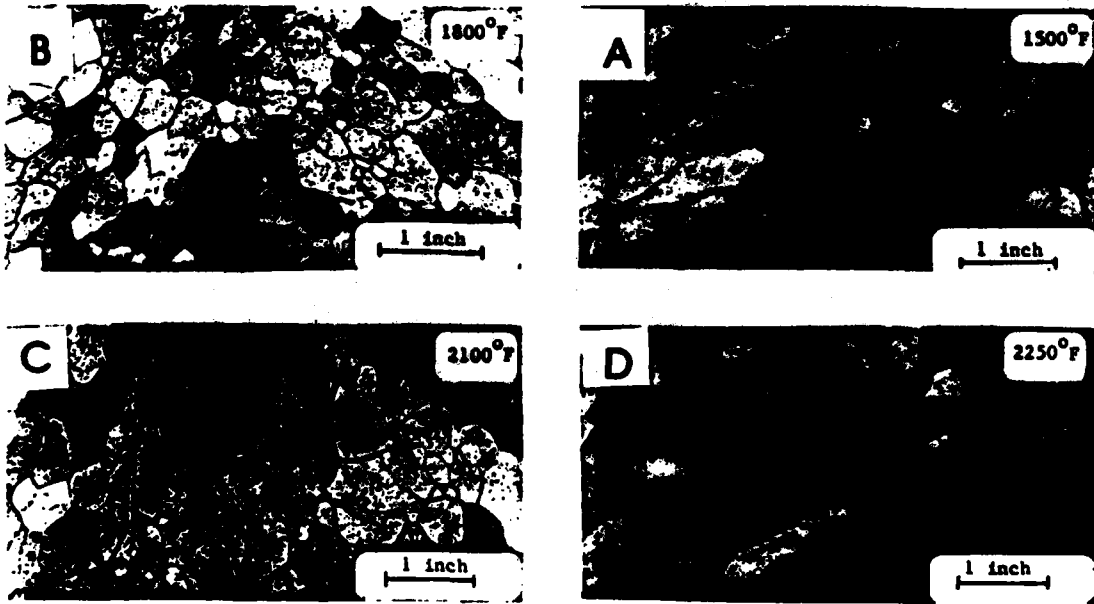


Fig. 3: Microstructure of samples forged to a 30% reduction at (A) 815°C, (B) 980°C, (C) 1150°C, (D) 1230°C.



A



A



B



C



D



D

Fig. 4: Microstructure of specimens forged at (A)  $815^{\circ}\text{C}$  ( $1500^{\circ}\text{F}$ ), (B)  $980^{\circ}\text{C}$  ( $1800^{\circ}\text{F}$ ), (D)  $1230^{\circ}\text{C}$  ( $2250^{\circ}\text{F}$ ) and subsequent annealed at  $1205^{\circ}\text{C}$  ( $2200^{\circ}\text{F}$ ) for 1 hr.

Fig. 5: Microstructure of specimens forged at (A)  $815^{\circ}\text{C}$  ( $1500^{\circ}\text{F}$ ), (C)  $1150^{\circ}\text{C}$  ( $2100^{\circ}\text{F}$ ), (D)  $1230^{\circ}\text{C}$  ( $2250^{\circ}\text{F}$ ) and subsequent annealed at  $1343^{\circ}\text{C}$  ( $2450^{\circ}\text{F}$ ) for 1 hr.

## V. MICROSTRUCTURE OF DEFORMED AND ANNEALED MATERIAL:

The microstructure of specimens forged at 815°C (1500°F) (Specimens-A), 980°C (1800°F) (Specimens-B), 1150°C (2100°F) (Specimens-C), and 1230°C (2250°F) (Specimens-D) and annealed for 1 hr at 1205°C (2200°F) and 1343°C (2450°F) are shown in Figures 4 and 5, respectively. Specimens A and D, initially having a columnar grain structure, and annealed at 1205°C (2200°F) resulted in a mixed grain structure as shown in Figures 4a and 4d. When annealed at 1343°C (2450°F) specimens A and D show a fully recrystallized grain structure as shown in Figures 5a and 5d. Specimens B and C, initially having a equiaxed grain structure, annealed at both 1205°C (2200°F) and 1343°C (2450°F) also show a fully recrystallized grain structure as shown in Figures 4b and 5c, respectively. This fully recrystallized microstructure apparently results from both the difference in deformation temperature that was used, 980°C (1800°F) and 1150°C (2100°F) compared to 815°C (1500°F) and 1230°C (2250°F), and the initial equiaxed microstructure. In both Figures 4 and 5 one can see the recrystallized grains superimposed on the "ghost boundaries" of the deformed grains. The larger recrystallized grains are the result of recrystallization and rapid grain growth occurring during annealing, as seen in Figures 4b and 5c.

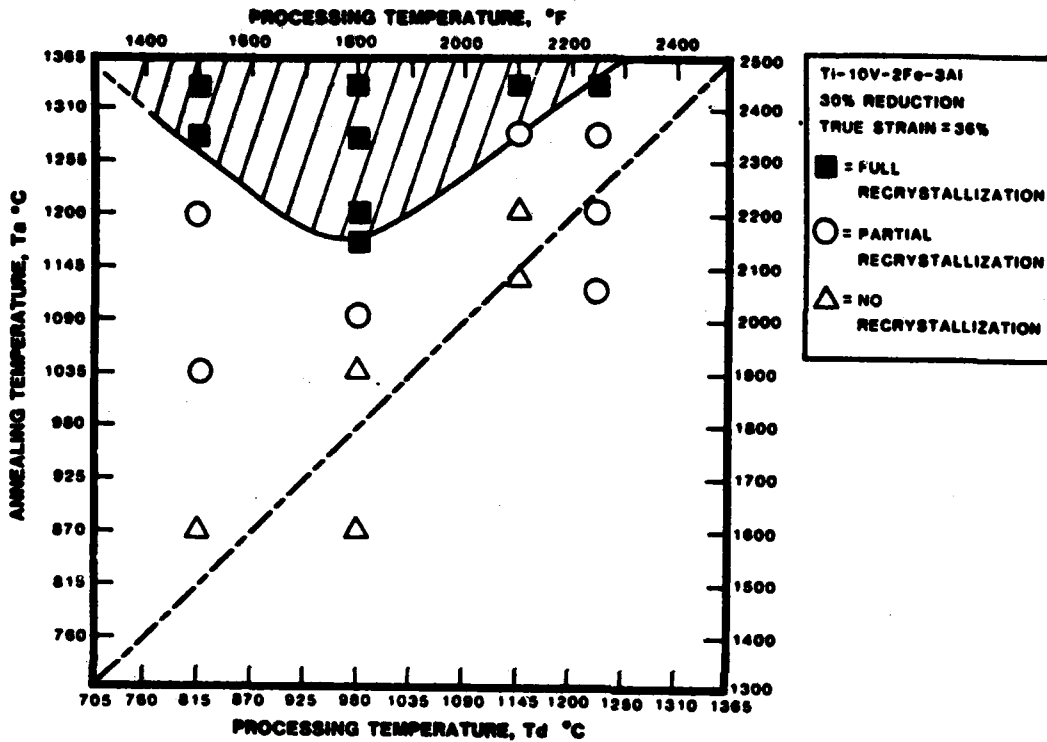
## VI. THE PROCESSING WINDOW:

Figure 6 shows the effect of processing and annealing temperatures on the microstructure of specimens forged to a

30% reduction. Specimens forged at 980°C (1800°F) with an initial equiaxed microstructure (Specimen B) were found to produce a fully recrystallized microstructure at a lower anneal temperature of 1175°C (2150°F) than specimens forged at 815°C (1500°F) and 1230°C (2250°F) (Specimens A and D, respectively). Specimens A and D, both having columnar grains initially, require annealing temperatures of 1290°C (2350°F) to produce a fully recrystallized, equiaxed microstructure. This shows that a "processing window" exists for which a uniform recrystallized microstructure results. This "processing window" is connected with (a) the forging and annealing temperatures and (b) the initial shape of the ingot grains, equiaxed or columnar.

#### VII. RECOMMENDATIONS:

The "processing window" found in this study considered the forging temperature, forging reduction and final annealing temperatures and time which resulted in the formation of an equiaxed recrystallized structure. This work did not consider the possible effect of initial grain shape, equiaxed or columnar, on the magnitude of the "processing window". In follow-on research we suggest that all of the starting material have the same initial microstructure, equiaxed or columnar and the amount of true strain and annealing temperature and time remain the same.



**Fig. 6: Processing Map**

The effect of processing and annealing temperature on the microstructure of specimens forged to 30% reduction.

## REFERENCES

1. F.H. Froes, C.P. Yolton, J.P. Hirth, R. Ondercin and D. Moracs, "Proceedings of the Beta and Near-Beta Alloys Symposium," TSM-AIME, Atlanta, GA, March (1983).
2. F.H. Froes, C.P. Yolton and J.P. Hirth, "Proceedings of the Beta and Near-Beta Alloys," Symposium, TSM-AIME, Atlanta, GA, March (1983).
3. H.J. McQueen and J.J. Jonas, "Treatise on Materials, Acad. Press, (1975).
4. I. Weiss, F.H. Froes and D. Eylon, To be submitted to Metall. Trans. (1984).

**1984 USAF-SCEEE GRADUATE STUDENT SUMMER SUPPORT PROGRAM**

**Sponsored by the  
AIR FORCE OFFICE OF SCIENTIFIC RESEARCH**

**Conducted by the  
SOUTHEASTERN CENTER FOR ELECTRICAL ENGINEERING EDUCATION**

**FINAL REPORT**

**VEHICLE AND CREW SCHEDULING IN AIRLIFT OPERATIONS**

**Prepared by:** Arthur M.B. Hogan  
Dr. M. Jeya Chandra

**Academic Rank:** Graduate Student (Hogan)  
Assistant Professor (Chandra)

**Academic Department:** Economics (Hogan)  
Industrial Engineering and Management (Chandra)

**University:** University of California at San Diego (Hogan)  
The Pennsylvania State University (Chandra)

**Research Location:** School of Aerospace Medicine  
Data Sciences Division  
Biomathematical Modeling Branch

**USAF Research:** Dr. Richard Albanese

**Date:** August 10, 1984

**Contract No.** F49620-82-C-0035

**VEHICLE AND CREW SCHEDULING IN AIRLIFT OPERATIONS**

by

Arthur M.B. Hogan  
Dr. M. Jeya Chandra

**Abstract**

This paper addresses the analytical solution of crew allocation and vehicle scheduling encountered by certain divisions of the United States Air Force. The paper reports the formulation of a general decision model as a mixed integer programming problem, the computational complexity involved in obtaining an analytical solution, and transformations to allow the application of heuristics in obtaining suboptimal solutions. A heuristic to solve the integer linear program formulation was implemented.

## Acknowledgement

The authors would like to thank the Air Force Systems Command, the Air Force Office of Scientific Research and the Southeastern Center for Electrical Engineering Education for providing them with an opportunity to spend a very worthwhile and interesting summer at the School of Aerospace Medicine, Brooks AFB, TX. We would like to acknowledge in particular the Biomathematical Modeling Branch for its hospitality and excellent working conditions. We would also like to thank the Aeromedical Library for their invaluable help.

Finally, we would like to thank Dr. Richard Albanese for suggesting this area of research and for his cooperation and guidance, and we would like to acknowledge many helpful discussions with Dr. Sherwood Samn and Mr. Ronald Wasserstein.

## 1.0 Introduction

The vehicle and crew scheduling and routing problems are encountered by certain divisions of the United States Air Force in airlift operations. A balance mix of missions must be maintained eg. a cargo of medical supplies is useless without the appropriate medical personnel. There are physical constraints upon aircraft operation; physiological, upon crews. The problem differs from that encountered by the airlines in that a fixed set of routed missions must be completed; however, there is no constraint upon flying times (1,2).

## 2.0 Objective

The objective is to minimize the makespan and resources employed in the airlift operations through mathematical modeling. We develop a model to optimize the usage of crews and vehicles and investigate the appropriate means to solve the model. The model is realistic in that it includes constraints upon the usage of crews and vehicles and the stochastic nature of these restrictions. The methods of solution investigated are computationally efficient, producing a solution in a reasonable time. It can be formulated as a multiple goal assignment problem with side constraints.

### 3.0 Model

The model assumes that the sequence of mission and legs are specified. Balancing of missions has not been directly incorporated into the model; however, this objective can be achieved by decomposing the problem into problems of shorter duration and by limiting the missions that can be undertaken upon completion of a specific mission. The problem is formulated as a multiple goal (3,4) chance constrained (5) generalized assignment model.

#### 4.8 Notation

For the purposes of this report a mission shall be defined as the completion of a route, by an vehicle, and the leags are the arcs that connect bases and are consistently labeled.

##### Objectives

T = makespan or total time to complete all missions  
C = number of crews  
A = number of airplanes

##### Input to Model

$\alpha_s$  = probability level that missions would have been on schedule  
 $N_h$  = number of legs in mission h  
M = number of missions  
TL = total number of legs  
 $t_k$  = flying time on leg k  
 $f_{hijkl}$  = forced delay of aircraft l between end of mission h leg i and mission j leg k  
 $R_{hijklm}$  = ground time of crew m between end of mission h leg i and mission j leg k  
Q = set of pairings of mission h leg i and mission j leg k that are allowed for aircraft  
Q' = set of pairings of mission h leg i and mission j leg k that are allowed for crews

##### Output from Model

$x_{hilm} = 1$ , if airplane l and crew m assigned to mission h leg i  
 $\emptyset$ , otherwise  
 $ta_{hil} =$  completion time of mission h leg i by aircraft l  
 $tc_{him} =$  completion time of mission h leg i by crew m  
 $dc_m = 1$ , if crew m assigned  
 $\emptyset$ , otherwise  
 $da_l = 1$ , if aircraft l assigned  
 $\emptyset$ , otherwise

## 5.0 Integer Linear Program

$$\begin{aligned} \min \quad & T \\ & \sum_{m=1}^{TL} dc_m \\ & \sum_{l=1}^M da_l \end{aligned}$$

$$\text{st.} \quad \sum_{l=1}^{TL} \sum_{m=1}^M x_{hilm} = 1 \text{ for all } (h,i) \quad (1)$$

$$1/TL \sum_{h=1}^M \sum_{i=1}^{N_h} \sum_{l=1}^M x_{hilm} \leq dc_m, \quad m=1, \dots, TL \quad (2)$$

$$1/TL \sum_{h=1}^M \sum_{i=1}^{N_h} \sum_{m=1}^{TL} x_{hilm} \leq da_l, \quad l=1, \dots, M \quad (3)$$

$$\begin{aligned} P\{ta_{jkl} - ta_{hil} \geq [t_k + f_{hijk}] \sum_{m=1}^{TL} x_{hilm}\} \geq \alpha_s \\ (h,i,j,k) \in Q, \quad l=1, \dots, M \end{aligned} \quad (4)$$

$$\begin{aligned} P\{tc_{jkm} - tc_{him} \geq [t_k + R_{hijkm}] \sum_{l=1}^M x_{hilm}\} \geq \alpha_s \\ (h,i,j,k) \in Q', \quad m=1, \dots, TL \end{aligned} \quad (5)$$

$$ta_{hil} \leq T, \text{ for all } (h,i,l) \quad (6)$$

$$ta_{hil} - tc_{him} + Lx_{hilm} - L \leq 0, \quad (7a)$$

for all  $(h,i,l,m)$

$$tc_{him} - ta_{hil} + Lx_{hilm} - L \leq 0, \quad (7b)$$

for all  $(h,i,l,m)$

where  $ta_{hil}, tc_{him} \geq 0$

$da_l, dc_m, x_{hilm} \in \{0,1\}$

$L = \text{some large number}$

- (1) specifies that all legs are covered (replace = with  $\geq$  if deadheading allowed)
- (2) determines if crew m has been used
- (3) determines if aircraft l has been used
- (4) chance constraint of aircraft arrivals: likelihood of schedule being correct given data from past is representative
- (5) chance constraint of crew arrivals: likelihood of schedule being correct given data from past is representative
- (6) determines last arrival time
- (7) links assigned crew and planes so that crews and planes that have been assigned to each other arrive at the same time

Note that the chance constraints (4) and (5) are of the form:

$$P\{b_i \leq \sum_j a_{ij} x_{ij}\} \geq \alpha_i, \text{ for all } i \quad (8)$$

In the case where b are normally distributed random variables with known mean and variance:  $E\{b\}$ ,  $\text{Var}\{b\}$ , the non-linear constraint (8) can be transformed into a linear constraint. Normalizing (8):

$$P\{[b_i - E\{b_i\}] / \sqrt{\text{Var}\{b_i\}} \leq [\sum_j a_{ij} x_{ij} - E\{b_i\}] / \sqrt{\text{Var}\{b_i\}} \geq \alpha_i; \quad (9)$$

for all i

This means that

$$P\{b_i \leq \sum_j a_{ij} x_j\} = \bar{\Phi} \left[ \frac{\sum_j a_{ij} x_j - E\{b_i\}}{\sqrt{\text{Var}\{b_i\}}} \right] \quad (10)$$

for all  $i$

where  $\bar{\Phi}$  represents the cumulative standard normal distribution. Let  $K\alpha_i$  be the standard normal value such that  $\bar{\Phi}(K\alpha_i) = \alpha_i$ . Then the statement (8) is equivalent to:

$$\left[ \sum_j a_{ij} x_j - E\{b_i\} \right] / \sqrt{\text{Var}\{b_i\}} \geq K\alpha_i \quad (11)$$

for all  $i$

Rearranging,

$$\sum_j a_{ij} x_j \geq E\{b_i\} + K\alpha_i \sqrt{\text{Var}\{b_i\}} \quad (12)$$

for all  $i$

The chance constraints (4) and (5) can now be written:

$$t_{jkl} - t_{hij} \geq [E\{t_k\} + E\{f_{hijkl}\}] + \quad (4')$$

$$K\alpha_s \sqrt{\text{Var}\{t_k\} + \text{Var}\{f_{hijkl}\} + 2\text{Cov}\{t_k, f_{hijkl}\}} \sum_{m=1}^{TL} x_{hilm}$$

for all  $(h, i, j, k) \in Q, l=1, \dots, M$

$$t_{jkm} - t_{hilm} \geq [E\{t_k\} + E\{R_{hijkm}\}] + \quad (5')$$

$$K\alpha_s \sqrt{\text{Var}\{t_k\} + \text{Var}\{R_{hijkm}\} + 2\text{Cov}\{t_k, R_{hijkm}\}} \sum_{l=1}^M x_{hilm}$$

for all  $(h, i, j, k) \in Q', m=1, \dots, TL$

Note that the only effect of introducing the stochastic nature of completion times is to increase the length of the times used for scheduling. The constraints (4') and (5') can be further simplified if the forced ground time and crew ground time are independent of the flying time, in which case the covariance terms drop out. Further simplifications

in the model are achieved by weighting one of the goals completely and fixing the other two (2,6,7,8,9).

Example: objective is to minimize the number of crews

$$\min \sum_{m=1}^{TL} dc_m$$

$$\text{st. } \sum_{l=1}^A \sum_{m=1}^{TL} x_{hil m} = 1, \text{ for all } (h,i) \quad (1'')$$

$$dc_m - 1/TL \sum_{h=1}^M \sum_{i=1}^{N_j} \sum_{l=1}^A x_{hil m} \geq 0, \quad (2'')$$

$$m=1, \dots, TL$$

$$ta_{jkl} - ta_{h,i,l} + [E\{t_k\} + E\{f_{h,i,jkl}\}] + \quad (4'')$$

$$K\alpha_s \sqrt{\text{Var}\{t_k\} + \text{Var}\{f_{h,i,jkl}\}} \sum_{m=1}^{TL} x_{hil m} \leq 0$$

for all  $(h,i,j,k) \in Q, l=1, \dots, A$

$$tc_{jkm} - tc_{him} + [E\{t_k\} + E\{R_{h,i,jkm}\}] + \quad (5'')$$

$$K\alpha_s \sqrt{\text{Var}\{t_k\} + \text{Var}\{R_{h,i,jkm}\}} \sum_{l=1}^A x_{hil m} \leq 0$$

for all  $(h,i,j,k) \in Q', m=1, \dots, TL$

$$ta_{hil} \leq T, \text{ for all } (h,i,l) \quad (6'')$$

$$ta_{hil} - tc_{him} + Lx_{hil m} - L \leq 0 \quad (7a'')$$

for all  $(h,i,l,m)$

$$tc_{him} - ta_{hil} + Lx_{hil m} - L \leq 0 \quad (7b'')$$

for all  $(h,i,l,m)$

The formulation of the model is in the form of the generalized assignment problem:

$$\begin{aligned} \min \quad & \sum_i \sum_j c_{ij} x_{ij} \\ \text{st.} \quad & \sum_j a_{ij} x_{ij} \leq b_i \quad i=1, \dots, m \\ & \sum_i x_{ij} = 1 \quad j=1, \dots, n \\ & x \in \{0,1\} \end{aligned}$$

Problems of this form are NP-complete (10,11,12): the computational effort to find the optimum grows exponentially with the problem size. The problem is strongly NP-complete: it can be transformed exponentially into an NP-complete problem. If one views the crews as traveling salesman and the plane flight legs to be serviced as cities the crew scheduling problem becomes a traveling salesman problem. However, since the crews do not have to start and finish at the same base, one can assign a zero distance between base pairs for crews for beginning and ending bases and then solve for each pairing and use the best of these solutions.

In problems of this type, heuristics whose computational effort grows as some low order polynomial of problem size have been used to explore the solution space. Hopefully, the sub-optimal solution thus obtained is within a few percent of the true optimum. The mixed integer formulation of the crew - vehicle scheduling problem can be solved

exactly and heuristically (13,14). The problem with both of these methods is that a relaxed version of the problem must be solved first using the Simplex method, and the number of computations involved in this algorithm grows exponentially with the number of constraints (15). The dual of the problem can be solved by making the computations grow with the number of variables; however, this method does not produce a feasible solution until it stops, whereas the primal is always feasible and may be close to optimal if computational time is restricted (at each iteration the new solution is an improvement over the previous solution).

The problem can be transformed from the mixed integer formulation to an integer problem by multiplying all the constraints by an appropriately large constant. This allow the application of integer programming heuristics (16,17,18) to obtain suboptimal solutions; however, Hillier's heuristic first solves a relaxed version of the problem using the Simplex method.

The constraints can be partitioned into two sets: one with all zero-one variables, and the other with mixed variables:

$$\begin{aligned} \min \quad & \sum_i \sum_j c_{ij} x_{ij} \\ \text{st.} \quad & \sum_i x_{ij} = 1, \text{ for all } j \\ & \sum_j a_{ij} x_{ij} \leq b_i, \text{ for all } i. \end{aligned}$$

The by Lagrangean relaxation:

$$\begin{aligned} \min \quad & \sum_i \sum_j c_{ij} x_{ij} - \sum_i \lambda_i (\sum_j a_{ij} x_{ij} - b_i) \\ \text{st.} \quad & \sum_i x_{ij} = 1, \text{ for all } j \end{aligned}$$

The Lagrangean multipliers can be determined iteratively (19) using either subgradient methods (20) or multiplier adjustment methods (21) and employing a zero-one programming heuristic to solve the problem at each iteration (22,23,24).

Example: objective is to minimize the number of crews

$$\begin{aligned}
 \min \quad & \sum_{m=1}^{TL} dc_m - \\
 & \sum_{(h,j,k)} \sum_{i=1}^A \lambda_{hijk} [ta_{jki} - ta_{hil} + [E\{t_k\} + E\{f_{hijk}\}] + \\
 & \quad [given (h,i,j,k) \in Q] \\
 & \quad K\alpha_2 \sqrt{\text{Var}\{t_k\} + \text{Var}\{f_{hijk}\}} \sum_{m=1}^{TL} x_{hilm} - \\
 & \sum_{(h,i,j,k)} \sum_{m=1}^{TL} \lambda'_{hijkm} [tc_{jkm} - tc_{him} + [E\{t_k\} + E\{R_{hijkm}\}] + \\
 & \quad [given (h,i,j,k) \in Q'] \\
 & \quad K\alpha_2 \sqrt{\text{Var}\{t_k\} + \text{Var}\{R_{hijkm}\}} \sum_{l=1}^M x_{hilm} - \\
 & \sum_{h=1}^M \sum_{i=1}^{N_h} \sum_{l=1}^A \lambda''_{hil} (T - ta_{hil}) - \\
 & \sum_{h=1}^M \sum_{i=1}^{N_h} \sum_{l=1}^A \sum_{m=1}^L \lambda'''_{hilm} (ta_{hil} - tc_{him} + Lx_{hilm} - L) - \\
 & \sum_{h=1}^M \sum_{i=1}^{N_h} \sum_{l=1}^A \sum_{m=1}^L \lambda''''_{hilm} (tc_{him} - ta_{hil} + Lx_{hilm} - L) \\
 \text{st.} \quad & \sum_{m=1}^{TL} \sum_{i=1}^A x_{hilm} = 1, \text{ for all } (h,i) \\
 & dc_m - 1/TL \sum_{h=1}^M \sum_{i=1}^{N_h} \sum_{l=1}^A x_{hilm} \geq 0, m=1, \dots, TL
 \end{aligned}$$

### 6.0 Implementation of Kochenberger Heuristic

A modification of Kochenberger's heuristic was implemented in ANSI standard FORTRAN IV. The algorithm was modified to include variables first that would remove infeasibilities and then those that would most rapidly improve the objective. This was done because occasionally Kochenberger's heuristic would end without a feasible

solution. The problem must be formulated as:

$$\begin{array}{ll} \max & \sum_i \sum_j c_{ij} x_{ij} \\ \text{st.} & \sum_j a_{ij} x_{ij} \leq b_i, \quad j=1, \dots, m \\ & x_{ij} \geq 0, \text{ and an integer} \end{array}$$

## Outline of Procedure

1. Cast the problem in the appropriate format
2. Set all  $x_j$ 's to zero
3. Compute  $\bar{b}_i = b_i - \sum_j a_{ij} x_j$ , for all  $i$
4. Compute  $\bar{a}_{ij} = a_{ij} / \bar{b}_i$ ;  $\bar{a}_{ij}$  = portion of slack consumed if problem is feasible, if infeasible and modification 1 calculate for only the infeasible constraints all others set to zero
5. Compute  $r_i = \sum_j \bar{a}_{ij}$ , for all  $i$
6.  $\bar{c}_i = c_i / r_i$ ;  $\bar{c}_i$  = effective gradient, if infeasible and modification 2 then set  $c$  be the number of constraints moved toward feasibility less the number moved toward infeasibility, if constraint is already feasible and addition of this variable cause an infeasible then set  $c = -1$
7. Choose greatest  $\bar{c}_i$ , if tie choose variable that makes greatest contribution to the objective
8. Use decision diagram on page following outline, unless using relaxed decision criteria: if infeasible, and addition of variable moves more constraints towards feasibility than infeasibility without making an infeasible, then increment variable
9. If a variable was incremented go back to 3, otherwise stop

(Note: all divisions by zero are set to some large number, unless numerator is zero in which case the result is one.)



The change in the algorithm was motivated by the fact that the algorithm failed to find a feasible solution to the following:

$$\begin{array}{ll} \max & 2x_1 + x_2 - x_3 \\ \text{st.} & x_3 \geq 1 \\ & x_1 - x_2 \geq 1 \\ & x_1 + 3x_2 = 7 \end{array}$$

The Kochenberger heuristic stops with  $x = 1$  and  $x = 2$ , modification 1 stops at  $x = 4$ ,  $x = 1$  and  $x = 1$ , and modification 2 stops at  $x = 7$  and  $x = 1$ , the optimum. The heuristic has been implemented in ANSI standard FORTRAN IV, a listing of which is contained in the second appendix and sample output is in the third appendix.

#### 7.0 Recommendations

The simplifications of the general model yield complex programs. Some of the models developed to optimize one of the goals appear to be less complex (2) and should probably be employed. The solutions obtained by the heuristic might be further improved through the use of more intelligent starting points than all variables set to zero and by adding a last phase of exchanging one or more variables at a time, similar to Peterson (25) or Hillier's phase III (16).

## References

1. Soyster, A.L. and R. Krishnan, "Airlift Crew-Ratio Scheduling," Report from Texas A and M Research Foundation(1981).
2. Armstrong, R.D., A. Charnes and S. Samn, "Airlift and Crew Scheduling During Airlift Operations," Final Report to Texas A and M Reseach Foundation(1981).
3. Ignizio, J.P. "Goal Programming: A Tool for Multiple Objective Anaglysis," Journal of Operations Research 29(2) 1109-1119 (1978).
4. Kornbluth, J.S.H. "A Survey of Goal Programming," Omega 1(2) 193-205 (1973).
5. Charnes, A. and W. Cooper, "Chance-Constrained Programming," Management Science 6 73-79 (1973).
6. Rubin, J., "A Technique for the Solution of Massive Set Covering Problems, with Application to Airline Crew Scheduling," Transportation Science 7(1) 34-48 (1973).
7. Nicoletti, B., "Automatic Crew Routing," Transportation Science 9(1) 33-44 (1975).
8. Marsten, R.E. and F. Shepardson, "Exact Solution of Crew Scheduling Problems Using Set Partioning Model: Recent Successful Applications," Networks 11 165-177 (1981).
9. Ginnessi, F. and B. Nicholetti, "The Crew Scheduling Problem: A Traveling Salesman Approach," Combinatorial Optimization, N. Christofides, A. Migozzi, P. Toth and C. Sandi ed., John Wiley, New York (1979).
10. Garey, M.R. and D.S. Johnson, Computers and Intractability: A Guide to NP-Completeness, W.F. Freeman, San Fransisco (1978).
11. Garey, M.R. and D.S. Johnson, "Approximation Algorithms for Combinatorial Problems: An Annotated Bibliography," Algorithms and Complexity: New Directions and Recent Results, J.F. Traub ed., Academic Press, New York (1976).
12. Lenstra, J.K. and A.H.G. Rinnooy Kan, "Complexity of

Scheduling Under Precedence Constraints," Operations Research 26 22-35(1978).

13. Ibaraki, T., T. Ohashi and H. Mine, "Heuristic Algorithm for Mixed Integer Programming," Mathematical Programming Study 2 115-136(1974).

14. Benders, J.F., "Partitioning Procedures for Solving Mixed Variables Programming Problems," Numerische Mathematik 4 238-252(1962).

15. Klee, V. and G.J. Minty, "How Good Is the Simplex Algorithm," Mathematical Note no. 643 Mathematics Research Laboratory, Boeing Scientific Labs, Feb. (1970).

16. Hillier, F.S., "Efficient Heuristic Procedures for Integer Linear Programming with an Interior," Operations Research 17 600-637(1969).

17. Kochenberger, G.A., B.A. McCarl and F.P. Wyman, "A Heuristic of General Integer Programming," Decision Sciences 5(1) 36-44(1974).

18. Zankis, S.H., "Heuristic 0-1 Linear Programming: An Experimental Comparison of Three Methods," Management Science 24(1) 91-104 (1977).

19. Fisher, M.L., "The Lagrangian Relaxation Method for Solving Integer Programming Problems," Management Science 27(1) 1-18 (1981).

20. Held, M., P. Wolfe and H.D. Gowder, "Validation of Subgradient Optimization," Mathematical Programming 6 62-88 (1974).

21. Fisher, M., R. Jaikmur and L. Van Wassenhove, "Multiplier Adjustment Method for the Generalized Assignment Problem," Decision Sciences Working Paper, University of Pennsylvania (May 1980).

22. Senju, S. and Y. Toyoda, "An Approach to Linear Programming with Zero-One Variables," Management Science 15(4) B196-B207 (1968).

23. Toyoda, Y., "A Simplified Algorithm for Obtaining Approximate Solutions to Zero-One Programming Problems," Management Science 21(12) 1417-1427 (1975).

24. Balas, E. and C.H. Martin, "Pivot and Complement - A Heuristic for 0-1 Programming," Management Science 26 86-96

(1980)

25. Petersen, C.C., "A Capital Budegeting Heuristic Algorithm Using Exchange Operations," AIIE Transactions, 6 143-150 (1974).

**APPENDIX A**  
**EXAMPLE PROBLEM**

Objective is to minimize the makespan of a three base problem with two routes with two flights each, three crews and two planes.

Model

Min T

st.  $\sum_{l=1}^A \sum_{m=1}^C x_{nilm} \geq 1$  for all (h,i)

$$t_{jkl} - t_{hil} + t_{\kappa} + f_{hijkl} \leq 0 -$$

(h,i,j,k) ∈ Q, l=1,...,A

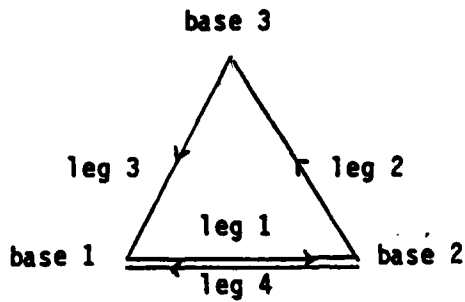
$$t_{jkm} - t_{him} + t + R_{hijkm} \leq 0$$

(h,i,j,k) ∈ Q', m=1,...,C

$$t_{hil} \leq T$$

$$t_{hil} - t_{him} + Lx_{nilm} - L \leq 0$$

$$t_{him} - t_{hil} + Lx_{nilm} - L \leq 0$$



leg	time
1	8
2	7
3	6
4	8

rest time=16  
no forced delay

The two routes are 1->2->1 and 1->2->3->1. Note that mission order has not been specified, therefore to solve some constraints must be deleted eg. mission 1 can't precede and succeed mission 3.

$$\begin{array}{ll}
 \text{Min} & T \\
 \text{st.} & x_{1111} + x_{1121} + x_{1112} + x_{1122} + x_{1113} + x_{1123} \geq 1 \\
 & x_{1211} + x_{1221} + x_{1212} + x_{1222} + x_{1213} + x_{1223} \geq 1 \\
 & x_{1311} + x_{1321} + x_{1312} + x_{1322} + x_{1313} + x_{1323} \geq 1 \\
 & x_{2111} + x_{2121} + x_{2112} + x_{2122} + x_{2113} + x_{2123} \geq 1 \\
 & x_{2211} + x_{2221} + x_{2212} + x_{2222} + x_{2213} + x_{2223} \geq 1 \\
 & x_{2311} + x_{2321} + x_{2312} + x_{2322} + x_{2313} + x_{2323} \geq 1 \\
 & x_{3111} + x_{3121} + x_{3112} + x_{3122} + x_{3113} + x_{3123} \geq 1 \\
 & x_{3411} + x_{3421} + x_{3412} + x_{3422} + x_{3413} + x_{3423} \geq 1 \\
 & x_{4111} + x_{4121} + x_{4112} + x_{4122} + x_{4113} + x_{4123} \geq 1 \\
 & x_{4411} + x_{4421} + x_{4412} + x_{4422} + x_{4413} + x_{4423} \geq 1 \\
 & ta_{111} - ta_{121} + 7\{x_{1211} + x_{1212} + x_{1213}\} \leq 0 \\
 & ta_{112} - ta_{122} + 7\{x_{1221} + x_{1222} + x_{1223}\} \leq 0
 \end{array}$$

$$\begin{aligned}
ta_{211} - ta_{122} + 7\{x_{2211} + x_{2212} + x_{2213}\} &\leq 0 \\
ta_{312} - ta_{222} + 7\{x_{2221} + x_{2222} + x_{2223}\} &\leq 0 \\
ta_{311} - ta_{341} + 6\{x_{3411} + x_{3412} + x_{3413}\} &\leq 0 \\
ta_{312} - ta_{342} + 6\{x_{3421} + x_{3422} + x_{3423}\} &\leq 0 \\
ta_{411} - ta_{441} + 6\{x_{4411} + x_{4412} + x_{4413}\} &\leq 0 \\
ta_{412} - ta_{442} + 6\{x_{4421} + x_{4422} + x_{4423}\} &\leq 0 \\
ta_{121} - ta_{131} + 6\{x_{1311} + x_{1312} + x_{1313}\} &\leq 0 \\
ta_{122} - ta_{132} + 6\{x_{1321} + x_{1322} + x_{1323}\} &\leq 0 \\
ta_{221} - ta_{231} + 6\{x_{2311} + x_{2312} + x_{2313}\} &\leq 0 \\
ta_{222} - ta_{232} + 6\{x_{2321} + x_{2322} + x_{2323}\} &\leq 0 \\
ta_{131} - ta_{311} + 8\{x_{3111} + x_{3112} + x_{3113}\} &\leq 0 \\
ta_{132} - ta_{312} + 8\{x_{3121} + x_{3122} + x_{3123}\} &\leq 0 \\
ta_{131} - ta_{411} + 8\{x_{4111} + x_{4112} + x_{4113}\} &\leq 0 \\
ta_{132} - ta_{412} + 8\{x_{4121} + x_{4122} + x_{4123}\} &\leq 0 \\
ta_{341} - ta_{411} + 8\{x_{4111} + x_{4112} + x_{4113}\} &\leq 0 \\
ta_{342} - ta_{412} + 8\{x_{4121} + x_{4122} + x_{4123}\} &\leq 0 \\
ta_{341} - ta_{111} + 8\{x_{1111} + x_{1112} + x_{1113}\} &\leq 0 \\
ta_{342} - ta_{112} + 8\{x_{1121} + x_{1122} + x_{1123}\} &\leq 0 \\
ta_{341} - ta_{211} + 8\{x_{2111} + x_{2112} + x_{2113}\} &\leq 0 \\
ta_{342} - ta_{212} + 8\{x_{2121} + x_{2122} + x_{2123}\} &\leq 0 \\
ta_{131} - ta_{211} + 8\{x_{2111} + x_{2112} + x_{2113}\} &\leq 0 \\
ta_{132} - ta_{212} + 8\{x_{2121} + x_{2122} + x_{2123}\} &\leq 0 \\
tc_{341} - tc_{411} + 24\{x_{4111} + x_{4121}\} &\leq 0 \\
tc_{342} - tc_{412} + 24\{x_{4112} + x_{4122}\} &\leq 0 \\
tc_{343} - tc_{413} + 24\{x_{4113} + x_{4123}\} &\leq 0
\end{aligned}$$

$$\begin{aligned}
tc_{341} - tc_{111} + 24\{x_{1111} + x_{1121}\} &\leq 0 \\
tc_{342} - tc_{112} + 24\{x_{1112} + x_{1122}\} &\leq 0 \\
tc_{343} - tc_{113} + 24\{x_{1113} + x_{1123}\} &\leq 0 \\
tc_{341} - tc_{211} + 24\{x_{2111} + x_{2121}\} &\leq 0 \\
tc_{342} - tc_{212} + 24\{x_{2112} + x_{2122}\} &\leq 0 \\
tc_{343} - tc_{213} + 24\{x_{2113} + x_{2123}\} &\leq 0 \\
tc_{441} - tc_{111} + 24\{x_{1111} + x_{1121}\} &\leq 0 \\
tc_{442} - tc_{112} + 24\{x_{1112} + x_{1122}\} &\leq 0 \\
tc_{443} - tc_{113} + 24\{x_{1113} + x_{1123}\} &\leq 0 \\
tc_{441} - tc_{211} + 24\{x_{2111} + x_{2121}\} &\leq 0 \\
tc_{442} - tc_{212} + 24\{x_{2112} + x_{2122}\} &\leq 0 \\
tc_{443} - tc_{213} + 24\{x_{2113} + x_{2123}\} &\leq 0 \\
tc_{131} - tc_{211} + 24\{x_{2111} + x_{2121}\} &\leq 0 \\
tc_{132} - tc_{212} + 24\{x_{2112} + x_{2122}\} &\leq 0 \\
tc_{133} - tc_{213} + 24\{x_{2113} + x_{2123}\} &\leq 0 \\
tc_{131} - tc_{311} + 24\{x_{3111} + x_{3121}\} &\leq 0 \\
tc_{132} - tc_{312} + 24\{x_{3112} + x_{3122}\} &\leq 0 \\
tc_{133} - tc_{313} + 24\{x_{3113} + x_{3123}\} &\leq 0 \\
tc_{131} - tc_{411} + 24\{x_{4111} + x_{4121}\} &\leq 0 \\
tc_{132} - tc_{412} + 24\{x_{4112} + x_{4122}\} &\leq 0 \\
tc_{133} - tc_{413} + 24\{x_{4113} + x_{4123}\} &\leq 0 \\
tc_{231} - tc_{311} + 24\{x_{3111} + x_{3121}\} &\leq 0 \\
tc_{232} - tc_{312} + 24\{x_{3112} + x_{3122}\} &\leq 0 \\
tc_{233} - tc_{313} + 24\{x_{3113} + x_{3123}\} &\leq 0 \\
tc_{231} - tc_{411} + 24\{x_{4111} + x_{4121}\} &\leq 0
\end{aligned}$$

$$\begin{aligned}
tc_{232} - tc_{412} + 24(x_{4112} + x_{4122}) &\leq 0 \\
tc_{233} - tc_{413} + 24(x_{4113} + x_{4123}) &\leq 0 \\
tc_{111} - tc_{121} + 23(x_{1211} + x_{1221}) &\leq 0 \\
tc_{112} - tc_{122} + 23(x_{1212} + x_{1222}) &\leq 0 \\
tc_{113} - tc_{123} + 23(x_{1213} + x_{1223}) &\leq 0 \\
tc_{211} - tc_{221} + 23(x_{2211} + x_{2221}) &\leq 0 \\
tc_{212} - tc_{222} + 23(x_{2212} + x_{2222}) &\leq 0 \\
tc_{213} - tc_{223} + 23(x_{2213} + x_{2223}) &\leq 0 \\
tc_{311} - tc_{121} + 23(x_{1211} + x_{1221}) &\leq 0 \\
tc_{312} - tc_{122} + 23(x_{1212} + x_{1222}) &\leq 0 \\
tc_{313} - tc_{123} + 23(x_{1213} + x_{1223}) &\leq 0 \\
tc_{311} - tc_{221} + 23(x_{2211} + x_{2221}) &\leq 0 \\
tc_{312} - tc_{222} + 23(x_{2212} + x_{2222}) &\leq 0 \\
tc_{313} - tc_{223} + 23(x_{2213} + x_{2223}) &\leq 0 \\
tc_{411} - tc_{121} + 23(x_{1211} + x_{1221}) &\leq 0 \\
tc_{412} - tc_{122} + 23(x_{1212} + x_{1222}) &\leq 0 \\
tc_{413} - tc_{123} + 23(x_{1213} + x_{1223}) &\leq 0 \\
tc_{411} - tc_{221} + 23(x_{2211} + x_{2221}) &\leq 0 \\
tc_{412} - tc_{222} + 23(x_{2212} + x_{2222}) &\leq 0 \\
tc_{413} - tc_{223} + 23(x_{2213} + x_{2223}) &\leq 0 \\
tc_{341} - tc_{341} + 22(x_{3411} + x_{3421}) &\leq 0 \\
tc_{342} - tc_{342} + 22(x_{3412} + x_{3422}) &\leq 0 \\
tc_{343} - tc_{343} + 22(x_{3413} + x_{3423}) &\leq 0 \\
tc_{441} - tc_{441} + 22(x_{4411} + x_{4421}) &\leq 0 \\
tc_{442} - tc_{442} + 22(x_{4412} + x_{4422}) &\leq 0
\end{aligned}$$

602

$$\begin{aligned}
tc_{413} - tc_{443} + 22\{x_{4413} + x_{4423}\} &\leq 0 \\
tc_{121} - tc_{131} + 22\{x_{1311} + x_{1321}\} &\leq 0 \\
tc_{122} - tc_{132} + 22\{x_{1312} + x_{1322}\} &\leq 0 \\
tc_{123} - tc_{133} + 22\{x_{1313} + x_{1323}\} &\leq 0 \\
tc_{221} - tc_{231} + 22\{x_{2311} + x_{2321}\} &\leq 0 \\
tc_{222} - tc_{232} + 22\{x_{2312} + x_{2322}\} &\leq 0 \\
tc_{223} - tc_{233} + 22\{x_{2313} + x_{2323}\} &\leq 0 \\
ta_{111} - tc_{111} + Lx_{1111} - L &\leq 0 \\
ta_{111} - tc_{112} + Lx_{1112} - L &\leq 0 \\
ta_{111} - tc_{113} + Lx_{1113} - L &\leq 0 \\
ta_{211} - tc_{211} + Lx_{2111} - L &\leq 0 \\
ta_{211} - tc_{212} + Lx_{2112} - L &\leq 0 \\
ta_{211} - tc_{213} + Lx_{2113} - L &\leq 0 \\
ta_{112} - tc_{111} + Lx_{1121} - L &\leq 0 \\
ta_{112} - tc_{112} + Lx_{1122} - L &\leq 0 \\
ta_{112} - tc_{113} + Lx_{1123} - L &\leq 0 \\
ta_{212} - tc_{211} + Lx_{2121} - L &\leq 0 \\
ta_{212} - tc_{212} + Lx_{2122} - L &\leq 0 \\
ta_{212} - tc_{213} + Lx_{2123} - L &\leq 0 \\
ta_{121} - tc_{121} + Lx_{1211} - L &\leq 0 \\
ta_{121} - tc_{122} + Lx_{1212} - L &\leq 0 \\
ta_{121} - tc_{123} + Lx_{1213} - L &\leq 0 \\
ta_{221} - tc_{221} + Lx_{2211} - L &\leq 0 \\
ta_{221} - tc_{222} + Lx_{2212} - L &\leq 0 \\
ta_{221} - tc_{223} + Lx_{2213} - L &\leq 0 \\
ta_{412} - tc_{413} + Lx_{4123} - L &\leq 0
\end{aligned}$$

$ta_{122} - tc_{121} + Lx_{1221} - L \leq 0$   
 $ta_{122} - tc_{122} + Lx_{1222} - L \leq 0$   
 $ta_{122} - tc_{123} + Lx_{1223} - L \leq 0$   
 $ta_{222} - tc_{221} + Lx_{2221} - L \leq 0$   
 $ta_{222} - tc_{222} + Lx_{2222} - L \leq 0$   
 $ta_{222} - tc_{223} + Lx_{2223} - L \leq 0$   
 $ta_{131} - tc_{131} + Lx_{1311} - L \leq 0$   
 $ta_{131} - tc_{132} + Lx_{1312} - L \leq 0$   
 $ta_{131} - tc_{133} + Lx_{1313} - L \leq 0$   
 $ta_{132} - tc_{131} + Lx_{1321} - L \leq 0$   
 $ta_{132} - tc_{132} + Lx_{1322} - L \leq 0$   
 $ta_{132} - tc_{133} + Lx_{1323} - L \leq 0$   
 $ta_{231} - tc_{231} + Lx_{2311} - L \leq 0$   
 $ta_{231} - tc_{232} + Lx_{2312} - L \leq 0$   
 $ta_{231} - tc_{233} + Lx_{2313} - L \leq 0$   
 $ta_{311} - tc_{311} + Lx_{3111} - L \leq 0$   
 $ta_{311} - tc_{312} + Lx_{3112} - L \leq 0$   
 $ta_{311} - tc_{313} + Lx_{3113} - L \leq 0$   
 $ta_{312} - tc_{311} + Lx_{3121} - L \leq 0$   
 $ta_{312} - tc_{312} + Lx_{3122} - L \leq 0$   
 $ta_{312} - tc_{313} + Lx_{3123} - L \leq 0$   
 $ta_{411} - tc_{411} + Lx_{4111} - L \leq 0$   
 $ta_{411} - tc_{412} + Lx_{4112} - L \leq 0$   
 $ta_{411} - tc_{413} + Lx_{4113} - L \leq 0$   
 $ta_{412} - tc_{411} + Lx_{4121} - L \leq 0$   
 $ta_{412} - tc_{412} + Lx_{4122} - L \leq 0$   
 $ta_{131} - tc_{132} + Lx_{1312} - L \leq 0$

$ta_{341} - tc_{341} + Lx_{3411} - L \leq 0$   
 $ta_{341} - tc_{342} + Lx_{3412} \leq 0$   
 $ta_{341} - tc_{343} + Lx_{3413} - L \leq 0$   
 $ta_{342} - tc_{341} + Lx_{3421} - L \leq 0$   
 $ta_{342} - tc_{342} + Lx_{3422} - L \leq 0$   
 $ta_{342} - tc_{343} + Lx_{3423} - L \leq 0$   
 $ta_{441} - tc_{441} + Lx_{4411} - L \leq 0$   
 $ta_{441} - tc_{442} + Lx_{4412} - L \leq 0$   
 $ta_{441} - tc_{443} + Lx_{4413} - L \leq 0$   
 $ta_{442} - tc_{441} + Lx_{4421} - L \leq 0$   
 $ta_{442} - tc_{442} + Lx_{4422} - L \leq 0$   
 $ta_{442} - tc_{443} + Lx_{4423} - L \leq 0$   
 $tc_{111} - ta_{111} + Lx_{1111} - L \leq 0$   
 $tc_{112} - ta_{111} + Lx_{1112} - L \leq 0$   
 $tc_{113} - ta_{111} + Lx_{1113} - L \leq 0$   
 $tc_{211} - ta_{211} + Lx_{2111} - L \leq 0$   
 $tc_{212} - ta_{211} + Lx_{2112} - L \leq 0$   
 $tc_{213} - ta_{211} + Lx_{2113} - L \leq 0$   
 $tc_{111} - ta_{112} + Lx_{1121} - L \leq 0$   
 $tc_{112} - ta_{112} + Lx_{1122} - L \leq 0$   
 $tc_{113} - ta_{112} + Lx_{1123} - L \leq 0$   
 $tc_{211} - ta_{212} + Lx_{2121} - L \leq 0$   
 $tc_{212} - ta_{212} + Lx_{2122} - L \leq 0$   
 $tc_{213} - ta_{212} + Lx_{2123} - L \leq 0$   
 $tc_{121} - ta_{121} + Lx_{1211} - L \leq 0$   
 $tc_{443} - ta_{442} + Lx_{4423} - L \leq 0$

$tc_{122} - ta_{12} + Lx_{1212} - L \leq 0$   
 $tc_{133} - ta_{131} + Lx_{1213} - L \leq 0$   
 $tc_{221} - ta_{221} + Lx_{2211} - L \leq 0$   
 $tc_{222} - ta_{221} + Lx_{2212} - L \leq 0$   
 $tc_{223} - ta_{221} + Lx_{2213} - L \leq 0$   
 $tc_{121} - ta_{121} + Lx_{1211} - L \leq 0$   
 $tc_{122} - ta_{121} + Lx_{1212} - L \leq 0$   
 $tc_{123} - ta_{121} + Lx_{1213} - L \leq 0$   
 $tc_{221} - ta_{221} + Lx_{2211} - L \leq 0$   
 $tc_{222} - ta_{221} + Lx_{2212} - L \leq 0$   
 $tc_{223} - ta_{221} + Lx_{2213} - L \leq 0$   
 $tc_{131} - ta_{131} + Lx_{1311} - L \leq 0$   
 $tc_{132} - ta_{131} + Lx_{1312} - L \leq 0$   
 $tc_{133} - ta_{131} + Lx_{1313} - L \leq 0$   
 $tc_{131} - ta_{132} + Lx_{1321} - L \leq 0$   
 $tc_{132} - ta_{132} + Lx_{1322} - L \leq 0$   
 $tc_{133} - ta_{132} + Lx_{1323} - L \leq 0$   
 $tc_{231} - ta_{231} + Lx_{2311} - L \leq 0$   
 $tc_{232} - ta_{231} + Lx_{2312} - L \leq 0$   
 $tc_{233} - ta_{231} + Lx_{2313} - L \leq 0$   
 $tc_{311} - ta_{311} + Lx_{3111} - L \leq 0$   
 $tc_{312} - ta_{311} + Lx_{3112} - L \leq 0$   
 $tc_{313} - ta_{311} + Lx_{3113} - L \leq 0$   
 $tc_{311} - ta_{312} + Lx_{3121} - L \leq 0$   
 $tc_{312} - ta_{312} + Lx_{3122} - L \leq 0$   
 $tc_{313} - ta_{312} + Lx_{3123} - L \leq 0$   
 $tc_{442} - ta_{442} + Lx_{4422} - L \leq 0$

$$tc_{313} - ta_{312} + Lx_{3123} - L \leq 0$$

$$tc_{411} - ta_{411} + Lx_{4111} - L \leq 0$$

$$tc_{412} - ta_{411} + Lx_{4112} - L \leq 0$$

$$tc_{413} - ta_{411} + Lx_{4113} - L \leq 0$$

$$tc_{414} - ta_{412} + Lx_{4121} - L \leq 0$$

$$tc_{412} - ta_{412} + Lx_{4122} - L \leq 0$$

$$tc_{413} - ta_{412} + Lx_{4123} - L \leq 0$$

$$tc_{341} - ta_{341} + Lx_{3411} - L \leq 0$$

$$tc_{342} - ta_{341} + Lx_{3412} - L \leq 0$$

$$tc_{343} - ta_{341} + Lx_{3413} - L \leq 0$$

$$tc_{341} - ta_{342} + Lx_{3421} - L \leq 0$$

$$tc_{342} - ta_{342} + Lx_{3422} - L \leq 0$$

$$tc_{343} - ta_{342} + Lx_{3423} - L \leq 0$$

$$tc_{441} - ta_{441} + Lx_{4411} - L \leq 0$$

$$tc_{442} - ta_{441} + Lx_{4412} - L \leq 0$$

$$tc_{443} - ta_{441} + Lx_{4413} - L \leq 0$$

$$tc_{441} - ta_{442} + Lx_{4421} - L \leq 0$$

$$ta - T \leq 0$$

## Variable Transformation for Algorithms

$X_{1111} \rightarrow X_1$

$X_{1121} \rightarrow X_2$

$X_{1112} \rightarrow X_3$

$X_{1122} \rightarrow X_4$

$X_{1113} \rightarrow X_5$

$X_{1123} \rightarrow X_6$

$X_{1211} \rightarrow X_7$

$X_{1221} \rightarrow X_8$

$X_{1212} \rightarrow X_9$

$X_{1222} \rightarrow X_{10}$

$X_{1213} \rightarrow X_{11}$

$X_{1223} \rightarrow X_{12}$

$X_{1311} \rightarrow X_{13}$

$X_{1321} \rightarrow X_{14}$

$X_{1312} \rightarrow X_{15}$

$X_{1322} \rightarrow X_{16}$

$X_{1313} \rightarrow X_{17}$

$X_{1323} \rightarrow X_{18}$

$X_{2111} \rightarrow X_{19}$

$X_{2121} \rightarrow X_{20}$

$X_{2112} \rightarrow X_{21}$

$X_{2122} \rightarrow X_{22}$

$X_{2113} \rightarrow X_{23}$

X<sub>2123</sub> → X<sub>24</sub>  
X<sub>2311</sub> → X<sub>25</sub>  
X<sub>2321</sub> → X<sub>26</sub>  
X<sub>2312</sub> → X<sub>27</sub>  
X<sub>2322</sub> → X<sub>28</sub>  
X<sub>2313</sub> → X<sub>29</sub>  
X<sub>2323</sub> → X<sub>30</sub>  
X<sub>3111</sub> → X<sub>31</sub>  
X<sub>3121</sub> → X<sub>32</sub>  
X<sub>3112</sub> → X<sub>33</sub>  
X<sub>3122</sub> → X<sub>34</sub>  
X<sub>3113</sub> → X<sub>35</sub>  
X<sub>3123</sub> → X<sub>36</sub>  
X<sub>3411</sub> → X<sub>37</sub>  
X<sub>3421</sub> → X<sub>38</sub>  
X<sub>3412</sub> → X<sub>39</sub>  
X<sub>3422</sub> → X<sub>40</sub>  
X<sub>3413</sub> → X<sub>41</sub>  
X<sub>3423</sub> → X<sub>42</sub>  
X<sub>4111</sub> → X<sub>43</sub>  
X<sub>4121</sub> → X<sub>44</sub>  
X<sub>4112</sub> → X<sub>45</sub>  
X<sub>4122</sub> → X<sub>46</sub>  
X<sub>4113</sub> → X<sub>47</sub>  
X<sub>4123</sub> → X<sub>48</sub>

X 4411 ->X 49

X 4421 ->X 50

X 4412 ->X 51

X 4422 ->X 52

X 4413 ->X 53

X 4423 ->X 54

X 2211 ->X 55

X 2221 ->X 56

X 2212 ->X 57

X 2222 ->X 58

X 2213 ->X 59

X 2 223 ->X 60

ta 111 ->X 61

ta 112 ->X 62

ta 211 ->X 63

ta 212 ->X 64

ta 121 ->X 65

ta 122 ->X 66

ta 221 ->X 67

ta 222 ->X 68

ta 311 ->X 69

ta 312 ->X 70

ta 411 ->X 71

ta 412 ->X 72

ta 341 ->X 73

ta 342 ->X 74  
ta 441 ->X 75  
ta 442 ->X 76  
ta 131 ->X 77  
ta 132 ->X 78  
ta 231 ->X 79  
ta 232 ->X 80  
tc 111 ->X 81  
tc 112 ->X 82  
tc 113 ->X 83  
tc 121 ->X 84  
tc 122 ->X 85  
tc 123 ->X 86  
tc 211 ->X 87  
tc 212 ->X 88  
tc 213 ->X 89  
tc 221 ->X 90  
tc 222 ->X 91  
tc 223 ->X 92  
tc 311 ->X 93  
tc 312 ->X 94  
tc 313 ->X 95  
tc 341 ->X 96  
tc 342 ->X 97  
tc 343 ->X 98

tc 411 ->x 99  
tc 412 ->x 100  
tc 413 ->x 101  
tc 441 ->x 102  
tc 442 ->x 103  
tc 443 ->x 104  
tc 131 ->x 105  
tc 132 ->x 106  
tc 133 ->x 107  
tc 231 ->x 108  
tc 232 ->x 109  
tc 233 ->x 110  
T ->x 111

**APPENDIX B**  
**FORTRAN LISTING**

PROGRAM KOCHHR

MAIN LINE CALLING ROUTINE TO IMPLEMENT THE KOCHENBERGER HEURISTIC ALGORITHM TO SOLVE THE INTEGER PROGRAMMING PROBLEM. THE PROGRAM WILL SOLVE AN INTEGER LP WITH N VARIABLES AND M (IMPLICIT) CONSTRAINTS. IT WILL ALSO RESTRICT THE FIRST INB VARIABLES TO BE BINARY.

REF. KOCHENBERGER, G.A., B.A. MCCARL AND F.P. WYMAN,  
"A HEURISTIC FOR GENERAL INTERGER PROGRAMMING"  
DECISION SCIENCES 5(1) 36-44(1974).

CALL READD  
CALL CONVRT  
CALL KOCH  
CALL WRITO  
GOTO10 .  
END  
SUBROUTINE READD

DESIGNED TO READ:

CARD 1 COL 2-80 TITLE DESCRIPTION OF PROBLEM USING  
ANY CHARACTERS  
CARD 2 COL 1-5 NO. BINARY VARIABLES (MUST BE FIRST)  
6-10 NO. CONSTRAINTS  
11-15 NO. VARIABLES  
16-20 NO. <= CONSTRAINTS  
21-25 NO. => CONSTRAINTS  
26-30 NO. = CONSTRAINTS  
31-35 0, MINIMIZATION  
1, MAXIMIZATION  
36-40 0, STRAIGHT KOCHENBERGER HEURISTIC  
1, MODIFICATION #1  
2, MODIFICATION #2  
41-45 0, KOCHENBERGER FEASIBILITY  
DECISION CRITERIA  
1, RELAXED CRITERIA  
CARD 3-T M SET OF CARDS, ONE SET FOR EACH CONSTRAINT  
CARD I COL 1-10 CODE(S) 0, <= CONSTRAINT  
1, => CONSTRAINT  
2, = CONSTRAINT  
11-20 B(I) CONSTANT IN CONSTRAINT  
CARD I+1 A(I,J) J COEFFIECIENTS OF CONSTRAINT  
PUNCH ROWWISE IN 1018 FORMAT, IF MORE  
CONTINUE ON NEXT CARD(S).

CARD T+1 C(J) COST COEFFICIENTS OF OBJECTIVE FUNCTION  
PUNCH ROWWISE IN 1018 FORMAT IF MORE VARIABLES  
CONTINUE ON NEXT CARD(S)

TO CALCULATE AND PRINT:  
Z, SUBOPTIMAL VALUE OF THE OBJECTIVE FUNCTION  
XB(I), SUBSCRIPT OF BASIC VARIABLES IN SUBOPTIMAL  
SOLUTION  
A(I,NPI), VALUE OF THE BASIC VARIABLES

PARAMETER N = NO. VARIABLES  
NM = NLET+NGET+2\*NEQ

WHERE

NLET = NO. <= CONSTRAINTS  
NGET = NO. => CONSTRAINTS  
NEQ = NO. = CONSTRAINTS

PARAMETER N=200,NM=500  
BYTE IT  
DIMENSION IC(N),IA(NM,N),IB(NM),IT(NM),TITLE(20)  
COMMON INB,IM,IN,ILET,IGET,IEQ,IMM,IMTH,ID,IC,IA,IB  
COMMON /CNVT/IT  
OPEN(UNIT=1,NAME='KOCH.IN',TYPE='OLD',READONLY,FORM='FORMATTED')  
READ(1,9000,END=2000)TITLE  
READ(1,9001)INB,IM,IN,ILET,IGET,IEQ,IMM,IMTH,ID  
IF((IGET+ILET+2\*IEQ).GT.NM)STOP '\*TOO MANY CONSTRAINTS\*'  
IF(IN.GT.N)STOP '\*TOO MANY VARIABLES\*'  
OPEN(UNIT=2,NAME='KOCH.OUT',TYPE='UNKNOWN',FORM='FORMATTED')  
WRITE(2,9000)TITLE  
WRITE(2,8004)  
WRITE(2,8000)INB,IM,IN  
WRITE(2,8001)ILET,IGET,IEQ  
WRITE(2,8009)IMTH,ID  
IF(IMM.EQ.0)WRITE(2,8002)  
IF(IMM.NE.0)WRITE(2,8003)  
DO 200 I=1,IM  
READ(1,9001)IID,IB(I)  
IT(I)=IID  
J=10  
IF(IN.LE.J)GOTO150  
DO 100 J=10,IN,10  
READ(1,9001)(IA(I,IJ),IJ=J-9,J)  
IF((J.GT.IN).AND.((J-10).NE.IN))READ(1,9001)(IA(I,IJ),IJ=J-9,IN)  
CONTINUE  
J=10  
IF(IN.LE.J)GOTO350  
DO 300 J=10,IN,10  
READ(1,9001)(IC(IJ),IJ=J-9,J)  
WRITE(2,9001)(IC(IJ),IJ=J-9,J)

```

IF((J.LE.IN).AND.((J-10).NE.IN))GOTO400
READ(1,9001)(IC(IJ),IJ=J-9,IN)
WRITE(2,9001)(IC(IJ),IJ=J-9,IN)
CLOSE(UNIT=1,DISPOSE='SAVE')
WRITE(2,8004)
WRITE(2,8005)
WRITE(2,8004)
DO 600 I=1,IM
IF(IT(I).EQ.0)WRITE(2,8006)IB(I)
IF(IT(I).EQ.1)WRITE(2,8007)IB(I)
IF(IT(I).EQ.2)WRITE(2,8008)IB(I)
J=10
IF(IN.LE.J)GOTO550
DO 500 J=10,IN,10
WRITE(2,9001)(IA(I,IJ),IJ=J-9,J)
IF((J.GT.IN).AND.((J-10).NE.IN))WRITE(2,9001)(IA(I,IJ),IJ=J-9,IN)
WRITE(2,8004)
CONTINUE
WRITE(2,8004)
RETURN
STOP '*NORMAL TERMINATION OF KOCH*'
FORMAT(1X,'NO. BINARY VARIABLES = ',I8,1X,'NO. OF CONSTRAINTS = '
1,I8,1X,'NO. OF VARIABLES = ',I8)
FORMAT(1X,'NO. <= CONSTRAINTS = ',I8,1X,'NO. => CONSTRAINTS = '
1,I8,1X,'NO. OF = CONSTRAINTS = ',I8)
FORMAT(1X,'MINIMIZE')
FORMAT(1X,'MAXIMIZE')
FORMAT(1X)
FORMAT(1X,'ST. ')
FORMAT(1X,I8,'=>')
FORMAT(1X,I8,'<=')
FORMAT(1X,I8,'=')
FORMAT(1X,'MODIFICATION = ',I8,1X,'DECISION CRITERIA = ',I8)
FORMAT(20A4)
FORMAT(10I8)
END
SUBROUTINE CONVRT

PUTS OBJECTIVE AND CONSTRAINTS IN APPROPRIATE FORM FOR THE
KOCHENBERGER HEURISTIC

      MAX Z=CX
      ST. AX<=B

PARAMETER N=200,NM=500
BYTE IT
DIMENSION IC(N),IA(NM,N),IB(NM),IT(NM)
COMMON INB,IM,IN,ILET,IGET,IEQ,IMM,IMTH,ID,IC,IA,IB
COMMON /CNVT/IT
NXEQ=IM

```

```
DO 500 I=1,IM
IF(IT(I)-1)500,100,200
```

```
=> CONSTRAINT CHANGE TO <= BY CHANGING SIGN
```

```
IS=I
IGET=IGET-1
GOTO300
```

```
= CONSTRAINT ADD ANOTHER <= WITH CHANGED SIGN
```

```
NXEQ=NXEQ+1
IEQ=IEQ-1
IS=NXEQ
IB(IS)=-IB(I)
DO 400 J=1,IN
IA(IS,J)=-IA(I,J)
CONTINUE
IF((IEQ.NE.0).OR.(IGET.NE.0))STOP '*INPUT ERROR ON CONSTRAINTS*'
IM=NXEQ
IF(IMM.GT.0)RETURN
```

```
MINIMIZATION PROBLEM CHANGE SIGN TO MAKE MAXIMIZATION PROBLEM
```

```
DO 600 J=1,IN
IC(J)=-IC(J)
RETURN
END
SUBROUTINE KOCH
```

IMPLEMENTS MODIFIED KOCHENBERGER DECISION CRITERIA TO DETERMINE WHICH VARIABLE TO INCREMENT: WILL FIRST ATTEMPT TO MAKE PROBLEM FEASIBLE AND THEN APPLY KOCHENBERGER'S CRITERIA.

```
PARAMETER N=200,NM=500
REAL*4 CBAR
LOGICAL*1 LPFEAS,LFEAS,LFEAS1,LM
DIMENSION IC(N),IA(NM,N),IB(NM),IX(N),IORD(N),IBBAR(NM),
LABAR(NM,N),R(N),CBAR(N)
COMMON INB,IM,IN,ILET,IGET,IEQ,IMM,IMTH,ID,IC,IA,IB,IX
COMMON /UPDAT/IBBAR,ABAR,R,CBAR,ICC,LPFEAS
COMMON /SORT/IORD
LPFEAS=.TRUE.
DO 100 I=1,IM
IBBAR(I)=IB(I)
LPFEAS=LPFEAS.AND.(IBBAR(I).GE.0)
CALL INIT
DO 300 I=1,IN
IORD(I)=I
```

```

FIND DECREASING ORDER OF CBAR
CALL KSORT (CBAR, IN, IORD)
JC=0
JC=JC+1

QUIT WHEN CAN'T INCREMENT A VARIABLE
IF (JC.GT.IN) RETURN
ICC=IORD(JC)

IF BINARY VARIABLE ALREADY SET TRY ANOTHER
IF ((IX(ICC).NE.0).AND.(ICC.LE.INB)) GOTO400

IS THE PROBLEM NOW FEASIBLE
IF (LPFEAS) GOTO700

WILL THE OBJECTIVE FUNCTION INCREASE
IF (IC(ICC).LE.0) GOTO400

WILL THE ADDITION OF THIS VARIABLE CAUSE INFEASIBILITY
DO 600 I=1,IM
IF (IBBAR(I).LT.IA(I,ICC)) GOTO400

INCREMENT VARIABLE
GOTO1000
LM=IMTH.EQ.2
IF (LM.AND.(CBAR(ICC).LT.0)) RETURN
IF (ID.EQ.1) GOTO910
LFEAS=.FALSE.
DO 900 I=1,IM

IS THE CONSTRAINT FEASIBLE
IF (IBBAR(I).LT.0) GOTO800

DOES THE PROBLEM REMAIN FEASIBLE FOR THIS CONSTRAINT
IF (IBBAR(I).LT.IA(I,ICC)) GOTO400
GOTO900

DOES THE VARIABLE MAKE AN IMPROVEMENT IN FEASIBILITY
LFEAS=LFEAS.OR.(IA(I,ICC).LT.0)
CONTINUE

```

```
IF (LFEAS) GOTO 1000
IF (IC (ICC) .LE. 0) GOTO 400
GOTO 1000
IF (LM) GOTO 1000
INFES = 0
DO 940 IJ = 1, IM
```

IS CONSTRAINT FEASIBLE

```
IF (IBBAR (IJ) .GE. 0) GOTO 930
```

COUNT UP NUMBER OF CONSTRAINTS THE VARIABLE  
MAKES FEASIBLE

```
IF (IA (IJ, I) .GT. 0) GOTO 915
IF (IA (IJ, I) .EQ. 0) GOTO 920
ICBAR = IGBAR + 1
GOTO 940
ICBAR = ICBAR - 1
GOTO 940
```

DOES VARIABLE MAKE CONSTRAINT INFEASIBLE

```
IF (IBBAR (IJ) .GE. IA (IJ, I)) GOTO 940
```

IS THERE ANY VARIABLE THAT COULD MAKE THIS  
CONSTRAINT FEASIBLE

```
LFEAS = .FALSE.
DO 935 J = 1, IN
LFEAS = LFEAS .OR. (IA (IJ, J) .LT. 0)
IF (LFEAS) GOTO 940
CONTINUE
GOTO 400
CONTINUE
IX (ICC) = IX (ICC) + 1
CALL UPDATE
GOTO 200
END
SUBROUTINE UPDATE
```

UPDATE IBBAR, ABAR, R, CBAR, IF INFEASIBLE  
AND METHOD2 RETURNS NUMBER OF CONSTRAINTS  
VARIABLE MAKES FEASIBLE IN CBAR (I)

```
PARAMETER N = 200, NM = 500
REAL*4 CBAR
LOGICAL*1 LZERO, LPFEAS, LFEAS
DIMENSION IC (N), IA (NM, N), IB (NM), IBBAR (NM), ABAR (NM, N), R (N),
ICBAR (N)
```

```

COMMON INB, IM, IN, ILET, IGET, IEQ, IMM, IMTH, ID, IC, IA, IB
COMMON /UPDAT/IBBAR, ABAR, R, CBAR, ICC, LPFEAS
LPFEAS=.TRUE.
DO 100 I=1, IM
IBBAR(I)=IBBAR(I)-IA(I, ICC)
LPFEAS=LPFEAS.AND.(IBBAR(I).GE.0)
ENTRY INIT
LPFEAS=.NOT.LPFEAS
IF((IMTH.EQ.2).AND.LPFEAS)GOTO400
DO 200 I=1, IN
R(I)=0.0
DO 200 IJ=1, IM
ABAR(IJ, I)=-SIGN(1.0E10, FLOAT(IA(IJ, I)))
LZERO=IBBAR(IJ).EQ.0
IF(.NOT.LZERO)ABAR(IJ, I)=FLOAT(IA(IJ, I))/FLOAT(IBBAR(IJ))
IF(LZERO.AND.(IA(IJ, I).EQ.0))ABAR(IJ, I)=1.0
IF((IMTH.NE.1).OR(.NOT.LPFEAS))GOTO150
IF(IBBAR(IJ).GE.0)GOTO200
R(I)=R(I)+ABAR(IJ, I)
CONTINUE
DO 300 I=1, IN
CBAR(I)=SIGN(1.0E10, FLOAT(IC(I)))
LZERO=ABS(R(I)).LE.1.0E-20
IF(.NOT.LZERO)CBAR(I)=FLOAT(IC(I))/R(I)
IF(LZERO.AND.(IC(I).EQ.0))CBAR(I)=1.0
RETURN
DO 700 I=1, IN
ICBAR=0
DO 600 IJ=1, IM

IS CONSTRAINT FEASIBLE

IF(IBBAR(IJ).GE.0)GOTO550

COUNT UP NUMBER OF CONSTRAINTS THE VARIABLE
MAKES FEASIBLE

IF(IA(IJ, I).GT.0)GOTO500
IF(IA(IJ, I).EQ.0)GOTO600
ICBAR=ICBAR+1
GOTO600
ICBAR=ICBAR-1
GOTO600

DOES VARIABLE MAKE CONSTRAINT INFEASIBLE

IF(IBBAR(IJ).GE.IA(IJ, I))GOTO600

IS THERE ANY VARIABLE THAT COULD MAKE THIS
CONSTRAINT FEASIBLE

```

```

LFEAS=.FALSE.
DO 575 J=1,IN
LFEAS=LFEAS.OR.(IA(IJ,J).LT.0)
IF(LFEAS)GOTO600
CONTINUE
ICBAR=-1
GOTO700
CONTINUE
CBAR(I)=FLOAT(ICBAR)
RETURN
END
SUBROUTINE WRITO

```

OUTPUTS VARIABLES IN BASIS AND VALUES  
AND SUBOPTIMAL VALUE OF Z THE OBJECTIVE.

```

PARAMETER N=200,NM=500
DIMENSION IC(N),IA(NM,N),IB(NM),IX(N),IBBAR(NM)
COMMON INB,IM,IN,ILET,IGET,IEQ,IMM,IMTH,ID,IC,IA,IB,IX
COMMON /UPDAT/IBBAR
WRITE(2,8001)
DO 100 I=1,IM
IF(IBBAR(I).GE.0)GOTO100
WRITE(2,8004)
STOP '*NO FEASIBLE SOLUTION FOUND*'
CONTINUE
WRITE(2,8000)
WRITE(2,8001)
DO 200 I=1,IN
IF(IX(I).LE.0)GOTO200
IOPT=IOPT+IC(I)*IX(I)
WRITE(2,8002)I,IX(I)
CONTINUE
IF(IMM.EQ.0)IOPT=-IOPT
WRITE(2,8001)
WRITE(2,8003)IOPT
CLOSE(UNIT=2,DISPOSE='SAVE')
RETURN
FORMAT(1X,'BASIC VARIABLES',6X,'VALUE')
FORMAT(1X)
FORMAT(7X,I8,7X,I8)
FORMAT(1X,'SUBOPTIMAL VALUE, Z = ',I10)
FORMAT(1X,'*NO FEASIBLE SOLUTION FOUND*')
END
SUBROUTINE KSORT
REAL*4 VERSION
TOURNAMENT SORT FOR DESCENDING ORDER
CBAR PRIMARY ARRAY TO BE SEQUENCED
C SECONDARY ARRAY TO BE SEQUENCED

```

```

      IM      NUMBER OF MEMBERS IN A
      IORD    INDEX TO BE REARRANGED ACCORDING TO THE ORDER OF A
PARAMETER N=200,NM=500
REAL*4 CBAR
DIMENSION IBBAR(NM),IORD(N),ABAR(NM,N),CBAR(N),R(N)
1,IA(NM,N),IB(NM),IC(N)
COMMON INB,IM,IN,ILET,IGET,IEQ,IMM,IMTH,ID,IC,IA,IB
COMMON /UPDAT/IBBAR,ABAR,R,CBAR
COMMON /SORT/IORD
IF(IN.GT.8)GOTO5
NN=3
GOTO20
NN=1
DO 10 I=1,1000
NN=2*NN+1
IF(NN.GE.IN)GOTO15
CONTINUE
NN=NN/2
NN=NN/2
IF(NN.EQ.0)RETURN
KK=IN-NN
K=1
I=K
J=I+NN
IX=IORD(I)
IY=IORD(J)
TEMP=CBAR(IX)-CBAR(IY)
IF(TEMP.GT.1E-20)GOTO50
IF((ABS(TEMP).LE.1E-20).AND.
1(IC(IX).GE.IC(IY)))GOTO50
IORD(I)=IY
IORD(J)=IX
I=I-NN
IF(I.GE.1)GOTO30
K=K+1
IF(K.LE.KK)GOTO25
GOTO20
END

```

APPENDIX C  
SAMPLE OUTPUT

TEST1

NO. BINARY VARIABLES =  
NO. <= CONSTRAINTS =  
MAXIMIZE

3 NO. OF CONSTRAINTS =  
2 NO. => CONSTRAINTS =

2 NO. OF VARIABLES = 2  
0 NO. OF = CONSTRAINTS = 0

1 3

S.T.

3=>  
1 1

11=>  
1 3

BASIC VARIABLES      VALUE

1 1  
2 2

SUBOPTIMAL VALUE, Z = 7

YAMA334

NO. BINARY VARIABLES =

NO. OF CONSTRAINTS =

NO. OF VARIABLES =

5

NO. <= CONSTRAINTS =

NO. => CONSTRAINTS =

NO. JF = CONSTRAINTS =

0

MAXIMIZE

3      2      -5      -2      3

S.T.

4=>  
1      1      1      2      1

8=>  
7      0      3      -4      3

3<=  
11      -6      0      3      -3

BASIC VARIABLES

VALUE

1      1  
2      1

SUBOPTIMAL VALUE, Z =

5

1984 USAF-SCEEE GRADUATE STUDENT SUMMER SUPPORT PROGRAM

Sponsored by the

AIR FORCE OFFICE OF SCIENTIFIC RESEARCH

Conducted by the

SOUTHEASTERN CENTER FOR ELECTRICAL ENGINEERING EDUCATION

FINAL REPORT

A Design for Minimum Eigenvalue Sensitivity

Subject to Selected Modal Insensitivity

Prepared by: Mr. Thomas H. Hopp  
Academic Department: Mechanical and Nuclear Engineering  
University: Northwestern University  
Research Location: Air Force Wright Aeronautical Laboratory  
Flight Control Division, Control Dynamics  
Branch, Control Analysis Group  
USAF Research Contact: Mr. James DeWeese  
Supervising Laboratory  
Member: Dr Siva S. Banda  
Date: 24 August 1984  
Contract No: F49620-82-C-0035

A Design for Minimum Eigenvalue Sensitivity

Subject to Selected Modal Insensitivity

by

Thomas H. Hopp

ABSTRACT

The problem of assigning eigenvalues with minimum sensitivity to system parameter changes is well represented in the literature, and traces its roots back to Jacobi. Designing a system with modes which are insensitive is a more recent development reported in the literature. When modal insensitivity is enforced on some of a system's eigenvalues it has been reported that the remaining eigenvalues become more sensitive to parameter changes. In this report the techniques of minimum eigenvalue sensitivity and modal insensitivity are combined to provide system designs which will not have increased sensitivity of the eigenvalues which were not made insensitive. The computer program MACSYMA, developed at MIT, is used extensively in calculating the example.

### Acknowledgement

The author would like to thank the Air Force Systems Command, the Air Force Office of Scientific Research, and the Southeastern Center for Electrical Engineering Education for providing him with the opportunity of doing research at the Flight Dynamics Laboratory, Wright-Patterson AFB OH. He would like to acknowledge the laboratory, in particular the Control Dynamics Branch and the Control Analysis Group, for their hoppitality.

Finally, he would like to thank Dr Siva S. Banda for his collaboration and guidance during the research effort, and he would like to acknowledge many helpful discussions with Capt D. Brett Ridgely.

## I. INTRODUCTION:

Robust control system theory is under study by the Air Force for use in the control of aircraft and large space structures. Design techniques that incorporate robustness are desirable since they allow the designer to compensate for inaccuracies in the design due to modelling errors and mechanical failures.

The topic of this report is robust eigenvalue placement. The techniques presented in this report can be considered robust for two reasons. First, the sensitivity to system parameter changes of some of the assigned closed-loop eigenvalues is minimized. Second, certain selected closed-loop eigenvalues may be made completely insensitive to parameter changes.

In this report we will consider systems of the form

$$\dot{x}(t) = A(\alpha) x(t) + B(\alpha) u(t) \quad (1)$$

where the state  $x$  is an  $n$ -vector and the control  $u$  is an  $m$ -vector. We will further assume that the entries of the  $A$  and  $B$  matrices may vary as a function of some parameter  $\alpha$  in such a way that the system may still be considered time invariant.

It is well known in multivariable systems theory that the state feedback matrix  $K$  which places eigenvalues is not unique. The minimization of eigenvalue sensitivities in control system synthesis was first used by Morgan [1] to exploit the nonuniqueness of the  $K$  matrix by selecting from all possible  $K$ 's the one which would

minimize some sensitivity functional. Further work in this area has been done by Porter [2], Crossley and Porter [3], Reddy [4], Ramar and Gourishankar [5], and Gourishanker and Ramar [6].

As in [6] we define the sensitivity of any eigenvalue  $s_i$  of the closed-loop system with respect to small variations in the element  $a_{jk}$  of the closed-loop system matrix  $\tilde{A}$  to be

$$S_{jk}^i = \frac{1}{g'(s_i)} \text{tr} \left[ R(s_i) \frac{\partial \tilde{A}}{\partial a_{jk}} \right] \quad (2)$$

where  $g'(s_i)$  is the derivative of the closed-loop characteristic polynomial with respect to  $s$  evaluated at  $s_i$ ,  $R(s_i)$  is the adjoint of  $(s_i I - \tilde{A})$ , and  $\text{tr}$  denotes the trace of the matrix. The sensitivity functional to be minimized is of the form

$$J = \sum_{i=1}^n \sum_{j=1}^n \sum_{k=1}^n |S_{jk}^i|^2 \quad (3)$$

This form of the functional represents the most general case where the sensitivity of all the eigenvalues is being minimized with respect to changes in all of the entries of  $\tilde{A}$ . In practice this usually will not be the case and the summation limits in (3) can be adjusted according to the requirements of a particular problem.

More recent work in the field has been concerned with control systems which provide eigenvalue and eigenvector insensitivity, this is called modal insensitivity. Howze and Cavin [7] defined and solved the modal insensitivity problem first. Sambandan and Chandrasekharan [8] and Calise and Raman [9] are others who have

worked with modal insensitivity.

From [7] we get the definition of modal insensitivity. Let  $ds_i$  be the change in eigenvalue  $s_i$  due to changes in the  $\tilde{A}$  matrix, and let  $dv_i$  be the change in the associated eigenvector  $v_i$  due to changes in the  $A$  matrix. If  $ds_i = 0$  and  $dv_i = \gamma_i v_i$  for some scalar  $\gamma_i$  i.e., the eigenvalue doesn't change and the eigenvector changes in magnitude only then the  $i$ th mode is considered insensitive. In this report we are only interested in the insensitivity of the eigenvalue, the additional benefit of the eigenvector insensitivity is a by-product of the design process. We will see later that the conditions for modal insensitivity give us a set of linear equality constraints on the entries of the feedback matrix  $K$ .

The work reported here was motivated by Calise and Raman [9]. They indicated that when a mode is made insensitive, the remaining eigenvalues tend to become more sensitive to parameter changes. In this report we will provide for some modes to be made insensitive while at the same time minimizing the sensitivities of the remaining eigenvalues.

## II. OBJECTIVES:

The problem statement is as follows. Given a set of  $n$  desired distinct and self-conjugate closed-loop eigenvalues for the system

(1) find the control law

$$u(t) = Kx(t) \quad (4)$$

which will:

a) make  $p < n$  of the desired eigenvalues insensitive

and

b) minimize the sensitivity of any or all of the remaining  $(n-p)$  eigenvalues.

The number of eigenvalues  $p$  which can be made insensitive must be calculated in the design procedure, while the number of remaining eigenvalue sensitivities which are to be minimized is the designer's choice. The following sections will provide the theory for the problem's set up and solution. The results will also be demonstrated with an illustrative example.

### III. MODAL INSENSITIVITY THEORY:

For modal insensitivity we must not only assign an eigenvalue  $s_i$ , but also its eigenvector  $v_i$ . This requires  $v_i$  to be in the set of achievable eigenvectors which was characterized by Moore [10]. From [9] we get the condition which must be satisfied for modal insensitivity and eigenvector assignability

$$\begin{bmatrix} (s_i I - A_0) & -B_0 \\ dA & dB \end{bmatrix} \begin{bmatrix} v_i \\ w_i \end{bmatrix} = D_i \begin{bmatrix} v_i \\ w_i \end{bmatrix} = 0 \quad (5)$$

where  $A_0$  and  $B_0$  are the nominal values of the matrices,

$$dA = \left. \frac{dA}{d\alpha} \right|_{\alpha_0}, \quad dB = \left. \frac{dB}{d\alpha} \right|_{\alpha_0}, \quad (6)$$

and  $KV_i = W_i$  for each  $i = 1, \dots, p$ . Furthermore, we require that the eigenvectors be linearly independent, and if there are pairs of complex eigenvalues then their eigenvectors must also be complex conjugates.

Equation (5) shows that the vectors  $[v_i, w_i]^T$  must be in the null space of  $D_i$ . Since the eigenvectors must also be linearly independent it is possible to assign only  $p = (n+m-r)$  modally insensitive eigenvectors where  $r$  is the rank of  $D$ . Also to be considered is that not any arbitrary set of  $p$  eigenvalues can be made insensitive. If an eigenvalue causes the null space of  $D_i$  to be the null vector then that eigenvalue cannot be made insensitive.

Once the  $p$  insensitive eigenvalues and their eigenvectors are calculated they can be arranged to give a set of equality constraints on the entries of  $K$ .

$$K [v_1 | v_2 | \dots | v_p] = [w_1 | w_2 | \dots | w_p]$$

or  $KV = W \quad (7)$

#### IV. MINIMUM EIGENVALUE SENSITIVITY THEORY:

To minimize the sensitivity of eigenvalues we use the technique described by Gourishankar and Ramar [6]. The reasoning behind this method is that only one row of the feedback matrix  $K$  is needed to place the eigenvalues while the rest of the rows of  $K$  can be chosen

to minimize their sensitivity.

Define a matrix  $\bar{K}$ , a row vector  $\hat{k}$ , a matrix  $\bar{B}$ , and a column vector  $\hat{b}$

$$\bar{K} = \begin{bmatrix} k_1 \\ \vdots \\ k_{i-1} \\ k_{i+1} \\ \vdots \\ k_m \end{bmatrix}, \quad \hat{k} = k_i \quad (8)$$

$$\bar{B} = [b_1 \quad b_2 \quad \dots \quad b_{i-1} \quad b_{i+1} \quad \dots \quad b_m], \quad \text{and } \hat{b} = b_i.$$

Next, let

$$\bar{u} = \bar{K}x, \quad \hat{u} = \hat{k}x \quad (9)$$

and form the equation

$$\dot{x} = Ax + \bar{B}\bar{u} + \hat{b}\hat{u} \quad (10)$$

Substituting into equation (10) using equation (9) we have

$$\dot{x} = (A + \bar{B}\bar{K})x + \hat{b}\hat{u} = \bar{A}(\bar{K})x + \hat{b}\hat{u} \quad (11)$$

which is a single input system.

When the system is redefined in equation (8) the resulting equation (11) must be controllable. Substituting for  $\hat{u}$  using equation (9) we get

$$\dot{x} = (\bar{A}(\bar{K}) + \hat{b}\hat{k})x = \tilde{A}x \quad (12)$$

which is the closed-loop system equation. We now need  $\hat{k}$  as a function of  $\bar{K}$ . This can be done by any of several different methods of eigenvalue assignment. It is suggested that the technique

presented by Gopinath [11] be used because it leads to the solving of just  $n$  linear equations for  $\hat{k}$  as a function of  $\bar{K}$  rather than solving nonlinear equations which is the case in other techniques. Once we have  $\hat{k}$  as a function  $\bar{K}$  then we have  $\tilde{A}$  as a function of  $\bar{K}$ , and therefore the sensitivity function  $S_{jk}^i$  given in equation (2) is also a function of  $\bar{K}$ .

The elements of  $\bar{K}$  are then chosen in such a way as to minimize the functional  $J$  in equation (3). The feedback matrix  $K$  that results from the procedure places the eigenvalues as desired while minimizing some or all of their sensitivities to parameter changes in the  $\tilde{A}$  matrix.

#### V. MATHEMATICAL PROBLEM FORMULATION AND SOLUTION:

From the problem of making eigenvalues insensitive we get a set of equality constraints on the entries of  $K$ . The problem of minimizing the sensitivities of eigenvalues provides us with a functional  $J$  which is to be minimized.

Combining these individual problems we arrive at a problem statement in the form of a nonlinear programming problem:

MINIMIZE  $J$  SUBJECT TO THE EQUALITY CONSTRAINTS  $KV=W$

which when solved will yield the matrix  $K$  which is the solution to our problem as stated in section II. The control law will place the closed-loop eigenvalues as desired while making  $p$  of them insensitive and minimizing the sensitivity of some or all of the

remaining eigenvalues.

The Karush-Kuhn-Tucker necessary conditions for constrained minimization [12] give us a method for solution. Since the problem is a nonlinear minimization there is no guarantee that a solution exists. The program MACSYMA was used in calculating the example which is in this report.

The solution algorithm goes as follows:

1) Find the equality constraints  $KV=W$  from the  $p$  eigenvalues which are being made insensitive. Remember  $p$  depends upon the dimension of the null space of  $D$ .

2) Redefine the system as a single input system, and find  $\hat{k}$  as a function of  $\bar{K}$ .

3) Find the sensitivities as a function of  $\bar{K}$  and calculate  $J$  as a function of  $\bar{K}$ .

4) Form the nonlinear programming problem, and carry out the minimization.

#### VI. EXAMPLE:

To illustrate the techniques in this report we look at the following fourth order system

$$\dot{x} = \begin{bmatrix} 0 & 1 & 0 & 0 \\ 0 & 0 & -1 & 0 \\ 0 & 0 & 0 & 1 \\ 0 & 0 & 1+\alpha & 0 \end{bmatrix} x + \begin{bmatrix} 0 & 0 \\ 1 & 0 \\ 0 & -1 \\ 0 & 0 \end{bmatrix} u \quad (13)$$

with two controls and an uncertainty in the (4, 3) position of the  $A$

matrix. We would like to place the closed loop eigenvalues at -1, -2, -3, and -4 using state feedback. Also, we want to make -1 insensitive to parameter changes, and minimize the sensitivity of -2.

To make -1 insensitive we form equation (5)

$$\begin{bmatrix} -1 & -1 & 0 & 0 & 0 & 0 \\ 0 & -1 & 1 & 0 & -1 & 0 \\ 0 & 0 & -1 & -1 & 0 & 0 \\ 0 & 0 & -1 & -1 & 0 & 0 \\ 0 & 0 & 0 & 0 & 0 & 0 \\ 0 & 0 & 0 & 0 & 0 & 0 \\ 0 & 0 & 0 & 0 & 0 & 0 \\ 0 & 0 & 1 & 0 & 0 & 0 \end{bmatrix} \begin{bmatrix} v_1 \\ w_1 \end{bmatrix} = 0$$

and solve for  $v_1$  and  $w_1$ ,

$$v_1 = \begin{bmatrix} -1 \\ 1 \\ 0 \\ 0 \end{bmatrix}, \quad w_1 = \begin{bmatrix} -1 \\ 0 \end{bmatrix}.$$

When we form the constraints  $KV=W$  we get

$$\begin{aligned} k_2 - k_1 + 1 &= 0 \\ k_6 - k_5 &= 0 \end{aligned}$$

where

$$K = \begin{bmatrix} k_1 & k_2 & k_3 & k_4 \\ k_5 & k_6 & k_7 & k_8 \end{bmatrix}.$$

To minimize -2's sensitivity we choose the first row of  $K$  as  $k$  and form the single input system of equation (11)

$$\dot{x} = \begin{bmatrix} 0 & 1 & 0 & 0 \\ 0 & 0 & -1 & 0 \\ -k_5 & -k_6 & -k_7 & 1-k_8 \\ 0 & 0 & 1 & 0 \end{bmatrix} x + \begin{bmatrix} 0 \\ 1 \\ 0 \\ 0 \end{bmatrix} \hat{u}.$$

Using Gopinath's eigenvalue placement techniques to assign -1, -2, -3, and -4 we can get  $\hat{k}$  as a function of  $\bar{k}$ . Next, we find the

sensitivity of -2 to changes in element (4, 3) of  $\tilde{A}$  as in equation (2). These steps require the use of MACSYMA in order to handle the magnitude of the matrix algebra required. The sensitivity  $S_{43}^{-2}$  is too large a function to be included here.

Finally, we form J as in equation (3)

$$J = |S_{43}^{-2}|^2 \quad (15)$$

which is a function of  $\bar{K}$ . In order to carry out the minimization we also need to reformulate the equality constraints (14) as functions of K. The minimization is carried out for the Karush-Kuhn-Tucker necessary conditions using MACSYMA. The results are:

$$k_5 = k_6 = \text{arbitrary},$$

$$k_7 = \text{arbitrary},$$

$$k_8 = \frac{23}{11},$$

$k_5 = k_6 = 1$  and  $k_7 = 0$  were chosen and the rest of the K matrix calculated

$$K = \begin{bmatrix} -9 & -10 & 15 & -\frac{24}{11} \\ 1 & 1 & 0 & \frac{23}{11} \end{bmatrix}.$$

The resulting closed-loop system which has -1, -2, -3, and -4 as it's eigenvalues is

$$\dot{X} = \begin{bmatrix} 0 & 1 & 0 & 0 \\ -9 & -10 & 14 & -\frac{24}{11} \\ -1 & -1 & 0 & -\frac{12}{11} \\ 0 & 0 & 11+\alpha & 0 \end{bmatrix} X$$

The value of -2's sensitivity in this case is zero. To check this design was allowed to vary and the change in the eigenvalues was observed. Table One summarizes the results.

Percent Change in:				
$a_{43}$	-1	-2	-3	-4
+10	0	0	36.5	27.4
+20	0	0	51.6	39.7
-10	0	0	23.5	17.6
-20	0	0	36.5	27.4

To contrast this a design was done to only make -1 insensitive without any sensitivity minimization. The design was done using an entire eigenstructure assignment method. The resulting K was

$$K = \begin{bmatrix} -4 & -5 & 0 & -\frac{3}{11} \\ 0 & 0 & 5 & \frac{17}{11} \end{bmatrix},$$

and the closed loop system becomes

$$\dot{X} = \begin{bmatrix} 0 & 1 & 0 & 0 \\ -4 & -5 & -1 & -\frac{3}{11} \\ 0 & 0 & -5 & -\frac{6}{11} \\ 0 & 0 & 11+\alpha & 0 \end{bmatrix} X.$$

Table Two shows the variations in the eigenvalues due to changes in

$a_{43}$ :

Percent Change in:				
$a_{43}$	-1	-2	-3	-4
+10	0	39.7	25.8	0
+20	0	54.8	36.5	0
-10	0	21.1	14.1	0
-20	0	35.2	23.5	0

Tables One and Two show that an improvement can be made upon the sensitivity of -2 and that in this case it's sensitivity becomes zero.

VII. RECOMMENDATIONS:

The procedure outlined in this report depends upon the formulation of a sensitivity function. This function is in general very complicated and unwieldy to handle. For large order systems the sensitivity function becomes so large as to be totally impracticable. Large in this case means about fourth order. This problem has been commented upon by many of the papers which discuss eigenvalue sensitivity. In light of this a more compact sensitivity function is highly desirable.

This report only covers the problem of state feedback. The ideas herein should be applicable to output feedback and observers. These could lead toward actual application of this theory.

## REFERENCES

1. Morgan, B.S., Jr., "Sensitivity Analysis and Synthesis of Multivariable Systems," IEEE Transactions on Automatic Control, Vol. AC-11, No. 3, July 1966, pp. 506-512.
2. Porter, B., "Eigenvalue Sensitivity of Modal Control Systems to Loop-Gain Variations," International Journal of Control, Vol. 10, No. 2, 1969, pp. 159-162.
3. Crossley, T.R. and Porter, B., "Eigenvalue and Eigenvector Sensitivities in Linear Systems Theory," International Journal of Control, Vol. 10, No. 2, 1969, pp. 163-170.
4. Reddy, D.C., "Eigenfunction Sensitivity and the Parameter Variation Problem," International Journal of Control, Vol. 9, No. 5, 1969, pp. 561-568.
5. Ramar, K. and Gourishankar, V., "Utilization of Design Freedom of Pole Assignment Feedback Controllers of Unrestricted Rank," International Journal of Control, Vol. 24, No. 3, 1976, pp. 423-430.
6. Gourishankar, V. and Ramar, K., "Pole Assignment with Minimum Eigenvalue Sensitivity to Plant Parameter Variations," International Journal of Control, Vol. 23, No. 4, 1976, pp. 493-504.
7. Howze, J.W. and Cavin, R.K., III., "Regulator Design with Modal Insensitivity," IEEE Transactions on Automatic Control, Vol. AC-24, No. 3, June 1979, pp. 466-469.
8. Sambandan, A. and Chandrasekharan, P.C., "Design of Output Feedback Controller with Eigenvalue and Eigenvector Insensitivity," International Journal of Control, Vol. 33, No. 5, 1981, pp. 935-943.
9. Calise, A.J. and Raman, K.V., "Modal Insensitivity with Optimality," Proceedings of the 1984 American Control Conference, San Diego CA, June 1984, pp. 949-953.
10. Moore, B.C., "On the Flexibility Offered by State Feedback in Multivariable Systems Beyond Closed Loop Eigenvalue Assignment," IEEE Transactions on Automatic Control, Vol. AC-21, Oct. 1976, pp. 689-692.
11. Gopinath, B., "On the Control of Linear Multiple Input-Output Systems," The Bell System Technical Journal, Vol. 50, No. 3, March 1971, pp. 1063-1081.
12. McCormick, G., Nonlinear Programming: Theory, Algorithms, and Applications, John Wiley and Sons, New York, 1983, pp. 210-211.

1984 USAF-SCEEE GRADUATE STUDENT SUMMER SUPPORT PROGRAM

Sponsored by the

AIR FORCE OFFICE OF SCIENTIFIC RESEARCH

Conducted by the

SOUTHERN CENTER FOR ELECTRICAL ENGINEERING EDUCATION

FINAL REPORT

DIGITAL LQR DESIGN FOR ADVANCED TACTICAL AIRCRAFT-STOL APPROACH

Prepared by: Robert F. Hoskin  
Academic Department: Mechanical Engineering  
University: Purdue University  
Research Location: Air Force Aero-Propulsion Laboratory,  
Components Division, Controls Branch  
USAF Research Contact: Charles Skira  
SFRP Supervising  
Faculty Member: Dr. Robert L. Kerr  
Date: August 9, 1984  
Contract No: F49620-82-C-0035

DIGITAL LQR DESIGN FOR ADVANCED  
TACTICAL AIRCRAFT - STOL APPROACH

by

Robert F. Hoskin

ABSTRACT

The integration of flight control and engine control subsystems for an advanced tactical fighter is an important topic under investigation. The use of Digital Linear Quadratic Regulator Theory to control a linear system model (STOL approach) of the advanced aircraft/engine model is investigated. Digital LQR design produced a system which is stable, but not completely satisfactory due to long settling times and large state deviations. Recommendations to improve simulation techniques and aircraft/engine performance are discussed.

### Acknowledgement

The author would like to thank the Air Force Systems Command, the Air Force Office of Scientific Research and the Southeastern Center for Electrical Engineering for providing the opportunity to pursue a research topic at the Aero-Propulsions Laboratory, Wright-Patterson AFB, Ohio. He would like to thank Charles Skira, Lester Small, and other members of the Components Division for an excellent working environment and worthwhile suggestions during the research period.

Finally, he would like to thank Dinesh Joshi, Peter Shaw, and Rod Davis of Northrop Corporation for providing the linear models used in the project, and also for their many suggestions and assistance.

## I. INTRODUCTION

One of the current topics under investigation by the Air Force is the integration of flight control and engine control subsystems of an advanced tactical fighter aircraft. Previous aircraft have depended upon the pilot to perform this integration, but increasing engine and aircraft complexity will not allow the pilot to coordinate engine/aircraft control without diverting attention from fulfilling mission requirements. Integrated Flight and Propulsion Control (IFPC) is a program designed to improve the performance of the engine/aircraft (by using automatic systems to control the combined engine/aircraft) while reducing pilot workload.

The aircraft to which IFPC is being applied is based upon the F/A-18A design. Improvements to the aircraft design include a variable cycle engine (VCE), thrust vectoring/thrust reversing (TV/TR) nozzle, variable geometry inlet and canards, all of which contribute to improving the engine/aircraft performance while extending the flight envelope.<sup>1</sup>

The first step in developing a control scheme for any system is to develop a mathematical model of the system to be controlled. In most cases a system as complex as the aircraft/engine in question can only be modeled as non-linear, and the control of non-linear systems can present the control engineer with control implementation problems (not from an analytical standpoint, but from practical limitations of typical computer hardware).<sup>2</sup> To alleviate this problem, the non-linear system is modeled as a group of linear models, each model being developed for a selected point within the flight envelope. The control scheme for this system of models is devised to provide control near each operating point, and to provide transitional control between operating points, providing full control throughout the entire flight envelope.<sup>2</sup> The method used to design a control law for each operating point is known as Digital Linear Quadratic Regulator Theory (transitional control is provided by a combination

of integral control and interpolation of feedback gains for regions between operating points - developing transitional control was not a part of this project).

Digital LQR theory is a method of modern control in which a continuous system described by a space state representation of the form

$$\dot{x}(t) = Fx(t) + Gu(t) \quad (1)$$

and

$$y(t) = Hx(t) + Du(t) \quad (2)$$

is controlled using a digital computer implementing full state feedback of the form

$$u(kT) = -Px(kT) \quad (3)$$

$$\text{where: } u(t) = u(kT) \quad kT \leq t < (k+1)T$$

To implement this full state feedback design, equations (1) and (2) must be discretized to form the equations

$$x[(k+1)T] = \phi(T)x(kT) + \theta(T)u(kT) \quad (4)$$

and

$$y[(k+1)T] = Hx(kT) + Du(kT) \quad (5)$$

where

$$\phi(T) = e^{FT} \quad (6)$$

and

$$\theta(T) = \int_0^T \phi(T-\tau)d\tau \quad (7)$$

Using this discretized form of the system equations, digital LQR theory seeks to minimize the performance index

$$J = \frac{1}{2} \sum_{k=0}^{\infty} [x(kT)^T Q x(kT) + u(kT)^T R u(kT)] \quad (8)$$

The state feedback matrix, P, is obtained by a recursive solution of the following equations.<sup>3</sup>

$$P(kT) = [ R + \theta^T K[(k+1)T] \theta ]^{-1} [ \theta^T K[(k+1)T] \theta ] \quad (9)$$

and

$$K(kT) = Q + \theta^T K[(k+1)T] \theta - [ \theta^T K[(k+1)T] \theta ]^T P(kT) \quad (10)$$

Starting with the condition that  $K(\infty) = 0$ , equations (9) and (10) are solved recursively backward until constant values are obtained for the coefficients of the P matrix (in other words,  $P(kT) = P[(k+1)T]$ ). The values of the coefficients in the P matrix will vary depending on the selection of sampling time, and on the values in the Q (state weighting) matrix and the R (control weighting) matrix. The sampling time is chosen such that it is representative of typical computer hardware used for control purposes, and matrices Q and R are selected to produce the desired type of output response.

There are several methods of selecting coefficients for the weighting matrices, and the method chosen for this project is known as Bryson's Rule.<sup>4</sup> Bryson's Rule chooses coefficients for the R and Q matrices based on the maximum state and control deviations (from a given equilibrium point) that are desired. The coefficients are initially chosen by using the following relationships:

$$R_{ii} = \frac{1}{[u_{\max_i}]^2} \quad (11)$$

and

$$Q_{ii} = \frac{1}{[x_{\max_i}]^2} \quad (12)$$

Where:  $u_{\max_i}$  = maximum control deviation  
 $x_{\max_i}$  = maximum state deviation

If the simulated time response using these initial weightings is unsatisfactory, the coefficients of the Q and R matrices can be re-selected using an iterative procedure to improve system response. This iterative procedure requires both engineering intuition and knowledge of the system to produce a satisfactory control law.

## II. OBJECTIVES

The main objective of this project was to develop a suitable control law for the linearized aircraft/engine model (described in the next section) using Digital LQR theory as presented in the Introduction. Additionally, an examination of the closed loop system (closed loop poles and simulated closed loop time response) when subjected to state perturbations was to be undertaken to determine the robustness of the control law. Finally, the effects of changing the sampling time were to be examined.

## III. MODEL DESCRIPTION AND SIMPLIFICATIONS

The aircraft/engine model used in this project is a linear model describing system operation for a Short Takeoff and Landing (STOL) situation. The model provided by Northrop was simplified somewhat to facilitate the Digital LQR design procedure. Simplifications were as follows:

- (1) Reduce the aircraft state matrix to five states (u, w, q,  $\theta$ , h). This simplification corresponds to the longitudinal component of aircraft motion.
- (2) Eliminate rudder and assuming all actuators to move symmetrically (left and right).
- (3) Eliminate inlet actuator /sensors and assume perfect pressure recovery.
- (4) Reduce the number of aircraft/engine outputs
- (5) Simplify the engine/nozzle actuators to first order systems (one state per actuator).
- (6) Eliminate TLA (propulsive lift) as a control.

With these simplifications, the final model was a system having 32 states, 60 outputs, and 14 inputs. The final form of the simplified model was:

$$\dot{x}(t) = Fx(t) + GYy(t) + Gu(t) \quad (13)$$

and

$$y(t) = Hx(t) + DYy(t) + Du(t) \quad (14)$$

As can be seen, equations (13) and (14) are not in standard state space form (see equations (1) and (2)).

#### IV. COMPUTER PROGRAMS

To implement the Digital LQR design methods computer programs were written to change the system equations (equations (13) and (14)) to standard form (the form of equations (1) and (2)), compute the state feedback matrix P, compute the open and closed loop eigenvalues, and simulate the time response of the closed loop system.

The first set of programs written utilized subroutines from the IMSL library<sup>5</sup>, and changed equations (13) and (14) to the form:

$$\dot{x}(t) = FSx(t) + Gu(t) \quad (15)$$

and

$$y(t) = HSx(t) + Du(t) \quad (16)$$

where

$$FS = ( F + GY [ I-DY ]^{-1}H ) \quad (17)$$

and

$$HS = [ I-DY ]^{-1}H \quad (18)$$

The second program utilized subroutines from the LQGLIB library.<sup>6</sup> This program discretized equations (15) and (16) (to the form of equations (4) and (5)), and designed the feedback matrix, P, given a selected sampling time and the selected values for the coefficients of the R and Q matrices. This program also returned the closed loop system matrix, ACL, where:

$$ACL = [ \phi - \theta P ] \quad (19)$$

The third program utilized subroutines from the LQGLIB library<sup>6</sup>, and simulated the closed loop system time response given a sampling time, the discretized system equations, and the following equation:

$$x[(k+1)T] = ACLx(kT) \quad (20)$$

The fourth program utilized subroutines from the LQGLIB library<sup>6</sup>, and computed the open and closed loop eigenvalues of the system (from the FS and ACL matrices respectively).

#### V. ITERATIVE PROCEDURE

As stated in the Introduction, Digital LQR design is an iterative process, in which the state and control weightings are varied until satisfactory system response is obtained. The computer programs described in the previous section were used to implement this procedure. To begin the procedure, the system was put into standard form and Bryson's Rule was used to select the initial weighting matrices. The initial weightings were based upon knowledge of the aircraft controls and states (for example, the horizontal rudder position was selected to have a maximum deviation of 30 degrees from equilibrium). After the state and control weighting matrices were obtained, a sampling time was selected (for most iterations the sampling time was 17 milli-seconds) and the state feedback matrix computed. Next the aircraft states were given an initial perturbation, and the closed loop response for the given P matrix was calculated. Finally, the closed loop poles of the system were examined.

The initial time simulation yielded a response in which most of the states returned to steady state within 5 seconds while deviating only slightly from equilibrium. The exception was the altitude of the aircraft, which varied by 100 feet from its equilibrium glidepath in 10 seconds of simulation time (the actual time response plots are not shown in order to maintain brevity). To compensate for this unacceptable deviation, more state and control weighting was placed on the aircraft states and controls (horizontal rudder, ailerons, etc.) and less weighting placed on engine states and controls in following iterations.

#### VI. FINAL CONTROL LAW

After a large number of iterations, a final control law for the system was selected. The open and closed loop poles of the system

are shown in Table 1 (note that the open loop poles are S plane poles, and the closed loop poles are Z plane poles).

OPEN LOOP EIGENVALUES (S plane)		CLOSED LOOP EIGENVALUES (Z plane)	
Real Part	Imag. Part	Real Part	Imag. Part
0.0	0.0	0.18268	0.0
-50.0	0.0	0.065086	0.0
-50.0	0.0	0.25663	0.0
-0.77631	0.0	0.356845	0.0
-20.0	0.0	0.356847	0.0
-100.0	0.0	0.64543	0.151146
-100.0	0.0	0.64543	-0.151146
-100.0	0.0	0.99937	0.005337
-160.603	0.0	0.99937	-0.005337
-2.6142	0.0	0.999978	0.0
-7.6226	0.0	0.965452	0.0
-14.9	0.0	0.948668	0.0
15.3186	0.0	0.934649	0.0
-15.3186	0.0	0.9035	0.0
-3.0999	0.0	0.94994	0.0
2.068	0.0	0.77071	0.000396
-0.035276	0.31402	0.77071	-0.000396
-0.035276	-0.31402	0.98689	0.0
-60.606	0.0	0.71177	0.0
-40.0	0.0	0.18268	0.0
-40.0	0.0	0.506505	0.0
-80.0	0.0	0.18268	0.0
-60.606	0.0	0.506505	0.0
-5.124	0.0	0.522028	0.0
-38.71	0.0	0.518509	0.0
-38.71	0.0	0.517743	0.0
-38.71	0.0	0.517732	0.0
-38.71	0.0	0.427415	0.0
-38.71	0.0	0.427415	0.0
-24.6	0.0	0.517848	0.0
-24.6	0.0	0.657999	0.0
-24.6	0.0	0.657999	0.0

Table 1 - Open and Closed Loop Eigenvalues  
Sampling Time = 17 milli-seconds

After examining Table 1, it can be seen that the open loop system has 2 poles in the right half plane, and is thus unstable. The closed loop system has all poles located inside the unit circle in the Z plane (the transformation between the S and Z planes is  $Z = e^{TS}$  : poles in the left half of the S plane map inside the unit circle in

the Z plane) and thus is an asymptotically stable system. However, 8 of the closed loop poles have magnitudes very close to 1, indicating that these poles will cause several states to have long settling times (including the aircraft altitude). Examining the time simulation confirms this statement.

Although the final system response is not completely satisfactory from a performance standpoint, it was chosen because the system stayed within physical limitations imposed upon the aircraft. Specifically, aircraft constraints limit horizontal rudder deflections, aileron deflections, leading edge flap deflections, trailing edge flap deflections, and canard deflections to a total range of approximately 100 degrees (in most cases less than this). Since a moderate perturbation of the final system model required feedback control signals approaching these physical limits, the system response could not be improved without requiring the system to behave in an impossible manner (for example requiring a canard deflection of 200 degrees—mathematically possible but not physically possible). In its final form the closed loop system is asymptotically stable, but the system response requires improvement before real time implementation can take place.

#### RECOMMENDATIONS

Since the final control scheme devised for the aircraft/engine linear model did not produce a completely satisfactory time response, further design work with this model needs to be completed. The model itself should be examined for possible errors which might have caused the time response of the linear model to be misrepresentative of the actual system (recall that the model used is based on the F-18A design—a design that has been successfully controlled). The Digital LQR design theory used should also be re-evaluated and re-examined for possible problems.

In addition to the above recommendations, there are several other items that deserve discussion. The first item has to do with the subroutine used to produce the digital time simulation (because of time limitations of the project, every effort was made to use existing soft-

ware rather than expend time to write new software). This subroutine produced the time simulation using the discretized system equations, including equation (3). Equation (3) computes the feedback control signal from the instantaneous state deviations. Equation (3) assumes this computation to be instantaneous, but in reality a digital computer implementing equation (3) in real time control would produce results more representative of the equation

$$u[(k+1)T] = -Px(kT) \quad (21)$$

because of time delays associated with multiplication. Figure 1 illustrates this phenomenon.

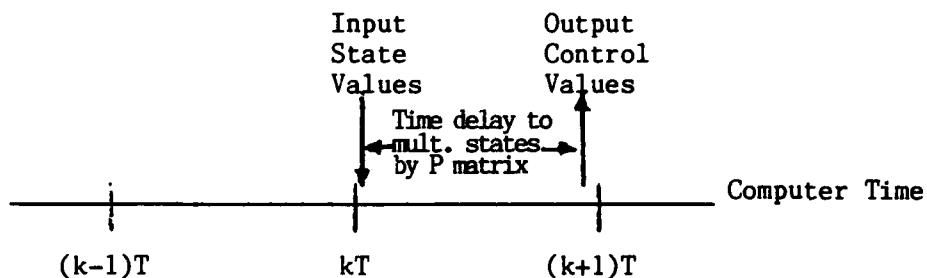


Figure 1 - Illustration of Computational Time Delay

This additional time delay produces an extra pole (at the origin in the Z plane) in the closed loop system, causing the time response to be different (usually less damped) than the response produced by using equation (3) for the simulation.<sup>3</sup> This time delay is inherent when digital computers are used for real time control, and a simulation subroutine that incorporates this delay should be used to produce an accurate time simulation (the effect of the delay becomes more pronounced as the sampling time is increased).

Another item that needs to be discussed also deals with a subroutine used for the time simulation, in this case the method in which the system is given perturbations. As discussed previously, the time

response is produced using equation (20). The use of this equation limits one to producing the closed loop response to a step input (the initial states are given a perturbation and the response is observed to see if the system returns to steady state). A more realistic simulation would allow ramp and other types of inputs (more representative of what an aircraft might encounter in flight) to be used.

Finally, the effects of changing the sampling time need to be examined in more detail. One of the initial objectives was to study changes in system response caused by varying the sampling time, but time limitations on the project restricted the study to one sampling time.

## REFERENCES

1. Design Methods For Integrated Control Systems. Midterm Industry Briefing Presented at AFWAL, Dayton, Ohio jointly by Northrop Corp., Systems Control Technology Inc., and General Electric, June 28, 1984.
2. Ronald L. De Hoff, W. Earl Hall, Jr., Richard J. Adams, Narendra K. Gupta, F100 Multivariable Control Synthesis Program, Volume 1 - Development of F100 Control system, Technical Report AFAPL-TR-77-35, Volume 1, (Government Printing Office, 1977), p. 110.
3. Benjamin C. Kuo, Digital Control Systems, (Holt, Rinehart and Winston, Inc., New York, 1980), pp. 617-618.
4. J.W. Fuller, J.H. Vincent, Advanced VSTOL Flight Control System Technology Assessment, SCT Report No. 5339-250-1 (SCT Publication, May 1982), p. 37.
5. ASD Computer Center Staff, CDC NOS User's Guide, Revision B, 1983.
6. Alphatech, Inc., LOGLIB User's Manual : A Description Of Computer Routines For Use In Linear Systems Studies, May 1984.

1984 USAF-SCEEE SUMMER FACULTY RESEARCH PROGRAM

Sponsored by the

AIR FORCE OFFICE OF SCIENTIFIC RESEARCH

SOUTHEASTERN CENTER FOR ELECTRICAL ENGINEERING EDUCATION

FINAL REPORT

THE ROLE OF ANTIOXIDANT NUTRIENTS IN PREVENTING HYPERBARIC  
OXYGEN DAMAGE TO THE RETINA

Prepared by : William L. Stone, Ph.D.  
and George Howard, Jr.

Academic Rank: Assistant Professor

Department and  
University: Department of Biomedical Sciences  
Meharry Medical College

Research Location: Brooks Air Force Base, School of Aerospace  
Medicine, Division of Hyperbaric Medicine.

USAF Research: Col. Richard Henderson, M.D., Chief of Clinical  
Investigations and Acting Director, Division  
of Hyperbaric Medicine

Date: September 6, 1984

Contract No. F49620-82-C-0035

George Howard, Jr.

ABSTRACT

Hyperbaric oxygen was found to affect adversely the electrophysiological response of the retina to light in rats fed a diet deficient in both vitamin E and selenium. Both vitamin E and selenium are micronutrients thought to play essential roles in preventing in vivo lipid peroxidation. Rats fed diets supplemented with vitamin E and/or selenium and treated with 2.0 ATA (atmospheres absolute) of 100 percent oxygen for 1.5 hours per day for 4 weeks did not show any decrease in electroretinogram response. The retina is known to be particularly susceptible to oxidative damage caused by in vivo lipid peroxidation. Dietary antioxidants appear to provide protection from hyperbaric oxygen damage to the rat retina.

## **I. INTRODUCTION:**

Hyperbaric oxygen treatment is currently being used by the School of Aerospace Medicine to treat a variety of clinical disorders. These clinical disorders include gas gangrene, gas embolism, decompression sickness, carbon monoxide poisoning and wound healing enhancement. The therapeutic benefits of long term hyperbaric oxygen treatment are potentially limited by the adverse clinical and pathological effects of high oxygen concentration upon the retina and lung. In addition, many drugs and toxins are known to directly promote oxidative damage or to interfere with enzymatic antioxidant mechanisms. This raises the possibility of adverse drug-hyperbaric oxygen interactions in patients undergoing long-term hyperbaric oxygen therapy.

Gable and Townsend (1) have observed pulmonary lesions in victims of fatal military aircraft accidents "possibly attributable to prolonged intermittent supplemental oxygen, stressing the potential hazard of oxygen toxicity for aviators" (2). Oxygen toxicity to retinal and pulmonary tissues most likely involves free radical damage to biological membranes. Vitamin E and selenium are nutrients that play a central role in physiological antioxidant mechanisms. Vitamin E effectively quenches free radicals generated by lipid peroxidation. Selenium is a cofactor for glutathione peroxidase which detoxifies lipid hydroperoxides. Humans deficient in vitamin E and/or selenium may be particularly susceptible to the pathophysiological consequences of hyperbaric oxygen. Conversely, dietary supplements of these micronutrients may offer considerable protection against oxygen toxicity.

The retina is more sensitive to toxic and environmental disorders than most tissues. The retina is particularly predisposed to the

toxic effects of lipid peroxidation initiated by oxy-radicals. This is because the retina has: a) a very high content of polyunsaturated fatty acids (about 30% 22:6n3) which are very susceptible to lipid peroxidation (6); b) a very high consumption of oxygen, about seven times more per g of tissue than the brain and ; c) the presence of pigments (e.g. retinal) capable of inducing photosensitized oxidation reactions (7). Retinal lipid peroxidation is likely to be accelerated under conditions of hyperbaric oxygen stress.

In animal models hyperbaric oxygen causes severe retinal pathology and, in humans, causes loss of visual fields and visual definition (8). The ability of the retina to resist oxidative damage is very dependent upon the functioning of both enzymatic and chemical antioxidant mechanisms (3). A number of important antioxidant mechanisms are very dependent upon micronutrient intake. We have previously shown that rat retinas have significant levels of vitamin E, glutathione-S-transferase, and the selenoenzyme glutathione peroxidase (3,4). Retinal vitamin E and glutathione peroxidase are decreased to very low levels by nutritional deficiency of vitamin E and selenium, respectively (7,9). Retinal glutathione-S-transferase activity is induced in the absence of dietary vitamin E and selenium (4).

Rats deficient in vitamin E and selenium (the B dietary group) show a decreased a- and b-wave electroretinogram (ERG) amplitude (9). Recent in vitro studies of Armstrong, et al. (10), have shown that intravitreal injections of synthetic lipid hydroperoxides into rabbit eyes causes a marked decrease in the amplitude of the a-, b-, and c-waves of the ERG. The retinal pigment epithelium of rats fed the diet deficient in both vitamin E and selenium also show a large

accumulation of lipofuscin pigment (9) as well as major ultrastructural alterations (11). Lipofuscin pigment is thought to be a by-product of in vivo lipid peroxidation and can be measured by fluorescent microscopy.

The information presented above suggests that hyperbaric oxygen damage to the retina would be greatly accelerated in cases of antioxidant nutrient deficiencies and inhibited by dietary supplementation with antioxidant nutrients.

## II. OBJECTIVES OF THE RESEARCH EFFORT:

The primary goal of this project was to determine if hyperbaric oxygen damage to the retina and lung is accelerated in organisms deficient in dietary antioxidant nutrients and inhibited in organisms supplemented with antioxidant nutrients. Rats will be used as an experimental model in this work. Damage to the retina will be determined noninvasively by measurement of electroretinograms (ERGs). When ERGs show evidence of retinal damage the rats will be sacrificed and the retinas and pulmonary tissues examined by fluorescent microscopy, as well as light and electron microscopy. Lung tissue samples will also be collected and biochemically characterized as described below.

## III. EXPERIMENTAL DESIGN:

Rats were fed diets deficient in antioxidant nutrients. The antioxidant nutrients tested in this initial study were vitamin E and selenium. A factorial design was utilized in which the dietary groups were:

- 1) a basal diet deficient in both vitamin E and selenium but adequate in all other nutrients (the basal or B diet)
- 2) a basal diet plus vitamin E (the B+E diet)
- 3) a basal plus selenium diet (the B+Se diet)
- 4) a basal plus vitamin E plus selenium diet (the B+E+Se diet)

The detailed composition of the basal diet is given in Table IV. Enough feed has been mixed to continue the nutritional experiments to the end of October, 1984 ; i.e. for a total of 16 weeks or 8 weeks beyond the end of the SFRP tenure.

Male, 30 g, inbred Fischer-344 (CDF) rats were obtained from Charles River Breeding Laboratory. The P.I. has utilized this rat strain in nutritional experiments analogous to those proposed here. The time course for development of nutritional deficiencies in vitamin E and selenium is well characterized in this strain. We have also performed extensive histopathology studies on Fischer-344 rats fed diets identical to those used in this study. It takes about 5 weeks for 50 g rats to lose half of their blood selenium and half of their plasma vitamin E content when fed the basal diet. After 10 weeks, the rats have only about 10% of their initial blood vitamin E and selenium. After 20 weeks, rats are almost totally depleted of both micronutrients and suffer retinal damage under nonstress conditions.

The animals were housed in suspended stainless steel, wire-bottomed cages and maintained at 25±2 C and 50% relative humidity. Lighting was on a 6:00 AM to 6:00 PM light period and a 6:00 PM to 6:00 AM dark

period. Upon arrival at Brooks AFB, the rats were fed a normal Purina laboratory chow (Rodent Laboratory Chow 5001, Ralston Purina Co., St. Louis, MO) and water ad libitum for 1 week. The rats were randomly divided into the four dietary groups designated above. Eight animals were used per dietary group (32 rats in total). The basal group was fed a Torula yeast-based diet having very low levels of vitamin E and Se but adequate levels of all other nutrients as proposed by the National Research Council for the Laboratory Rat. The basal+vit E+Se group was fed an identical diet but supplemented with 50 mg vitamin E per kg of diet (1.1 IU per mg of DL-alpha-tocopherol) and 0.4 ppm Se (added as sodium selenite). All dietary supplies were purchased from U.S. Biochemical Co, Cleveland, OH. The Torula-based diets were prepared in small batches by slowly mixing the constituents to avoid heating, and stored at 4 C. The glass and stainless steel feeders, obtained from Hazelton Systems, Aberdeen, MD, were filled every 2 days and any uneaten food discarded to minimize rancidity. The glass and stainless steel feeders as well as a small (2 kg capacity) Hobart food mixer were shipped to Brooks AFB from the P.I.'s laboratory at Meharry Medical College. Rats in all the dietary groups were provided with deionized water to which 3 ppm chromium (as CrCl<sub>3</sub>) was added. Both diet and drinking water were provided ad libitum. Half the rats from each dietary group were treated with 2.0 ATA of pure oxygen for 1.5 hr per day. This treatment began 2 weeks after the start of the dietary regimens. The other half of the rats provide a nonHBD control groups to monitor retinal damage that might be due to antioxidant deficiency alone.

At weeks 2, 4, and 6 and 8, electroretinograms (ERGs) of rats in each dietary group were recorded. ERG measurements were made using an

aluminized mylar plastic positive electrode placed on the cornea of each rat. This electrode effectively eliminates the possibility of corneal damage. The ground electrode was attached to the rat ear lobe. A negative pin electrode was inserted under the scalp. We used a ganzfeld (whole field) flash, a Grass photostimulator and a Tektonix model 4512 recording oscilloscope with a 5A22N differential amplifier and a 5B10N time base amplifier. The animals were placed in a dark room for 1 hr before measuring ERGs. About 10 min before recording an ERG, each rat was anesthetized (IM injection) with 0.1 ml of ketamine (50 mg/ml). At least six's a- and b-wave amplitude measurements were made for each eye and the results (at least 12 measurements per rat) averaged. The P.I. and Mr. George Howard were responsible for these measurements.

Rats from each dietary group have been evaluated for plasma vitamin E, plasma glutathione peroxidase (GSHPX), and red blood cell glutathione peroxidase at week 3. Plasma and RBC samples were collected at week 7 and will be analyzed on the P.I.'s return to Meharry Medical College. Glutathione peroxidase is a selenoenzyme and its activity in plasma and red blood cells (RBCs) is a good measure of selenium status. Blood is obtained from each rat after cutting (under methoxyfluorane anesthetization) off a small section from the end of the tail. This process is relatively untraumatic and can easily be done on the same rat on a biweekly basis. Blood is separated into plasma and washed RBCs. The glutathione peroxidase assays on plasma, and RBCs as well as plasma vitamin E assays will be done at Meharry Medical College by the P.I. and Mr. George Howard, a summer graduate student SCEEE fellow.

When the rats exposed to hyperbaric oxygen and deficient in vitamin E and/or selenium showed signs of retinal damage (such as diminished ERG a- and b-wave amplitudes), they were sacrificed (by overdose of methoxyfluorane) for detailed biochemical and cytopathology studies. Control animals, not exposed to hyperbaric oxygen were also sacrificed. Rats fed the diet deficient in both vitamin E and selenium and treated with HBO (the B+HBO group) have already shown decreased ERG a-wave amplitudes compared with the nonHBO B group. Rats from the B and B+HBO group have therefore been sacrificed for future biochemical and cytopathology studies.

#### IV. THE EFFECTS OF HYPERBARIC OXYGEN ON ELECTRORETINOGRAMS:

At weeks 2 and 4, hyperbaric oxygen treatment had no apparent effect on ERGs recorded from rats on any of the dietary regimens. As shown in Table I, rats exposed to hyperbaric oxygen treatment for 4 weeks, and fed a basal diet (B diet) deficient in vitamin E and selenium for 6 weeks, have decreased ERG a-wave amplitudes ( $P < 0.05$ ) and b-wave amplitudes compared to age-matched rats fed an identical diet but not treated with hyperbaric oxygen. Rats fed diets deficient in vitamin E (B+Se diet) or selenium alone (B+E diet) did not show any decline in ERG a- or b-wave amplitudes when exposed to hyperbaric oxygen at this time (see Table I). We anticipate, however, that rats deficient in vitamin E or selenium will eventually show decreased retinal function as they become progressively more deficient in these micronutrients. Acute deficiency of vitamin E and selenium takes no longer than 15 weeks on the dietary regimens.

#### V. THE EFFECT OF HYPERBARIC OXYGEN ON WEIGHT AND WEIGHT GAIN:

Rats fed the B diet deficient in both vitamin E and selenium for 5 weeks, and treated with hyperbaric oxygen (HBO) for 3 weeks show a decreased weight and weight gain compared with age-matched rats fed an identical diet but not receiving HBO treatment (see Table II). Similarly, rats fed the vitamin E deficient diet and treated with HBO (B+Se+HBO) are also beginning to demonstrate a reduced weight and weight gain which might indicate the onset of chronic HBO toxicity and retinal damage. HBO treatment does not appear to be adversely affecting the weight or weight gain of rats fed the vitamin E and selenium supplemented diet (the B+E+Se diet) or the diet supplemented with vitamin E alone (the B+E diet).

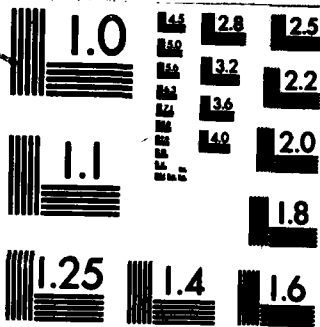
#### VI. ANTIOXIDANT STATUS OF RATS:

Plasma vitamin E, red blood cell and plasma Se-glutathione peroxidase activities were measured in rats, in all dietary groups, 3 weeks after the start of the nutritional regimens. As expected, rats fed the B diet have significantly lower plasma vitamin E as well as plasma and RBC Se-glutathione peroxidase activities compared to rats fed the B+E+Se diet (see Table III). We have recently obtained plasma and RBC samples at week 7 and plan to measure plasma vitamin E, plasma and RBC glutathione peroxidase and RBC glutathione levels in these samples. This work will be done at Meharry Medical College in the P.I.'s laboratory.

#### VII. RECOMMENDATIONS:

Dietary deficiencies of both vitamin E and selenium were found to adversely effect the electrophysiological response of the retina to light. Rats are generally considered a species very resistant to





MICROCOPY RESOLUTION TEST CHART  
NATIONAL BUREAU OF STANDARDS-1963-A

oxidative damage. Our preliminary results suggest that nutritional supplementation of patients with antioxidant nutrients could diminish the oxygen toxicity problems associated with HBO therapy. We do not yet know if deficiency of vitamin E or selenium alone will be associated with hyperbaric oxygen damage to the rat retina. We recommended that the nutritional experiments be continued for an additional 4 to 6 weeks so that ERG measurements can be made on rats treated with hyperbaric oxygen and acutely deficient in vitamin E (B+Se group) or selenium (B+E group).

It is also recommended that the follow-on biochemical studies of lung tissue, and light/electron microscopy studies of lung and retinal tissues, be pursued as detailed in the RESEARCH INITIATION PROPOSAL.

Animals in the B and B+HBO groups were euthanized at week 6 and samples of lung tissue stored at -70 C for biochemical analyses (see below). The rats were perfused with Karnofsky's fixative. Retinal and lung tissues were embedded in Epon for future analyses by fluorescent microscopy, phase contrast microscopy, and electron microscopy.

Rats have enzymatic antioxidant mechanisms that can be induced in response to oxidative stress (3,4,5). The degree to which an organism can induce these enzymatic antioxidant mechanisms may be an important parameter in determining an organism's susceptibility to oxygen toxicity. These potential physiological responses must be characterized before the relevancy of our results to humans can be understood. Glutathione-S-transferase activity in the rat lung increases in response to hyperoxia (5). A number of glutathione-S-transferase isozymes have a "nonselenium glutathione peroxidase" activity that may protect against damaging in vivo lipid

peroxidation reactions. We therefore recommend that the glutathione-S-transferase isozyme profiles in the lungs of antioxidant deficient and supplemented rats be measured and characterized. Mr. George Howard, Jr. and the P.I. have developed high pressure liquid chromatographic procedures for the rapid separation and purification of glutathione-S-transferase isozymes. These biochemical determinations should be done on rats treated with hyperbaric oxygen (HBO) and on control nonHBO rats raised under normal conditions.

The results of the light/electron microscopy studies of lung and retinal tissues would certainly benefit by quantitative computer-image analysis.

#### 9. REFERENCES:

- 1) Gable, W.D., Townsend, F.M. (1962) *Aerospace Med.* 33, 1344.
- 2) Balentine, J.D. in *Oxygen and Physiological Function*, ed. by F.F Jobsis, Professional Information Library, Dallas, TX (1976).
- 3) Stone, W.L. and Dratz, E.A. (1982) *Exp. Eye Res.*, 35, 405-412.
- 4) Stone, W.L., and Dratz, E.A. (1980) *Biochim. Biophys. Acta*, 631, 503-506.
- 5) Jenkinson, S.G., Lawrence, R.A., Burk, R.F. and Gregory, P.E.

(1983) *Toxicol. and Applied Pharmacol.*, 68, 399-404

6) Farnsworth, C.C., Stone, W.L., and Dratz, E.A. (1978)  
*Biochim. Biophys. Acta*, 552, 281-293.

7) Stone, W.L., Katz, M.L., Lurie, M., Marmor, M.F. and  
Dratz, E.A. (1979) *Photochem. Photobiol.*, 29, 725-730.

8) Nichols, C.W. and Lambertson, C.J. (1969)  
*New Engl. J. Med.*, 281, 25-30.

9) Katz, M.L., Stone, W.L., and Dratz, E.A. (1978) *Invest.  
Ophthalmol.*, 17, 1049-1058.

10) Armstrong, D., Hiramitsu, T., Gutteridge, J.,  
and Nilsson, S.E. (1982) *Exp. Eye Res.*, 35, 157-171.

11) Katz, M.L., Parker, K.R., Handelman, G.J., Brasel, T.L.  
Dratz, E.A. (1982) *Exp. Eye Res.*, 34, 339-369.

## **ACKNOWLEDGEMENTS**

The authors would like to thank the Air Force System Command, the Air Force Office of Scientific Research and the Southeastern Center for Electrical Engineering Education for the honor and opportunity of contributing our scientific expertise. We thank the School of Aerospace Medicine, and particularly the Division of Hyperbaric Medicine at Brooks AFB, for their hospitality and assistance in our experimental endeavors.

Finally, we would like to thank Col. Richard A. Henderson for his detailed collaborative efforts in all aspects of this project. We also acknowledge the collaborative efforts of Dr. Howard Davis and Dr. Richard Harris in the Veterinary Pathology Division at Brooks AFB. Capt. Fanton in the Veterinary Services Division is also acknowledged for his role as a consultant in this project.

Table 1. The effect of hyperbaric oxygen (HBO) on a- and b-wave electroretinogram amplitudes (mean±SEM) in rats fed diets deficient or supplemented with vitamin E and/or selenium.

Dietary group 1	a-wave	b-wave
	microvolts	
B+HBO(3)	88±9*	251±41
B(4)	139±13	381±37
B+E+HBO(4)	153±8	315±37
B+E(4)	166±7	312±13
B+Se+HBO(4)	140±16	306±54
B+Se(4)	141±6	266±16
B+E+Se+HBO(4)	143±18	294±37
B+E+Se(4)	147±11	281±37

1 Pure oxygen at 2.0 ATA for 1.5 hr per day was given for 5 days per week for 4 weeks prior to measurement of ERGs. Rats were fed the indicated diets for 6 weeks prior to the measurement of ERGs. Selenium and vitamin E supplementation was 0.4 ppm and 50 mg/kg diet, respectively. The number of rats used in determining a data entry is given in parentheses.

\* P<0.05

Table II. Weights and weight gains (mean±SEM) of rats fed diets deficient or supplemented with vitamin E and/or selenium and with or without hyperbaric oxygen treatment.

Dietary group <sup>1</sup>	weight gain	weight
	g/100 g/week	g
B+HBO	7.2	170±3
B	10.9	188±2
B+E+HBO	12.5	204±7
B+E	12.5	198±4
B+Se+HBO	9.3	180±3
B+Se	14.4	199±5
B+E+Se+HBO	13.9	190±4
B+E+Se	11.1	187±3
LC	9.7	199±5

<sup>1</sup> Hyperbaric oxygen was provided as in Table I but for 3 weeks prior to weight measurements. Rats were on the indicated diets for 5 weeks prior to weight measurements. Dietary supplementation was as described in Table I.

Table III. Antioxidant levels (mean±SEM) in rats fed diets supplemented or deficient in vitamin E and/or selenium and with or without hyperbaric oxygen (HBO) treatment.

Dietary group <sup>1</sup>	plasma vitamin E ug/ml of plasma	glutathione peroxidase	
		plasma milli e.u./ul	RBC milli e.u./mg Hb
B+HBO	1.6±0.2	0.5±0.2	219±55
B	1.9±0.2	0.5±0.2	244±42
B+E+HBO	4.9±0.3	NM	NM
B+E	5.7±0.3	NM	NM
B+Se+HBO	1.5±0.3	3.4±0.4	637±147
B+Se	1.5±0.3	2.2±0.2	658±217
B+E+Se+HBO	5.0±0.8	3.0±0.4	986±180
B+E+Se	5.4±0.4	2.6±0.5	1417±110

<sup>1</sup> Hyperbaric oxygen was provided as in Table I but for 1 week prior to measurement of antioxidant levels. Rats were on the indicated diets for 3 weeks prior to measurement of antioxidant levels. Eight rats were in each dietary group and half were treated with HBO. Milli e.u. for glutathione peroxidase activity is nanomoles of NADPH oxidized per min. NM indicates not measured at this time point.

Table IV. Composition of basal diet.

Ingredient	g/100g
Touria yeast	36.00
Sucrose	43.05
Corn oil, tocopherol stripped	14.50
Vitamin mix 1	2.20
Mineral mix Draper 2	4.00
L-Methionine	0.25

1. The vitamin mixture provided: (in mg/100 g of diet) ascorbic acid, 99; inositol, 11; choline chloride, 16.5; p-aminobenzoic acid, 11; niacin, 9.9; riboflavin, 2.2; pyridoxine-HCl, 2.2; thiamin HCl, 2.2; calcium pantothenate, 6.6; biotin, 0.05; folic acid, 0.2; vitamin B-12, 0.003. In addition the vitamin mixture contains: (in units /100 g of diet) vitamin A acetate, 1980; calciferol (D3), 220.

2. The salt mix provided (in mg/100 g of diet):  $\text{CaCO}_3$ , 654;  $\text{CuSO}_4 \cdot 5\text{H}_2\text{O}$ , 0.72;  $\text{Ca}_3(\text{PO}_4)_2$ , 1422; Ferric citrate  $\cdot 3\text{H}_2\text{O}$ , 64;  $\text{MnSO}_4 \cdot \text{H}_2\text{O}$ , 5.5; potassium citrate  $\cdot \text{H}_2\text{O}$ , 946; KI, 0.16;  $\text{K}_2\text{HPO}_4$ , 309; NaCl, 432;  $\text{ZnCO}_3$ , 1.8; and  $\text{MgCO}_3$ , 164.

1984 USAF-SCEEE GRADUATE STUDENT SUMMER SUPPORT PROGRAM

Sponsored by the

AIR FORCE OFFICE OF SCIENTIFIC RESEARCH

Conducted by the

SOUTHEASTERN CENTER FOR ELECTRICAL ENGINEERING EDUCATION

FINAL REPORT

THE DISTRIBUTIONAL ANALYSIS OF CONTRAST SENSITIVITY MEASURES

Prepared by: Marc W. Hunter  
Academic Department: Psychology  
University: Southern Illinois University  
Research Location: Air Force Human Resources Laboratory  
Operations and Training Division  
Williams AFB, Arizona  
USAF Research Contact: Dr. Robert T. Nullmeyer  
3FRP Supervising  
Faculty Member: Dr. David L. Kohfeld  
Date: October 20, 1984  
Contract No: F49620-82-C-0035

THE DISTRIBUTIONAL ANALYSIS OF CONTRAST SENSITIVITY MEASURES

by

Marc W. Hunter

ABSTRACT

Visual contrast sensitivity measures were obtained using a video display that generated vertical sine-wave gratings. Threshold contrasts were determined using three different methods of stimulus presentation: Bekesy Tracking (Experiment 1), and the methods of adjustment and increasing contrast (Experiment 2). An inverted-U described the general form of contrast sensitivity functions for all three psychophysical methods, thus confirming that visual resolving power is best at intermediate spatial frequencies and progressively less keen at relatively extreme frequencies. The data from the Bekesy Tracking procedure were collected into separate distributions for the ascending and descending trials, and deconvolving the former distribution from the latter resulted in a model that was exponential in form. This analysis of component processes suggested that contrast sensitivity measures are comprised of at least two component processes, only one of which reflects sensory sensitivity, the other(s) having to do with undesired response-criterion bias. In general, the results indicate that the method of increasing contrast generates the most "criterion-free" measures of contrast sensitivity. These measures could serve as the best predictor of the contrast sensitivity required in other tasks, such as performance in a visual simulator, in which precise visual resolution is essential.

### Acknowledgements

The data collection, analyses and preparation of this paper were generously supported by the Air Force Systems Command, the Air Force Office of Scientific Research, and the Southeastern Center for Electrical Engineering Education during the author's work as a Summer Research Fellow at the Human Resources Laboratory, Williams AFB, Arizona. Computer time and routines, including graphics, were funded by a research grant to the author from the Office of Research and Projects in the Graduate School at Southern Illinois University, Edwardsville. I am indebted to the research staff at AFHRL, Williams AFB, for their encouragement and support, including travel funds, without which this research could not have been accomplished. Special thanks are extended to my colleague, Dr. Robert Nullmeyer, for his close collaboration prior to and during this research assignment. Dr. George Geri provided the raw data for Experiment 1 and also offered incisive comments about the procedures used to generate and analyze contrast sensitivity functions. Finally, Mr. Glen York gave generously of his office space, computer-software expertise, and actual time to use his minicomputer terminal at AFHRL.

## I. INTRODUCTION

An important aspect of visual perception is the resolving power of the visual system, that is, its ability to determine very small spatial patterns, or to discriminate fine detail in a visual display. Visual acuity is particularly essential when a person is required to detect and identify objects and events in a visual environment where detailed information is sparse or fleeting. Some examples are driving an automobile at night, inspecting electronic microchips, or monitoring distant events as they are being displayed on a video screen. For the Air Force, the obvious example is pilot performance in either a visual simulator or the aircraft itself; objects and patterns that "approach" from a distance must be identified rapidly and accurately in order to accomplish a mission without adverse consequences.

One way to measure spatial resolution is to present a grating of vertical black test bars on a white background and to reduce the difference between the luminance of the light bars and the luminance of the dark bars until a person can no longer detect the dark bars on the white background. The coarseness of the grating can easily be varied, and the entire test field is presented on an ordinary video display. A crude example of this task is to consider the vertical black stripes on a zebra; if one could vary both the number and darkness of these stripes, what effect would this have on one's ability to detect the presence of stripes on this animal? Of course, if the recognition of "zebra" instead of "horse" were somehow important, this kind of visual resolving power would be essential. More specifically, the difference in luminance at which such striations are just resolved is the contrast threshold.

Contrast is usually defined as  $(L_{\max} - L_{\min}) / (L_{\max} + L_{\min})$ , where  $L_{\max}$

is the luminance of the brightest part of the grating ("white stripes") and  $L_{\min}$  is the luminance of the darkest part ("black stripes"). The reciprocal of this contrast value is usually computed and is plotted as contrast sensitivity.<sup>1</sup> Contrast threshold measurements are usually obtained for a number of sinusoidal gratings of increasing spatial frequency, in cycles per degree (increasing number of stripes on the zebra). The resulting data are presented in the form of contrast sensitivity functions (CSFs), in which either contrast threshold<sup>2</sup> or contrast sensitivity<sup>3,4</sup> is plotted on a logarithmic ordinate against spatial frequency on a logarithmic abscissa.

Recent research by Ginsburg and his associates<sup>3,5,6</sup> has explored several psychophysical methods for obtaining contrast sensitivity measures, as well as demonstrating the relationship between CSFs and performance measures ranging from threshold detection and identification of letters to a pilot's skill in detecting a target during fighter-aircraft simulation. As evidence for the applied value of these procedures, Ginsburg and Cannon<sup>3</sup> also reported that visual abnormalities caused by brain lesions, multiple sclerosis, and cataracts are apparent in measures of threshold contrast sensitivity, but not necessarily in Snellen-type tests of visual acuity. Ginsburg consistently concluded that CSFs are superior to standard clinical tests (e.g., the Snellen test of visual acuity) in predicting performance in realistic visual environments.

## II. RESEARCH OBJECTIVES

The present research involved a distributional analysis of the data obtained with the three psychophysical methods studied by Ginsburg and Cannon; i.e., Bekey Tracking, the method of adjustment, and the method of increasing contrast. According to Ginsburg and Cannon, the method of

increasing contrast was the best of the three methods because the instructions to subjects were easiest to follow, less time was needed for data collection, the measures were most consistent (lowest variability), and perhaps most importantly in the present context, the contrast threshold values were least influenced by the response-criterion bias that obscures the "pure" relation between CSFs and sensory processes only. It should be noted, however, that none of the psychophysical methods provides data that are criterion free, primarily because an operator's disposition to respond to a detectable change in stimulation (i.e., contrast changes) tends to vary from trial to trial. In this vein, the separation of perceptual sensitivity and response bias from overall measures of threshold sensitivity is an enduring problem in signal detection theory and psychophysical measurement.

In the present investigation, entire distributions of contrast sensitivity measures were evaluated. A system identification method of deconvolution was used to decompose the distributions into component densities that presumably reflected the separate influence of "pure" contrast sensitivity and response bias on threshold detections. The general research objective was the same as Ginsburg's: to develop a valid predictor of contrast sensitivity in other tasks, such as performance in a visual simulator, in which precise visual resolution is essential.

### III. EXPERIMENT 1

A. Method. The operators (highly motivated, professional people) were three pilot trainees at Williams AFB, Arizona. Each operator had normal or fully-corrected vision. Testing was conducted in a darkened, quiet room in the Human Resources Laboratory.

The apparatus was an Optronix Model 200 Vision Tester, which has been

described elsewhere.<sup>3</sup> Briefly, this equipment is capable of displaying sinusoidal gratings at different spatial frequencies. Contrast at the video screen is defined as  $(L_{\max} - L_{\min}) / (L_{\max} + L_{\min})$ . In the present experiment, the display screen had an average luminance of 100 cd/m<sup>2</sup>, or the equivalent of 87 decibels (51 millilamberts) of white light.<sup>7</sup> Seven spatial frequencies were employed: 0.5, 1.0, 2.0, 4.0, 8.0, 11.4, and 22.8 cycles per degree. The operators viewed the screen from a distance of three meters.

The psychophysical method employed in Experiment 1 is known as Beksy Tracking.<sup>2,3</sup> This method is available in a preprogrammed mode of operation in the Optronix Vision Tester. Specifically, the contrast either increased or decreased at a fixed rate of 4 dB per second, as determined by the position of the operator's hand-held switch. A block of trials was comprised of ten ascending and ten descending responses at a given spatial frequency. During a trial block, if a pattern on the screen was not detectable, the switch was held in one position until the grating was just barely visible (ascending), at which point the operator abruptly changed the switch direction until the grating seemed to disappear (descending). The Optronix microcomputer recorded a contrast threshold measurement whenever a change in switch position (threshold decision) occurred.

An experimental session was divided into five series of trial blocks, with a rest period between each series. Within a series, the seven programmed spatial frequencies were administered in order (0.5 to 22.8 cycles per degree). A total of 50 ascending measures and 50 descending measures for each of the seven spatial frequencies was obtained from each operator.

B. Results and Discussion. Figure 1 presents log threshold contrast sensitivity as a function of log spatial frequency, in cycles per degree,

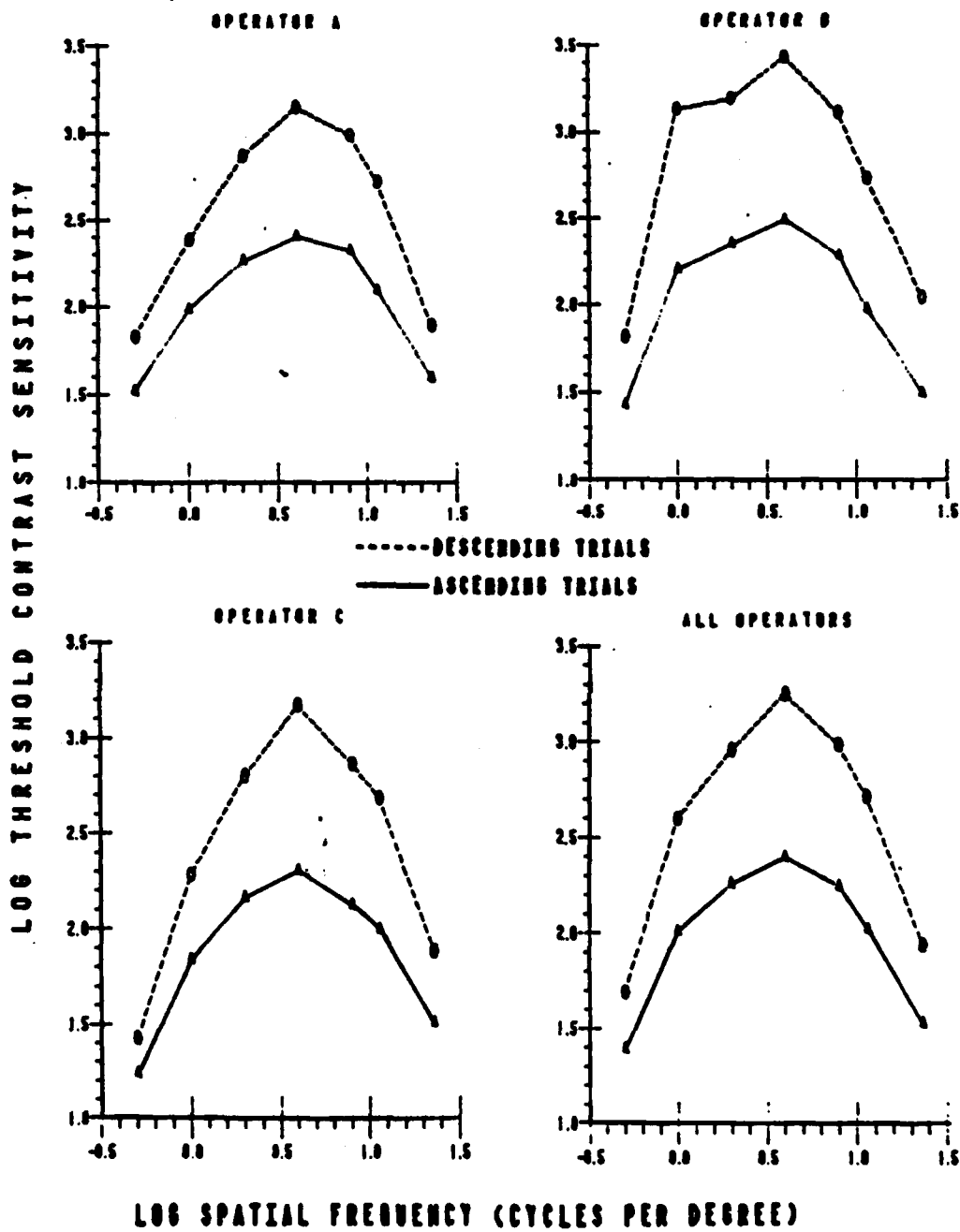


Figure 1. Contrast sensitivity functions for the Bakesy Tracking method

for the Beksy Tracking method. Each operator's data are plotted separately (50 measures per data point), and the data means are pooled in the lower-right panel (150 measures per data point). The top function in each panel (dashed line) is for the descending trials (decreasing contrast), and the bottom function (solid line) is for the ascending trials (increasing contrast). The data form contrast sensitivity functions (CSFs) across the seven spatial frequencies (0.5, 1.0, 2.0, 4.0, 8.0, 11.4, and 22.8 cycles per degree) that are plotted on the logarithmic abscissa.

At least three conclusions may be drawn from the data shown in Figure 1. First, the CSFs reveal the characteristic inverted-U shape found in previous research.<sup>3,4</sup> This indicates that the resolving power of the visual system is best at intermediate frequencies (2-8 cycles per degree) and progressively less keen at relatively extreme frequencies (0.5 and 22.8 cycles per degree). Second, the CSFs for the descending trials suggest considerably greater contrast sensitivity than those for the ascending trials. This difference was also noted by Ginsburg and Cannon,<sup>3</sup> and is probably attributable to the exaggerated response bias that occurs when descending trials are coupled with ascending trials, as required by the Beksy Tracking procedure. This particular consideration will be evaluated subsequently more fully. Finally, the CSFs are both uniform and consistent across the three operators. However, this observation is based on graphic presentation of mean values, and deserves further evaluation based on the assessment of variability as well.

Figure 2 provides a detailed presentation of the same data that are shown in Figure 1. The data are now plotted as histograms (bin widths of 0.1 log sensitivity), with proportion of threshold detections on the ordinate as a function of log threshold contrast sensitivity on the

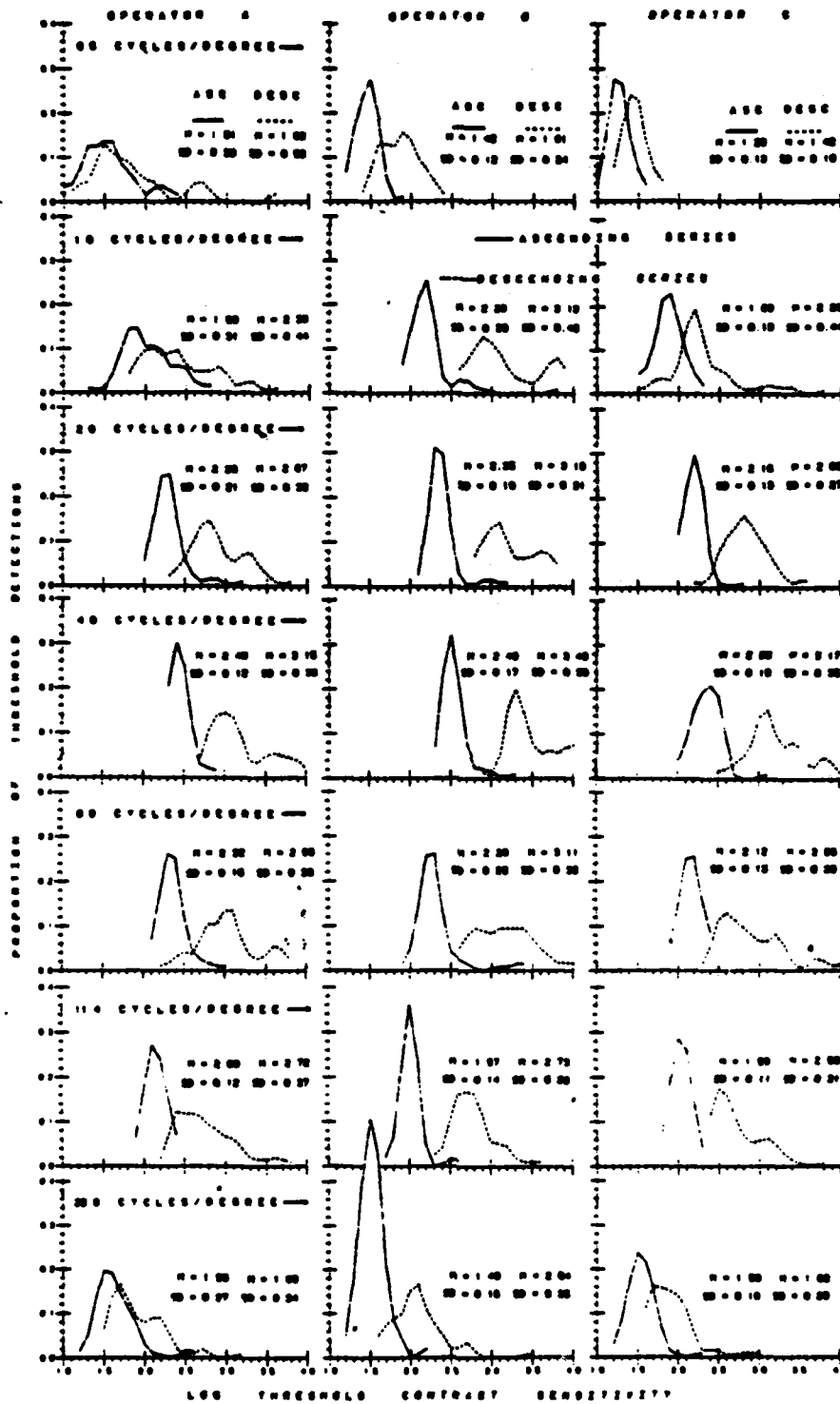


Figure 2. Individual distributions at each spatial frequency for the Bekesy Tracking method

abscissa. Figure 2 also shows the mean and standard deviation for the ascending and descending series for the three operators (rows) in each of the seven spatial frequencies (columns). It may be seen that in every instance the standard deviations are larger for the distributions of descending measures. In other words, although the operator's responses indicated higher mean contrast sensitivity in the descending (decreasing contrast) trials, the variability of these threshold measures was always greater.

The value of presenting entire distributions of data, as shown in Figure 2, is based on the assumption that the particular form of a histogram sometimes provides valuable information about the nature of the processes that give rise to a particular distribution of measures. Clearly, the shapes of the descending distributions are different than those of the ascending distributions, i.e., the former are generally flatter and more skewed than the latter. This raises the possibility that the operators were behaving differently in the ascending and descending modes. Perhaps the operators were perceiving the stimulus gratings differently, or, as suggested by Ginsburg and Cannon,<sup>3</sup> they may have adopted different response strategies. Based on these considerations, it seemed appropriate to pursue the matter of distributional analysis in more detail.

Although the individual histograms in Figure 2 are somewhat irregular, viewing down a column reveals that the shapes of the ascending and descending distributions are fairly consistent across spatial frequencies. Accordingly, the histograms were collapsed across spatial frequencies by adjusting the 50 raw scores in each distribution to a common origin of 1.0 on the log sensitivity scale, and then collecting these values across the seven spatial frequencies. Although this procedure eradicates infor-

mation about the actual positions of individual spatial frequency distributions on the contrast sensitivity axis, it does not sacrifice vital information about the nature of log sensitivity as a continuous random variable. The outcome is shown in Figure 3, which has the same axes and bin widths as in Figure 2. Thus, each operator's ascending and descending distribution in Figure 3 is comprised of 350 measures, and the pooled data of all three operators (lower-right panel) includes 1,050 measures per distribution.

In general, the ascending and descending histograms displayed in Figure 3 are most likely from the same Pearson "family" of distributions. That is, both distributions appear gamma in form; i.e., their means, standard deviations, and positive skewness are correlated. These properties suggest that both distributions were generated by common underlying processes that almost certainly have to do with the Bekey Tracking procedure for obtaining contrast sensitivity thresholds. But it is equally apparent that when descending thresholds are obtained, one or more of the component processes is behaving quite differently (larger mean, variance, and skewness), or perhaps another process emerges in addition to those required for ascending threshold estimations. In short, the shapes of the histograms in Figure 3 pointed to the feasibility of a deconvolution procedure which could reveal additional information about the processes that underlie contrast sensitivity distributions.

C. Distributional Analysis. The next step in this investigation was to identify and separate the component processes that characterize the difference between the ascending and the descending distributions shown in Figure 3. The convolution method employed for this task was the Z transform method<sup>8</sup> which is often associated with linear systems identifi-

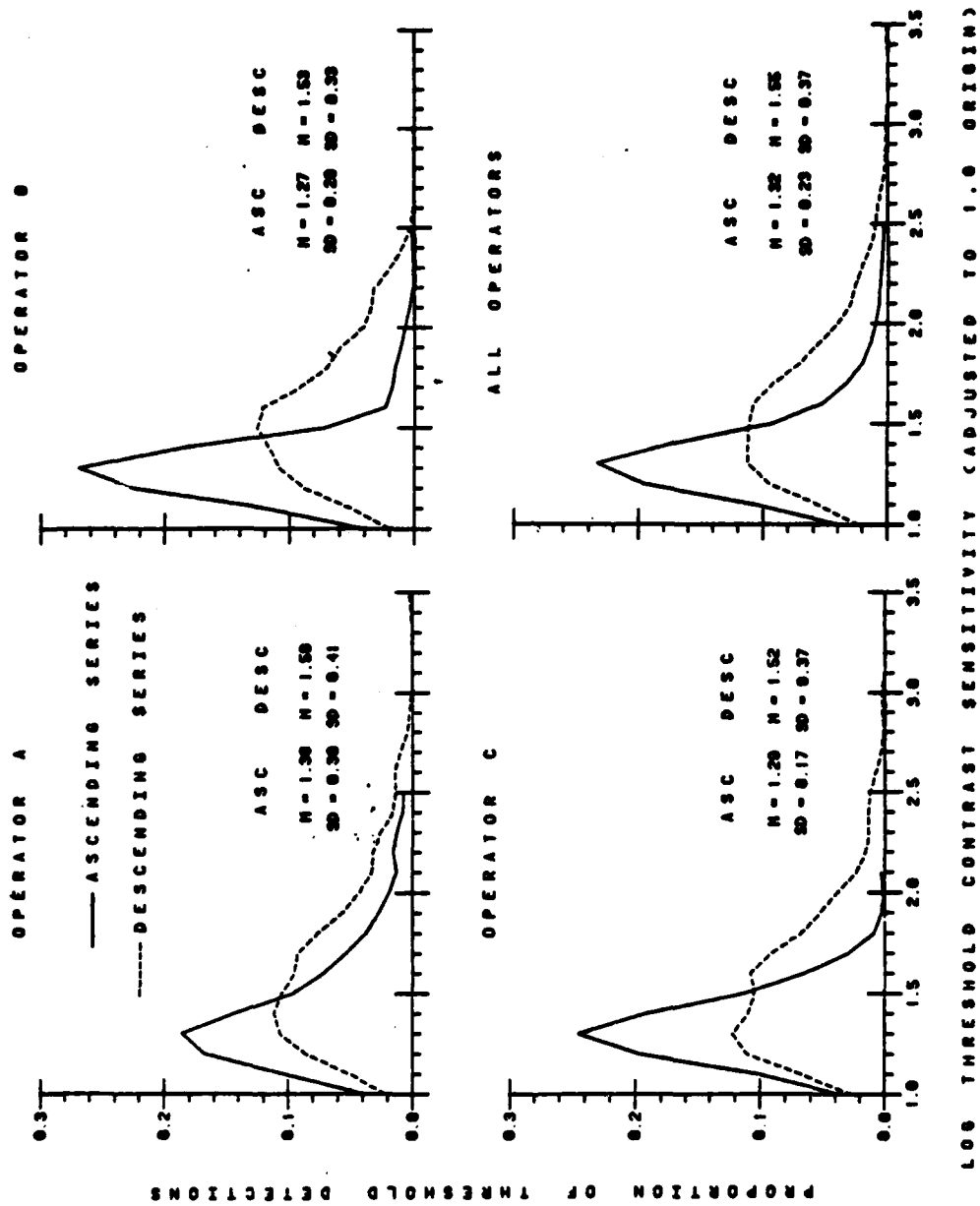


Figure 3. Individual distributions collapsed across spatial frequencies for the Bekesy Tracking method

cation in engineering.<sup>9,10</sup> This approach incorporates the idea that an observed distribution (e.g., the descending series distribution) is often the convolution of a known distribution (e.g., the ascending series distribution) and another hypothetical process (e.g., a response bias component) for which one seeks to identify a model. Conceptually, convolution methods are similar to ordinary subtractive procedures except that the former involve the deconvolution (or "subtraction") of entire distributions rather than just measures of central tendency. Examples of the application of linear systems identification to the analysis of reaction time distributions are provided elsewhere.<sup>11,12,13,14</sup>

Using the Z transform method of convolution, a model of the difference between the ascending and the descending distributions in Figure 3 was obtained by deconvolving the ascending series distribution for all operators (lower-right panel) from their corresponding descending series distribution (same panel). The resulting difference model is shown in the middle panel of Figure 4. The ascending series distribution in the top panel of Figure 4 is the same as in the lower-right panel of Figure 3, and the distribution that is plotted as a solid line in the bottom panel of Figure 4 is the same as in the lower-right panel of Figure 3. The difference model selected by the convolution method was also the one whose reconvolution with the ascending distribution gave the closest approximation to the descending distribution from which it was identified. This reconvolution is the distribution composed of the dashed lines, as seen in the bottom panel of Figure 4. Although tests for goodness of fit were not made, the fit is obviously quite good, which supports the idea that the model describes a linear, additive component that accounts for the difference between the ascending and descending thresholds obtained in this research.

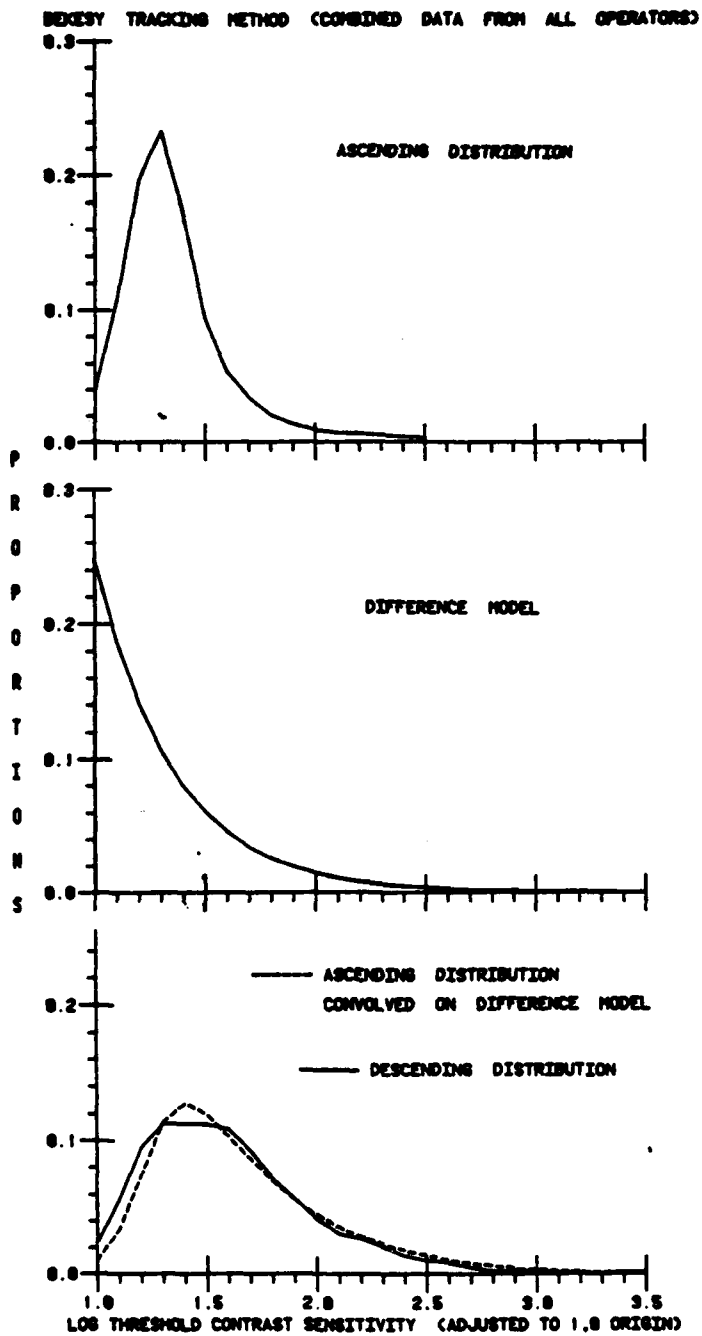


Figure 4. Difference model resulting from deconvolution of Bekesy ascending distribution from Bekesy descending distribution

The difference model that is shown in the middle panel of Figure 4 is exponential in form. An exponential model of the component process which separates the descending distribution from the ascending distribution implies that this underlying event operates much like a constant, conditional probability mechanism. Although this model is sharply bounded from below, the plotted location of this lower bound (1.0 log unit) on the contrast sensitivity axis is arbitrary, since the distributions from which it was derived were adjusted to a common 1.0 origin. The exponential form of this model, however, suggests a process that generates increasingly larger contrast sensitivity measures over a range of about 2.0 log sensitivity units. Moreover, the conditional probability that this process will influence the contrast threshold measures in the descending series becomes progressively lower according to a fixed probability rule. Finally, an exponential model provides a description of a single underlying event or process. As applied to the present analysis, this means that the higher and more variable contrast sensitivity thresholds in the descending series may be attributable to one categorical process.

#### IV. EXPERIMENT 2

The purpose of the second experiment was to obtain contrast threshold data for the method of increasing contrast and the method of adjustment. The goal was to compare these results with those obtained from the Bekey Tracking procedure, as was reported in Experiment 1.

A. Method. The operators were three Research Psychologists employed at the Human Resources Laboratory, Williams AFB, Arizona. All had normal or fully-corrected vision. DK, the principal investigator, was 43; a graduate student, MH, was 24; and a colleague, RN, was 34 years old. The three operators were familiar with the research aims and had extensive

experience with psychophysical methodology. The apparatus and general procedures were the same as in Experiment 1, except that only six spatial frequencies were utilized (0.5, 1.0, 3.0, 6.0, 11.4, and 22.8 cycles per degree).

The method of increasing contrast was utilized in the first experimental session. This method is essentially the same as the ascending series part of Bekesy Tracking, except that no descending series are included. Briefly, the contrast increased at a fixed rate of 4 dB per second from below threshold to where the operator could first detect the presence of the test grating. The time between each threshold detection and the onset of the next trial was varied to discourage the operator from guessing the contrast threshold based on a fixed time interval from the last detection. The operator depressed a switch when the grating on the screen was just barely detectable. A block of trials consisted of 10 increasing presentations at each of the six spatial frequencies. There was a rest period at the end of each series of six trial blocks. As before, an experimental session was comprised of five series of trial blocks (six series for DK), yielding a total of 50 measures for each of the six spatial frequencies (60 for DK).

The method of adjustment was employed in a subsequent experimental session. The operator was given a hand-held switch with an adjustable knob that allowed him to either increase or decrease the contrast between the dark bars and the light bars on the screen until he could just barely detect the presence of the grating. The operator was instructed to turn the knob as far as it would go below the threshold before a trial began. He then increased the contrast and "bracketed" the threshold point, using as much time as was needed to achieve the desired setting. The operator

then depressed a button which stored the desired value in the microcomputer and reset the contrast on the screen to zero. All three operators reported making their threshold decisions quite rapidly, at a rate of about one every five seconds for the middle frequencies, but somewhat less rapidly at the extreme frequencies where threshold decisions seemed more difficult. As before, RN and MH generated 50 measures at each frequency, and DK recorded 60 values.

B. Results and Discussion. Figure 5 shows the mean threshold values, plotted in the same manner as in Figure 1. Because of the obvious similarity of the CSFs for each individual, the data were collapsed across operators, thus yielding 160 measures in each CSF data point for the adjustment method and increasing contrast method. The third CSF in Figure 5, labeled "Bekey ascending trials," is the same as the one in the lower-right panel of Figure 1. This latter CSF is composed of data points with 150 measures, and is presented for comparison with the two CSFs obtained in the present experiment.

The most compelling feature of Figure 5 is the overall similarity of the CSFs for the three methods shown. This similarity is somewhat surprising when one considers that each CSF was composed of data taken from only three operators, and indeed, a separate trio of operators in the Bekey ascending trials. These results suggest at least three important conclusions. First, the three different psychophysical methods generated such similar CSFs that one's confidence in the validity of these measures is improved considerably. Second, the elevated CSF for the Bekey descending trials in Experiment 1 is probably based on properties of the method itself rather than "true" differences in contrast sensitivity. That is, the descending trials appear to be the "outliers" relative to three other

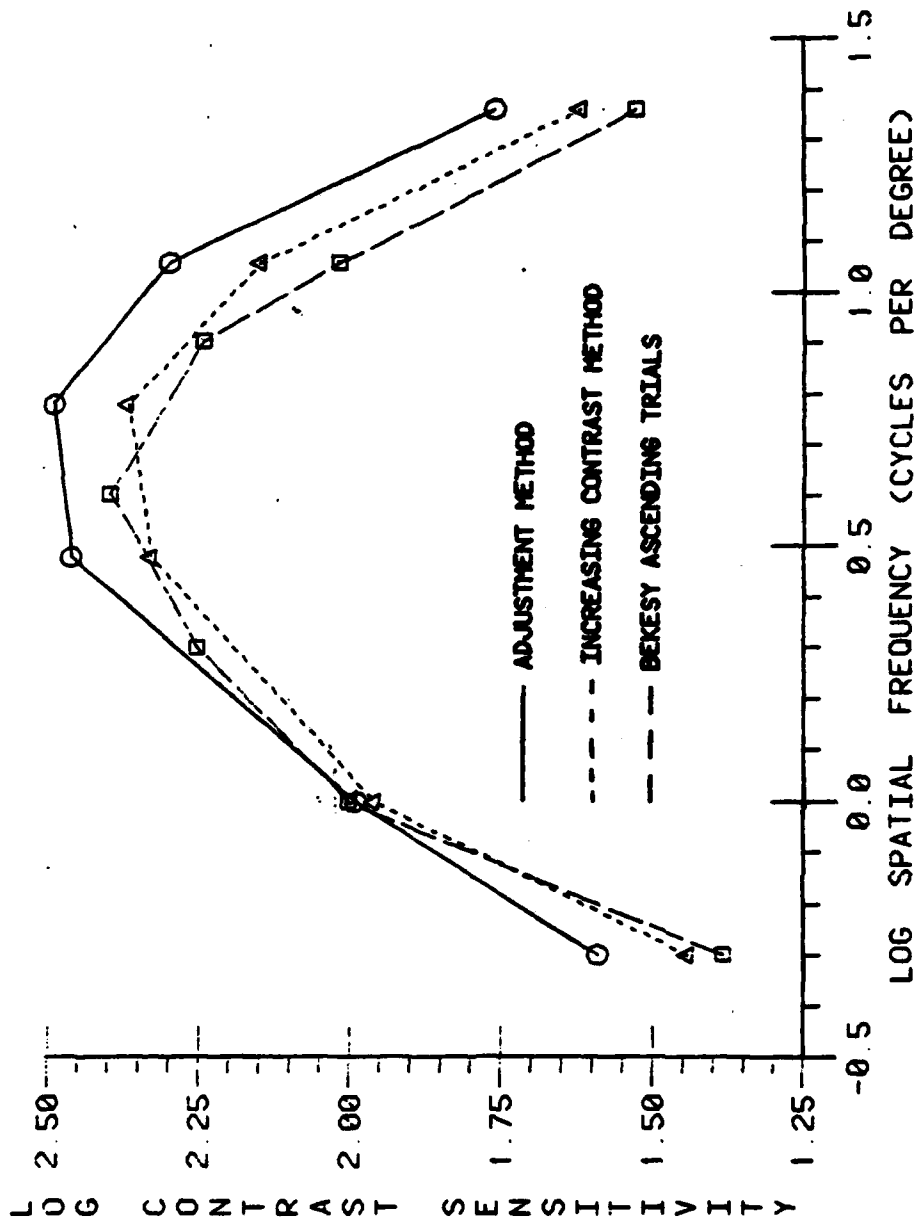


Figure 5. Contrast sensitivity functions for the adjustment and increasing contrast methods (Experiment 1) and for Bekesy Tracking (Exper. 2)

procedures. Finally, it now seems possible that representative CSFs can be generated from relatively few operators, at least if these individuals are familiarized with the testing procedures and can generate a reasonably large sample of contrast threshold measures at each spatial frequency.

Figure 6 provides a comparison of the distributions of data for the same three methods that are depicted in Figure 5. The threshold values were adjusted to the 1.0 origin on the log sensitivity axis, just as they were in Experiment 1, Figure 3. The distribution composed of Bekesy ascending trials (1,050 measures) is the same as the one plotted in the lower-right panel in Figure 3, and in the top panel of Figure 4. Each of the distributions for the increasing contrast method and the adjustment method contain 960 values. The similarities between the general forms of the distributions shown in Figures 3 and 6 are quite apparent.

The results shown in Figure 6 lead to some important conclusions. First, all three distributions are gamma in form, with characteristic positive skewness. As noted previously, this implies that the processes or events which underlie each distribution are similar for the three psychophysical methods, as one might expect. Second, the Bekesy ascending trials and the adjustment method produced distributions that are similar in form, whereas the distribution of increasing contrast measures is more peaked, less variable, and less skewed. By implication, the perceptual and response processes which characterize the Bekesy ascending measures and the method of adjustment values should be similar, whereas the selective influence of at least one of these two processes on the threshold decisions obtained from the increasing contrast method should be reduced. Finally, if one accepts the view that a distribution of measures with the lowest possible variability is the most desirable in terms of measure-

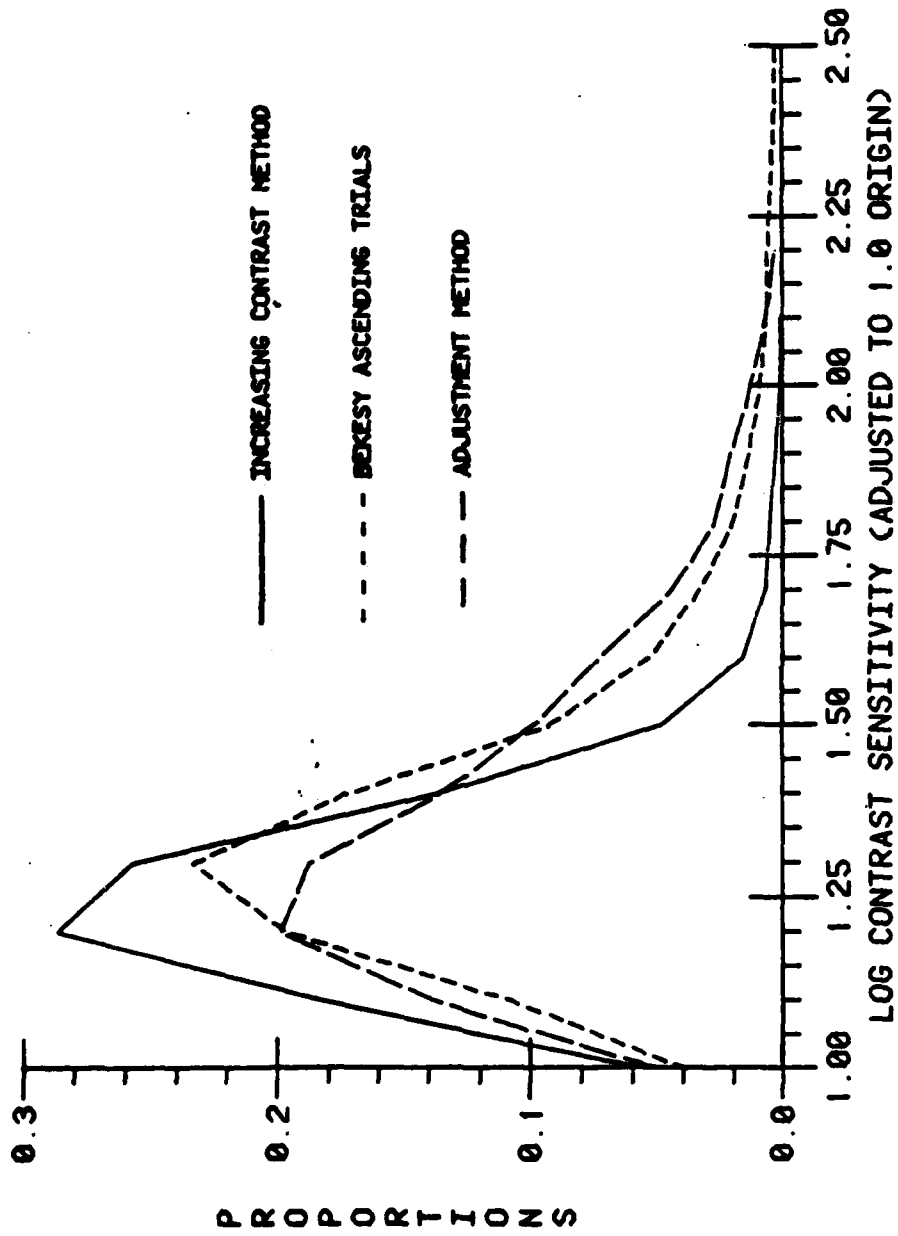


Figure 6. Distributions of the same data shown in Figure 5

mental precision, the method of increasing contrast could serve as the most predictive method for determining contrast sensitivity skills. Indeed, Ginsburg and Cannon<sup>3</sup> offered this conclusion for reasons quite similar to those presented in this report.

#### V. GENERAL DISCUSSION

In 1963, McGill<sup>15</sup> proposed that the form of some distributions would provide a kind of "signature" that reflects the nature of the processes that comprised these distributions. Since then, a number of investigators have demonstrated that simple reaction time is the convolution of two main components: sensory detection and response execution.<sup>11,14,16,17</sup> The present analysis of contrast sensitivity thresholds was influenced by this previous reaction time work in two important ways. First, the linear systems identification, and the associated Z transform method of convolution employed by Kohfeld, provided the analytic framework for decomposing the distributions of contrast sensitivity measures. Second, the reaction time process is sometimes discussed in terms of a response threshold that triggers the reaction; this is conceptually similar to the idea of the decision threshold that is determined with contrast sensitivity measures. In this vein, one can explore the parallels between the two reaction time stages, sensory detection and response execution, and the corresponding two stages in contrast sensitivity decisions.

The theory of signal detectability (TSD) provides one way to conceptualize the behavior of individuals in both reaction time and contrast sensitivity tasks. According to TSD, the operator is both a sensor and a decision maker, and therefore, the evaluation of threshold measurements would require an independent assessment of the operator's sensory sensitivity,  $d'$ , and response criterion,  $\beta$ .<sup>18,19</sup> TSD assumes further that  $d'$

and  $\beta$  are independent aspects of task performance, and are selectively influenced by different factors. With respect to contrast sensitivity, the visual contrast at the video screen determines  $d'$ , whereas  $\beta$  is characterized by the operator's strategy in responding to task demands. As such, the logic of TSD may prove useful in describing the forms of the distributions of threshold contrast sensitivity. Because of the nature of this threshold task, one can suppose that these distributions reflect the behavior of both sensory mechanisms ( $d'$ ) and a response process ( $\beta$ ). In other words, the distributions shown in Figures 2, 3, and 6 are a composite of at least two component densities,  $d'$  and  $\beta$ , each of which is an independent random variable.

It should be noted that no prior predictions were made about the shapes of the distributions actually obtained in this research. That is, no theoretical formulation dictated that particular forms of histograms should be generated, e.g., exponential, gamma, or normal. Thus, when the convolution method resulted in a model that was exponential in form (middle panel of Figure 4), no a priori logic suggested that this model was part of the sensory component ( $d'$ ), the response component ( $\beta$ ), or perhaps a third component altogether. However, both TSD logic and common intuition provide guidance in this matter. When one serves as an operator in the descending series part of the Beksy Tracking task, it is at once apparent that deciding when the grating has disappeared is considerably more difficult than when ascending threshold decisions are required. The consensus of the operators can be offered in the quote: "I held the switch down until I was sure that the bars were gone." This sounds very much like response bias, or in TSD terminology, the operators adopted a more lenient criterion in the descending trials, thus yielding inflated contrast thresholds.

These considerations lead one to conclude that deconvolving the ascending distribution from the descending distribution resulted in a difference model that reflects a response bias component. As noted previously, its exponential form implies that it represents a single process or categorical event. This interpretation does not imply that the ascending trials are free of response bias; rather, it supports the view that descending thresholds are influenced by at least two sources of undesired response bias. The separation of the  $d'$  and  $\beta$  components from the distributions generated with Bekesy ascending trials, the method of adjustment, and the preferred method of increasing contrast (see Figure 6) is a matter for future research.

#### VI. RECOMMENDATIONS

The main goal of this investigation was to determine the psychophysical procedure and data analytic method that will provide the most valid measure of contrast sensitivity. The results suggest that the method of increasing contrast, coupled with the analysis of the forms of response distributions, is the recommended procedure for assessment of "pure" contrast sensitivity. An important implication is that the resulting measures will serve as a better predictor of the contrast sensitivity required in other tasks, such as performance in a visual simulator, in which precise visual resolution is essential. That is, when response bias is either reduced or analytically removed from contrast sensitivity measures, better prediction should result, primarily because the response bias in a specific predictor task (e.g., threshold determinations) will not necessarily correlate with the unique response bias in a different criterion task (e.g., identifying objects during simulated flight). Accordingly, two related lines of research are recommended at this juncture, one of which would deal with further

refinements of the contrast sensitivity measure itself, and the other having to do with using the measure as a predictor in an applied setting.

A. Refinements of Contrast Sensitivity Measures. There are a number of analytic procedures and different experimental approaches that deserve future research; three are mentioned here.

1. Hazard-function estimation. Considerable progress has already been made in estimating the hazard functions of the three distributions shown in Figure 6. While discussion of this work is beyond the scope of the report, it should be noted that all three distributions can be decomposed further by determining the form of their hazard functions. <sup>17,20,21,22</sup> These results suggest that all three distributions in Figure 6 represent the convolution of sensory and response components whose separate distributional forms can be estimated.

2. Experimental manipulation of task components. Established experimental procedures are available for selective experimental manipulation of the response bias component in measures of contrast sensitivity. The goal would be to provide empirical verification of the selective influences of sensory sensitivity ( $d'$ ) and response bias ( $\beta$ ) on these measures, which thus far in this investigation has been a matter of mathematical inference only.

3. Contrast discrimination thresholds. Almost all of the previous research with CSFs deals with measures of threshold detection. However, a more realistic task might include the operator's skill in discriminating different spatial frequencies. Consider an operator who continuously scans a visual display for new information. On the one hand, detection refers to the perceptual process of noting that "something" has appeared, disappeared, or changed, but this process is non-specific as to what it

was. On the other hand, discrimination is the more complicated process of identifying exactly what did appear, disappear, or change. Realistically, if a fighter pilot first detects something, subsequent identification of what it was (e.g., a "friendly aircraft" and not an "enemy fighter") may likely be the behavior one seeks to predict. In this vein, I have designed a series of experiments in which the operator's task would be to identify the particular visual frequency (number of vertical bars) as well as performing the preceding task of merely detecting that something had appeared on the video display.

B. Predicting Simulated Flight. An important research interest of Marc W. Hunter, who was assigned to this project as part of the GSSSP, was to explore the possibility that an operator's CSF could be used to predict the criterion skill of detecting and identifying objects during simulated flight. Previous research has shown that there is usually only moderate variation among different individuals' sensitivity to relatively high spatial frequency patterns (e.g., 22.8 cycles per degree). However, there are sometimes considerable individual differences in the low frequency range (e.g., 0.5 cycles per degree). It is to be noted that fog, haze, dust, and cloud cover has the effect of changing the spatial frequency of an object when introduced between some viewer and the object. Specifically, a haze or particulate will lower the spatial frequency of the object, having the effect of a "blurring" or spreading of the edges of the object by means of a property called atmospheric attenuation. Thus, for example, a pilot approaching some group of targets (e.g., aircraft) in a fog or light mist will usually first detect a group of masses that are nearly elliptical in shape, rather than perceiving them immediately as aircraft. If attenuation had not occurred the target aircraft would have appeared as being an object

having relatively high spatial frequency, with crisper lines showing more detail. Obviously, target aircraft will always be identified more quickly and accurately in a relatively clear atmosphere in which visual detail is keenest.

If contrast sensitivity measures had revealed significant differences in sensitivity to lower, and on occasion middle and upper spatial frequencies, it seems reasonable to assume that targets consisting of these frequencies would be detected and identified at differing distances. That is, those pilots with relative insensitivity to low spatial frequency patterns may require more time to detect targets composed of those low frequencies than those pilots shown to possess greater sensitivity in that specific frequency range. Obviously, the benefits of rapid and accurate target detection and identification are clear with respect to tactical air missions. Whether or not performance in a simulated environment would generalize to real-world environments is also a matter for further research.

Based on these considerations, Mr. Hunter explored the feasibility of a study to be performed at the Human Resources Laboratory on one of the aircraft simulation systems available there. It was determined that (a) the visual system currently used on the Advanced Simulator for Pilot Training (ASPT) has a setting regarded as "fog." However, this procedure merely changes the contrast of the scene produced. Since contrast change does not constitute spatial frequency change, it seems that the "fog" setting does not adequately simulate real fog effects precisely enough to manipulate it as the independent variable of primary interest; and (b) the Digital Image Generation System (DIGS) presently does not have the capability to produce atmospheric attenuation, and the necessary hardware and software changes were economically infeasible for a summer pilot study.

There is some indication that the Human Resources Laboratory is attempting to implement a visual system that could produce the necessary images for our recommended research. Even if this visual system did not allow for "flight" into the scene, the procurement of this system would allow research that would prove useful in determining the predictive relationship between contrast sensitivity functions and the detection of spatial frequency changes during simulated flight.

## REFERENCES

1. J. P. Thomas, "Spatial Resolution and Spatial Interaction," in E. C. Carterette and M. P. Friedman (Eds.), Handbook of Perception V, New York, Academic Press, 1975.
2. R. Sekuler and P. Tynan, "Rapid Measurement of Contrast-Sensitivity Functions," American Journal of Optometry & Physiological Optics, Vol. 54, pp. 573-575, 1977.
3. A. P. Ginsburg and M. W. Cannon, "Comparison of Three Methods for Rapid Determination of Threshold Contrast Sensitivity," Investigative Ophthalmology & Visual Science, Vol. 24, pp. 798-802, 1983.
4. F. W. Cambell and J. G. Robson, "Application of Fourier Analysis to the Visibility of Gratings," Journal of Physiology, Vol. 197, pp. 551-566, 1968.
5. A. P. Ginsburg, "Spatial Filtering and Vision: Implications for Normal and Abnormal Vision," in L. M. Proenza, J. M. Enoch, and A. Jampolsky (Eds.), Clinical Application of Visual Psychophysics, New York, Cambridge University Press, 1981.
6. A. P. Ginsburg, D. W. Evans, R. Sekuler, and S. A. Harp, "Contrast Sensitivity Predicts Pilots' Performance in Aircraft Simulators," American Journal of Optometry and Physiological Optics, Vol. 59, pp. 105-109, 1982
7. D. L. Kohfeld, "Simple Reaction Time as a Function of Stimulus Intensity in Decibels of Light and Sound," Journal of Experimental Psychology, Vol. 88, pp. 251-257, 1971.
8. E. I. Jury, Theory and Application of the Z-Transform Method, Harrington, New York, Krieger, 1964.

9. T. C. Hsia, System Identification: Least Squares Methods, Lexington, Massachusetts, Heath, 1977.
10. A. P. Sage and J. L. Melsea, System Identification, New York, Academic Press, 1971.
11. D. L. Kohfeld, J. L. Santee, and N. D. Wallace, "Loudness and Reaction Time: II. Identification of Detection Components at Different Intensities and Frequencies," Perception and Psychophysics, Vol. 29, pp. 550-562, 1981.
12. D. L. Kohfeld, "Stages of Reaction Time in Adults and Children," Paper Presented at the 22nd Annual Meeting of the Psychonomic Society, Philadelphia, Pennsylvania, November, 1981.
13. D. L. Kohfeld, "Reaction-Time Stages of Auditory Intensity," Paper Presented at the 23rd Annual Meeting of the Psychonomic Society, Minneapolis, Minnesota, November, 1982.
14. D. L. Kohfeld, "Sensory-Detection Models of Auditory and Visual Reaction Time Processes," Paper Presented at the 17th Annual Meeting of the Society for Mathematical Psychology, Chicago, Illinois, August, 1984.
15. W. J. McGill, "Stochastic Latency Mechanisms," in R. D. Luce, R. R. Bush, and E. Galanter (Eds.), Handbook of Mathematical Psychology, Vol. 1, New York, Wiley, 1963.
16. D. M. Green and R. D. Luce, "Detection of Auditory Signals Presented at Random Times: III.", Perception and Psychophysics, Vol. 9, pp. 257-268, 1971.
17. S. L. Burbeck and R. D. Luce, "Evidence from Auditory Simple Reaction Times for Both Change and Level Detectors," Perception and Psychophysics, Vol. 32, pp. 117-123, 1982.

18. D. M. Green and J. A. Swets, Signal Detection Theory and Psychophysics, New York, Wiley, 1966.
19. W. N. Dember and J. S. Warm, Psychology of Perception (2nd Edition), New York; Holt, Rinehart, and Winston, 1979.
20. B. Bloxom, "Estimating an Unobserved Component of a Serial Response Time Model," Psychometrika, Vol. 44, pp. 473-484, 1979.
21. B. Bloxom, "Some Problems in Estimating Response Time Distributions," In H. Wainer and S. Messick (Eds.), Principles of Modern Psychological Measurement: A Festschrift in Honor of Frederick M. Lord, Hillsdale, New Jersey, Lawrence Erlbaum Associates, 1983.
22. D. R. Miller and N. D. Singpurwalla, "Failure Rate Estimation Using Random Smoothing," Sankhya (Indian Journal of Statistics), Vol. 42B, pp. 217-228, 1980.

**1984 USAF-SCREE SUMMER FACULTY RESEARCH PROGRAM**

**Sponsored by**

**AIR FORCE OFFICE OF SCIENTIFIC RESEARCH**

**Conducted by the**

**SOUTHEASTERN CENTER FOR ELECTRICAL ENGINEERING EDUCATION**

**FINAL REPORT**

**INDIVIDUAL AND GROUP DYNAMICS: A CONSIDERATION OF  
CLIMATE, TASK DESIGN, AND COMBAT READINESS FACTORS OF THE OAP/OAS**

**Prepared by:** Joseph F. Kager  
**Department and** Management Dept.  
**University:** Auburn University  
**Research Location:** Leadership and Management Development Center,  
Directorate of Research and Analysis,  
Maxwell Air Force Base, Alabama  
**USAF Research Contacts:** Maj. Hickey Dansby and  
Capt. Michael Cox  
**SFRP Supervising** Dr. Kevin Hossholder  
**Faculty Member:** Associate Professor  
**Date:** August 23, 1984  
**Contract No:** F9620-82-C-0035

**INDIVIDUAL AND GROUP DYNAMICS: A CONSIDERATION OF  
CLIMATE, TASK DESIGN, AND COMBAT READINESS FACTORS OF THE OAP/OAS**

Joseph F. Kager

**ABSTRACT**

The purpose of this review was to explore individual and group dynamics underlying the measurement and feedback processes employed by the Leadership and Management Development Center's consulting service. Factors examined were climate, task design, and combat readiness. Findings suggest that additional understanding of the processes may be gained by considering individual and group influences independently, and that aggregating individual, perceptually measured factors to group level constructs may not always be justified. Recommendations were made concerning factor measurement, through the Organizational Assessment Package (OAP), and feedback of each of the enumerated factors.

### **ACKNOWLEDGEMENTS**

I would like to thank the personnel at the Leadership and Management Development Center at Maxwell Air Force Base. In particular, appreciation is due Major Mickey Dansby, Captain Michael Cox, and Master Sergeant John Kopek for providing the resources and guidance necessary in writing this report. Special thanks go to Dr. Kevin Mossholder whose support and suggestions were instrumental in completing this report. Finally, appreciation is given to the Air Force Systems Command, the Air Force Office of Scientific Research, and the Southeastern Center for Electrical Engineering Education for providing the opportunity to spend an interesting and worthwhile summer.

## I-INTRODUCTION

### Goals and Objectives of the LMDC

A primary task of the Leadership and Management Development Center (LMDC) is to supply management consultant services to United States Air Force Organizations. These services are designed to improve leadership and management skills of Air Force personnel and enhance combat readiness through increased motivation and productivity.<sup>1</sup>

This is accomplished through visits by the LMDC consultant teams. The principle assessment device employed is a survey known as the Organizational Assessment Package (OAP). The survey assesses perceptions of individuals on work-related variables, such as; organizational climate, work characteristics, supervisory characteristics, and job satisfaction. A revision of the OAP, the Organizational Assessment Survey (OAS), will measure similar areas as well as stress and combat readiness.

After the assessment of these areas, feedback is given to supervisors at all levels of the organization concerning how their units compare with a sample of similar units contained in the LMDC database. From these comparisons, consultants select units which could benefit from consulting interventions involving techniques tailored to the the units' needs. Workshops may be scheduled if enough supervisors demonstrate a particular need.

## Survey Feedback Approach to Organizational Change

The survey feedback technique of organizational change was introduced by Mann and his associates.<sup>2,3</sup> The three basic components of survey feedback interventions are data collection, group meetings, and process analysis. The unique role of each component is now briefly discussed.

**Data Collection.** Survey feedback data usually deal with organizational issues such as group relations, supervision, organizational policy, employee satisfaction, and performance. Information derived is mostly attitudinal and is used to corroborate or disconfirm the client's beliefs about the state of the organization, thereby unfreezing attitudes and encouraging inquiry concerning results from the data. A key in making survey feedback a powerful change tool is the relevancy of the information.<sup>4</sup> More relevant information increases the likelihood that organizational members will commit themselves to subsequent change.

**Group Meetings.** The importance of group meetings in survey-feedback was demonstrated by Klein and his associates.<sup>5</sup> They found that meetings, as opposed to written reports, resulted in more satisfaction with feedback processes and perceptions of greater information utilization. Direct involvement of the family work group members (i.e. people who interact frequently and often perform related work) was shown to enhance

groups' potential to change.<sup>6</sup> Once subordinates have openly discussed problems with their supervisors, it becomes easier to do so in the future.

**Process Analysis.** The consultant's role is to stimulate the group to analyze its own process during the feedback session. Facilitation rather than domination may provide for useful group learning experiences and can significantly improve the group's output.<sup>5</sup>

### **Major Considerations of Survey Feedback**

Golembiewski and Hilles<sup>7</sup> point to two considerations that must be stressed in using survey feedback. First, the survey should be rooted in a clear statement of values or goals prescribing what the organization should be. The key in accomplishing this lies in the specificity of organizational goals. Without specificity, a survey can not ask meaningful questions. Second, the survey must be rooted in a comprehensive model of reality. This means the model should specify: (1) Dimensions that best describe organizational life; (2) The organizational importance of these dimensions; and (3) Processes and dynamics useful for moving the organization towards its goals.<sup>7</sup> Thus, the survey should reflect the best model available, and the analysis should extract maximally useful information from the data.

Golembiewski and Hilles<sup>7</sup> go on to state that a comprehensive model must be actively pursued by researchers to facilitate development of even better models. The idea of seeking out more comprehensive models is supported by Nader<sup>8</sup> and Huse.<sup>9</sup>

## **II OBJECTIVES**

The main goal of this review is to advance recommendations to the LMDC that will aid in improving their consulting services. To accomplish this goal individual and group dynamics underlying the measurement and feedback processes are generally discussed. Specifically examined are climate, task design, and combat readiness factors of the OAP/OAS survey. By viewing individual and group dynamics of these factors, a more comprehensive understanding of the underlying issues of measurement and feedback processes will be gained.

When warranted, a multi-level perspective is used to attain insight into issues concerning individual and group dynamics. Basically this perspective states that attitudes and behaviors can, in some instances, be best explained from both individual and group levels of measurement. Benefits of this approach are an improved specification of relationships among variables, and an increased generalization of cause and effect relationships by specifying more than one level of cause.<sup>10</sup>

### **III-INDIVIDUAL AND GROUP DYNAMICS OF ORGANIZATIONAL CHANGE**

In advancing models of behavior, organizational theorists have long acknowledged that the needs of the group and of the individual interact.<sup>11,12</sup> It is important, therefore, to consider individual behavior as possibly being influenced by individual and group needs. "The more we can find out of the effect of one on the other (individual and group), the better we can understand the behavior of the individual".<sup>12</sup>

Organizational change theory specifies how altered inputs, internal developments, or various contextual changes will influence the system under study.<sup>13</sup> Basically, organizational change can operate in one of three manners; individual approaches to organizational change, group approaches to organizational change, and direct change of organizational variables. Since the latter method involves manipulation of the role structure in the organization, due to practical considerations of the Air Force, only the first two will be discussed.

Changing the organization solely through its individual members generally has not been successful. This failure stems from a disregard of the systematic properties of organizations.<sup>13</sup> The basic problem lies in the lack of precise concepts for distinguishing between behavior determined by situational constructs of the organization and behavior determined from individual personality needs and constructs. Katz and Kahn<sup>13</sup> note that to effect organizational change from an individual focus, it must be assumed that individuals can be provided with new insight, that the insights gained will cause altered behaviors, and that the insights will persist upon return to the job.

The second, and seemingly more fruitful approach to organizational change involves the use of the group as a means of increasing learning and heightening commitment to things learned. Kurt Lewin and his followers first demonstrated the utility of group methods in modifying individual behavior. They found subordinate participation via a group was superior in enhancing

organizational change when compared to change initiated without group participation.<sup>13</sup> One additional point needs to be emphasized in relation to group change. Maximal group involvement will occur only when decisions in which subordinates participate, have a direct influence on their work.<sup>13</sup> For example, soliciting rank and file subordinate input on upper level financial decisions would probably not facilitate group change.

#### **IV. CLIMATE**

##### **Distinction Between Individual and Organizational Climate**

Several organizational researchers have found it useful to distinguish between individual and organizational climate.<sup>14, 15, 16</sup> Individual climate refers to descriptions of organizational practices and procedures from a single member's point of view. Organizational climate refers to a collective description of the organization's environment, most often assessed through an averaging of organizational member's perceptions.

##### **Climate As Measured by the OAP/OAS**

The OAP separates climate into two subfactors: Organizational Communications Climate, the degree to which a worker perceives the communication environment as open and rich; and General Organizational Climate, an individual's perception of the overall organizational environment.<sup>17</sup> These definitions are given at the beginning of the climate section to aid the reader in understand-

ing how the research to be presented applies to OAP/OAS climate measurement.

#### **Relationship to Satisfaction and Performance**

Past research has demonstrated relationships between climate and such variables as satisfaction and performance.<sup>10</sup> Given the apparent significance of climate with respect to job satisfaction and performance, it would seem important to identify the determinants of climate. With knowledge of these determinants, it would become feasible to initiate organizational changes leading to a better climate. The meaningfulness of the level at which these factors are measured must first be assessed to understand these relationships.

#### **Situational and Situational-Individual Approaches to Climate**

At the individual level of measurement, climate is reflected by individual perceptions of the work environment. Past research has supported two approaches in specifying the sources of climate perceptions. The first approach emphasizes the situational characteristics of the organization (e.g. size, span of control) in influencing climate perceptions. From this perspective, climate should change as the characteristics of the organization change from setting to setting.<sup>11</sup>

It has also been postulated that climate perceptions are reflected in individual differences in perception, as well as the characteristics of the situation.<sup>12</sup> This point has been asply

supported by studies showing that climate perceptions within an organization reflect differences in personality attributes and ability,<sup>20,21</sup> as well as age, race, and intelligence.<sup>22</sup>

The situational approach to perceived climate says it is permissible to aggregate individual perceptions, assuming that individually measured climate is the same as organizational climate. That is, if every individual in a group is operating within a similar setting, individual and organizational climates should be isomorphic. On the other hand, if individual climate perceptions are influenced by both individual and situational parameters, an organization containing members with diverse individual characteristics would be expected to yield a range of climate perceptions. In this case, aggregation of individual perceptions would be in error. Because of the greater support for both situational and individual dimensions of individual climate, the influence of both factors is considered in the following discussion.

#### **Meaningfulness of Aggregated Climate Scores**

The rationale for aggregating individual climate scores to measure organizational climate rests on three assumptions: individual climate scores describe perceived situations; individuals exposed to the same set of situational conditions will describe these conditions in similar ways; and aggregation will emphasize perceptual similarities and minimize individual differences.<sup>19</sup> Based on this logic, empirically demonstrating agreement among

different individuals justifies aggregation of perceptual scores.<sup>23</sup>

Researchers in this area have generally adopted the group mean in aggregating perceptual climate scores. Using the mean is appropriate as long as the point of reference is the situation and not the individual.<sup>16</sup> In other words, the scale items must be worded to elicit objective responses rather than subjective reactions to events or attributes. Techniques used to demonstrate interperceiver agreement have stressed that significant mean differences between organizations or organizational subgroups connote that the perceptual scores reflect situational rather than individual influences. Unfortunately, while this approach appears logical, meaningful guidelines have not been developed for determining what level of statistical agreement justifies aggregation.

Due to the lack of consensus on agreement necessary to aggregate individual scores, this author recommends a construct validity approach to validate aggregate climate measures. The criteria advanced by Jones and James<sup>15</sup> should be demonstrated before any inferences from individual perceptions to organizational climate are made: first, significant differences across different organizational subunits should exist; second, interperceiver agreement among group members demonstrated through intraclass correlation coefficients should be present; third, homogeneous situational characteristics such as context (i.e. technology, goals), structure (i.e. size, span of control), and

job type should be shared among group members; and fourth , meaningful relationships between the aggregate scores and group measures of satisfaction and productivity should be proven.

### **Implications**

As noted earlier in this section, the OAP/OAS divides climate into two subfactors; Organizational Communications Climate, and General Organizational Climate. Both of these are measured at the individual level of perception. Scores for work groups, sections, branches and squadrons are aggregated within an Air Force Wing to yield composite scores. For example, a Deputy Commander will receive a composite score of his/her deputation and a score for each squadron under his/her command. Squadron scores received represent aggregations of branches and sections within that unit.

The climate research reviewed would seem at odds with some of the reporting procedures employed. Specifically, reporting aggregated individual scores to represent organizational climates at different levels. In a related military study by the U.S. Navy, Jones and James<sup>15</sup> found aggregation was meaningful only at a division level. This is roughly equivalent to a section at an air base. Additionally, in reporting that a composite squadron score is not significantly different from the database norm comprised of similar units, no normative information about sections and branches within the squadron is obtained. This may hide problems from higher-level supervisors that are apparent to supervisors at lower levels of command.

It seems important to address the meaning of aggregated scores given as feedback in the consultant process. This issue is relevant to any of the perceptual measures obtained from the OAP/OAS. Examining the level of aggregation from the construct validity approach discussed earlier would be one way to do this. In order for this technique to be useful, a procedure demonstrating at which hierarchical level meaningful organizational climate exists, for each base visited, would be required. Since each base differs in size and personnel make-up, a generalized level across all bases would not be possible.

An alternate strategy that could be employed to aid consultants in giving meaningful feedback to supervisors high in the organizational hierarchy would be simply to give a break-out concerning each command level. This would provide a more comprehensive view and expose problems existing at various levels. A strengthening of organizational commitment to change could also result. Supervisors at lower levels may be more apt to correct problems if higher level involvement is present.

Of course, the issue of response anonymity and possible retribution must be considered. It is suggested in providing supervisors with comprehensive feedback that scores not be identified with specific groups. For example, supervisors would receive scores for unidentified groups A, B, C, and so on, for each command level. However, certain situations, such as a small number of groups per level, could render this strategy ineffective. A possible alternative would be to provide a range of

scores for each level. By employing either of these methods of reporting feedback, a more overall view of the organization is provided to supervisors, while preserving the anonymity of the respondents.

One final point needs to be made in regard to the climate measure (in particular; statements eighty-nine and ninety-seven of the General Organizational Climate subfactor), Payne et al.<sup>16</sup> stated that in using the mean as a climate aggregate, items should elicit objective rather than subjective responses. The enumerated items, measuring pride and motivation, may result in affective responses. If a truly descriptive scale is desired, elimination or rewording of the items mentioned is suggested.

#### V. TASK DESIGN

##### Task Design As Measured By The OAP/OAS

Task design is conceptualized on the OAP/OAS by three factors: Need for Enrichment, focusing on job characteristics desirable to individuals; Task Characteristics, measuring several job aspects (i.e. task identity, feedback); and Task Autonomy, focusing on the amount of discretion afforded individuals in planning and performing their jobs.<sup>17</sup> This model is similar to the job characteristics approach to task design,<sup>20</sup> which will be elaborated in a following section.

### Outcomes of Task Redesigns

As with climate, redesigning tasks has been shown to be associated with beneficial work outcomes. Variables positively influenced by job redesign are satisfaction, productivity, and commitment.<sup>24</sup> Task redesign can lead to high internal motivation in workers. Research supporting this proposition has found that job satisfaction increased as a result of task manipulations. Similarly, it has been argued that changing jobs can lead to heightened commitment to the organization and increased productivity. The relationship of these desirable organizational properties and enriched tasks demonstrates the merit in considering task redesign as a viable organizational intervention technique.

### Competing Approaches to Task Design

Presently, two competing approaches to changing jobs in organizations exist. The older and more researched approach emanates from the job characteristics model.<sup>24</sup> Briefly, the job characteristics model examines individual responses to jobs as a function of job characteristics moderated by individual differences. The second, and more recent approach to task design is the social information processing model developed by Salancik and Pfeffer.<sup>25</sup> This perspective emphasizes the effects of the social context and the consequences of past choices in explaining job responses.

## **The Job Characteristics Model**

This overview is based on Hackman and Oldham's model.<sup>26</sup> Drawing on previous task design research,<sup>26,27</sup> the job characteristics model states that interactions between jobs and individuals determine work outcomes. Dependent variables, or work outcomes, include satisfaction, turnover, absenteeism, and performance. Job characteristics, or core dimensions, are posited to describe motivational components of work which satisfy individual needs. These include skill variety, task significance, task identity, feedback, and autonomy. Jobs must be high on all dimensions for positive outcomes to occur.<sup>28</sup> Ideally both horizontal and vertical changes to jobs are recommended. Horizontal changes involve increasing the number of different things individuals do, while vertical changes imply increasing the degree to which individuals are responsible for decisions.

Applying the job characteristics model as does the Air Force, assumes that specific jobs are invariant across individuals. That is, since individual perceptions are aggregated and composite scores formed, individuals' scores are subsumed within that composite. People may perceive certain job characteristics differently. For instance, a job requiring extensive travel would probably be viewed differently by an unmarried employee than an employee with a family. However, certain job characteristics can be similarly perceived by workers. A building with temperature above ninety degrees will result in similar perceptions concerning the heat. Therefore task redesign should take into account both individual and group influences.

This point was raised in recent attacks on the job characteristics model. For instance, criticisms stating that the model does not specify the determinants of individual needs nor individual perceptions,<sup>28</sup> and that the model neglects situational influences on perceptions,<sup>29</sup> are representative of the recent controversy.

#### Social Information Processing Model

Partially because of dissatisfaction with the job characteristics model, a social information processing approach evolved. This approach attributes job attitudes and needs as originating from two sources. First, individuals develop attitudes and needs associated with a job as a function of the information available to them at the time the attitude or need is expressed. One important source for information is the immediate social environment. The social context of the situation generally has two effects: (1) it directly allows for construction of meaning through socially acceptable beliefs, attitudes, and actions; (2) it indirectly causes individuals to focus attention on certain information, making that information more salient.<sup>25</sup>

For instance an individual's perceptions can be directly influenced by overt statements of coworkers as to monotony or some other characteristic of the job. Indirect influences are contained in everyday conversations. In noting certain aspects of the job, coworkers cue an individual as to what to consider in the work setting. Calling attention to the social importance

of the organization's service may make the job seem significant. In both instances, coworkers are giving social cues to the individual.

The second source of job attitudes and needs is individuals' past behaviors attributed to the environment. The process of attributing attitudes from past behavior depends on commitment to the behavior. Commitment is greatest when behavior occurs under conditions of choice, when it is public, and when its occurrence cannot be denied. Commitment causes information about past behavior to become salient leading to possible influences on attitudes and needs.<sup>23</sup>

Straw<sup>30</sup> found this effect in that individuals committed to ROTC programs because of binding contracts, developed more favorable attitudes towards the program after they received a high draft number, compared to those not bound by contracts. This is surprising since the individuals joined ROTC to avoid conscription. Presumably the high draft number should have caused the program to lose its appeal since it no longer fulfilled a personal goal. However, attitudes became more favorable, possibly resulting from the individuals' need for attitudes justifying remaining in the program.

Three important conclusions are implied from this approach. First, task redesign programs cannot be successfully accomplished over night. Changing employee attitudes towards salient job dimensions involves a long-term, managed social process. Secondly, the dimensions made salient must be capable of being per-

ceived as changed. Those dimensions that cannot be acted upon because of either role or technology constraints should not be addressed. Lastly, the social information processing approach is individually-oriented. Social contexts can be perceived differently by individuals. In particular an individual's past behaviors contribute to attitudes unique to that person. However, small groups, characteristicly with high interaction, may perceive social contexts similarly. Demonstrating consensus of job attitudes by a validation procedure, like the one discussed in the climate section, may allow groups to become the focal unit of task redesign.

#### **Recent Research in Task Design**

Generally the research done in this area is laboratory based, comparing the relative effects of the two models in changing job attitudes. Studies by White and Mitchell<sup>31</sup> and O'Reilly and Caldwell<sup>32</sup> are representative of the laboratory studies. Both studies found social cues and direct task manipulations to affect job attitudes. Social cues accounted for somewhat more variation in satisfaction and productivity than task manipulations. In one of the few field experiments conducted in this area, Griffin<sup>33</sup> found evidence for both social cues and task manipulations in changing job attitudes. Social cues were verbally given by supervisors directed towards reinforcing the core dimensions of feedback, task variety, autonomy, and task identity inherent in the jobs. The objective manipulations involved

implementing new technology and restructuring of organizational roles.

Results indicated that both social cues and task manipulations influenced job perceptions. Task manipulations appeared to influence productivity, while no relationships between productivity and social cues were detected. This study demonstrated that the relationships hypothesized by the social information processing model are not restricted to the laboratory. Also, organizations should consider this approach, in addition to direct manipulations, in task redesigns.

### Implications

It is recommended that both the job characteristics and social information processing approaches to task design be considered by the LHDC. This means that when task interventions are appropriate, effort should be directed towards changing perceptions through a managed social process as well as actually changing the task. In adopting groups as focal units for change, aggregation considerations arise. Whether task perceptions are specific to individuals, groups, or both, as advocated by a multi-level perspective, deserves consideration. If task perceptions are to collectively describe a group of people working at the same job, homogeneity of group perceptions should be demonstrated.

Adopting both approaches to task design theoretically makes sense, but in application actually changing tasks is not always

possible. This may especially be true in the Air Force where organizational roles or technology may limit actual task changes. Here, influencing task perceptions may be a viable alternative. The most obvious source of potential social cues is the supervisor. Cues could be specifically directed at the core task dimensions of feedback, variety, autonomy, identity, and significance. It is important for supervisors to understand that cues should be given only in relevant instances, and in the case of feedback, as performance warrants. Griffin's field study<sup>33</sup> demonstrated supervisory cueing's impact on task perceptions.

Social cueing should begin when individuals enter the organization. Employing job previews that emphasize the positive aspects of the job is one possibility. For example, the Air Force should emphasize, in as relevant terms as possible, how jobs help protect the country, or how jobs offer a wide variety of useful experiences. This would immediately make salient those positive dimensions inherent in the job. Another example would be communicating career ladders to new personnel, and specifying the importance of performance for promotion. This is undoubtedly important to individuals upon entering the Air Force.

Social cues can come from a variety of sources too numerous to be discussed here. Something as simple as erecting a bulletin board may change a perception of lack of information flow in an organization. Of course certain people could construe such manipulations to be somewhat unethical. This issue, though relevant, is beyond the scope of this review and therefore not considered.

## **VI. COMBAT READINESS**

### **Combat Readiness As Measured by the OAP/OAS**

The OAP/OAS divides combat readiness into combat related training, group cohesion, morale, and combat motivation. These subfactors, as with climate and task design, are measured at the individual perceptual level. It is important to note that objective criteria, such as logistics, are omitted. The measures used in composite criterion are psychological and therefore subjective in nature. While this section will emphasize the individual and group components of combat readiness, a strict multi-level view is not discussed because of the lack of information in the combat readiness area concerning this perspective.

### **Assumptions of the Present Review**

Before discussing the literature on combat readiness, a few comments are in order. First, the majority of literature on combat readiness is based on studies conducted by the Army. Although overall missions of Army and Air Force personnel are conceptually different, basic similarities are assumed to allow generalizations. Second, published research discusses combat readiness of experienced combat personnel. Combat readiness of support personnel was not discussed in any of the readings and generalizations to them may be limited. Finally much of the writing in this area consists of subjective opinions as opposed to empirical research. Views advanced in these articles will be

reported; however their findings will not be stressed in advancing implications in the last section.

### **The Problem of Combat Readiness**

Preparing individuals for stresses they will encounter in a combat situation has always been important to military leaders. The ability of a unit to adapt to high stress in combat is a major determinant of its success. Stress encountered by infantry units was discussed by Marshall<sup>34</sup> when he observed an astounding seventy-five percent of the men in any given combat unit would not fire, or persist in firing against the enemy. Thus, a major task for leaders is to determine variables facilitating stress reduction in combat.

### **Stress and Its Components**

Grinker and Spiegel<sup>35</sup> assert that universal stresses of combat tend to reduce all individuals to a common denominator, termed the combat personality. The authors base their ideas on findings from an extensive study of both successful and unsuccessful adaptations to combat. Stress affects the combat personality by producing fear, anxiety, and to a lesser extent, hostility.<sup>35</sup>

The difference between fear and anxiety is an important issue. First, fear is an emotional response to a real stimulus that either threatens the individual at the moment or portends actual danger. In most circumstances, individuals are able to

reduce fear through action.<sup>35</sup> Since fear occurs in response to actual danger, it is an emotion of self-preservation, serving as an integral part in individuals' defense mechanisms. Anxiety is an anticipation of danger, occurring when individuals are reminded or forewarned of traumatic experiences, and respond as if the danger was truly present.<sup>35</sup> Low levels of anxiety can prepare individuals for possible dangers in combat. However, when high levels of anxiety exist, individuals may become obsessed with dangers both real and unreal. Individuals in this condition cannot distinguish between dangers that are real (fear) and those that are not based in reality (anxiety). Thus, to increase combat readiness, factors acting to decrease individuals' anxiety must be distinguished. The remainder of this section will discuss parameters that facilitate reduction of anxiety (i.e. increase psychological combat readiness) from both individual and group perspectives.

#### Individual Perspectives

**Individual Stress Limits.** An individual perspective of measurement assumes that stress affects individuals differently. Standish<sup>36</sup> took this view, reasoning that each individual develops a mental stability limit in childhood based on security and discipline received from the parents. By adolescence, the limit is fixed. An individual's adaptation to a stressful situation is dependent on the sum of situational stresses and the individual's mental stability limit. Since an individual's mental stability

limit is not flexible, the situation, or the match between individual and situation, must be changed to decrease the individual's stress.

**Learned Habits.** Hausser<sup>37</sup> advocated the individual as the focal point to enhance combat readiness. He lists four factors which propel men into combat: submission to authority; fear of both punishment for desertion and of disgrace; loyalty to the unit; and personal pride. The author advocates a behavior modification approach to decreasing stress, namely individuals should be rewarded for appropriate behavior and punished for inappropriate behavior. Through this approach, along with longer and more intensive training, individuals should master the task at hand, resulting in less anxiety in actual combat.<sup>37</sup>

**Self-Confidence.** Additionally, strengthening individuals' self-confidence is suggested as a means of stress reduction.<sup>35,38,39</sup> If individuals can be made more confident during training and indoctrination of their stamina, skill, and ability as combat participants, anxiety will resultantly decrease.<sup>38</sup> This view differs from the learned habits approach in that cognitive processes are stressed.

Stouffer and his associates,<sup>38</sup> in their study of social psychology during World War II, found that those individuals who exhibited high levels of self-confidence after completing training, were rated significantly better performers in combat by their superiors than those who reported low self-confidence following training.

## **GROUP PERSPECTIVES**

Understanding group impact on individuals is important in formulating a comprehensive measure of combat readiness. As is often the case, accurate predictions of individuals' behavior will not necessarily afford accurate predictions of individuals' behavior when they are members of a group. Group effects on individual behavior can take a variety of forms. For example, extinction of personal feelings, higher levels of emotion, and a feeling of decreased responsibility for actions are characteristic of individuals in groups.<sup>40</sup> Therefore, in adapting a comprehensive model of combat readiness, the group, as well as the individual, should be taken into account.

**GROUP Cohesion and Loyalty.** In relation to combat readiness, effects of group cohesion are often cited.<sup>35, 36, 41</sup> Situational influences of combat, namely the existence of an outside threat, often results in a feeling of group solidarity. Individuals in combat come to depend on the group, not only for survival, but also for various affectional needs.<sup>36</sup> Through this dependence the group is able to enforce its standards and goals on individuals. Grinker and Spiegel<sup>35</sup> identify an individual's attachment to the group as the most important factor in controlling anxiety. They state that as long as an individual's interests remain devoted to the group, high levels of anxiety will not develop.

**GROUP Size.** Individuals' abilities to form strong group ties are moderated by group size, in that cohesion seems to be

found strongest at the primary group level.<sup>35,41</sup> Primary groups characteristically have high interactions and a shared dependence (e.g. bomber crews and combat squads). High levels of teamwork are also characteristic of primary groups. In most instances teamwork is necessary for successful performance of the primary group's mission. Group size moderates cohesion in that individuals are unable to identify with large intangible groups such as an Air Force Wing or the Air Force taken as a whole. Therefore, to reduce anxiety through feelings of group cohesion and loyalty, emphasis must be placed at the primary group level.<sup>41</sup>

**Morale.** Factors discussed as influences on individual stress levels have primarily concerned group cohesion and self-confidence. These elements collectively result in morale.<sup>35</sup> Morale is defined as a group's capacity to pull together persistently for a common purpose.<sup>35</sup> It can also be thought of as a collective state of motivation experienced throughout the group. An additional component of morale is subordinate confidence in leadership. Eighty-eight percent of the combat flyers interviewed by Shaffer<sup>39</sup> voiced that confidence in the ability of their commanding officer aided in controlling fear. The management and supervision factor of the OAP/OAS, to some extent, measures this construct. Specifically, support, guidance received, and the overall quality of supervision are assessed through the instrument.

## Implications

In measuring combat readiness a contingency approach is advocated. Factor assessment, and the manner in which feedback is given, should depend on the group's mission. Specifically, a differentiation needs to be made between groups in which tasks demand high levels of teamwork and those that do not. Combat units, or groups in which tasks are largely conjunctive, need to be assessed at both individual and group levels. Assessing individual perceptions of combat readiness is crucial, since only one group member who is experiencing high stress may hinder overall group performance. This could occur even if the majority of group members perceived the unit as combat ready. A composite score of this hypothetical group would reflect the majority's perceptions, but hide the individual's negative evaluation of combat readiness. It is suggested that individual influences of combat readiness such as confidence in one's training and abilities be assessed individually for members of groups performing conjunctive tasks.

Collective measures of combat readiness also are important for groups performing conjunctive tasks. Throughout the literature, the construct of group cohesion and loyalty is noted for reducing stress. The phenomenon seems strongest at the primary group level. It can be argued that the nature of conjunctive tasks causes feelings of group cohesion and loyalty, since unit success is dependent on each group member working together. Therefore aggregating primary groups for feedback concerning

cohesion is not advised when tasks performed within groups are characteristically high in required teamwork.

Measuring combat readiness of groups whose missions do not demand high levels of teamwork suggests a different approach. Individual determinants of combat readiness may be more important than group considerations. Since successful performance is dictated by the individual's effort, group influences will play a lesser part in combat readiness. Individual aspects of combat readiness, such as confidence in training and personal abilities, would seem to be more influential in explaining combat readiness in low teamwork groups.

Other potential determinants of combat readiness, such as trust in leadership abilities, are important to both high and low teamwork groups. Confidence in leadership is not directly measured by the combat readiness scale; however, overall supervision is assessed through the management and supervision factor. Statements in this factor concern supervisory processes, but fail to measure outcomes such as confidence and trust in leaders' judgement and abilities. Statements assessing leadership outcomes deserve consideration on the combat readiness scale.

Finally, although objective indices of combat readiness are not considered in the survey, subjective aspects of logistics deserve mention. Shaffer<sup>30</sup> found confidence in equipment as a factor related to reduced stress. This factor may be especially important for primary groups performing conjunctive tasks. An obvious example would be a flight crew that perceives it's air-

craft as being in less than satisfactory condition. Stresses in this situation would be enormous. This factor may operate in the framework suggested in Herzberg's two factor theory of motivation,<sup>42</sup> in that equipment perceived as functioning well may not heighten individuals' feelings of combat readiness, but equipment that is thought to be less than adequate will certainly depress motivation for combat.

### VII. SUMMARY

This review discussed individual and group dynamics underlying the measurement and feedback processes employed by the LMDC management consulting service. Specifically examined were climate, task design, and combat readiness factors of the OAP/OAS survey. Both individual and group perspectives were reviewed for each factor in order to illustrate individual and group influences on individual behavior. Consequently, a better understanding of the multiple determinants influencing individual behavior was gained.

#### Climate

Researchers in the climate area differentiate between individual climate, descriptions of organizational practices from a single member's point of view; and organizational climate, a collective description of the organizational environment, most often assessed by averaging organizational members' perceptions. By aggregating individual perceptions one assumes that organiza-

tional members perceive climate similarly, and that these similarities outweigh individual differences in perception. It becomes necessary to assess the degree of perceptual agreement among individuals whose scores are aggregated. Aggregate climate measures should be construct valid to assure that agreement exists to warrant feedback at various organizational levels.<sup>15</sup>

Aggregation procedures characteristically give no information about subunits that are subsumed within the larger unit. In the Air Force, supervisors high in the command hierarchy are given a narrow view of their organizations. Giving these supervisors a break-out of scores at each command level would offer them a more comprehensive view of their organizations. Confidentiality of respondents could be maintained by giving anonymous representation of group scores, or by giving a range of scores of the groups at any particular organizational level. A final point regarding climate aggregation concerns the wording of statements. If responses are aggregated, the statements should elicit objective rather than subjective responses.<sup>16</sup> Individual differences are minimized if this guideline is followed. Specifically, statements measuring pride and motivation should not be used to assess organizational climate.

### **Task Design**

Two approaches to changing jobs in organizations exist. The job characteristics model states that individuals' job attitudes are a function of job characteristics (i.e. task identity, task

significance, skill variety, feedback and autonomy) moderated by individual differences.<sup>24</sup> Actual changes in the job characteristics are necessary to affect job attitudes. Research on this approach has treated job attitude change as occurring at the group level. The other view, the social information processing model, states that the social context and individuals' past actions explain job attitudes.<sup>25</sup> In order to change job attitudes, jobs must only be perceived as changed. Social cues given by supervisors or coworkers are postulated to affect change. This approach operationalizes change as occurring at the individual level. However perceptions may be collectively held. As with climate, the level at which aggregation is appropriate should be validated in task design measures. Evidence exists supporting both models' influence on workers' job satisfaction and productivity.

#### Combat Readiness

Combat readiness is determined by individuals' abilities to cope with stress. Individual determinants of combat readiness are a person's self-confidence in their stamina, skill, and ability as a combat participant. Group determinants concern cohesion and loyalty. Feelings of group solidarity, characteristic of cohesive groups, appear strongest at the primary group level (i.e. groups typically having high interaction, tasks demanding high levels of teamwork, and a shared dependence). In measuring combat readiness, groups whose tasks demand high levels of team-

work, and groups which perform tasks characteristically demanding little teamwork should be assessed differently. The former groups should be measured by both individual and group constructs. Here, individual self-confidence is important since one group member who is not confident and/or combat ready could affect the group's collective performance. Group cohesion should be assessed because of its stress controlling properties. Combat readiness of low teamwork groups should primarily be assessed through individual determinants. Aspects such as confidence in training and personal abilities would seem more influential in determining combat readiness in these groups than constructs of cohesion and loyalty.

Lastly two other determinants of combat readiness may affect stress levels of both groups. First, subordinates' trust in the abilities of their leaders should be assessed. In addition, individuals' confidence in their equipment may affect stress reduction. Both of these constructs were found to be important in controlling stress of combat air crew members.<sup>39</sup>

#### **VIII. RECOMMENDATIONS**

The reviews of climate, task design, and combat readiness referred to above, demonstrate the importance of considering both individual and group dynamics in the measurement and consulting processes. In light of this review, the following recommendations are warranted:

1) Determine the level at which aggregate climate and task design feedback scores are meaningful by demonstrating agreement using a construct validity approach. Present methods assume homogeneity of group members' perceptions.

2) Expand the climate feedback given to supervisors to encompass each level of their command. Confidentiality of respondents can be maintained by giving anonymous representation of group scores or by reporting ranges of scores. This will allow a more comprehensive view of the organization, and not violate the participants' confidence.

3) Rework items eighty-nine and ninety-seven of the General Organizational Climate factor. These statements, measuring pride and motivation may be eliciting subjective responses, which should not be used if average climate scores are reported.

4) Adopt a social information processing approach for task redesign interventions in addition to objective task changes. Social cues have a proven influence on job attitudes.

5) Differentiate in measuring combat readiness between groups which perform tasks demanding high levels of teamwork and those groups whose tasks are identifiably low in teamwork characteristics. Low teamwork groups should primarily be assessed at individual levels, while for high teamwork groups, assessment at both individual and group levels may be important.

6) In determining combat readiness, assess confidence in leadership and equipment at the individual level for both high and low teamwork task groups. These constructs may be important in measuring psychological combat readiness.

## REFERENCES

1. Hendrix, W.H. and Halverson, V.B., Organizational Survey Assessment Package for Air Force Organizations, (AFHRL-TR-78-93) Brooks AFB TX: Air Force Human Resources Laboratory, 1979.
2. Mann, F.C., "Studying and Creating Change: A Means to Understanding Social Organizations, In Research in Industrial Human Relations, Industrial Relations Research Association, No. 17, pp. 146-167, 1957.
3. Mann, F.C. and Likert, R., "The Need for Research on Communicating Research Results", Human Organization, Vol. 11, pp. 15-19, 1952.
4. Nerf, P.W., "Survey Research: A Tool for Problem Diagnosis and Improvement in Organizations", In M.D. Dunnette (Ed.), Handbook of Industrial and Organizational Psychology, (Wiley and Sons, New York, 1967), pp. 947-949.
5. Klein, S.H., Kraut, A.I., and Wolfson, A., "Employee Reactions to Attitude Survey-Feedback" In M.D. Dunnette (Ed.), Handbook of Industrial and Organizational Psychology, (Wiley and Sons, New York, 1967), pp. 947-949.
6. French, W.L. and Bell, C.H., Organizational Development, (Prentice-Hall, Englewood, 1978), p. 93.
7. Golombiewski, R.T., and Hilles, R.J., Toward the Responsive Organization: The Theory and Practice of Survey Feedback, (Brighton, Salt Lake City, 1979), pp. 78-85.
8. Nader, D.A., Feedback and Organization Development Using Data-Based Methods, (Addison-Wesley, Reading, 1977), p. 59.
9. Huse, E.F., Organization Development and Change, (West, New York, 1980), p. 121.
10. Rousseau, D.H. "Issues of Level in Organizational Research: Multi-Level and Cross Level Perspectives", In B. Straw & L.L. Cummings (Eds.), Research on Organizational Behavior, (JAI Press, New York, 1983).
11. Argyris, C., "Personality and Organizational Theory Revisited", Administrative Science Quarterly, pp. 141-166, 1973.
12. Whyte, W.H., The Organizational Man, (Doubleday, New York, 1957), pp. 130-132.

13. Katz, D., and Kahn, L.R., The Social Psychology of Organizations, 2nd. Ed., (Wiley and Sons, New York, 1978), pp. 186-199.
14. James, L.R., "Aggregation Bias in Estimates of Perceptual Agreement", JOURNAL of Applied Psychology, Vol. 67, pp. 219-229, 1982.
15. Jones, A.P., and James L.R., "Psychological Climate: Dimensions and Relationships of Individual and Aggregated Work Environment Perceptions", Organizational Behavior and Human Performance, Vol. 23, pp. 201-250, 1979.
16. Payne, R.L., Fineman, S., and Wall, T.D., "Organizational Climate and Job Satisfaction: A Conceptual Synthesis", Organizational Behavior and Human Performance, Vol. 16, pp. 45-62, 1976.
17. Bahr, T.A., Manual for the Organizational Assessment Package Survey, (LMDC-TR-82-1560), Maxwell AFB, AL: Leadership and Management Development Center, 1982.
18. Schneider, B. and Snyder, R. "Some Relationships Between Job Satisfaction and Organizational Climate", JOURNAL of Applied Psychology, Vol. 60, pp. 318-328, 1975.
19. Schnieder, B. and Reichers, A., "On the Etiology of Climates", Personnel Psychology, Vol. 36, pp. 19-40, 1983.
20. Kerr, S. and Schriesheim, C., "Consideration, Initiating Structure and Organizational Criteria-An Update of Korman's 1966 Review", Personnel Psychology, Vol. 27, pp. 555-568, 1974.
21. Johnston, H.B., "Some Personality Correlates of the Relationships Between Individuals and Organizations", JOURNAL of Applied Psychology, Vol 59, pp. 623-632, 1974.
22. Hellriegel, D. and Slocum, J.W., "Organizational Climate: Measures, Research, and Contingencies", Academy of Management Journal, Vol. 17, pp. 255-280, 1974.
23. James, L.R. and Jones, A.P., "Organizational Climate: A Review of Theory and Research", Psychological Bulletin, Vol. 81, pp. 1096-1112, 1974.
24. Hackman, J.R. and Oldham, G.R., "Motivation Through the Design of Work: Test of a Theory", Organizational Behavior and Human Performance, Vol. 16, pp. 250-279, 1976.
25. Salancik, G.R., and Pfeffer, J.A., "A Social Information Processing Approach to Job Attitudes and Task Design", Administrative Science Quarterly, Vol. 23, pp. 224-253, 1978.

26. Turner, A.H. and Lawrence, P.R., Industrial Jobs and the Worker, (Harvard Graduate School of Business, Boston, 1965).
27. Hulin, C.L. and Blood, H.R., "Job Enlargement, Individual Differences, and Worker Responses", Psychological Bulletin, Vol. 69, pp. 41-55, 1968.
28. Hackman, J.R. and Lawler, E.E., "Employee Reactions To Job Characteristics", Journal of Applied Psychology, Vol 55, pp. 259-286, 1971.
29. Roberts, K.H. and Glick, W., "The Job Characteristics Approach to Task Design: A Critical Review", Journal of Applied Psychology, Vol. 66, pp. 193-217, 1981.
30. Strav, B.H., "Attitudinal and Behavioral Consequences of Changing a Major Organizational Reward: A Natural Field Experiment", Journal of Personality and Social Psychology, Vol. 29, pp. 742-751, 1974.
32. White, S.E., and Mitchell, T.R., "Job Enrichment Versus Social Cues: A Comparison and Competitive Test", Journal of Applied Psychology, Vol. 64, pp. 1-9, 1979.
32. O'Reilly, C.A. and Caldwell, D.F., "Informational Influence as a Determinant of Perceived Task Characteristics and Job Satisfaction", Journal of Applied Psychology, Vol. 61, pp. 157-165.
33. Griffin, R.W., "Objective and Social Sources of Information in Task Redesign: A Field Experiment", Administrative Science Quarterly, Vol. 28, pp. 184-200, 1983.
34. Marshall, S.L.A., Men Against Fire, (William Morrow, New York, 1947), p. 83.
35. Grinker, R.R. and Spiegel, J.P., Men Under Stress, (McGraw-Hill, New York, 1979), pp. 30-62.
36. Standish, A., "The Crisis in Courage", U.S. Army Combat Forces Journal, pp. 40-48, 1952.
37. Hausser, W.L., "Combat Effectiveness", In S.C. Sarkesian (Ed.), Combat Effectiveness: Cohesion, Stress and the Volunteer Military, (Sage Publications, Beverly Hills, 1980), pp. 92-121.
38. Stouffer, S.A., Lunsdaine, A.A. Lunsdaine, H.H., Williams, R.H., Janis, I.L., Smith, H.B., Star, S.A., and Cottrell, L.S., The American Soldier: Combat and Its Aftermath, Vol 2, (Princeton Press, New Jersey, 1949) pp. 120-187.

39. Shaffer, L.F., "Fear and Courage in Aerial Combat", JOURNAL of Consulting Psychology , Vol. 11, pp. 137-142, 1947.
40. Stouffer, S.A., Suchman, E.A., DeVinney, L.C., Star, S.A., and Williams, E.H., The American Soldier: Adjustment During Army Life , Vol 1, (Princeton Press, New Jersey, 1942) pp. 240-253.
41. Hoskos, C.C., The American Enlisted Man , (Sage Publications, New York, 1970), 78-96.
42. Herzberg, F., "Work and the Nature of Man", in M.D. Dunnette (Ed.), Handbook of Industrial and Organizational Psychology , (Wiley and Sons, New York, 1976) pp. 136-140.

\*P END BIM 154 JOB 566 NN159JKK 0002 0001 LOCAL 7206

41 PAGES 10.05.2

1984 USAF-SCEEE GRADUATE STUDENT SUMMER SUPPORT PROGRAM

Sponsored by the

AIR FORCE OFFICE OF SCIENTIFIC RESEARCH

Conducted by the

SOUTHEASTERN CENTER FOR ELECTRICAL ENGINEERING EDUCATION

FINAL REPORT

EXPERIMENTAL ANALYSIS OF PRESSURE SWING ADSORPTION

Prepared by: John C. Kayser  
Academic Department: Chemical Engineering  
University: Ohio State  
Research Location: USAF School of Aerospace Medicine  
Brooks AFB  
USAF Research Contact: Dr. Kenneth G. Ikels  
SFRP Supervising Faculty Member: Dr. Kent S. Knaebel  
Date: September 19, 1984  
Contract No.: F49620-82-C-0035

EXPERIMENTAL ANALYSIS OF PRESSURE SWING ADSORPTION

by

John C. Kayser

ABSTRACT

The United States Air Force is currently assessing the separation of oxygen from air using pressure swing adsorption (PSA) for use on board aircraft. A recently developed theoretical model for PSA (Knaebel and Hill [1]) is experimentally tested by separating oxygen from air at 45°C and 45 psia (feed pressure). Molecular sieve 5A adsorbent is used in a two-bed, six-step PSA cycle. The theory accurately predicts the maximum recovery of oxygen as a function of the pressure ratio within 8%. In simple breakthrough experiments the model predicts the slope of six linear equilibrium isotherms with an average deviation from the actual values of 5%. The model should be a useful tool in future USAF performance studies of PSA units.

The experimental work is performed under conditions favorable to the assumptions of the theoretical model. Recommendations are given for future theoretical and experimental development under less favorable conditions. Additional experimental work could significantly expand the utility of the theory.

### ACKNOWLEDGEMENTS

I would like to thank the Air Force Systems Command, the Air Force Office of Scientific Research and the Southeastern Center for Electrical Engineering Education for sponsoring this work. Special thanks are extended to the U.S. Air Force School of Aerospace Medicine, Brooks A.F.B., Texas. In particular, the technical and laboratory support of Dr. Kenneth G. Ikels and Mr. Clarence Theis was invaluable to this project.

Finally, I would like to thank Dr. Kent S. Knaebel for his help in every aspect of this study. His theoretical work formed a framework for the study and his experimental guidance was indispensable.

## I. INTRODUCTION

Pressure swing adsorption (PSA) is an attractive technique for separating gas mixtures. It requires little energy input and is capable of providing pure product. The Air Force is presently assessing PSA as a method of supplying oxygen on demand to crew members on board aircraft. An important part of the Air Force effort is to understand the performance of PSA units under a variety of conditions. A theoretical analysis of PSA was recently developed by Knaebel and Hill [1]. If accurate, the theory would be a useful tool in studying the performance of PSA units. This work evolved naturally out of the Air Force need for increased understanding of PSA performance and the necessity of testing the available theory.

## II. OBJECTIVES

The primary objective of this project was to test the PSA theory of Knaebel and Hill [1]. The constraints and assumptions of the theory formed an excellent guideline for the experimental study. Using the theory the following experimental objectives were defined.

1. To predict the slope of the equilibrium adsorption isotherms of a component of a binary gas mixture by running a dynamic breakthrough experiment.
2. To construct a PSA system to separate oxygen from air and compare the experimental performance with the predictions of the theory.

## III. BACKGROUND

PSA works on the basis of preferential adsorption of one component of a mixture on an adsorbent solid. An adsorbed component can be partially removed from the solid by decreasing the pressure of the gas around the solid. Hence, by "swinging the pressure" from high to low a strongly adsorbed component can be trapped via adsorption at high pressure and released via desorption at low pressure.

The measure of the quantity of a component adsorbed on a solid at equilibrium is represented by the adsorption isotherm. Adsorption isotherm information is necessary for fundamental study of PSA. In the sections which follow all comments pertain to a binary gas mixture. Additionally, the heavier component, species A, means that more of component A adsorbs than component B if each were at the same partial pressure. It follows that species B is sometimes referred to as the light component of the binary mixture.

In a two-bed PSA process (see Figure 1) a gas mixture is fed to bed 1 while bed 2 is depressurized and purged with product gas to regenerate the adsorbent. Pressurization of the regenerated bed can be performed either with feed gas or product gas. After pressurization of bed 2, bed 1 is depressurized and purged while the feed is diverted to bed 2. So, each bed undergoes identical cycles but are  $180^\circ$  out of phase. In this study pressurization with product is performed for two reasons:

1. the theoretical equations for pressurization with product are analytic solutions of continuity (i.e. not numerical) and
2. the theory predicts greater recovery of product gas by pressurization with product as compared to pressurization with feed gas.

Knaebel and Hill [1] extended the analysis of PSA significantly by developing equations applicable to arbitrary compositions of a binary feed gas. The applicability of the theory is defined by the constraints and assumptions involved in the derivation. A list and brief discussion of these follows.

1. Local equilibrium: During the dynamic operation of the PSA process it is assumed that the gas mixture is in local equilibrium with the solid adsorbent. Local equilibrium is equivalent to assuming instantaneous adsorption and desorption. The assumption is a reasonable one if the gas velocity is low enough through the packed bed to enable equilibrium to

approximately occur. As a result, the assumption will be supported if the feed rate is low resulting in slower cycling of the process.

2. Linear, uncoupled isotherms: The requirement of uncoupled isotherms means that the adsorption of each component is only a function of its partial pressure and is independent of the adsorption of the other component. Miller [2] showed that for the nitrogen-oxygen binary at 24°C and up to 2000 mm Hg the coupling is negligible. The constraint of linear isotherms passing through the origin is favored at high temperatures and low pressures.

3. Negligible dispersion - The dispersion coefficient, which is a measure of the dispersion forces in a flowing system, can be roughly broken into two components: one due to mixing at high velocities and one due to molecular diffusion. By operating the PSA system with long cycles (i.e. low velocities) the mixing component should be small. Additionally, the molecular diffusion dispersion component should not be significant.

4. Zero pressure drop along a packed bed during feed and purge steps: In reality this cannot be achieved but it can be approximated. Slow cycling of the process also favors this assumption and the average pressure can be used in calculations with little loss in accuracy.

5. Isothermal operation: The heats of adsorption of nitrogen and oxygen on molecular sieve 5A (adsorbent used in this study) are less than 5<sup>kcal</sup>/gmole. Consequently, the thermal effects of adsorption are mild but quite noticeable. Also, during depressurization there is a significant temperature drop. In general, at pressures less than 45 PSIA and temperatures above 20°C the temperature of the PSA process designed for this study is maintained within a ±4°C range. At lower pressures and higher temperatures the quantity of material adsorbed decreases resulting in a better approximation of isothermal operation.

6. Binary mixture: The theory is limited to binary mixtures. In actuality air contains three main components: nitrogen (~78%) oxygen (~21%) and argon (~1%). Argon adsorption on molecular sieve 5A is essentially identical to that of oxygen (i.e. the adsorption isotherms are coincident). As a result, oxygen and argon can be treated as a single component and the mixture as a binary.

In the following section the experiments and relevant theoretical equations are presented. The derivation of the theoretical equations is not included.

#### IV. EXPERIMENTAL SUMMARY

##### A. Void Fraction Determination

An important parameter in the analysis of flow through packed beds is the void fraction. Simultaneously measuring the void fraction and the bulk density allows calculation of the particle density. The particle density is a fundamental number and once it is determined the void fraction can be calculated for any packed bed if the bulk density is known. The three parameters are related by the following equation:

$$(1-\epsilon) \rho_p = \rho_B \quad [1]$$

The experimental determination of the void fraction and bulk density and thus the particle density is performed using the apparatus in Figure 2. The glass column is packed with molecular sieve 5A and filled with cyclohexane ( $C_6H_{12}$ ). With knowledge of the pertinent volumes and weight of solids the void fraction can be determined. Cyclohexane was chosen since its large molecular diameter indicates that it cannot enter the crystal cages of the zeolite. The void fraction is thus defined as all the voids outside of the zeolite crystal lattice divided by the total volume. To test the hypothesis that cyclohexane is excluded from the zeolite crystal, n -  $C_{18}H_{38}$

was used in the identical experiment. It is reasonable to assume that  $n\text{-C}_{18}\text{H}_{38}$  cannot significantly enter the zeolite lattice. A statistically equal void fraction was determined in the  $n\text{-C}_{18}\text{H}_{38}$  experiment as Table 1 indicates.

Table 1: Results of Void Fraction Experiments

Run #	Liquid	$\epsilon$
1	$\text{C}_6\text{H}_{12}$	.492
2	$\text{C}_6\text{H}_{12}$	.477
3	$\text{C}_6\text{H}_{12}$	.463
4	$\text{C}_6\text{H}_{12}$	.476
Cyclohexane $\bar{\epsilon}$ - .477 $\pm$		.012
5	$n\text{-C}_{18}\text{H}_{38}$	.481
$\text{C}_6\text{H}_{12} + n\text{-C}_{18}\text{H}_{38}$		$\bar{\epsilon} = .478 \pm .010$
		$\bar{P}_s = .810 \pm .002$
		$\bar{P}_p = 1.552 \pm .03$

#### B. Equilibrium Isotherm Measurement

Nitrogen and oxygen isotherms were measured at  $30^\circ\text{C}$ ,  $45^\circ\text{C}$ , and  $60^\circ\text{C}$ . The apparatus constructed to perform the measurements is shown in Figure 3. The isotherms are presented in Figures 4 and 5. The measurement procedure involves the addition of a known amount of gas to bomb A followed by the distribution of the gas in bombs A and B where bomb B contains a known weight of zeolite. Given the particle density, volumes of the apparatus, and the equilibrium pressure and temperature the isotherms can be determined.

As noted earlier, the applicability of the theory is limited to linear isotherms. The nitrogen isotherms are approximately linear at  $45^\circ\text{C}$  and  $60^\circ\text{C}$  in the pressure domain studied. Oxygen is linear for each isotherm in the pressure

domain studied. The isotherms indicate that PSA operation to separate air at 45°C up to pressures of 2500 mm Hg would adequately support the requirement of linear isotherms.

### C. Breakthrough Experiments

A breakthrough experiment consists of imposing a square wave change in feed gas composition and studying the composition versus time profile of the effluent gas. If the feed gas is enriched in species A and enters a bed dilute in A, then the square wave in composition is maintained along the bed and the effluent gas composition undergoes a square wave or shock change. The theory predicts the composition shock phenomenon and it is approximated in the laboratory. The time that it takes the shock to travel the length of the bed enables calculation of the slope of the equilibrium isotherm. The theory predicts the following relation if the bed is saturated in pure B prior to the square wave change to component A:

$$K_A = \left( \frac{U_{IN} t_{SH}}{L} - 1 \right) \left( \frac{\epsilon}{1-\epsilon} \right) \quad [2]$$

By measuring the parameters on the right hand side of equation [2] the slope of the isotherm can be determined. The apparatus shown in Figure 6 was built to perform breakthrough experiments. Additionally, the two-bed PSA system discussed in the next section can be used to determine equilibrium isotherms. The feed step in PSA cycle using pressurization with pure product is identical to the breakthrough experiment described above. Table 2 compares the results of six breakthrough measurements of K to actual equilibrium isotherm slopes. The results support the validity of the theory for the conditions of the experiments.

Table 2: Equilibrium Isotherms From Breakthrough

System	Method*	P(psia)	T°C	U <sub>in</sub> <sup>cm/s</sup>	K <sub>break</sub>	K <sub>eq</sub>	Δ%rel.to K <sub>eq</sub> **
N <sub>2</sub> (A)-O <sub>2</sub> (B)	1	3.0	24	14.64	24.42	23.62	+3.4
N <sub>2</sub> (A)-O <sub>2</sub> (B)	2	45	45	7.46	8.56	8.24	+3.9
N <sub>2</sub> (A)-O <sub>2</sub> (B)	2	45	60	6.45	7.27	7.55	-3.7
O <sub>2</sub> (A)-Ar(B)	1	14.7	20	3.88	7.22	6.94	+4.0
O <sub>2</sub> (A)-Ar(B)	1	14.7	45	4.24	4.99	4.73	+5.5
O <sub>2</sub> (A)-Ar(B)	1	14.7	60	4.44	4.05	3.71	+9.2

Ave. absolute Δ% = 4.95%

\*1-breakthrough, 2-PSA

$$**\Delta\% = \left( \frac{K_{\text{break}} - K_{\text{eq}}}{K_{\text{eq}}} \right) 100$$

#### D. PSA Studies

A schematic of the process built to produce oxygen from air is given by Figure 7. The process operates on the six-step cycle shown in Figure 1. An important performance characteristic of a PSA unit is the recovery of the product. Recovery is the ratio of the product flow of the light component divided by the feed rate of the light component. The theory predicts a maximum theoretical recovery given by equation [3]:

$$R = (1 - \beta) \left( 1 - \frac{1}{\rho(1 - Y_F)} \right) \quad [3]$$

where

$$\beta = \frac{1 + \left( \frac{1 - \epsilon}{\epsilon} \right) K_B}{1 + \left( \frac{1 - \epsilon}{\epsilon} \right) K_A} \quad [4]$$

and

$$\rho = \frac{P_H}{P_L} \quad [5]$$

Figure 8 compares equation [3] with experimentally determined values of the recovery. The theory closely approximates the experiments. The average absolute % error of the theory relative to the experimental is 7.8%. The equilibrium properties appear in the term  $\beta$ . Small values of  $\beta$  and large values of  $\rho$  are desired for large recoveries of product. Since  $\beta$  is fixed at a given temperature,  $\rho$  is the important design variable.

Typical times for each step in the PSA cycle (refer to Fig. 1) are given in Table 3. The slow cycling assures that the local equilibrium assumption is approximated.

Table 3: Typical Cycle Times  
 $P_H = 45$  psia,  $T = 45^\circ\text{C}$ ,  $L = 30$  in,  $D = .900$  in

Step	Time (sec)	
1	35	} feed time to a single bed
2	65	
3	5	
4	35	
5	65	
6	5	
210 sec		

#### V. RECOMMENDATIONS

The experimental data presented indicate that the PSA model of Knaebel and Hill [1] is quite accurate for the experimental conditions tested. The theory identifies the important parameters which influence the performance of a PSA process. The pressure ratio ( $\rho$ ) and a separation factor ( $\beta$ ) were discussed here. More generally, the theory may be used to determine all of the operating parameters of a PSA process (including cycle times) given a desired product rate or a fixed feed rate.

The constraints and assumptions of the model are an excellent framework for further study. The effect of nonlinear

isotherms and faster cycling are good places to start. Even if the constraints and assumptions are violated the parameters of the model (perhaps in a modified form) will still be important.

#### NOMENCLATURE

$\beta$	a separation factor
D	inside diameter of bed
$\epsilon$	void fraction
$K_i$	slope of equilibrium isotherm
L	length of bed
$P_H$	pressure of the feed step
$P_L$	pressure during purge step
$\rho$	pressure ratio
$\rho_B$	bulk density
$\rho_P$	particle density
$t_{SH}$	time for concentration shock to traverse bed
$U_{IN}$	interstitial gas velocity at inlet to bed
$Y_F$	mole fraction of heavy component in feed

#### REFERENCES

1. Knaebel, K.S., and F.B. Hill, Chem. Eng. Sci., (Submitted 1983).
2. Miller, G.W., Master's Thesis, The Ohio State University, 1984.

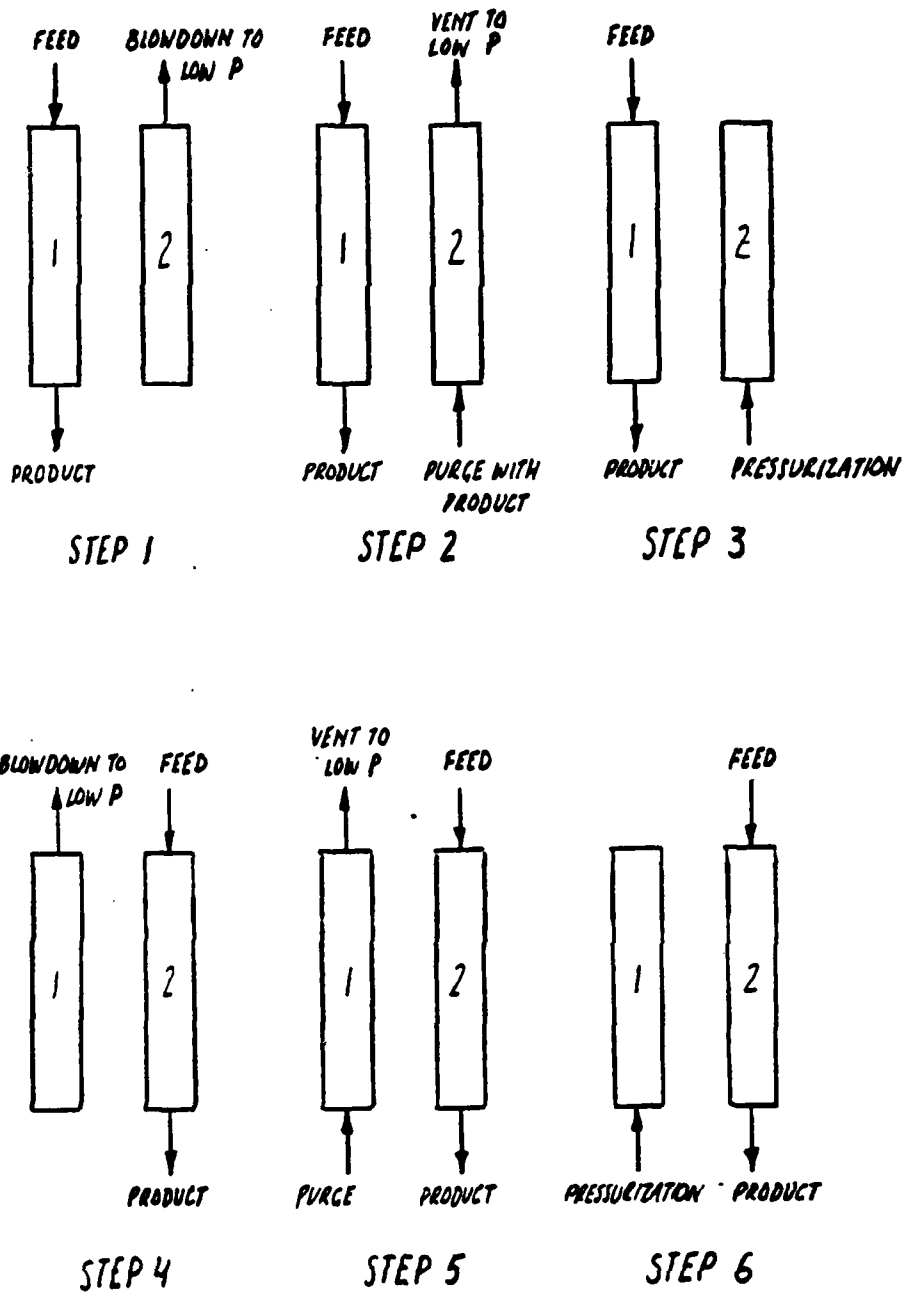


FIGURE 1: SIX-STEP, TWO-BED PSA CYCLE

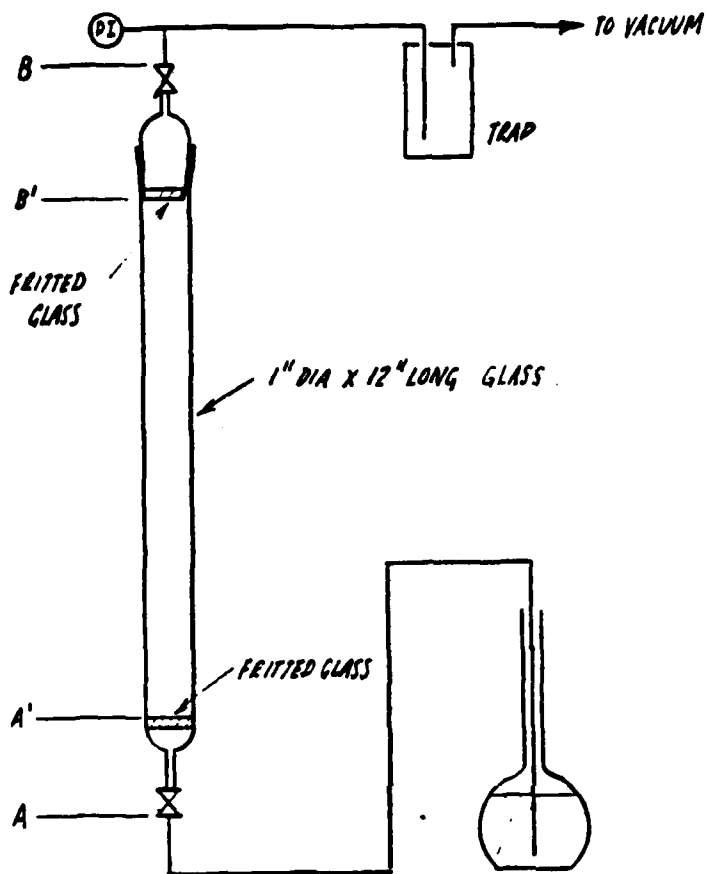
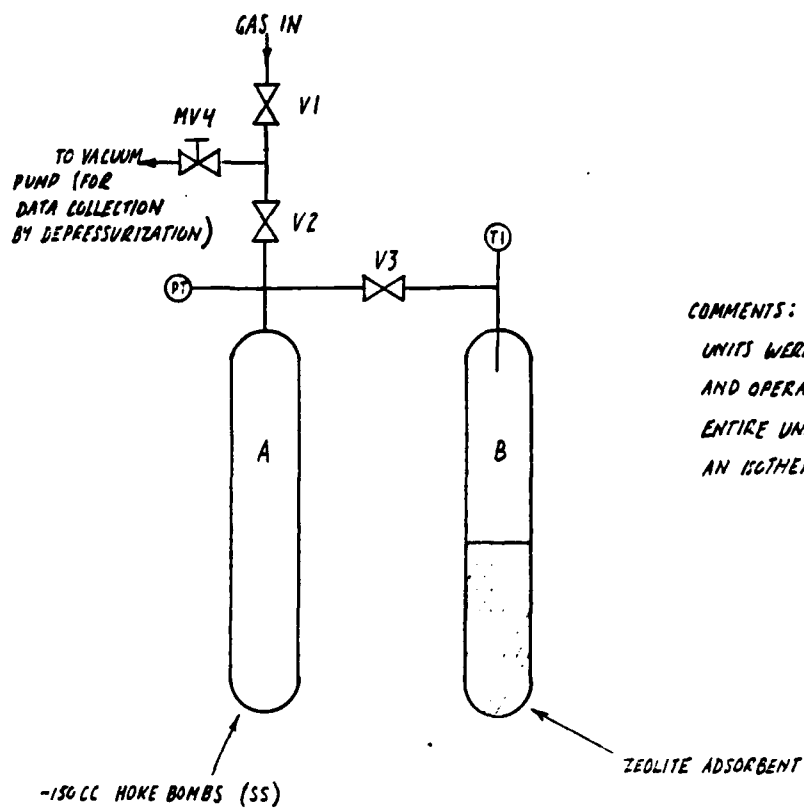


FIG. 2: APPARATUS USED TO DETERMINE VOID FRACTION



COMMENTS: TWO EQUILIBRIUM  
UNITS WERE CONSTRUCTED  
AND OPERATED SIMULTANEOUSLY.  
ENTIRE UNIT SUBMERGED IN  
AN ISOTHERMAL BATH.

FIG. 3: APPARATUS USED TO MEASURE EQUILIBRIUM ISOTHERMS

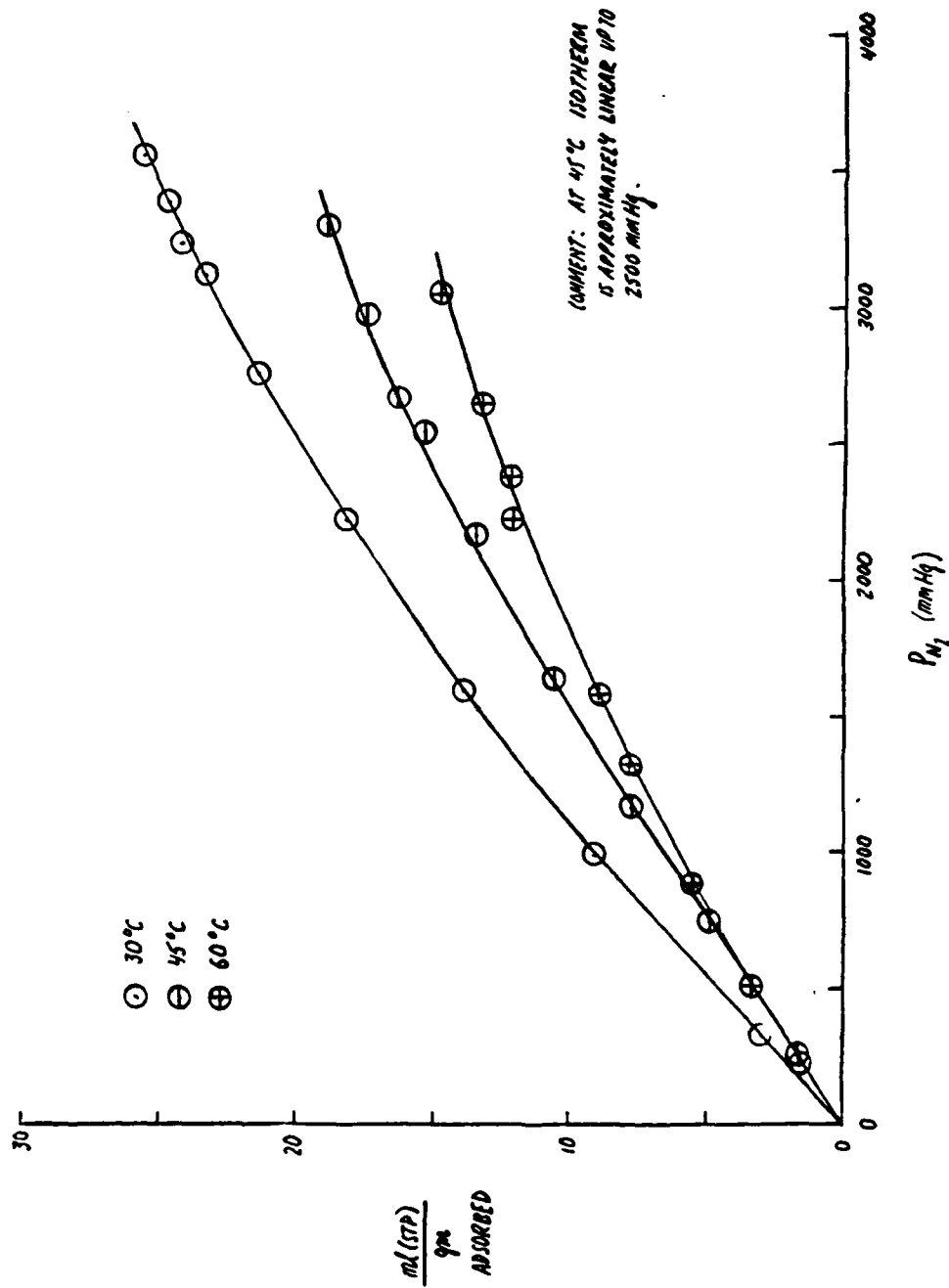


FIG. 4: EQUILIBRIUM ISOTHERMS FOR NITROGEN ON ZEOLITE 5A

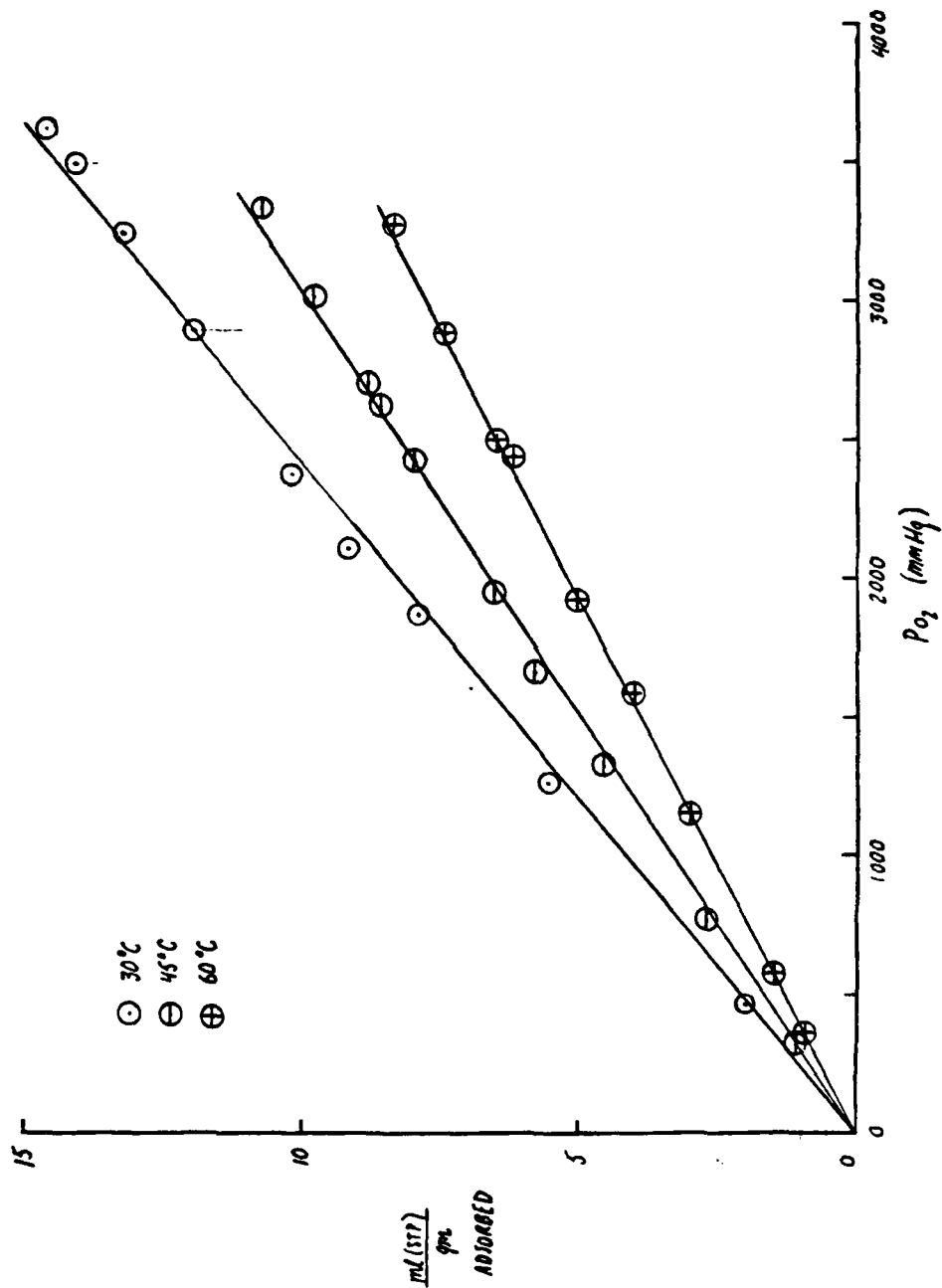
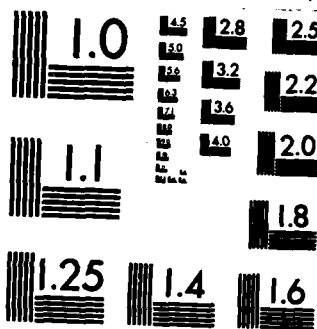


FIG. 5 : EQUILIBRIUM ISOTHERMS FOR OXYGEN ON ZEOLITE 5A





MICROCOPY RESOLUTION TEST CHART  
 NATIONAL BUREAU OF STANDARDS-1963-A

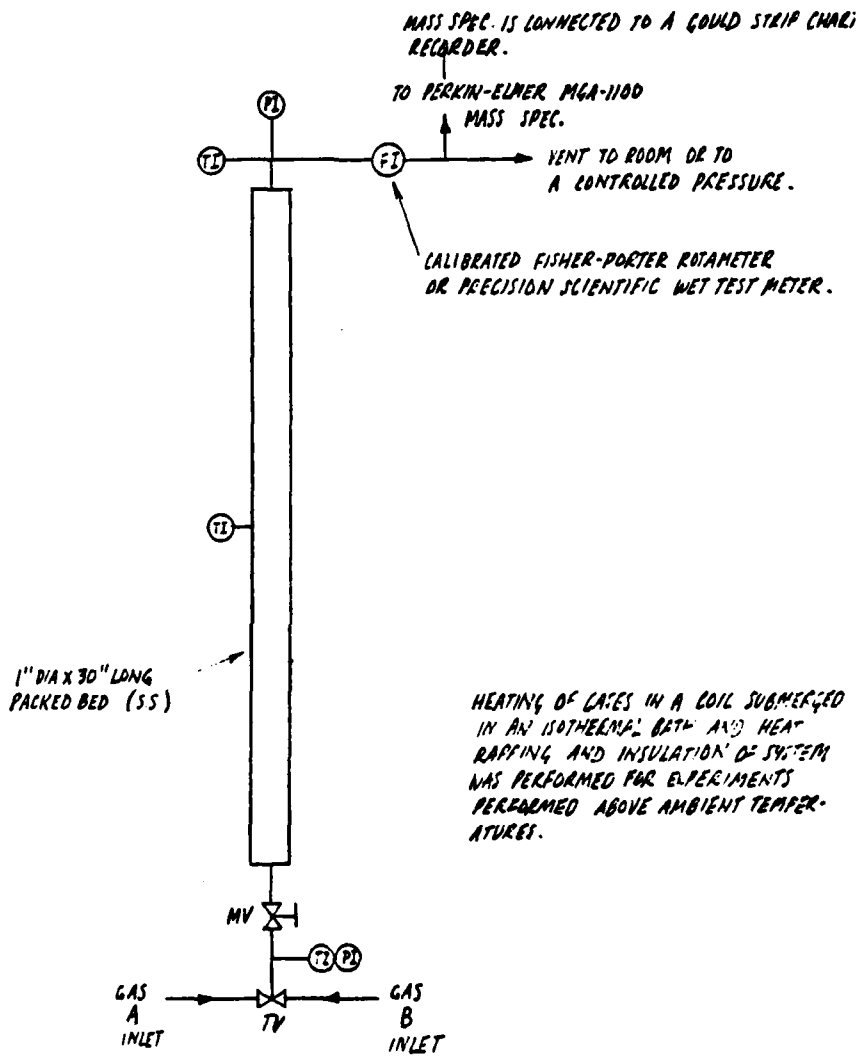


FIG. 6: SCHEMATIC OF SYSTEM USED TO STUDY BREAKTHROUGH PHENOMENA



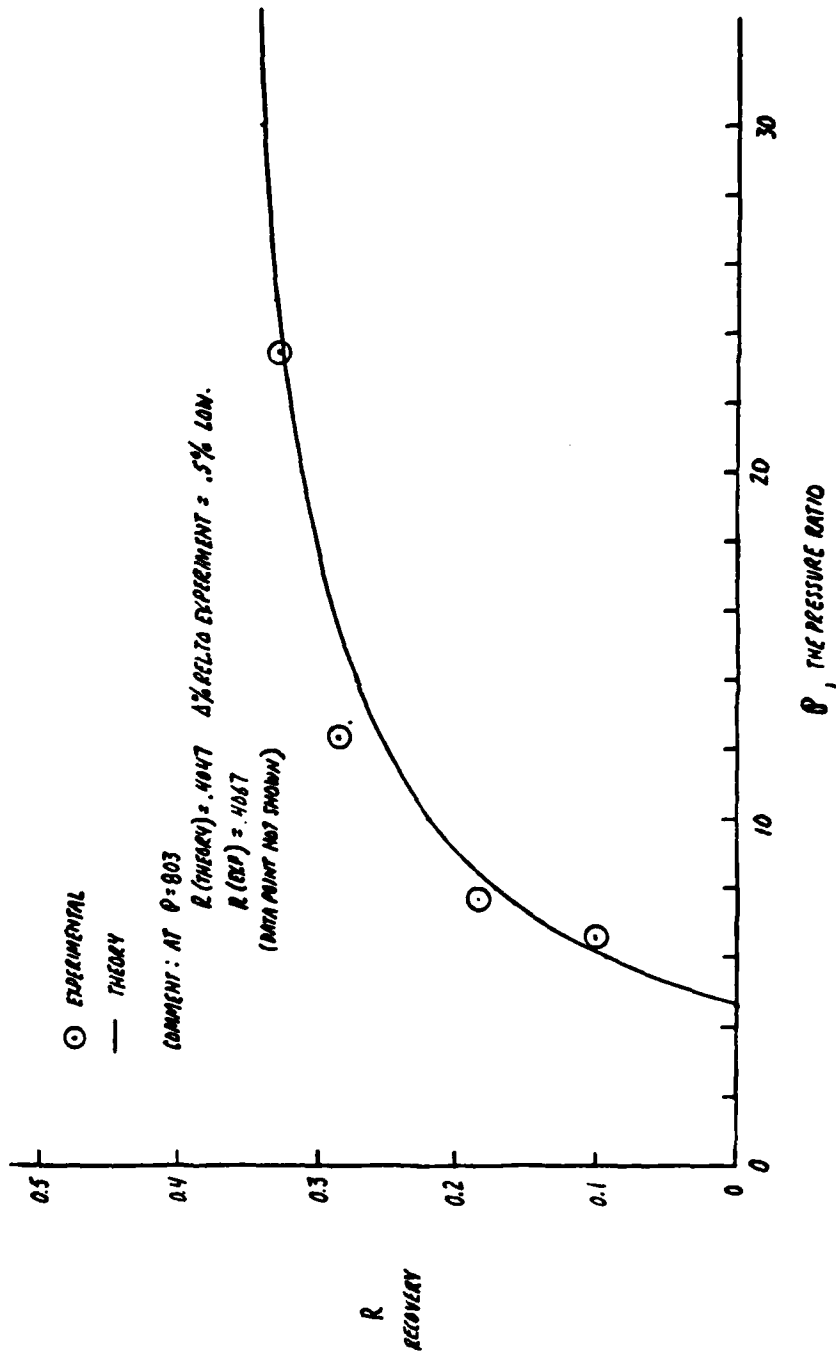
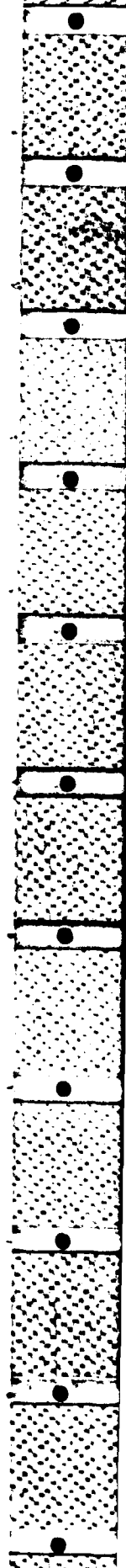


FIG. 8: OXYGEN RECOVERY AT 45°C,  $P_M = 45$  PSIA - THEORY-VS-EXPERIMENT



1984 USAF-SCEEE GRADUATE STUDENT SUMMER SUPPORT PROGRAM

Sponsored by the

AIR FORCE OFFICE OF SCIENTIFIC RESEARCH

Conducted by

SOUTHEASTERN CENTER FOR ELECTRICAL ENGINEERING EDUCATION

FINAL REPORT

TACKLING THE I/O BOTTLENECK

Prepared by: Nancy K. Kirkwood

Academic Department: Mathematics

University: Colorado State University

Research Location: Distributed Systems Section,  
Command and Control Division,  
Rome Air Development Center,  
Griffiss AFB, New York.

SFRP Supervising  
Faculty Member: Dr. Raymond A. Liuzzi

Date: August 14, 1984

Contract No.: F49620-82-C-0035

## TACKLING THE I/O BOTTLENECK

by

Nancy K. Kirkwood

### ABSTRACT

Knowledge-based expert systems make heavy demands on the machines supporting them. In particular, when a large body of knowledge is paged into secondary storage, the critical problem is the "I/O bottleneck" as the pages of data are brought in for processing. In the following, I review research into handling this problem, covering the range from hardware to software, and including new decentralized machines, VLSI memories, database machines and other special purpose architectures, pipelining and parallelisms, locality of reference, and cognitive economy. Proposals are made for increased knowledge about patterns of reference, a survey of current symbolic languages, implementation of promising "paper" machines, and generally a closer harmony between the architecture of the machine and the architecture of the algorithms for its use.

ACKNOWLEDGEMENTS

I wish to thank the Air Force Systems Command, the Air Force Office of Scientific Research, the Southeast Center for Electrical Engineering Education, and Rome Air Development Center for the opportunity to do this research. In particular, I want to express my appreciation to Dr. Ray Liuzzi of RADC for his help and support in this endeavor. I also want to thank the other members of the Knowledge Base Engineering Group: Dr. Gerard Capraro, Dr. Northrup Fowler, and Robert Schrag of RADC, Dr. John Minor of the University of Oklahoma, and Dr. Bruce Berra of Syracuse University for many helpful comments and valuable information.

## I. INTRODUCTION

In recent years it has finally become possible to realize a dream of scientists in many fields--an expert assistant program to aid in fact retrieval and problem-solving. Such artificial intelligence systems were envisioned in the 1960's, but neither the machines nor the conceptual tools were ready. We are now gaining the capability to realize them with tremendously larger and faster machines, the experience of the database community in the organization and access to large bodies of knowledge, and new conceptual models and heuristics for dealing with complex problems.

An expert system consists firstly of a body of facts from the specific domain and relations between the facts, and generally is so large in size that it cannot be contained in memory but must be paged into secondary storage. This is termed the extensional database (edb), and may resemble a standard relational database. The second part of an expert system is a body of rules of inference, which may include problem-solving heuristics and "beliefs" of the system. This is termed the intensional database (idb), and is generally much smaller in size than the edb.

There are a number of well-accepted expert systems, among them those in the fields of medical diagnosing (MYCIN), VLSI design, electronic fault diagnosis, molecular analysis (DENDRAL), and natural language understanding (HEARSAY II). For an excellent tutorial on expert systems, see Stefik et al, 1982 [A12].

Future and currently developing systems include robot planning, expert assistants for Air Force pilots, automatic programming and program verification, image processing systems, and machine translation from one natural language to another. The widely-known Japanese "Fifth Generation" research effort is a serious and well financed project to implement, among other things, very large scale expert systems and machines capable of running them [see H13].

Many expert systems are implemented in the framework of symbolic logic programming, rather than the better-known procedural programming used in "number-crunching" applications. Non-procedural languages such as Lisp and Prolog are often used. (Prolog and its

variants were chosen by the Japanese Fifth Generation researchers.)

The basic unit in logic programming is the Horn clause, of the general form

```
P <-- Q1,Q2,Q3,...,Qn
<Head>    <Body>
```

signifying that P is true if Q1 up to Qn are true. The Qi's may be facts or other Horn clauses, requiring proofs of their own. A fact is represented by a clause with no body but a head containing only constants. A rule is a clause with a head and a body which contains variables. A clause with a body only, containing constants, is called a ground goal and may be submitted to the edb for verification of its constituents. A clause with a body only, containing variables, is called a goal or query.

The process of satisfying a query is called resolution, and proceeds by the rules of first-order logic, gradually reducing the query to a list of unit ground clauses or facts which need to be shown (ground goal), and then accessing the edb for the truth-value of these clauses. Traditionally in logic programming, the set of facts (edb) and rules (idb) with the same header name are stored together in procedures, and the set of these procedures (the program) is small enough to fit in main memory. (For a tutorial on logic programming, see Kowalski [A8].)

A relational database stores information as relations, which are two-dimensional arrays. Columns represent fields or attributes, and rows represent individual records, also called tuples. All data is represented in this fashion, as flat files. The fundamental operations of relational algebra are: select (choose a set of tuples from a relation); project (form a new relation leaving out certain fields, then eliminate duplicate tuples); and join (the set of tuples formed by the cartesian product of two relations).

Relational database has a well-developed theoretical basis, and is the most popular database model today. Other common models are network and hierarchical, and their use seems more natural in some applications.

The database community has long been dealing with the problems of organizing large amounts of data and retrieving them from storage in a fast and efficient manner. As intelligent

systems have moved from hypothesis to reality, it has become clear to some AI workers that they share many of these concerns. Database applications have also been moving toward more complex queries and data models, involving some degree of intelligence on the part of the system, as well as an actively helpful user interface. In fact, logic programming languages have been successfully used as database query languages [L4]. The overlap of database and artificial intelligence activities is known as knowledge base, and is generally conceived to consist of a large body of facts, and their associated rules of inference.

## II. OBJECTIVES

As soon as the knowledge base program gets big enough to overrun memory onto secondary storage, which is the case in most intelligent systems, the problem of speed of access to the facts and rules becomes critical. This is the "I/O bottleneck," and the objective of my summer research was to explore the various techniques, running through the spectrum from hardware to software, being considered to ameliorate this problem.

In Section III, the following hardware design ideas are examined:

- \* memory large enough to hold entire database
- \* content-addressable memories and memory machines
- \* new massively parallel machines
- \* high-speed database machines and accelerators
- \* use of special purpose function architectures (SPFA's)

Section IV concerns logical design and optimizations at the interface between hardware and software:

- \* compiled or proof-plan approach and its variants
- \* partial and multiple key hashing
- \* promises and difficulties of parallelisms
- \* pipelined implementations
- \* query optimization, both semantic and syntactic
- \* comprehensive cached directories

In Section V, I discuss algorithmic issues, including:

- \* locality of reference and continuity of reference
- \* multiple data views, inducing continuity of reference
- \* meta-expert systems to extract and organize information from a human expert
- \* cognitive economy--system self-optimization

Section VI contains recommendations for future research into specific topics chosen from these subjects. The knowledge base applications field is very active now, in a variety of directions, and one of its most pressing needs is a general overview integrating the interests and knowledge of the various groups involved: the hardware and software groups, and the artificial intelligence and database groups. Without coordination, cooperation and mutual understanding between disciplines, we cannot keep the strategic edge in future development. My recommendations include calls for this kind of coordination, as well as specific software and hardware projects.

### III. HARDWARE DESIGN

Much of the thrust in current hardware research is to develop a high degree of parallelism. A large number of new machines have been designed and a few implemented. The usual organization has a large number ( $10^3$  to  $10^6$ ) of processing and/or memory elements, which may or may not be under central control. A sequential machine is limited to one focus of attention and operates SISD (single instruction, single data stream). Opposed to this is MIMD (multiple instruction, multiple data streams), which can either have a central controller or run by data flow. In data-flow operation, each processing element works on a job when it has all the necessary data, and sends its results on to the next one. (See [H9] for an introduction to data-flow architecture.) As in a human group endeavor, coordination between these processors is a major problem. Following is a brief description of a number of these and other parallel architectures.

As memory becomes cheaper and denser, it becomes practical to look at machines with main memory so large that they do not need secondary storage. The I/O bottleneck is eliminated, to be replaced by at least two other problems: the need for non-volatile storage, and organization of and access to such a large internal store. The latter can be a bottleneck of its own, but orders of magnitude faster.

The ESP MMM (Massive Memory Machine [H7]) is one effort at such a machine. There are up to 100 processors, each with large local memory and caches. It is ordinarily run SISD, with each processor having a copy of the program. The processor which owns the current data has the lead, broadcasting its data to the others. This machine is still theoretical.

The Connection Machine [H8] has a large front-end processor, with the Connection Memory handling references. This is composed up millions of tiny cells, passing messages through their neighbors. Each cell has a few words of memory, a small list of known addresses, a state vector and a rule table telling it how to behave when messages arrive. If a cell knows one of its neighbors is faulty, it will not route messages through it, so other than the loss of local information, the network will survive faults.

Data in the Connection Memory is organized as nodes which are balanced binary trees of cells. The nodes are connected in a semantic network, to enable match, partial match, tree search, and other symbol processing in a natural way. There are plans to build a slice of this memory and it will be interesting to see its operation if it is built.

DIRECT [H5] is another architecture for implementing large relational databases. There are query processors and memory processors, and an interconnection matrix with shared associative memory. Data is in mass storage and brought into the pages with high bandwidth. DIRECT has been built, and exhibited considerable overhead for concurrency control, due to its centralized architecture [H3].

The Delta machine has been built by ICOT. It has a very large cache memory, from 16 to 128 Mbyte, said to be fail-safe. There is an intelligent disk controller, and pipelined data streams. Data is indexed both by address and attribute values. Parallelism is implemented in fetch of pages from secondary memory, and trans-

fer back to the hierarchical cache memory after processing. The designers are considering the use of redundancy in data storage, rather than just multiple indexing, to speed up access [H12].

The MPP is being built by Goodyear for image processing [H4]. It contains  $2^{14}$  processing elements (PEs) with their own memories and a central program and data management unit, and has SIMD operation. Tuples in the relations are stored one to a PE, so selections, projections and joins can be highly parallel.

The Boltzmann machine has large numbers of value-passing processors [H6]. This highly innovative theoretical architecture is patterned largely on what is known of the activities of the brain. Information is stored as patterns of weighted links between nodes. This machine has the potential for handling set operations, best match, and other AI/knowledge base activities in a unique fashion, and it will be interesting to see an implementation of it.

ZMOB has a ring architecture with up to 256 Z-80 microprocessors, a host VAX and a conveyor-belt type message-passing communication system. Data may be accessed by address or by content. This has been partly implemented at the University of Maryland [H11].

There are a number of database machines and parallel accelerators about, some available in the marketplace. Sequential machines such as the Britton-Lee IDM 500 are designed especially for fast and efficient database operations, and sometimes include pipelining for greater speed. The STARAN and ASPRO projects use content-addressable internal store for parallel processing, but data must still be loaded from disks. Database machines give fast handling of sorts and joins and other data manipulations. However, unless a much higher bandwidth can be attained in the transfer of data from secondary storage, we still have the I/O bottleneck problem ([H1]). There are physical considerations preventing much more speed gain in disk access, and implementation of parallelism involves a lot of concurrency control.

Generally, it may be noted that some tasks are inherently sequential, regardless of the researcher's desire to introduce parallelism. It is thus pointless to impose the considerable overhead in control needed to implement parallelisms unless the task at hand requires it. Even in a parallel machine, facility

must be maintained for efficient sequential processing as well.

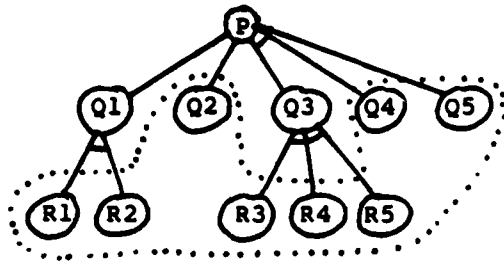
An evolutionary way to improve architectures for knowledge base is by means of special purpose function architectures (SPFA's, see [H2]). Starting with a computer which has a number of high-level knowledge-base functions implemented in software, the specific functions causing bottlenecks can be implemented in hardware using appropriate parallelism (for instance merge sorting, text search or data directories). Eventually a series of plug-in modules is envisioned to tailor a computer to the execution of its tasks. An SPFA development facility has been proposed in [H10], where candidate SPFA's can be designed, emulated, built and moved into the working environment.

Inherent in a lot of these new machines and architectures are VLSI chip designs, and certainly as such chips get denser and cheaper, and improved design methods are developed, architectures will benefit. Another common theme is content-addressable or associative memories. These are currently very expensive, and are usually put to use in a cache in central memory to which data is paged. However, in this arrangement, the time-cost of moving pages in far overshadows the benefits of associative search. There is still a promising future for these devices if costs are brought down so that it is practical to have much, or all, of memory associative.

#### IV. LOGICAL DESIGN AND HARDWARE/SOFTWARE INTERFACE

Many of the present and proposed future knowledge base and expert systems are based in logic programming, and there are a number of ways to optimize their use of the machine. I will discuss these first, and then other subjects in this area.

As stated in the introduction, satisfying a user's query proceeds by first-order logic until ground goals are reached, at which point the edb is queried as to the truth (or existence) of facts satisfying these goals. There are several ways to organize this process. The figure below shows a logical proof-tree.



P is true if Q1 OR Q2 OR  
 (Q3 + Q4 + Q5) are true  
 Q1 is true if R1 + R2 are  
 true  
 Q3 is true if (R3 + R4 + R5)  
 are true

Figure 1. AND-OR logical tree. AND branches are connected by an extra line. The leaves of the tree (inside the dotted line) are ground goals, and will be checked against the facts in the edb.

The interpreted method proceeds depth-first, following the logical AND-OR tree out to a leaf, checking that fact, and proceeding left-to-right. Failure of a fact to be true causes backtracking to the last choice point, and examination of another branch. This is the original implementation of Prolog [L14]. It is exhaustive, but can end up in a loop due to recursion, or spend a lot of time in unfruitful parts of the tree, and often runs very slowly.

The compiled or proof-plan approach [L4] does all the logical deduction at one time, following every possible path out to the sets of facts that have to be true to satisfy the query. Then when a user query comes in, the appropriate plan and set of facts is pulled out, and all the edb accesses are made at one time. These can be optimized, and a look-ahead done to bring in pages anticipating their use. However, any change to the idb will require recompiling the proof-plans, so this method is impractical for a volatile idb.

These two methods do not exhaust the possibilities. Plans may be generated to order upon user query, and the edb accesses grouped and optimized. These plans may be saved for future reference, though in an evolving knowledge base, some means must be used to keep track of the truth or relevance of the plans over time. Partial proof-trees may be indexed and stored, and patched together quickly upon user queries [L7].

Proof-plan generation could also take place to a certain point (depending on the application), generating a group of edb

accesses which could be optimized together. Upon the success or failure of this portion, further deduction in one direction or another would then take place. This method has the advantage of pruning a large search-tree, and would spend little time in an unfruitful area. It has been little-explored by researchers, although it seems to be much like human problem-solving, and I believe it merits further consideration.

Other approaches to hardware/software optimization include parallelisms and pipelining, and various means of indexing and accessing data. There is considerable present research into parallelisms of logic programming, especially by the Fifth Generation group. On paper, AND and OR parallelisms in logical trees are easy to implement. But once these are implemented on actual machines, the control overhead between the processes competing for data and resources often overwhelms the advantages gained [L11].

Lower-level pipelining seems a much more promising direction. Tick and Warren's design [L12] utilizes pipelined micro-instructions, an interleaved memory access, and copying of execution structures rather than structure-sharing. Optimizations of this type well below the user level require little concurrency control and give significantly faster operation.

Proof-trees are often short and bushy, and in this case parallel edb access (which is currently being done by advanced database techniques and machines) can mean a big improvement. For this reason, the compiled proof-plan technique and its variants are a promising direction for research. Since the idb is conceived to be much smaller than the edb, storage of proof-plans is a small price to pay for the gain in speed.

Optimization of sets of queries of relational database and knowledge base can be done by the careful combination of operations and correct choice of their precedence (see [L1], [L5], [L10], [L13]). A lot of work is being done in this area. Additionally, look-ahead can be done to bring in pages prior to their use and save on page faults.

At a lower level, and independently of whether parallelism is used, several kinds of indexing and hashing can improve search performance. Superimposed codewords [L15] may be generated for each item in the database, and a directory kept of these words

with pointers to the item. A query (which often involves a partial match) will also generate a codeword, and matching of codewords quickly produces a list of relevant records (and possibly some others, called "false drops"). A hashing function may be keyed on several fields in the record, rather than just the primary key, aiding retrieval of information without costly inverted indices. A descriptor file may be kept for each page of memory, which determines what records are present (by the logical OR-ing of descriptors of all the records on that page). See [L8] and [L9] for implementation of these methods to simulate content-addressability without paying the hardware price.

Another means to gain speed in knowledge-base access is a comprehensive directory kept in cache memory. Humans know instantly when they do not know something [S1] and do not waste time searching in memory for it. For example, I know my grandmother's first name, and I know I do not know her middle name, and although I don't recall her maiden name, I could find it in memory with a search. If a system kept a directory of facts, listed by various indices, it would save time spent searching in slow secondary storage for facts that were not in the database. In addition, storage of semantic relations (rules), with information as to number and type of arguments, would immediately eliminate a number of ill-formed queries (Stanley Su, personal communication, and [L5]). For instance, mother-of(chair) would be invalid since chairs are not living, and mother-of(george) would return only one answer and not continue to search the knowledge base for others. A disadvantage of directories is the update problem in an evolving or changing database, which could be quite costly in time and effort. Usefulness of this method would depend heavily on the characteristics of the application. For an architecture designed to keep these directories, see [L3].

## V. ALGORITHMIC ISSUES

The theme of the algorithmic issues is the optimally efficient representation of knowledge. Tackling the I/O bottleneck here means minimizing the difficulties of search. There are two

kinds of search in knowledge-base programming--fact retrieval, and heuristic search or search for a proof-plan or an answer using the rules of inference. See Eastman's paper [A6] for a comprehensive review of searching.

Fact retrieval benefits from specialized data structures which represent the "world" in a way that promotes locality of reference. A complex expert system may involve several representations or views of its world. (See [A10] for an implementation of views in Prolog.) The views should be designed so that a small change of input data or query remains local (causes only small changes) to at least one view. For instance, Randall Davis [A3] describes an electronic trouble-shooter that considers physical adjacency, thermal adjacency, and functional organization. These views are layered, with paths of causality between them, and the expert system considers the most restrictive view first. Data structures which store information on complex systems by a well-designed hierarchy of views can optimize the program's use of memory. Redundancy may be used to advantage, saving time at the expense of space (storage space is comparatively cheap).

Heuristic search can benefit enormously from the pruning of search trees by meta-knowledge, i.e., knowledge about problem-solving techniques, suggestions about profitable and unprofitable branches, past experience, decomposition of tasks into subtasks, and generalization and analogy. A program that uses higher-level problem-solving techniques can avoid the combinatorial explosion of search trees that will occur with the brute-force techniques. An expert system should also be able to communicate its meta-knowledge to the user [S1].

Knowledge-compilers can also be used to translate one representation into another that can be used more efficiently [A11]. Another form of knowledge compiling is an evolutionary knowledge base, where the results of queries are added to the knowledge of the program. In many expert systems, conclusions must be based upon incomplete information, and subsequently revised as new information comes in. Classic monotonic logic, in which beliefs are based on axioms and previously proved beliefs and always remain true, lacks the tools to deal with this situation. Some system for routine revision of beliefs, such as Doyle's

Truth Maintenance [A4], is needed for knowledge base programs that deal with incomplete worlds. Current research is touching on systems that revise their opinions and learn from their mistakes.

The use of very high level non-monotonic rules (hints), from user or programmer, can be a valuable heuristic for certain types of problems [A7].

The question of physical locality of reference is a serious one in large applications. Physical locality implies that as a program executes over time, it stays generally within a small subset of pages in virtual memory, only gradually moving its center of interest. Clearly a program whose memory references are nearly at random over a large database, causing constant page faults, will be ineffective and perhaps so slow as to be useless.

It is presently unknown to what extent large knowledge-base systems exhibit physical locality of reference. An important and little-studied subject is that of methods of knowledge engineering that maximize such locality, and thus promote operating efficiency.

In general, we cannot hope to gain the kind of performance we need from knowledge-based programming unless there is a natural and simple mapping from high-level knowledge representations in software to the hardware architecture supporting it. Buchanan [A2], in an excellent paper on knowledge engineering, states, "The choice of representation for the expert's knowledge must be a compromise between what is natural and easy for the expert and what is natural and easy for the programmer." This is true, but we must go further than that and write a program whose abstractions convert to a fast-running and efficient utilization of the machine.

The presently used methods to transfer human expert knowledge to the expert system are 1) handcrafting--the programmer either becomes an expert or confers with one; 2) interactive dialog--for an instructive example see [A5]; 3) automatic rule formation--the empirical generation of rules from examination of a large number of facts [A2].

The principle of cognitive economy (Lenat et al., [A9]) may be used with any of the above methods to optimize the data representation. The classic goal in data representation is expres-

sability, typified by very high level language, multiple levels of abstraction, minimal non-redundant representations, and inference by pattern-directed knowledge sources. For cognitive economy, the second goal of efficiency is added. Lenat suggests relaxing the tighter constraints of expressability, and gaining efficiency by three methods:

1) dynamic self-monitoring and self-modification, including program constructs, data representation and physical data storage (a very difficult subject and not one from which we can expect quick results);

2) the caching of computed results, i.e., frequently computed values (easily done), successful search paths and algorithms for later use, and preliminary or partial results which are needed often (here a belief revision system might be necessary).

3) expectation-filtering, valuable in diagnosis or exploratory systems, in which unexpected results should cause belief revision.

Cognitive economy is a difficult but potentially rewarding subject. The methodology of building expert systems, and meta-knowledge for the user, are receiving a good deal of attention at present. I believe research into locality of reference is the most pressing need in the software area, both as to the locality evidenced by running systems, and methods of increasing this locality.

## VI. RECOMMENDATIONS

+ A study into physical locality of reference is my strongest recommendation. It is not presently known to what extent working systems exhibit physical locality of reference, and what can be done to increase this. I suggest the examination of a number of knowledge-base programs running on their host machines, counts of page faults, and analysis of which program operations cause them. Research into optimal page sizes and paging strategies should also be done specific to knowledge-base-type systems.

The types of knowledge representation that lead to easy implementation of locality of reference should also be examined.

We cannot afford the luxury of awkward and time-consuming mappings from higher-level data structures to lower-level models of computation. Browne, in an excellent article [L2], states: "The cost-effectiveness of an architecture for execution of an algorithm is heavily influenced by the mapping between the models of computation of the algorithm and the architecture."

+ A parallel recommendation from the hardware side is to examine and promote architectures that lead to locality of reference. New architectures should be based on knowledge of execution patterns of living programs. When more is known about these execution patterns, machines can be designed that better avoid bottlenecks and clumsy execution.

+ A test set of medium to large-scale knowledge-base-type programs is needed in order to evaluate existing and simulated machines, as well as enhancements and improvements to existing machines. These should be large enough to adequately exercise the secondary storage and paging facilities. A standard representative set will allow realistic comparisons of machines to be made, which are presently difficult or impossible. They should be coded in several languages (not a trivial task) and be fairly straightforward to adapt to specific hardware situations.

+ An investigation of the use of cached directories which include semantic knowledge in order to eliminate paging-in of useless data. In a relatively non-volatile knowledge-base, these directories should be worth their cost.

+ An investigation into the selective use of redundancy in data representations. In order to index items by several attributes, multi-key hashing and descriptors can be used, or inverted indices may be kept. Access by means other than primary keys is improved, but still may generate an unacceptable level of page faults. In a relatively stable knowledge base, storing duplicate copies of some or all data, by secondary keys or content, may make sense. These should be stored so that physical locality of reference from at least one viewpoint is maintained. It seems likely,

however, that in a volatile or highly-connected knowledge base, the price of consistency between these copies will outweigh their advantages.

+ Encouragement for the building of promising paper machines into silicon. Emulation of these machines can be helpful, but still a number of practical considerations cause problems (sometimes fatal) when the machines are actually built.

+ An examination of the feasibility of VLSI main-frame memory to eliminate the use of secondary storage. It seems quite probable that this hardware will arrive in due course of time. There are a number of concerns associated with this type of architecture, including:

Protocols for use of non-volatile memory for storage and error recovery;

Bus architecture for fast access to the very large memory;

Problems of reliability in data storage, necessitating error-control coding.

+ An unbiased examination should be made of the benefits of Prolog vs. Lisp for knowledge-base programming. Lisp has a strong programmer support facility. If Prolog is to gain more popularity, especially in the U.S., it will have to develop the same. There are also a number of variants and hybrids of both Lisp and Prolog, including Loglisp (Syracuse University), IC-Prolog [P2], Epilog [P3], and meta-Prolog [P1], intended to handle artificial intelligence and/or parallelism. A survey of the uses, advantages and disadvantages of these would be helpful. Since Lisp and Prolog are both inherently sequential, and parallelisms are added on artificially, new truly parallel languages may be needed eventually to program truly parallel machines.

+ Further communication between database researchers and artificial intelligence researchers should be encouraged. The questions of knowledge representation (data models), consistency (integrity), temporal factors, as well as machines capable of handling very large bodies of knowledge, are of vital concern

to researchers from both disciplines.

+ Further communication between hardware designers and software designers is necessary if we are ever to achieve the levels of performance necessary to handle artificial intelligence applications. The implementation of machine intelligence requires far more hardware support than was originally believed. This support cannot be forthcoming unless there is an easy logical mapping between the machine and its applications.

Glushkov wrote (quoted in [P3]):

The long life of Princeton type computers is attributed to a profound matching of their structural and program organization and to the mutual harmony of the von Neumann principles. Any partial revision of these principles inevitably involves contradictions between machine architecture and computational process organization.

If we are to achieve success in knowledge-based, nonprocedural applications, we must also achieve that kind of harmony between the architecture and its use.

## REFERENCES

### HARDWARE DESIGN

- H1. Agrawal, R., and D.J. DeWitt, "Whither Hundreds of Processors in Database Machine?" Proceedings of the Workshop on High-Level Computer Architecture, Los Angeles, 1984, pp. 6.21-6.32.
- H2. Berra, P.B., "On Computer Architectures For Knowledge Based Expert Systems," Unpublished report, RADC Post-doctoral Program/AFOSR/Syracuse University, 1983.
- H3. Boral, H., and D.J. DeWitt, "Applying Data Flow Techniques to Data Base Machines," Computer, Vol. 3, No. 6, August 1982, pp. 57-63.
- H4. Davis, E., "Application of the Massively Parallel Processor to Database Management Systems," AFIPS Conference Proceedings, Anaheim, California, 1983, pp. 299-307.
- H5. DeWitt, D.J., "DIRECT--A Multiprocessor Organization for Supporting Relational Database Management Systems," IEEE Transactions on Computers, Vol. C-28, No. 6, June 1979, pp. 395-405.
- H6. Fahlman, S.E., G.E. Hinton and T.J. Sejnowski, "Massively Parallel Architectures for AI: NETL, Thistle and Boltzmann Machines," Proceedings of the AAAI National Conference on Artificial Intelligence, Washington, D.C., 1983, pp. 109-113.
- H7. Garcia-Molina, H., R.J. Lipton, and J. Valdes, "A Massive Memory Machine," IEEE Transactions on Computers, Vol. C-33, No. 5, May 1984, pp. 391-399.
- H8. Hillis, W.D., "The Connection Machine," A.I. Memo No. 646, Artificial Intelligence Laboratory, MIT, 1981.

- H9. Lerner, E., "Data-flow Architecture," IEEE Spectrum, April 1984, pp. 57-62.
- H10. Liuzzi, R.A., "The Specification of a Data Base Machine Architecture Development Facility and a Methodology for Developing Special Purpose Function Architectures," Report No. RADC-TR-80-256, Rome Air Development Center, Griffiss AFB.
- H11. Rieger, G., R. Trigg, B. Bane, "ZMOB: A New Computing Engine for AI," Memo TR-1028, Maryland Artificial Intelligence Group, Dept. of Computer Science, University of Maryland, 1981.
- H12. Scheppe, H., from Institut fur Theoretische und Praktische Informatik, West Germany, in presentation given at 1984 Syracuse University Minnowbrook Workshop on Database Machines.
- H13. Treleaven, P.C., and I.G. Lima, "Japan's Fifth-Generation Computer Systems," Computer, August 1982, pp. 79-88.

#### LOGICAL DESIGN AND HARDWARE/SOFTWARE INTERFACE

- L1. Bitton, D., H. Boral, D.J. DeWitt and W.K. Wilkinson, "Parallel Algorithms for the Execution of Relational Database Operations," ACM Transactions on Database Systems, Vol. 8, No. 3, pp. 324-353.
- L2. Browne, J.C., "Understanding Execution Behavior of Software Systems," Computer, Vol. 17, No. 7, July 1984, pp. 83-87.
- L3. Capraro, G.T., "A Database Management Modelling Technique and Special Function Hardware Architecture," Ph.D.

dissertation, Syracuse University, March 1978.

- L4. Chakravarthy, U.S., J. Minker, and D. Tran, "Interfacing Predicate Logic Languages and Relational Databases," Proceedings of First International Logic Programming Conference, Marseille, 1982, pp. 91-98.
- L5. Grant, J., and J. Minker, "Optimization in Deductive and Conventional Relational Database Systems," in Advances in Data Base Theory-Volume 1, H. Gallaire et al., eds., Plenum Press, New York, 1981, pp. 195-234.
- L6. King, J.J., "Modelling Concepts for Reasoning about Access to Knowledge," Proceedings of Workshop on Data Abstraction, Databases and Conceptual Modeling, Pingree Park, Colorado, 1980, pp. 138-140.
- L7. Klahr, P., "Planning Techniques for Rule Selection in Deductive Question-Answering," in Pattern-directed Inference Systems, D.A. Waterman and F. Hayes-Roth, eds., Academic Press, 1978, pp. 223-239.
- L8. Lloyd, J.W., "Implementing Clause Indexing in Deductive Database Systems," Technical Report 81/4, Dept. of Computer Science, University of Melbourne, 1981.
- L9. Ramamohanarao, K., J.W. Lloyd, and J.A. Thom, "Partial-Match Retrieval Using Hashing and Descriptors," ACM Transactions on Database Systems, Vol. 8, No. 4, Dec. 1983, pp. 552-576.
- L10. Smith, J.M., and P.Y. Chang, "Optimizing the Performance of a Relational Algebra Database Interface," Communications of the ACM, Vol. 18, No. 10, pp. 568-579.
- L11. Tick, E., "Towards A Multiple Pipelined Prolog Processor," Proceedings of the Workshop on High-Level Computer Architecture, Los Angeles, 1984, pp. 4.7-4.17.

- L12. Tick, E., and D.H.D. Warren, "Towards a Pipelined Prolog Processor," IEEE International Symposium on Logic Programming, IEEE Computer Science Press, 1984, pp. 29-40.
- L13. Warren, D.H.D., "Efficient Processing of Interactive Relational Database Queries Expressed in Logic," Proceedings of 7th International Conference on Very Large Data Bases, France, 1981, pp. 272-281.
- L14. Warren, D.H.D., "Implementing Prolog," Research Report 39, Department of Artificial Intelligence, University of Edinburgh, 1977.
- L15. Wise, M.J., and D.M.W. Powers, "Indexing Prolog Clauses via Superimposed Code Words and Field Encoded Words," IEEE International Symposium on Logic Programming, IEEE Computer Science Press, 1984, pp. 203-210.

#### ALGORITHMIC DESIGN

- A1. Barr, A., "Meta-knowledge and Cognition," Proceedings of the 6th International Joint Conference on Artificial Intelligence, Tokyo, 1979, vol. 1, pp. 31-33.
- A2. Buchanan, B.G., "Issues of Representation in Conveying the Scope and Limitations of Intelligent Assistant Programs," in Machine Intelligence 9, J.E. Hayes et al., ed., Ellis Horwood Ltd., Chichester, 1979, pp. 407-425.
- A3. Davis, R., "Diagnosis via Causal Reasoning: Paths of Interaction and the Locality Principle," Proceedings of the AAAI National Conference on Artificial Intelligence, Washington, D.C., 1983, pp. 88-94.
- A4. Doyle, J., "A Truth Maintenance System," Artificial Intelligence, Vol. 12(1979), No. 3, pp. 231-272.

- A5. Eick, C., "From Natural Language Requirements to Good Data Base Definitions--A Data Base Design Methodology," International Conference on Data Engineering, Los Angeles, 1984, pp. 327-331.
- A6. Eastman, C., "Search Problems in Logic Based Systems," Final Report, 1980 USAF-SCEEE Summer Faculty Research Program, Air Force Office of Scientific Research.
- A7. Goguen, J.A., "On Fuzzy Robot Planning," in Fuzzy Sets and Their Applications, L.A. Zadeh et al., eds., Academic Press Inc., New York, 1975, pp. 429-447.
- A8. Kowalski, R.A., Logic for Problem Solving, North-Holland, 1979.
- A9. Lenat, D.B., F. Hayes-Roth, and P. Klahr, "Cognitive Economy," Memo HPP-79-15, Heuristic Programming Project, Computer Science Dept., Stanford University, 1979.
- A10. Nakashima, H., "Knowledge Representation in Prolog/KR," IEEE International Symposium on Logic Programming, IEEE Computer Science Press, 1984.
- A11. Rich, C., "Multiple Points of View in Modelling Programs," Proceedings of the Workshop on Data Abstraction, Databases and Conceptual Modelling, Pingree Park, Colorado, 1980, pp. 177-179.
- A12. Stefik, M., J. Aikins, R. Balzer, J. Benoit, L. Birnbaum, F. Hayes-Roth, and E. Sacerdoti, "The Organization of Expert Systems: A Prescriptive Tutorial," Artificial Intelligence, Vol. 18, No. 2, March 1982, pp. 135-173.

- P1. Bowen, K.A., and R.A. Kowalski, "Amalgamating Language and Meta-Language in Logic Programming," in Logic Programming, K.L. Clark and S.-A. Tarnlund, Academic Press Inc., London, 1982, pp. 153-172.
- P2. Clark, K.L., F.G. McCabe, S. Gregory, "IC-Prolog Language Features," in Logic Programming, K.L. Clark and S.-A. Tarnlund, eds., Academic Press Inc., London, 1982, pp. 253-266.
- P3. Wise, M.J., "Epilog: Re-interpreting and Extending Prolog for a Multiprocessor Environment," in Implementations of Prolog, J.A. Campbell, ed., Ellis Horwood Ltd., Chichester, 1984, pp. 340-351.

1984 USAF-SCEEE GRADUATE STUDENT SUMMER SUPPORT PROGRAM

Sponsored by the

AIR FORCE OFFICE OF SCIENTIFIC RESEARCH

Conducted by the

SOUTHEASTERN CENTER FOR ELECTRICAL ENGINEERING EDUCATION

FINAL REPORT

A Range Update Algorithm for the Data Handling/Recording System

Prepared by: Guy F. Klose

Academic Affiliation: Department of Computer Science  
and Electrical Engineering  
University of Vermont

Research Location: Rome Air Development Center  
Intelligence and Reconnaissance Division  
Image Exploitation Section

USAF Research Contact: Andrew R. Pirich

SFRP Supervisor: Dr. David C. Lai

Date: 20 July, 1984

Contract Number: F49620-82-C-0035

A Range Update Algorithm for the Data Handling/Recording System

by

Guy F. Klose

ABSTRACT

The Harris Data Handling/Recording System (DH/RS), by using the Westinghouse Auto-Q, is capable of real-time screening and classification of targets from forward-looking infrared imagery, but presently has no provision for automatically updating target range and velocity. An algorithm is developed for the estimation and tracking of range and velocity given target cue information provided by the Auto-Q. Range is estimated from target size and velocity is estimated from the relation of changes in range and time elapsed between estimations. After a suitable model of target dynamics is developed, tracking is provided by the one-step prediction of target states. The classic  $\phi$  Tracker is then implemented as part of the DH/RS software. Suggestions for the continuation of this project have also been presented.

ACKNOWLEDGEMENTS

The author wishes to thank the Air Force Systems Command, Air Force Office of Scientific Research, and the Southeastern Center for Electrical Engineering Education for providing the opportunity for summer research at the Rome Air Development Center, Griffiss Air Force Base, New York.

The author also wishes to thank the Image Exploitation Section and its DH/RS Group, in particular, Andy Pirich, Mike Hinman, and Lt. Bruce Pratt, and John Due'll of Harris Corporation for their invaluable cooperation with this project.

## I. Introduction

The Harris Data Handling/Recording System (DH/RS) is capable of semi-automatic, high-speed exploitation of reconnaissance imagery from airborne forward-looking infrared (FLIR) sensors. Target screening and classification is accomplished by the Westinghouse Auto-Q automatic target cueing unit which is part of the DH/RS Real-Time Processing Module. Presently, the Auto-Q is given an average range and velocity by the operator upon initialization, however it has no provision for automatically updating this information. It is desired to design a suitable estimation/tracking algorithm to be implemented as part of the DH/RS software.

The problem of designing a range update algorithm for the DH/RS is twofold. First, one wants to find an estimate from target cue information provided by the Auto-Q. Secondly, one wants to use that range estimate to update a one-step predictor which is used as a target tracker. One-step prediction is necessary since the range estimate will occur after a target cue is received, and the Auto-Q needs a range estimate before it can analyze imagery and return the cue. Previously, several versions of tracking algorithms have been designed and analyzed,<sup>1-10</sup> the simplest of which is the so-called "αβ Tracker."<sup>3,5-10</sup> The αβ Tracker can be shown to be a special case of the Kalman Filter,<sup>10</sup> and while the Kalman Filter can provide greater tracking accuracy, it utilizes a more complex tracking model,<sup>9</sup> and hence, is not as desirable computationally. Analysis of the DH/RS will provide necessary constraints which will aid selection and design of a tracking algorithm.<sup>11</sup> In the design of tracking filters, one must compromise between the conflicting requirements of good noise smoothing and of good maneuver-following or transient capability.<sup>6</sup>

## II. Objectives of Research Effort

Initial effort was to be spent on familiarization with the DH/RS and the Auto-Q which would help establish direction towards a solution to the problem, designing an automatic range update algorithm for the system. The software and operational characteristics of the system would have to be analyzed in order to determine the propriety of certain classic estimation and tracking schemes. Once the system requirements had been established, the estimation/tracking algorithm was to be implemented in FORTRAN IV Plus in the DH/RS software. Once the operation had been observed and analyzed, performance could be monitored and perhaps enhanced, by changing estimation or tracking schemes, if the algorithm did not offer suitable properties.

## III. Estimation

The Auto-Q provides the following information on each target it classifies: target class, size (length and width measured in pixels), location (pixel coordinates), confidence of classification, and imagery frame number. The Auto-Q uses premission data describing the FLIR sensor vehicle such as altitude, bearing, velocity, and range to target. Ideally, one would like to estimate some of these quantities from target cue information. This project considers the estimation of range and velocity from target size and the time elapsed between cued frames.

Range may be estimated from target size in a couple of different ways; velocity can then be estimated by relating changes in range to the time lapse. Both methods of range estimation considered rely on the acquisition of experimental data (from realistic missions) correlating range and target size. The simplest method would be to create a table of data relating range to average target size and to interpolate

between data values with a polynomial curve-fitting technique. Another method, more realistic in terms of estimation theory, would be to estimate conditional probability density functions (pdf) from the experimental data. Once a family of pdf's have been estimated over all values of range, one may use an estimator such as the Maximum Likelihood test to determine which range is most probable given a particular target size.<sup>1,2</sup> Choice of either method depends heavily upon the nature of the experimental data. The curve fitting technique would be acceptable if the experimental data is closely populated. On the other hand, if the data is not closely populated, assuming a Gaussian distribution of the data and describing the pdf by mean and variance may work well, but accuracy increases with the number of data points. If not much data is available, then the conditional pdf estimate may be poor.

#### IV. Tracking

The first step in designing a tracking algorithm is to model the system. Here it is necessary to make a number of assumptions about the dynamics of the system. Most tracking algorithms have been designed for use with a radar track-while-scan system that has fixed sensors and moving targets. In this case, sensors and targets may move, so movement of the targets will be considered negligible compared to that of the sensors, and any target movement may be resolved as sensor movement. Also, the assumption will be made that the sensors will be slowly maneuvering (i.e., straight line of flight and constant velocity) so that any maneuver may be described as random acceleration modelled as additive maneuver noise. The observation will be a single measure of current range and velocity, estimated from target cues as described in the previous section, with additive noise describing the uncertainty of the measurement.

Next, the state equations of the system have to be defined such that they will describe the transition from one step to the next. Then the tracking filter becomes a recursive estimator that minimizes some sort of error between a signal and its estimate. The following notation is used for modelling the system<sup>3,5,8-10</sup>

message model:  $\langle x(k+1) \rangle = \underline{A} \langle x(k) \rangle + \langle n(k) \rangle$  (4.1)

where:  $\langle x(k) \rangle = \begin{bmatrix} r(k) \\ \dot{r}(k) \end{bmatrix} = \begin{bmatrix} \text{range at time } k \\ \text{velocity at time } k \end{bmatrix}$  (state vector)

$\underline{A} = \begin{bmatrix} 1 & T \\ 0 & 1 \end{bmatrix}$  (state transition matrix)

$\langle n(k) \rangle = \begin{bmatrix} 0 \\ n(k) \end{bmatrix}$  (model noise vector)

observation model:  $\langle y(k) \rangle = \langle x(k) \rangle + \langle u(k) \rangle$  (4.2)

where:  $\langle y(k) \rangle = \begin{bmatrix} y_1(k) \\ y_2(k) \end{bmatrix} = \begin{bmatrix} \text{meas. range at } k \\ \text{meas. velocity at } k \end{bmatrix}$  (meas. vector)

$\langle u(k) \rangle = \begin{bmatrix} u_1(k) \\ u_2(k) \end{bmatrix}$  (observation noise vector)

$n$ ,  $u_1$ , and  $u_2$  are independent noise sequences with zero mean and variances  $\sigma_m^2$ ,  $\sigma_1^2$ ,  $\sigma_2^2$ , respectively. Figure 1 shows the block diagram of the complete system model.

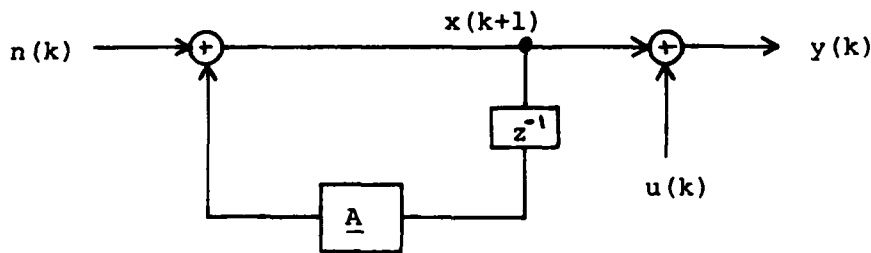


Figure 1: System Model

If the observation and model noises are white, then the Kalman Filter is an optimum recursive estimator that minimizes the mean-squared error between the signal  $x$  and its estimate  $\hat{x}$ .<sup>1,4,10</sup> One Kalman Filter feature is its variable gain matrix (called the Kalman Gain,  $\underline{K}$ ) that minimizes the mean-squared error at every step. If the Kalman Gain is fixed, then the Kalman Filter can be shown to be equivalent to an  $\alpha\beta$  Tracker.<sup>10</sup>  $\alpha$ , the range error gain, weights the difference between predicted and measured values of range, and  $\beta$ , the velocity error gain, does the same for velocity. The problem that remains is the choice of optimum values for  $\alpha$  and  $\beta$ , which has been treated by several sources.<sup>6-10</sup> One such source<sup>6</sup> determines the optimum choice for  $\beta$  given  $\alpha$ , where  $\alpha$  is left as a design parameter. The following predictor model is used:

$$\text{predicted estimate: } \hat{x}(k+1|k) = \underline{A}\hat{x}(k|k) \quad (4.3)$$

$$\text{filtered estimate: } \hat{x}(k|k) = \hat{x}(k|k-1) + \underline{K}[y(k) - \hat{x}(k|k-1)] \quad (4.4)$$

$$\text{initial condition: } \hat{x}(1|1) = \begin{bmatrix} y(1) \\ (1/T)[y(1) - y(0)] \end{bmatrix}$$

A block diagram of the predictor model is shown in Figure 2.

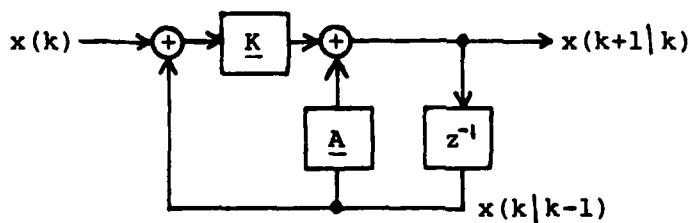


Figure 2: Predictor Model

For the  $\alpha\beta$  Tracker, the gain matrix  $\underline{K}$  is defined in the following manner:

$$\underline{K} = \begin{bmatrix} \alpha & 0 \\ \beta/T & 0 \end{bmatrix}$$

## V. Analysis

To design an estimator/tracker, the DH/RS needed to be thoroughly analyzed in terms of system performance. Several features needed to be isolated and tested. The first feature was the system's tolerance to range and velocity error. The robustness of the Auto-Q directly affects the accuracy needed for the estimation/tracking algorithm. The second feature to be tested was the system's limits of range and velocity, which would help define the usable range of the algorithm. The timing requirements of the system was also an important consideration, since system timing must not be impeded in order to preserve the speed of classification. Lastly, several target identification missions needed to be analyzed in order to obtain the experimental data necessary for the estimation scheme.

Once the above analysis had been completed, the estimation/tracking algorithm could be implemented in software, as described in the next section. The only items left unaddressed are the actual mapping from size to range and the choice of the tracker's design parameters, i.e.,  $\alpha$  and  $\beta$ .

The above analysis was in fact attempted and the results are presented in the section covering discussion and recommendations.

## VI. Software Modifications

The DH/RS software is implemented in FORTRAN IV Plus using the RSX-11M Operating System on a Digital Equipment Corporation PDP-11/44. The system software is highly modularized and so it was analyzed to reveal the most appropriate places to modify for the addition of an estimation/tracking algorithm. Refer to the Appendix for necessary subroutines and existing software modifications.

The Man-Machine Interface/Real-Time Processing Module Configuration module (MCNRTP) is used to initialize the Auto-Q with sensor vehicle data such as initial range and velocity, which are both entered by the operator through a menu. The modification needed in this case is to make RANGE a global parameter by use of a named common block (TRK), and hence, available to initialize the tracking algorithm. Velocity is already available in common block.

The Real-Time Processing Module Screening and Exploitation module (RTPMSE) handles the receipt of target cues. The most appropriate time to make a one-step prediction to update range would be immediately after a target cue has been received by RTPMSE. Hence, the modification needed in this case is the addition of a call to SUBROUTINE TRACK, passing appropriate arguments, near label 450 in RTPMSE.

The only other modification needed is the addition of two subprograms, SUBROUTINE TRACK and FUNCTION STRMAP. SUBROUTINE TRACK is accessed by RTPMSE and handles the tracking algorithm and the message handling to and from the Auto-Q. FUNCTION STRMAP is accessed by TRACK and is used to estimate range by mapping from target size to range.

As one can readily see, the above software modifications are fairly transparent, and hence, are easily implemented in system software. However, some general comments are in order. Firstly, the Communications Interface Send and Receive modules (CISEND and CIRECV) are used by TRACK to communicate with the Auto-Q, rather than using the tedious configuration of messages by the Real-Time Processing Module Message Handler (RTPMMH). Secondly, according to an Auto-Q designer at Westinghouse, the Auto-Q will accept a message for range update during target screening without inhibiting screener performance. If this was not the case, the software would have to stop screening, send the update message, and then restart the screening. Not only would this be much more complex to implement, it would also severely inhibit the real-time performance of the system.

## VII. Discussion and Recommendations

The DH/RS has been in very limited operation for most of this calendar year, so the author was afforded limited opportunity of quantitative system evaluation, and hence, was limited in the implementation and refinement of a real-time estimation/tracking algorithm.

Some characteristics were found that will severely limit the performance of a tracking algorithm. The system will only detect and classify targets correctly less than 50% of the time. It will not recognize targets if the Auto-Q has been initialized with values of range less than 2000 meters or velocity greater than 100 miles per hour. If the Auto-Q is initialized with a range of over approximately 4000 meters, a very high rate of false alarms occur. These limitations circumvent the original intent of the estimator/tracker.

In conclusion, at this moment, the DH/RS is mostly limited by the characteristics of the Auto-Q. Although software modifications of the existing system can be considered minor, automatic update of range is best implemented within the Auto-Q. However, the Auto-Q is a Westinghouse proprietary device and even Harris Corporation, the system contractor, has limited knowledge of its operation. The author suggests that for improved DH/RS operation, the Auto-Q should be upgraded by Westinghouse. The material presented in this paper may be best utilized by Westinghouse after improved performance of the Auto-Q is realized.

VIII. Appendix: Program Listings

a) add to MCNRTP:

COMMON/TRK/ RANGE

b) add to RTPMSE:

CALL TRACK(RCVDTC(3),RCVDTC(6),RCVDTC(7),RCVDTC(8))

c) SUBROUTINE TRACK(FRAME,CLASS,XSIZE,YSIZE)

IMPLICIT INTEGER(A-Z)

INTEGER NAME(3),RCVBUF(64),DATTIM(7),TSKODR(5),TARPRS(20,2)

INT\*4 NAVFR,ACALT

BYTE SENTYP(2),FOV(2)

REAL ACDRFT,ACHEAD,ACPTCH,ACROLL,DEPNGL,VELHGT

REAL\*8 FRMLL(2),MISID

COMMON/TRK/ RANGE

COMMON/FRANAV/ NAVFR,ACALT,ACDRFT,ACHEAD,ACPTCH,ACROLL,

1 DATTIM,DEPNGL,FOV,FRMLL,VELHGT

COMMON/MISDAT/ ENGOFF,MISID,SENTYP,TARPRS,TSKODR

C

C INITIALIZE COUNTER AND FRAMES/SECOND

C

DATA I/1/,FPS/30/

C

C DO NOT TRACK IF THIS IS NOT A FLIR MISSION

C

IF (SENTYP(1).EQ.'C') RETURN

C

C OTHERWISE, GO AHEAD AND TRACK

C

IF (I.GT.1) GO TO 100

C

T = (FRAME-1)/FPS

V = VELHGT\*ACALT\*0.3048

RANGE = RANGE - T\*V

GO TO 200

C

100 T = (FRAME-PFRAME)/FPS

IF (CLASS.EQ.-1) GO TO 150

AREA = XSIZE\*YSIZE

MRANGE = STRMAP(AREA)

V = V + (BETA/T)\*(MRANGE-RANGE)

RANGE = RANGE + ALPHA\*(MRANGE-RANGE) - T\*V

GO TO 200

C

150 RANGE = RANGE - T\*V

C

```
200 ANGLE = (DEPNGL*1000)*0.0174532925/20.0
    ALT = ACALT*0.3048
C
    RCVBUF(1) = 4
    RCVSIZ = 10
    RCVBUF(2) = RANGE
    RCVBUF(3) = ANGLE
    RCVBUF(4) = ALT
    RCVBUF(5) = V
C
    CALL CISEND(RCVSIZ,2,RCVERR,RCVBUF)
    IF (RCVERR.EQ.0) GO TO 300
    CALL DBMRHE(817,NAME,0)
    GO TO 500
C
300 RCVTO = 10
    CALL CIRECV(RCVSIZ,2,RCVERR,RCVTO,RCVBUF)
    IF (RCVERR.EQ.0) GO TO 400
    CALL DBMRHE(818,NAME,RCVTO)
C
400 CALL DBMRHE(713,NAME,RCVERR)
C
500 I = I + 1
    PFRAME = FRAME
    RETURN
    END
```

IX. References

1. Schwartz, Mischa and Leonard Shaw, Signal Processing: Discrete Spectral Analysis, Detection, and Estimation, McGraw-Hill, 1975, pp. 343-382.
2. Srinath, M.D. and P.K. Rajasekaran, An Introduction to Statistical Signal Processing with Applications, John Wiley and Sons, 1979.
3. Cadzow, James A., Discrete Time Systems: An Introduction with Interdisciplinary Applications, Prentice-Hall, 1973, pp. 272-279.
4. Bozic, S.M., Digital and Kalman Filtering, John Wiley and Sons, 1979.
5. Bhagavan, B.K. and R.J. Polge, "Performance of the g-h Filter for Tracking Maneuvering Targets," IEEE Trans. on Aerospace and Electronic Systems, vol. AES-10, pp864-866; Nov. 1974.
6. Benedict, T.R. and G.W. Bordner, "Synthesis of an Optimal Set of Radar Track-While-Scan Smoothing Equations," IRE Trans. on Automatic Control, vol. AC-7, pp. 27-32; July, 1962.
7. Sklansky, Jack, "Optimizing the Dynamic Parameters of a Track-While-Scan System," RCA Review, vol. 18, pp. 163-185; June, 1957.
8. Schooler, C.C., "Optimal  $\alpha\beta$  Filters for Systems with Modelling Inaccuracies," IEEE Trans. on Aerospace and Electronic Systems, vol. AES-11, pp. 1300-1306; Nov., 1975.
9. Singer, Robert A. and Kenneth W. Behnke, "Real-Time Tracking Filter Evaluation and Selection for Tactical Applications," IEEE Trans. on Aerospace and Electronic Systems, vol. AES-7, pp. 100-110; January, 1971.
10. Kanyuk, Allen J., "Transient Response of Tracking Filters with Randomly Interrupted Data," IEEE Trans. on Aerospace and Electronic Systems, vol. AES-6, pp. 313-323; May, 1970.
11. Zimmerman, Andrew C., "An Evaluation of the Data Handling and Recording System," Final Report, 1983 USAF-SCEEE Graduate Student Summer Support Program; August, 1983.

1984 USAF-SCEEE GRADUATE STUDENT SUMMER SUPPORT PROGRAM

Sponsored by the

AIR FORCE OFFICE OF SCIENTIFIC RESEARCH

Conducted by the

SOUTHEASTERN CENTER FOR ELECTRICAL ENGINEERING EDUCATION

FINAL REPORT

PATTERN MATCHING ALGORITHMS IN ADA

Prepared by: John Kreuter  
Department and Computer Science  
University: Tulane University  
Research Location: Air Force Human Resources  
Laboratory,  
Lowry Air Force Base,

Denver, CO

USAF Research Contact: Maj. Hugh Burns  
SFRP Supervising  
Faculty Member: Dr. Larry Reeker  
Date: July 20, 1984  
Contract No: F49620-82-C-0035

John Kreuter

Abstract

When the Dod issued the directive making Ada the standard high level computer language, a need was created to determine the capabilities of Ada in such areas as artificial intelligence. Libraries of packages both with general application and with specific usefulness to artificial intelligence need to be developed. One approach is to develop Ada packages which will mirror the capabilities of languages such as Lisp and Snobol which have proven their utility in solving AI questions. Our summer research group took this approach and began the development of Lisp-like list processing packages -- undertaken by my colleague Ken Wauchope -- and Snobol-like pattern matching packages -- undertaken by this author. Viewing pattern matching as an extended parsing problem, Ada packages for pattern matching utilizing the more efficient (time-wise) Earley Algorithm were developed, as well as packages implenting the more traditional backtracking (recursive descent) approach. Since the full Ada language was not available to us this summer at Lowry AFB, these efforts should be considered as preliminary, with the implementation of the algorithms in the richness of the full Ada language, and an analysis of the run time space requirements still needing to be accomplished.

## I Objectives

Brian Dallman, a Research Psychologist for the Training Systems Division of the Air Force Human Resources Laboratory, in a paper delivered to the Joint Services Workshop on Artificial Intelligence in Maintenance, defined three principal goals for the Air Force program for the development of AI technology as it applies to maintenance aiding and training:

"First, the program will apply AI technology to real Air Force problems in the maintenance aiding and training domains through an integrated system. The rationale for this integrated system has been documented by Richardson (1983). The principal initial demonstrations will be conducted as a part of AFHRL's Integrated Maintenance Information System (IMIS) program (Johnson, 1982). The second goal is to establish a capability for the conduct and examination of artificial intelligence research. AI is a multidisciplinary field with the principal contributions being made by cognitive psychologists and computer scientists. Because of the scarcity of experts, it will be necessary to educate Air Force personnel and maximize the sharing of resources and information. This can be accomplished through jointly funded research activities and participation with AI researchers as in the case of the Intelligent Computer-Assisted Instruction Network. The third goal will be to assist/consult with other Air Force organizations in the development and exploitation of the

evolving AI technology. As the technology becomes more refined and personalized, it will also become more distributed. There will be a need for contacts for information and assistance."

These goals defined the objectives of our summer research project. To meet the first goal we brought with us an expert system developed independently at Tulane University, and participated in workshops conducted by General Dynamics at the AFHRL, in an effort to synthesize the results of our research with theirs. The third goal mentioned above will be met as our and other research continues, is published and distributed. The bulk of our summer research was devoted to meeting the second goal. The area for this research was further defined in the same paper by Mr. Dallman:

PROBLEM:

Since Ada recently became the DoD standard computer language, ideally it should be used for all programming applications within DoD. However, there are some applications for which Ada is not currently practical. One of these areas is artificial intelligence. In DoD, the majority of programming for AI applications is done in LISP. Consequently, if LISP remains the primary AI language, then Ada's usage and acceptance in a critical new area of software engineering will be severely limited and DoD's effort to establish a common high order language will be

hampered.

#### OBJECTIVE

To develop an extension of the Ada language which will provide the capabilities for AI programming applications. This extension can involve possibly only an Ada package or collection of packages.

To meet this objective we defined two major areas for summer research, to be undertaken in Ada: development of LISP-like list processing and tree matching algorithms, undertaken by my colleague Mr. Ken Wauchope; and development of SNOBOL-like pattern matching algorithms. It was in this second area that my own research effort was conducted.

#### II Definition of Patterns

Before any pattern matching algorithm could be implemented, a suitable definition -- one that can be represented in Ada -- had to be developed. The packaging facilities of Ada then allow the representation and pattern building functions to be developed and compiled independently from the pattern matching routines. Although the packaging allowed by the Irvine compiler is very primitive it was sufficient to allow for at least this much encapsulation. Programming in a fully certified Ada will be able to make more extensive use of the package to build hierarchies of libraries of packages, with each library at a given level containing packages useful to the applications at the next higher level. Thus at the bottom level the

libraries would contain packages of generally useful abstract data types such as stacks, queues, linked lists, sequences, strings (a more complex variety of string than that offered by the Ada compiler), matrices, etc. At the next higher level would be packages that could use these types (which themselves use the primitive types provided by the Ada compiler). For instance, the pattern matching packages would be defined at this level. At the next higher level would be packages utilizing complex structures such as patterns -- for instance, a compiler could be defined at this level, using the pattern matching algorithms to do the parsing.

Despite its limitations, the Irvine compiler did allow for development of complex data structures using Pascal-like records and arrays with a new twist: constraints need not be introduced initially. Using these structures, the first working definition of a pattern was:

- A PATTERN is an (unconstrained) array of  
ALTERNATIVES.
- An ALTERNATIVE is an (unconstrained) array of BEADS.  
(Bead is used here to correspond to SNOBOL terminology.)
- A BEAD is any of
  - (i) a string
  - (ii) a PATTERN
  - (iii) a primitive function  
(primitive functions selected corresponded

to the most useful SNOBOL primitives.)

The Irvine compiler, though it supports unconstrained arrays, does not support size-variant records, so the utility of using unconstrained arrays in a package is limited. The next working definition for a pattern therefore made an Alternative a linked list of Beads. Unfortunately, without generic packages, a linked list could not be conveniently defined outside the pattern package. Thus, although the type Alternative was implemented as a linked list, a Linked List type was never explicitly defined. The working definition for a Pattern, then became

```
type prim-func is (ARB1, REMAIN1, POS1, SPAN1, ANY1,  
                  NOTANY1, BREAK1, TAB1);
```

```
type Primitive is record
```

```
    Name : prim-func;
```

```
    Arg  : string-pointer;
```

```
end record;
```

```
type Pattern;
```

```
type Kinds is (terminal, non-terminal, operation,  
              R, L);
```

```
-- R and L are used to hold the left and right
```

```
-- unmatched sub-strings
```

```
type Bead(Kind : Kinds) is record
```

```
    case Kind is
```

```
        when non-terminal => Choice : Pattern;
```

```

        when terminal => Str   : string-pointer;
        when operation => Op   : Primitive;
        when R => null;
        when L => null;
    end case;
end record;

type alt-pointer;
type Alternates is record
    C      : Bead;
    next   : alt-pointer;
end record;
type alt-pointer is access Alternates;

type pats is array(Positive range <>) of Alternates;
type Pattern is access pats;

```

This provided the basic representation for patterns. To complete the definition of pattern as an abstract data type, some pattern building functions also had to be defined. There are two basic pattern building functions: "+", which concatenates its operands, and "or", which alternates the operands, both operators functioning as they do in SNOBOL. Since Ada allows for overloading, these operations could retain the same symbols and form for all the various possible combinations of operands.

Finally a type Sys-Pat was introduced, so that the

pattern building functions could distinguish between internally generated sub-patterns and actual user defined patterns. For example the pattern  $P = ("a" + "b" + "c")$  should have a length of 3, but the pattern  $P = (A + "c")$ , where  $A = ("a" + "b")$  should have a length of 2. By overloading the pattern building functions, the compiler is forced to choose the proper representation in both cases.

The problem of pattern matching is, given a pattern and a target string, to find a sub-string such that for each set of alternatives a bead can be found which matches the sub-string starting at the point where the last set of alternatives leaves off. In some schemes the sub-string may start either flush left, flush right, or anywhere within the target string, depending on a positional indicator passed to the pattern matching algorithm along with the pattern and the target string. Since the patterns used here include the ARE primitive function (which matches any arbitrarily long string of characters) positional indicators have been left out of this initial work. All patterns are matched flush left; however, provision has been made to include positional indicators in future versions.

### III A First Algorithm

The most intuitive approach to the pattern matching problem is to try every possibility individually. This leads to the "backtracking" method, -- that is for each set of alternatives, each bead is tried until a match is found. Then for the next set of alternatives each bead is tried,

etc., until all sets of alternatives have been matched. If for any set of alternatives no bead matches, then the algorithm backtracks -- that is, the previous set of alternatives is tried again, starting from the bead that just matched. Clearly every possible parse of the string will be found in this fashion, but there are several problems which arise with this method which will be discussed later.

A typical way of implementing the backtracking method, and the way that I chose, is the so called recursive descent algorithm. As the name implies, recursion is used extensively by this method, especially if the bead being matched is itself a pattern. (Recall that a bead may be either a string, a pattern, or a primitive function.) In this case the recursive descent algorithm calls itself (i. e. recursion), passing the value of the bead (i. e. the pattern) and the cursor position of the string. The positional indicator, if used, would be flush left. In this fashion the algorithm "descends" with recursive calls until the bead being matched is not a pattern. At this point, if the bead is a string it is matched against the target. If the bead is a primitive function, then a string is derived from the function, the target string and the cursor position. This derived string is then matched against the target. If this matching is successful the next set of alternatives at this level of descent is tried. (This may be done by recursion also, by iteration, or by co-routines.)

After each set of alternatives is matched (or if no match is found) the algorithm returns to the next higher level with the matched sub-string (or the null string if no match is found).

An elegant way of implementing the backtracking aspect of the algorithm -- that is when no match is found, returning to a previous set of alternatives and resuming where the algorithm left off -- is through the use of co-routines which in Ada is handled by the Task. The Task starts by examining each bead in the first set of alternatives. For each bead that successfully matches, a new Task is started, which examines the remainder of the string and the remaining sets of alternatives. When the last set of alternatives has been examined, the task passes back the matching sub-strings (or the null string if no match has occurred) and terminates. The parent task then adds its sub-string to the beginning of each tree on the list which has been passed to it. This new list of trees is then passed back, and the task terminates, etc., until the top-most task completes all possible parse trees. Thus although backtracking takes place (each possibility is considered individually) it occurs with a degree of concurrency dependent on the run-time environment.

Unfortunately, the Irvine compiler also does not have Tasking as one of its features. The process described above can be implemented as a function, but with the loss of (psuedo) concurrency and elegance. Furthermore, as shown in

the analysis below, backtracking can be a very costly way of conducting pattern matching. Some of this cost can be absorbed with concurrency, but the implementation and run-time analysis of this must await a certified Ada (so that concurrent tasks can be incorporated into the algorithm). The run-time analysis could then consider both time and resource utilization. As multiprocessors appear this analysis could provide some interesting insights into time consumption versus resource demands.

Two noteworthy problems exist with the pattern matching method outlined above. The first occurs if the pattern itself is left recursive -- that is it has the form  $P = P' + A$ , where  $P'$  is a pattern which can produce  $P$ , and  $A$  is any pattern (possibly null). The recursive descent algorithm will examine  $P$  by first considering its first set of alternatives, i. e.  $P'$ . This will cause a recursive call, so that  $P'$  is considered. Since  $P'$  can produce  $P$ , eventually the algorithm will recursively consider  $P$ , which then causes a recursive call to  $P'$ , eventually leading to another call to  $P$ , etc. without ever having advanced the target string cursor. Thus the recursive descent method goes into an infinite loop if it encounters a left recursive pattern. Fortunately this is not a major problem since it has been shown that any pattern can be generated by a pattern in Greibach Normal Form, which means the pattern has one of the following forms:

$$P = a + P_1 + P_2 + \dots + P_n$$

P = a

P = null

where a is any string or primitive function, and the P's are all patterns. Clearly a pattern in Greibach Normal Form cannot be left recursive, so if any given pattern is first massaged into this form, the recursive descent algorithm will work.

#### IV A More Practical Algorithm

Although this problem of handling left recursion is not major since any pattern can be massaged into Greibach Normal Form, the problem of the time requirements of the backtracking algorithm in the most general cases of patterns remains. Consider as an example the pattern  $P = ("a" + P + P)$  or null. Suppose this pattern is to be matched against a string of a's. Clearly the leftmost 'a' will be matched by the "a" of P. All other a's can be matched by either the first (recursive) occurrence of P, or by the second, independent of how any previous or subsequent a's are matched. Thus if the string is L long, combinatorics tells us that the number of possible parses is  $1 + 2^{*(L-1)}$  -- that is the number of parses is exponential. Since the backtracking algorithm considers each possible parse individually, it will require exponential time to parse such a pattern. So, although the backtracking method may be useful given certain restrictions on the allowable patterns, in the most general case the time constraints become unreasonable.

Obviously, the way to reduce the time costs of parsing is to not treat each individual possibility by itself, rather to group them into classes. In the above example, for instance, there is no need to consider both of the recursive P's individually since they both reduce to the same tree. Both P's can be considered in parallel, and then the above example will parse in linear time! Even with more complex examples, it can be shown that by developing a scheme to consider similar possibilities in parallel, parsing can be accomplished in polynomial time, a vast improvement over the exponential time required by the backtracking method. One such scheme, which can be implemented without any initial manipulation of the pattern is known as Earley's algorithm.

Earley's algorithm is described in its mathematical details in Harrison's "Introduction to Formal Language Theory", where he calls it simply "a good practical algorithm". The main problem I encountered in implementing this algorithm was developing reasonable data structures to represent the rather complex mathematical formulas introduced -- patterns must be converted to "dotted rules", a triangular matrix of dotted rules must be created, and the functions 'x', '\*', and 'predict' must be implemented. Once again the effort was hampered by the lack of generic packaging facilities in the Irvine compiler. The development process certainly could have made good use of a lower level of abstract data types which included sets and

matrices. As it was these structures had to be developed along with the rest of the algorithm.

Another problem encountered in implementing Harrison's version of Earley's algorithm is that this version (as most are) is developed for a context-free grammar, not for pattern matching. Although for the most part context-free parsing is analogous to pattern matching, the analogy breaks down when the primitive functions are considered. These primitive functions are in general string and cursor dependent, and so have no context free representation. Since they are at most dependent on the string and cursor, though, it was possible to alter the 'predict' function so as to produce simple string derivations of each primitive function as it is encountered during the parse. This increases the time requirements as compared to a simple context-free parsing problem, but the modified algorithm still requires no more than polynomial time.

As can be readily seen from the above discussion, although Earley's algorithm is faster than the backtracking method, the price is paid in the complexity of algorithm and the space it takes while running. The complexity also will make it more difficult to develop Earley's algorithm in a concurrent environment. Now that the algorithms have been developed into working programs, it remains to be studied whether the difficulties of Earley's algorithm outweigh its benefits.

V Recommendations

Although the summer research effort has been quite successful, producing working programs utilizing two different methods for pattern matching, more work remains to be done. As mentioned throughout this paper, the primitive state of the Irvine Ada compiler, in use at the Human Resources Laboratory at Lowry Air Force Base, proved most inadequate in accomplishing the primary goal of the research -- to produce a hierarchy of Ada packages for pattern matching (or for Mr. Wauchope, a hierarchy of packages for list processing). To provide maximum utility to future users and researchers, the programs developed this summer should be rewritten in a fully certified Ada, making use of the packaging facilities as detailed in the Dod specifications for the language. In the specific case of the backtracking algorithm for pattern matching, the rewrite should also include the use of Tasks, again not available for use this summer, but detailed in the Dod Ada specifications. It is in this full Ada environment that the two methods of pattern matching could be best tested against each other in real time, to provide a comparison of their relative merits in time, space and concurrency. It is to address these questions that the accompanying proposal is made. With a certified Ada compiler and an additional year of research time the questions raised by this summer's research may be fully answered.

Brian Dallman, in the previously cited call for research also asked for an evaluation of Ada's ability to meet the

challenge of AI programming, and suggestions for a possible superset of Ada to meet the challenge. In this regard two recommendations are made: First, Ada makes no provision for treating functions as data types. Such a treatment is especially useful in pattern matching, where it is desirable to associate an action to be taken with a pattern to be matched. Second, when producing large systems as is often the case in AI programming it would be beneficial to be able to declare subprograms within a package to be external, so as to be able to compile them separately from the rest of the package. Although the separate compilation of the packages themselves is very useful, in complex systems the package itself may grow to a cumbersome point, with each update requiring inordinate amounts of compile time. A facility for external compilation would relieve this load.

## REFERENCES

- 1) Dallman, Brian (1983). AFHRL program for artificial intelligence applications to maintenance and training. Paper delivered at Joint Services Workshop: Artificial Intelligence in Maintenance, Boulder, Colorado (Proceedings forthcoming).
- 2) Harrison, Michael A., Introduction to Formal Language Theory, Berkeley, California, Addison-Wesley Publishing Company, 1978).

1984 USAF-SCEEE GRADUATE STUDENT SUMMER SUPPORT PROGRAM  
Sponsored By  
AIR FORCE OFFICE OF SCIENTIFIC RESEARCH  
Conducted by  
SOUTHEASTERN CENTER FOR ELECTRICAL ENGINEERING EDUCATION

FINAL REPORT  
OPTICAL THIN FILM COATING DAMAGE VIA PULSED LASERS

Prepared By: M. R. Lange  
Academic Department: Institute For Modern Optics, Physics Dept.  
University: University of New Mexico  
Albuquerque, NM 87131

Research Location: Air Force Weapons Laboratory  
Kirtland Air Force Base  
Albuquerque, New Mexico 87117

USAF Research Contact: Dr. A. H. Guenther, Dr. J. K. McIver  
SFRP Supervisor: John Ungvarsky  
Date: July, 23, 1984  
Contract No.: F49620-82-C-0035

OPTICAL THIN FILM COATING DAMAGE VIA PULSED LASERS

By

Michael R. Lange

Abstract

The absorbing inclusion model of pulsed laser induced damage in thin films is revisited and generalized. A solution is derived that can facilitate arbitrary absorption functions and pulse shapes. It is also shown that this model applies to regions previously excluded when the wavelength dependence of Mie absorption by an inclusion in a thin film is taken into account. The model reveals that fluoride film damage is thermally dominated with absorption that appears generally material independent, but wavelength dependent. Furthermore, it also shows that thermal diffusion plays an important part in oxide film damage, however, there is apparently some material dependence not accounted for in the present model. It is postulated that this material dependence enters through the absorption process. As might be expected, absorption in oxide films is also shown to be wavelength dependent.

ACKNOWLEDGEMENT

The author would like to thank the Air Force Systems Command, the Air Force Office of Scientific Research and the Southeastern Center for Electrical Engineering Education for providing him with the support and facilities to perform this fruitful research effort at the Air Force Weapons Laboratory in Albuquerque, New Mexico.

In particular, he wishes to thank his supervisor John J. Ungvarsky and the invaluable scientific guidance of Arthur H. Guenther, Chief Scientist of AFWL and John K. McIver, Theoretical Physicist with the Institute for Modern Optics at the University of New Mexico.

## I. Introduction

The damage of optical thin films by localized highly absorbing regions is the primary limitation in the development of high energy lasers. The model presented here is not a new model<sup>1</sup>. This model incorporates a small localized region within the film that absorbs the incident laser radiation at a rate far above the surrounding film. The absorbed energy subsequently diffuses through the surrounding film. The cross section of the absorbing center presenting itself to the radiation along with the diffusion capability of the film determines the rate at which the region reaches a critical temperature at which damage results.

This model has been successful in describing the way in which single shot damage thresholds scale with respect to the laser pulse duration and the thermal properties of the absorbing region for fluoride films. Thus far, comparisons between the prediction of the model and experimental data have been restricted to cases where the laser pulse duration is long in comparison to the time required for heat to diffuse from the center to the edge of the absorbing region.

In this presentation, previous work on this model is generalized. In the next section an analytical expression for the damage threshold is derived that is valid for arbitrary shapes of an incident laser pulse. The particular example of a single flat top pulse is then discussed.

Predictions of this model are then compared with two different sets of experimental data. The implication and conclusions that can be drawn from this model are then summarized in the final section.

## II. Objectives

The Main objective of this effort was to further develop a model and theory of laser damage in optical thin films. A general description of the problem is illustrated in Figure 1. A spherical inclusion of radius 'a' is embedded in a surrounding material of different optical and thermal properties. Only the inclusion is permitted to absorb radiation. The size of the absorbing region is assumed to be much smaller than the laser spot size so that absorption can be thought of as occurring in a field with a constant radial intensity.

The thermal properties of the system are described by the thermal conductivity 'k' and the thermal diffusivity 'D' of each region. These properties in concert with the rate at which radiation is absorbed are taken to be independent of temperature. The system is said to be damaged when the interface between the two regions reaches some critical temperature (e.g., the melting temperature of the film). This condition is chosen because an interface between a film and an inclusion would be a weak and stressful point.

## III. Theory

Mathematically the temperature distribution in the system is described by the following thermal diffusion equations;

$$\frac{1}{D_i} \frac{\partial T_i(r,t)}{\partial t} = \frac{1}{r} \frac{\partial^2}{\partial r^2} (rT_i)_i + \frac{A}{K} \quad r < a \quad (1)$$

$$\frac{1}{D_h} \frac{\partial T_h(r,t)}{\partial t} = \frac{1}{r} \frac{\partial^2}{\partial r^2} (rT_h) \quad a < r \quad (2)$$

$$T_i(r,0) = T_h(r,0) = 0 \quad (3)$$

where the subscripts i and h refer to inclusion and host respectively.

The interface condition between the impurity and host is assumed to be

$$T_i(a,t) = T_h(a,t) \quad (4)$$

$$K_i \left. \frac{dT_i}{dr} \right|_a = K_h \left. \frac{dT_h}{dr} \right|_a \quad (5)$$

The solution for this system may be found by Laplace (temporal) transform as presented in a previous paper<sup>2</sup> or by intergral (spatial) transform as is presented here. The intergral transform technique<sup>3</sup> is more general because no specific form of the absorption profile need be assumed.

The intergral transform technique involves expanding the solution in appropriate eigenfunctions of the region. The appropriate eigenfunctions are spherical Bessel functions. Because of assumed spherical symmetry we specify the problem to spherical Bessel functions of order zero. These may be written as sines and cosines.

The appropriate eigenfunctions for this region are:

$$\psi_i = \sin(\alpha r)/r \quad (6)$$

and

$$\psi_h = [A \sin(\beta r) + B \cos(\beta r)]/r \quad (7)$$

The overall temporal eigenvalue must be the same in both regions i.e.,

$$D_i \alpha^2 = D_h \beta^2 \equiv \lambda^2 \quad (8)$$

The coefficients 'A' and 'B' may now be determined from the interface conditions for which we find

$$A = \frac{1}{b\lambda} [b\lambda \sin(\alpha a) \sin(\beta a) - \frac{\sqrt{D_h}}{a} c \sin(\alpha a) \cos(\beta a) + \lambda \cos(\alpha a) \sin(\beta a)] \quad (9)$$

$$B = \frac{1}{b\lambda} [b\lambda \sin(\alpha a) \cos(\beta a) + \frac{\sqrt{D_i}}{a} c \sin(\alpha a) \sin(\beta a) - \lambda \cos(\alpha a) \sin(\beta a)] \quad (10)$$

where  $b = \frac{K_h \sqrt{D_i}}{K_i D_h}$ ,  $c = 1 - \frac{K_h}{K_i}$

The eigenfunction normalization may be shown to be

$$N(\alpha) = \frac{2\pi^2 K_h}{\sqrt{D_h D_i}} (A^2(\alpha) + B^2(\alpha)) \quad (11)$$

which works out to be

$$N(y) = \frac{2\pi^2 K_i}{D_i b y^2} ( (c \sin y - y \cos y)^2 + b^2 y^2 \sin^2 y ) \quad (12)$$

with  $y = \frac{\lambda a}{\sqrt{D_i}} = \alpha a$ .

The solution expanded in the eigenfunctions is of the form

$$T_R(\vec{r}, t) = \int d\lambda C(\lambda, t) \Psi_R(\lambda, \vec{r}); R = i, h. \quad (13)$$

The coefficients of the composite region then satisfy

$$C(\lambda, t) = \frac{1}{N(\lambda)} \sum_{R=i, h} \int dr_R \Psi_R(\lambda, \vec{r}) T_R(\vec{r}, t) \quad (14)$$

where use has been made of the orthogonality of the composite

eigenfunction.

The time evolution of this coefficient is found by applying this transform operator to equations (1) through (5). With the aid of Green's theorem the system and boundary conditions transform to an ordinary differential equation with the solution

$$C(\lambda, t) = \frac{\text{Exp}(-\lambda^2 t)}{N(\lambda)} \hat{A}(\lambda, t) \quad (15)$$

where

$$\hat{A}(\lambda, t) \equiv \int_0^t dt' \text{Exp}[\lambda^2 t'] \bar{A}(\lambda, t')$$

and

$$\bar{A}(\lambda, t) = 4\pi \int_0^a dr r \bar{A}(r, t') \sin(\alpha, r) \quad (16)$$

thus we find a solution of the form

$$T_R = \int_0^\infty d\alpha C(\lambda, t) \psi_R(\lambda, r) \quad (17)$$

and specifically for the impurity region

$$T_I(\vec{r}, t) = \frac{D_I b}{2\pi^2 r a K_I} \int_0^\infty dy \left( \frac{y^2 \sin(yr/a) \text{Exp}(-y^2 t/\gamma) \hat{A}(y, t)}{(c \sin y - y \cos y)^2 + b^2 y^2 \sin^2 y} \right) \quad (18)$$

where  $\gamma = \frac{a^2}{D_I}$

Now, if we assume that  $A(r, t) = A(t)$  (i.e., absorption within the region is independent of radius)  $\hat{A}$  becomes

$$\hat{A}(y, t) = \frac{4\pi a^2}{y^2} (\sin y - y \cos y) \int_0^t dt' A(t') \text{Exp}\left(\frac{y^2 t'}{\gamma}\right) \quad (19)$$

Thus

$$T_i(\vec{r}, t) = \frac{2D_i b a}{\pi r K_1} \int_0^\infty dy F(y) \text{Exp}(-y^2 t/\gamma) \int_0^t dt' A(t') \text{Exp}(y^2 t'/\gamma) \quad (20)$$

with

$$F(y) = \frac{(\sin y - y \cos y) \sin(y r/a)}{(C \sin y - y \cos y)^2 + b^2 y^2 \sin^2 y} \quad (21)$$

Note that no assumptions have been made as to the temporal behavior of the absorption profile.

As with previous works<sup>4,5</sup>, the source term is written in terms of the incident intensity

$$\int_{V_i} dr^3 A(r, t) = Q\left(\frac{2\pi a}{\lambda}, n'\right) I(t) \quad (22)$$

where  $Q$  is the absorption cross section computed from electromagnetic theory and  $n'$  is the imaginary part of the index of refraction. The damage threshold is then defined as  $E \equiv \int_0^{t_p} dt I(t')$  in (J/cm<sup>2</sup>), where  $t_p$  is the pulse length required to reach the critical temperature  $T_c$  at the radius 'a' of the absorbing region. Thus  $T_c t_p = f(r, Q, E)$  is inverted to give  $E = g(T_c, t_p, r, Q)$  for the damage threshold in (J/cm<sup>2</sup>).

For the particular case of a repetitively square pulsed laser the last term of equation (19),

$$\int_0^t dt' A(t') \text{Exp}(y^2 t'/\gamma) = \frac{\gamma A_0}{y^2} (\text{Exp}(y^2 t/\gamma) - 1) \frac{(1 - e^{-N T y^2/\gamma})}{(1 - e^{-T y^2/\gamma})} \quad (23)$$

where  $N$  is the Number of Pulses and  $T$  Equals  $t_p + t_d$ , where  $t_p$  is the pulse length and  $t_d$  is the delay time between pulses. A derivation of this will be presented in a future publication.

#### IV. Results

As shown in a previous work<sup>6</sup>, for a single square pulse ( $N=1$ ) such that  $\frac{t_p}{\gamma} > 1$  an appropriate expression for the integral solution may easily be computed. The damage in ( $J/cm^2$ ) is then found by the method described in reference 6 to be given by

$$E_1 = 16T_c \frac{\sqrt{\rho_h C_{ph} K_h t_p}}{\pi} \frac{1}{1 + \frac{\pi \rho_f C_{pf}}{120 \rho_h C_{ph}} \left( \frac{15 \rho_h C_{ph} - 10 - K_h}{\rho_f C_{pf} K_f} \right)} \quad (24)$$

where the second term in the denominator is usually quite small. Thus we may write

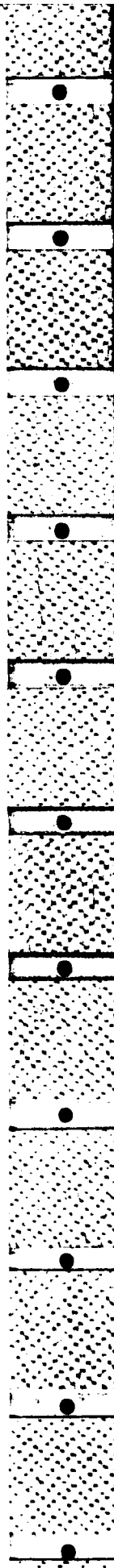
$$E_0 = 16T_c \frac{\sqrt{\rho_h C_{ph} K_h t_p}}{\pi} \quad (25)$$

This term has been plotted against measured damage thresholds in several previous works. In Reference 4 it was mentioned that this scaling would not apply to the shorter pulse length data of Walker et. al.<sup>1</sup>. This is not due to the pulse length being too short, since as pointed out by Milam<sup>7</sup> this scaling should apply to most of Walker's Data<sup>1</sup>. This is more because of the strong wavelength dependence in absorption of small particles predicted by Mie theory<sup>4</sup>. Small particles refers to inclusions which are small enough that absorption begins to be volumetric as opposed

to cross sectional. That is, the inclusion becomes small enough that the optical field cannot be fully attenuated within its bounds. This occurs either if the film thickness is decreased (for a fixed wave length) forcing the inclusion to decrease, or if the pulse length is decreased (i.e., the size particle most likely to damage is decreased)<sup>4</sup>. In the latter case the absorption should affect the size particle most likely to damage<sup>4</sup> so that the problem becomes further complicated. However, if similar films are compared the problems as predicted by Mie Theory<sup>4</sup> are avoided (by similar films we mean comparison of half wave with halfwave ect.). That is, the cross sections should be similar and no wavelength dependence should be observed. The range of validity of this is limited because as the film becomes much thinner than the particle most likely to damage, a smaller particle damages at a slightly higher threshold<sup>4</sup> (see Figures 5, 6, and 7). This in fact is not observed. A wave Length dependence still remains.

When the data is plotted against the scaling (Eq. 25) for half wave, quarterwave and fullwave films, a clear splitting by wavelength occurs in each of the three types of films. This scaling fits flourides best for reasons unknown to the author.

The wavelength dependence can be realized by comparing Figures 2 through 4 with Figures 5 through 7. The only free parameter between Figures 5, 6 and 7 is the imaginary part of the index of refraction. Since absorption  $\alpha$  (cm<sup>-1</sup>)  $\cong \frac{4\pi n''}{\lambda}$ , the nonlinear dependence n'



on  $\lambda$  indicates that the absorption is a function of wavelength. This is not unreasonable. Absorption is a function of wavelength in most theories of absorption that may apply here<sup>1</sup>. The specifics of the wavelength dependence cannot be hypothesized, though, until the precise mechanism or mechanisms are known. It should be noted that the imaginary part of the index of refraction is simply a phenomenological measure of absorption and does not make a statement about the choice of mechanisms for absorption.

As stated above, the specifics of wavelength dependence cannot be hypothesized. It is interesting to note, though, that the theory of optics of metals can give absorption coefficients on the right order and roughly the same general trends of wavelength dependence noted in the data. This point is interesting, but should not be emphasized. The absorbing region is not a simple metallic sphere and this wavelength trend was not observed in previous data<sup>4</sup> (though the previous data was from two separate experiments and at longer pulse lengths). It is likely that the absorbing region evolves during irradiation to a highly absorbing state and that no simple classical theory will suffice to explain its behavior.

For oxides (see Figure 8) there is a splitting of scaling for both wavelength and material, though  $\text{HfO}_2$  scales on the same line as  $\text{Al}_2\text{O}_3$ . If oxides are scaled strictly against  $\sqrt{\epsilon_p}$  times some additional material dependent constant (other than  $\sqrt{k_0 C_p}$ ) the oxides also scale as Equation 25. According to the data<sup>1</sup> this constant is highly material dependent, it does not seem to depend upon the film thickness, but it does appear to

depend upon the incident wavelength to some fractional power ( $\approx 1/2$ ). All of this indicates that oxides also scale as the square root of pulse length, but that some other material dependent properties enter that are not strictly thermal (because of the wavelength dependence of the constant). In other words, the mechanisms for absorption in fluoride films are similar enough between the various fluorides that the thermal properties dominate the damage evolution while oxides differ from film to film in some way other than the obvious thermal properties. This same behavior is exhibited in Figure 9 of fluoride and oxide data from a different source<sup>8</sup>.

When the fluoride data<sup>1</sup> is plotted against the scaling (Eq. 26) for a given wave length, films that are fullwave (at 1.06  $\mu\text{m}$ ) have damage thresholds that are similar to those of halfwave, but as we go to quarterwave or smaller the difference becomes greater. This difference may be explained by reference to Figures 5 through 7. These are plots of the exact solution of the diffusion equation using Mie scattering theory to compute the absorption cross section. That is, it seems to require a combination of electromagnetic theory and thermal diffusion to explain the increase in damage threshold for thinner films at fixed incident wavelengths. However, this behavior may be simply understood. As the film, and therefore the absorbing regions, become small with respect to the wavelength, the regions absorb proportional to their volumes. On the other hand, regions on the order of a half wavelength or greater absorb as the cross section<sup>4</sup>. Thus as the film thickness decreases, absorption

decreases as the cross section up until some point and then decreases more quickly as the volume tending towards higher damage thresholds.

#### V. Discussion

The different behavior of oxides versus fluorides suggests at least one of three things. Either there is a major oxide dependent difference in thin film properties as opposed to bulk properties, there are structural or chemical complexities not accounted for, or there is simply a mechanism for absorption in oxides such that the absorption appears highly material dependent. The latter two seem more likely because of the wavelength dependence for the missing material constant.

It should be pointed out here that the more predictable behavior of the fluorides does not necessarily prove that an absorbing inclusion exists. It does, however, strongly suggest a central absorbing region common to the various fluorides that thermally diffuses the absorbed energy such that damage thresholds for fluorides are thermally dominated. This region should have properties that are either initially different from the surrounding film or are quickly altered by an enhanced field, a mechanical process, or an increased temperature in the region. An enhanced field could be caused by a microcrack or local defect<sup>9,10</sup>.

The theoretical evidence that the size of the absorbing region that damages is on the order of the film thickness<sup>6</sup> does not exclude the

possibility that a smaller absorbing region expands to the thickness of the film as damage ensues. An expanding absorbing region has been suggested by Komolov<sup>11</sup> and expanding damage regions have been observed by Foltyn and Jolin<sup>10</sup>.

It is interesting to note in Figure 2 of the  $\frac{\lambda}{4}$  films, the stray  $\text{ThF}_4$  points. These same points are plotted on Figure 7 for damage threshold at  $\lambda = 1.06 \mu\text{m}$  versus film thickness. They are anomalously high on this plot also indicating that they are unique points not following the trends of the surrounding data.

#### VI. Recommendations

Although the model presented here is not new and has been presented previously, the continued success of fitting data to this model in different regions has provided more insight into the important parametric behavior of laser damage. This indicates that the efforts to generalize the model to include arbitrary spatial and temporal absorption and other significant parameters should also prove fruitful.

The model strongly suggests that regions in fluoride films absorb in a manner that is nearly material independent and damage threshold is primarily thermally dominated, while the absorption is wavelength dependent. Oxides, however, seem to absorb in a manner that is both material and wavelength dependent. The square root of pulse length

dependence does tend to show that thermal diffusion also plays a measurable part in the damage thresholds of oxide films.

The difference in behavior of oxides tends to suggest a structural or chemical complexity, possibly involving the absorption of radiation, that has not been accounted for. It is recommended that further work in the field of deposition and testing of oxide and flouride films be carried out. Particularly work using some sort of real time monitoring of the damage process for both single and repeating pulses.

It should be pointed out here that there are fundamental differences in oxides and flourides which exhibit themselves through macroscopic properties of the materials. For example the index of refraction of flouride films is usually less than that of oxide films. The melting temperature is also less for flourides than oxides. Furthermore the ultra-violet cut-off of absorption occurs for shorter wavelengths in flourides than oxides and thus multi-photon effects would appear sooner in oxides as wavelength decreases. There are other possible differences like the structural properties, elasticities or the thermo-mechanical response of the materials. One final apparant difference is the fact that flourides probably have oxide impurities, but oxide impurities are unknown. The implication or significance of these various differences are unknown to the author at present.

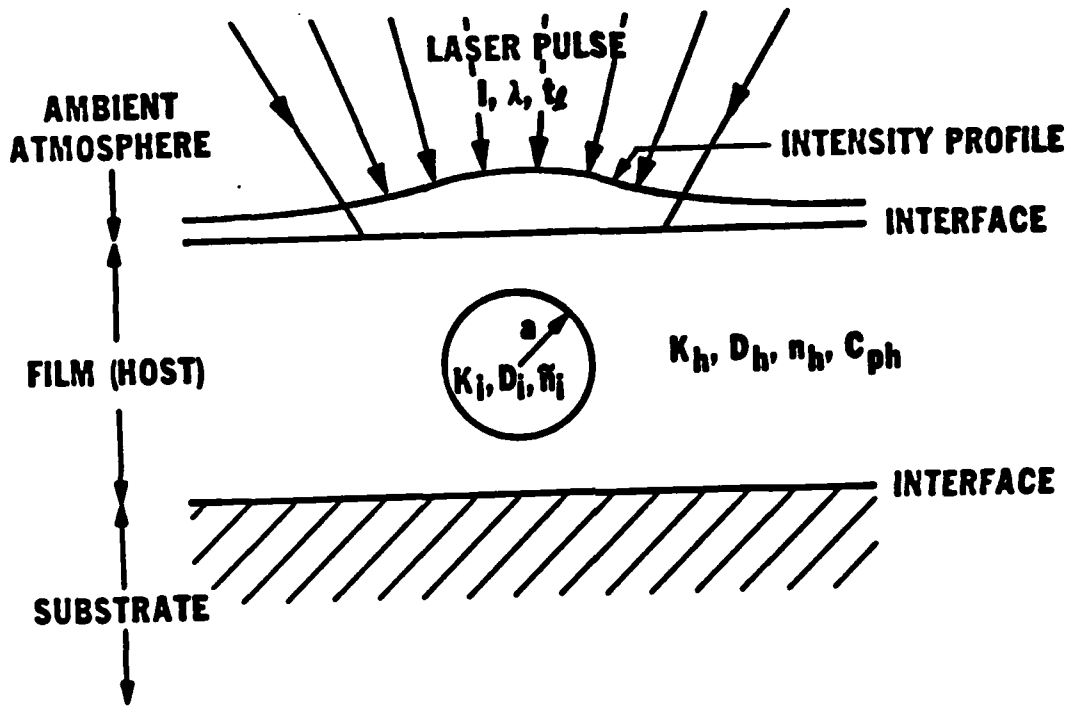


Figure 1

1. Schematic of the spherical inclusion model

2. Scaling of experimentally measured<sup>1</sup> damage threshold of fluorides versus a theoretically derived parameter of thermal properties for  $\lambda/4$  films at two different wavelengths (note anomalously high ThF<sub>4</sub> points).

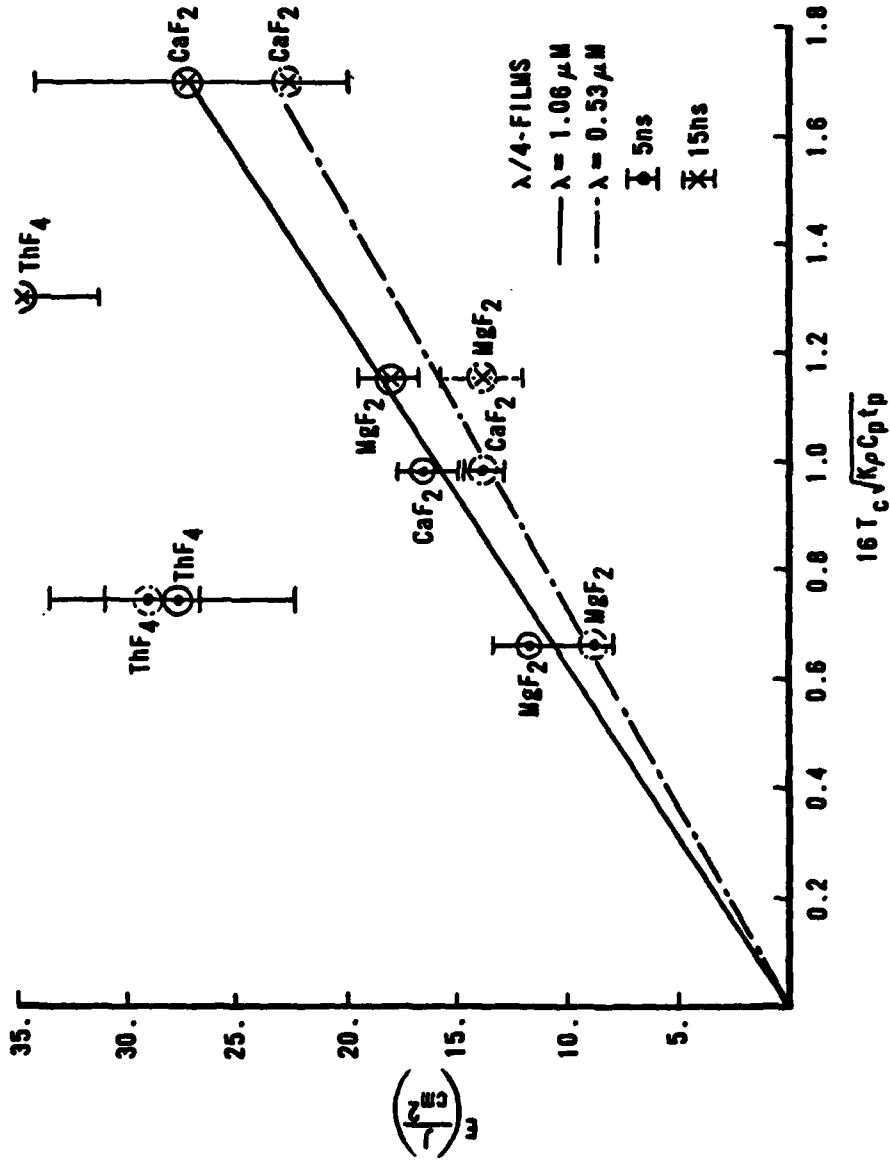


Figure 2

4. Scaling of experimentally measured<sup>1</sup> damage threshold of fluorides versus a theoretically derived parameter of thermal properties for  $\lambda$  films at three different wavelengths.

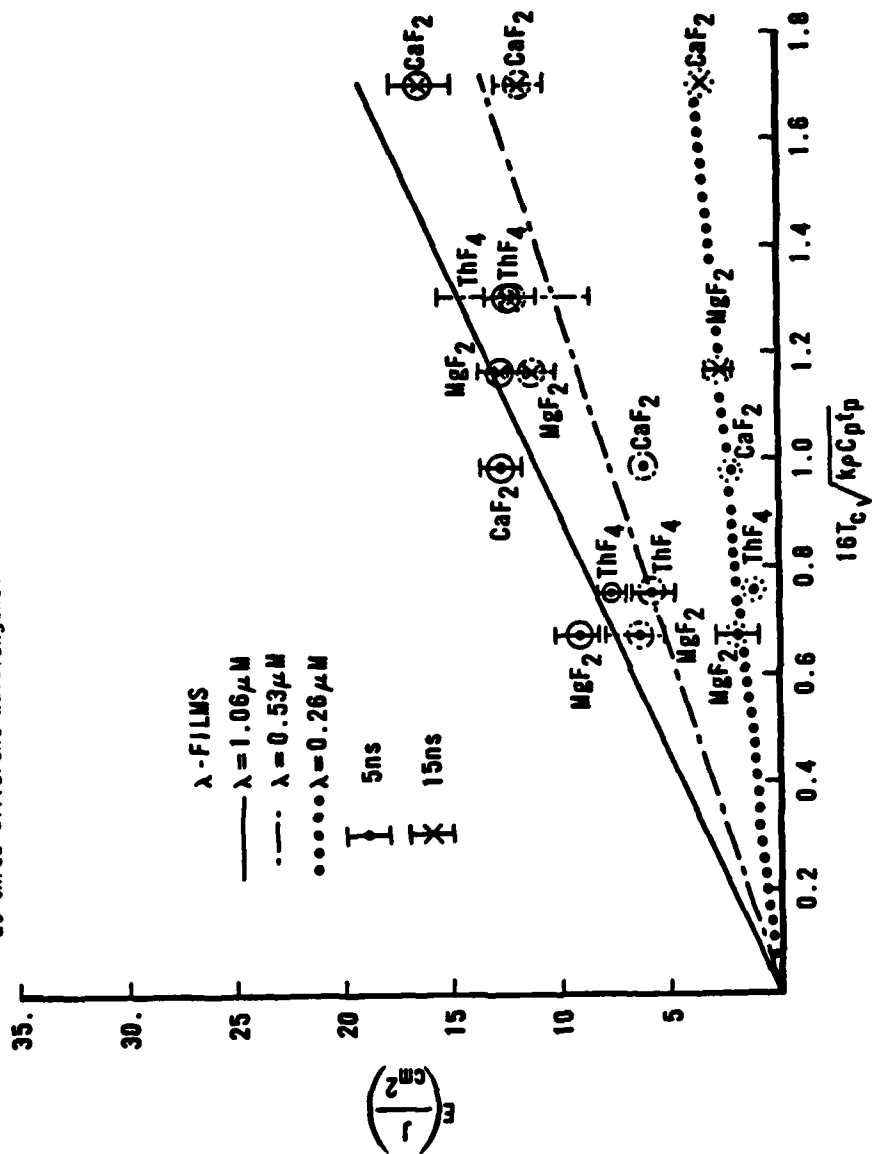


Figure 4

3. Scaling of experimentally measured<sup>1</sup> damage threshold of fluorides versus a theoretically derived parameter of thermal properties for  $\lambda$  films at four different wavelengths.

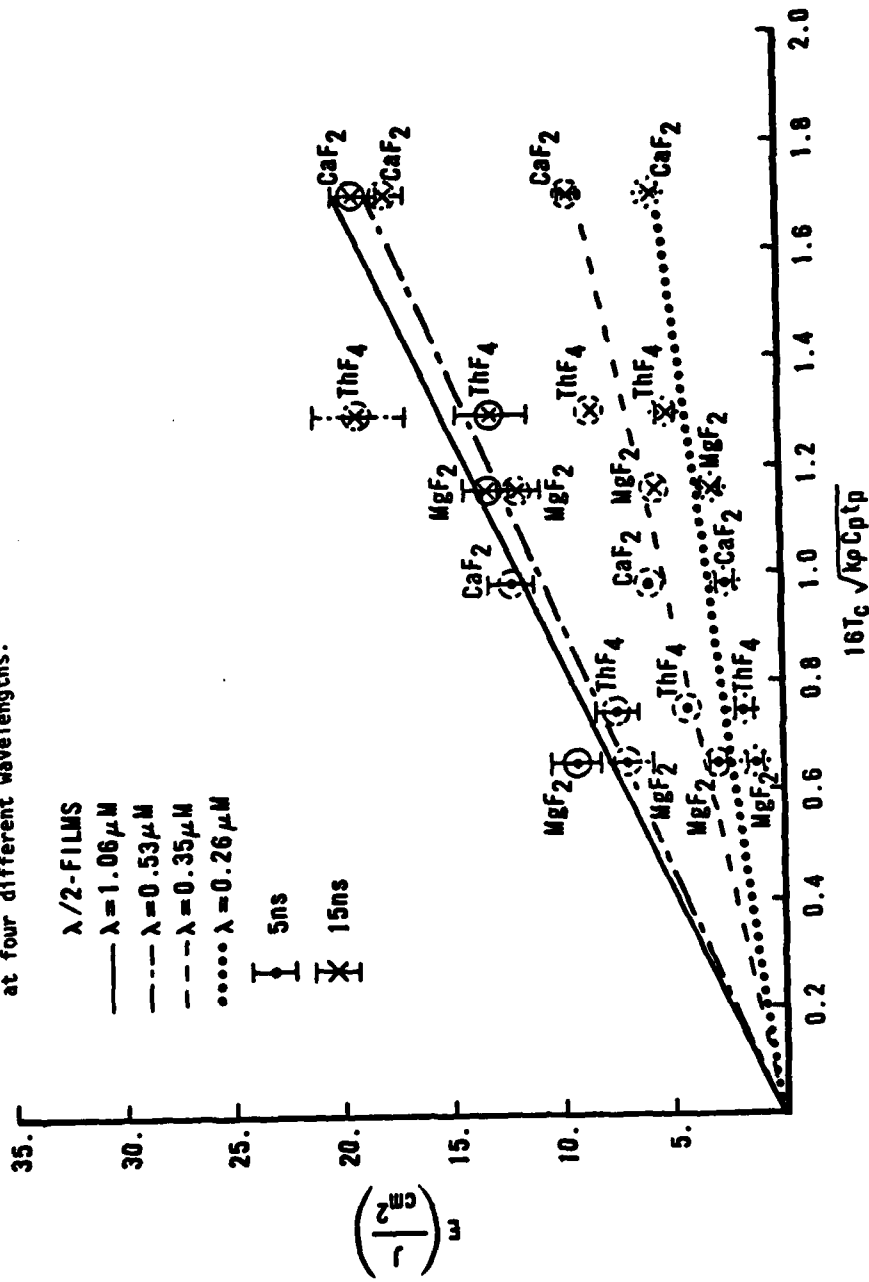


Figure 3

6. Damage threshold data<sup>1</sup> and theory versus film thickness for  
 $\lambda = 0.353 \mu\text{m}$  (measured in units of  $\lambda$  at  $1.06 \mu\text{m}$ ).

$\tilde{n} = 1.3-18$   
 $\lambda = 0.353 \mu\text{m}$

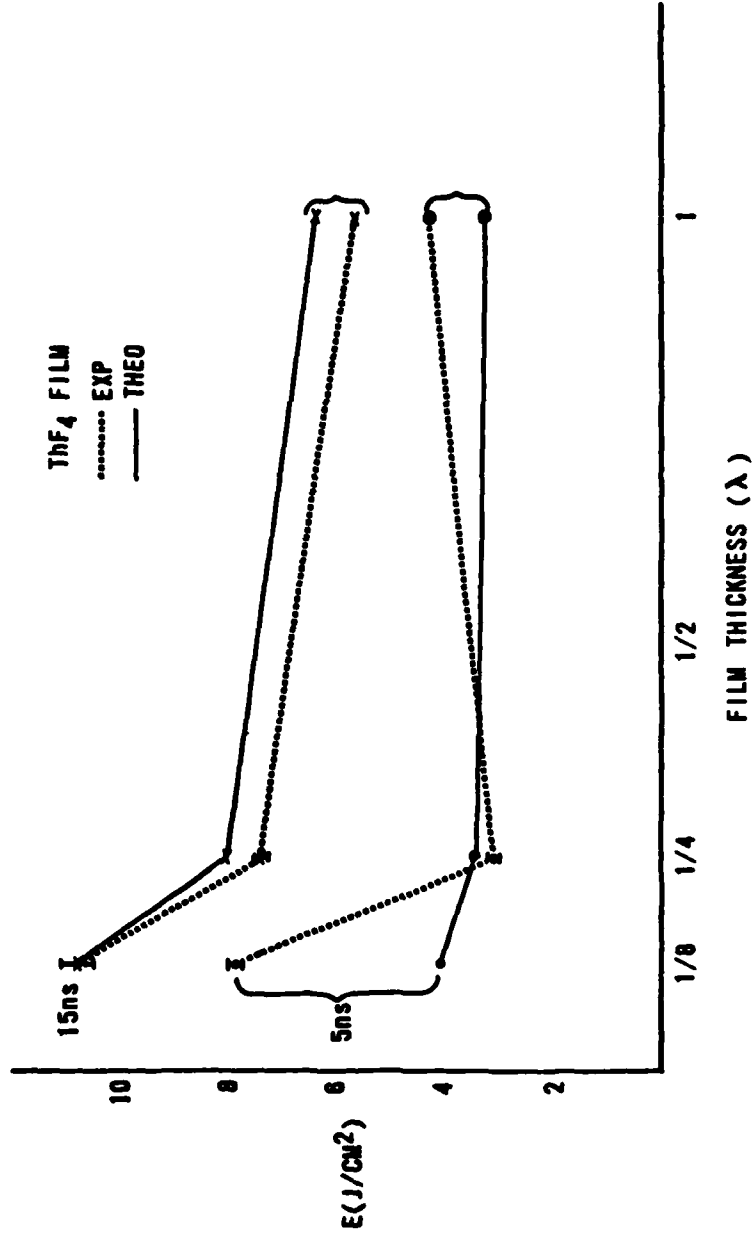


Figure 6

5. Damage threshold data<sup>1</sup> and theory versus film thickness  
 for  $\lambda = 0.26 \mu\text{m}$  (measured in units of  $\lambda$  at  $1.06 \mu\text{m}$ ).

$\bar{n} = 1.3 - i4.8$   
 $\lambda = 0.26 \mu\text{m}$

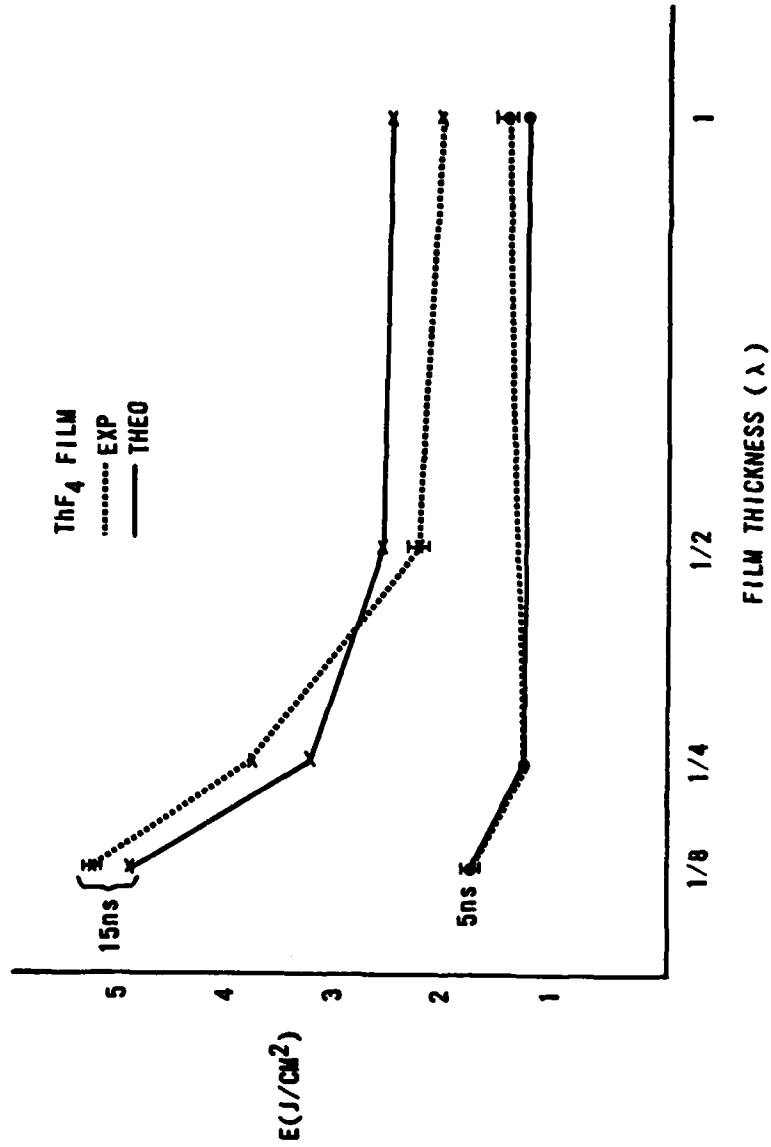


Figure 5

8. Scaling of experimentally measured<sup>1</sup> damage threshold of oxides versus a theoretically derived parameter of thermal properties for  $\lambda/2$  films at four different wavelengths.

$\lambda/2$ -FILMS  
 —  $\lambda = 1.06 \mu\text{M}$   
 - -  $\lambda = 0.53 \mu\text{M}$   
 - -  $\lambda = 0.35 \mu\text{M}$   
 .....  $\lambda = 0.26 \mu\text{M}$

I 5ns  
 II 15ns

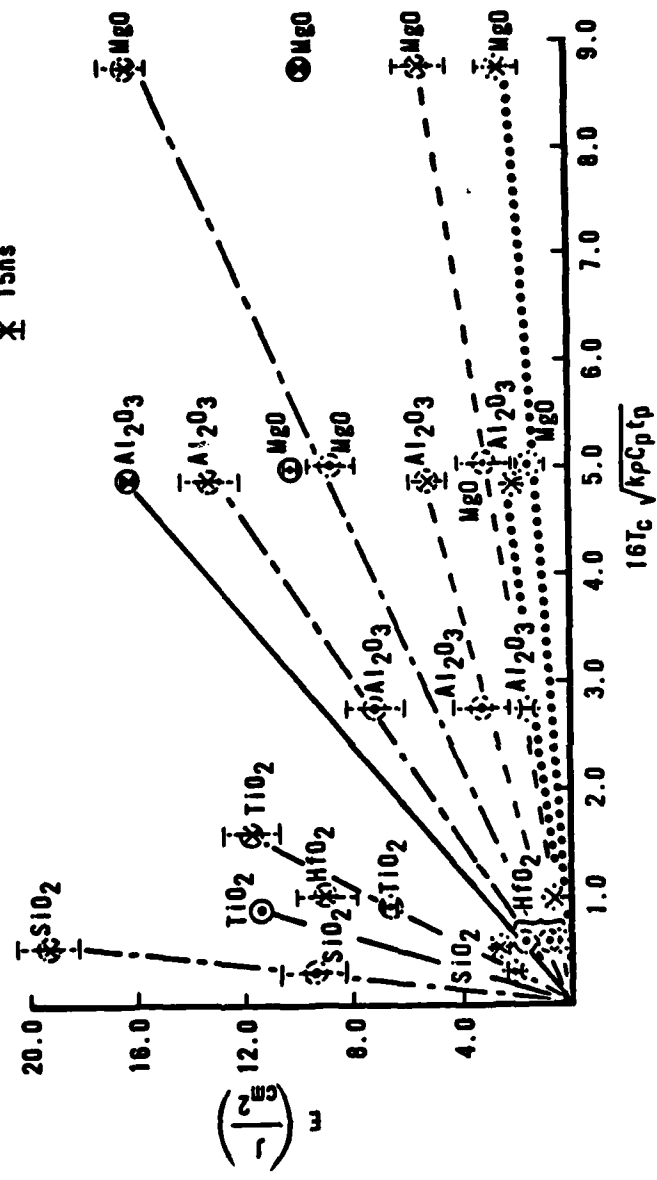


Figure 8

7. Damage threshold data<sup>1</sup> and theory versus film thickness for

$\lambda = 1.06 \mu\text{m}$  (measured in units of  $\lambda$  at  $1.06 \mu\text{m}$ ).

$\tilde{n} = 1.3-113$

$\lambda = 1.06 \mu\text{m}$

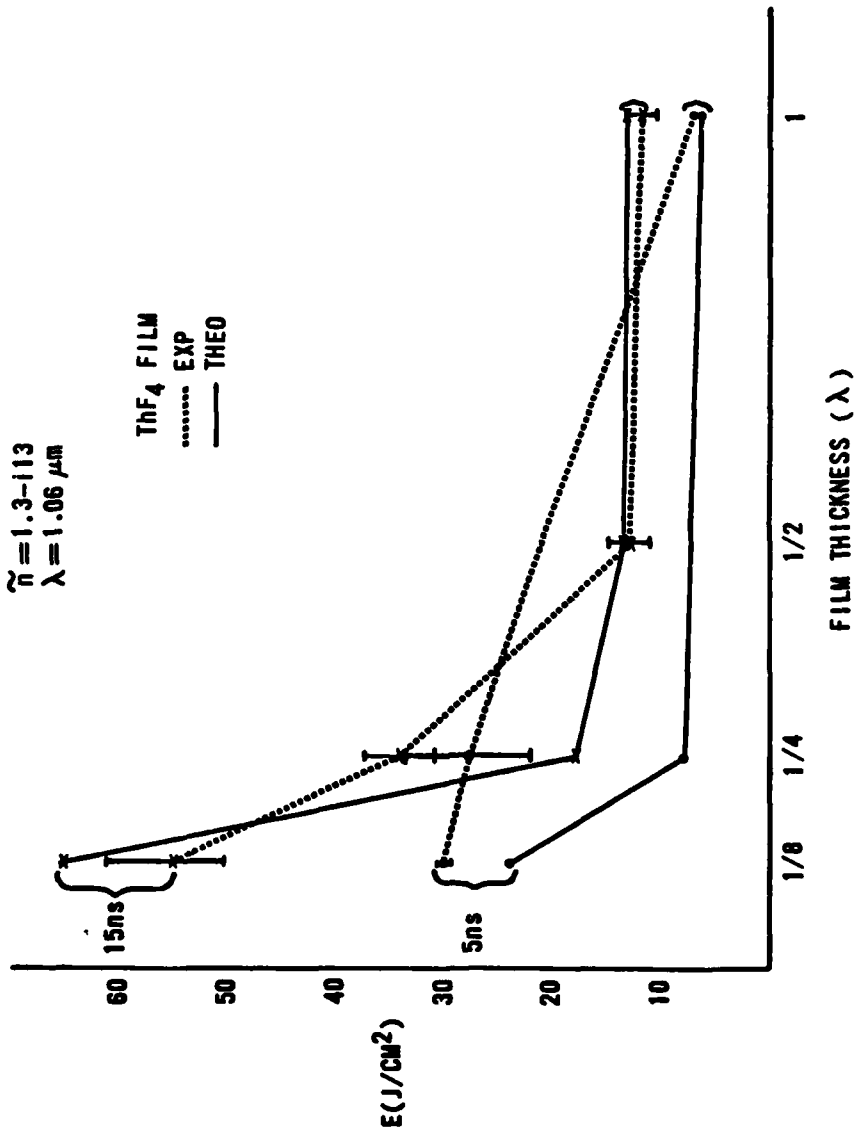


Figure 7

## References

1. T.W. Walker, A.H. Guenther, P.E. Nielson, IEEE J. Quan. Electron, 17 No. 10 (1981), p. 2041.
2. H. Goldenberg and J.C. Tranter, Brit. J. Appl. Phys., 3 (1952) pp.296.
3. N. Dzişik, Heat Conduction, John Wiley, N.Y., 1st Edn, 1980.
4. M.R. Lange, J.K. McIver, A.H. Guenther, In H.E. Bennett, A.H. Guenther, D. Milam, B.E. Newnam (Ed.), NBS Spec. Pub. 1983, (to be published).
5. M.R. Lange, J.K. McIver, A.H. Guenther, J. Thin Solid Films, 1984, (to be published).
6. M.R. Lange, J.K. McIver, A.H. Guenther, In H.E. Bennet, A.H. Guenther. D. Milan, B.E. Newnam (Ed.), NBS Spec. Pub. 669, 1982 pp. 380.
7. D. Milam, Private Communications, Lawrence Livermore Laboratory.

9. Scaling of experimentally measured<sup>8</sup> damage threshold of both fluorides and oxides versus theoretically derived parameter of thermal properties

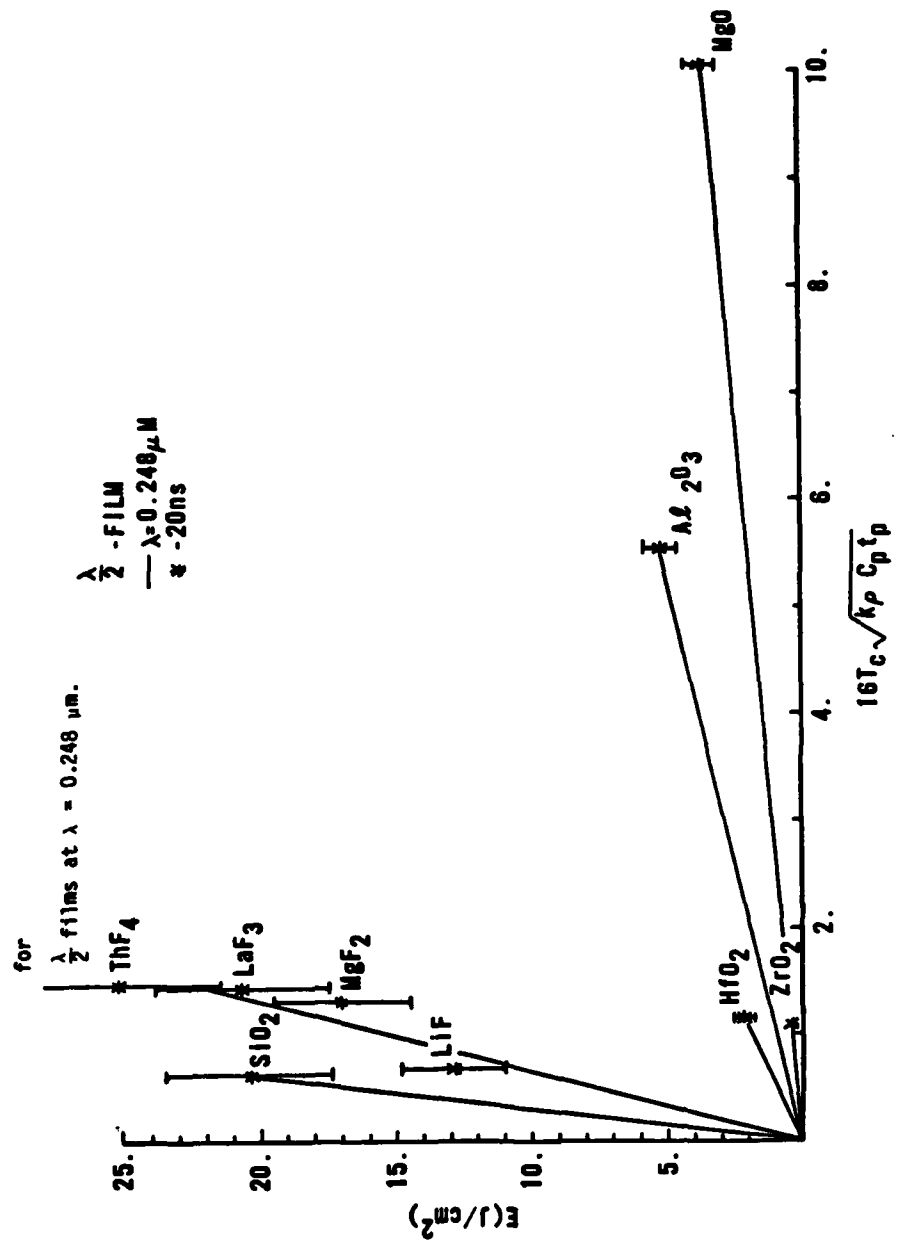


Figure 9

8. F. Rainer, W.H. Lowdermilk, D. Milam, 14th Boulder Damage Symposium, 1982.

9. J. Bettis, A.H. Guenther, A.J. Glass, IEEE '74 Region Six Conf. (1974) pp. 43.

10. S.R. Foltyn, L.J. Jolin, In H.E. Bennet, A.H. Guenther, D. Milam, B.E. Newman (ED.), NBS Spec. Pub. 1983, (to be published)

11. V.L. Komolov, Sov. Phys. Tech. Phys. 27 No. 3, 1982, pp. 311.

1984 USAF-SCEEE GRADUATE STUDENT SUMMER SUPPORT PROGRAM

Sponsored by the

AIR FORCE OFFICE OF SCIENTIFIC RESEARCH

Conducted by the

SOUTHEASTERN CENTER FOR ELECTRICAL ENGINEERING EDUCATION

FINAL REPORT

REPROCESSING OF BARNES TRANSMISSOMETER DATA

Prepared by: Barry R. Lemieux and Martin A. Patt

Academic Department: Electrical Engineering

University: University of Lowell

Research Location: Air Force Weapons Laboratory, Advanced  
Control Division, Advanced Laser Optics  
Branch

USAF Research Contact: Dr. Eric P. Shettle

SFRP Supervising  
Faculty Member: Martin A. Patt, Associate Professor

Date: September 2, 1984

Contract No: F49620-82-C-0035

REPROCESSING OF BARNES TRANSMISSOMETER DATA

by

Barry R. Lemieux  
and  
Martin A. Patt

ABSTRACT

Under NATO project OPAQUE, large data files were collected for subsequent processing by the Air Force Geophysics Laboratory. The validity of some of the supplemental 1400-meter Barnes transmissometer data stored in processed hourly-files was suspect. The data has been carefully studied and a determination has been made that the 1400-meter Barnes data was not valid. The processing error which resulted in the bad data was found, and the hourly data files were subsequently reprocessed.

## ACKNOWLEDGEMENTS

The authors would like to thank the Air Force Systems Command, The Air Force Office of Scientific Research and the Southeastern Center for Electrical Engineering Education for providing the opportunity to spend a worthwhile and productive summer at the Air Force Geophysics Laboratory, Hanscom Air Force Base, Massachusetts. The laboratory, and in particular the Optical Physics Division is hereby acknowledged for its hospitality and excellent working conditions. Thanks are extended to Mr. Eric P. Shettle for his cheerful guidance throughout the course of this effort.

Very special thanks go to Mr. Robert L. Honohan, Jr., formerly a research assistant contracting with A.F.G.L. Mr. Honohan met with us on his own time on a number of occasions to inform us of the location of various pertinent documents, and assist us in the use of a number of existing A.F.G.L. computer procedures.

## I. INTRODUCTION

The OPAQUE program was a joint NATO program designed to make measurements of the optical and infrared properties of the atmosphere over a period of several years at several locations in Europe. A.F.G.L. was responsible for the measurements at one of these sites in Northern Germany. The reduced data (on an hourly basis) from this station was put into one-month data files for subsequent analysis, and written to magnetic tape for exchange with the other national groups responsible for the measurements at the other sites.

The OPAQUE hourly-file is a data file containing hourly data for a one month period. Each file contains 31 records, one for each day of the month. For months containing less than 31 days, the extra records are merely disregarded. Each daily record contains an array dimensioned 85 x 24. There are 85 entries for each hour of the day, the entries being derived from a ten minute period during the hour. The data entries reported for each hour are defined in Table 1. The 85 entries are initialized as follows:

1. (station number) 71
2. (date) year,month,day,packed into the six rightmost digits
3. (time) hour (0 to 23)
4. (duration of measurement cycle)
- 5-10. (comments on scattering-filter-humidity) 0
- 11-57. (measurement values)  $-1 \times 10E+30$
- 58-77. (weather data)  $-1 \times 10E+30$
- 78-84. (data quality) appropriate number of 9's
85. (rain data)  $-1 \times 10E+30$

With the exceptions of entries 76 and 85, entries 58 through 85 are not recorded by the measurement system data logger. The processing of measurement values are of several types:

1. The AEG Point Visibility Meter, Eltro, Horizontal Luxmeter, Night Path Luminance, and the east direction Variable Path Function Meter require the beginning value, end value, maximum value, minimum value, and number of samples obtained in the ten minute period.
2. The vertical Luxmeter requires one value from each of the four compass points.
3. The VPFM samples in the south, west, and north compass points are required in addition to the five values above for the east direction.
4. The direct Epply and Barnes instrument require values entered, depending on the filter being used for the measurement.

All data values are entered in the daily arrays except if the value was not physically present, or the data could not be interpreted, or the data was out of range, and then a distinguishable flag value is entered in its place. Hence, if a scientific value is not entered for one of these reasons, one of the following values will be entered in its place:

-1 x 10E+30 raw data for that time does not exist  
-9 x 10E+99 raw data exists, but it is impossible to  
interpret  
+8 x 10E+88 the calibrated scientific value is over-range  
-8 x 10E+88 the calibrated scientific value is under-  
range

## II. OBJECTIVES OF THE RESEARCH

The validity of some of the 1400-meter Barnes Transmissometer data stored in words 64 and 65 and in words 28 and 29 beginning 7/1/80, of the processed hourly files was suspect because of apparent continuing erratic fluctuations. The objective of the research effort presented here centers around a thorough analysis of the processed minute-file data together with station-logs and supplemental information to determine whether or not the data stored in the minute-files truly reflects the scientific measurements of the Barnes transmissometer, and if valid to further determine why this validity is not reflected in the hourly-files, and to make the necessary corrections to the hourly data files.

## III Overview of the Hourly File Generating Process

An overview of the programs used to generate and examine the hourly-files is shown in Figure 1. The boxes show the permanent files

involved, and the directed lines show the procedures necessary to accomplish the task.

Before values can be placed in the hourly-file, it must be initialized with the INERIK procedure. The initial values have been listed previously.

The first step in the creation of an hourly data file is the accumulation of the raw data in a Raw Data File. The data usually appears for a three to five day period arranged chronologically on the tape with each measurement time followed by data collected by all instruments at that time. In general the chronological rather than instrument oriented organization of the raw data makes it impractical for obtaining desired outputs such as plots, lists, and special arrays of data. For this reason Stripped Minute Channel Files, Stripped Luxmeter Files, and Stripped Vislab Files are created. The stripping software takes data from these Raw Data Files and arranges it by files consisting of up to sixty-two half days.

The hourly-file is generated from the three stripped data files: the Stripped Minute Channel File, the Stripped Luxmeter File, and the Stripped Vislab File. The three corresponding procedures used to accomplish this are ERIK, LUXERIK, and VISERIK. These procedures generally depend on the time periods of the data.

Before the Hourly file generation is done, it is necessary to modify the Stripped Minute Channel File with the procedure CLEANLX.

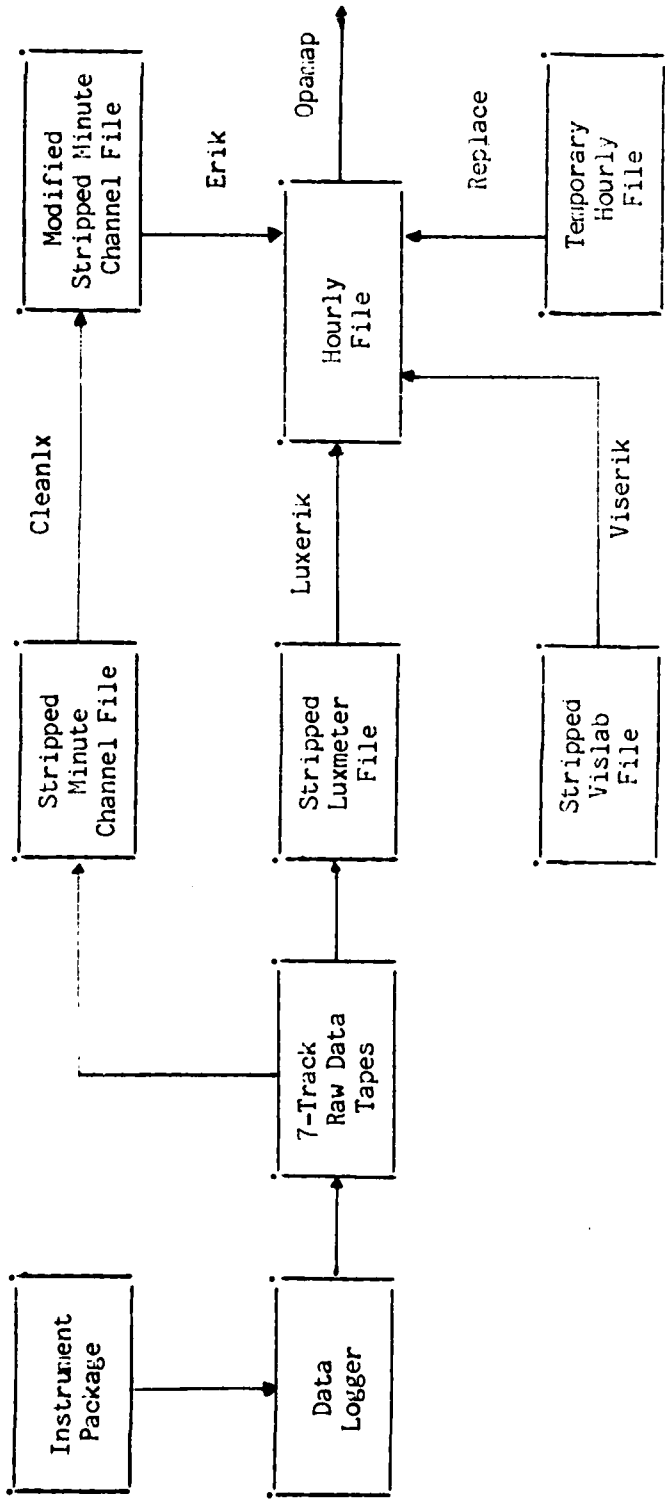


Figure 1: Programs Used to Generate and Examine Hourly-Files

This is done to remove invalid data resulting from the time constant associated with range changes in the non-rotating luxmeter.

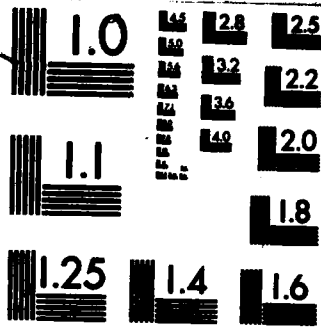
Sometimes it is desirable to change a few entries in the hourly-file while leaving the others intact. This can be accomplished with the REPLACE procedure. A temporary hourly-file containing the required new data values is generated exactly as the hourly-file. Values in this temporary file can then replace corresponding values in the hourly-file. In general, one or more (up to all 85) words can be changed between any two times in the month.

The contents of the hourly-file can be examined with the OPAMAP procedure. Outputs that can be generated include daily maps or summaries of the contents of the data files (either for individual days or for a complete month) and numerical data in various forms.

#### IV. DESCRIPTION OF THE REVISED HOURLY OPAQUE DATA BANK FILE

The instrumentation for the atmospheric optical measurements at the Meppen OPAQUE site was changed significantly in the Fall, 1980. The reconfiguration of the instruments and the additional measurements added to the data set required a redefinition of the contents of the data words in the post-OPAQUE data bank files. These changes are reflected in Table 1: "Format of the Revised Hourly OPAQUE Data Bank File"





MICROCOPY RESOLUTION TEST CHART  
NATIONAL BUREAU OF STANDARDS-1963-A

## V. REPROCESSING TO INCLUDE THE CORRECTED BARNES 1400 METER INSTRUMENT

An intensive investigation was launched in May and June of 1984 to ascertain the validity of the 1400 meter Barnes instrument data that had been stored in hourly-file data-words 64, 65, 28, and 29.

The investigation showed that both the sparsity of data in these data-words, and the seeming inconsistency of the data were a result of a software problem in reading the 1400 meter Barnes filter-wheel position. Improvements were made in the software, and results were verified by comparison with station log entries. Reprocessing of the data was undertaken and completed prior to the end of July, 1984. The corrections were handled as replacements to the already existing hourly files which had been produced by (or for) A.F.G.L. and subsequently further processed at A.F.G.L. The following minute-data was incorporated in the hourly-files:

Word	Description
64	Beginning April, 1978, 1400 meter Barnes 3-5 micron filter (position 1) Analog Channel 22
65	Beginning April, 1978, 1400 meter Barnes 8-12 micron filter (position 3) Analog Channel 22
28	Beginning July, 1980, 1400 meter Barnes 8-13 micron filter (position 2) Analog Channel 22

29 Beginning July, 1980, 400 meter Barnes

4 micron or open (position 0) Analog Channel 22

## VI DESCRIPTION OF OPERATING SYSTEM

The Cyber computer under operating system NOS/BE was used to run all hourly-file procedures and, as such, formed the major working component of this project. Its speed and efficiency were the primary determinants of the pace at which any work could progress. Components of the NOS/BE operating system are illustrated in Figure 2.

Commands for altering the status of a file from one operating system status-type to another are as follows:

Attach- makes a "permanent" file accessible as a "local" file.

Batch- changes file status from local to input queue or from output queue to local status.

Edit- copies a local file to the editor buffer.

Save- places a copy of edit file buffer in local status.

Catalog- gives a local file "permanent" status.

Files are stored in any of the following ways:

- a) on a nine track Computer Center (CC) Tape
- b) on the system disk using a catalog statement
- c) on a disc-pack

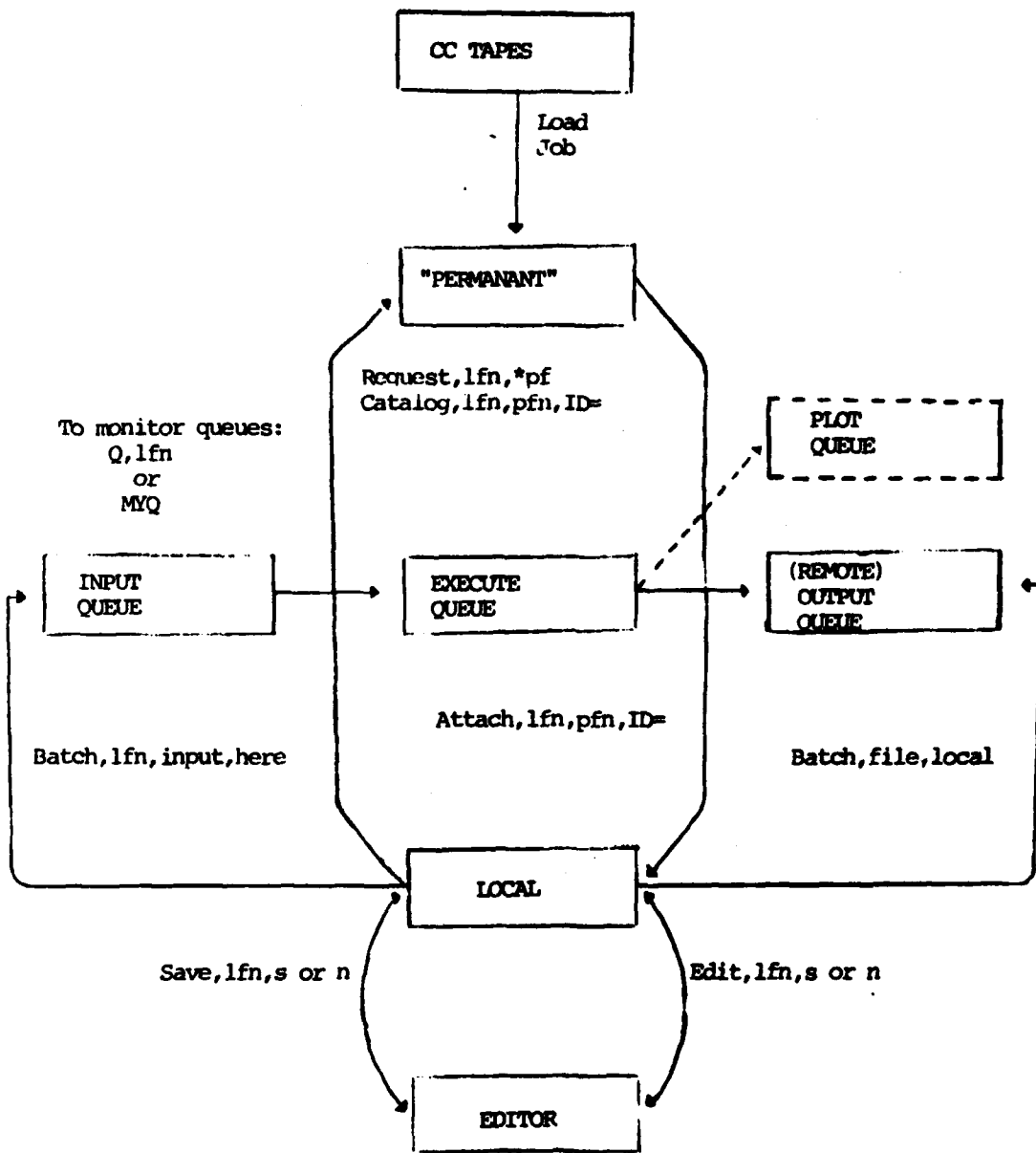


Figure 2: NOS/BE Operating System

Our collection of "permanent" files was limited by restrictions on size (accounts varied from 15,000 to 45,000 PRUs) and time ( files remaining for two weeks without being attached were dropped from the system).

"Permanent" files must be attached as local files to be used in a processing job. This may be accomplished through the Attach statement:

ATTACH,local file name,permanent file ID=user name

Local files can be placed in the editor buffer using the Edit command:

EDIT,lfn,s or n

where s and n refer to sequenced and nonsequenced lines.

The editor is the heart of the Operating System, for it is here that files can be created, examined, checked for correctness, changed, modified, updated, saved, and batched to the input queue; and from here that they can be tracked as well. A file judged satisfactory in the editor is given local status through use of the Save statement:

SAVE,file name,s or n

If the file happens to be a job it may be sent to the processor's

input queue via

BATCH,ifn,input,here

The final parameter, "here", allows the job to be monitored by the user as it is run. The command MYQ displays the progress of all jobs batched in under the user's ID. This progress is reported as the job's position in one of four queues. The input queue holds jobs which have been batched in but have not yet begun to be processed, the execute queue lists jobs which are currently being run, and the output queue lists jobs which have been completed. The plot queue holds data associated with jobs requiring graphed material and are currently being plotted or waiting to be plotted. In each of these queues a job is referred to by a seven letter name which consists of a five letter prefix listed in the first line of the job, followed by two suffix characters added by the system at the time of the batch to input. Using this name the progress of a specific job may may be checked by the QUEUE command:

Q,jobname

From the output queue a job may be given local status using the Batch command:

BATCH,file,local

then placed in the editor for examination before being batched to the printer buffer.

A local file may be given "permanent" status through Request and Catalog statements:

```
REQUEST,lfn,*pf
```

```
CATALOG,lfn,pfn,ID=user name
```

#### VII. SPECIFIC SYSTEM USED TO PROCESS FILES

Because this research project was concerned with the creation and revision of hourly data files a logical, speedy system was developed to allow the process to proceed as simply and efficiently as possible. From starting data to finished product a multitude of steps were involved. Various CC tapes, differing amounts of reprocessing, and determination of time periods for any one file were among the complications which had to be dealt with.

All these factors combined to make careful bookkeeping a must. The process began with a chart showing all of the steps which could be necessary, as well as the CC tapes necessary to create any one month's hourly file. Since efficiency was a prime consideration, many months were processed at the same time. Figure 3 is a sample chart used during this processing. The fifth and sixth columns reflect data

needed for the begin statements of a job to create an hourly file. (See figure 4). The days of the year are referred to by number, and the data necessary to complete any one monthly file usually spans two months of minute data. The day's numbers and hence the minute files needed to create any one month's hourly file were the same from year to year, except for 1980, a leap year.

The jobs to create temporary files and replace their data into existing hourly files were of a general nature (see figure 4). Certain parameters were left unspecified and changed from month to month. This "general job" method proved advantageous for two reasons. First accuracy and completeness were assured. The basic procedures were not changed from one job to another. Once the first job met with success, the later versions were virtually guaranteed to run. Secondly the chance of error was diminished by the reduced amount of typing required to create the job. The only errors possible were in naming files specific to any one job.

The changes needed to make the general jobs specific were made in the editor using the change statement:

`/string 1/=string 2/, line no.`

They were occasionally made by retyping an entire line. An updated job to create hourly file is shown in figure 5. The processing of files is depicted in the flow graph of figure 6.

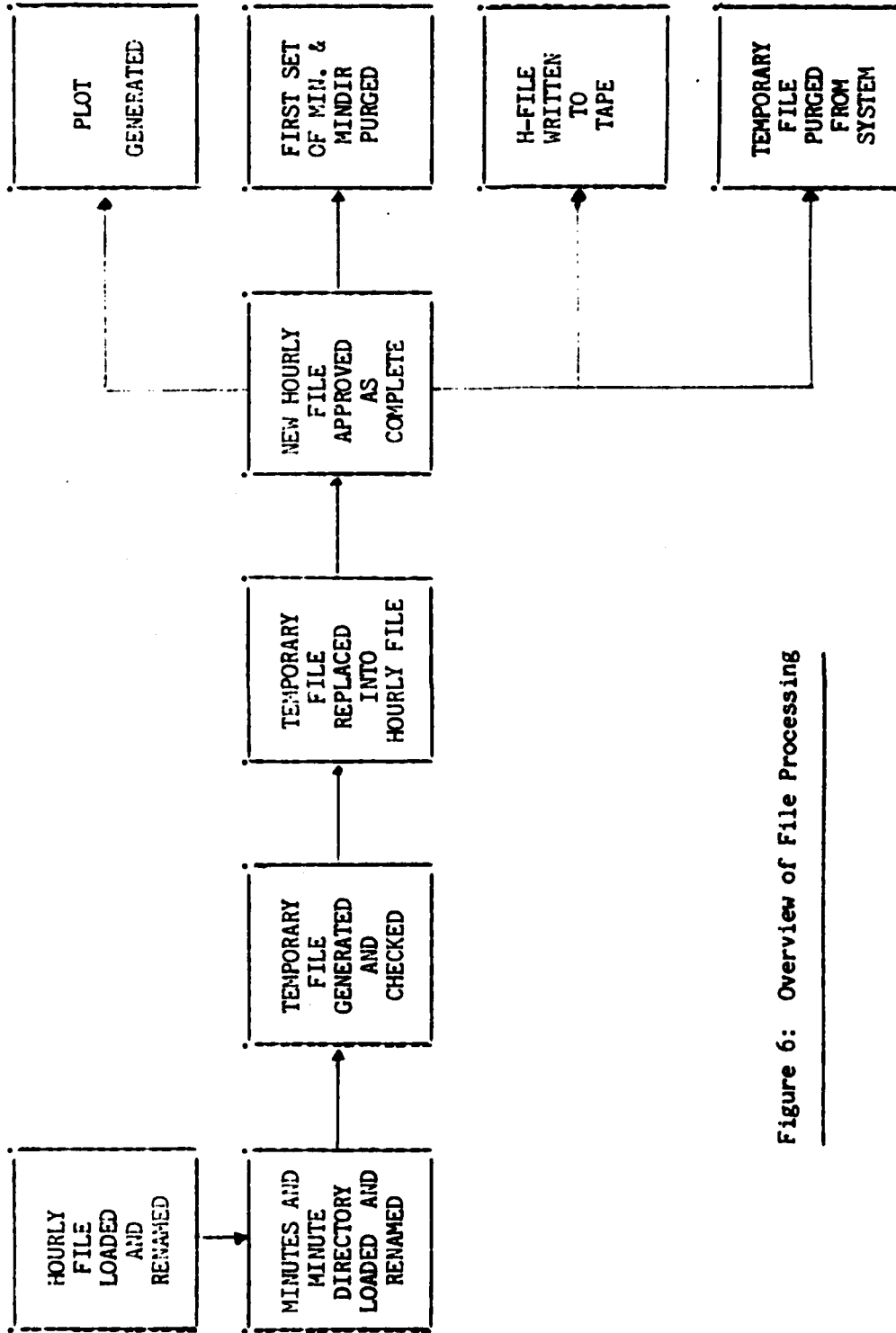


Figure 6: Overview of File Processing

The file making/updating process itself is initiated with the creation of the minutes and minute directory files from the seven-track magnetic tapes containing on-site raw data files from Meppen, Germany. Then the files are renamed XMMYYmin and XMMYYmindir (where MM is the three letter abbreviation for the month and YY the last two digits of the year) so the general job programs will be able to attach them. Sample commands used are:

```
Attach,a,apr78min,id=Lowell,pw=a,b.  
Rename,a,xxapr78min  
Return,a
```

When the ID is not specified in the Rename statement the file remains under it's original listing, and pw defines a user password. The minute files and minute directory files are usually loaded in groups of three (there are three pairs to a CC tape) and purged as the jobs which attach them are judged to be correct. However, the last set of minutes and minute directory must be kept for the first job of the next set. Each set of minutes and directory used about 12,000 PRU's so four sets couldn't fit in even our largest computer account. For this reason the last set had to be moved, space permitting, to one of the smaller accounts until the first set could be purged, when the last set could again be loaded to the Lowell account.

### VIII. SPECIFIC JOBS USED

It was necessary to regenerate and replace data words 64 and 65 of the hourly files for April 1978 through June 1980, and data words 28, 29, 64 and 65 of the hourly files for July 1980 through October 1980. This process required two steps; the generation of a temporary file formatted like an hourly file but containing only the regenerated data words, and the replacement of these data words into the original hourly file. For the period from November 1980 through March 1983 the replacement scheme was not followed. Rather a new hourly file was generated with software corrections for data words 28, 29, 64, and 65. New hourly files were easy to generate for these months because both the VPFM and the Luxmeter had been removed from operation.

The job to generate an hourly file (or a temporary hourly file) illustrated below and in figure 5 begins with a standard type first line which identifies it. The line consists of a five letter prefix, a maximum run time in seconds, an estimate of core memory required, and the account number and ID of the user. It first attaches W6465FIXPROCS, a procedure file containing all of the specific procedures needed to run the job, (see figure 7), as local file XX. There are four begin statements which identify the individual procedures needed, where they can be found, and one or more parameters used in the procedure. The begin statements are followed by an end of record mark; then the data necessary for each procedure is listed, separated by done and end of record marks.

100=LEMIE,T100,CM177000.

3159 LEMIEUX

110=ATTACH,XX,W6465FIXPROCS,ID=PATT,MR=1.

120=BEGIN,INERIK,TYMMEB.

130=BEGIN,??,XX,MM1Y1,TYMMEB.

140=BEGIN,??,XX,MM2Y2,TYMMEB.

150=BEGIN,OPAMAP,XX,HYMMEB.

160=\*EOR

170= MO YR

180=\*EOR

190=BEG,DB1,HB1,MB1\$END,DE1,HE1,ME1\$PICK

200=DONE

210=\*EOR

220=BEG,DB2,HB2,MB2\$END,DE2,HE2,ME2\$PICK

230=DONE

240=\*EOR

250=DISPLAY,1,31,4,64,65,28,29.

260=DONE

270=\*EOR

280=\*EOF

First to be run is INERIK. The parameter supplied is H301EB, (see figure 5) the name to be given to the file which this procedure will create. It will be identified as parameter P1 (see the first line of

the INERIK procedure file located in W6465FIXPROCS) then substituted into the procedure wherever P1 appears. On other jobs this parameter will be changed only one time in the hourly job, but will be substituted into the INERIK procedure automatically and the new files will be named accordingly. The INERIK procedure itself attaches a binary program INITERIKFILEX3664 and renames it as a local file INITOP each time it runs. This program does the actual initializing of the file to be created. The MAP(OFF) statement suppresses information provided by the system to aid in debugging jobs. This information is not necessary in the case of jobs which have proven successful in the past. The "INITOP" statement uses the data between the first set of EORs to run INITERIKFILESX3664. Finally the procedure names the file being created with a catalog statement, and returns the local files it had attached.

Next the job runs ENOV80 twice, once for each month of minute data necessary to create the hourly file. This procedure requires two parameters: the month of minute data being used, and the name of the file into which the generated data words are to be placed. The minute directory, minutes, and hourly file are attached and renamed, then three binary programs use the minute data to generate hourly data and substitute it into the hourly file created by the INERIK procedure. The map is then switched off, the memory cleared with the LDSET command, the binary programs combined, the entire group executed, and the local files returned.

Each time it is run, this procedure uses a BEG statement which supplies the day, hour, and minute at which the data for the hourly month begins and ends.

The last procedure attached is OPAMAP. It requires one parameter and attaches five binary programs in order to display data words from the hourly file just created. The parameter here is the name of the file containing the desired information. After the memory is cleared, the five binary files are combined and executed together as in ENOV80. The statement provided as data lists the first and last day for which data is to be displayed and the number of data words to be displayed, and identifies by number the individual words to be displayed.

The replace job shown in figure 4 also begins with an identifying line and immediately attaches W6465FIXPROCS. It first uses OPAMAP, described earlier, to display the questionable data words. Then REPLAC2 is called to perform the actual replacement. This procedure file requires three parameters: the file into which the replacements are to be made, the file from which the replacement data will come, and the year of the data. The year is specified in order that the correct CAL binary program will be attached - there is one for each year. The procedure attaches the CAL program and four others, blocks unwanted output with MAP(OFF), clears the memory, combines the characters, and executes them. The EXIT(U) command is an unconditional exit which allows the statements following it to be run even if a problem occurs earlier in the procedure. Finally the files

are returned. Each line of data supplied gives a word to be replaced and the day and hour of the first and last replacements to be made. As a check on the replacements, the OPAMAP procedure is run again, displaying the same words as before, Thus the second set of data displayed in the replace job should be different from the first, and the same as that displayed in the temporary job.

IX. DIRECTORY OF HOURLY FILES BEFORE REPLACEMENTS

The hourly-files to which replacements have been made were taken from magnetic tapes issued, catalogued, and housed at the A.F.G.L. Computer Center, as well as hourly-files already on the A.F.G.L. computer system as permanent files. the following tape directories document the replacement process.

	JAN	FEB	MAR	APR	MAY	JUN	JUL	AUG	SEP	OCT	NOV	DEC
1977	a	a	a	a	a	a	a	a	a	a	a	a
1978	a	a	a	1784	1784	1784	1784	1784	1784	1784	1784	b
1979	b	b	b	b	b	b	b	b	b	b	b	b
1980	b	b	b	4894	4894	4894	4894	4894	4894	4894	c	c
1981	c	c	c	c	c	c	c	c	c	c	c	c
1982	c	c	c	c	c	c	c	c	c	c	c	c
1983	c	c	c									

Key: a = Replacement not applicable because 1400 meter Barnes measurements began April, 1978.

b = Replacements were made to hourly-files already on the A.F.G.L. Cyber computer system as permanent files.

c = Replacement process was not used. New hourly files were generated.

#### X. DIRECTORY OF HOURLY-FILES AFTER REPLACEMENTS

	JAN	FEB	MAR	APR	MAY	JUN	JUL	AUG	SEP	OCT	NOV	DEC
1977	2460	2460	2460	2460	2460	2460	2460	2460	2460	2460	2460	2460
1978	1784	1784	1784	4822	4822	4822	4822	4822	4822	4822	4822	4822
1979	4822	4822	4822	4822	4822	4822	4822	4822	4822	4822	4822	4822
1980	4822	4822	4822	4876	4876	4876	4876	4876	4876	4876	4876	4876
1981	4876	4876	4876	4876	4876	4876	4876	4876	4876	4876	4876	4876
1982	4876	4876	4876	4876	4876	4876	4876	4876	4876	4876	4876	4876
1983	4876	4876	4876									

Notes: Hourly-files stored on tape CC4876 do not contain MET data.

Backup tapes of the hourly-files were made as follows:

NOS/BE TAPE	NOS/BE BACKUP	NOS BACKUP
CC4822	CC4825	CC4946
CC4876	CC4825	none

#### XI. INCIDENTAL MAGNETIC TAPES GENERATED

CC4838	NOS/BE	Backup of Honohan's system of 1983
CC4839	NOS/BE	Daily backup of Patt, Summer 1984
CC4875	NOS/BE	Continuation of CC4839
CC4899	NOS	Sources, NOS compilations, and procedures
PAT401	NOS	Same as CC4899

#### XII. RECOMMENDATIONS

1. It is recommended that further processing of the hourly-files begin at once to exploit the large OPAQUE data base. Additional software should be created as soon as possible to automate the view toward the development of an authentic atmospheric model.

2. It is strongly recommended that the procedures used under operating system NOS/BE be updated to run under the more modern NOS operating system currently being installed on the CYBER computer at A.F.G.L.

## IX. REFERENCES

1. F. Baer and P.J. Sheau, "Optimal Spatial Representations For Numerical Weather Prediction Models Based On Normal Mode Analyses", Optical Physics Division, A.F.G.L., Air Force Systems Command, USAF, Hanscomb AFB, Mass., 1982. AFGL-TR-82-0028
2. M.A. Patt, "Analysis of the Validity of Barnes Transmissometer Data", Atmospheric Physics Division, A.F.G.L., Air Force Systems Command, USAF, Hanscom AFB, Mass., 1984. F49620-82-C-0035
3. J.E. Powers, R.J. Dirkman, and M.A. Patt, "The Processing and Analysis of the Data From an Air Force Geophysics Laboratory Atmospheric Optical Measurement Station and Maintenance of The Central Data Logger System", Optical Physics Division, A.F.G.L., Air Force Systems Command, USAF, Hanscom AFB, Mass., 1984.  
AFGL-TR-84-0081
4. J.E. Powers and R.J. Dirkman, "The Reduction and Analysis of Raw Data Tapes from the AFGL Project OPAQUE Data Processor", Optical Physics Division, A.F.G.L., Air Force Systems Command, USAF, Hanscom AFB, Mass., 1981. AFGL-TR-81-0130
5. J.E. Powers and R.J. Dirkman, "The Development and Support of the NATO Project OPAQUE U.S.A.F. Systems Control Programs", Optical Physics Division, A.F.G.L., Air Force Systems Command, USAF, Hanscom AFB, Mass., 1978. AFGL-TR-78-0176

Table 1. Hourly-File Word Allocation

Word No.	Data Item	
1	Station No.	= 71
2	Date - Year,Month,Day	
3	Time	
4	Duration of Measurement cycle	010
5	Comment Numbers	
6	Comment Numbers	
7	Comment Numbers	
8	Comment Numbers	
9	Comment Numbers	
10	Scattering x 100 + Filter x 10 + Humidity	
11	S <sub>s</sub> BEG	AEG Point
12	S <sub>s</sub> FIN	Visibility Meter
13	S <sub>s</sub> MAX	
14	S <sub>s</sub> MIN	
15	NV	Number of Measurements
16	E <sub>g</sub> BEG	
17	E <sub>g</sub> FIN	Eltro
18	E <sub>g</sub> MAX	Transmissometer
19	E <sub>g</sub> MIN	
20	NV	
21	E <sub>L</sub> BEG	
22	E <sub>L</sub> FIN	Horizontal
23	E <sub>L</sub> MAX	Luxmeter
24	E <sub>L</sub> MIN	
25	NV	
26	E <sub>v</sub> <sup>N</sup> (North)	Vertical Luxmeter
27	E <sub>v</sub> <sup>E</sup> (East)	Off after 6/30/80

28	B <sub>15-2</sub>	Barnes	8-13 mm (1500 m)
29	B <sub>15-4</sub>	(eff. 7/1/80)	Open (1500 m)
30	L <sub>p</sub>	BEG	
31	L <sub>p</sub>	FIN	
32	L <sub>p</sub>	MAX	Night Path Luminance
33	L <sub>p</sub>	MIN	
34	NV		
35	F <sub>p</sub>	BEG	Variable Path Function Meter
36	F <sub>p</sub>	FIN	
37	A2	BEG	AEG, 2 meter
38	A2	FIN	(eff. 11/1/80)
39	A8	BEG	AEG, 8 meter
40	A8	FIN	(eff. 11/1/80)
41	A16	BEG	AEG, 16 meter
42	A16	FIN	(eff. 11/1/80)
43	A48	BEG	AEG, 48 meter
44	A48	FIN	(eff. 11/1/80)
45	A80	BEG	AEG, 80 meter
46	A80	FIN	
47	A80	MAX (10')	(eff. 11/1/80)
48	A80	MIN (10')	
49	SEL	BEG	Slant ELTRO
50	SEL	FIN	
51	SEL	MAX (10')	(eff. 11/1/80)
52	SEL	MIN (10')	

53	T <sub>1</sub>	3-5 $\mu$ m BEG
54	T <sub>2</sub>	8-12 $\mu$ m Barnes Transmissometer (500m)
55	T <sub>3</sub>	8-13 $\mu$ m
56	T <sub>x</sub>	Open or 4 $\mu$ m
57	T <sub>8</sub>	3-5m FIN
58	X	Aerosol Data
59	A	
60	B	
61	C	
62	D	
63	E	
64	B <sub>15-1</sub>	3-5 $\mu$ m Barnes Transmissometer (1500m)
65	B <sub>15-3</sub>	8-12 $\mu$ m (1500)
66	H	Turbulence Data
67	I	
68	N	Cloud Cover
69	dd	Wind Direction at 10 m
70	ff	Wind Speed at 10 m
71	d <sub>2</sub> d <sub>2</sub>	Wind Direction at 2 m
72	f <sub>2</sub> f <sub>2</sub>	Wind Speed at 2 m
73	ppn <sup>2</sup>	Pressure
74	TTT	Temperature
75	T <sub>r</sub> T <sub>d</sub> T <sub>d</sub>	Dew Point Temperature
76	r <sub>r</sub> r <sub>d</sub> r <sub>d</sub>	Rain Rate
77	E	General Ground State
78	QQQQ	Packed MRI Data
79	QQQQ	Packed EItro Data
80	QQQQQQQQ	Packed Luxmeter
81	QQQQ	Packed Night Path
82	QQQQQQQ	Packed Vis Lab
83	QQQQQQQQQQ	Packed Eppley Data
84	QQQQQ	Packed Barnes Data
85	PRR	Total Rain

month/yr	location of second set of mines		location of new mines loaded & Erik-file renamed to be loaded		Erik-file loaded & renamed hourly		Start/end time from first set of mins	Start/end time from second set of mins	Job to create temporary hourly	Job to replace	First set of mins purged	U465minny written to CC 4-8-85	PURGE temporary hourly
	CC	min number	CC	min number	CC	min number							
JUN 78	2720	✓	1784	✓	✓	9/1/80	12/19/59	✓	✓	✓	✓	✓	✓
JUN 78	466	✓	1784	✓	✓	12/1/80	12/22/0	✓	✓	✓	✓	✓	✓
JUN 78	766	✓	1784	✓	✓	152/1/80	159/1/0	✓	✓	✓	✓	✓	✓
JUL 78	766	✓	1784	✓	✓	153/1/80	182/1/57	✓	✓	✓	✓	✓	✓
JUL 78	1442	✓	1784	✓	✓	182/1/80	183/1/59	✓	✓	✓	✓	✓	✓
AUG 78	442	✓	1784	✓	✓	213/1/80	241/1/51	✓	✓	✓	✓	✓	✓
AUG 78	442	✓	1784	✓	✓	241/1/80	241/1/80	✓	✓	✓	✓	✓	✓

Figure 3: Sample Processing Chart

Figure 4: General Replace Job and Job To Create Hourly File

```
100=LENIR,T100,CHI77000.                                3159  LEMIEUX
110=ATTACH,XX,U646SFIXPROCS,ID=PATT,MR=1.
120=BEGIN,OPANAP,XX,HYHMEB.
130=BEGIN,REPLAC2,XX,HYHMEB,TYHMB,YY.
140=BEGIN,OPANAP,XX,HYHMEB.
150=RETURN,XX.
160=*EOR
170=DISPLAY,1,31,4,64,65,28,29.
180=DONE
190=*EOR
200=REPLACEXX,64,1,1,31,23.
210=REPLACEXX,65,1,1,31,23.
220=DONE
230=*EOR
240=DISPLAY,1,31,4,64,65,28,29.
250=DONE
```

```
100=LENIE,T100,CHI77000.                                3159  LEMIEUX
110=ATTACH,XX,U646SFIXPROCS.ID=PATT,MR=1.
120=BEGIN,INERIK,XX,HYHMEB.
130=BEGIN,??,XX,MM1Y1,HYHMEB.
140=BEGIN,??,XX,MM2Y2,HYHMEB.
150=BEGIN,OPANAP,XX,HYHMEB.
160=*EOR
170=  MD  YR
180=*EOR
190=BEG,DB1,MB1,MB1$END,DE1,ME1,ME1$PICK
200=DONE
210=*EOR
220=BEG,DB2,MB2,MB2$END,DE2,ME2,ME2$PICK
230=DONE
240=*EOR
250=DISPLAY,1,31,4,64,65,28,29.
260=DONE
270=*EOR
280=*EOF
```

Figure 5: Specific Job To Create Hourly File

```
100=LENIE,T100,CN177000.                3159  LEMIEUX
110=ATTACH,XX,U6465FIXPROCS,ID=PATT,MR=1.
120=BEGIN,INERIK,XX,H301EB.
130=BEGIN,ENC090,XX,JAN83,H301EB.
140=BEGIN,ENC090,XX,FEB83,H301EB.
150=BEGIN,OPANAP,XX,H301EB.
160=*EOR
170=  01  83
180=*EOR
190=BEG,1,0,0*END,31,9,59%PICK
200=DONE
210=*EOR
220=BEG,31,10,0*END,31,23,59%PICK
230=DONE
240=*EOR
250=DISPLAY,1,31,10,64,65,26,29,53,54,13,14,18,19.
260=DONE
270=*EOR
280=*EOF
```

Figure 7: W6465FLXPROCS

```
100=.PROC,EAPR79,P1=MMYY,P2=TEMPMMYYHOURLY.
110=ATTACH(TAPE2,XX_PI_MIN,ID=LOWELL,SN=PERM,PW=A,B,MR=1)
120=ATTACH(TAPE3,XX_PI_MINDIR,ID=LOWELL,SN=PERM,PW=A,B,MR=1)
130=ATTACH(TAPE6,P2,[D=PATT,PW=A,B])
140=ATTACH(ERIC,ERIC3455MIN73X3664,ID=PATT,MR=1)
150=ATTACH(CMND,CMNDX3664,ID=PATT,MR=1)
160=ATTACH(CAL,CAL79X3664,ID=PATT,MR=1)
170=ATTACH(SUBS,SUBSX3664,ID=PATT,MR=1)
180=MAP(OFF)
190=LOSET(PRESET=ZERO)
200=LOAD(ERIC,CMND,CAL,SUBS)
210=EXECUTE,,PL=15000.
220=RETURN,TAPE2,TAPE3,TAPE6,ERIC,CMND,CAL,SUBS.
230=*EOR
240=.PROC,E79,P1=MMYY,P2=TEMPMMYYHOURLY.
250=ATTACH(TAPE2,XX_PI_MIN,ID=LOWELL,SN=PERM,PW=A,B,MR=1)
260=ATTACH(TAPE3,XX_PI_MINDIR,ID=LOWELL,SN=PERM,PW=A,B,MR=1)
270=ATTACH(TAPE6,P2,[D=PATT,PW=A,B])
280=ATTACH(ERIC,ERIC3455MIN77X3664,ID=PATT,MR=1)
290=ATTACH(CMND,CMNDX3664,ID=PATT,MR=1)
300=ATTACH(CAL,CAL82X3664,ID=PATT,MR=1)
310=ATTACH(SUBS,SUBSX3664,ID=PATT,MR=1)
320=MAP(OFF)
330=LOSET(PRESET=ZERO)
340=LOAD(ERIC,CMND,CAL,SUBS)
350=EXECUTE,,PL=15000.
360=RETURN,TAPE2,TAPE3,TAPE6,ERIC,CMND,CAL,SUBS.
370=*EOR
380=.PROC,EJUL90,P1=MMYY,P2=TEMPMMYYHOURLY.
390=ATTACH(TAPE2,XX_PI_MIN,ID=LOWELL,SN=PERM,PW=A,B,MR=1)
400=ATTACH(TAPE3,XX_PI_MINDIR,ID=LOWELL,SN=PERM,PW=A,B,MR=1)
```

410=ATTACH(TAPE6,P2, ID=PATT, PU=A, B)  
 420=ATTACH(ERIC, ERIKMINJUL90THRUOCT80X3664, ID=PATT, MR=1)  
 430=ATTACH(CMND, CMNDX3664, ID=PATT, MR=1)  
 440=ATTACH(CAL, CAL82X3664, ID=PATT, MR=1)  
 450=ATTACH(SUBS, SUBSX3664, ID=PATT, MR=1)  
 460=MAP(OFF)  
 470=LDSET(PRESET=ZERO)  
 480=LOAD(ERIC, CMND, CAL, SUBS)  
 490=EXECUTE, , PL=15000.  
 500=RETURN, TAPE2, TAPE3, TAPE6, ERIC, CMND, CAL, SUBS.  
 510=\*EOR  
 520=.PROC, ENOV90, P1=MMYY, P2=TEMPMMYYHOURLY.  
 530=ATTACH(TAPE2, XX\_P1\_MIN, ID=LOWELL, SN=PERM, PU=A, B, MR=1)  
 540=ATTACH(TAPE3, XX\_P1\_MINDIR, ID=LOWELL, SN=PERM, PU=A, B, MR=1)  
 550=ATTACH(TAPE6, P2, ID=PATT, PU=A, B)  
 560=ATTACH(ERIC, ERIKMINNOV30T-RUX3664, ID=PATT, MR=1)  
 570=ATTACH(CMND, CMNDX3664, ID=PATT, MR=1)  
 580=ATTACH(CAL, CAL32X3664, ID=PATT, MR=1)  
 590=ATTACH(SUBS, SUBSX3664, ID=PATT, MR=1)  
 600=MAP(OFF)  
 610=LDSET(PRESET=ZERO)  
 620=LOAD(ERIC, CMND, CAL, SUBS)  
 630=EXECUTE, , PL=15000.  
 640=RETURN, TAPE2, TAPE3, TAPE6, ERIC, CMND, CAL, SUBS.  
 650=\*EOR  
 660=.PROC, INERIK, P1=TEMPMMYYHOURLY.  
 670=REQUEST(TAPE6, \*PF)  
 680=ATTACH(INITOP, INITERIKFILEX3664, ID=PATT)  
 690=MAP(OFF)  
 700=INITOP.  
 710=CATALOG(TAPE6, P1, ID=PATT, EX=A, MD=B)  
 720=RETURN, TAPE6, INITOP.  
 730=\*EOR  
 740=.PROC, OPANAP, P1=FILENAME.  
 750=ATTACH(TAPE6, P1, ID=PATT, PU=A, B)  
 760=ATTACH(ERIC, ERIC00RX3664, ID=PATT, MR=1)  
 770=ATTACH(CMND, CMNDX3664, ID=PATT, MR=1)  
 780=ATTACH(CAL, CAL79X3664, ID=PATT, MR=1)  
 790=ATTACH(SUBS, SUBSX3664, ID=PATT, MR=1)

```

800=MAP(OFF)
810=LDSET(PRESET=ZERO)
820=LOAD(ERIC,CMND,CAL,SUBS)
830=EXECUTE,,PL=15000.
840=RETURN,TAPE6,ERIC,CMND,CAL,SUBS.
850=*EOR
860=.PROC,REPLACE,P1=W6465MMHYHOURLY,P2=TEMPMMHYHOURLY,P3=YR.
870=ATTACH,TAPE6,P1,ID=PATT,PW=A,B.
880=ATTACH,TAPE10,P2,ID=PATT,PW=A,B.
890=ATTACH,ERIC,ERIKX3664,ID=PATT,MR=1.
900=ATTACH,CMND,CMNDX3664,ID=PATT,MR=1.
910=ATTACH,CAL,CAL_P3_X3664,ID=PATT,MR=1.
920=ATTACH,REPLAC,REPLACX3664,ID=PATT,MR=1.
930=ATTACH,SUBS,SUBSX3664,ID=PATT,MR=1.
940=MAP(OFF)
950=LDSET(PRESET=ZERO)
960=LOAD(ERIC,CMND,CAL,REPLAC,SUBS)
970=EXECUTE,,PL=15000.
980=EXIT(U)
990=RETURN,TAPE6,TAPE10,ERIC,CMND,CAL,REPLAC,SUBS.
1000=*EOR
1010=.PROC,REPLAC2,P1=W6465MMHYHOURLY,P2=TEMPMMHYHOURLY,P3=YR.
1020=ATTACH,TAPE6,P1,ID=PATT,PW=A,B.
1030=ATTACH,TAPE10,P2,ID=PATT,PW=A,B.
1040=ATTACH,ERIC,REPLACEJOBX3664,ID=PATT,MR=1.
1050=ATTACH,CMND,CMNDX3664,ID=PATT,MR=1.
1060=ATTACH,CAL,CAL_P3_X3664,ID=PATT,MR=1.
1070=ATTACH,SUBS,SUBSX3664,ID=PATT,MR=1.
1080=MAP(OFF)
1090=LDSET(PRESET=ZERO)
1100=LOAD(ERIC,CMND,CAL,SUBS)
1110=EXECUTE,,PL=15000.
1120=EXIT(U)
1130=RETURN,TAPE6,TAPE10,ERIC,CMND,CAL,SUBS.
1140=*EOR

```

1984 USAF-SCEEE GRADUATE STUDENT SUMMER SUPPORT PROGRAM

Sponsored by the

AIR FORCE OFFICE OF SCIENTIFIC RESEARCH

Conducted by the

SOUTHEASTERN CENTER FOR ELECTRICAL ENGINEERING EDUCATION

FINAL REPORT

A COMPUTER SEARCH FOR  $M_{11}$  AS A GALOIS GROUP OVER  $\mathbb{Q}$

Prepared by: Eric E. Liverance  
Academic Department: Mathematics  
University: Yale University  
Research Location: WPAFB Flight Dynamics Laboratory,  
Structures and Dynamics Division,  
Analysis and Optimization Branch  
USAF Research Contact: Mr. James DeWeese  
SFRP Supervising  
Faculty Member: Dr. Paul J. Nikolai  
Date: September 15, 1984  
Contract No: F49620-82-C-0035

A COMPUTER SEARCH FOR  $M_{11}$  AS A

GALOIS GROUP OVER  $\mathbb{Q}$

by

Eric E. Liverance

ABSTRACT

Two methods of calculating Galois groups of polynomials are presented. Their use in conjunction with one another is discussed and is probably the most efficient means known to compute Galois groups. Stauduhar's method is improved for degree  $n \leq 5$  by explicit calculation of resolvents. Finally, an unsuccessful computer search for  $M_{11}$  as a Galois group over  $\mathbb{Q}$  is presented. The search is based on Van der Waerden's method.

### ACKNOWLEDGEMENTS

I would like to thank the Air Force Systems Command, the Air Force Office of Scientific Research and the Southeastern Center for Electrical Engineering Education for providing me with the opportunity to carry out research for this paper at the Flight Dynamics Laboratory, Wright-Patterson AFB, Dayton, Ohio. I would like to acknowledge the laboratory for its hospitality and excellent working conditions. In particular, I would like to thank the Computer Support Group there for the lavish amount of computer time and for the untiring assistance given to my project. All computations done in this paper were obtained with the aid of MACSYMA, a large symbolic manipulation program developed at the MIT Laboratory for Computer Science and support from 1975 to 1983 by the National Aeronautics and Space Administration under grant NSG1323, by the Office of Naval Research under grant N00014-77-C-0641, by the U.S. Department of Energy under grant ET-78-C-02-4687, and by the U.S. Air Force under grant F49620-79-C-020, and since 1982 by Symbolics, Inc. of Cambridge, Mass.

I would also like to thank Joe P. Buhler and John McKay for their invaluable guidance in researching this area. Finally, I would like to give special thanks to Paul J. Nikolai for his helpful direction in the inner workings of the laboratory and for making this research project possible.

I. INTRODUCTION:

The following are the two main problems of Galois theory over the rationals:

- (1) To determine  $\text{Gal}(f)$ , the Galois group of  $f(x)$ , given the polynomial  $f(x)$ .
- (2) To find a polynomial  $f(x)$  having a given permutation group  $G$  as Galois group.

The first has been solved by many people in various ways. In Section III we examine a couple of these. When used in conjunction they provide the most effective method known of computing Galois groups. One of the methods - Stauduhar's method - is improved upon for degree  $n \leq 5$  in Section IV by explicit calculation of Galois resolvents.

The second problem listed above is as yet unsolved. Partial results do exist. For example, Schafarevich [6] has shown that all solvable groups can be realized as Galois groups. Also, it is easy to show that  $A_n$  and  $S_n$  can always be realized as Galois groups. See Tschebotarow [11]. There have also been isolated cases of someone realizing some particular group as a Galois group. See Erbach [4], La Macchia [7]. Also Feit (unpublished) has recently realized  $\text{PSL}(3,p)$ ,  $p \neq -1 \pmod{24}$  as Galois groups. However, no one has yet developed a method powerful enough to show all finite groups can be realized as Galois groups.

In Section V, a computer search for  $M_{11}$ , the Mathien group of degree 11, is presented. It is intended to be a contribution to the second problem above. The method of search is based on Van der Waerden's method of computing Galois groups, presented in Section III.

## II. OBJECTIVES:

The main objective of this project was to investigate methods of calculating Galois groups of polynomials, and to try to apply these methods to the unsolved problem in Galois theory mentioned in the Introduction. In particular, I had hoped to develop some sort of method of realizing  $M_{11}$  as a Galois group. Rather than directly attack this problem, I carried out a computer search for  $M_{11}$  based on one the methods of calculating Galois groups I investigated.

## III. THE METHODS OF VAN DER WAERDEN AND STAUDUHAR:

The following development is essentially a condensation of the excellent paper by Van der Linden [8]. For proofs of the theorems, see Van der Linden's paper.

We discuss two methods of calculating the Galois group of a polynomial  $f(x)$ . We shall see that when used in conjunction they provide a very effective method of calculating Galois groups.

We place the following restrictions on  $f(x)$ .  $f(x)$  must be a monic, irreducible polynomial with integer coefficients. Let  $G$  denote the Galois group of  $f(x)$ , and let  $f(x)$  be of degree  $n$ , so that  $G \subset S_n$ .

The first method is due to Van der Waerden [13].

Let  $d_1, \dots, d_r$  be positive integers with  $\sum_{i=1}^r d_i = n$ . We say  $\sigma \in S_n$  has cycle pattern  $(d_1, \dots, d_r)$  if  $\sigma$  is the product of  $r$  disjoint cycles of lengths  $d_1, \dots, d_r$ . Let  $p$  be a prime number. Suppose that  $\bar{f} = (f \bmod p) \in \mathbb{F}_p[x]$  factorizes as

$$\bar{f} = \prod_{i=1}^r \bar{f}_i \quad \text{with degree } (\bar{f}_i) = d_i,$$

where the  $\bar{f}_i$  are distinct monic irreducible polynomials in  $\mathbb{F}_p[x]$ . In

this situation we say  $p$  belongs to the cycle pattern  $(d_1, \dots, d_r)$ . We also want to speak of the cycle pattern belonging to the "prime at infinity". This can be done by replacing in the above definition  $\mathbb{F}_p[x]$  by  $\mathbb{R}[x]$  and  $(f \bmod p)$  by  $f$ . In this case all  $d_i$  are 1 or 2.

Theorem 1. Suppose that  $p$  is a, possibly infinite, prime, which belongs to the cycle pattern  $(d_1, \dots, d_r)$ . Then there exists an element  $\sigma$  of  $G$  of cycle pattern  $(d_1, \dots, d_r)$ .

To apply the theorem, we make a list of all transitive subgroups of  $S_n$  which contain elements with the encountered cycle pattern. Such a list can be formed from Butler [2]. (His paper contains a list of transitive subgroups and the cycle patterns occurring in each one for groups of degree  $n \leq 11$ .) By Theorem 1 we know  $G$  is in this list. This is not sufficient to determine  $G$  in general, unless we find  $G = S_n$  (or  $G = A_n$  if  $\text{disc}(f)$  is a square as we shall see). However, the following theorem allows us to make a reasonably certain guess as to which member of the list  $G$  is.

Theorem 2. (Tschebotaröw Density Theorem). Let  $(d_1, \dots, d_r)$  be a cycle pattern. Let  $C$  be the set of elements of  $G$  with cycle pattern  $(d_1, \dots, d_r)$ , and let  $P$  be the set of primes belonging to  $(d_1, \dots, d_r)$ . Then

$$\lim_{x \rightarrow \infty} \frac{\#\{p \leq x : p \in P\}}{\#\{p \leq x : p \text{ prime}\}} = \frac{\#C}{\#G}.$$

Bounds do exist for the least prime belonging to a given cycle type, however at present they are not very good.

This theorem, then lets us narrow our list down (with moral certainty) to those whose cycle frequencies match those encountered. Often

this narrowed down list contains only one subgroup of  $S_n$ . However, it is only with the following method that we obtain certainty.

We now discuss the method of Stauduhar. This method is actually much older than Stauduhar [10] (see for example Dehn [3]) and is based on the use of Galois resolvents. These are defined as follows. Write  $\underline{u} = (u_1, \dots, u_n)$ , where the  $u_i$  are indeterminates over  $Q$ . Consider the field  $Q(\underline{u})$ . We have an action of  $S_n$  on  $Q(\underline{u})$  by permuting the  $u_i$ . For every subgroup  $H$  of  $S_n$  we denote by  $Q(\underline{u})^H$  the fixed field of  $H$ . By Galois theory, we have  $\text{Gal}(Q(\underline{u})/Q(\underline{u})^H) = H$ . Let  $H'$  be a subgroup of  $H$ ; then we have  $Q(\underline{u})^{H'} = Q(\underline{u})^H(F(\underline{u}))$  for some  $F(\underline{u}) \in Q(\underline{u})^{H'}$ . We may choose  $F(\underline{u}) \in Z[\underline{u}]$ . Let  $\Phi_{H,H'}(z, \underline{u}) =$

$\prod (z - \sigma F(\underline{u}))$ , where  $R$  is a set of left coset representatives of  $\sigma \in R$  in  $H$ , i.e.  $H$  is the disjoint union of  $\sigma H'$  for  $\sigma \in R$ . We call  $\Phi_{H,H'}$  the Galois resolvent of  $H'$  in  $H$  corresponding to  $F(\underline{u})$ .

Theorem 3. Let  $f(x) \in Z[x]$  be monic and irreducible, and  $G \subset S_n$  its Galois group. Let  $H \subset S_n$  be a subgroup containing  $G$ , and  $H' \subset H$  a subgroup. Let  $\sigma \in H$ . Write  $\underline{\alpha} = (\alpha_1, \dots, \alpha_n)$ , where the  $\alpha_i$  are the roots of  $f(x)$ . Then

- a)  $\Phi_{H,H'}(z, \underline{\alpha}) \in Z[z]$ ,
- b) if  $G \subset \sigma H' \sigma^{-1}$  then the root  $\sigma F(\underline{\alpha})$  of  $\Phi_{H,H'}(z, \underline{\alpha})$  is in  $Z$ ,
- c) conversely, if  $\sigma F(\underline{\alpha}) \in Z$ , and  $\sigma F(\underline{\alpha})$  is not a double root of  $\Phi_{H,H'}(z, \underline{\alpha})$ , then  $G \subset \sigma H' \sigma^{-1}$ .

We apply this theorem in the following way. Suppose one knows that  $G \subset H$ , where  $H$  is a transitive subgroup of  $S_n$  (for example, one knows this for  $H = S_n$ ). Using Galois resolvents and Theorem 3, we can determine whether or not  $G \subset \sigma H' \sigma^{-1}$  for some maximal transitive

subgroup  $H' \subset H$  and some  $\sigma \in H$ . If this occurs for no maximal subgroup, then  $G = H$ . If however,  $G \subset \sigma H' \sigma^{-1}$ , we replace  $H$  by  $\sigma H' \sigma^{-1}$  and repeat the procedure.

We compute  $\Phi_{H,H'}(z, \underline{\alpha})$  with the help of its roots which we compute using the roots of  $f$ . Because we know that  $\Phi_{H,H'}(z, \underline{\alpha}) \in \mathbb{Z}[z]$ , we can calculate it exactly on a computer using high precision arithmetic. If a zero of  $\Phi_{H,H'}(z, \underline{\alpha})$  is "almost" an integer, we can round it to an integer. With the help of long integer arithmetic we can show that this integer is a root of  $\Phi_{H,H'}(z, \underline{\alpha})$ . Our improvement in Section IV of Stauduhar's method calculates these resolvents in terms of the coefficients of  $f$  when degree  $f = n \leq 5$ .

If we get  $G \subset \sigma H' \sigma^{-1}$  for some  $\sigma \in H$ , we merely renumber the roots of  $f$  to get  $G \subset H'$ .

In the rare case (see Van der Linden [8]) that  $\Phi_{H,H'}(z, \underline{\alpha})$  has a double integral root one has to take another Galois resolvent of  $H'$  in  $H$ .

One special case of Galois resolvents is the resolvent of  $A_n$  in  $S_n$ . In this case, we take  $F = \prod_{1 \leq i < j \leq n} (u_i - u_j)$ . Then

$$\begin{aligned} \Phi_{S_n, A_n}(z, \underline{u}) &= (z - F)(z + F) \\ &= z^2 - \prod_{1 \leq i < j \leq n} (u_i - u_j)^2. \end{aligned}$$

So  $\Phi_{S_n, A_n}(z, \underline{\alpha}) = z^2 - d$ , where  $d = \text{disc}(f)$ , the discriminant of  $f$ . So we have  $G \subset A_n$  iff  $d$  is a square in  $\mathbb{Z}$ . We also see that in this case,  $\Phi_{S_n, A_n}$  cannot have a double integral root because  $d \neq 0$ .

Stauduhar [10] gives data for using his method for  $4 \leq n \leq 7$ .

We now discuss the use of both methods together. Van der Waerden's method gives us a list of possible subgroups of  $S_n$  for  $G$ . Now we can use the Galois resolvent of Stauduhar's method to show that  $G$  is contained in one of the conjugates of one of the subgroups of the list. If this is the case we know  $G$  exactly. If not,  $G$  must be bigger than our first guess.

This method is in practice the most efficient procedure in general because it usually avoids calculating resolvent equations of high degree. Also it avoids the most difficult part, computationally, of the Van der Waerden method - factoring modulo large primes.

#### IV. EXPLICIT CALCULATION OF THE GALOIS RESOLVENTS FOR DEGREE $n = 4, 5$ .

We first consider the cases  $n = 2, 3$  for completeness. In these cases, the Galois group depends entirely on  $\text{disc}(f)$ .

If  $f(x) = x^2 + bx + c$ , then the irreducibility of  $f$  implies that  $\text{disc}(f) = b^2 - 4c$  is not a square in  $\mathbb{Z}$ . Hence  $G = S_2$ .

If  $f(x) = x^3 + bx^2 + cx + d$ , then  $G = A_3$  or  $S_3$  depending on whether or not

$$\text{disc}(f) = -4b^3d + b^2c^2 + 18bcd - 4c^3 - 27d^2$$

is a square in  $\mathbb{Z}$ .

#### The case $n = 4$ .

Let

$$f(x) = x^4 + bx^3 + cx^2 + dx + e$$

be a monic irreducible polynomial in  $\mathbb{Z}[x]$ . The tree of transitive subgroups of  $S_4$  is displayed below in Figure 1.

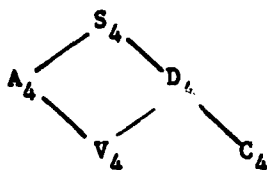


FIGURE 1 - TRANSITIVE SUBGROUPS OF  $S_4$

We shall show that it is sufficient to compute  $\Phi_{S_4, D_4}(z, \underline{\alpha})$  and  $\Phi_{D_4, C_4}(z, \underline{\alpha})$  in order to determine  $G$ .

To compute  $\Phi_{S_4, D_4}(z, \underline{\alpha})$ , the so-called cubic resolvent of  $f$ , we set  $F(\underline{u}) = u_1 u_2 + u_3 u_4$ . Then

$$\begin{aligned} \Phi_{S_4, D_4}(z, \underline{\alpha}) &= (z - (\alpha_1 \alpha_2 + \alpha_3 \alpha_4))(z - (\alpha_1 \alpha_3 + \alpha_2 \alpha_4))(z - (\alpha_1 \alpha_4 + \alpha_2 \alpha_3)) \\ &= z^3 + a_1 z^2 + a_2 z + a_3 \end{aligned}$$

where

$$a_1 = -c, \quad a_2 = bd - 4e, \quad a_3 = -b^2 e - d^2 + 4ce.$$

It can now be verified that by our choice of  $F$  we have  $\text{disc}(\Phi_{S_4, D_4}) = \text{disc}(f)$ . Hence  $\Phi$  cannot have multiple roots. Also, if  $\Phi$  has no rational roots, then  $G = S_4$  or  $A_4$ , depending on whether  $\text{disc}(\Phi)$  is a square in  $\mathbb{Z}$  or not. If  $\Phi$  has 3 rational roots, then  $G$  is contained in all 3 conjugates of  $D_4$  and hence is equal to  $V_4$ . If  $\Phi$  has exactly one rational root, then  $G \subset D_4$ . Note that in this case,  $\text{disc}(\Phi)$  is not a square in  $\mathbb{Z}$ , for if it were we would have  $G \subset A_4$  and hence  $G \subset A_4 \cap D_4 = V_4$ . This would imply that  $\Phi$  have 3 rational roots.

Thus we find it necessary to compute  $\Phi_{D_4, C_4}(z, \underline{\alpha})$ . In this case we assume  $G \subset D_4$  and that

$$\Phi_{S_4, D_4}(z, \underline{\alpha}) = (x^2 + c_1 x + c_2)(x + c_3)$$

is the factorization of  $\Phi_{S_4, D_4}$  over the integers.

Let  $F(\underline{u}) = u_1 u_2^2 + u_2 u_3^2 + u_3 u_4^2 + u_4 u_1^2$ . Then we have

$$\Phi_{D_4, C_4}(z, \underline{a}) = (z-s_1)(z-s_2),$$

where

$$s_1 = a_1 a_2^2 + a_2 a_3^2 + a_3 a_4^2 + a_4 a_1^2$$

$$s_2 = a_1 a_4^2 + a_4 a_3^2 + a_3 a_2^2 + a_2 a_1^2.$$

Then  $G = C_4$  iff  $\text{disc}(\Phi_{D_4, C_4})$  is a square in  $\mathbb{Z}$ .

$$\begin{aligned} \text{disc}(\Phi_{D_4, C_4}) &= (s_1 - s_2)^2 \\ &= c_1^2 b^2 - 4c_2 b^2 + 4c_1^3 - 16c_1 c_2. \end{aligned}$$

The case  $n = 5$ .

Let

$$f(x) = x^5 + bx^4 + cx^3 + dx^2 + ex + f$$

be a monic irreducible polynomial in  $\mathbb{Z}[x]$ . The tree of transitive subgroups of  $S_5$  is given in Figure 2 below.

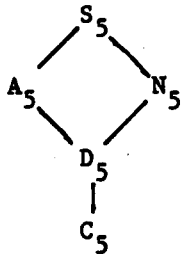


FIGURE 2 - TRANSITIVE SUBGROUPS OF  $S_5$

The Galois resolvents we need to compute are  $\Phi_{S_5, A_5}$  (i.e.  $\text{disc}(f)$ ),

$\Phi_{S_5, N_5}$ ,  $\Phi_{D_5, C_5}$ .

$$\text{disc}(f) = 3125f^4 + A_3 f^3 + A_2 f^2 + A_1 f + A_0$$

where

$$A_3 = -2500be + 2000b^2d - 3750cd + 2250bc^2 - 1600b^3c + 256b^5$$

$$A_2 = (2000c - 50b^2)e^2 + (2250d^2 + (160b^3 - 2050bc)d - 900c^2 + 1020b^2c^2 - 192b^4c)e - 900bd^3 + (825c^2 + 560b^2c - 128b^4)d^2 + (144b^3c^2 - 630bc^3)d + 108c^5 - 27b^2c^4$$

$$A_1 = (-1600d + 160bc - 36b^3)e^3 + (1020bd^2 + (560c^2 - 746b^2c + 144b^4)d + 24bc^3 - 6b^3c^2)e^2 + ((24b^2 - 630c)d^3 + (356bc^2 - 80b^3c)d^2 + (18b^2c^3 - 72c^4)d)e + 108d^5 + (16b^3 - 72bc)d^4 + (16c^3 - 4b^2c^2)d^3$$

$$A_0 = 256e^5 + (-192bd - 128c^2 + 144b^2c - 27b^4)e^4 + ((144c - 6b^2)d^2 + (18b^3c - 80bc^2)d + 16c^4 - 4b^2c^3)e^3 + (-27d^4 + (18bc - 4b^3)d^3 + (b^2c^2 - 4c^3)d^2)e^2.$$

As always,  $G \subset A_5$  iff  $\text{disc}(f) = D^2$  for some  $D \in \mathbb{Z}$ .

Next we compute  $\Phi_{S_5, N_5}$  the so-called sextic resolvent of  $f$ .

In order to do this, we first compute  $\Phi_{A_5, D_5}$ . Set

$$F(\underline{u}) = u_1u_2 + u_2u_3 + u_3u_4 + u_4u_5 + u_5u_1 - u_1u_3 - u_3u_5 - u_5u_2 - u_2u_4 - u_4u_1.$$

$F$  belongs to  $D_5$ . It can be seen that  $F^2$  belongs to  $N_5$ . Thus, if we compute  $\Phi_{A_5, D_5}$ , we can get  $\Phi_{S_5, N_5}$  by forming the polynomial whose roots are the squares of the roots of  $\Phi_{A_5, D_5}$ .

$$\Phi_{A_5, D_5}(z, \underline{a}) = z^6 + a_1z^5 + a_2z^4 + a_3z^3 + a_4z^2 + a_5z + a_6$$

where

$$a_1 = a_3 = 0 \quad a_5 = 32D$$

$$a_2 = -3c^2 + 8bd - 20e$$

$$a_4 = 3c^4 - 16bc^2d + 16b^2d^2 + 16b^2ce - 64b^3f$$

$$+ 16cd^2 - 8c^2e - 112bde + 240bcf + 240e^2 - 400df$$

$$\begin{aligned}
a_6 = & -c^6 + (8bd + 28e)c^4 + (-16b^2e - 16d^2 + 48bf)c^3 \\
& + (-16b^2d^2 - 112bde - 80df - 176e^2)c^2 \\
& + (64b^3de - 192b^2df + 64bd^3 + 224b^2e^2 - 640bef \\
& \quad + 224d^2e + 400f^2)c \\
& - 64b^4e^2 + 384b^3ef - 128b^2d^2e - 1600b^2f^2 \\
& + 640bd^2f - 64bde^2 - 64d^4 - 1600def + 320e^3.
\end{aligned}$$

Now let  $\Phi_{A_5, D_5}(z, \underline{a}) = \prod_{i=1}^6 (z - z_i)$ . By the comment above,

$$\Phi_{S_5, N_5}(z, \underline{a}) = \prod_{i=1}^6 (z - z_i^2).$$

This allows us to calculate the coefficients of  $\Phi_{S_5, N_5}$  in terms of those of  $\Phi_{A_5, D_5}$ . Write

$$\Phi_{S_5, N_5}(z, \underline{a}) = z^6 + b_1z^5 + b_2z^4 + b_3z^3 + b_4z^2 + b_5z + b_6.$$

Then we find that

$$\begin{aligned}
b_1 &= 2a_2 \\
b_2 &= a_2^2 + 2a_4 \\
b_3 &= 2a_2a_4 + 2a_6 \\
b_4 &= a_4^2 + 2a_2a_6 \\
b_5 &= -1024 \operatorname{disc}(f) + 2a_4a_6 \\
b_6 &= a_6^2.
\end{aligned}$$

One can show that  $\Phi_{A_5, D_5}$  and hence  $\Phi_{S_5, N_5}$  can never have multiple roots. See Tschebotarow [11].

It remains to calculate  $\Phi_{D_5, C_5}$ . Unfortunately, I was unable to carry out this calculation. To see why, we need to look at our original discussion of Galois resolvents.

$\Phi_{H, H'}$  taken with respect to  $F(\underline{u})$  is really the minimal polynomial for  $F(\underline{u})$  over  $\mathbb{Q}(\underline{u})^H$ . Thus the coefficients of  $\Phi_{H, H'}$  are in

$\mathbb{Q}(\underline{u})^H$ . However, we can show that in fact the coefficients are in a subring of  $\mathbb{Q}(\underline{u})^H$ .

Let  $R = \mathbb{Z}[p_1, \dots, p_n]$  where the  $p_i$  are the elementary symmetric functions of the  $u_i$ ,

$$p_1 = \sum_{i=1}^n u_i, p_2 = \sum_{1 \leq i < j \leq n} u_i u_j, \dots, p_n = \prod_{i=1}^n u_i.$$

We call an element of  $\mathbb{Q}(\underline{u})$  R-integral if its unique monic minimal polynomial over  $\mathbb{Q}(\underline{u})^S$  has coefficients in R. The R-integral elements A of  $\mathbb{Q}(\underline{u})$  form a ring (see Jacobson [5]). In particular, since

$$x^n - p_1 x^{n-1} + p_2 x^{n-2} \dots + (-1)^n p_n = \prod_{i=1}^n (x - u_i),$$

each  $u_i \in A$ . A obviously also contains R. Since A is a ring, it contains any polynomial of the  $u_i$  with integer coefficients. Thus we see that  $F(\underline{u}) \in A$  and similarly so are all the roots of  $\Phi_{H,H'}$ . Consequently, the coefficients of  $\Phi_{H,H'}$  are in A. Thus we can conclude that the coefficients of  $\Phi_{H,H'}$  are in  $\mathbb{Q}(\underline{u})^H \cap A$ .

We found in all the other cases that we were able to go still farther and could write the coefficients of  $\Phi_{H,H'}$  in  $R[E(\underline{u})]$  where  $E(\underline{u})$  is a polynomial of the  $u_i$  with integer coefficient, invariant under H. So, in other words we would like to show that for  $H = D_5$ ,  $H' = C_5$ ,  $\mathbb{Q}(\underline{u})^H \cap A = R[E(\underline{u})]$ . However, I was actually able to show that the constant term of  $\Phi_{D_5, C_5}$  does not lie in  $R[E(\underline{u})]$ . Hence

$$\mathbb{Q}(\underline{u})^H \cap A \not\supseteq R[E(\underline{u})].$$

The determination of  $\mathbb{Q}(\underline{u})^H \cap A$  is necessary in order to calculate  $\Phi_{D_5, C_5}$ . If no assumptions are made, the calculation is nearly impossible.

Thus in this case, one must use the methods described in Section III to distinguish  $D_5$  and  $C_5$ .

V. A COMPUTER SEARCH FOR  $M_{11}$ :

We extract Tables 1 and 2 from Butler [2]. We wish to find a polynomial  $f$  whose Galois group  $G$  is  $M_{11}$ . Rather than just generate polynomials and compute Galois groups blindly, we should like to find some characteristic of  $M_{11}$  which would show up in the polynomial  $f$  if  $G = M_{11}$ , and use this characteristic to generate polynomials. The Van der Waerden method of computing Galois groups gives us a very simple characteristic of  $f$ .

TABLE 1 - GROUPS OF DEGREE 11

Butler's notation for group	name	order	even
T1	$C_{11}$	11	+
T2		22	
T3	half metacyclic	55	+
T4	metacyclic	110	
T5	$L(2,11)$	660	+
T6	$M_{11}$	7920	+
T7	$A_{11}$	$(1/2)11!$	+
T8	$S_{11}$	$11!$	

TABLE 2 - CYCLE TYPE DISTRIBUTION

	$1^{11}$	$1^3 2^4$	$1 \cdot 2^5$	$1^2 3^3$	$1^3 4^2$	$1 \cdot 5^2$	$2 \cdot 3 \cdot 6$	$1 \cdot 2 \cdot 8$	$1 \cdot 10$	$11$
T1	1	.	.	.	.	.	.	.	.	10
T2	1	.	11	.	.	.	.	.	.	10
T3	1	.	.	.	.	44	.	.	.	10
T4	1	.	11	.	.	44	.	.	44	10
T5	1	55	.	110	.	264	110	.	.	120
T6	1	165	.	440	990	1584	1320	1980	.	1440

From Table 2 we note that of the 6 groups listed,  $M_{11}$  is the only group with the cycle types  $1^3 4^2$  and  $1 \cdot 2 \cdot 8$  occurring. Thus if, for a polynomial  $f$ ,  $p$  belongs to either cycle type  $1^3 4^2$  or  $1 \cdot 2 \cdot 8$ , then  $G = M_{11}$ ,  $A_{11}$ , or  $S_{11}$ . We note also that if some  $p$  belongs to cyclic type  $11$ , then  $f$  is guaranteed to be irreducible.

The above facts form the basis for the computer search. If we force  $f$  to satisfy

$$f \equiv g \pmod{2}$$

$$f \equiv h \pmod{3}$$

where  $g$  is irreducible modulo 2 and  $h$  belongs to cycle type  $1 \cdot 2 \cdot 8$  or  $1^3 4^2$ , then we are guaranteed by the congruence relation modulo 2 that  $f$  is irreducible, and we are guaranteed by the congruence relation modulo 3 that  $G = M_{11}$ ,  $A_{11}$ , or  $S_{11}$ . Then such polynomials can be tested to see if they have a square determinant. If so, then  $G = M_{11}$  or  $A_{11}$ .

To distinguish these last two cases requires a bit more work. Usually the method of Van der Waerden will indicate that  $G$  is one or

the other. However, to be absolutely sure, at this point we use a method that appears in McKay [9].

We can distinguish  $A_{11}$  and  $M_{11}$  by their transitivity -  $A_{11}$  is nine-fold transitive whereas  $M_{11}$  is only four-fold transitive. Consider the set of sums of roots of  $f$  five at a time.  $A_{11}$  acts transitively on this set, but  $M_{11}$  does not. Thus if we form the polynomial  $g$  whose roots are sums of the roots of  $f$  five at a time, then  $g(x)$  is irreducible iff  $G = A_{11}$ . If  $G = M_{11}$ , then  $g(x)$ , which is of degree  $\binom{11}{5} = 462$  has an irreducible factor of degree 66 corresponding to the Steiner system  $S(4,5,11)$ .

Admittedly, this last test is very difficult, but it would only be applied to polynomials which we were already very sure were  $M_{11}$ .

In the search that was actually carried out, I chose  $h$  to belong to cycle type  $1 \cdot 2 \cdot 8$  since it occurs more commonly than  $1^3 4^2$ . To generate the polynomials  $f$ , I merely generated all mod 2 polynomials irreducible of degree 11, denoted  $P(11,2)$ ; and all mod 3 polynomials irreducible of degrees 1, 2, and 8, denoted  $P(1,3)$ ,  $P(2,3)$ , and  $P(8,3)$  respectively. Then one member from each set was chosen and  $f$  was forced to satisfy the previously mentioned congruence relations mod 6. The coefficients of  $f$  were chosen to be between -2 and +3 inclusive.

We note that an arbitrary number of congruence relations could have been forced on  $f$ , so that the first few primes could be made to belong to cycle types that best approximate their occurrence in  $M_{11}$ . Then by "keeping in line" with the Tschebotarow Density Theorem, one would hope to produce an  $f$  for which  $G = M_{11}$ . However, such a polynomial must still undergo all the testing described above. With so many

congruence relations forced on  $f$ , the coefficients of  $f$  are bound to get large and thus increase the computation time. Furthermore, in view of Van der Waerden's proof (Van der Waerden [12]) that as the coefficients of  $f$  become large, the probability that  $G = S_{11}$  is 1, it is in our interest to keep the coefficients of  $f$  small. Thus only two congruences relations were forced on  $f$  and the coefficients were taken as small as possible - between -2 and +3 inclusive.

We now calculate the total number of polynomials such a search would generate. We have the well-known formula for the number  $I(n,p)$  of irreducible polynomials of degree  $n \bmod p$ , a prime (see Jacobson [5], p. 145 or Berlekamp [1], p. 83-84):

$$I(n,p) = \frac{1}{n} \sum_{d|n} \mu(d) p^{n/d},$$

where  $\mu(d)$  is the Mobius function.

We have

$$I(11,2) = \frac{2^{11}-2}{11} = 186$$

$$I(8,3) = \frac{3^8-3^4}{2} = 810$$

$$I(2,3) = \frac{3^2-3}{2} = 3$$

$$I(1,3) = \frac{3}{1} = 3.$$

Hence the complete search examines  $186 \cdot 810 \cdot 3 \cdot 3 = 1,355,940$  polynomials. This is a vast reduction over a totally blind search of degree 11 polynomials mod 6. There  $6^{11} = 362,797,056$  of these.

Due to time constraints and the fact that I was working in a very high level (hence inefficient) language, my search was necessarily incomplete. I used approximately 120 hours of computer time to examine approximately 72,000 polynomials - about 5% of the total intended.

The search was unsuccessful, however, it did manage to find a polynomial for which  $G = A_{11}$ . We now present this polynomial.

$$f(x) = x^{11} + 3x^{10} + 3x^0 + x^7 - 2x^6 + 3x^5 - 2x^4 - 2x^2 - x + 1.$$

The roots of  $f$  are

$$\begin{aligned} \alpha_1 &= 0.4855 & \alpha_4, \alpha_5 &= -0.1299 \pm 0.9416i \\ \alpha_2 &= 0.6345 & \alpha_6, \alpha_7 &= 0.6173 \pm 0.7089i \\ \alpha_3 &= 0.8491 & \alpha_8, \alpha_9 &= -0.5146 \pm 0.9311i \\ & & \alpha_{10}, \alpha_{11} &= -1.8223 \pm 0.9535i \end{aligned}$$

$$\begin{aligned} \text{disc}(f) &= 57,630,486,432,885,025 \\ &= 5^2 \cdot 11^2 \cdot 4,364,791^2. \end{aligned}$$

We factor  $f$  mod selected primes:

$$\begin{aligned} f(x) &\equiv x^{11} + x^{10} + x^9 + x^7 + x^5 + x + 1 \pmod{2} \\ &\equiv (x+1)(x^2+1)(x^8 - x^7 - x^4 - x^3 - x^2 + x + 1) \pmod{3} \\ &\equiv (x-8)(x-6)(x+2)(x^2 - 5x + 7) \cdot \\ &\quad (x^6 + 3x^5 + x^4 - 3x^3 + 8x^2 - 2x + 2) \pmod{17}. \end{aligned}$$

Since  $\text{disc}(f)$  is a square,  $G \subset A_{11}$ . However the factorization mod 17 implies that  $G = A_{11}$ .

## VI. RECOMMENDATIONS:

There are at least 2 ways the results of this paper could be extended:

- (1) The problem of determining the structure of  $\mathbb{Q}(\underline{u})^H \cap A$ , for  $H = D_5$  (mentioned in Section IV) could be worked on. Then  $\mathfrak{F}_{D_5, C_5}$  could be calculated.
- (2) There is no reason to believe the computer search of Section V cannot be completed in a reasonable amount of time if carried out in a low-level language.

I should also like to add that an excellent reference to related literature is Van der Linden [8].

#### REFERENCES

1. Berlekamp, E.R., Algebraic Coding Theory, McGraw-Hill, New York, 1968.
2. Butler, Gregory and John McKay, "The Transitive Groups of Degree up to Eleven," Comm. in Alg. 11 (8), 863-911 (1983).
3. Dehn, E., Algebraic Equations, Columbia Univ. Press, New York; reprint, Dover, New York, 1960.
4. Erbach, D.W., J. Fischer and J. McKay, "Polynomials with  $PSL(2,7)$  as Galois Group," J. Num. Th. 11, 69-75 (1979).
5. Jacobson, Nathan, Basic Algebra I, W.H. Freeman and Co., San Francisco, 1974.
6. Krasner, M., Math Reviews, Vol. 16 (1955), pp. 571-572.
7. LaMacchia, Samuel E., "Polynomials with Galois Group  $PSL(2,11)$ ," Comm. in Alg., 9(6), 613-625 (1981).
8. Linden, F.J. Van der, "The Computation of Galois Groups," Computational Methods in Number Theory, part II, edited by H.W. Lenstra and R. Tijdeman, Mathematical Centre Tracts, Mathematische Centrum, Amsterdam 1982.
9. McKay, J., "Some Remarks on Computing Galois Groups," Siam J. Comput., Vol. 8, No. 3, p. 344-347, August 1979.
10. Stauduhar, R.P., "The Determination of Galois Groups," Math. Comp. 27, 981-996 (1973).
11. Tschebotaröw, N., Grundzuge der Galois'schen Theorie, P. Noordhoff, Groningen, 1950.
12. Waerden, B.L. Van der, "Die Seltenheit der Gleichungen mit Affekt," Math. Ann. 109, p. 13-16 (1934).
13. Waerden, B.L. Van der, Modern Algebra, Vol. 1, Ungar, New York, 1953.

**END**

**FILMED**

**7-85**

**DTIC**